Development of Photo-Induced C–H Activation by Copper and Ruthenium Catalysis

Dissertation

for the award of the degree

"Doctor rerum naturalium"

of the Georg-August-Universität Göttingen

within the doctoral program of chemistry

of the Georg-August-University School of Science (GAUSS)

submitted by

Julian Koeller

from Göttingen

Göttingen, 2019

Thesis Committee

Professor Dr. Lutz Ackermann, Institute of Organic and Biomolecular Chemistry

Professor Dr. Konrad Koszinowski, Institute of Organic and Biomolecular Chemistry

Members of the Examination Board

Reviewer:

Professor Dr. Lutz Ackermann, Institute of Organic and Biomolecular Chemistry

Second Reviewer:

Professor Dr. Konrad Koszinowski, Institute of Organic and Biomolecular Chemistry

Further Members of the Examination Board

Professor Dr. Dr. h.c.mult. Lutz F. Tietze, Institute of Organic and Biomolecular Chemistry

Professor Dr. Dietmar Stalke, Institute of Inorganic Chemistry

Dr. Holm Frauendorf, Institute of Organic and Biomolecular Chemistry

Dr. Michael John, Institute of Organic and Biomolecular Chemistry

Date of the Oral Examination: 29 October, 2019

Acknowledgments

First and foremost, I sincerely thank Professor Lutz Ackermann for all the opportunities he has provided me with over the last five years. I am especially thankful for the opportunity to work on this thesis under his mentorship and guidance. Furthermore, I thank Professor Lutz Ackermann for providing excellent working conditions and his style of leadership that shaped a research group and work environment that was always characterized by colleagueship and mutual support. I am particularly thankful for the time I got to spend during the research stay at the Academia Sinica.

Secondly, I thank Professor Konrad Koszinowski for readily taking the time to additionally supervise this thesis. I am very thankful for his time and the thoughtful suggestions he provided during our meetings. Furthermore, I thank Professor Dr. Dr. h.c.mult. Lutz F. Tietze, Professor Dr. Dietmar Stalke, Dr. Holm Frauendorf and Dr. Michael John for agreeing to be part of the examination board and for the time they invested in this.

Additionally, I thank the analytical departments of the institute for the swift and precise handling of countless of analytical samples and for their kind support in case of any problems.

Furthermore, I am grateful to Gabriele Keil-Knepel for all her support regarding any administrative tasks and similar requirements. I particularly thank Stefan Beußhausen and Karsten Rauch for all their hard work, which substantially contributes to the excellent working conditions.

I am profoundly thankful to all my former and present colleagues in the Ackermann group, especially my former lab members, namely Dr. Gandeepan Parthasarathy, Dr. Thomas Müller, Isaac Choi, Dr. Parthasarathi Subramanian, and Dr. Marc Moselage. I am very thankful to Isaac Choi, Dr. Lars Finger, Joachim Loup, Dr. Thomas Müller, Torben Rogge, Maximilian Stangier, Ralf Steinbock, Julia Struwe, Cong Tian, Dr. Hui Wang, and Wei Wang for the proofreading of this thesis.

To my parents and Melina, I am eternally grateful for their constant and unconditional support, especially during the last decade.

Content

List of Abbreviations

4-CzPN	3,4,5,6-tetra(9*H*-carbazol-9yl)phthalonitrile
Ac	acetyl
Acr–Mes	9-mesityl-10-methylacridinium
Ad	adamantyl
Alk	alkyl
AMLA	ambiphilic metal-ligand activation
API	active pharmaceutical ingredient
Aq	8-aminoquinoline
Ar	aryl
ATR	attenuated total reflectance
BHT	2,6-di-*tert*-butyl-4-methylphenol
BIES	base-assisted internal electrophilic substitution
Bn	benzyl
Boc	*tert*-butyloxycarbonyl
bpy	2,2'-bipyridine
Bu	butyl
CFL	compact fluorescent lamp
CMD	concerted metalation-deprotonation
Cp	cyclopentadienyl
d	doublet
DABCO	1,4-diazabicyclo[2.2.2]octane
dap	2,9-bis-(4-methoxy-phenyl)-1,10-phenanthroline
DCE	1,2-dichloroethane
DCN	1,4-dicyanonaphthalene
dd	doublet of doublets
$dFCF_3ppy$	2-(2,4-difluorophenyl)-5-(trifluoromethyl)pyridine
DG	directing group
DMA	dimethylacetamide
DMF	dimethylformamide
dmg	dimethylglyoxime

DMPU	*N*,*N*'-dimethylpropyleneurea
DMSO	dimethyl sulfoxide
dtbbpy	4,4'-bis(tert-butyl)-2,2'-bipyridine
equiv	equivalent
ESI	electrospray ionization
Et	ethyl
GC	gas chromatography
i	*iso*
IES	intramolecular electrophilic substitution
IR	infrared
LED	light-emitting diode
m	*meta* or multiplet
M. p.	melting point
m/z	mass-to-charge ratio
Me	methyl
Mes	mesityl
MS	mass spectrometry
MTBE	2-methoxy-2-methylpropane
NBS	*N*-bromosuccinimide
NMO	4-methylmorpholine 4-oxide
NMP	1-methylpyrrolidin-2-one
NMR	nuclear magnetic resonance
Ns	nosyl
o	*ortho*
p	*para*
PA	picolinamide
Ph	phenyl
phen	1,10-phenanthroline
PIDA	(diacetoxyiodo)benzene
Piv-Val	*N*-pivaloyl-valine
ppy	2-phenylpyridinato

Pr	propyl
Py	pyridyl
pym	pyrimidyl
R	rest
SET	single electron transfer
t	*tert* or triplett
TEMPO	(2,2,6,6- tetramethylpiperidin-1-yl)oxidanyl
Tf	triflyl
TFA	trifluoroacetic acid
THF	tetrahydrofuran
TLC	thin layer chromatography
tpy	2-(*p*-tolyl)pyridine
UV	ultraviolet

1 Introduction

Along with the continuous growth of the global population, humankind is constantly increasing its demand for energy, food, and consumables. The economic development over the last century has contributed to an unprecedented level of wealth and quality of life for billions of people. Among the natural sciences, chemistry has been one of the major driving forces for this development.

In 1913, only four years after Haber's initial demonstration of his ammonia synthesis, Bosch had managed to establish the commercial production of ammonia at BASF.[1] Since then, the Haber-Bosch-process laid the foundation for the production of nitrogen fertilizers, which were and still are a key to global agricultural productivity.[1-2] Accordingly, Haber and Bosch were awarded the Nobel Prize in Chemistry in 1918[3] and 1931,[4] respectively. This is but one example of the enormous impact that large-scale chemical processes can have on a global scale. Throughout the last century, chemical processes kept contributing to economic and social development.

Unfortunately, the ecological impact was not always directly realized. Beginning in the 1960s, society became increasingly aware of the environmental issues associated with the widespread use of chemicals and their production processes.[5] As a response to these growing problems, changes in the design of chemical production were gradually introduced. Thus, these efforts resulted in the continuous development of new concepts and more sustainable approaches during the following decades. In 1991, Trost introduced the concept of atom economy,[6] which reformed how chemists approached organic synthesis.[7] His idea was then essentially incorporated into the 12 Principles of Green Chemistry published by Anastas and Warner in 1998.[8]

Within their work, Anastas and Warner also established catalysis as a fundamental tool to achieve more sustainable development. In the years prior to the publication of the 12 Principles of Green Chemistry, the field of catalysis had witnessed a tremendous development. Thus, the Nobel Prize for Chemistry in 2001 was awarded to W. S. Knowles,[9] R. Noyori,[10] and B. Sharpless[11] for their work on asymmetric hydrogenation and oxidation methods.[12] The recognition catalysis received was further increased when Y. Chauvin,[13] R. Grubbs,[14] and R. R. Schrock[15] received the Nobel Prize for Chemistry in

2005,[16] acknowledging their work regarding olefin metathesis. Finally, in 2010, R. F. Heck, E.-i. Negishi,[17] and A. Suzuki[18] were honored for the development of palladium-catalyzed cross-couplings in organic synthesis.[19] In this context, the Nobel Prize for Chemistry in 2007 awarded to G. Ertl[20] should also be mentioned.[21] Especially, the impact of cross-coupling reactions on organic synthesis can hardly be overestimated as it fundamentally changed the way chemists addressed the synthesis of structurally complex molecules such as drugs and agrochemicals. These Nobel Prizes further underline the importance Anastas and Warner already attributed to the field of catalysis.

As mankind is nowadays still facing the consequences of its increased demand for energy and resources, the race for the development of new and more sustainable methods is still ongoing. As in the last century, chemistry will continue to be a key factor for a sustainable and environmentally benign growth, of both wealth and improved living conditions of the global population.

1.1 Transition Metal-Catalyzed C–H Activation

C–C and C–Het bond formations enabled by metal-catalyzed cross-coupling reactions had a tremendous influence on the production of fine chemicals, active pharmaceutical ingredients (APIs), and agrochemicals and are nowadays a well-established tool in organic synthesis.[22] Despite the indisputable impact, cross-coupling strategies have innate drawbacks.

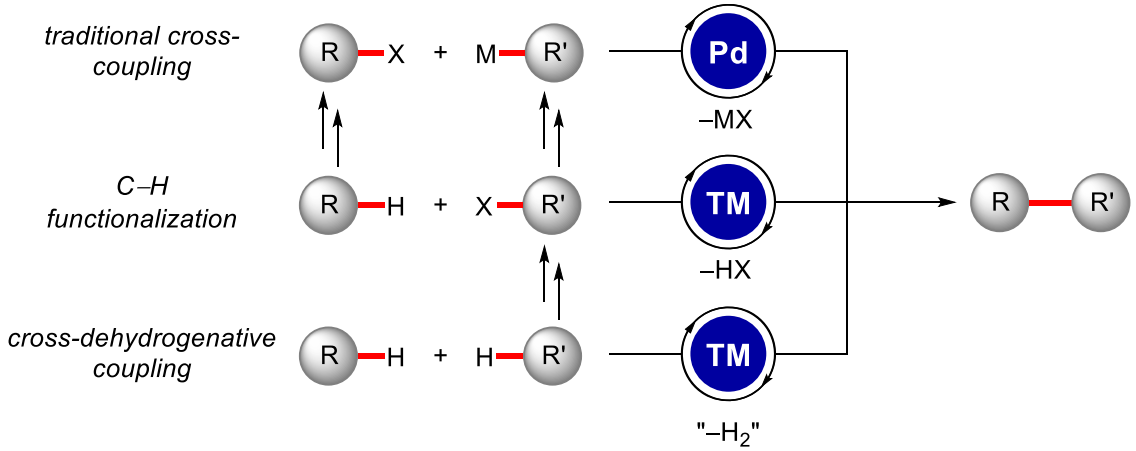

Figure 1.1: Comparison between cross-coupling strategies and C–H activation.

As it becomes evident from Figure 1.1, traditional cross-coupling strategies greatly rely on the use of prefunctionalized starting materials. As these have to be prepared in additional synthetic steps, their use inherently lowers the step-economy[23] as well as the atom-economy of the overall synthesis. In addition, the cross-coupling reaction itself generates stochiometric amounts of by-products.[24] Furthermore, the required organometallic reagents cause problems of their own, as they display adverse properties in regard to stability or toxicity.

Accompanying the increasing emphasis on sustainability, the recent decades have witnessed tremendous advances in the field of transition metal-catalyzed C–H functionalization reactions.[25] The direct site-selective functionalization of C–H bonds circumvents the need for pre-functionalization and thereby reduces waste generation, hence lowering the economic and ecologic costs of the synthesis. The overall higher resource economy[26] of the C–H functionalization strategy has been the major driving force behind its development during the last decades.

Yet, the avoidance of pre-functionalized starting materials creates a new challenge regarding the desired C–H functionalization. As C–H bonds are ubiquitous in organic molecules[27] and their respective bond dissociation energies (BDEs) are usually quite similar,[28] effective discrimination among the C–H bonds is crucial for a selective functionalization. This is usually achieved in one of three ways (Figure 1.2). Two out of the three strategies rely on the use of either electronically or sterically biased substrates. Although effective, these two methods are severely limited in their substrate scope and therefore in their general applicability. More broadly applicable and therefore of considerably higher significance is the directing group-based approach.[29] By pre-coordination of the transition metal, this strategy allows for the site-selective functionalization of C–H bonds in close proximity to the Lewis-basic directing group.[30]

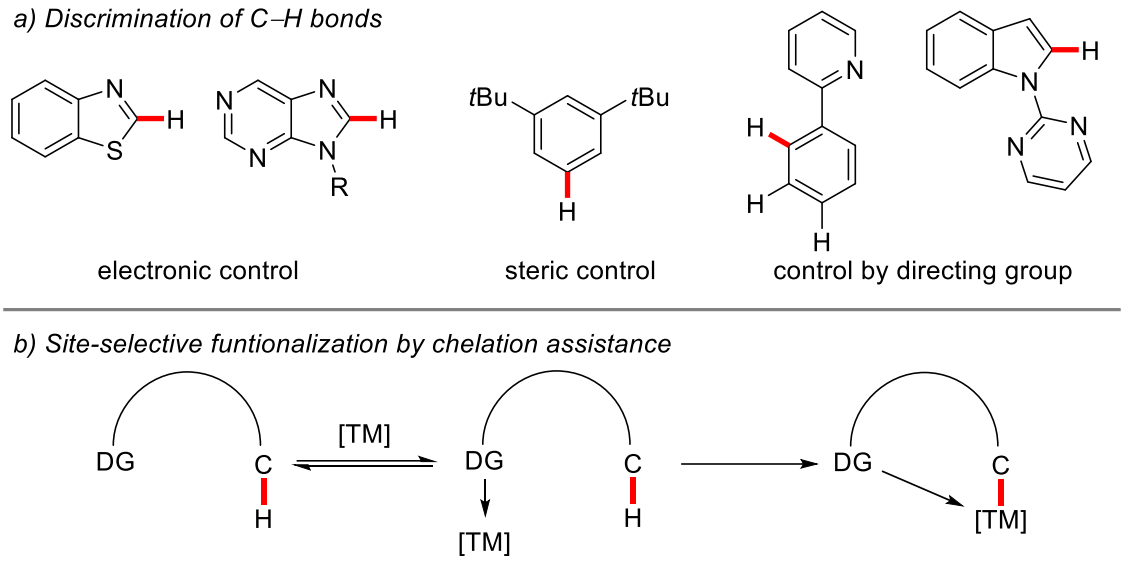

Figure 1.2: a) Discrimination between C–H bonds. b) Mode of action of the directing group.

The tremendous potential of this approach is displayed by the late-stage functionalization of complex and highly functionalized molecules such as peptides,[31] functional materials,[32] and complex alkaloids.[33]

As the transition metal-facilitated cleavage of the C–H bond is the common key step in the above-mentioned C–H functionalization strategies, it has been heavily studied. These efforts resulted in a profound knowledge of the underlying mechanisms which are depicted in Figure 1.3.[34] A C–H bond cleavage by a) oxidative addition is commonly encountered with electron-rich, low-valent complexes of late transition metals.[34c,34f] Since an oxidative process is not feasible for early transition metals with a d^0 electron configuration the predominant mechanism regarding the C–H cleavage is b) *σ*-bond metathesis or d) 1,2-addition.[34d,34f] In contrast to the early transition metals, electron-deficient late transition metals usually react *via* c) an electrophilic activation process.[34c,34d] Especially during the last two decades e) base-assisted C–H metalation received increased attention.[34b,34c]

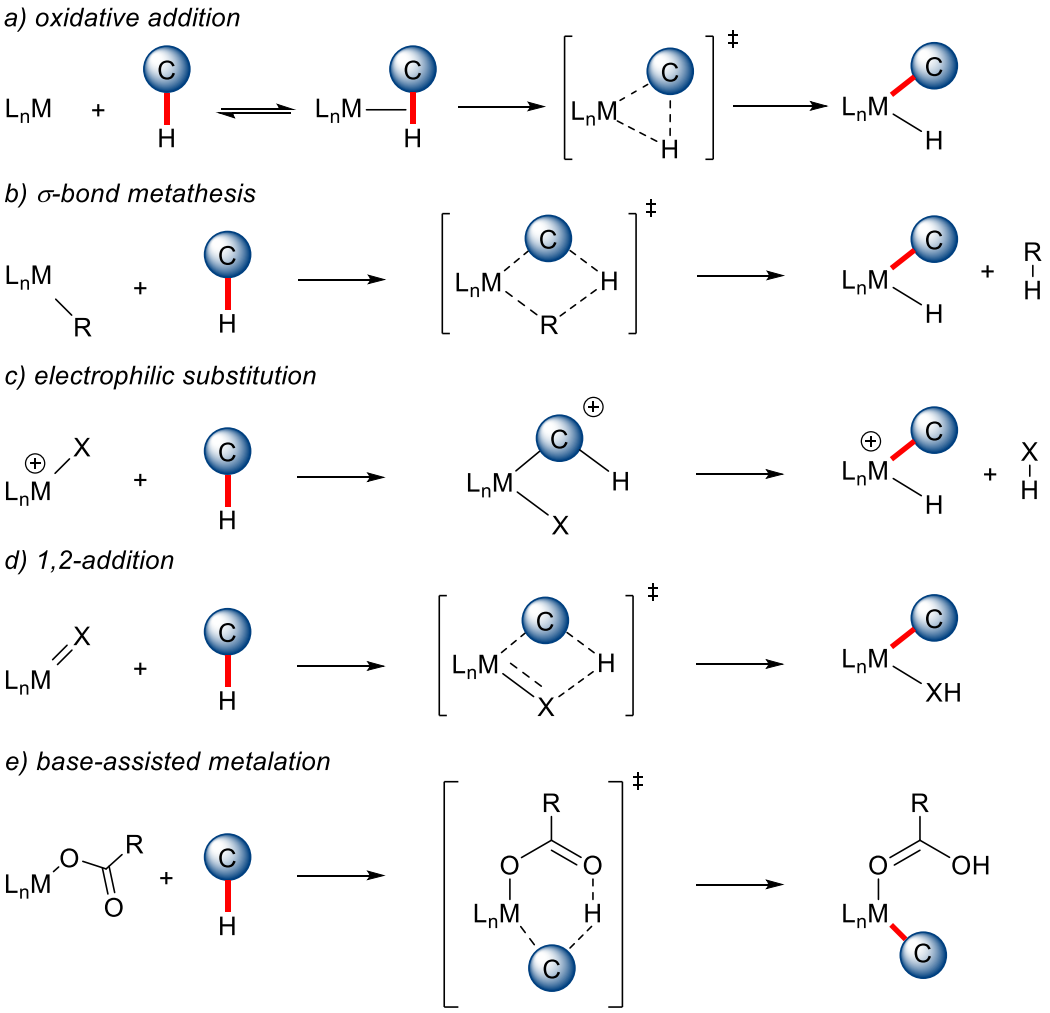

Figure 1.3: Mechanistic pathways for the C–H cleavage step.

Within the regime of base-assisted C–H metalation, several distinct mechanistic scenarios for the key C–H bond cleavage have been proposed (Figure 1.4). Concerted metalation-deprotonation (CMD),[35] ambiphilic metal-ligand activation (AMLA),[34e,36] and base-assisted internal electrophilic substitution (BIES)[34a,37] describe the interaction between C–H bond, metal center and carboxylate ligand. While they all proceed *via* a six-membered transition state, CMD and AMLA are usually associated with electron-deficient substrates and are controlled by intrinsic C–H acidity, whereas BIES is commonly assigned to electron-rich substrates. In stark contrast, intramolecular electrophilic substitution (IES)[38] proceeds *via* a four-membered transition state and is usually encountered with metal-alkoxide complexes.

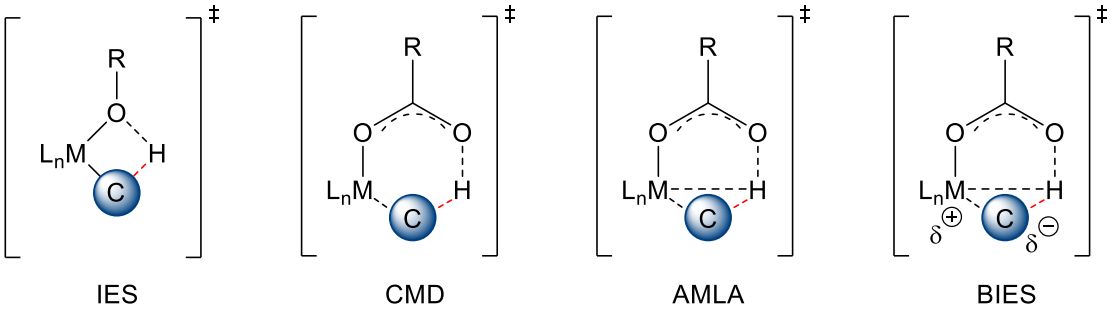

Figure 1.4: Transition states for the C–H cleavage in base-assisted C–H metalation.

Yet, a considerable amount of the disclosed C–H functionalization reactions during the last decades exploited the high reactivity of precious transition metal catalysts based on palladium,[39] iridium,[40] and rhodium.[41] Despite their high potential for C–H functionalization, these metals are expensive and display considerable toxicity.[25] The search for suitable alternatives is therefore an ongoing and highly active research topic within the field of transition metal-catalyzed C–H functionalization.[25]

1.2 Copper-Catalyzed C–H Functionalization

In comparison to the precious transition metals, copper has several considerable advantages. First, its high natural abundance[42] results in a price which is only a fraction of the one of the precious transition metals. Second and of equal importance are its benign properties regarding toxicity. In addition, its readily accessible oxidation states allow for facile one- or two-electron processes. Thus, radical pathways and pathways relying on bond formation *via* organometallic intermediates are well established with copper catalysts.[43] These properties make copper-based catalysts highly attractive and led to their widespread use in chemistry.[44] Since a comprehensive discussion of their use in organic chemistry is beyond the scope of this introduction, this chapter will focus on the applications of copper catalysts for C–H arylations and the formation of C–Het bonds.

1.2.1 Copper-Catalyzed C–H Arylations

Groundbreaking studies regarding transition metal-enabled arylations date back to the beginning of the 20th century.[45] As early as 1901, Ullmann reported the reductive

coupling of haloarenes. Using stoichiometric amounts of copper, he was able to prepare symmetrically substituted biaryls from bromoarenes **1** (Scheme 1.1a).[45e] Notably, chloroarenes were also viable substrates. Two years later Ullmann also disclosed a protocol for the N–H arylation of anilines **2** to yield diphenylamines.[45d]

In 1905 Ullmann and Sponagel disclosed their work regarding the phenylation of phenol (**3a**) (Scheme 1.1b).[45c] Notably, this represents the first example of the catalytic use of copper for C–X (X = N, O) bond formations. Only one year later Goldberg published her remarkable work on *N*–arylation reactions with aniline derivative **2a**, thereby substantially broadening the scope of copper-catalyzed reactions (Scheme 1.1c).[45b]

a) Biphenyl synthesis (Ullmann, 1901)

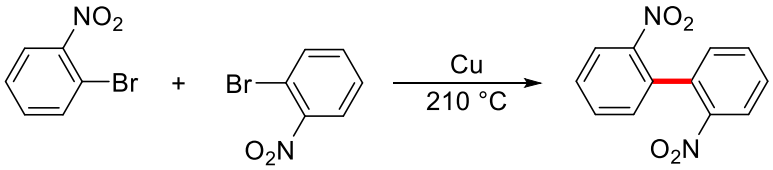

1b **1b** **4bb**: 76%

b) Arylation of phenol with aryl bromides (Ullmann, 1905)

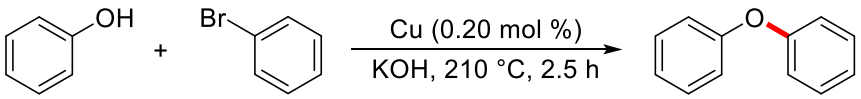

3a **1a** **5aa**: 90%

*c) Arylation of amine **2b** (Goldberg, 1906)*

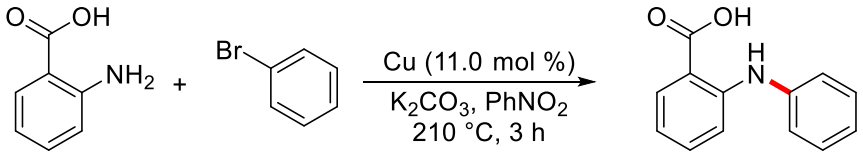

2b **1a** **6ba**: 99%

Scheme 1.1: Ullmann and Goldberg's seminal work on arylation reactions.

In this context, the copper-catalyzed condensation of 2-bromobenzoic acid with *β*-dicarbonyls as reported by Hurtley in 1929 should also be mentioned.[46] These early examples for copper-catalyzed C–C, C–O, and C–N bond formations developed by Ullmann, Goldberg and Hurtley exemplify the potential of copper for regioselective arylations. The mechanism of the Ullmann condensation reactions has been intensively

investigated since their first appearance but is still disputed.[47] Commonly accepted by now is the role of copper(I) ions as the primary catalytically active species, as proposed by among others Paine[48] and Jutand.[49] The larger part of the mechanism is still subject to debate and the proposals include a) oxidative addition of the aryl halide to the copper(I) species, b) the formation of aryl radical intermediates resulting from either single electron transfer (SET) or halide atom transfer (AT), c) *σ*-bond metathesis trough a four-membered intermediate, and d) *π*-complexation of copper(I) by the aryl halide.[47]

Initial evidence for the feasibility of copper-catalyzed C–H arylations was provided by stoichiometric reactions reported by Nilsson[50] and Wahren[51] in 1968 and 1973 respectively. In their work on palladium-catalyzed arylations of *N*-methylimidazole (**7a**), Miura and coworkers observed a pronounced effect of copper(I) iodide on the regioselectivity of the reaction (Scheme 1.2a).[52] While in both cases the formation of the diarylated *N*-methylimidazole **8aa** was observed, the reaction did not deliver the C-2 arylated product **9aa** in the absence of copper. *Vice versa* in the presence of 2.00 equivalents of copper(I) iodide, the regioselectivity was altered and no C-5 arylated product **10aa** was obtained.

a) Influence of CuI on the regioselectivity of the arylation

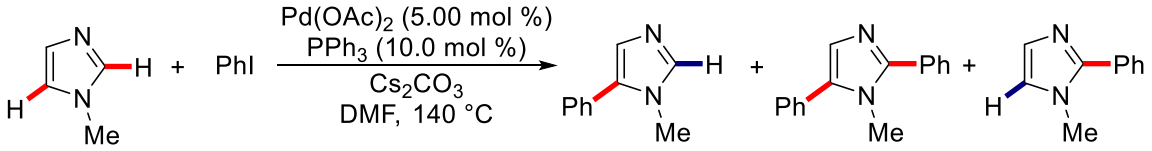

7a **11a**

	10a	**8aa**	**9aa**
no CuI	54%	24%	0%
CuI (2.00 equiv)	0%	40%	37%

b) Copper-mediated arylation of N-methylbenzimidazole

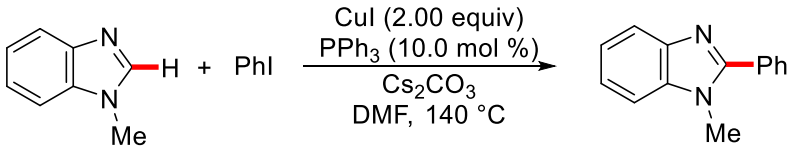

12a **11a** **13aa**: 89%

Scheme 1.2: Palladium-catalyzed arylation of imidazole **7a** and copper-mediated arylation of **12a**.

In addition, copper(I) iodide itself proved capable of mediating the C-2 arylation of *N*-methylbenzimidazole (**12a**) (Scheme 1.2b).The authors attributed the highly effective formation of benzimidazole **13aa** to an aromatic nucleophilic substitution reaction of the iodobenzene (**11a**) assisted by the base and a copper(I) species.[53]

After rationalizing that the observations of Miura and coworkers could result from the involvement of organocopper intermediates, Daugulis and coworkers started to investigate the possibility of a copper-catalyzed arylation protocol. These efforts led to their report of the copper-catalyzed C–H arylation in 2007 (Scheme 1.3).[54] Key to their success was the use of alkoxide bases which allowed for a facile generation of the proposed organocopper intermediate in a catalytic fashion. Notably, mechanistic experiments suggested that a benzyne-type mechanism was operative when the stronger alkoxide base KO*t*Bu was employed.[54]

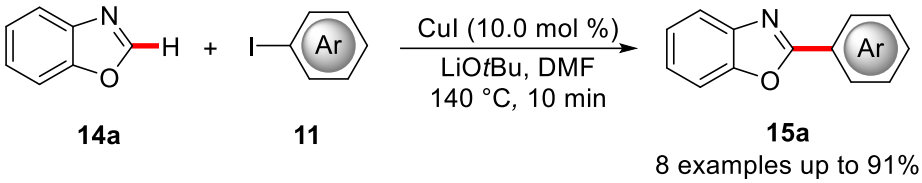

Scheme 1.3: C–H Arylation of benzoxazole (**14a**) with aryl iodides as reported by Daugulis.

This seminal report renewed the interest in copper-catalyzed arylation reactions. Thus in 2008 the scope was extended to electron-deficient as well as polyfluorinated arenes[55] and later in the same year, both electron-rich and electron-poor heterocycles were proven to be viable substrates (Scheme 1.4).[56]

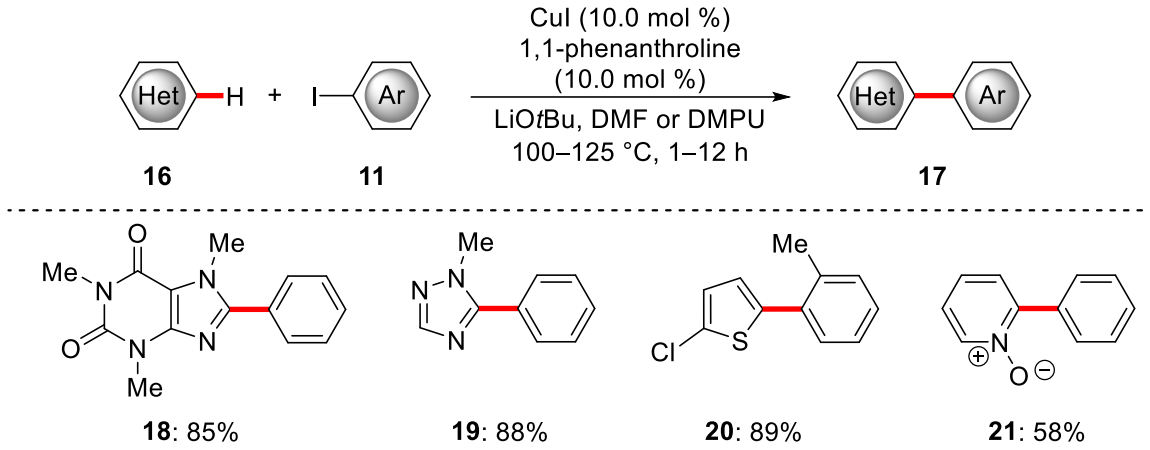

Scheme 1.4: Selected examples of copper-catalyzed C–H arylations.

As a part of this work, Daugulis and coworkers described the synthesis of a pentafluorophenyl-copper phenanthroline complex **22** from copper(I) chloride (Scheme 1.5a). The authors could show that complex **22** was also formed *in situ* under the catalytic conditions. Furthermore, it was shown that arylcopper complex **22** reacts with aryl iodides **11** to yield the biaryl products .[56]

Based on their mechanistic studies, the authors proposed that the heterocyclic C–H bond could either undergo direct cupration with the *in situ* formed copper(I) *tert*-butoxide, or that copper-assisted deprotonation of benzothiophen (**23**) followed by lithium-copper transmetalation would lead to the formation of the arylcopper species **24**. The reaction of **24** with aryl iodide **11** then delivers the biaryl product **25** (Scheme 1.5b).

a) Synthesis of arylcopper complex ***22***

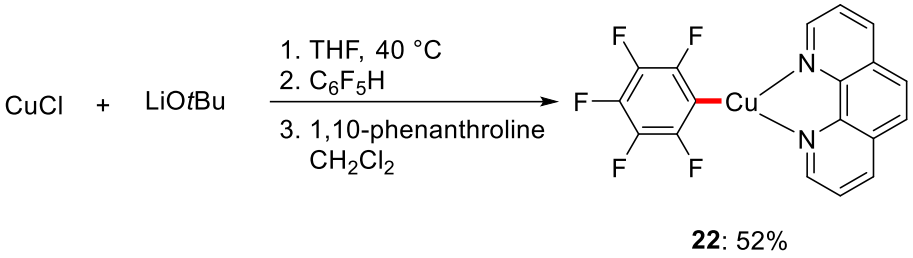

22: 52%

b) Mechanistic proposal from Daugulis

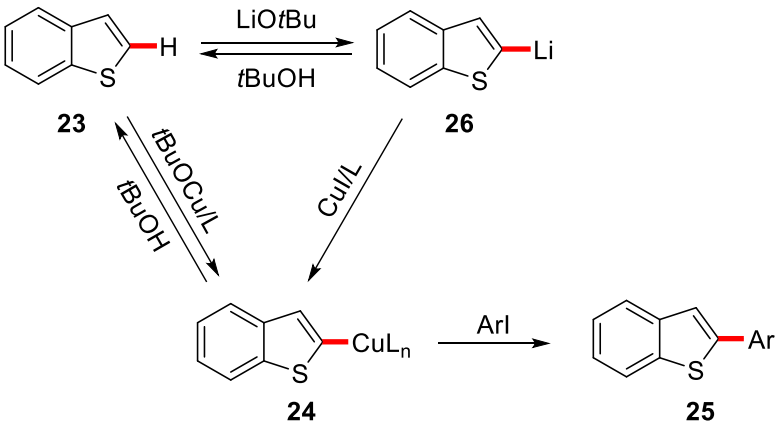

Scheme 1.5: Synthesis of aryl copper complex **22** and mechanistic proposal.

Also in 2008, Miura and coworkers independently reported a similar copper-mediated C–H arylation.[57] Contributing to the further development of the field, Ackermann independently published the C–H arylation of triazoles **27** by copper catalysis, thereby providing an easy route to fully substituted 1,2,3-triazoles **28** (Scheme 1.6).[58]

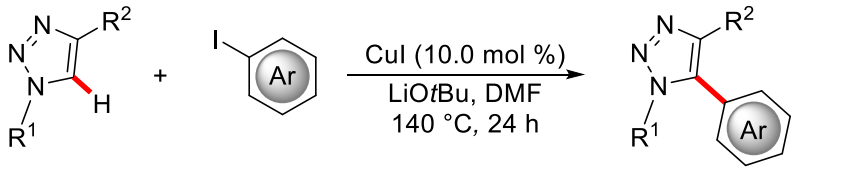

27 **11** **28**

9 examples up to 91%

Scheme 1.6: Copper-catalyzed C–H arylation of triazoles **27**.

By now these seminal reports by Daugulis, Miura, and Ackermann have led to a manifold of copper-catalyzed arylation protocols and the field is well-established as of today (Figure 1.5).[25,59]

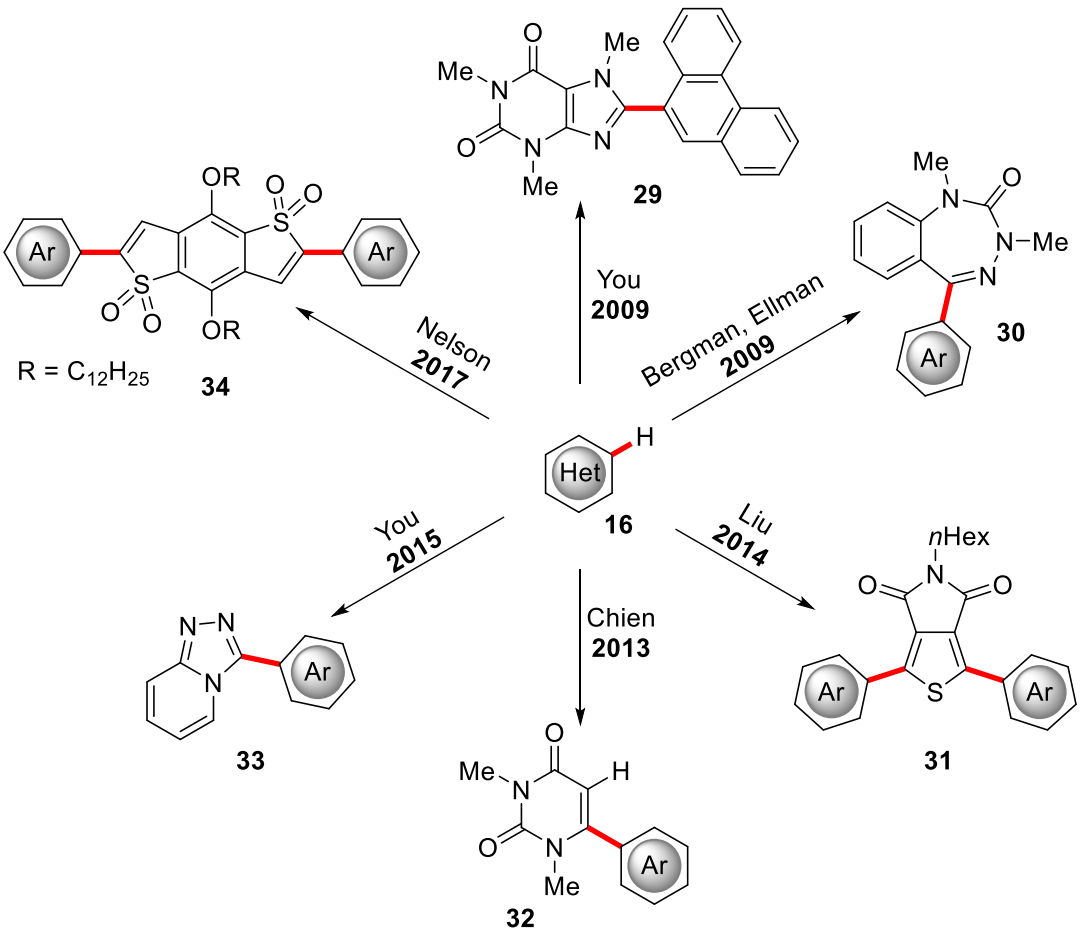

Figure 1.5: Applications of copper-catalyzed C–H arylations with aryl halides.

Despite the tremendous achievements in the field, these copper-catalyzed C–H arylation protocols require the use of elevated temperatures to achieve satisfying results. This requirement still constitutes a major drawback in the field.

1.2.2 Copper-Catalyzed C–X Bond Formations

The above discussed early examples disclosed by Ullmann and Goldberg not only showed the potential of copper-catalysts for arylation reactions, but also underlined the potential of copper-catalysts for C–N and C–O bond formations in general. While these reactions usually required high reaction temperatures, the development of suitable ligands, as pioneered by the groups of Liebeskind,[60] Buchwald,[61] Taillefer,[62] and Ma,[63] allowed for considerably lower reaction temperatures and catalyst loadings.

The following chapter will address the utilization of copper catalysts for the conversion of C–H bonds into C–X (X = N, O, S, Se) bonds, with a focus on the use of copper catalysts for C–N bond formations and C–H chalcogenation reactions. In 2006, the groups of Yu and Chatani independently reported an aerobic copper-promoted *ortho*-C–H functionalization of phenylpyridine (**35a**) with tosyl amide and aniline respectively (Scheme 1.7).[64]

*a) Amidation of phenylpyridine (**35a**) with tosyl amide (Yu, 2006)*

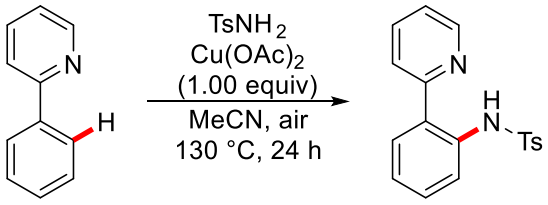

35a **36a**: 74%

*b) Amination of phenylpyridine (**35a**) with aniline (Chatani, 2006)*

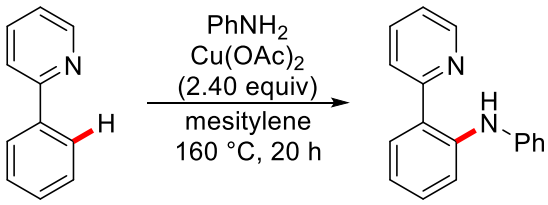

35a **37a**: 55%

Scheme 1.7: Copper-mediated C–H amination reactions reported by Yu and Chatani.

These seminal reports showcased for the first time the potential of simple copper salts for C–Het formations, yet in a stoichiometric fashion. In 2009, the scope of these copper(II)-mediated transformations was expanded to a variety of heterocycles possessing slightly acidic C–H bonds by the group of Schreiber.[65]

The field was further advanced by among others the group of Daugulis. In 2013, Daugulis and coworkers disclosed their work on copper(II)-catalyzed aminations. By exploiting the strongly coordinating, bidentate directing group 8-aminoquinoline (AQ), the authors were able to achieve the amination of benzamide **38b** with morpholine (**39**) in very good yields (Scheme 1.8a).[66] Additionally, their developed protocol displayed a broad substrate scope and high functional group tolerance.

Thus, electron-rich and electron-deficient substrates were well tolerated and a range of diversely substituted secondary and primary alkyl amines could be employed in the

reaction. Yet, the latter gave considerably lower yields. Furthermore, picolinamide **40a** also proved to be a competent substrate and the corresponding product **41a** could be isolated in 43% yield (Scheme 1.8b). Remarkably, the copper-catalyzed amination only delivered the mono-functionalized products.

*a) Copper-catalyzed amination with benzamide **38b***

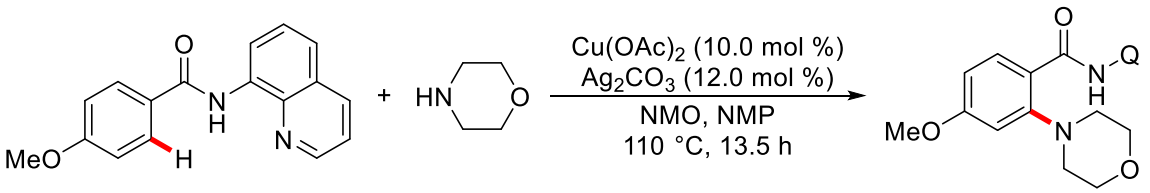

38b **39** **42a**: 83%

*b) Copper-catalyzed amination with picolinamide **40a***

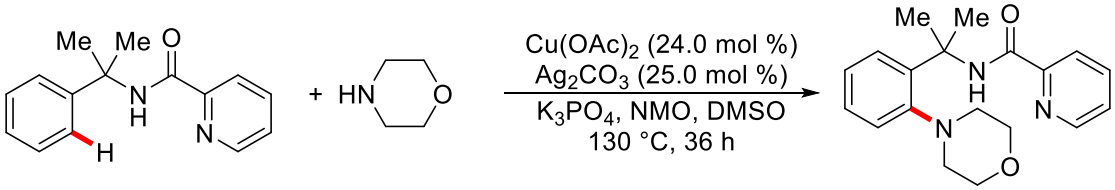

40a **39** **41a**: 43%

Scheme 1.8: Copper-catalyzed aminations with bidentate directing groups reported by Daugulis.

Since Daugulis' seminal contribution, the field of chelation-assisted copper-mediated or copper-catalyzed C–H amination reactions of (hetero)arenes was significantly advanced by among others the groups of Carretero, Chen, and Yu.[67] While requiring stochiometric amounts of copper, Yu's protocol tolerated an exceptionally wide range of heteroarenes (Scheme 1.9).[67a]

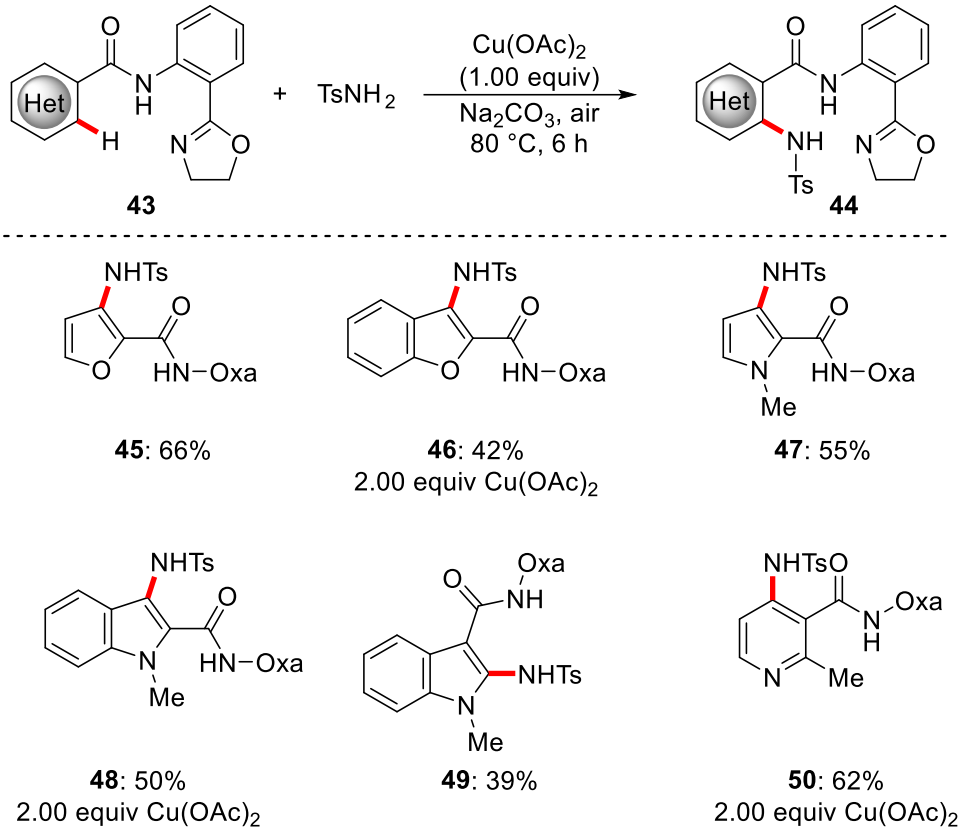

Scheme 1.9: Selected examples of heteroarene C–H amidation.

In his early work from 2006, Yu also disclosed an example of a copper(II)-catalyzed *ortho*-acetoxylation of 2-arylpyridines **35** (Scheme 1.10).[64a] Using O_2 as terminal oxidant, the authors were able to convert a range of decorated 2-arylpyridines **35** to the corresponding acetoxylated products. By employing a stoichiometric amounts of copper(II) acetate, the authors were also able to obtain mono-hydroxylated products.

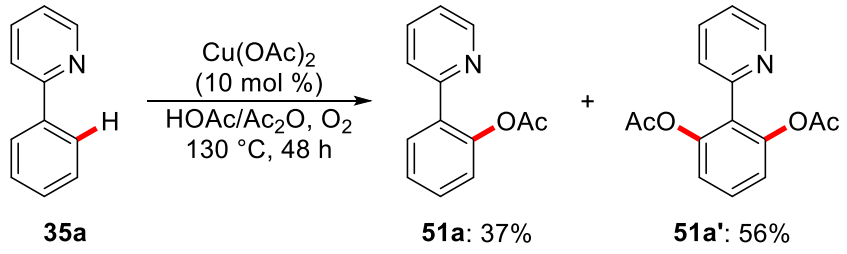

Scheme 1.10: Catalytic acetoxylation as reported by Yu.

As for the field of copper(II)-mediated amination reactions, the contribution by Yu and coworkers sparked further interest in copper(II)-mediated or catalyzed C–O bond formations. Thus, the area underwent tremendous advances in the following years.[68] Yet, the underlying mechanisms remained unclear for a prolonged time.

Employing the well-defined macrocyclic copper(III)-aryl complexes reported by Ribas in 2002,[69] the Stahl group was able to generate compelling evidence for the involvement of copper(III)-intermediates,[70] in both the C–O and the C–N[70c] bond coupling reactions. Within their mechanistic studies, they could show that arylcopper(III)-complex **52** delivered the methoxylated arene **53** in quantitative yield upon treatment with methanol (Scheme 1.11).[70b]

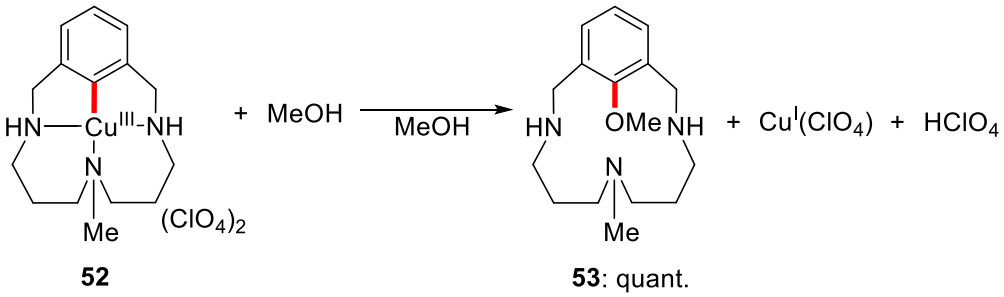

52 **53**: quant.

Scheme 1.11: Stoichiometric reaction using well-defined copper(III)-aryl complex **52**.

In 2013, the Daugulis group reported the 8-aminoquinoline-directed copper(II)-catalyzed aryloxylation of benzamides **38**.[71] The copper-catalyzed C–H bond formation tolerated a wide range of decorated phenols **3**, including thioethers, halogen-substituents and esters, and the corresponding products **54** were usually obtained in moderate to good yields (Scheme 1.12). In addition to phenol derivatives, the copper(II)-catalytic regime also proved applicable to several alkoxides.

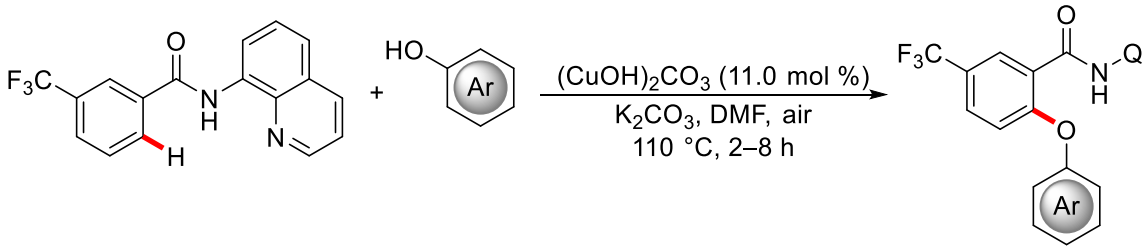

38c **3** **54c**
9 examples
56 to 88% yield

Scheme 1.12: Copper(II)-catalyzed aryloxylation as reported by Daugulis.

Yu's work from 2006 not only sparked the interest in C–H aminations and oxygenations but also included the first examples of a directed copper(II)-mediated thioetherfication.[64a] Both thiophenol (**55a**) and dimethyldisulfide (**56a**) proved to be suitable substrates to deliver the corresponding thioethers **57** and **58** (Scheme 1.13).

*a) Thioetherfication of **35a** using thiophenol (**55a**)*

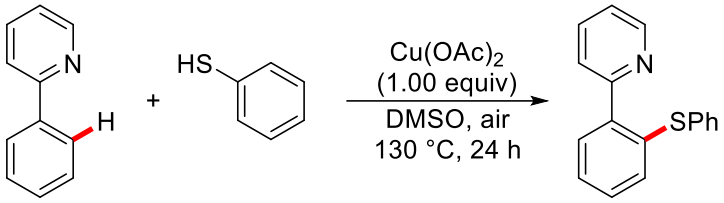

35a **55a** **57aa**: 40%

*b) Thioetherfication of **35a** using dimethyldisulfide (**56a**)*

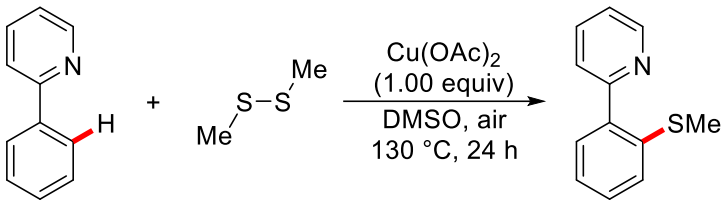

35a **56a** **58aa**: 51%

Scheme 1.13: Copper(II)-mediated C–S bond formation using different sulfur reagents.

In 2009, Fukuzawa and coworkers used diphenyl disulfide (**59a**) as a benign reagent for the sulfenylation of benzoxazoles **14**.[72] Catalytic amounts of copper(I) iodide in the presence of a bipyridine ligand under an atmosphere of oxygen were able to deliver the sulfenylated products in excellent yields (Scheme 1.14).

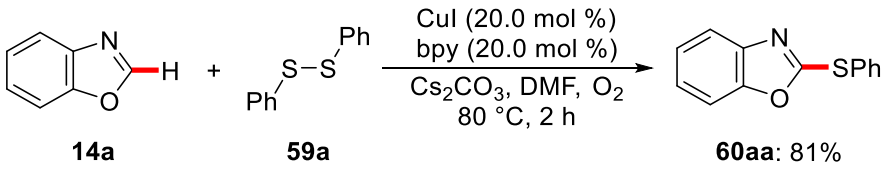

14a **59a** **60aa**: 81%

Scheme 1.14: Copper-catalyzed sulfenylation of benzoxazoles **14**.

One year later, the group of Cheng reported an undirected C–H chalcogenation of electron-rich arenes (Scheme 1.15).[73] The performed mechanistic studies included a reaction of **61** with stoichiometric amounts copper(I) thiophenolate in the presence of catalytic amounts of copper(I) iodide which delivered the product **62** in 65% yield. Additionally, the reaction was effectively catalyzed by copper(I) thiophenolate as well. These findings led the authors to propose a catalytic cycle with copper(I) thiophenolate as a key intermediate.[73]

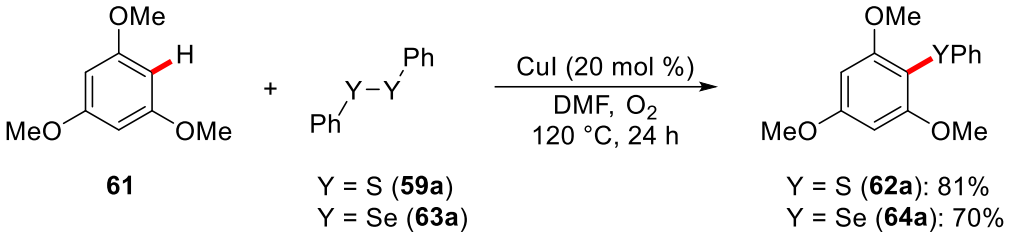

Scheme 1.15: Undirected copper-catalyzed chalcogenation of electron-rich arene **61**.

The group of Daugulis rationalized that DMSO might not only be used as sulfenylation reagent for thiomethylation reactions,[74] but might also be a suitable solvent for these reactions, as it can promote thiol oxidation and thereby regenerate the disulfide *in situ*.[75]

Thus in 2012, they disclosed the copper(II)-promoted sulfenylation of various C(sp^2)–H bonds (Scheme 1.16).[76] Besides a variety of alkyl and aryl disulfides, trifluoromethyl disulfide (**56b**) also proved to be a suitable sulfenylation reagent and the resulting trifluoromethyl thioether **65db** could be isolated in 63% yield (Scheme 1.16a). In addition, the copper(II)-promoted sulfenylation could also be performed when the bidentate picolinamide-based directing group was employed (Scheme 1.16b).

*a) Trifluoromethylsulfenylation of benzamide **38d** with $(CF_3S)_2$ (**56b**)*

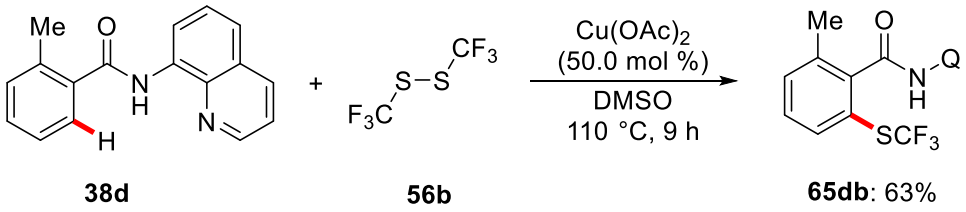

*b) Sulfenylation of piconlinamide **40b** with dibutyldisulfide (**56c**)*

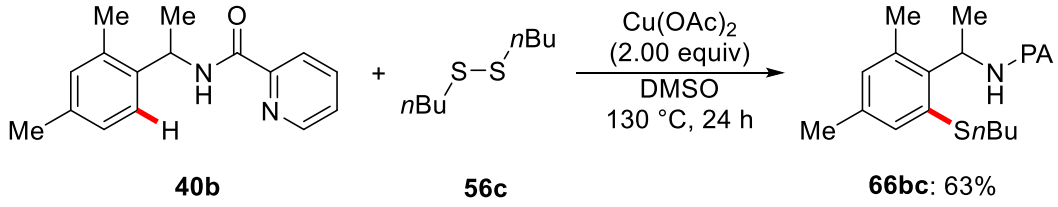

Scheme 1.16: Copper(II)-mediated sulfenylation with bidentate directing groups.

In stark contrast to this protocol relying on strong bidentate chelation, Ackermann and coworkers reported a copper(I)-mediated chalcogenation by triazole assistance.[77] In this remarkable work from 2016, the authors were able to show that weak coordination by the carbonyl group is able to outcompete strong coordination by the *N,N*-bidentate

coordination site. Thus, selective selenylations and sulfenylations of the C-5 position of the triazole ring were achieved, thereby providing facile access to fully substituted triazole **67aa** (Scheme 1.17).[77]

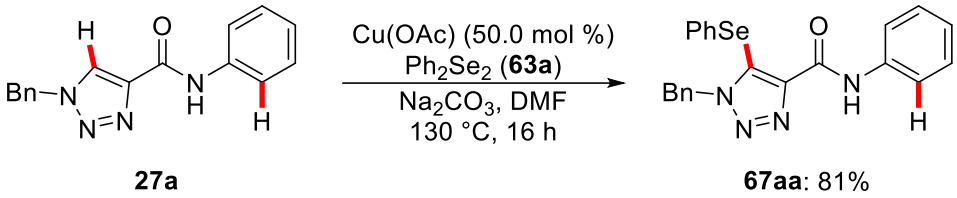

Scheme 1.17: Facile copper(I)-promoted selenylation of triazole **27a**.

In 2015, the group of Kambe had reported a copper(II)-mediated thiolation of pyrimidyl-substituted carbazoles and related heterocycles.[78] Although two equivalents of copper were required to achieve satisfying yields, their protocol allowed for the successful functionalization of valuable heterocycles, such as indole, carbazole, and benzo[*h*]quinolone (Scheme 1.18).

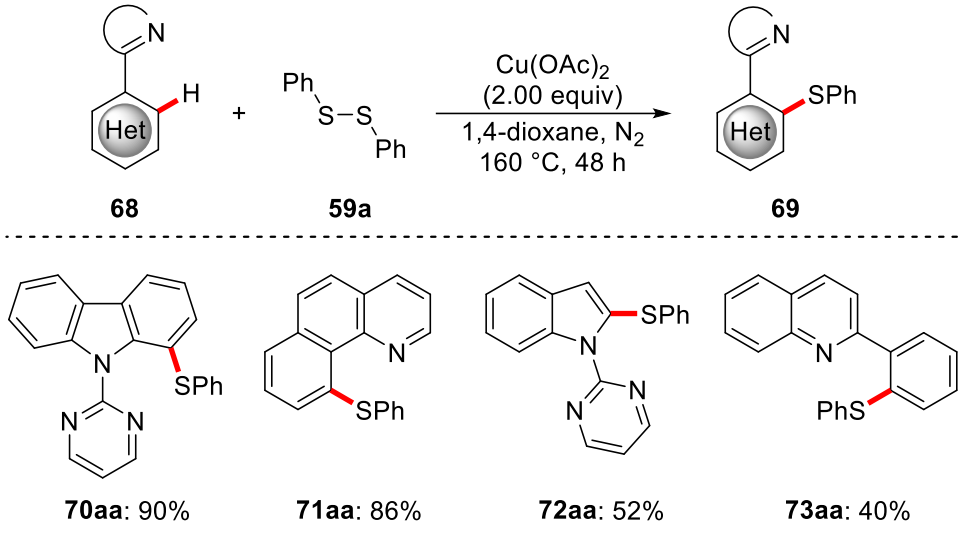

Scheme 1.18: Copper(II)-mediated thiolation of valuable heterocycles as reported by Kambe.

The selected examples in this chapter display only a fraction of the tremendous advances in the field of copper-mediated and copper-catalyzed C–H functionalizations. However, a large part of these reactions still requires the use of superstoichiometric amounts of copper salts and is often conducted at high temperatures. In addition, the often-observed reliance on strongly coordinating, bidentate directing groups remains a substantial limitation to the general applicability of the developed protocols.

1.3 Ruthenium-Catalyzed *meta*-C–H Functionalization

While early contributions to the emerging field of C–H functionalization relied on precious palladium[79] and rhodium catalysts,[41b-d,80] the pursuit of cheaper and more sustainable catalysts soon led to the rise of ruthenium catalysts for C–H functionalization reactions.[81]

The work of Murai, Chatani, and Kakiuchi regarding the ruthenium-catalyzed hydroarylation of alkenes[82] and Inoeu's work on ruthenium-catalyzed arylation reactions[83] constitute two early examples in the field of ruthenium-catalyzed C–H bond functionalization. While a ruthenium-catalyzed hydroarylation of ethylene had been previously described by Lewis and Smith in 1986 (Scheme 1.19a),[84] the Murai reaction displayed a higher level of generality. Adapting the earlier work of Lewis and Smith, Murai and coworkers were able to obtain a wide range of hydroarylation products **74** in often quantitative yields and with excellent levels of selectivity.

In 2001, Oi and Inoue reported the direct arylation of phenyl pyridines **35** with aryl bromides **1** (Scheme 1.19b).[83b] The benign properties of those bench-stable ruthenium(II)-catalysts in combination with their efficiency led to their widespread adaption in the context of C–H functionalization reactions.[81] Thus, the following years witnessed tremendous developments in the field of ruthenium-catalyzed C–H activation.[81,85]

Despite the impact of the work of Oi and Inoue, it has to be acknowledged in this context that their work displayed low levels of reproducibility.[86] In 2008, Ackermann and coworkers reported a highly robust ruthenium-catalyzed C–H arylation protocol and elucidated the influence of carboxylic acids as additives,[87] this pronounced influence was later further elaborated by detailed mechanistic investigations.[88] In 2011, a research group at Merck was able to provide further insights into the reproducibility issues associated with Oi and Inoue's work. Through careful analysis of the employed solvent NMP, they were able to trace back the observed effect to low-level impurities of γ-butyrolactone.[86]

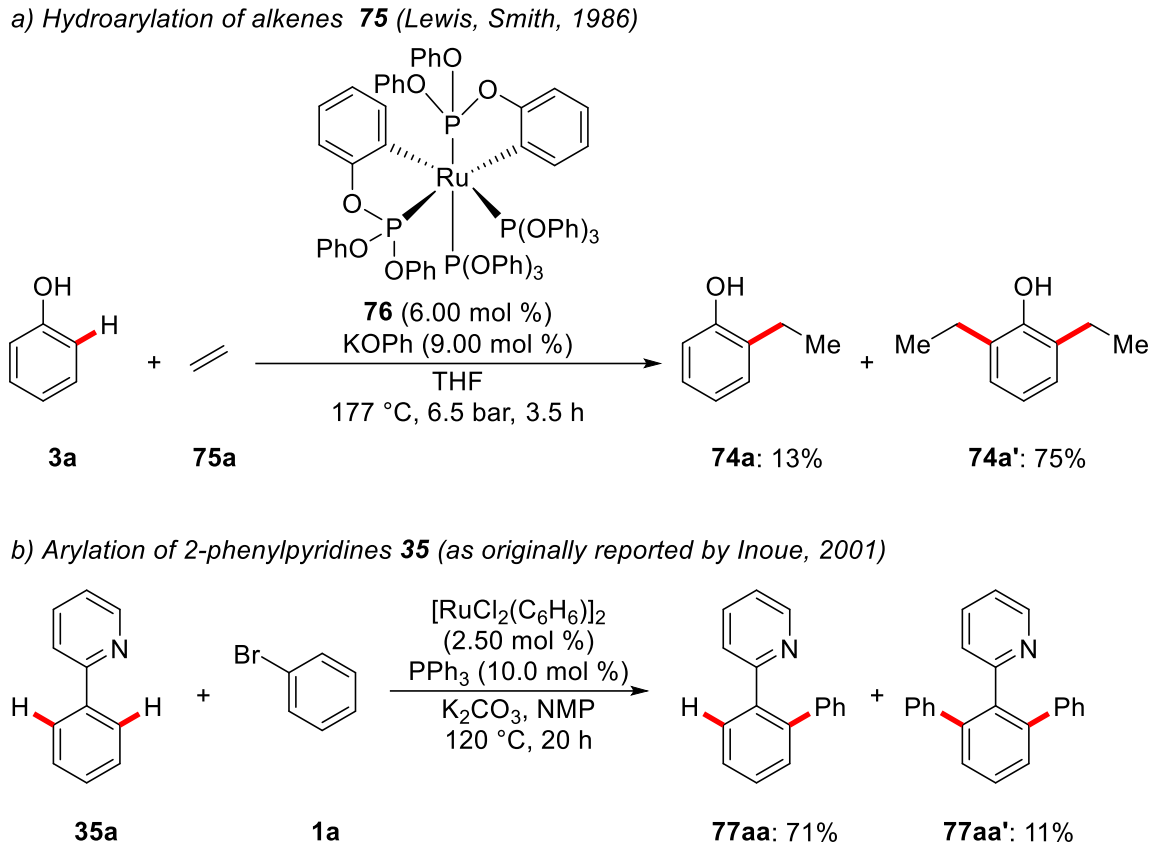

Scheme 1.19: Early work in the field of ruthenium-catalyzed C–H functionalization.

Besides their high versatility and efficiency and thus their application in a plethora of transformations, nowadays ruthenium-catalysts receive a large part of their attention due to their unique ability to enable *meta*-C–H functionalization reactions. While *meta*-selective C–H functionalizations have been realized with other metals, the applied strategies mainly rely on the principles depicted in Figure 1.6.[89]

A straightforward strategy to obtain *meta*-decorated products is the use of a traceless directing group (Figure 1.6a). After initial *ortho*-functionalization, *in situ* removable of the directing group furnishes the *meta*-substituted product. At the beginning of this decade, examples featuring this strategy were reported by the group of Satoh and Miura.[90] Yet, the ensuing decarboxylation step required stoichiometric amounts of silver additives. Recently, Ackermann and coworkers reported a ruthenium(II)-catalyzed formal *meta*-selective alkenylation.[91] In this case, the decarboxylation could be achieved without the traditionally employed silver or copper salts.

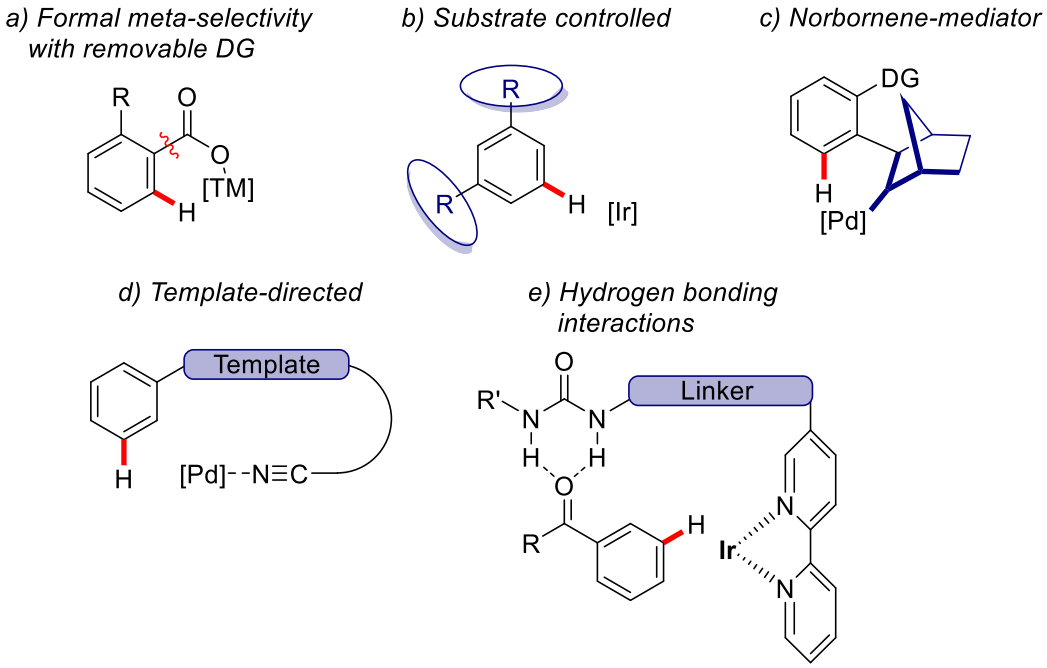

Figure 1.6: Strategies enabling *meta*-selective C–H bond functionalization.

Substrate-controlled *meta*-selectivity (Figure 1.6b) is reliant on the substrate's inherent reactivity and hence its substitution pattern. This approach has been achieved by iridium-catalyzed C–H borylations[92] and more recently in rhodium-catalyzed C–H silylations.[93] As this strategy is clearly highly dependent on the properties of the substrate it is not broadly applicable.

Since Catellani's seminal reports,[94] the Catellani reaction has been broadly studied and has been used in for various applications.[39c,95] In this approach, norbornene acts as a transient mediator allowing for facile *meta*-C–H activation (Figure 1.6c). Already in 2005, the group of Lautens reported the synthesis of *meta*-substituted arenes using the Catellani reaction.[96] In this instance, a sequence of palladium-catalyzed alkylation and subsequent hydride reduction led to the formation of various *meta*-decorated arenes. More recently, protocols for the Catellani reaction based on a C–H activation approach have been published by the groups of Dong[97] and Yu (Scheme 1.20).[98]

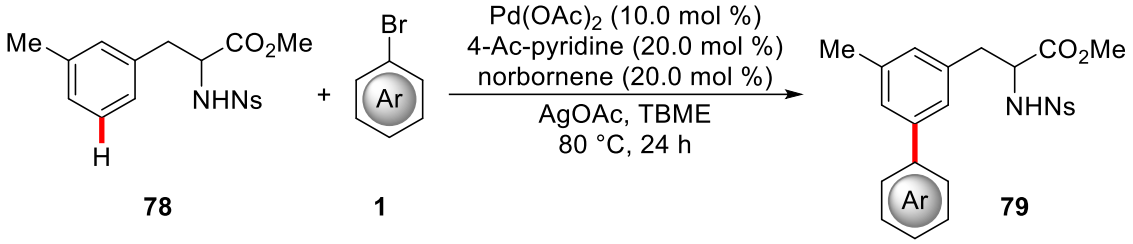

Scheme 1.20: Catellani reaction delivering *meta*-substituted arenes.

The group of Yu also developed the synthesis of *meta*-decorated arenes by C–H activation using engineered auxiliary structures (Figure 1.6d).[99] A different approach was established by the Kanai group in their work on the C–H borylation of benzamide derivatives in 2015.[100] The key of their strategy was the use of a structurally elaborate ligand. While the ligand itself is binding to the substrate by hydrogen-bonding secondary interactions, it simultaneously directs the transition metal catalyst towards the *meta*-C–H bond (Figure 1.6e).

However, both methods require the synthesis of high molecular weight and structurally complex motifs which negatively impacts step and atom economy and therefore the overall footprint of the strategies.[89,101] In contrast to the strategies shown in Figure 1.6, ruthenium-catalyzed *meta*-C–H bond activation does not require any additional templates or complex ligands. Instead, cycloruthenation in the *ortho*-position of the directing group induces a *σ*-activation of the arene ring (Figure 1.7). This electronic influence facilitates the functionalization of the C–H bond *para* to the ruthenium center and therefore allows an overall *meta*-functionalization in respect to the directing group.[101]

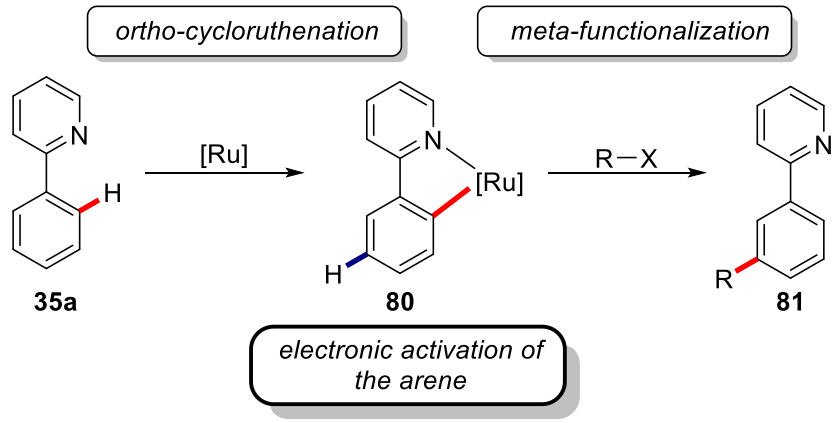

Figure 1.7: *σ*-Activation by cycloruthenation, exemplified with phenylpyridine (**35a**).

Early examples for stochiometric ruthenium *σ*-activation date back to the 1990s. In 1994, a report by Roper showed that the organometallic ruthenium complex **82** undergoes nitration *para* to the ruthenium center (Scheme 1.21a).[102] Notably, within the same month, van Koten independently reported the formation of a *para*-chlorinated product, which they had observed during their investigations of copper(II) mediated oxidative couplings with cyclometalated ruthenium complexes.[103]

In 1998, Coudret and coworkers reported the preparation of complex **84** *via* electrophilic bromination of the ligand backbone (Scheme 1.21b), within this work the authors also demonstrated a related iodination.[104]

*a) Nitration of ruthenium-bezene complex **82** (Roper, 1994)*

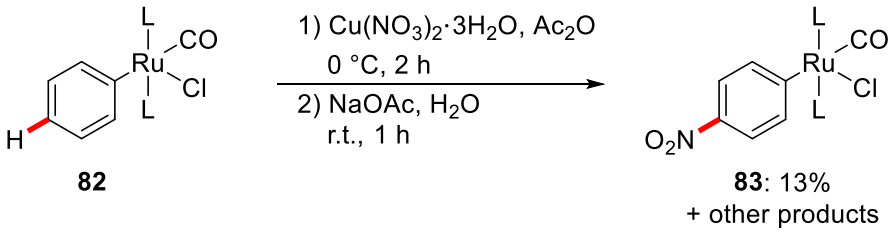

82 **83**: 13% + other products

*b) Electrophilic C–H bromination with ruthenium complex **84** (Coudret, 1998)*

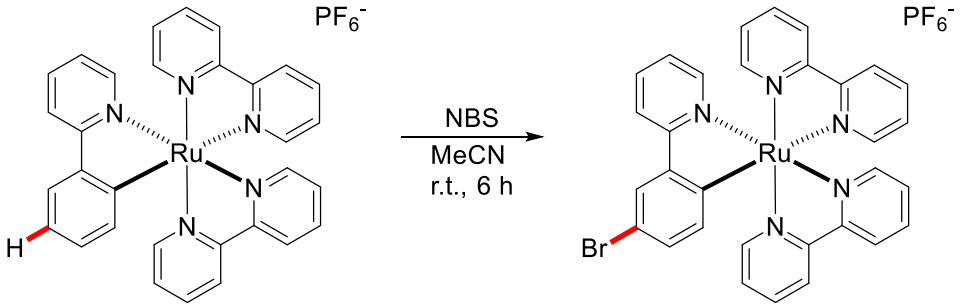

84 **85**: 95%

*c) Bromination of cyclometalated ruthenacycle **86** (Roper and Wright, 1999)*

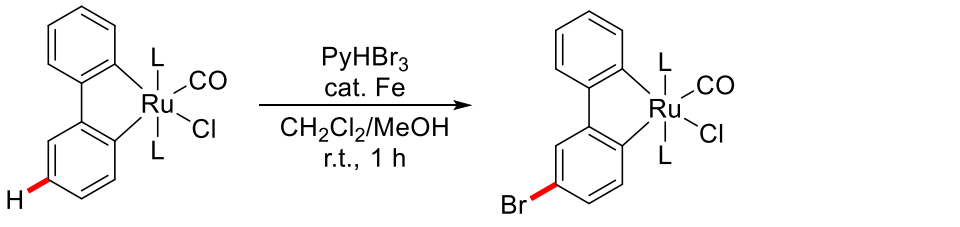

86 **87**: 69% L = PPh_3

Scheme 1.21: Early examples of C–H functionalizations involving ruthenium *σ*-activation.

Only one year later, Roper and Wright extended their initial work and disclosed the bromination of complex **86** (Scheme 1.21c). Additionally, the authors also reported the nitration of complex **86**. Interestingly, a corresponding osmium complex displayed analogous reactivity.[105]

Regardless of these early examples, the whole potential of ruthenium-enabled *σ*-activation was not fully recognized until 2011. In this year, Ackermann and coworkers reported the observation of the *meta*-functionalized product **88** in their investigations regarding the ruthenium-catalyzed *ortho*-alkylation of ketimine derivatives with primary alkyl bromides **89** (Scheme 1.22).[106] Although the *meta*-functionalized product was only obtained in minor quantities, this represents the first example of a ruthenium-catalyzed *meta*-C–H functionalization through *σ*-activation.

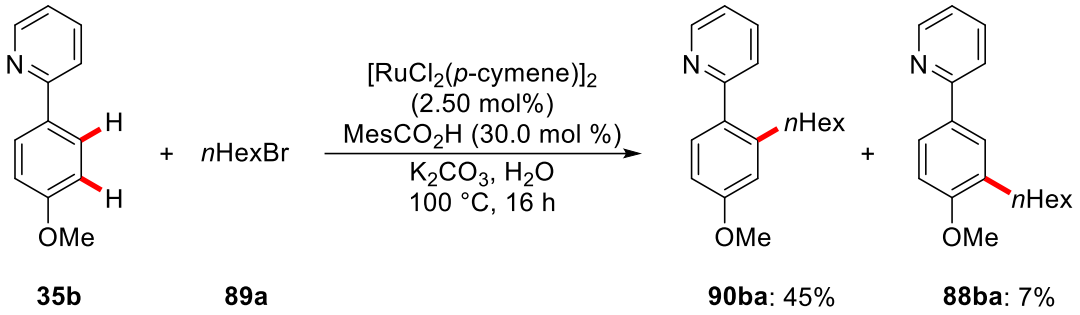

35b **89a** **90ba**: 45% **88ba**: 7%

Scheme 1.22: First observation of *meta*-selectivity in ruthenium-catalyzed C–H alkylations.

Later the same year, Frost disclosed a *meta*-selective ruthenium-catalyzed C–H sulfonation of phenylpyridines **35**.[107] This subsequent report proved that ruthenium-catalyzed *meta*-functionalizations could be achieved with synthetically meaningful yields (Scheme 1.23). Furthermore, the authors could show that the ruthenium complex resulting from C–H cycloruthenation underwent quantitative sulfonation when treated with tosyl chloride (**91**). However, the yields in the subsequent report by Frost were found significantly reduced.

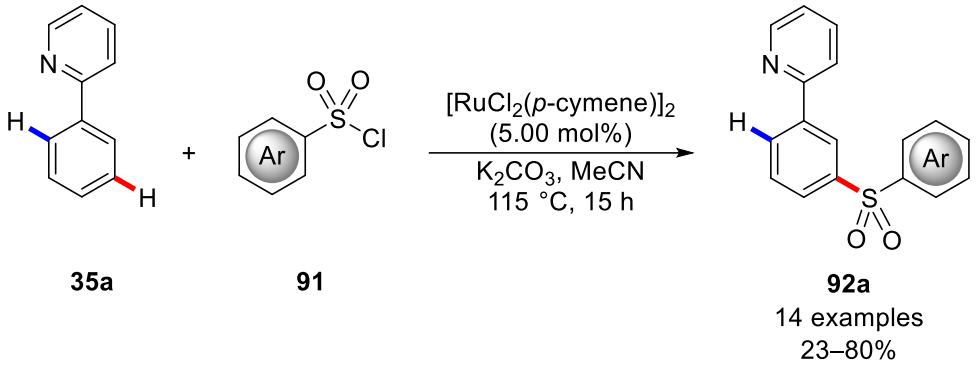

Scheme 1.23: Ruthenium-catalyzed *meta*-selective sulfonation as reported by Frost.

In 2013, Ackermann and coworkers published a *meta*-selective ruthenium-catalyzed C–H alkylation with challenging secondary alkyl halides **93** (Scheme 1.24).[108] In addition to the broad scope with respect to the alkyl halides **93** and heteroarenes, the authors also provided substantial evidence for the involvement of a radical process. Catalytic amounts of TEMPO significantly inhibited the reaction, while a stoichiometric amount of TEMPO completely suppressed the catalytic activity.[108]

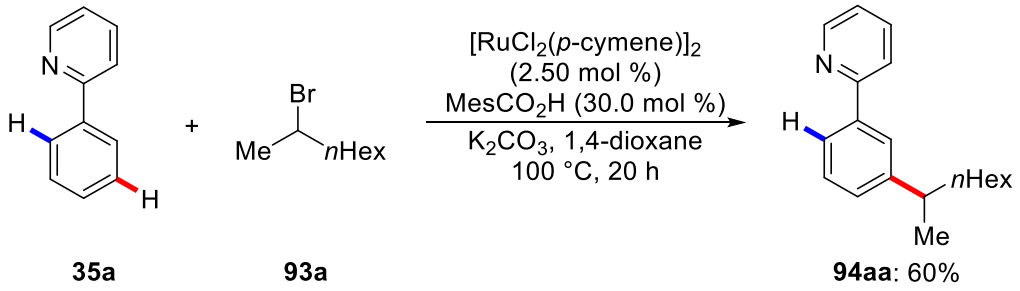

Scheme 1.24: Ruthenium-catalyzed *meta*-selective secondary alkylation.

In 2015, the groups of Ackermann and later Frost reported a related *meta*-C–H alkylation using tertiary alkyl halides (Scheme 1.25a).[109] The detailed mechanistic studies presented by Ackermann and coworkers, together with the results obtained by the Frost group, provided further evidence for a homolytic cleavage of the C–Br bond of the alkyl halide **93**. Experiments with stereochemically defined *cis*- and *trans*-cyclohexanes **93b**, delivered the same diastereomeric product mixture, thereby indicating the involvement of a common cyclohexyl radical intermediate (Scheme 1.25b).[109a]

Based on their observations, both groups proposed a bifunctional role of the employed ruthenium catalyst. In addition to its role in the C–H cleavage, the ruthenium catalyst is also involved in the cleavage of the C–Br bond of the alkyl halide *via* a SET-type process.

These new insights into ruthenium-catalyzed *meta*-C–H functionalization enabled by *σ*-activation sparked a great interest into the field.[101]

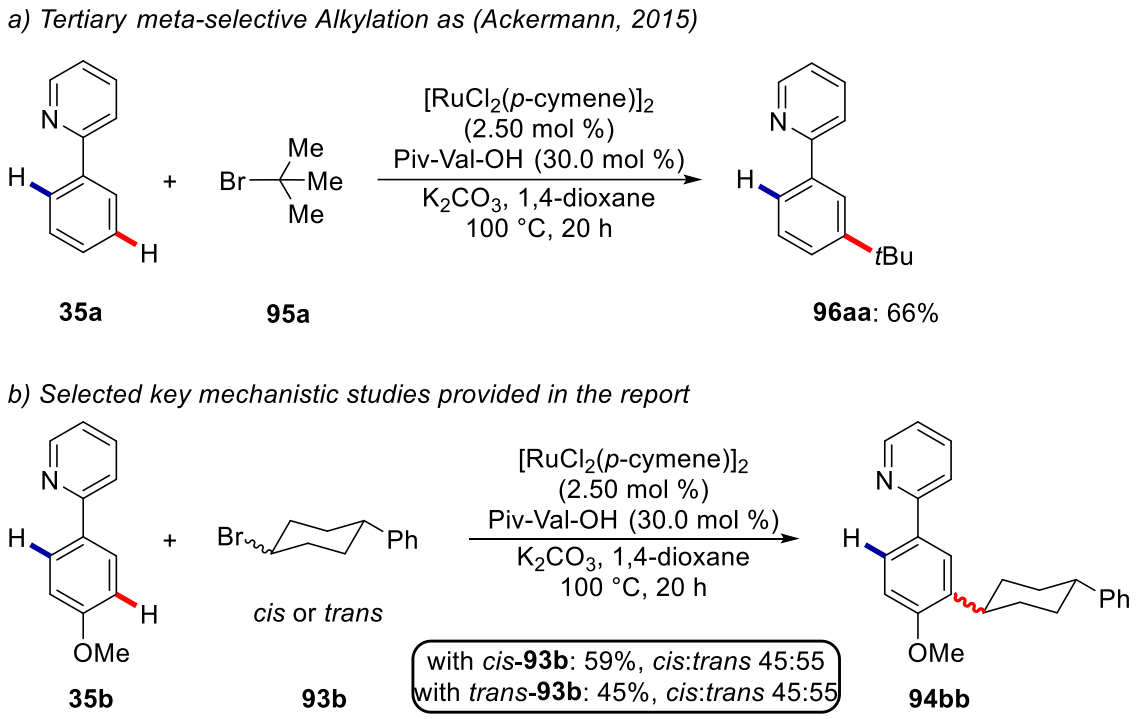

Scheme 1.25: Ruthenium(II)-catalyzed tertiary C–H alkylation and key mechanistic studies.

Within the same year, a *meta*-selective bromination protocol was independently reported by the groups of Greaney and Huang.[110] In 2017, this methodology was for the first time achieved with a reusable catalyst when Ackermann and coworkers introduced a heterogenous ruthenium-catalyst for the *meta*-C–H bromination (Scheme 1.26).[111] The robust, heterogeneous ruthenium on silica catalyst proved highly versatile and could be recycled up to five times without a notable loss of activity.

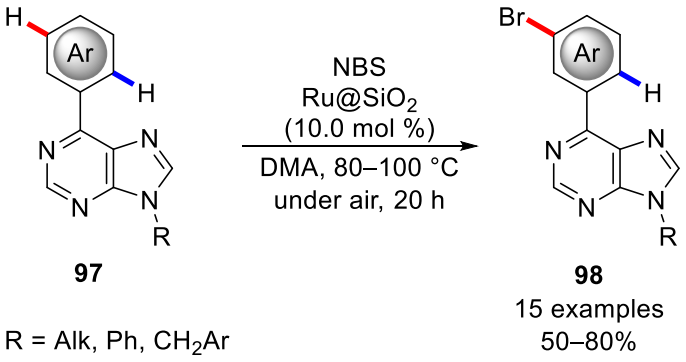

Scheme 1.26: *meta*-C–H bromination catalyzed by a heterogeneous ruthenium catalyst.

The scope of ruthenium-catalyzed *meta*-selective C–H functionalizations has by now been extended to, among others, mono- and difluoroalkylations,[112] the alkylation of structurally complex substrates,[113] and nitrations.[114] The protocol disclosed by Ackermann and coworkers not only allowed for the functionalization of a wide range of pyridyl-substituted substrates, but also delivered a range of functionalized purine derivatives **99** (Scheme 1.27).[112a]

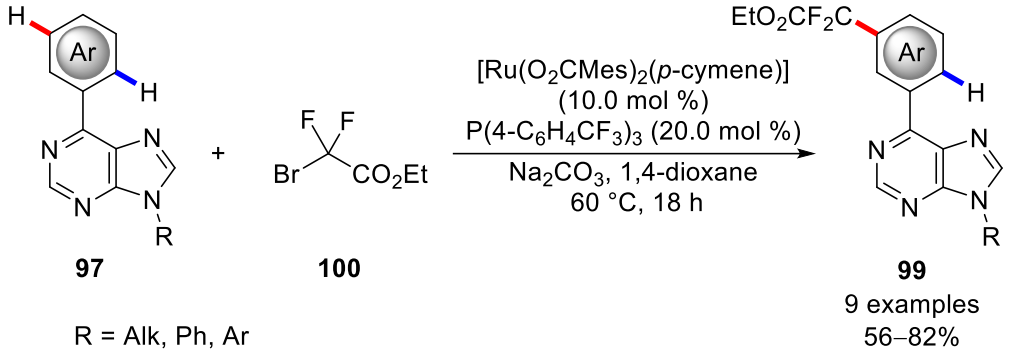

Scheme 1.27: Ruthenium(II)-catalyzed *meta*-C–H difluoromethylation.

While the field of ruthenium-catalyzed *meta*-C–H functionalization underwent considerable progress since Ackermann's seminal observation in 2011, one persistent drawback so far has been the elevated reaction temperature. Given that nowadays a radical pathway is commonly accepted to be involved in the underlying mechanism of these transformations, it appears promising to investigate whether these transformations could be enabled by visible-light photocatalysis.

1.4 Photoredoxcatalysis in Organic Transformations

As light is usually an abundant and readily accessible energy source, the idea of utilizing it to drive chemical reactions has attracted the attention of generations of chemists.[115] Exemplary for this is that, already at the beginning of the 20th century, the Italian chemist and visionary Ciamician described a fascinating projection of the future. In his scenario, chemical production would solely rely on solar energy.[116] Accordingly, classical production sites would be replaced by vast reactors and buildings exclusively made from glass.

In the 1940s, Schenck and Ziegler disclosed their work regarding the synthesis of the natural product ascaridole (**101**).[117] Upon exposure to sunlight, a solution containing the precursor *α*-terpinene (**102**) and chlorophyll would yield meaningful quantities of ascaridole (**101**) after two to three days of irradiation with sunlight (Scheme 1.28).[117-118]

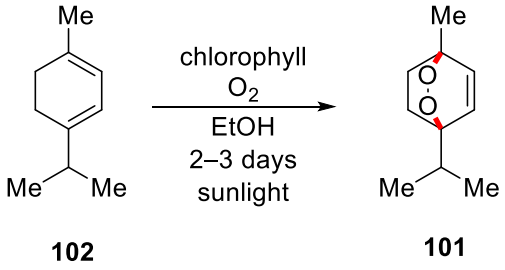

Scheme 1.28: Synthesis of ascaridole (**101**) as reported by Schenck and Ziegler.

This early example for the utilization of solar irradiation for the large-scale production of an API clearly underlines Ciamician's vision. Especially the last two decades have witnessed tremendous advances in the field of photoredox catalysis with a particularly strong influence on organic synthesis.[115,119] Thus, a plethora of transformations using UV or visible light have since been reported. The following discussion will focus on the merger of photoredox and transition metal catalysis, coined metalla-photoredox catalysis.

One of the earliest reports highlighting the potential of combining photocatalysis with classical transition metal-catalyzed coupling chemistry surfaced in 2007.[120] Within this seminal contribution, Akita and Osawa disclosed their findings regarding the influence of $Ru(bpy)_3^{2+}$ on the palladium-catalyzed Sonogashira coupling of phenylacetylene (**130a**) with bromobenzene (**1a**) (Scheme 1.29).[121]

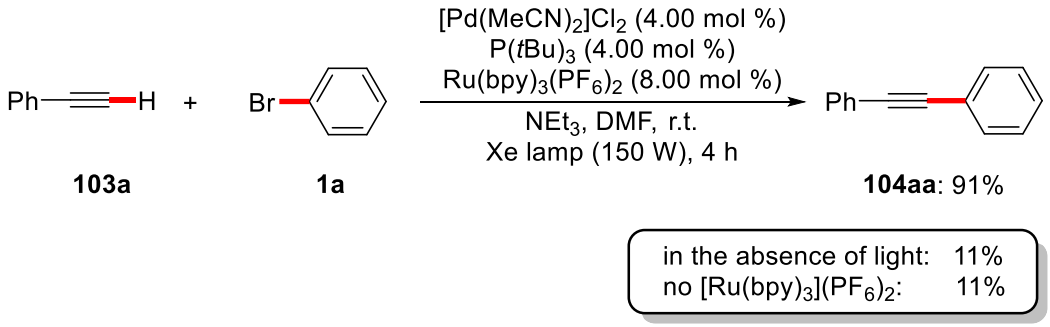

Scheme 1.29: Effect of visible light on the palladium-catalyzed Sonogashira coupling.

As depicted in Scheme 1.29 the authors observed a pronounced effect of the photocatalyst on the efficacy of the Sonogashira coupling. When the photocatalyst was omitted or the reaction was conducted in the dark, the yield dropped drastically to 11%. Moreover, through monitoring the conversion during irradiation and in the absence of light, the authors could clearly show that visible light promoted the reaction.[121] However, Akita and coworkers did not disclose a full catalytic cycle, yet proposed that a facilitated formation of the active palladium(0) species *via* SET with the excited-state photocatalyst might be the underlying reason for the observed increase in reactivity.[120-121]

In 2011, the group of Sanford published a dual photoredox C–H arylation protocol enabled by palladium-catalyzed C–H activation (Scheme 1.30).[122] The successful merger of transition metal-catalyzed C–H activation and photoredox catalysis allowed for the arylation to proceed at ambient temperature and in the absence of an external strong oxidant. Yet, in some cases, the reaction also proceeded in the absence of the ruthenium catalyst.

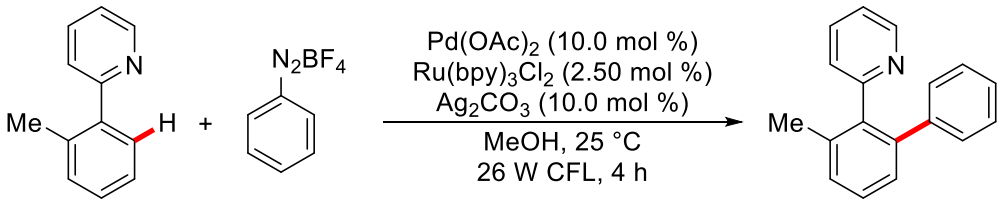

35c **105a** **77ca**: 76%

Scheme 1.30: Visible light-promoted palladium-catalyzed arylation of **35c** with diazonium salt **105a**.

In their mechanistic proposal, Sanford and coworkers assigned a dual role to the employed photocatalyst. First, oxidative quenching of the excited photocatalyst by the diazonium salt **105** results in the fragmentation of **105** and thereby delivers an aryl radical **106** (Scheme 1.31). Subsequently, the aryl radical adds to the palladacycle **107** generated by C–H palladation. The resulting palladium(III) intermediate **108** is further oxidized to a palladium(IV) species *via* a SET with $[Ru(bpy)_3]^{3+}$, thereby regenerating the photocatalyst and closing the photoredox cycle. Facile reductive elimination from this high-valent palladium(IV) species **109** delivers the product **77** and the catalytically active palladium(II) species **110**. The proposal of Sanford and coworkers that the photocatalyst was not only responsible for the initial aryl radical formation but was also capable of modulating the

oxidation state of palladium in the coupling cycle further increased the interest in the emerging field.[120,122]

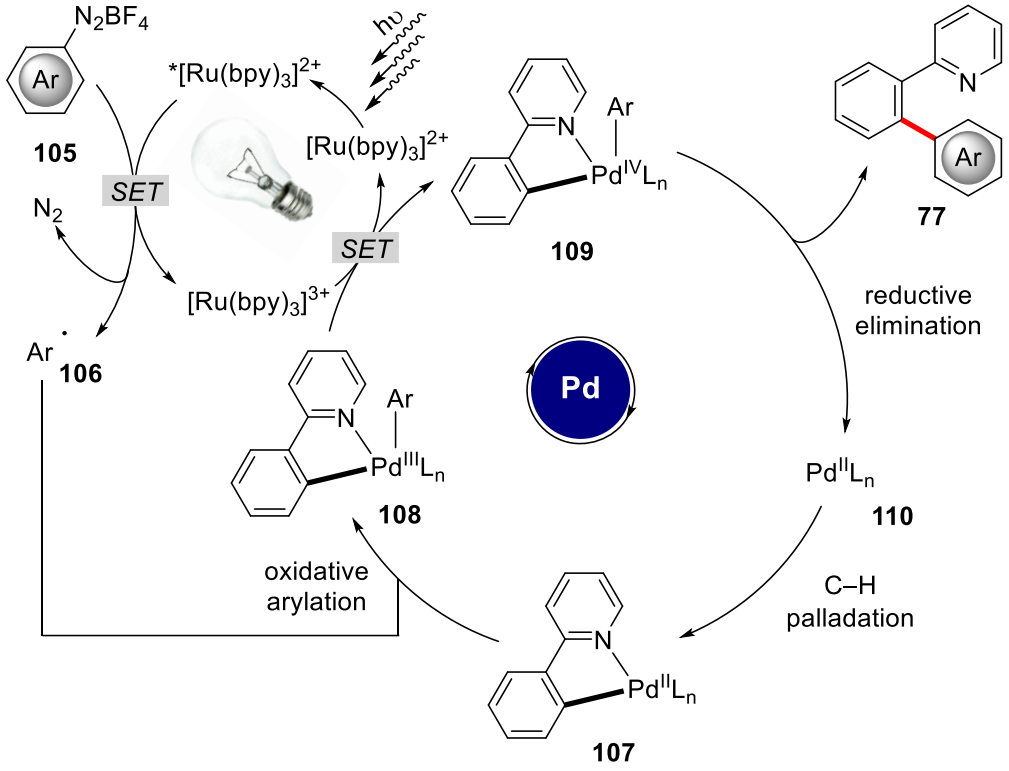

Scheme 1.31: Mechanistic proposal for the visible-light enabled palladium-catalyzed arylation.

One year later Sanford and coworkers were able to apply the previously established principle to the copper-catalyzed coupling of aryl boronic acids **111**. Utilizing photoredox catalysis for the formation of the $CF_3^{\cdot}$ radical, as reported earlier by the MacMillan group,[123] the authors were able to achieve the trifluoromethylation of arylboronic acids **111** at ambient temperature (Scheme 1.32).[124]

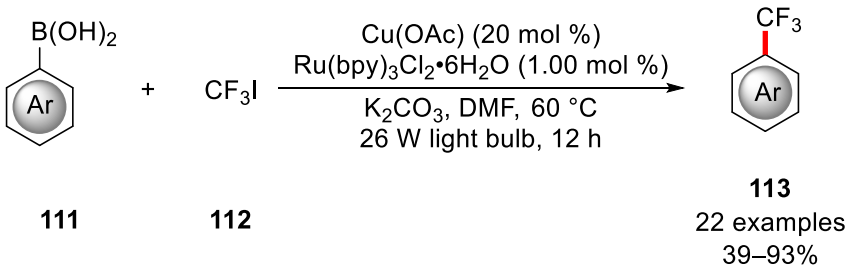

Scheme 1.32: Copper-catalyzed trifluoromethylation of **111** enabled by photoredox catalysis.

Also in 2012, Fu and Peters reported their findings concerning a photoinduced Ullmann C–N coupling.[125] In this initial work, they could show that the copper(I)-carbazolide

complex **114** undergoes arylation in the presence of iodobenzene (**11a**) when irradiated (Scheme 1.33a). Additionally, they demonstrated that complex **114** was also a capable catalyst for the arylation reaction itself (Scheme 1.33b).[125]

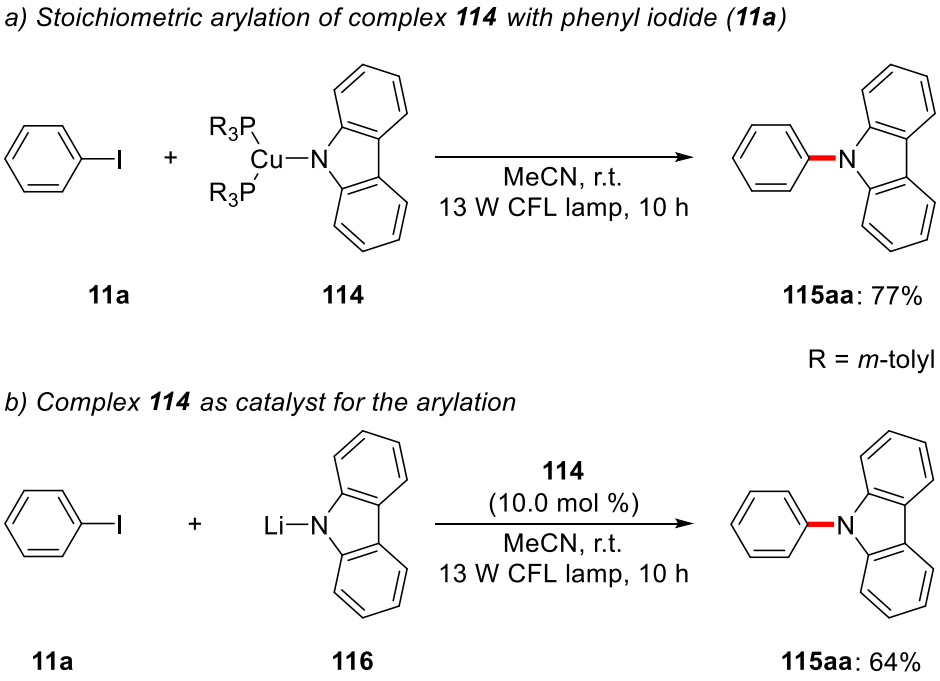

Scheme 1.33: Fu and Peters' initial results regarding the photo-induced Ullmann C–N coupling.

After having established this proof of concept, Fu and Peters were able to further extend the range of photo-induced Ullmann couplings to additional arylations,[126] alkylations,[127] and C–O bond formations.[128]

In 2015, the group of Kobayashi provided two further examples for copper-photoredox catalysis, namely the visible light-enabled Chan-Lam coupling[129] and a visible light-mediated Ullmann C–N coupling of carbazole derivatives **117**.[130] Taking the work from Fu and Peters as the outset for their own investigations, they could show that the presence of $Ir(ppy)_3$ enabled the transformation to proceed under visible light irradiation, thus eliminating the need to use high-energy light sources (Scheme 1.34).[130] In this case, the authors proposed that the excited state $Ir(ppy)_3$* would be quenched by an energy-transfer mechanism with the *in situ* generated copper(I)-carbazolide complex. However, due to the lack of experimental support, the authors could not decisively rule out other possible mechanistic scenarios.

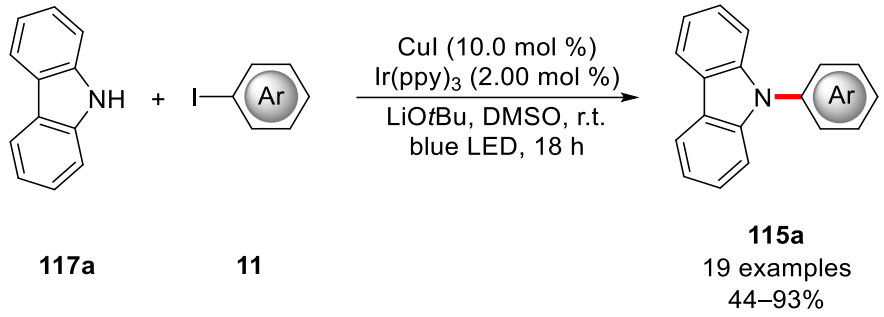

117a **11** **115a**
19 examples
44–93%

Scheme 1.34: Visible light-mediated Ullmann-type C–N coupling reported by Kobayashi.

While the earlier examples of metallaphotoredox catalysis[120] were achieved using palladium- or copper-based transition metal catalysts, the group of Rueping successfully applied the concept to rhodium- and ruthenium-catalyzed C–H functionalization.[131] By exploiting the photocatalyst's ability to modulate the oxidation state of the transition metal involved in the catalytic bond forming process, they could significantly facilitate the required reoxidation of the transition metal catalyst. Thus, they reported the rhodium- and ruthenium-catalyzed C–H olefination with air as benign oxidant (Scheme 1.35).[132] However, at these elevated reaction temperatures, such reactions are also viable in the absence of light.[29a,133]

a) Rhodium-catalyzed oxidative C–H olefination enabled by photoredox catalysis

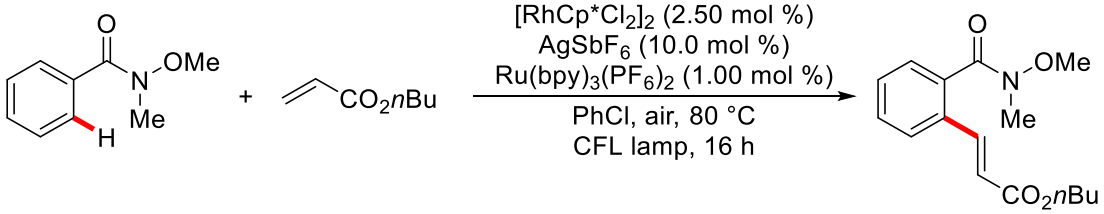

118a **119a** **120aa**: 91%

*b) Ruthenium-catalyzed C–H olefination of phenol ethers **121***

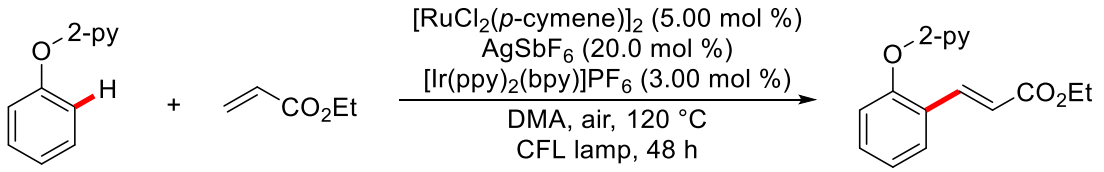

121a **119b** **122ab**: 61%

Scheme 1.35: Examples for rhodium- and ruthenium-photoredox catalysis by Rueping.

In both cases, the authors could avoid the use of commonly employed external oxidants such as copper(II) or silver(I) salts. Through the action of the photoredox catalyst, the

oxygen present in the reaction could serve as a competent oxidant, thereby allowing the required reoxidation of the intermediate rhodium and ruthenium hydride complexes. Still, both transformations required elevated temperatures to ensure satisfactory conversion.

Within the field of metallaphotoredox-catalysis, the combination of nickel- and photoredox catalysis with iridium-based photocatalysts has proven uniquely fruitful.[134] In 2014, the groups of Molander[135] and Doyle as well as MacMillan[136] simultaneously reported nickel-catalyzed couplings of alkyl radicals derived from alkyl trifluoroborates **123** or in the case of the report from Doyle and MacMillan, from carboxylic acids, such as proline (**124**).

*a) Nickel-catalyzed coupling with potassium trifluoroborates **123** (Molander, 2014)*

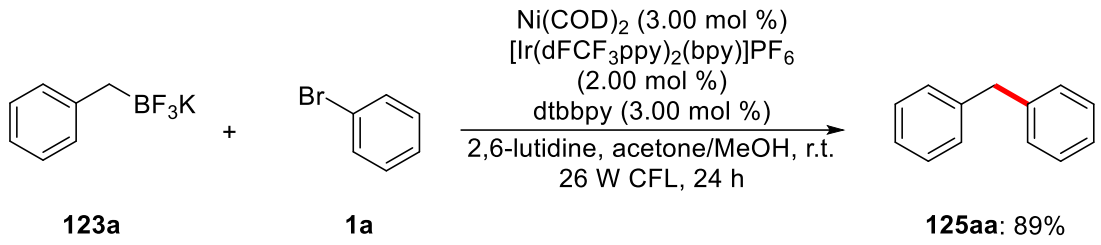

*b) Nickel-catalyzed decarboxylative coupling with proline (**124**) (Doyle, Macmillan, 2014)*

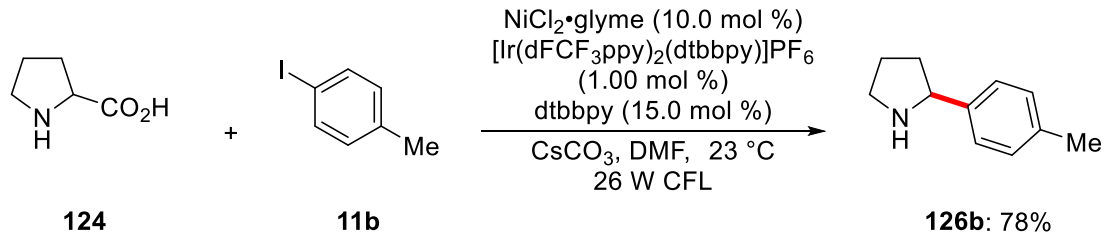

Scheme 1.36: Dual nickel-photoredox catalysis.

Both couplings displayed broad scope and high functional group tolerance. More importantly, both proposed mechanistic scenarios implied a dual role of the iridium-based photoredox catalysts (Scheme 1.37). In each case, the photoredox catalyst is involved in the generation of the alkyl radical **127** through a one-electron-oxidation of the alkyl substrate. The resulting radical is then captured by the nickel(II)-aryl species **128** generated by oxidative addition of aryl halide **129**. The photoredox catalyst is also responsible for the required reduction of the nickel(I)-species **130** generated by reductive elimination from nickel(III)-complex **131**.

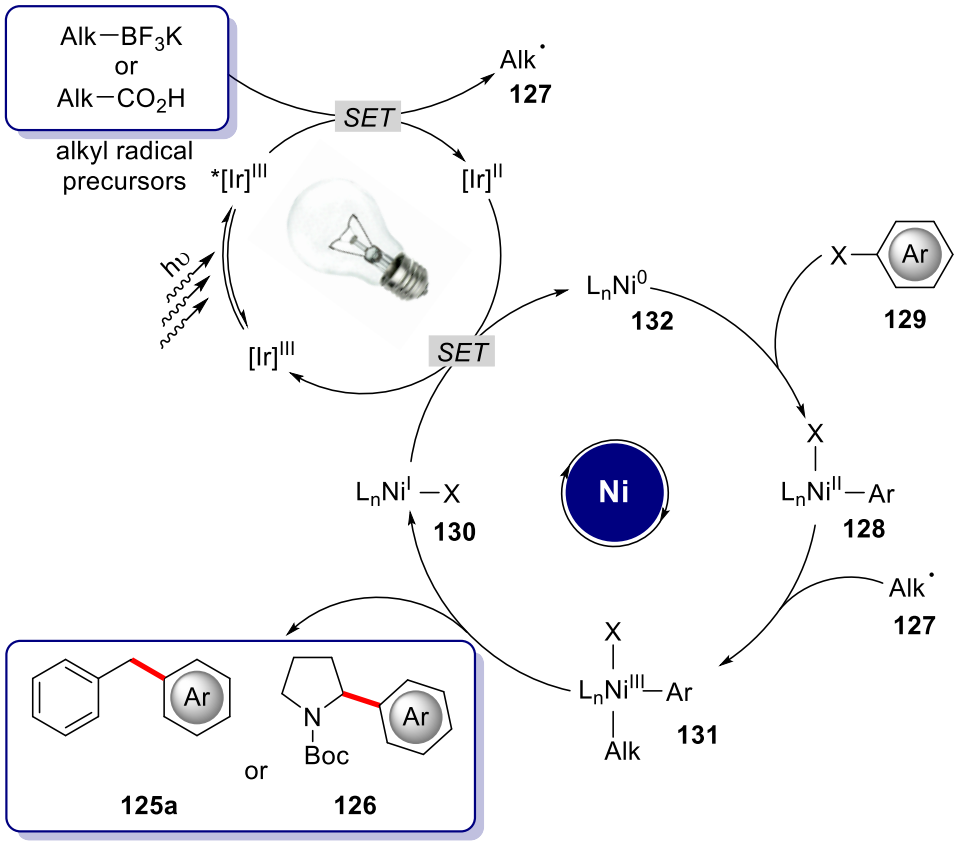

Scheme 1.37: Initially proposed mechanistic scenario for the dual nickel-photoredox couplings.

Since Molander's initial proposal for the mechanism of the nickel-catalyzed cross-coupling of aryl halides **129** and alkyl trifluoroborates, additional studies have highlighted the possibility of alternative mechanistic scenarios. In an ensuing report, Molander and Kozlowski have outlined a possible mechanism in which the alkyl radical **127** is captured by the nickel(0)-species **132**.[137] Subsequent oxidative addition of the aryl halide **129** would then result in the formation of intermediate **131**.

Furthermore, a recent report by the MacMillan group indicated that reductive elimination can also occur from an electronically excited nickel(II)-species.[138] Upon an energy transfer from the excited state photocatalyst, the resulting electronically excited nickel(II)-species can directly undergo reductive elimination, yielding the product and regenerating the active nickel(0) catalyst.

In conclusion, the merger of transition metal catalysis and photoredox catalysis has proven to be a versatile tool for organic synthesis. Despite undeniable advances, the drawbacks inherent to cross-coupling reactions remain. In addition, the careful selection of each catalyst with respect to its properties remains a cumbersome endeavor.[139] This

is further complicated by the fact that the rates of the different steps within the catalytic cycles have to be matched precisely to ensure efficient transformations. To this end, the previously discussed work from Fu and Peters is noteworthy as it displays the ability of copper-based transition metal catalysts to enable otherwise challenging transformations, even in the absence of exogenous photocatalysts.[126-128] Furthermore, metallaelectrocatalysis as recently pioneered by Ackermann and coworkers is nowadays becoming a valuable addition to the toolbox of organic chemistry and has been established as a benign alternative to photoredox catalysis.[26,140]

2 Objectives

As outlined in the previous chapter, copper catalysts have a long-standing and successful history in C–H functionalization reactions due to their benign properties.[43,44b,44c] Despite the fact that copper catalysts have been previously reported to enable C–H sulfenylation and selenylation reactions,[64a,72-74,76] their use for the selective chalcogenation of the C-7 position of indolines **133** has proven elusive thus far. Additionally, previously reported protocols often relied on stoichiometric amounts of copper complexes or bidentate directing groups. Furthermore, the protocol should also be applicable to the C-2 chalcogenation of indoles 1**34** (Scheme 2.1). In addition, oxidation of the sulfenylated indolines **135** would grant access to the corresponding C-7 sulfenylated indoles **136**. When employing diselenides **63**, the copper-catalyzed C–H chalcogenation would also yield the selenylated indolines **137** and indoles **138**, therefore the development of such a methodology is highly desirable.

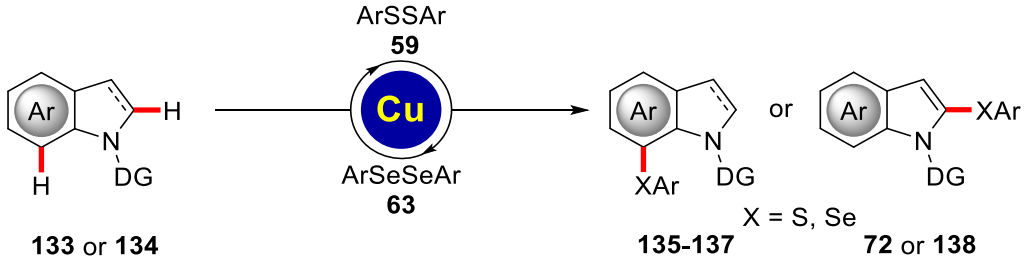

Scheme 2.1: Copper(II)-catalyzed chalcogenation of indolines **133** and indoles **134**.

Ruthenium and iridium polypyridyl complexes are prominently used in photoredox catalysis, yet the use of organic chromophores is often a valuable alternative.[119c,141] Among organo-photocatalysts, acridinium-based photocatalysts as pioneered by Fukuzumi,[142] offer unique opportunities.[143] Recently they have been used in dual catalytic systems with cobaloximes **139** to enable oxidative C–N and C–P couplings without the need of an external oxidant.[144] Previous photocatalytic Minisci-type alkylations are reliant on strong oxidants or precious transition metal catalysts.[145] As the dual acridinium cobalt catalytic system does not suffer these drawbacks, its application to decarboxylative C–H alkylation reactions appears highly beneficial (Scheme 2.2).

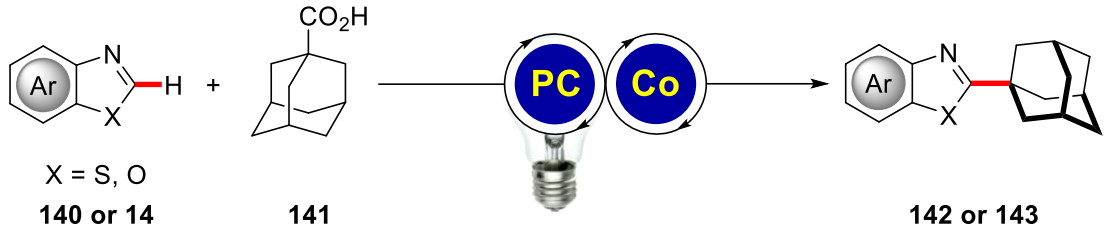

Scheme 2.2: Decarboxylative alkylation enabled by dual cobalt photoredox catalysis.

Copper-catalyzed arylation reactions are known since the pioneering studies from Ullmann and Goldberg.[45a,45b,45e] Nearly one century later Miura, Daugulis and Ackermann introduced copper-catalysts for the C–H arylation of azoles **7, 12 and 14** and triazoles **27**.[52,54,56-58] Despite the considerable advances, copper-catalyzed arylations were still dependent on harsh reaction conditions, namely high reaction temperatures. The recent work from Fu and Peters[125-126,127b] indicated the ability of *in situ* generated copper-complexes to undergo excitation by light, thereby enabling Ullmann-type couplings at ambient temperature. Since a related photo-induced copper-catalyzed C–H arylation could possibly also proceed at room temperature, establishing first photo-induced copper-catalyzed C–H transformations is highly desirable (Scheme 2.3).

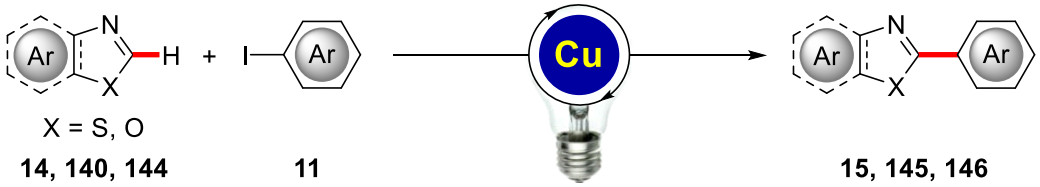

Scheme 2.3: Photo-induced copper-catalyzed C–H arylation.

Since Ackermann's seminal report of a ruthenium-catalyzed *meta*-selective C–H alkylation in 2011,[106] *σ*-activation by cycloruthenation has emerged as a powerful tool to facilitate *meta*-selective transformations.[101] Subsequent reports by Ackermann delivered conclusive evidence for a radical pathway and the involvement of the C–H cycloruthenated intermediate in the generation of the alkyl radical.[109] Despite the already achieved advances, the use of visible light to induce the key SET process might significantly lower the required temperatures and therefore lead to unprecedented mild

conditions for ruthenium-catalyzed *meta*-C–H alkylations. Ideally, this transformation would be achieved without an external photosensitizer and with visible light.

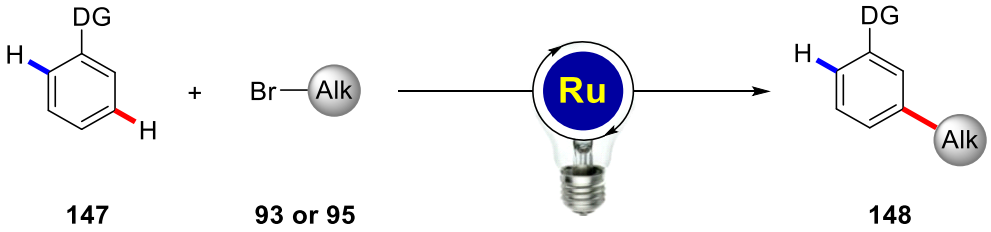

Scheme 2.4: Visible light-enabled ruthenium-catalyzed *meta*-C–H alkylation.

3 Results and Discussion

3.1 Copper-catalyzed C–H Chalcogenation of Indolines and Indoles

The indole motif represents one of the most ubiquitous heterocyclic structures found in nature[146] and is often a key structure in compounds of interest to medicinal chemistry.[147] Since it is apparent that the diverse substitution patterns on the indole ring are the reason for the observed wide array of biological properties, the recent years have witnessed great efforts towards the direct, positional-selective functionalization of indoles.[148] Yet, the majority of those transformations, including among others arylations,[149] cyanations,[150] or alkenylations,[151] exploits the innate reactivity of the indole core and is therefore restricted to the electron-rich C-2 or C-3 positions.

Hence, C–H functionalization reactions regarding the C-7 position are considerably less explored. Nevertheless, the use of sterically demanding directing groups at the nitrogen atom allowed for the direct functionalization of the C-7 position.[152] Another approach is the C-7 functionalization of the corresponding indoline **133** and subsequent oxidation to the corresponding indole **136**. The viability of this method has so far been elaborated with palladium,[153] rhodium,[154] iridium,[155] and ruthenium,[156] yet more favorable first-row transition metal-based catalysts have remained elusive for these transformations.

3.1.1 Optimization Studies and Evaluation of *N*-Substitution

Orienting optimization studies were performed by Dr. P. Gandeepan and revealed that, among the investigated solvents, only aromatic solvents proved viable for the desired transformation.[157] While both copper(I) and copper(II) salts were suitable precatalysts, $Cu(OAc)_2 \cdot H_2O$ delivered the best results. In addition, further screening of additives yielded no further enhancement.[157] Therefore, the simple and user-friendly catalytic system depicted in Scheme 3.1 was chosen as a starting point for the ensuing studies.

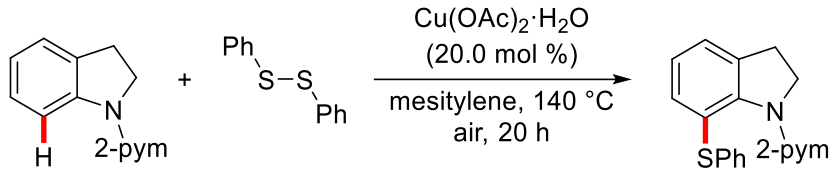

Scheme 3.1: Initial conditions for the copper-catalyzed thiolation of indolines.[157]

To further investigate the influence of additional oxidants, several oxidants were probed (Table 3.1).

Table 3.1: Effect of oxidants on the copper-catalyzed C–H thiolation.[a]

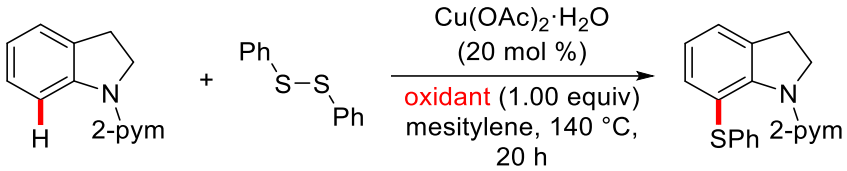

Entry	Oxidant	Yield (%)
1	$PhI(OAc)_2$	23
2	MnO_2	69[b]
3	$K_2S_2O_8$	57
4	oxone	--
5	air	66

[a] Reaction conditions: **133a** (0.30 mmol), **59** (0.30 mmol), $Cu(OAc)_2·H_2O$ (20.0 mol %), mesitylene (1.5 mL), oxidant (0.30 mmol), 140 °C, 20 h, yield of isolated product. [b] **59a** (0.36 mmol).

While the organic oxidant (diacetoxyiodo)benzene (PIDA) significantly lowered the catalytic efficacy (entry 1), the inorganic oxidants MnO_2, $K_2S_2O_8$, and oxone showed either no significant effect (entries 2 and 3) or completely diminished the catalytic efficiency (entry 4).

These results suggested that ambient air is a sufficiently strong oxidant for the transformation (entry 5). Although oxygen is often considered as an ideal oxidant,[158] reactions in flammable organic solvents involving pure oxygen pose a certain safety hazard, especially at elevated temperatures.[159] However, the significantly lower oxygen

concentration in ambient air reduces the associated risks significantly. Since many previously disclosed copper based thiolation reactions required considerably higher catalyst loadings, [64a,74,76,78,160] the comparatively low catalyst loading of only 20 mol % is also noteworthy.

Finally, the *N*-substitution pattern was evaluated. Acetyl and carboxamide substitution failed to deliver the desired thiolation products **151a** and **152a**, thus proving ineffective for the desired C–H thiolation (Scheme 3.2).

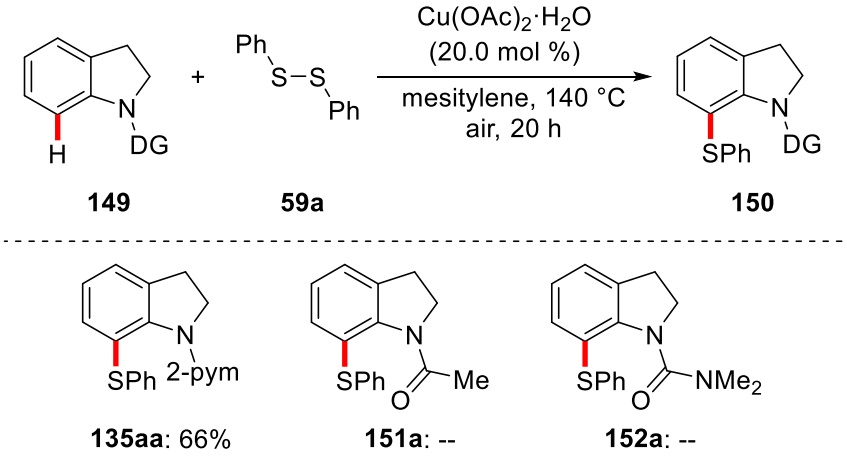

Scheme 3.2: Evaluation of the directing group in the copper(II)-catalyzed C–H thiolation. Reaction conditions: **149** (0.30 mmol), **59a** (0.30 mmol), $Cu(OAc)_2 \cdot H_2O$ (20.0 mol %), mesitylene (1.5 mL), 140 °C, 20 h, yield of isolated product.

3.1.2 Scope of the Copper-Catalyzed C–H Chalcogenation

With the optimized catalytst, the scope of the copper-catalyzed thiolation was explored. First, a range of diversely substituted disulfides **56** and **59** was investigated (Table 3.2).

Table 3.2: Scope of the copper(II)-catalyzed C–H thiolation with disulfides **56** and **59**.[a]

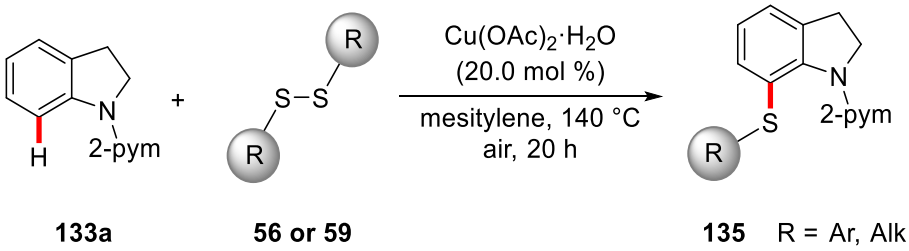

Entry	Disulfide	Product	Yield [%]
1	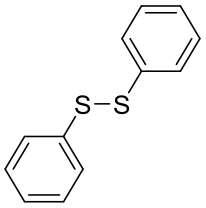 **59a**	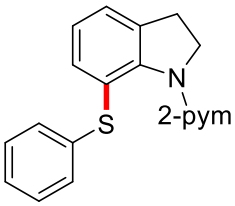 **135aa**	66
2	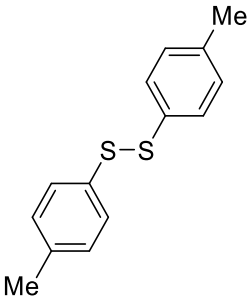 **59b**	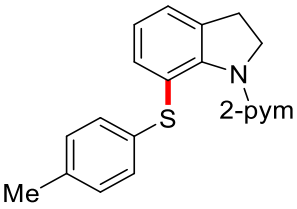 **135ab**	63
3	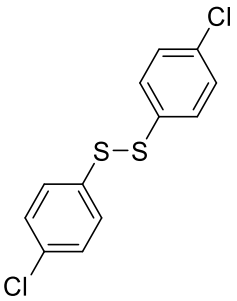 **59c**	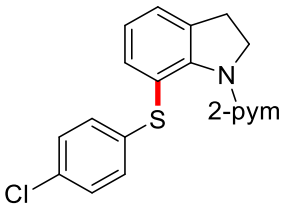 **135ac**	40
4	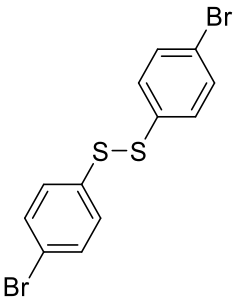 **59d**	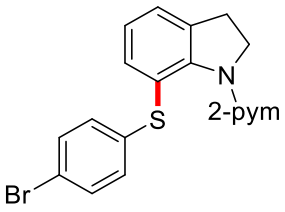 **135ad**	51

Entry	Disulfide	Product	Yield [%]
5	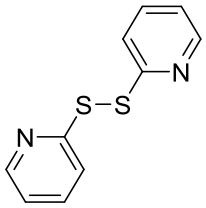 **59e**	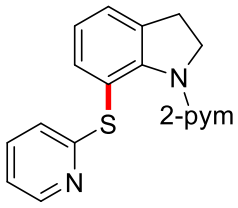 **135ae**	--
6	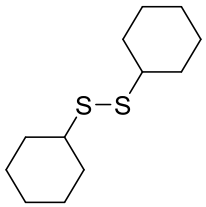 **56d**	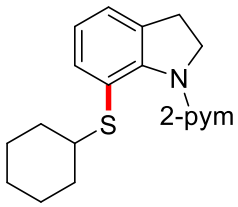 **135af**	--

[a] Reaction conditions: **135a** (0.30 mmol), **56** or **59** (0.30 mmol), $Cu(OAc)_2 \cdot H_2O$ (20.0 mol %), mesitylene (1.5 mL), 140 °C, 20 h, yield of isolated product.

While a methyl group in the 4-position of the diaryl disulfide **59b** had no significant influence on the outcome of the reaction and was well tolerated (entry 2), halogen substitution at the 4-position resulted in lowered yields (entries 3–4). Yet, the bromo-substituted diaryl disulfide **59d** still yielded the corresponding indoline **135ad** with a satisfactory yield, which is of significance in respect to possible further derivatization of the corresponding product **135ad**. 2-Pyridyl- or alkyl substituted disulfides **59e** and **56d** completely failed to deliver the corresponding products (entries 5–6). In case of the 2-dipyridyl substituted disulfide **59e**, this can most likely be attributed to competing coordination of **59e** to the copper(II)-catalyst.

In addition to the studied disulfides **59**, the scope of the copper(II)-catalyzed C–H thiolation in regard to the substitution pattern of the indoline was thoroughly investigated. To this end, a broad range of diversely substituted indolines **133** was subjected to the optimized reaction conditions (Table 3.3).

Table 3.3: Scope of the copper(II)-catalyzed C–H thiolation with indolines **133**.[a]

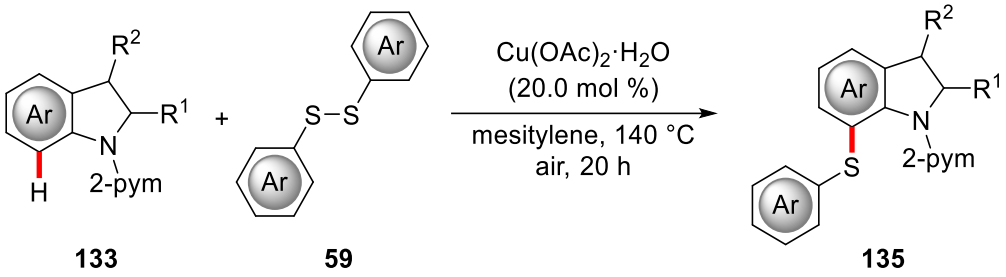

133 **59** **135**

Entry	Indoline	Product	Yield [%]
1	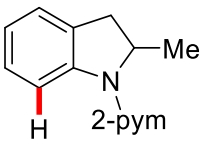	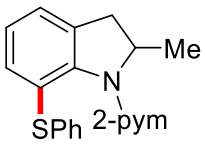	72
	133b	**135ba**	
2	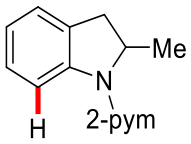	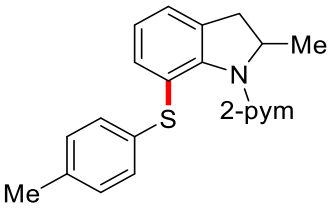	66
	133b	**135bb**	
3	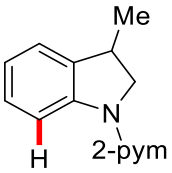	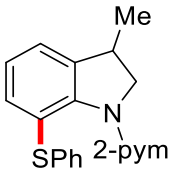	52
	133c	**135ca**	
4	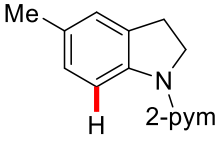	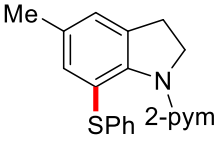	62
	133d	**135da**	

Entry	Indoline	Product	Yield [%]
5	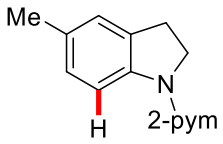 **133d**	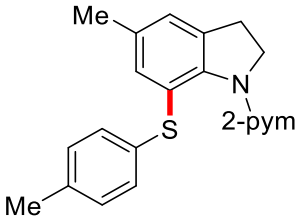 **135db**	60
6	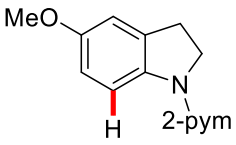 **133e**	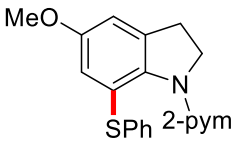 **135ea**	62
7	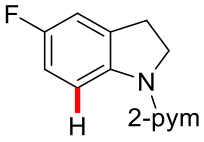 **133f**	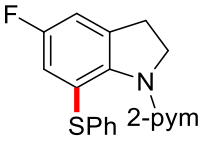 **135fa**	69
8	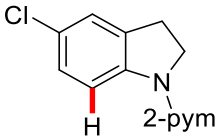 **133g**	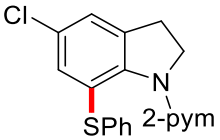 **135ga**	65
9	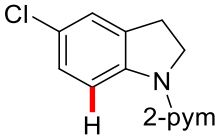 **133g**	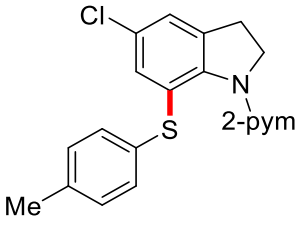 **135gb**	63

Entry	Indoline	Product	Yield [%]
10	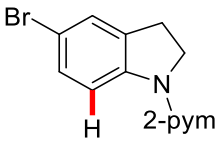	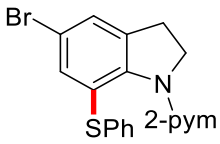	55
	133h	**135ha**	

[a] Reaction conditions: **133** (0.30 mmol), **59** (0.30 mmol), $Cu(OAc)_2 \cdot H_2O$ (20.0 mol %), mesitylene (1.5 mL), 140 °C, 20 h, yield of isolated product.

Methyl substituents in the C-2 or C-5 position of the indolines **133b** and **133d** had no pronounced effect on the outcome of the reaction. Only with the methyl group in the 3-position a slightly lower yield was observed (entries 1–5). Furthermore, electron-withdrawing functional groups, as well as electron-donating groups were well tolerated (entries 6–7). In addition to the fluoro-substituted indoline **133f**, the synthetically meaningful chloro- and bromo-substituents were also well accepted, and the corresponding products **135ga** and **135ha** were obtained in satisfying yields (entries 8–10).

Organoselenium compounds have received considerable attention due to their possible applications in medicinal research.[161] Therefore, it is noteworthy that the catalyst was not limited to disulfides **59**. Thus, a range of substituted indolines **133** and diselenides **63** could be employed to give efficient access to indoline-7-selenol derivatives **137** (Table 3.4).

Table 3.4: Scope of the copper(II)-catalyzed C–H selenylation with diselenides **63**.[a]

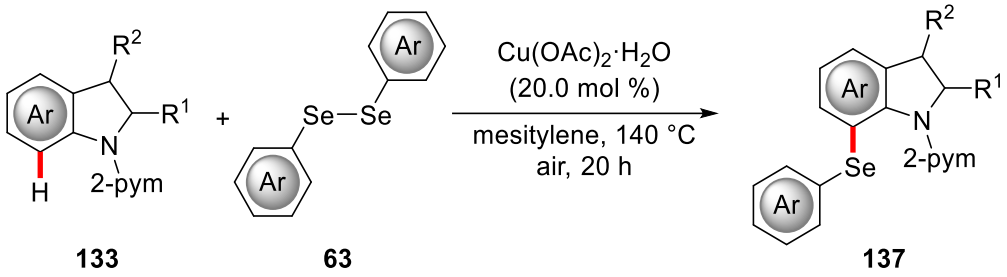

133 **63** **137**

Entry	Indoline	Product	Yield [%]
1	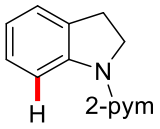	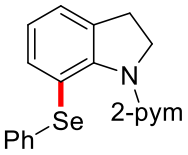	57
	133a	**137aa**	
2	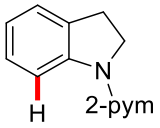	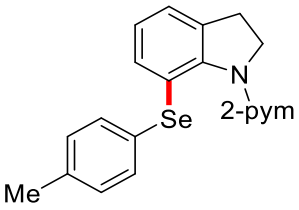	53
	133a	**137ab**	
3	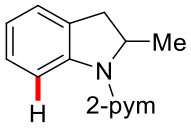	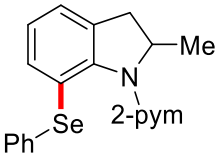	56
	133b	**137ba**	
4	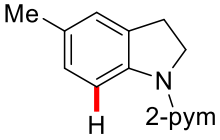	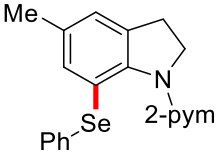	54
	133d	**137da**	

Entry	Indoline	Product	Yield [%]
5	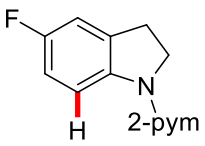 **133f**	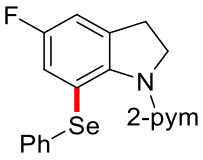 **137fa**	62
6	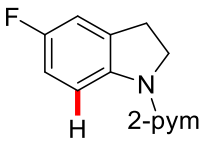 **133f**	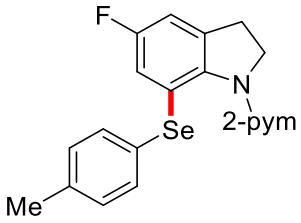 **137fb**	63
7	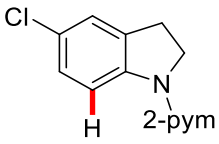 **133g**	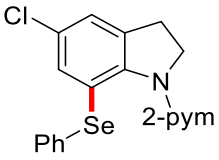 **137ga**	53

[a] Reaction conditions: **133** (0.30 mmol), **63** (0.30 mmol), $Cu(OAc)_2 \cdot H_2O$ (20.0 mol %), mesitylene (1.5 mL), 140 °C, 20 h, yield of isolated product.

In general, the copper(II)-catalyzed C–H selenylation showed similar applicability compared to the previously discussed thiolation, yet with slightly lowered yields (entry 1). While methyl substitution on either indoline **133** or diselenide **63** had little influence (entries 2–4), halogen substituents were well tolerated again (entries 5–7). Overall, the copper(II)-catalyzed C–H chalcogenation proceeded with good yields and high levels of positional selectivity.

Additionally, it was investigated if the copper(II)-based catalyst could also be utilized to achieve the direct thiolation of indoles **134**. To this end, a variety of diversely decorated indoles **134** and diaryl disulfides **59** was utilized (Table 3.5 and Table 3.6).

Table 3.5: Scope of the copper(II)-catalyzed C–H thiolation of indoles **134** with disulfides **59**.[a]

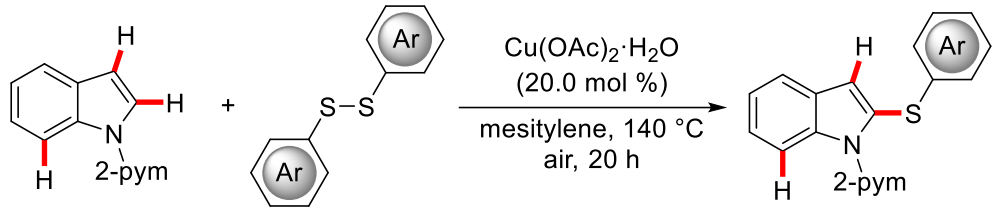

134a **59** **72**

Entry	Disulfide	Product	Yield [%]
1	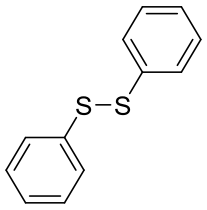	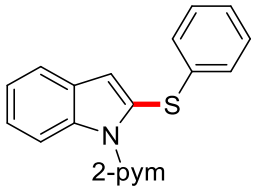	62
	59a	**72aa**	
2	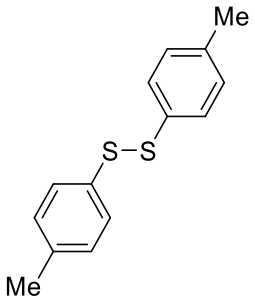	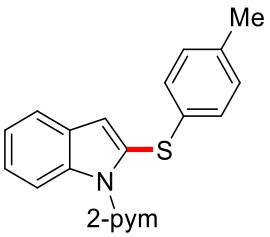	68
	59b	**72ab**	
3	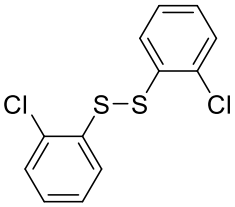	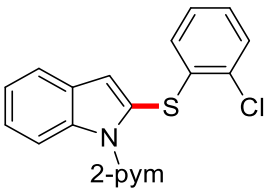	25
	59f	**72af**	

Entry	Disulfide	Product	Yield [%]
4	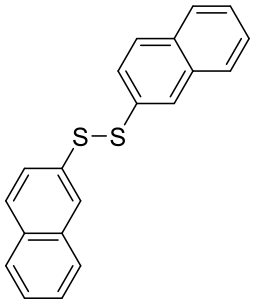	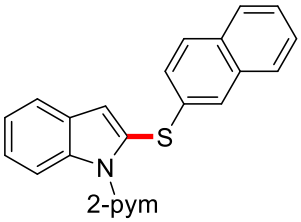	60
	59g	**72ag**	

[a] Reaction conditions: **134** (0.30 mmol), **59** (0.30 mmol), $Cu(OAc)_2 \cdot H_2O$ (20.0 mol %), mesitylene (1.5 mL), 140 °C, 20 h, yield of isolated product.

All employed disulfides **59** were competent substrates for the copper(II)-catalyzed C–H thiolation. Apart from the reaction with the *ortho*-substituted substrate **59f** (entry 3), all products **72** were obtained with moderate yields, again in a comparable fashion to the yields observed in the C–H thiolation of indolines **133**.

Table 3.6: Scope of the copper(II)-catalyzed C–H thiolation of indoles **134**.[a]

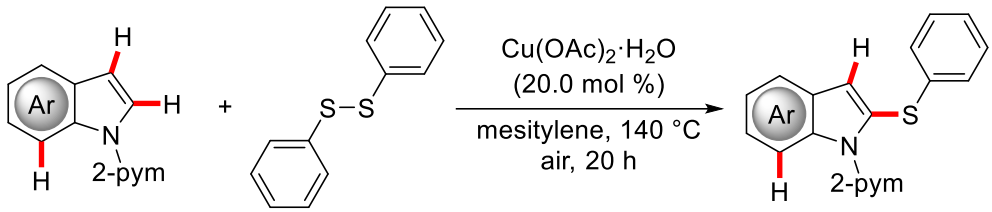

134 **59a** **72**

Entry	Indole	Product	Yield [%]
1	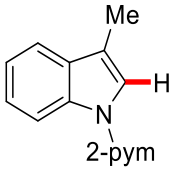	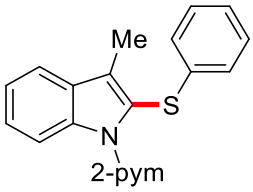	75
	134b	**72ba**	

Entry	Indole	Product	Yield [%]
2	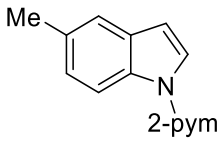 **134c**	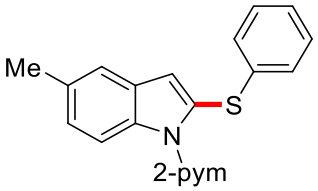 **72ca**	63
3	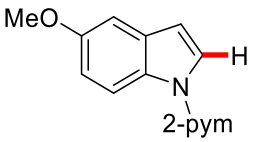 **134d**	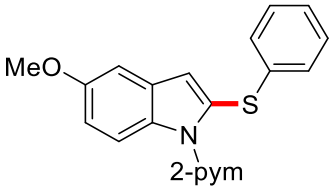 **72da**	48
4	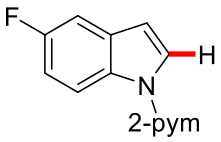 **134e**	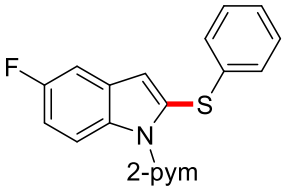 **72ea**	57
5	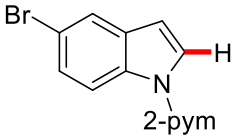 **134f**	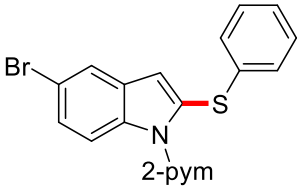 **72fa**	51

[a] Reaction conditions: **134** (0.30 mmol), **59a** (0.30 mmol), $Cu(OAc)_2 \cdot H_2O$ (20.0 mol %), mesitylene (1.5 mL), 140 °C, 20 h, yield of isolated product.

All the probed indoles **134** delivered the corresponding C-2-substituted products **72** in moderate to good yields. For the 3-methyl substituted indole **134b** an increased yield was observed (entry 1). In addition, a methyl group in the 5-position did not exert a pronounced effect but was well tolerated (entry 2), as were halogen substituents (entries 4–5). Although the C-3 functionalized products were not observed in any of the other cases, the result with indole **134b** might indicate the presence of a competing

reaction involving the more electron-rich C-3 position. Given the electronic properties of the C-3 position, a cleavage of the S–S bond of the disulfide **59** *via* an electrophilic substitution involving the electron-rich C-3 position of the indole core can be considered as a likely side reaction.

Besides this finding, the copper(II)-catalyzed thiolation showed complete C-2 selectivity, and no evidence for the formation of the C-3 or C-7 substituted product was obtained. This further illustrates the preferred formation of the 5-membered metallacycle involved in the functionalization of the C-2 position over the 6-membered metallacycle involved in the C-7 functionalization.[152a]

The overall robust nature of the copper(II) catalyst was further showcased by the facile selenylation of indole **134b**. Both diselenides **63a** and **63b** could be employed in the copper(II)-catalyzed selenylation and the resulting products were obtained in good yields (Scheme 3.3).

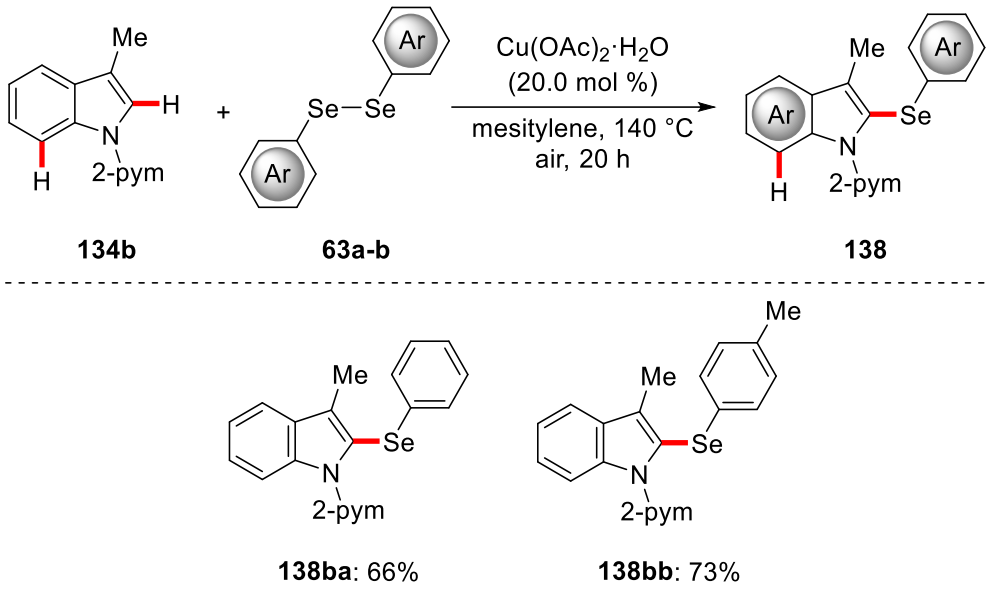

Scheme 3.3: Copper(II)-catalyzed C–H selenylation of indole **134** with diselenides **63**. Reaction conditions: **134b** (0.30 mmol), **63** (0.30 mmol), $Cu(OAc)_2 \cdot H_2O$ (0.06 mmol, 20.0 mol %), mesitylene (1.5 mL), 140 °C, 20 h, yield of isolated product.

However, in case the diselenides **63** were used, it was necessary to block the C-3 position. A reaction with unsubstituted indole **134a** resulted only in sluggish product formation. In comparison to the previously employed disulfides **59**, diselenides **63** possess a considerably higher electrophilicity and an overall increased reactivity towards S_N2 type

reactions.[162] It is, therefore, likely that a selenylation of the electron-rich C-3 position[163] is competing when the C-3 position is not blocked.

Despite the broad applicability of the copper(II)-catalyzed chalcogenation, some limitations were encountered during the attempts to further widen the scope of the developed methodology. Thus, ditellurides **153** could not be employed in the reaction, and furthermore the copper(II)-catalyzed thiolation of other biologically relevant nitrogen-containing heterocycles, such as carbazole (**155a**) or tetrahydroquinoline **156a** delivered the corresponding products only in low yields (Scheme 3.4).

*a) Copper-catalyzed tellurylation of indoline **133a***

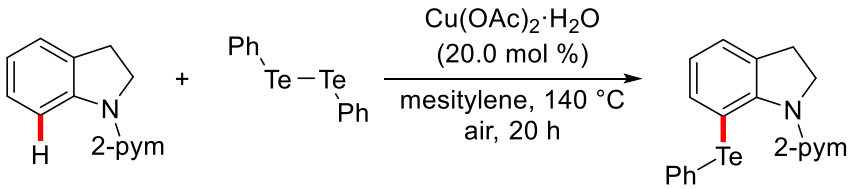

133a **153a** **154aa**: --

*b) Copper-catalyzed thiolation of carbazole **155a***

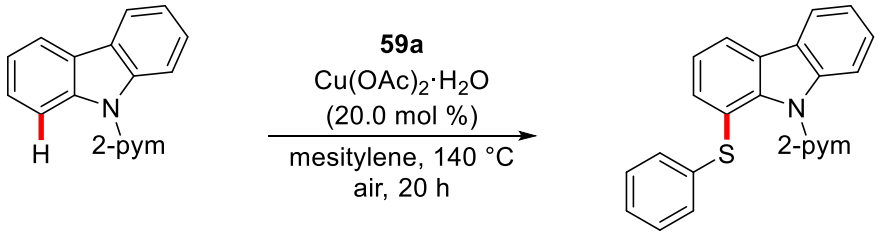

155a **70aa**: 20%

*c) Copper-catalyzed thiolation of tetrahydroquinoline **156a***

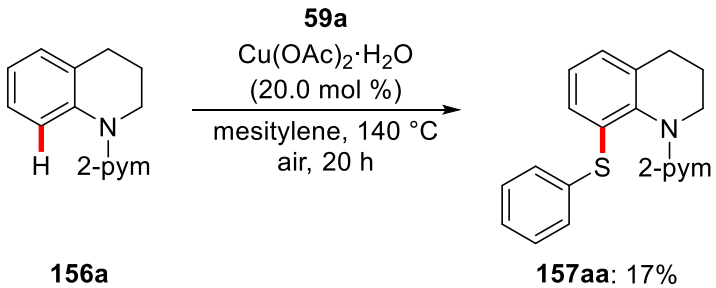

156a **157aa**: 17%

Scheme 3.4: Limitations of the copper(II)-catalyzed C–H chalcogenation. Reaction conditions: **133**, **155a** or **156a** (0.30 mmol), **59a** or **153a** (0.30 mmol), $Cu(OAc)_2 \cdot H_2O$ (20.0 mol %), mesitylene (1.5 mL), 140 °C, 20 h, yield of isolated product.

3.1.3 Mechanistic Studies

With the scope of the copper-catalyzed C–H chalcogenation established, several mechanistic experiments were conducted in order to delineate the copper catalyst's mode of action. In addition, these findings may also yield further insights into the observed regioselectivity.

3.1.3.1 Reaction in the Presence of Typical Radical Scavengers

Radical intermediates are frequently proposed to be key intermediates in copper-catalyzed C–X bond forming reactions (X = N, O, S).[68] It was therefore examined, whether the copper(II)-catalyzed chalcogenation involves the formation of radical intermediates and therefore proceeds *via* a SET-type mechanism. To this end, several reactions with commonly employed radical scavengers were conducted (Table 3.7).

Table 3.7: Effect of radical scavengers on the copper(II)-catalyzed C–H thiolation.[a]

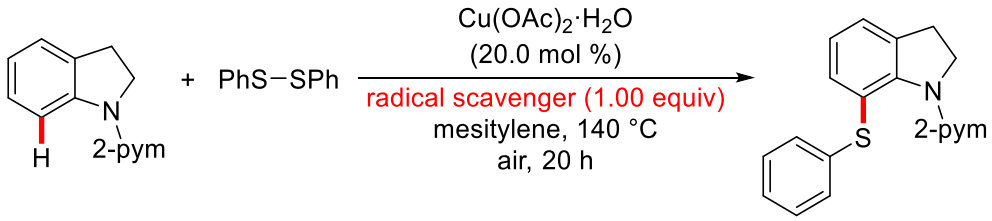

133a **59a** **135aa**

Entry	Radical scavenger	Yield [%]
1	--	66
2	TEMPO	23
3	BHT	--
4	galvinoxyl free radical	--

[a] Reaction conditions: **133a** (0.30 mmol), **59a** (0.30 mmol), $Cu(OAc)_2 \cdot H_2O$ (20.0 mol %), mesitylene (1.5 mL), radical scavenger (0.30 mmol), 140 °C, 20 h, yield of isolated product.

In all cases, the catalytic reaction was significantly inhibited. When TEMPO was used as radical scavenger, the catalyst's activity was drastically reduced (entry 2), furthermore the presence of either BHT or galvinoxyl completely suppressed product formation (entries 3–4). Although no adduct of the radical scavengers with possible radical intermediates

was observed in the ESI-HRMS analysis of the reaction mixture, these findings suggest that a SET-type mechanism is involved in the reaction.

3.1.3.2 H/D-Exchange Experiments

Deuteration studies were conducted, using fully isotopically labeled CD_3OD as co-solvent. First, an experiment involving indoline **133a** and disulfide **59a** was conducted, revealing a considerable deuterium incorporation of 47% in the C-7 position of the reisolated substrate. Expectedly, no deuterium incorporation in the product **135aa** was detected (Scheme 3.5).

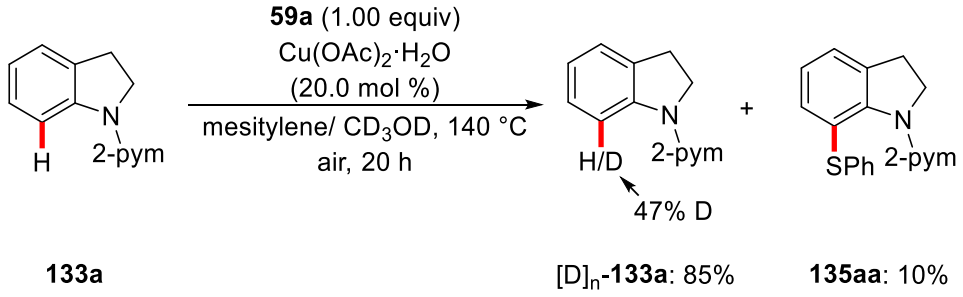

Scheme 3.5: H/D-exchange experiment with isotopically labeled co-solvent CD_3OD.

An additional experiment in the absence of the disulfide **59a** resulted in increased deuterium incorporation of 67% at the C-7 position of the indoline $[D]_n$-**133a** (Scheme 3.6), indicating that disulfide **59a** has no major role in the observed deuteration.

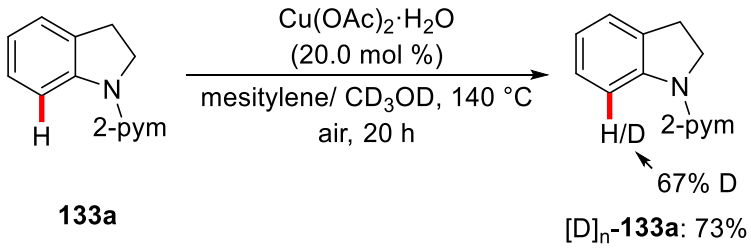

Scheme 3.6: H/D-exchange experiment in the absence of disulfide **59a** using indoline **133a**.

An otherwise identical experiment using indole **134a** as substrate led to deuterium incorporation exclusively in the C-2 position of the indole structure, thereby reconfirming the previously observed regioselectivities (Scheme 3.7).

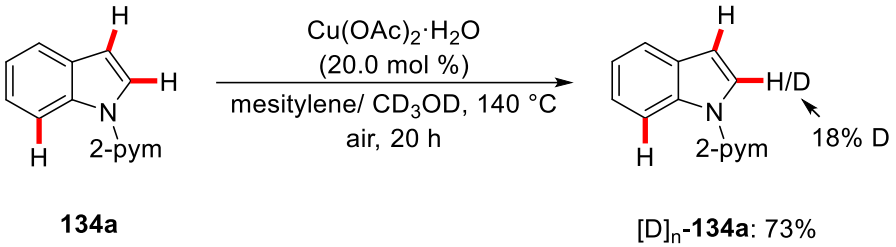

134a

$[D]_n$**-134a**: 73%

Scheme 3.7: H/D-exchange experiment in the absence of disulfide **59a** using indole **134a**.

This result can be rationalized when the ring size of the intermediate metallacycle is considered. While C–H metalation in the C-2 position results in the formation of a 5-membered cupra(II) cycle, C–H metalation of the C-7 position would deliver an unfavorable 6-membered metallacycle.[152c]

3.1.4 Proposed Catalytic Cycle

Based on the mechanistic findings, the following catalytic cycle was proposed (Scheme 3.8). First, facile and reversible chelation-assisted C–H cleavage with the substrate **133a** delivers the cyclometalated copper(II) species **158**. In a second step, **158** is oxidized by a sulfenyl radical **159** thereby generating copper(III) complex **160**. This proposal is supported by prior reports of copper(III) complexes stabilized by sulfide ligands.[76,164] Subsequent reductive elimination yields the desired product **135aa** and generates the corresponding copper(I) species. The regeneration of the active catalyst is achieved by interaction of the copper(I) species with the disulfide **59a** and air. The copper(I) species is reoxidized by a SET-type process with the disulfide, thereby regenerating the active copper(II) catalyst. Meanwhile, the associated cleavage of the disulfide S–S bond generates the sulfenyl radical and an arylthiolate anion. Finally, thiolate oxidation by O_2[165] delivers the disulfide.

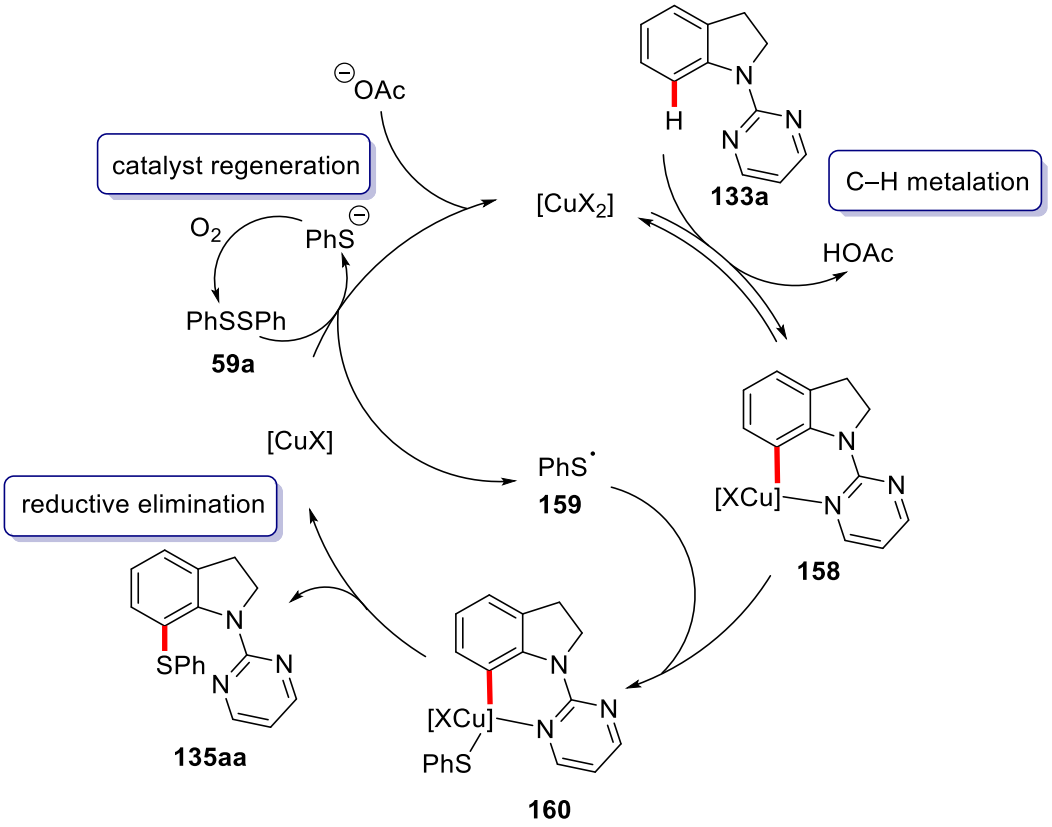

Scheme 3.8: Proposed catalytic cycle of the copper(II)-catalyzed C–H chalcogenation. X = OAc.

3.2 Visible-Light-Induced Decarboxylative C–H Adamantylation

First isolated from crude oil in 1933,[166] the adamantane scaffold rapidly received considerable attention from the chemical community. After the first chemical synthesis in 1941,[167] Schleyer's seminal synthesis in 1957[168] made the adamantane moiety widely available and it quickly found application in medicinal chemistry.[169] Similarly, benzothiazole and benzoxazole are key structures in numerous biologically active compounds.[170]

Despite the general availability of protocols for the C-2 selective alkylation of benzazoles, most of them rely on the use of alkyl halides.[171] Minisci-type alkylations of heteroarenes, utilizing carboxylic acids and their derivatives as environmentally more benign alkyl sources, have emerged as a versatile tool for organic synthesis,[172] starting from Minisci's seminal report in 1971.[173] Although light-induced Minisci-type C–H alkylation protocols have been disclosed recently, these methods often rely on the use of precious transition metals as the catalysts.[145,174] The use of a dual catalytic system comprised of an acridinium salt as organic photocatalyst and a cobaloxime for the reoxidation of the photocatalyst had not been disclosed for Minisci-type C–H alkylation reactions so far.

3.2.1 Optimization Studies and Scope

Orienting preliminary optimization studies regarding the visible-light-induced decarboxylative C–H adamantylation were performed by P. Gandeepan. The effect of different solvents, photocatalysts, and base additives was hence investigated, leading to the catalyst depicted in Scheme 3.9.[175] The key feature of the catalyst is the combination of an acridinium based photocatalyst **161** and cobaloxime **139a**.

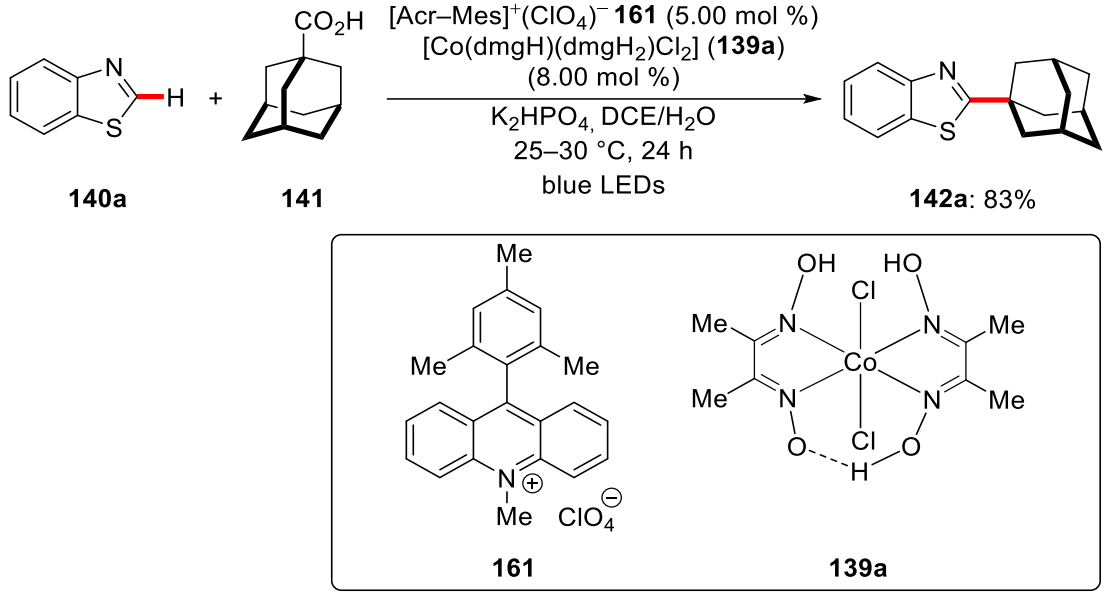

Scheme 3.9: Optimized catalyst of the decarboxylative C–H Adamantylation.

With the optimized conditions in hand, the scope of the visible-light-induced C–H adamantylation regarding benzothiazoles was explored (Table 3.8).

Table 3.8: Visible-light-induced decarboxylative C–H adamantylation with benzothiazoles **140**.[a]

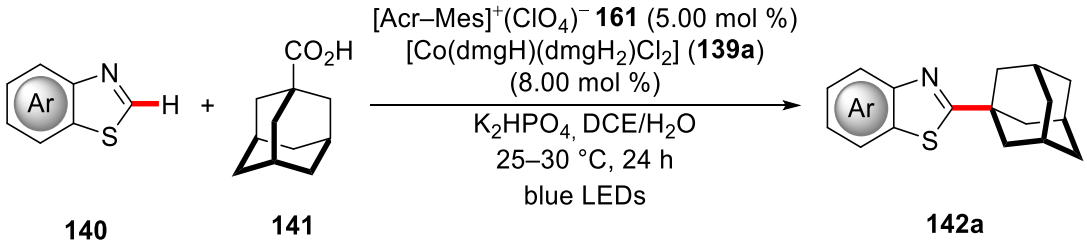

Entry	Benzothiazole	Product	Yield [%]
1	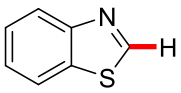 **140a**	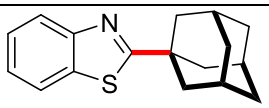 **142a**	83
2	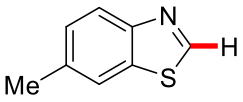 **140b**	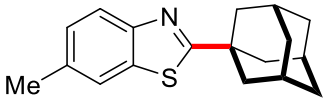 **142b**	53

Entry	Benzothiazole	Product	Yield [%]
3	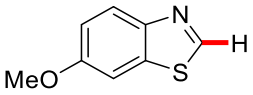	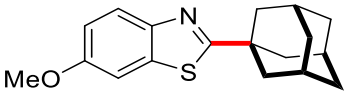	59
	140c	**142c**	
4	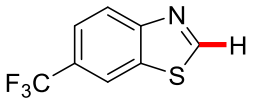	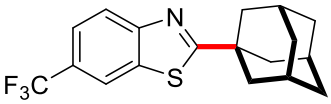	71[b]
	140d	**142d**	
5	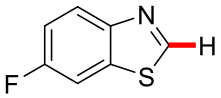	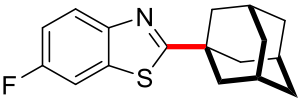	54
	140e	**142e**	
6	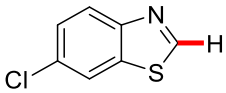	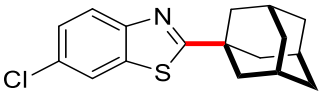	59
	140f	**142f**	
7	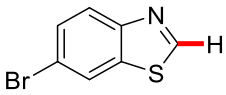	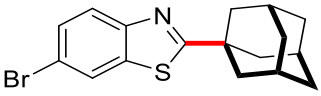	54
	140g	**142g**	
8	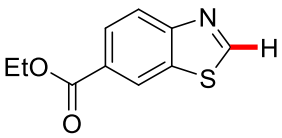	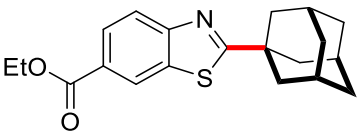	44[b]
	140h	**142h**	

Entry	Benzothiazole	Product	Yield [%]
9	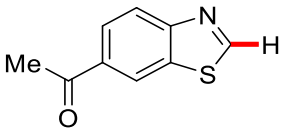 **140i**	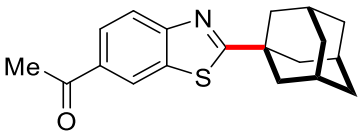 **142i**	32[b]
10	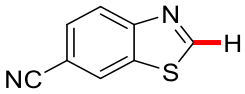 **140j**	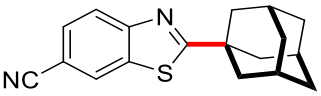 **142j**	18

[a] Reaction conditions: **140** (0.40 mmol), **141** (1.20 mmol), **161** (5.00 mol %), **139a** (8.00 mol %), K_2HPO_4 (1.20 mmol), DCE/H_2O (3:1, 2.0 mL), 24 h, yield of isolated product. [b] 48 h.

Both electron-donating as well as electron-withdrawing substituents in the C-6 position of the benzothiazoles **140** were well tolerated, delivering moderate to good yields, while electron-donating substituents delivered slightly higher yields (entries 2–3). In the case of benzothiazole **140d**, the reaction time had to be increased to 48 h in order to ensure a satisfying conversion (entry 4).

Halogen substituents were also accepted and no significant difference in the respective yields was observed. Thus, the benzothiazoles **140f** and **140g** containing synthetically meaningful chloro- and bromo-substituents delivered the corresponding products with 59% and 54% yield, respectively (entries 6 and 7). Unfortunately, a free hydroxyl group in the C-6 position diminished the catalytic efficacy.

In addition, valuable carbonyl groups, such as ester or ketone, were tolerated to some extent, although the reaction time had to be increased to 48 h to guarantee a meaningful conversion (entries 8–9). The cyano-substituted benzothiazole **140j** failed to deliver the product **142j** in synthetically useful yields. In this case the corresponding 2,3-dihydrobenzothiazole could be isolated with 30% yield.

This result indicates that strongly electron-withdrawing groups, such as cyano, may decrease the electron density of the proposed intermediate to a level that interferes with the postulated reoxidation of the intermediate resulting from the radical attack *vide infra* (chapter 3.2.3).

Furthermore, a range of diversely-substituted benzoxazoles **14** was subjected to the established reaction conditions (Table 3.9).

Table 3.9: Visible-light-induced decarboxylative C–H adamantylation with benzoxazoles **14**.[a]

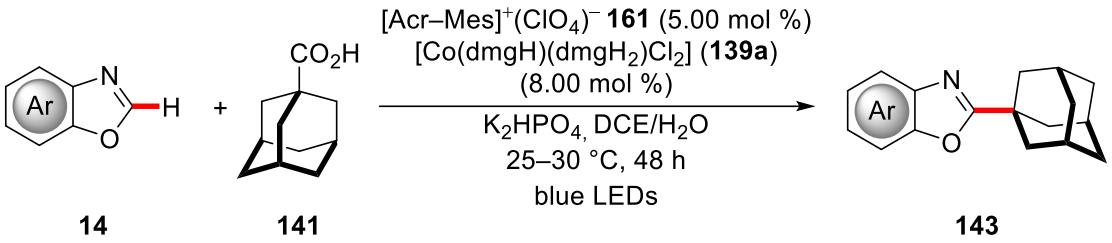

14 **141** **143**

Entry	Benzoxazole	Product	Yield [%]
1	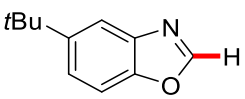 **14b**	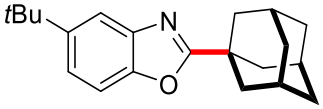 **143b**	45
2	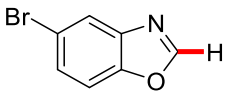 **14c**	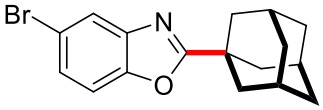 **143c**	42
3	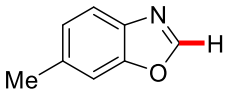 **14d**	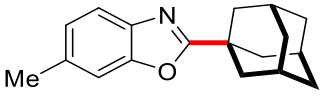 **143d**	50

Entry	Benzoxazole	Product	Yield [%]
4	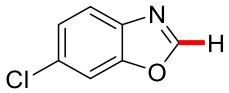	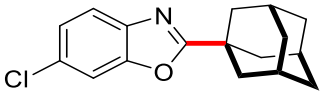	46
	14e	**143e**	
5	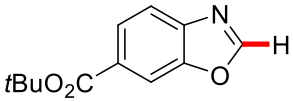	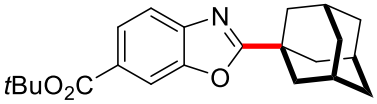	40
	14f	**143f**	

[a] Reaction conditions: benzoxzazole **14** (0.40 mmol), **141** (1.20 mmol), **161** (5.00 mol %), **139a** (8.00 mol %), K_2HPO_4 (1.20 mmol), DCE/H_2O: 3:1 (2.0 mL), 48 h, yield of isolated product.

The probed benzoxazoles **14** were converted with lower efficiency and the reaction time had to be extended to 48 h. With the prolonged reaction time, the C-5 and C-6 substituted benzoxazoles delivered the corresponding products in moderate yields. Alkyl substituents in the C-5 or C-6 position were well tolerated (entries 1 and 3). In addition, bromo- and chloro-substituents were also accepted (entries 2 and 4). Benzoxazole **14f** containing the valuable ester group delivered the product **143f** in 40% yield (entry 5).

Next, it was probed whether the visible-light-induced decarboxylative adamantylation could be extended to further biologically relevant nitrogen-containing heterocycles (Scheme 3.10). Accordingly, the biologically active purine alkaloid **162** and its derivative **163** were subjected to the optimized reaction conditions. The caffeine derivative **164** was obtained in good yield, and even the structurally complex analog **165** could still be isolated in 43% yield.

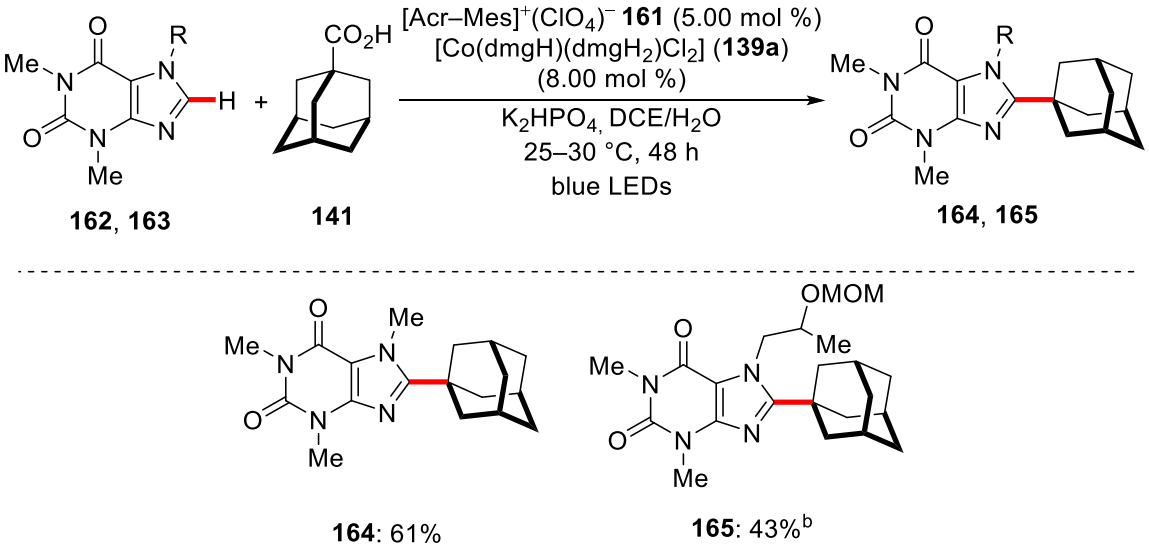

Scheme 3.10: Visible-light-induced decarboxylative C–H adamantylation of purine derivatives **162** or **163**. Reaction conditions: **162** (0.40 mmol), **141** (1.20 mmol), **161** (5.00 mol %), **139a** (8.00 mol %), K_2HPO_4 (1.20 mmol), DCE/H_2O: 3:1 (2.0 mL), yield of isolated product. [b] **163** (0.30 mmol).

Additionally, it was shown by Dr. P. Gandeepan that benzimidazoles could be employed as substrates.[175] However, limitations were encountered while probing further heterocycles. Thus, benzofuran, indole, imidazole, pyridine, and quinoline substrates remained unreactive in the visible-light-induced C–H adamantylation.

An additional limitation is the restriction to adamantane carboxylic acid as no other carboxylic acids could be employed in the decarboxylative C–H alkylation. Since it is expected that at least other tertiary carboxylic acids should display similar reactivity, this result is surprising to some extent. In the case of benzyl-substituted carboxylic acids, the dibenzylic species resulting from the radical-radical coupling was observed by GC-MS analysis. This observation suggests that the decarboxylative process is still operative even though no product formation was detected in these cases.

Minisci-type alkylations[173] are usually performed under acidic conditions.[172a,172c] This ensures protonation of the *N*-heterocyclic substrate and the associated lowering of the LUMO energy drastically increases the reactivity towards nucleophilic radicals.[172a] In sharp contrast to this, the visible-light-induced decarboxylative C–H adamantylation is performed under neutral to slightly basic conditions and hence lacks this additional

activation of the heterocyclic substrates. This lack of additional activation might be responsible for the observed limitations.

Still, the visible-light-induced decarboxylative C–H adamantylation allowed the facile adamantylation of a range of diversely decorated benzothiazoles **140** and benzoxazoles **14** and even allowed the functionalization of naturally occurring as well as synthetic purine alkaloids.

3.2.2 Mechanistic Studies

Regarding the intriguing findings concerning the C–H adamantylation, an investigation of the underlying mechanism was conducted next. In order to gain mechanistic insights into the reaction and to delineate its mode of action, a series of experiments was conducted.

3.2.2.1 Influence of Radical Scavengers on the C–H Adamantylation

Because of the high probability that the reaction involves several SET-type processes and the assumption that the adamantane radical is a key intermediate, a series of experiments in the presence of radical scavengers was conducted (Table 3.10). In all cases, the catalytic efficiency was significantly reduced. Yet, only in the presence of galvinoxyl the catalytic activity was completely diminished (entry 3). Nevertheless, these results are highly indicative of a SET-type process being operative.

Table 3.10: C–H Adamantylation in the presence of typical radical scavengers.[a]

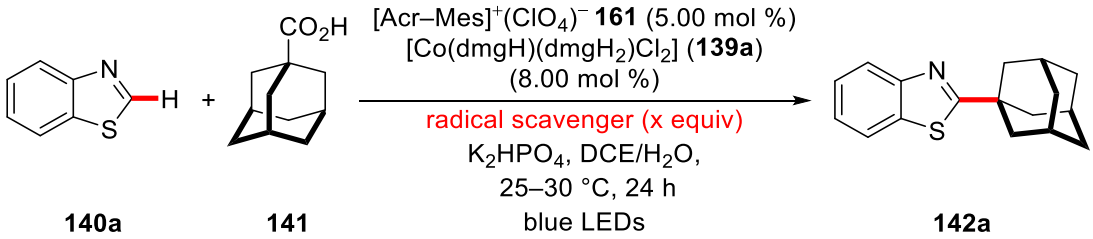

140a **141** **142a**

Entry	Radical scavenger (X equiv)	Yield [%]
1	--	83
2	TEMPO (1.00 equiv)	34

Entry	Radical scavenger (X equiv)	Yield [%]
3	galvinoxyl free radical (1.00 equiv)	--
4	BHT (1.00 equiv)	53
5	BHT (3.00 equiv)	36

[a] Reaction conditions: **140a** (0.40 mmol), **141** (1.20 mmol), **161** (5.00 mol %), **139a** (8.00 mol %), K_2HPO_4 (1.20 mmol), radical scavenger (X equiv), DCE/H_2O (3:1, 2.0 mL), yields of isolated product.

Additional evidence for the formation of the adamantane radical was obtained through ESI-HRMS analysis (Figure 3.1). In a sample removed from the reaction mixture after irradiation, the radical adduct **166** of the radical scavenger TEMPO and the adamantane radical could be detected.

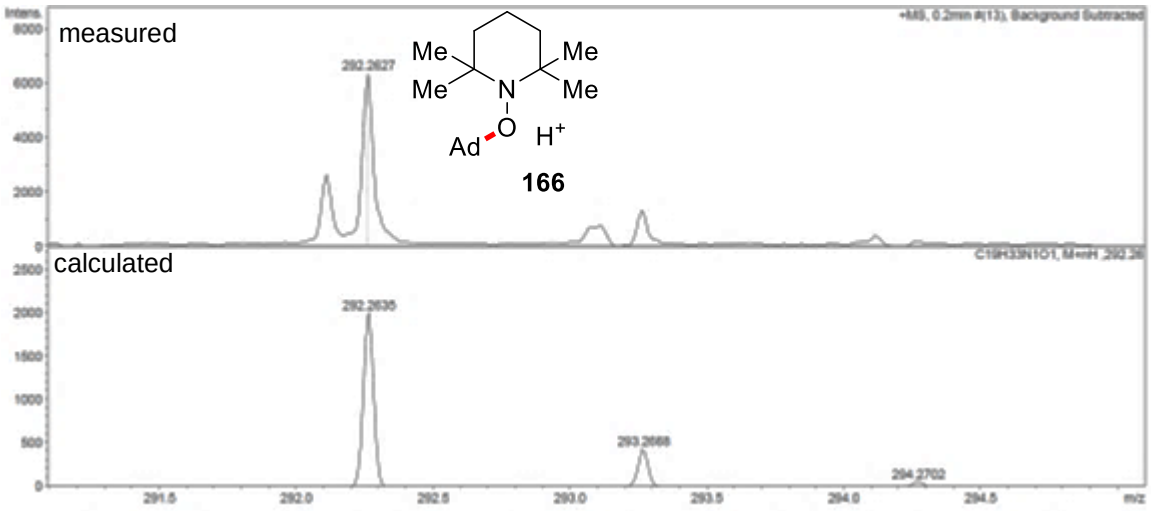

Figure 3.1: ESI-HRMS spectra of a sample taken from the reaction mixture.

3.2.2.2 Competition Experiment Between Benzothiazoles

In order to investigate the influence of the electronic nature of the benzothiazoles **140** an intermolecular competition experiment with electron-rich and electron-deficient benzothiazoles **140e** and **140b** was conducted (Scheme 3.11). Although no big difference between the reactivity of the two substrates was observed, the experiment revealed electron-deficient benzothiazoles to be slightly preferentially converted. This finding is in agreement with the postulated attack of the nucleophilic adamantane radical at the C-2 position of the corresponding benzothiazole.

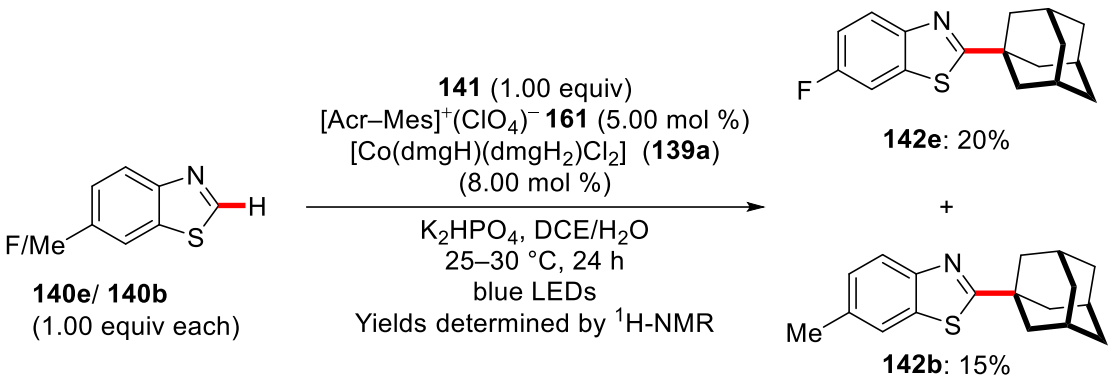

Scheme 3.11: Intermolecular competition experiment between benzothiazoles **140e** and **140b**.

3.2.2.3 Influence of Light by On/Off-Plot

To clearly determine the visible light-dependent nature of the C–H adamantylation, the reaction progress was monitored during several cycles of irradiation and stirring in the dark (Figure 3.2). No product formation was observed in the absence of light, while in contrast, the reaction proceeded smoothly when beeing irradiated. This finding provides additional strong evidence for the light-driven nature of the decarboxylative C–H adamantylation.

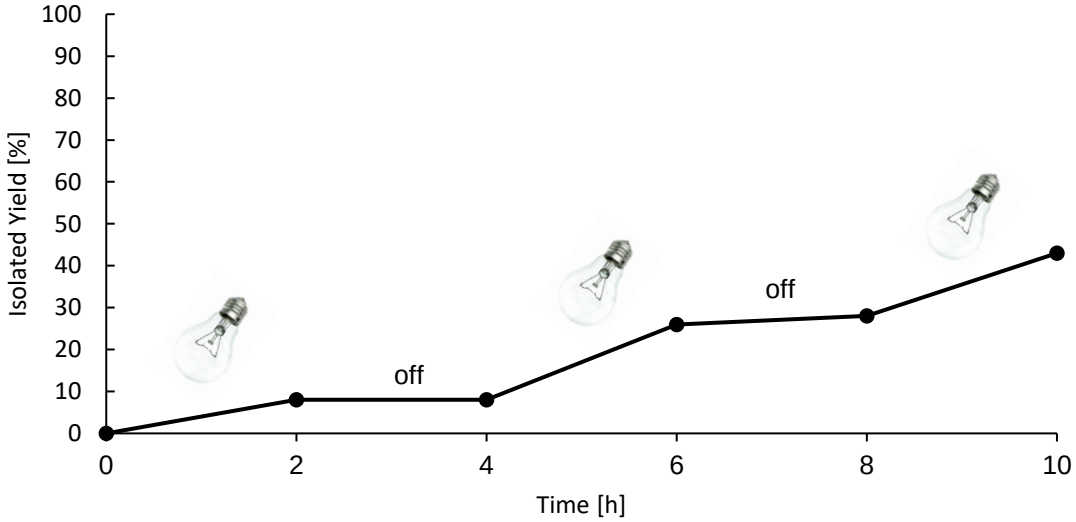

Figure 3.2: Effect of visible-light irradiation on the C–H adamantylation.

3.2.2.4 Fluorescence-Quenching Experiments

To obtain a better understanding of the exact effect of the visible-light irradiation, a series of fluorescence-quenching experiments was conducted. These experiments should allow to identify key interactions of the excited state photocatalysts with the substrates. Benzothiazole (**140a**) displayed a clear quenching effect, while 1-adamantane-carboxylic acid showed no quenching of the excited state photocatalyst (Figure 3.3). Based on the conducted experiments it cannot be distinguished whether a dynamic or static quenching process is operative in this case.[176]

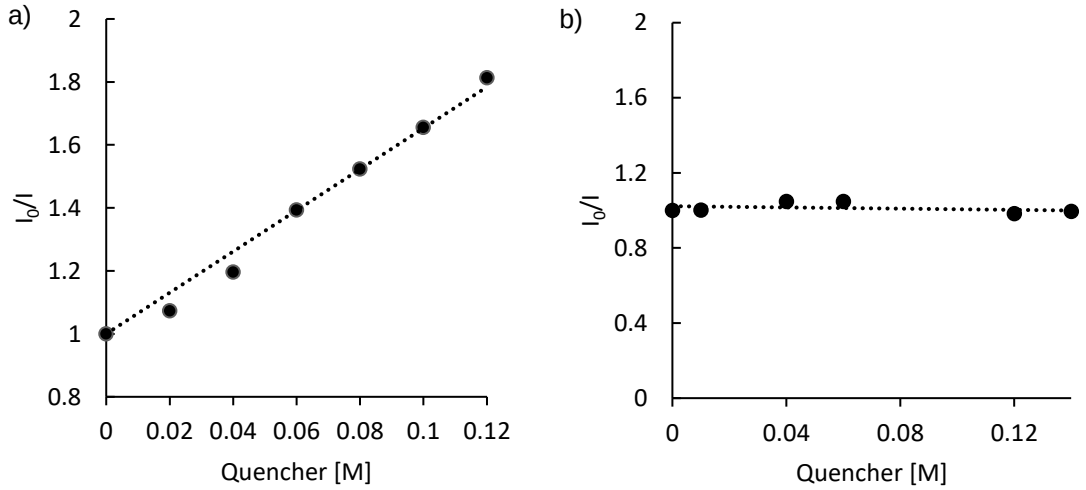

Figure 3.3: Fluorescence-quenching of **161** with a) benzothiazole (**140a**) and b) with 1-adamantanecarboxylic acid (**141**).

It has been previously reported by Nicewizc that benzothiazole (**140a**) can be oxidized by the excited state of an acridinium based photocatalysts.[177] Therefore the obtained results are coherent with the previously published ones. Furthermore, it is expected that the adamantanecarboxylate undergoes oxidation by the exited photocatalyst prior to decarboxylation. Thus, 1-adamantanecarboxylic acid should not display any quenching effect. Accordingly, this finding is also in agreement with the proposed underlying mechanism *vide infra*.

During the attempt to study the properties of the adamantanecarboxylate salts major solubility issues in the organic solvent were encountered. Thus, the adamantanecarboxylate tetrabutyl-ammonium salt **167**[178] was prepared and subsequently studied (Figure 3.4). The TBA salt displayed significant quenching

capabilities even at significantly lower concentrations. Yet, in this case, no linear correlation was observed. This result indicates that both static and dynamic quenching processes are operative in this case, leading to the observed non-linear correlation between the quencher concentration and the quotient of the fluorescence intensities.[176]

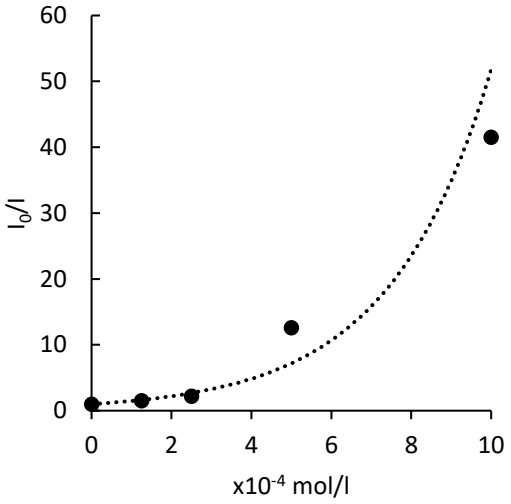

Figure 3.4: Fluorescence-quenching of **161** adamantanecarboxylate tetrabutyl-ammonium salt **167**.

Fluorescence-quenching experiments with acridinium salt **161** and a similar cobaloxime **139** have recently been reported by Lei[179] and suggest that a quenching process between the excited acridinium catalyst and the cobaloxime **139a** is also a likely possibility in the present C–H adamantylation.

3.2.3 Proposed Catalytic Cycle

Based on literature precedence and the results from the mechanistic studies, the following catalytic cycle was proposed (Figure 3.5). Initially, excitation of the acridinium photocatalyst by blue light takes place and generates the excited species of the photocatalyst [Acr-Mes]$^{+}$*. Given the high oxidation potential (E_{red} = 1.88 V vs SCE)[180] of the excited state of the Fukuzumi catalyst,[142-143,181] subsequent one-electron oxidation of the adamantanecarboxylate **168** (E_{ox} = 1.20 vs SCE)[178] delivers the oxygen-centered carboxyl radical. Further evidence for the step is found in recently reported protocols[181-182] and the result of the fluorescence-quenching experiment regarding adamantane carboxylate. The following decarboxylation yields the adamantane radical **169**, as supported by the outcome of the experiments with radical scavengers.

Subsequent attack of the radical at the C-2 position of benzothiazole **140a** delivers intermediate **170**. Simultaneously, the reduced state of the photocatalyst [Acr–Mes]$^{\cdot}$ **161**$^{\cdot}$ is reoxidized by a SET-type process with the cobalt(III)-species **171**, yielding the active photocatalyst and a cobalt(II)-species **172**. Oxidation of intermediate **170** by the cobalt(II)-species **172** and subsequent deprotonation and rearomatization delivers the product **142a** and generates a cobalt(I) species. The following reaction of the cobalt(I) species **173** with a proton generated during the reaction, delivers a cobalt(III)-hydride complex **174**. At last, hydrogen evolution from complex **174** closes the catalytic cycle.

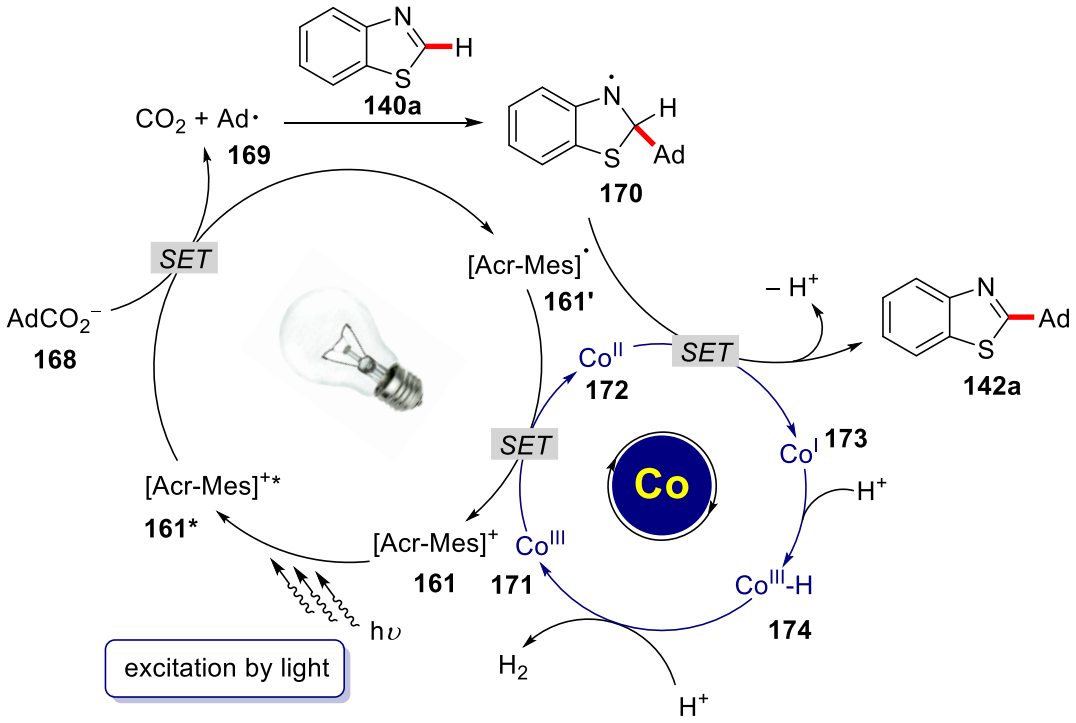

Figure 3.5: Proposed catalytic cycle of the decarboxylative C–H adamantylation.

As it becomes evidently clear from the proposed catalytic cycle, the properties of the attacking radical are of major importance. This offers another possible explanation for the reactivity observed during the investigations of the scope of the C–H adamantylation. Although alkyl radicals are generally considered to possess a nucleophilic character,[172a] the actual nucleophilicity for each radical may still vary considerably.[183] In addition to the inherent nucleophilicity, originating from its tertiary character,[184] it might be that the reactivity of the adamantane radical is further enhanced by its distinct structural properties that do not allow for a planar geometry of the radical.[185]

3.3 Light-Induced Copper-Catalyzed C–H Arylation of Azoles at Room Temperature

Since Ullmann's and Goldberg's pioneering studies[45b,45e] regarding copper-catalyzed arylation reactions, copper catalysts have become a highly versatile platform for a large range of organic transformations.[25,43,44c,44d,68,186] In 1998, an initial report by Miura and coworkers revealed the effect of copper(I) iodide on the regioselectivity of the studied palladium-catalyzed arylation of *N*-methylimidazole (**7a**).[52] Given the drastic changes in regioselectivity, their findings suggested the involvement of an organocopper intermediate in the arylation reaction. In 2007, Daugulis and coworkers reported the direct copper-catalyzed C–H arylation.[54] This seminal report of Daugulis demonstrated, for the first time, the viability of inexpensive and environmentally benign copper catalysis for heterocyclic C–H arylation reactions. In the following years the scope of copper-catalyzed C–H arylations was extended to electron-deficient polyfluorinated arenes,[55] and other prominent heterocycles by the groups of *inter alia* Daugulis,[56] Miura[57,187] and Ackermann.[58,188] Despite the undisputable progress in the field, all these reactions still require relative harsh conditions and elevated reaction temperatures. A copper-catalyzed C–H arylation proceeding at room temperature had thus far not been reported.

3.3.1 Copper-Catalyzed C–H Arylation of Azoles Under UV-Irradiation

3.3.1.1 Optimization and Scope

Optimization studies regarding the copper-catalyzed C–H arylation were largely performed by Dr. Fanzhi Yang. Among the various tested conditions, the combination of copper(I) iodide and *N*-methylated glycine ($Me_2NCH_2CO_2H$) in the presence of Li*O*t*B*u in Et_2O proved to be ideal (Scheme 3.12a).[189] In addition, it was shown by Dr. Yang that the reaction could be conducted under visible light when $Ir(ppy)_3$ was employed as photocatalyst (Scheme 3.12b).

a) Copper-catalyzed C–H arylation without exogenous photocatalyst

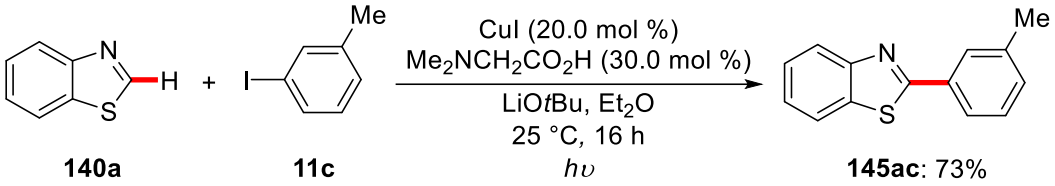

b) Copper-catalyzed C–H arylation in the presence of $Ir(ppy)_3$

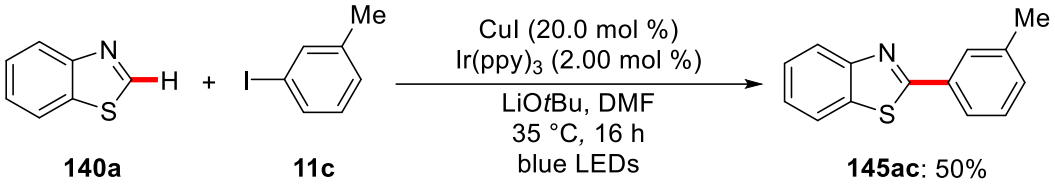

Scheme 3.12: Copper-catalyzed C–H arylation of benzothiazole (**140a**) with a) no exogenous photocatalyst and b) in the presence of $Ir(ppy)_3$.

The optimized conditions shown in Scheme 3.12 were chosen as a starting point for further improving the catalyst. Especially the influence of the concentration and the catalyst loading were investigated (Table 3.11).

Table 3.11: Influence of solvent, concentration and scale on the copper-catalyzed C–H arylation.[a]

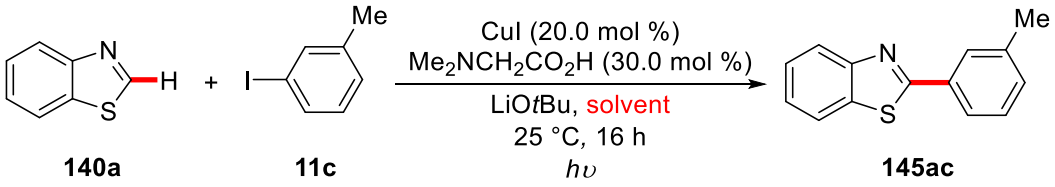

Entry	Solvent	Yield [%]
1	Et_2O	70
2	Et_2O	34[b]
3	nBu_2O	52
4	Et_2O	85[c]
5	Et_2O	84[d]
6	Et_2O/H_2O (9:1)	--

[a] Reaction conditions: **140a** (0.25 mmol), **11c** (1.25 mmol), CuI (20.0 mol %), $Me_2NCH_2CO_2H$ (30.0 mol %), LiO*t*Bu (0.75 mmol), solvent (1.0 mL), 254 nm, 16 h, yield of isolated product. [b] **140a** (0.50 mmol). [c] Et_2O (0.75 mL). [d] Under air.

First, the previously developed conditions were reaffirmed (entry 1). The reaction proved sensitive to changes in scale or concentration. If conducted at a larger scale the yield of the reaction dropped to 34% (entry 2). Yet, an increase in concentration led to a significantly improved isolated yield of 85% (entry 4). In addition, the reaction proved insensitive to air (entry 5) but did not tolerate the addition of water (entry 6). Regarding these new findings it was investigated if the catalyst loading could be decreased (Table 3.12).

Table 3.12: Influence of the catalyst loading on the copper-catalyzed C–H arylation.[a]

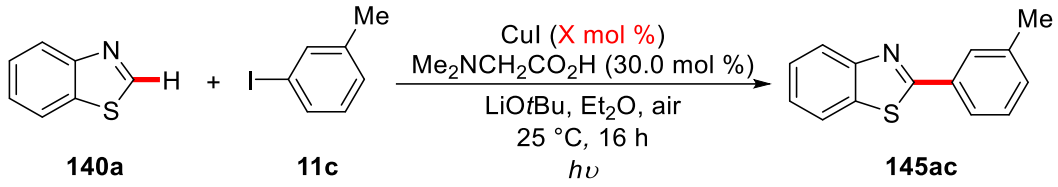

140a **11c** **145ac**

Entry	CuI (X mol %)	Yield [%]
1	20	73
2	20	73[b]
3	15	59
4	10	60

[a] Reaction conditions: **140a** (0.25 mmol), **11c** (1.25 mmol), CuI (20 mol %), $Me_2NCH_2CO_2H$ (30.0 mol %), LiO*t*Bu (0.75 mmol), Et_2O (0.75 mL), 254 nm, 16 h, yield isolated product. [b] Et_2O (0.50 mL).

While a further increase in the concentration had no positive effect on the catalyst's efficiency (entries 1 vs 2), a reduction of the catalyst loading had a detrimental effect on the yield (entries 3 and 4).

To investigate the catalyst's versatility the slightly modified catalyst was applied to the synthesis of the natural product texamine (**146a**) and its derivatives (Table 3.13).

Table 3.13: Copper-catalyzed C–H arylation of oxazoles **144** in the synthesis of texamine derivatives.[a]

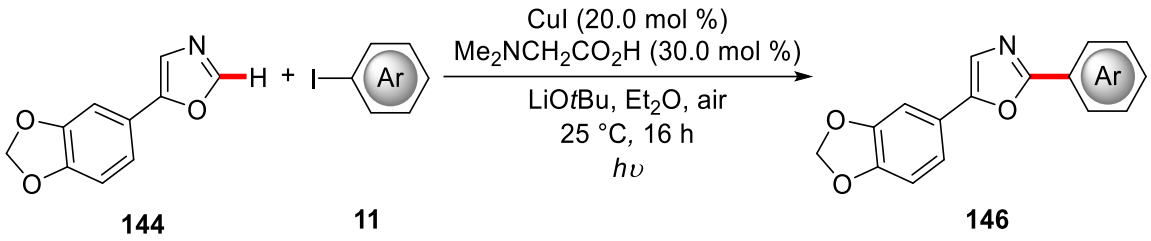

144 **11** **146**

Entry	Aryl iodide	Product	Yield [%]
1	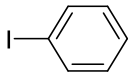	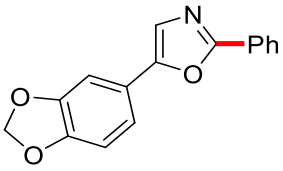	62
	11a	texamine (**146a**)	
2	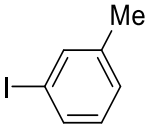	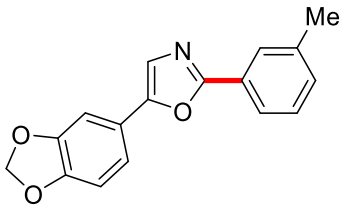	60
	11c	**146c**	
3	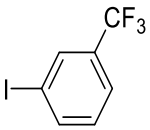	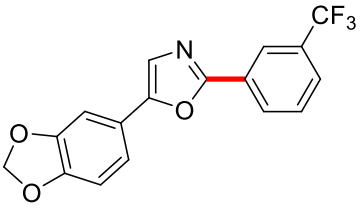	64
	11d	**146d**	
4	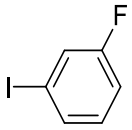	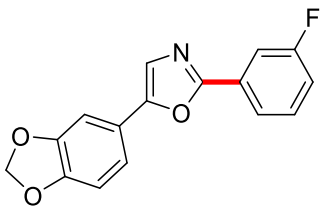	71
	11e	**146e**	

Entry	Aryl iodide	Product	Yield [%]
5	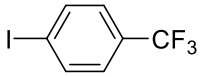 **11f**	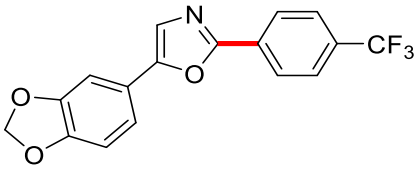 **146f**	72
6	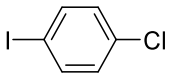 **11g**	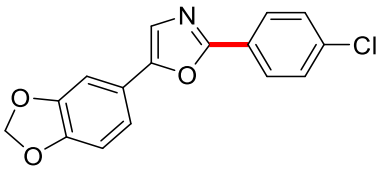 **146g**	69

[a] Reaction conditions: **144** (0.25 mmol), **11** (1.25 mmol), CuI (20.0 mol %), $Me_2NCH_2CO_2H$ (30.0 mol %), LiO*t*Bu (0.75 mmol), Et_2O (1.0 mL), air, 254 nm, 16 h, yield of isolated product.

The copper-catalyzed photo-induced C–H arylation protocol tolerated a wide range of diversely decorated aryl iodides **11** and the texamine derivatives **146** were obtained in moderate to good yields. It is especially noteworthy that the 1-chloro-4-iodobenzene (**11g**) was well-tolerated and no product associated to a possible protodehalogenation was observed (entry 6). The investigation of the scope also revealed a slight preference for electron-deficient aryl iodides **11**.

In addition, the newly found conditions were also tested in the C–H arylation of benzoxazole **14** (Scheme 3.13). Halogen substituents in the *meta*- or *para*-position of the iodoarenes **11e** and **11g** were well tolerated and the corresponding products **15ge** and **15gg** were obtained in good yields. Although the reactions were conducted under ambient atmosphere, the yields proved to be comparable to the other investigated substrates.[189] This further highlights the robust nature of the copper catalyst.

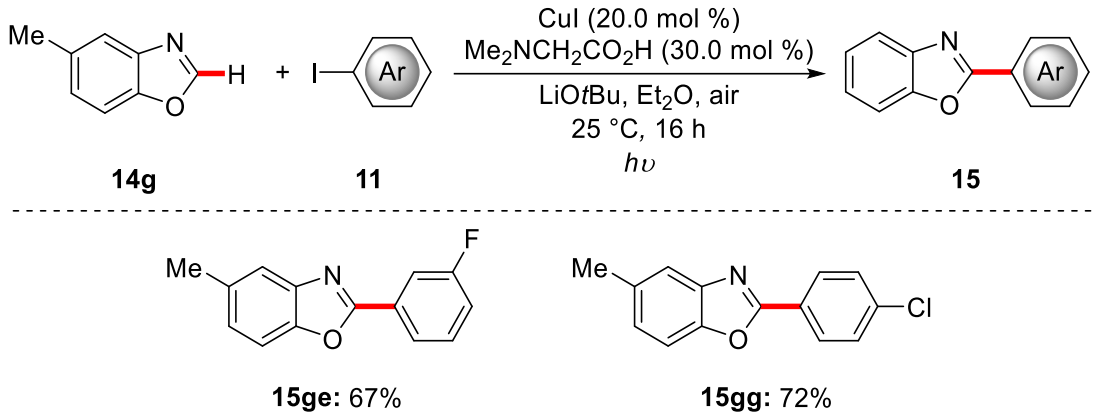

Scheme 3.13: Copper-catalyzed C–H arylation of benzoxazole **14g**. Reaction conditions: **14g** (0.25 mmol), **11** (1.25 mmol), CuI (20.0 mol %), $Me_2NCH_2CO_2H$ (30.0 mol %), LiO*t*Bu (0.75 mmol), Et_2O (1.0 mL), air, 254 nm, 16 h, yield of isolated product.

In a later study, the influence of the electronic nature of the benzothiazole substrates **140** was investigated by N. Imse as part of his bachelor thesis.[190] To this end, a range of diversely substituted benzothiazoles **140** was subjected to the optimized conditions established in the work of Dr. Fanzhi Yang (Table 3.14).[189]

Table 3.14: Copper-catalyzed C–H arylation of benzothiazoles **140**.[a]

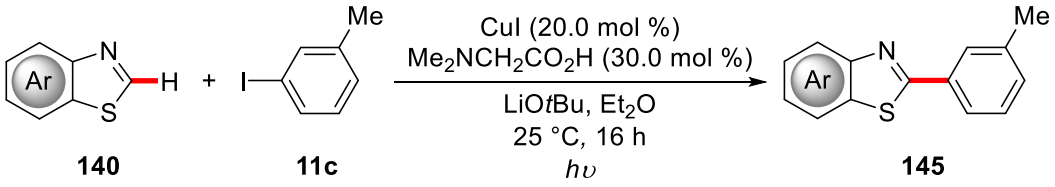

Entry	Benzothiazole	Product	Yield [%]
1	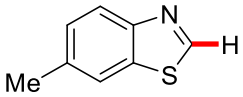	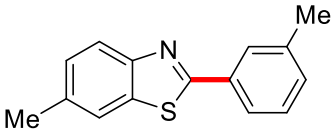	57
	140b	**145bc**	
2	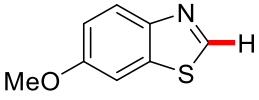	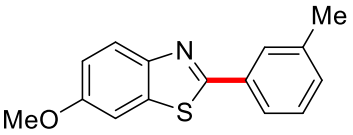	46
	140c	**145cc**	

Entry	Benzothiazole	Product	Yield [%]
3	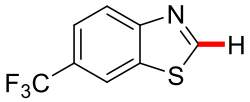	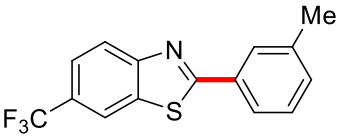	55
	140d	**145dc**	
4	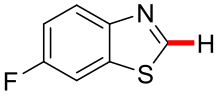	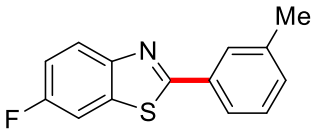	39
	140e	**145ec**	
5	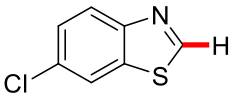	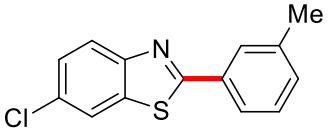	44
	140f	**145fc**	
6	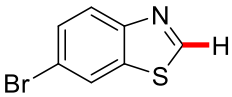	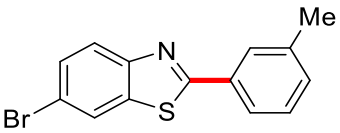	21
	140g	**145gc**	
7	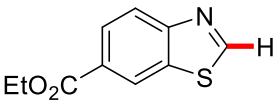	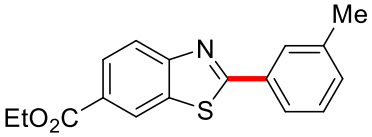	23
	140h	**145hc**	

[a] Reaction conditions: **140** (0.25 mmol), **11c** (1.25 mmol), CuI (20.0 mol %), $Me_2NCH_2CO_2H$ (30.0 mol %), LiO*t*Bu (0.75 mmol), Et_2O (1.0 mL), 254 nm, 16 h, yield isolated product.

In stark contrast to the results obtained with substituted aryl iodides **11**, the electronic nature of the substituents on the benzothiazole **140** had a significant influence on the performance of the C–H arylation. In all cases, the yield was clearly reduced compared to the unsubstituted benzothiazole **140a**. Even a methyl substituent in the C-6 position led

to a lowered yield (entry 1). When halogen substituents were present, the obtained yields decreased to the range of 40% (entries 4 and 5). Interestingly, both fluoro- and chloro-substituents did not have a negative impact on the catalytic efficiency, if present on the aryl iodide.[189] Bromo-substitution in the C-6 position further decreased the yield, as did an ester group (entries 6 and 7).

In conclusion, these results indicate that the photo-induced C–H arylation protocol is sensitive to the electronic nature of the benzothiazole **140** or the azole substrate in general. This pronounced substrate dependence was already briefly discussed by Peters and Fu in their work on photo-induced copper-catalyzed N–H arylation reactions,[126] and will be discussed in more detail in chapter 3.3.3.

3.3.2 Visible-Light-Induced Copper-Catalyzed C–H Arylation

In 2012, Ackermann and coworkers demonstrated the viability of a copper-catalyzed intramolecular arylation of triazoles in their studies regarding the synthesis of annulated triazoles.[188] Thus, it was investigated whether the previously established light-induced copper-catalyzed arylation protocol could be employed for the intramolecular arylation of triazoles. The iodo-substituted triazole **27b** was chosen as a model substrate and subjected to a range of reactions conditions (Table 3.15).

Table 3.15: Intramolecular C–H arylation of triazole **27b**.[a]

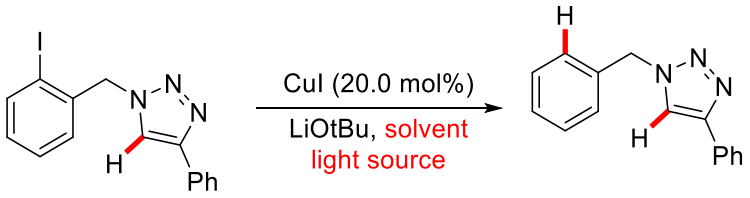

27b **175**

Entry	Solvent	Light source	Yield [%]
1	Et_2O	UV-C lamps (λ_{max}=254 nm)	10
2	Et_2O	UV-C lamps (λ_{max}=254 nm)	11[b]
3	THF	UV-C lamps (λ_{max}=254 nm)	38
4	DMF	UV-C lamps (λ_{max}=254 nm)	(47)

Entry	Solvent	Light source	Yield [%]
5	1,4-dioxane	UV-C lamps (λ_{max}=254 nm)	19
6	THF	blue LEDs	24
7	THF	UV-C lamp (λ_{max}=254 nm)	43[c]
8	DMF	blue LEDs	36
9	THF	--	--
10	THF	UV-C lamps (λ_{max}=254 nm)	33[c,d]
11	THF	blue LEDs	--, 96% rsm.[c,d]

[a] Reaction conditions: **27b** (0.25 mmol), CuI (20.0 mol %), Li*O*t*Bu (0.75 mmol), Et_2O (1.0 mL), 254 nm, 16 h. Yields determined by ^{1}H-NMR with mesitylene as internal standard, isolated yield in brackets. [b] $Me_2NCH_2CO_2H$ (30.0 mol %). [c] No CuI. [d] No base.

While the annulated product was not observed in any case, the corresponding dehalogenated product **175** was frequently obtained. The highest yield of the undesired byproduct was obtained when DMF was used as the solvent (entry 4), but the use of THF also delivered the byproduct in similar yields (entry 7). Interestingly, the dehalogenation reaction occurred independently of the presence of copper iodide or base when the reaction was conducted under UV-C irradiation (entries 7 and 10). While the dehalogenation did also occur when blue LEDs were used as light source (entries 6 and 8), it required the presence of copper iodide and base (entry 11), indicating that the copper catalyst was vital for the C–I bond cleavage in this case.

Although the formation of the annulation product was not observed, these findings suggested that a visible light-induced arylation protocol without the use of an additional photocatalyst might be feasible. To investigate this possibility, benzothiazole **140a** was chosen as a model substrate and subjected to a range of reaction conditions (Table 3.16).

Table 3.16: Preliminary results for the visible light-induced C–H arylation of benzothiazole **140a**.[a]

140a **11e** **145ae**

Entry	Ligand	Yield [%]
1	--	45
2	1,10-phenanthroline	12
3	PPh_3	trace
4	IPr HCl	39
5	$Me_2NCH_2CO_2H$	40

[a] Reaction conditions: **140a** (0.25 mmol), **11e** (1.25 mmol), CuI (20.0 mol %), ligand (30.0 mol %), LiO*t*Bu (0.75 mmol), Et_2O (1.0 mL), yield of isolated product.

The initial experiments revealed that the C–H arylation could be performed under visible-light irradiation. Furthermore, the reaction proceeded most efficiently in the absence of an additional ligand (entry 1), while prominent ligands, like 1,10-phenanthroline or triphenylphosphine, significantly lowered the catalytic performance (entries 2 and 3). Subsequently, the influence of the copper salt was investigated. Besides the initially tested copper(I) iodide a variety of copper salts gave the desired arylated product **145ae** with comparable yields (Table 3.17).

Table 3.17: Influence of the copper salt on the visible light-induced C–H arylation of **140a**.[a]

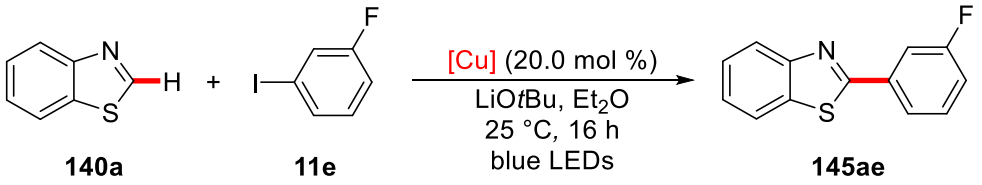

140a **11e** **145ae**

Entry	[Cu]	Yield [%]
1	--	--
2	CuCl	54
3	CuBr	50
4	CuTc	34

Entry	[Cu]	Yield [%]
5	$Cu(MeCN)_4PF_6$	42
6	$CuCl_2$	45
7	$Cu(OTF)_2$	43
8	$Cu(OAC)_2 \cdot H_2O$	51
9	$Cu(TFA)_2 \cdot H_2O$	42

[a] Reaction conditions: **140a** (0.25 mmol), **11e** (1.25 mmol), [Cu] (20.0 mol %), LiO*t*Bu (0.75 mmol), Et_2O (1.0 mL), air, yield of isolated product.

In the absence of a copper catalyst, the arylated product **145ae** was not detected (entry 1). Among the investigated copper(I) salts (entries 2–5), copper (I) chloride proved to be ideal (entry 2). Notably, several copper(II) salts were also suitable copper sources (entries 6–9). When copper(II) acetate monohydrate was employed a nearly identical yield was obtained (entry 8). Furthermore, the influence of the solvent was investigated (Table 3.18).

Table 3.18: Influence of the solvent on the visible light-induced C–H arylation.[a]

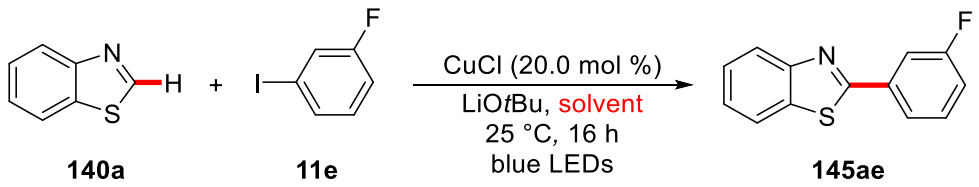

140a **11e** **145ae**

Entry	Solvent	Yield [%]
1	THF	20
2	*n*Bu_2O	17
3	DME	28
4	1,4-dioxane	--
5	MeCN	12
6	PhMe	trace
7	mesitylene	--
8	DMF	--
9	DCE	--

[a] Reaction conditions: **140a** (0.25 mmol), **11e** (1.25 mmol), CuI (20.0 mol %), LiO*t*Bu (0.75 mmol), solvent (1.0 mL), air, yield of isolated product.

The visible-light-induced C–H arylation proved to be highly dependent on the solvent. All the probed solvents performed considerably worse than the previously used Et_2O. Among the range of probed solvents, nearly only ethereal solvents were tolerated (entries 1–3), while other commonly used solvents failed to deliver the arylated product (entries 4–9). In addition, other bases proved unsuitable for the reaction (Table 3.19).

Table 3.19: Influence of the base on the visible light-induced C–H arylation of **140a**.[a]

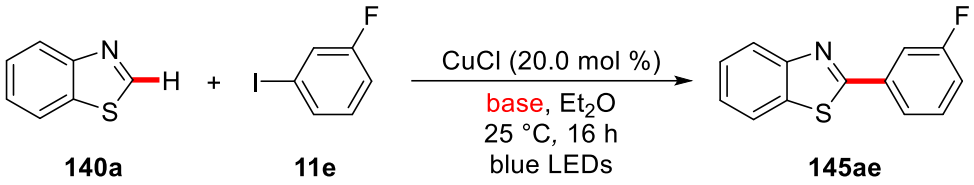

140a **11e** **145ae**

Entry	Base	Yield [%]
1	NaOMe	--
2	NaOEt	--
3	KO*t*Bu	--
4	K_3PO_4	--

[a] Reaction conditions: **140a** (0.25 mmol), **11e** (1.25 mmol), CuI (20.0 mol %), base (0.75 mmol), solvent (1.0 mL), air, yield of isolated product.

Since no synthetically meaningful yields could be achieved by the sole use of a copper-catalyst, a series of commonly used photocatalyst was evaluated in the visible-light-induced copper-catalyzed C–H arylation. Although the use of an additional photocatalyst has drawbacks regarding the cost efficiency and overall economy of the reaction, its use might allow a more effective light absorption and therefore higher yields. To this end, a series of organic and transition metal-based photocatalysts varying in their excited state oxidation and reduction capabilities were investigated in the visible-light-induced C–H arylation (Table 3.20).

Table 3.20: Influence of additional photocatalysts on the visible light-induced C–H arylation.[a]

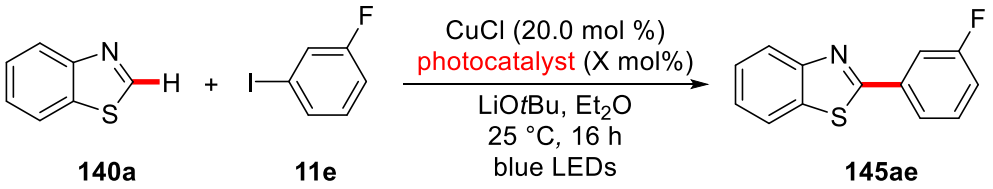

140a **11e** **145ae**

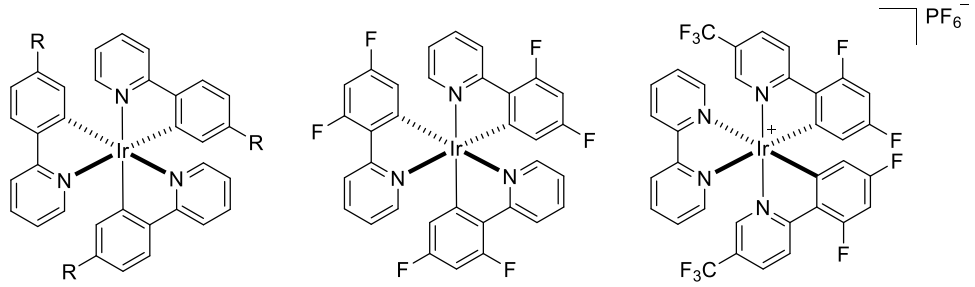

R = Me: **176**
R = *t*Bu: **177**
R = F: **178**

179 **180**

Entry	Photocatalyst (X mol %)	Yield [%]
1	--	54
2	DCN (5.00 mol %)	38
3	Eosin Y (sodium salt) (5.00 mol %)	39
4	Rhodamine 6G (5.00 mol %)	19
5	4,4-Dimethoxybenzophenone (5.00 mol %)	37
6	Rose Bengal (5.00 mol %)	41
7	$[Acr–Mes]^+(ClO_4)^-$ (5.00 mol %)	27
8	TiO_2 (50.0 mol %)	47
9	$Ru(bpy)_3Cl_2$ (5.00 mol %)	35
10	$Ir(ppy)_3$ (2.00 mol %)	54
11	$Ir(ppy)_3$ (2.00 mol %)	--[b]
12	**176** (2.00 mol %)	43
13	**177** (2.00 mol %)	53
14	**178** (2.00 mol %)	47
15	**179** (2.00 mol %)	48
16	**180** (2.00 mol %)	32

[a] Reaction conditions: **140a** (0.25 mmol), **11e** (1.25 mmol), CuI (20 mol %), photocatalyst, LiO*t*Bu (0.75 mmol), Et_2O (1.0 mL), air, yield of isolated product. In case of Ir-based photocatalyst, the reaction was conducted under N_2 and in DMF. [b] No base.

In case an organic photocatalyst was employed slightly lower yields were obtained (entries 2–7), the strong excited state oxidant acridinium photocatalyst however performed significantly worse (entry 7). The heterogeneous photocatalyst TiO_2 had no significant effect (entry 8). If a ruthenium-based photocatalyst was employed, a slightly lower yield was obtained (entry 9). Next, a series of diverse iridium-based photocatalysts was investigated. The reaction with the commonly used $Ir(ppy)_3$ delivered the product in 54% yield (entry 10), a nearly identical result to the reaction in the absence of a photocatalyst. In this case, the presence of LiO*t*Bu was still required (entry 11). The *tert*-butyl-substituted iridium photocatalyst **177** delivered the product in a nearly identical yield compared to $Ir(ppy)_3$, while the methyl-substituted **176** showed a slightly lower performance (entries 12 and 13). In general, iridium complexes with electron poor phenylpyridine ligands possess a lower excited state reduction potential but an increased lifetime of the excited state of the photocatalyst,[119d] which might lead to higher efficiency of the key SET step.[191] Yet, the fluoro-substituted iridium complexes **178** and **179** showed similar activity in the C–H arylation (entries 14 and 15). Only the cationic iridium complex **180** displayed significant lower activity (entry 16). In summary, the use of an additional photocatalyst did not improve the outcome of the visible-light-induced C–H arylation. Although this is the first example of an external-photocatalyst free, copper-catalyzed visible light-induced arylation by means of C–H activation, the project was not further pursued, since it seemed questionable whether the reaction could deliver synthetically meaningful yields.

3.3.3 Mechanistic Studies and Proposed Catalytic Cycle

During his seminal study on the photo-induced copper-catalyzed arylation of azoles, Dr. Fanzhi Yang performed several mechanistic experiments. In summary, the C–H arylation proved sensitive to the presence of the radical scavenger galvinoxyl, indicating that a SET-type process might be operative in the transformation.[189]

Unfortunately, attempts to isolate or to independently prepare possible reaction intermediates failed. However, the catalytic system utilizing $Ir(ppy)_3$ as photocatalyst allowed for further mechanistic investigations regarding the effect of the photoredox catalyst. To this end, fluorescence-quenching experiments were conducted with $Ir(ppy)_3$

and a series of potential quenchers (Figure 3.6. and Figure 3.7). Neither 3-iodotoluene (**11c**) nor benzothiazole (**140a**) showed any quenching capability indicating that there is no interaction of them with the excited state of the photocatalyst $Ir(ppy)_3$.

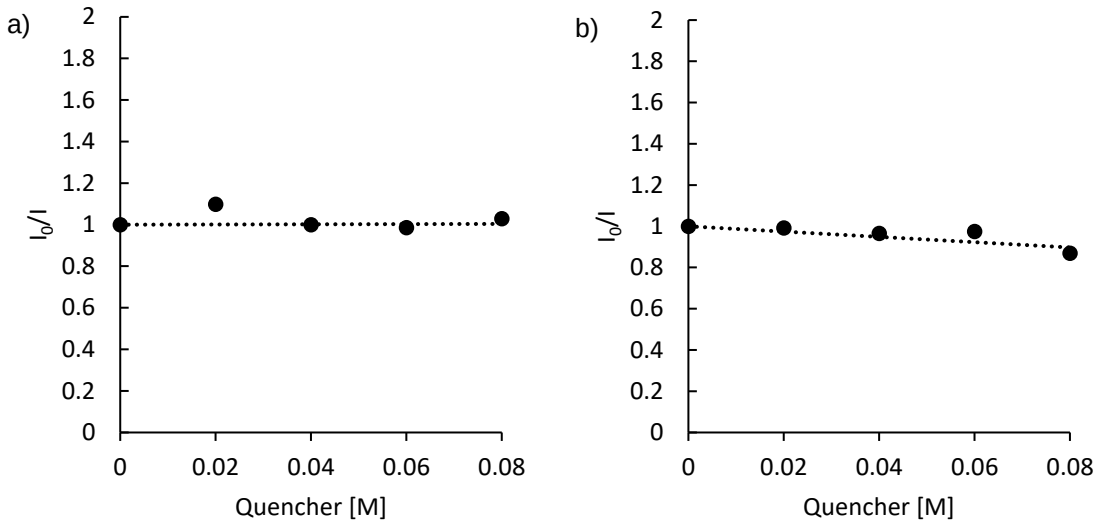

Figure 3.6: Fluorescence-quenching of $Ir(ppy)_3$ with a) with 3-iodotoluene (**11c**) and b) with benzothiazole (**140a**).

Interestingly, when the fluorescence-quenching studies were performed in MeCN as solvent, copper(I) iodide displayed no quenching (Figure 3.7a). This can most likely be attributed to the formation of an unreactive copper-acetonitrile complex.[192] In DMSO copper(I) iodide showed quenching of the excited state of $Ir(ppy)_3$ (Figure 3.7b). These results are in agreement with studies by Kobayashi and coworkers regarding the visible-light-induced N-arylation of heterocycles.[130] Since 3-iodotoluene (**11c**) does not show any quenching, these results also indicate that the proposed aryl radical is not formed by an oxidative quenching process of the excited state of $Ir(ppy)_3$.

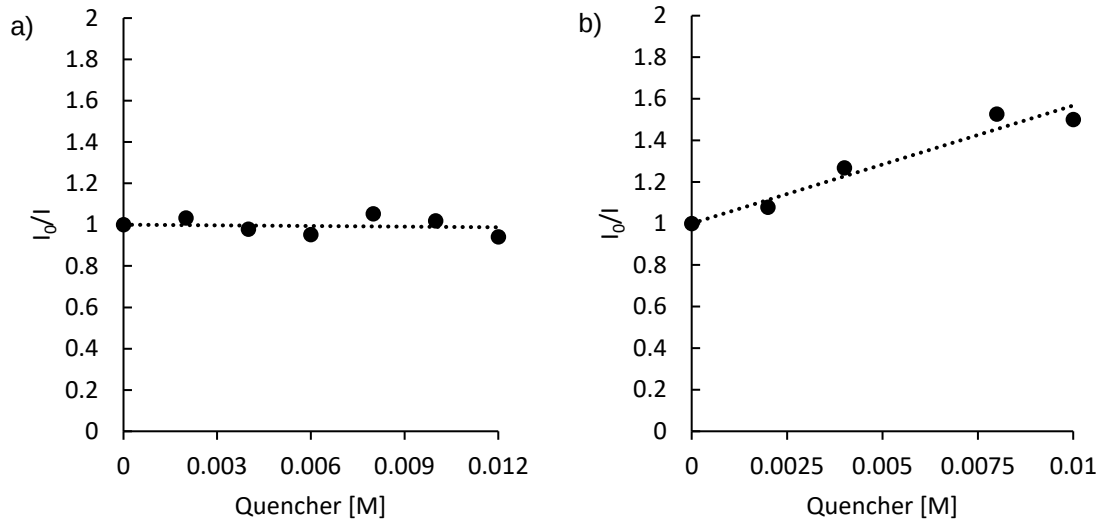

Figure 3.7: Fluorescence-quenching of $Ir(ppy)_3$ with a) copper(I) iodide in MeCN and b) with copper(I) iodide in DMSO.

Based on these initial results and literature precedence a catalytic cycle can be proposed (Scheme 3.14). The reaction of copper(I) chloride with an excess of LiO*t*Bu delivers a copper(I) ate complex **181**.[193] This step has also been shown to be operative for copper(II) chloride,[194] which explains the small difference between the different copper salts observed during the optimization. In a second step, the copper(I) ate-complex promotes facile C–H cleavage generating copper complex **182**. This copper complex **182** undergoes excitation by either visible or UV-light yielding the excited complex **182***. A subsequent SET generates copper(II) complex **183** and after homolytic cleavage of the C–I bond the aryl radical **106a**. The aryl radical attacks the copper(II) complex **183** thereby generating copper(III) complex **184**. Subsequent reductive elimination liberates the product and regenerates the active catalyst through reaction with an additional molecule LiO*t*Bu, thereby closing the catalytic cycle.

Since the key step is the SET process from the excited copper(I) complex **182*** to the aryl iodide **11a**, the reaction heavily depends on the reduction potential of this species and therefore on the electronic nature of **182***. Because substituents on the benzothiazole are likely to significantly influence these electronic properties, the proposed catalytic cycle offers a satisfying explanation for the observed strong influence of substituents on the benzothiazole **140** on the obtained yield.

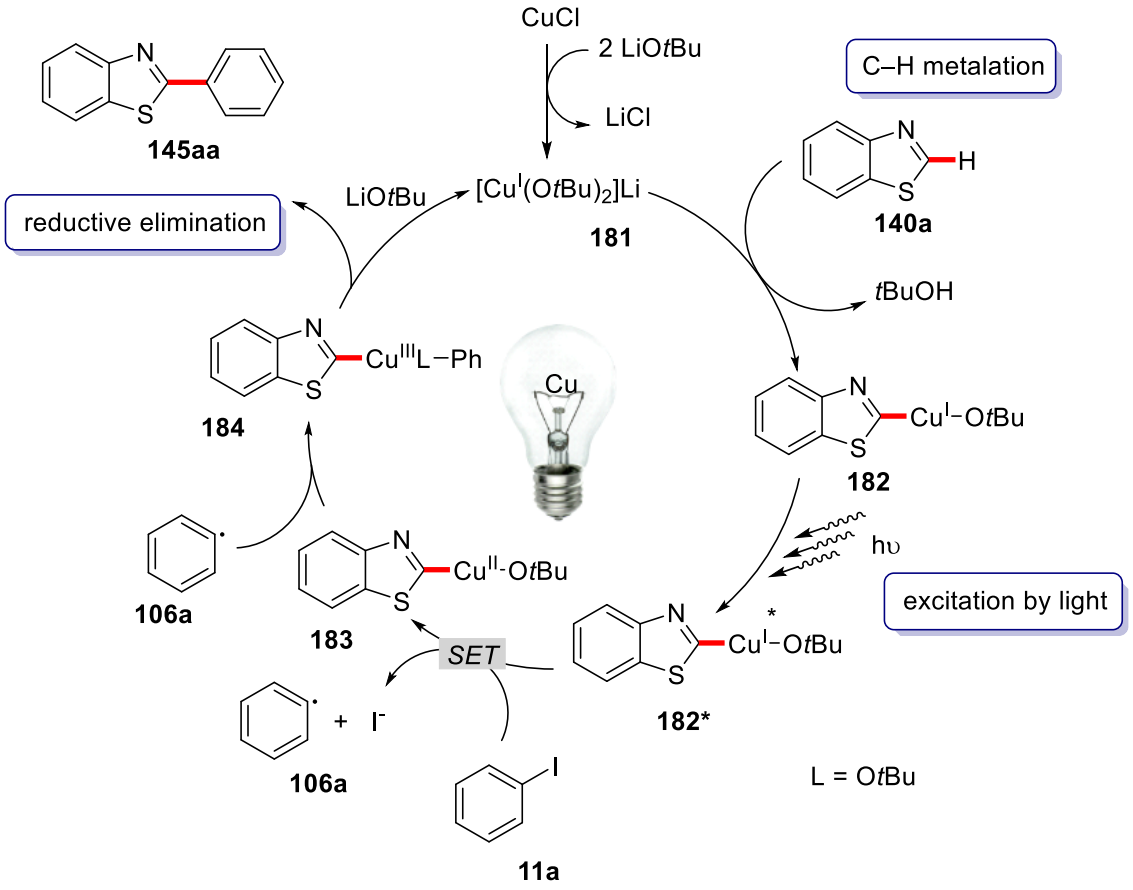

Scheme 3.14: Proposed catalytic cycle for the light-induced copper-catalyzed C–H arylation.

3.4 Visible-Light-Induced Ruthenium-Catalyzed *Meta*-C–H Alkylation

While the use of well-established directing groups allowed for the development of a plethora of *ortho*-selective C–H functionalization reactions,[81,195] the corresponding *meta*-selective C–H functionalizations continue to be scarce. However, *meta*-functionalized products are accessed by either exploiting the steric properties, the use of a hydrogen-bonding enabling linker, or the use of templates.[89,101] While the first approach is inherently limited in its scope, the other two methodologies suffer severe drawbacks regarding atom economy, caused by the necessity to introduce and remove the linker or template. Seminal work by Ackermann et al. revealed that ruthenium complexes can be employed for the *meta*-selective functionalization of arenes.[108] Based on this *σ*-activation strategy,[89,101] several C–H functionalization reactions have been disclosed by now.[109a,110b,111-112,113,196] Yet, a transformation proceeding at ambient temperature had remained elusive until recently.[197] By merging the ruthenium-based *σ*-

activation strategy with visible-light photocatalysis, this limitation might be overcome as will be discussed in the following chapter.

3.4.1 Ruthenium-Catalyzed *meta*-C–H Difluoromethylation

As the starting point for the investigations regarding the viability of a visible light-enabled ruthenium-catalyzed C–H functionalization reaction, the difluoromethylation of arenes (Scheme 3.15) previously reported by Ackermann was selected.[112a]

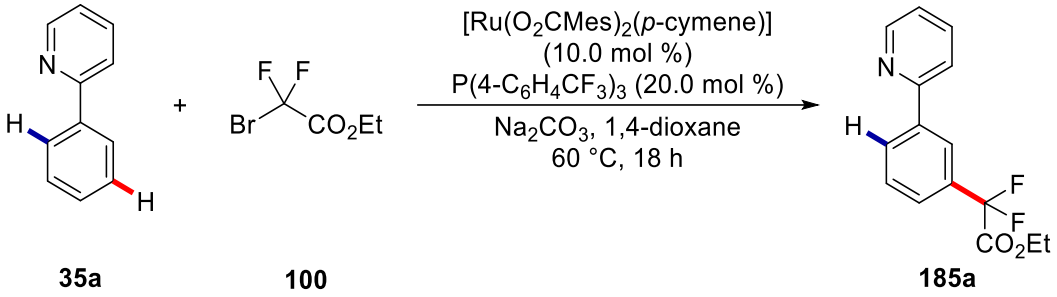

Scheme 3.15: Ruthenium-catalyzed difluoromethylation as reported by Ackermann.

Given the comparatively low reaction temperature and reports describing the feasibility of the C–H cycloruthenation step at ambient temperature,[198] it was expected that an intermediate ruthenacycle could be formed. Subsequent reaction of this ruthenacycle with a photochemically generated difluoroalkyl radical would further drive the reaction. This hypothesis was additionally backed by reports disclosing the use of difluoro bromoacetate (**100**) in photochemical protocols.[199] Thus, initial optimization revealed that small amounts of the desired product could be obtained under the probed reaction conditions (Table 3.21).

Table 3.21: Initial experiments regarding the visible-light-induced ruthenium-catalyzed C–H difluoromethylation.[a]

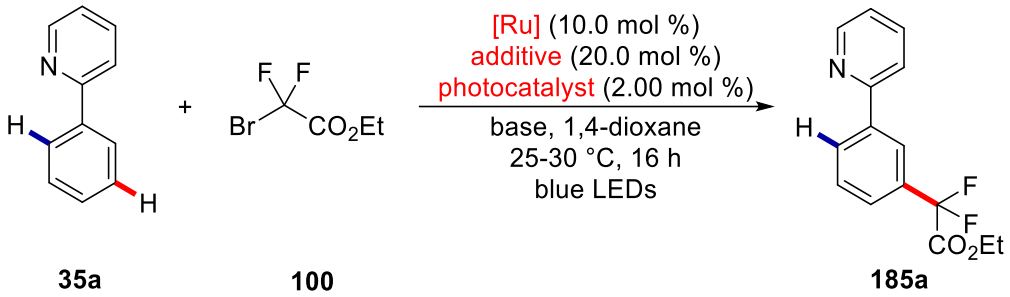

35a **100** **185a**

Entry	[Ru]	Photocatalyst	Additive	Base	Yield [%]
1	$[Ru(OAc)_2(p\text{-cymene})]$	--	PPh_3	K_2CO_3	8
2	$[Ru(OAc)_2(p\text{-cymene})]$	$Ir(ppy)_3$	PPh_3	K_2CO_3	7
3	$[Ru(OAc)_2(p\text{-cymene})]$	$Ru(bpy)_3Cl_2{\cdot}6\,H_2O$	PPh_3	K_2CO_3	11
4	$[Ru(OAc)_2(p\text{-cymene})]$	$Ir(ppy)_3$	*i*-$PrNEt_2$	Na_2CO_3	3
5	$[Ru(OAc)_2(p\text{-cymene})]$	$Ir(ppy)_3$	NEt_3	Na_2CO_3	--
6	$[Ru(OAc)_2(p\text{-cymene})]$	$Ru(bpy)_3Cl_2{\cdot}6\,H_2O$	*i*-$PrNEt_2$	Na_2CO_3	traces
7	$[Ru(O_2CMes)_2(p\text{-cymene})]$	--	PPh_3	K_2CO_3	4
8	$[Ru(O_2CMes)_2(p\text{-cymene})]$	$Ir(ppy)_3$	PPh_3	K_2CO_3	5
9	$[Ru(O_2CMes)_2(p\text{-cymene})]$	$Ru(bpy)_3Cl_2{\cdot}6\,H_2O$	PPh_3	K_2CO_3	2

[a] Reaction conditions: **35a** (0.30 mmol), **100** (0.90 mmol), [Ru] (10.0 mol %), additive (20.0 mol %), photocatalyst (2.00 mol %), base (0.60 mmol), 1,4-dioxane (1.5 mL), 25–30 °C, 16 h. Yield by ^{19}F-NMR with 2-chloro-4-fluorotoluene as internal standard.

While the initially probed conditions confirmed that the proposed difluoromethylation reaction was indeed possible, no distinct correlation was observed during these preliminary studies. Both investigated ruthenium carboxylate complexes, $[Ru(OAc)_2(p\text{-cymene})]$ and $[Ru(O_2CMes)_2(p\text{-cymene})]$ delivered the product **185a** in comparable yields (entries 1–6 and 7–9). Yet, a clear influence of the remaining factors, namely the photocatalyst and additive could not be recognized. Therefore, the additive was omitted in the following, more detailed investigations (Table 3.22).

Table 3.22: Investigations regarding the influence of the ruthenium- and photocatalyst.[a]

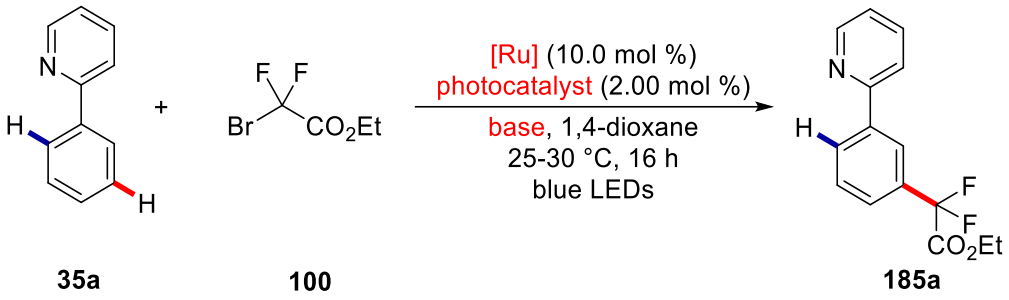

35a **100** **185a**

Entry	[Ru]	Photocatalyst	Base	Yield [%]
1	$[Ru(OAc)_2(p\text{-cymene})]$	$Ir(ppy)_3$	Na_2CO_3	40 (36)
2	$[Ru(OAc)_2(p\text{-cymene})]$	$Ir(ppy)_3$	Na_2CO_3	traces[b]
3	$[Ru(OAc)_2(p\text{-cymene})]$	--	Na_2CO_3	2
4	$[Ru(OAc)_2(p\text{-cymene})]$	--	Na_2CO_3	5[c]
5	--	$Ir(ppy)_3$	Na_2CO_3	1
6	$[Ru(O_2CMes)_2(p\text{-cymene})]$	$Ir(ppy)_3$	Na_2CO_3	2
7	$[Ru(OAc)_2(PPh_3)_2]$	$Ir(ppy)_3$	Na_2CO_3	12
8	$[Ru(O_2CAd)_2(PPh_3)_2]$	$Ir(ppy)_3$	Na_2CO_3	7
9	$[RuCl_2(PPh_3)_2]$	$Ir(ppy)_3$	Na_2CO_3	2
10	$[Ru(MeCN)_6](BF_4)_2$	$Ir(ppy)_3$	Na_2CO_3	5
11	$RuCl_3 \cdot x\ H_2O$	$Ir(ppy)_3$	Na_2CO_3	13
12	$[RuCl_2(p\text{-cymene})]_2$	$Ir(ppy)_3$	Na_2CO_3	16
13	$[Ru(OAc)_2(p\text{-cymene})]$	$Ir(ppy)_3$	Na_2CO_3	32[d]
14	$[Ru(OAc)_2(p\text{-cymene})]$	$Ru(bpy)_3Cl_2 \cdot 6\ H_2O$	Na_2CO_3	3
15	$[Ru(OAc)_2(p\text{-cymene})]$	$Ru(bpy)_3Cl_2 \cdot 6\ H_2O$	K_2CO_3	7
16	$[Ru(OAc)_2(p\text{-cymene})]$	$Ir(ppy)_3$	Na_2CO_3	41[e]

[a] Reaction conditions: **35a** (0.30 mmol), **100** (0.90 mmol), [Ru] (10.0 mol %), photocatalyst (2.00 mol %), base (0.60 mmol), 25–30 °C, 1,4-dioxane (1.5 mL), 16 h. Yield by ^{19}F-NMR with 2-chloro-4-fluorotoluene as internal standard, yield of isolated product in brackets. [b] No light. [c] 60 °C. [d] **100** (1.50 mmol). [e] Two Kessil A-A360N.

With [Ru(OAc)$_2$(*p*-cymene)] along with Ir(ppy)$_3$ as photocatalyst, and Na_2CO_3 as base the desired product **185a** could be isolated in 36% yield (entry 1). Control experiments revealed the essential nature of the light irradiation (entry 2), the photocatalyst (entries 3 and 4) and the ruthenium complex (entry 5) and. In addition, even at a reaction temperature of 60 °C no significant product formation was observed (entry 4). Other ruthenium complexes proved to be inferior to the initially employed [Ru(OAc)$_2$(*p*-cymene)] complex (entries 6–12). Furthermore Ir(ppy)$_3$ showed a significantly higher catalytic efficacy than the commonly used $Ru(bpy)_3^{2+}$ photocatalyst (entries 14 and 15). Lastly, a larger excess of **100** (entry 13) or an increase in the irradiation intensity (entry 16) did not improve the outcome of the reaction. Furthermore, the influence of the solvent and base was investigated (Table 3.23).

Table 3.23: Influence of the solvent and base on the ruthenium-catalyzed difluoromethylation.[a]

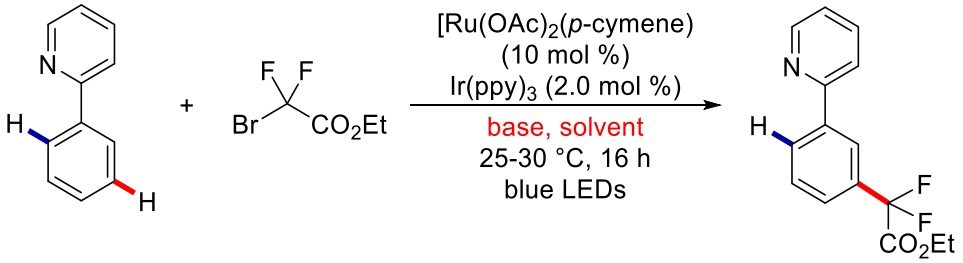

35a **100** **185a**

Entry	Solvent	Base	Yield [%]
1	DMF	Na_2CO_3	6
2	DCE	Na_2CO_3	10
3	MeCN	Na_2CO_3	9
4	DCM	Na_2CO_3	11
5	*o*-xylene	Na_2CO_3	34
6	*m*-xylene	Na_2CO_3	traces
7	*t*-BuPh	Na_2CO_3	7
8	1,4-dioxane/MeCN (2:1)	Na_2CO_3	12
9	1,4-dioxane/MeCN (4:1)	Na_2CO_3	11
10	1,4-dioxane	NaOAc	5
11	1,4-dioxane	KOAc	2

Entry	Solvent	Base	Yield [%]
12	1,4-dioxane	K_2CO_3	13
13	1,4-dioxane	Cs_2CO_3	2
14	1,4-dioxane	K_2HPO_4	13
15	1,4-dioxane	$NaHCO_3$	7
16	1,4-dioxane	2,4,6-collidine	--
17	1,4-dioxane	DABCO	2

[a] Reaction conditions: **35a** (0.30 mmol), **100** (0.90 mmol), [$Ru(OAc)_2$(*p*-cymene)] (10.0 mol %), $Ir(ppy)_3$ (2.00 mol %), base (0.60 mmol), solvent (1.5 mL), 16 h. Yield by ^{19}F-NMR with 2-chloro-4-fluorotoluene as internal standard.

Among the investigated solvents (entries 1–9), only *o*-xylene delivered comparable results (entry 5) while most of the solvents were ineffective in promoting the reaction. The same result was obtained when different bases were probed (entries 10–17). In conclusion, the combination of Na_2CO_3 and 1,4-dioxane proved to be ideal for this transformation.

Finally, the influence of different photoredox catalysts was investigated (Table 3.24). Among the probed photoredox catalysts only the derivatives of $Ir(ppy)_3$ were competent in promoting the reaction. Alkyl substituted **176** and **177** (entries 1 and 2) showed a slightly higher catalytic efficiency than the fluoro-substituted derivatives **178** and **179** (entries 3 and 4). The more electron-withdrawing phenylpyridine ligands in **180** and **186** further had a detrimental effect on the performance of the photocatalyst (entries 5 and 6). Unfortunately, the employed organic photoredox catalysts failed to promote the reaction (entries 8–10). Furthermore, the copper(I)-based photocatalysts were also not competent to catalyze the reaction (entries 11 and 12).

Table 3.24: Influence of the photocatalyst on the visible light-enabled ruthenium-catalyzed C–H difluoromethylation.

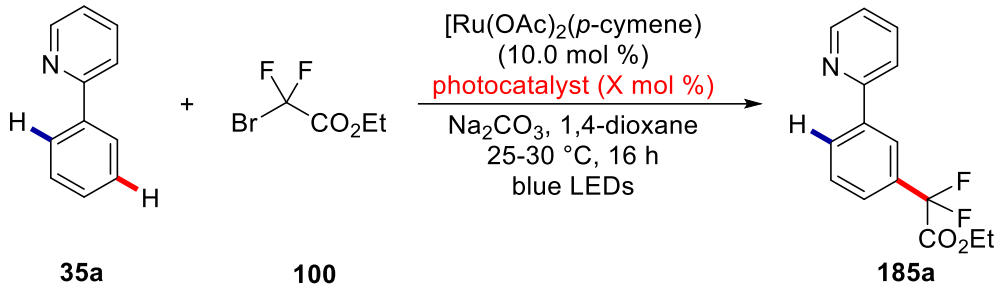

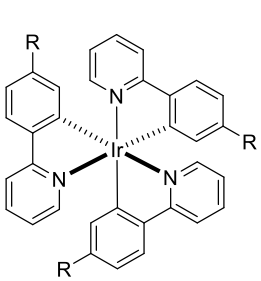

R = Me: **176**
R = *t*Bu: **177**
R = F: **178**

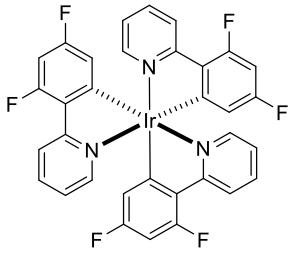

179

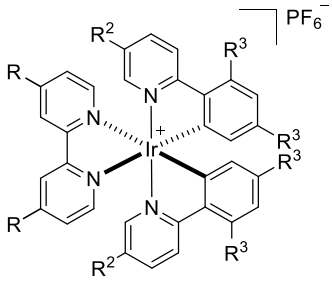

R = H, R^2 = CF_3, R^3 = F: **180**
R = *t*-Bu, R^2 = CF_3, R^3 = F: **186**
R = *t*-Bu, R^2 = H, R^3 = H: **187**

Entry	Photocatalyst	Yield [%]
1	**176** (2.00 mol %)	23
2	**177** (2.00 mol %)	26
3	**178** (2.00 mol %)	12
4	**179** (2.00 mol %)	6
5	**180** (2.00 mol %)	4
6	**186** (2.00 mol %)	traces
7	**187** (2.00 mol %)	8
8	4-CzPN (2.00 mol %)	--
9	Rhodamine 6G (5.00 mol %)	--
10	Rose Bengal (5.00 mol %)	--
11	[Cu(Me-phen)$_2$]Cl (5.00 mol %)	--
12	[Cu(dap)$_2$]Cl (5.00 mol %)	3

[a] Reaction conditions: **35a** (0.30 mmol), **100** (0.90 mmol), [Ru(OAc)$_2$(*p*-cymene)] (10.0 mol %), photocatalyst (X mol %), Na_2CO_3 (0.60 mmol), 1,4-dioxane (1.5 mL), 25–30 °C, 16 h. Yield by ^{19}F-NMR with 2-chloro-4-fluorotoluene as internal standard.

Since no synthetically meaningful yields could be obtained, the optimization was not further pursued at this point. Nevertheless, preliminary mechanistic experiments were conducted to gain insights into the underlying mechanism. To this end, fluorescence quenching experiments with $Ir(ppy)_3$ indicated that the excited state of $Ir(ppy)_3$ can be quenched by ethyl bromodifluoroacetate (**100**), suggesting an oxidative quenching scenario to be operative in the investigated reaction (Figure 3.8).

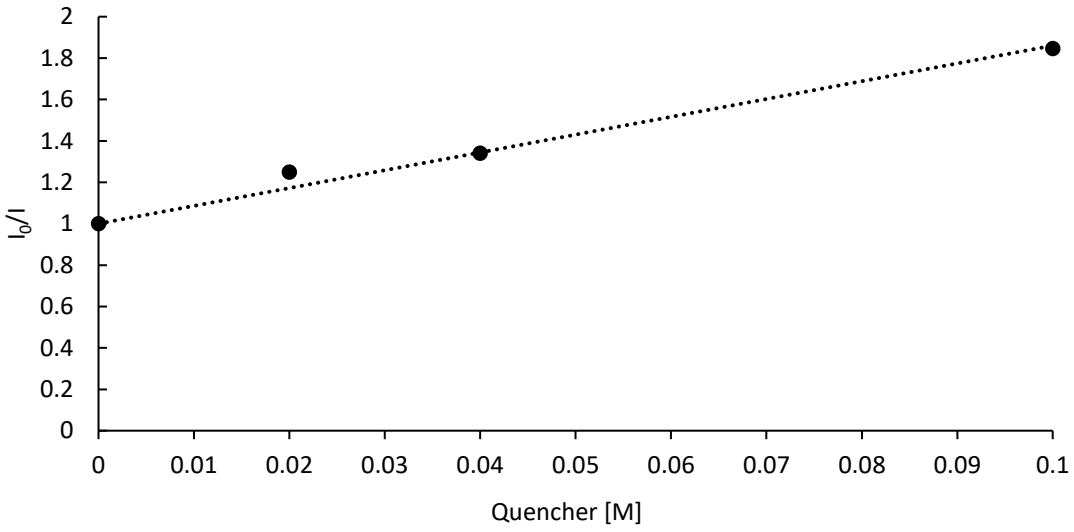

Figure 3.8: Fluorescence quenching of $Ir(ppy)_3$ with ethyl dibromofluoroacetate (**100**).

One explanation for the poor performance of the ruthenium-catalyzed C–H difluoromethylation could be a rapid deactivation of the photocatalyst. A possible pathway for catalyst deactivation is the difluoroalkylation of the phenylpyridine ligands on the iridium center. This additional functionalization would most likely affect the catalyst's redox potential and thereby might render it inactive. This proposed deactivation pathway has been recently investigated by Stephenson and coworkers.[200] An alternative scenario, that would result in the same outcome, is a ligand exchange at the iridium(III) center. Upon product formation, the alkylated product would exchange one or more of the coordinated phenylpyridine moieties and thereby induce catalyst deactivation.

3.4.2 Ruthenium-Catalyzed *meta*-C–H Alkylation

3.4.2.1 Optimization

After the initial investigation regarding the activated difluoro bromoacetate (**100**), further studies by Dr. P. Gandeepan revealed that unactivated secondary alkyl bromides **93** could deliver the corresponding *meta*-alkylated phenylpyridines **94** under blue light irradiation, yet at temperatures in the 60 °C range. Unfortunately, when the reaction temperature was decreased to ambient temperature, considerably lower yields of the products were obtained.

Thus, it was probed whether tertiary alkyl bromides **95** could actually provide the *meta*-alkylation products **96** at room temperature. To this end, several conditions, including parameters such as solvent (Table 3.25), base (Table 3.26) and transition metal (Table 3.27) were investigated.

Table 3.25: Influence of the solvent on the *meta*-C–H alkylation with **95a**.[a]

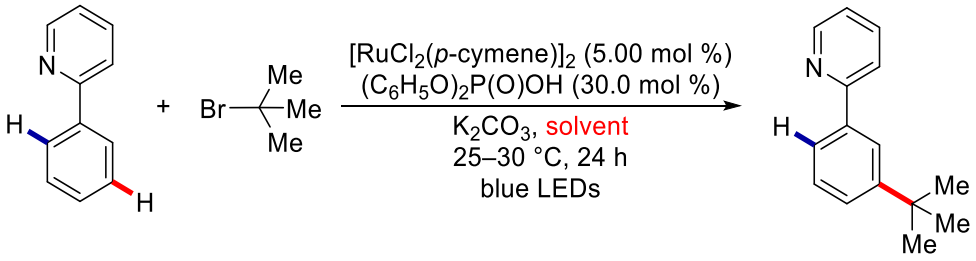

35a **95a** **96aa**

Entry	Solvent	Yield [%]
1	1,4-dioxane	80
2	DME	70
3	THF	61
4	DMA	79
5	DCE	--
6	DMF	21
7	MeCN	traces
8	PhMe	--

Entry	Solvent	Yield [%]
9	*m*-xylene	--
10	*t*BuPh	--

[a] Reaction conditions: **35a** (0.40 mmol), **95a** (1.20 mmol), $[RuCl_2(p\text{-cymene})]_2$ (5.00 mol %), $(C_6H_5O)_2P(O)OH$ (30.0 mol %), K_2CO_3 (0.80 mmol), solvent (2.0 mL), 25–30 °C, 24 h, yield of isolated product.

Probing a set of various solvents revealed that ethereal solvents were best suited for the reaction (entries 1–3). In addition, among the other probed solvents only DMA delivered comparable results (entry 4). Other prominently used solvents, such as DMF, MeCN, or the chlorinated solvent DCE were also ineffective for the *meta*-C–H alkylation (entries 5–7). Furthermore, aromatic solvents were also not suitable (entries 8–10).

Next, a range of bases, commonly used in ruthenium-catalyzed *meta*-C–H functionalization reactions, was investigated in the tertiary C–H alkylation (Table 3.26).

Table 3.26: Influence of the base on the *meta*-C–H alkylation with **95a**.[a]

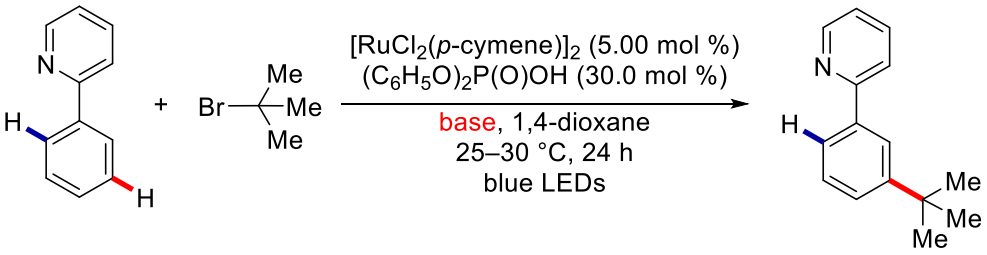

35a **95a** **96aa**

Entry	Base	Yield [%]
1	--	--
2	K_2CO_3	80
3	Na_2CO_3	47
4	KOAc	19
5	NaOAc	30
6	K_3PO_4	70

[a] Reaction conditions: **35a** (0.40 mmol), **95a** (1.20 mmol), $[RuCl_2(p\text{-cymene})]_2$ (5.00 mol %), $(C_6H_5O)_2P(O)OH$ (30 mol %), base (0.80 mmol), 1,4-dioxane (2.0 mL), 25–30 °C, 24 h, yield of isolated product.

While the presence of a base proved essential for the transformation to proceed (entry 1), a range of bases could be employed. Potassium carbonate proved ideal (entry 2), but the reaction with sodium carbonate also delivered the corresponding product in 47% yield (entry 3). In contrast, the corresponding acetates delivered the product in considerably lower yields (entries 4-5). Potassium phosphate showed a similar effectiveness as potassium carbonate (entry 6).

Furthermore, the influence of the transition metal catalyst was investigated. To this end, a range of different ruthenium complexes and other prominent transition metal catalysts was probed in the visible light-induced *meta*-C–H alkylation (Table 3.27)

Table 3.27: Influence of the transition metal catalyst on the *meta* C–H alkylation with **95a**.[a]

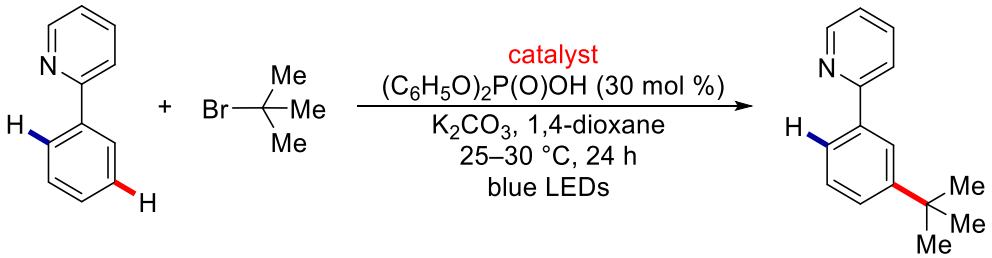

35a **95a** **96aa**

Entry	Catalyst	Yield [%]
1	$[RuCl_2(p\text{-cymene})]_2$ (5.00 mol %)	80
2	$[Ru(OAc)_2(p\text{-cymene})]$ (10.0 mol %)	35[b]
3	$[Ru(O_2CMes)_2(p\text{-cymene})]$ (10.0 mol %)	18[b]
4	$[Ru(NC\textit{t}Bu)_6][PF_6]_2$ (10.0 mol %)	--
5	$[Ru_2Cl_3(p\text{-cymene})_2][PF_6]$ (5.00 mol %)	83
6	$Pd(OAc)_2$ (10.0 mol %)	--
7	$[Cp^*RhCl_2]_2$ (10.0 mol %)	--
8	$[Cp^*IrCl_2]_2$ (10.0 mol %)	--

[a] Reaction conditions: **35a** (0.40 mmol), **95a** (1.20 mmol), catalyst, $(C_6H_5O)_2P(O)OH$ (30.0 mol %), K_2CO_3 (0.80 mmol), 1,4-dioxane (2.0 mL), 25–30 °C, 24 h, yield of isolated product. [b] Yield by ^{1}H-NMR with CH_2Br_2 as internal standard.

The $[Ru(OAc)_2(p\text{-cymene})]$ or $[Ru(O_2CMes)_2(p\text{-cymene})]$ complexes showed significantly lower activities in comparison to $[RuCl_2(p\text{-cymene})]_2$ (entries 1–3). The cationic

$[Ru(NCtBu)_6][PF_6]_2$ nitrile complex did not give any reactivity (entry 4). In contrast, the cationic $[Ru_2Cl_3(p\text{-cymene})_2][PF_6]$ complex showed similar activity to the dimeric $[RuCl_2(p\text{-cymene})]_2$ complex (entry 5). Interestingly, palladium-, rhodium- and iridium-based catalysts all failed to deliver the desired product **96aa** (entries 6–8), thus highlighting the unique power of the employed ruthenium catalysts.

Furthermore, the influence of an additional photocatalyst was investigated by Dr. P. Gandeepan, yet improved results were not obtained.[197a] At last, a series of control experiments was conducted to further investigate the influence of each reaction parameter (Table 3.28).

Table 3.28: Control experiments.[a]

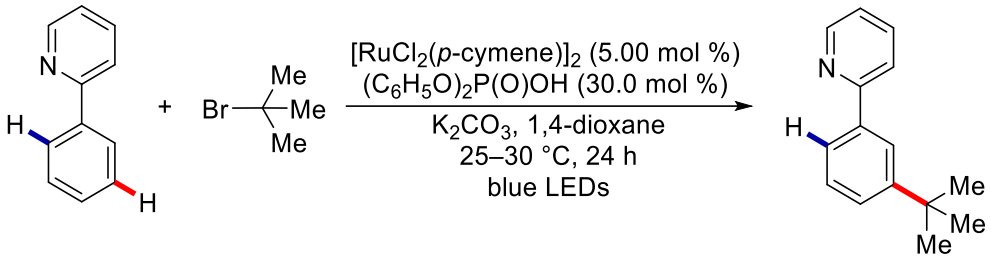

35a **95a** **96aa**

Entry	Deviation from standard conditions	Yield [%]
1	none	80
2	20 h instead of 24 h	76
3	16 h instead of 24 h	74
4	no $[RuCl_2(p\text{-cymene})]_2$	--
5	no light	--
6	no light, but 40 °C	--
7	no light, but 60 °C	--
8	no light, but 80 °C	--
9	no ligand	24
10	PPh_3 (30.0 mol %) instead of $(C_6H_5O)_2P(O)OH$	trace

[a]Reaction conditions: **35a** (0.40 mmol), **95a** (1.20 mmol), $[RuCl_2(p\text{-cymene})]_2$ (5.00 mol %), $(C_6H_5O)_2P(O)OH$ (30.0 mol %), K_2CO_3 (0.80 mmol), 1,4-dioxane (2.0 mL), 25–30 °C, 24 h, yield of isolated product.

A reduction of the reaction time led to slightly reduced yields (entries 2 and 3). Importantly, the *meta*-C–H alkylation did not proceed in the absence of the ruthenium

catalyst (entry 4). The same result was obtained when the reaction was conducted in the dark (entry 5), even if the temperature was stepwise increased to 80 °C (entries 6–8). While the transformation proceeded in the absence of an additional ligand (entry 9), triphenyl phosphine completely diminished the catalytic efficiency (entry 10). The conducted control experiments provided strong support for the proposed light-dependent nature of the transformation as no conversion could be achieved in the absence of light, even at significantly elevated temperatures.

Finally, the performance of different directing groups was explored under the established conditions (Scheme 3.16). Pyrazole **189a** was obtained in a satisfying yield, given that the temperature was raised to 60 °C. Under otherwise identical conditions, pyrimidine **191a** could only be isolated in low yield, while imidazole **188a** and triazole **190a** were not obtained. In regard to further late-stage functionalizations of the obtained products, the reaction yielding pyrazole **189a** is of high significance, since the pyrazole ring can be readily converted to the valuable amino group.[201]

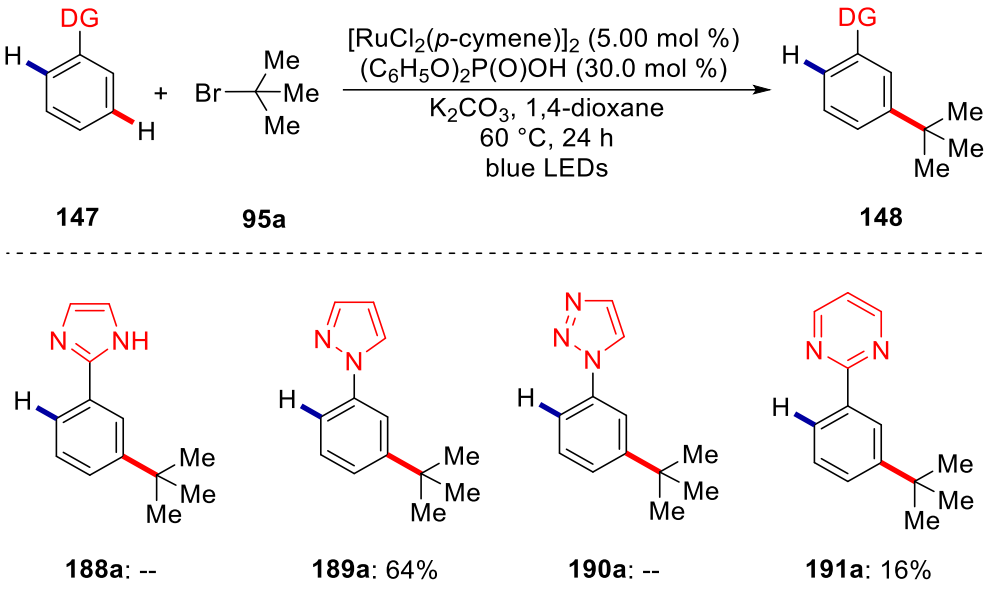

Scheme 3.16: Competence of diverse directing groups in the visible-light-driven ruthenium-catalyzed *meta*-C–H alkylation. Reaction conditions: **147** (0.40 mmol), **95a** (1.20 mmol), $[RuCl_2(p\text{-cymene})]_2$ (5.00 mol %), $(C_6H_5O)_2P(O)OH$ (30.0 mol %), K_2CO_3 (0.80 mmol), 1,4-dioxane (2.0 mL), 24 h, yield of isolated product.

3.4.2.2 Substrate Scope

With the optimized reaction conditions established through thorough investigations, the scope of the visible-light-promoted ruthenium-catalyzed *meta*-C–H alkylation was investigated. To this end, a variety of tertiary alkyl bromides **95** was subjected to the previously determined reaction conditions (Table 3.29).

Table 3.29. Scope of the ruthenium-catalyzed *meta*-selective C–H alkylation with alkyl bromides **95**.[a]

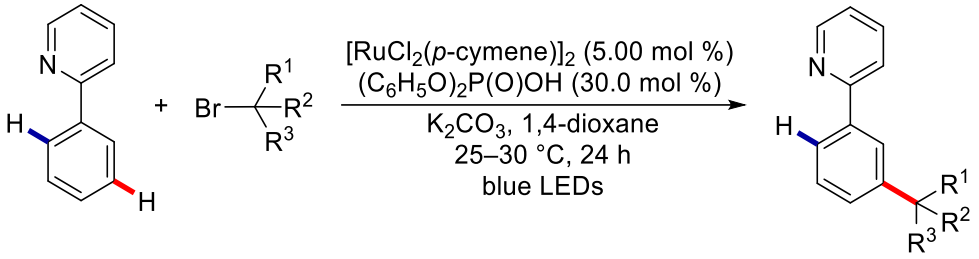

35a **95** **96**

Entry	Alkyl bromide	Product	Yield [%]
1	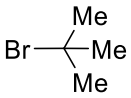 **95a**	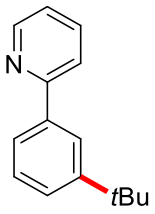 **96aa**	80
2	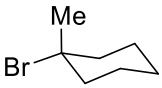 **95b**	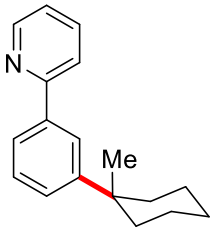 **96ab**	63
3	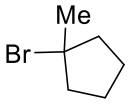 **95c**	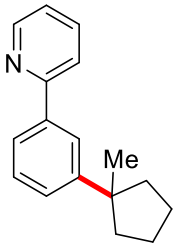 **96ac**	82

Entry	Alkyl bromide	Product	Yield [%]
4	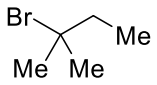 **95d**	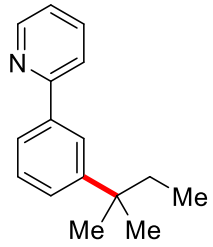 **96ad**	71
5	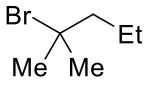 **95e**	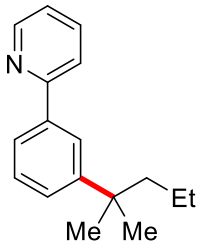 **96ae**	82
6	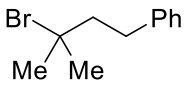 **95f**	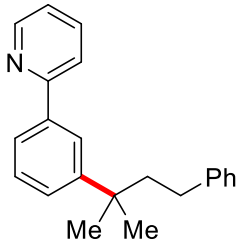 **96af**	80
7	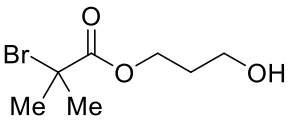 **95g**	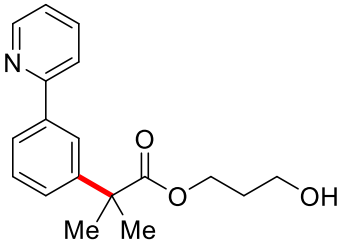 **96ag**	25[b]

[a] Reaction conditions: **35a** (0.40 mmol), **95** (1.20 mmol), $[RuCl_2(p\text{-cymene})]_2$ (5.00 mol %), $(C_6H_5O)_2P(O)OH$ (30.0 mol %), K_2CO_3 (0.80 mmol), 1,4-dioxane (2.0 mL), 25–30 °C, 24 h, yield of isolated product. [b] 48 h.

Most of the probed alkyl bromides **95** delivered the products in good to very good yields, comparable to the reaction with *tert*-butyl bromide (**95a**). Cyclic alkyl bromides **95b** and **95c** were also well tolerated (entries 2 and 3), with the cylcopentyl-substituted bromide **95c** giving slightly better results. Furthermore, different chain lengths or an aryl substituent in the alkyl bromide **95f** delivered the corresponding products **96ad**-**96af** in

very good yields (entries 4–6). However, in case the challenging free hydroxyl group was present in the alkyl bromide **95g**, the reaction time had to be extended to 48 h and the obtained yield dropped to 25% (entry 7). Yet the hydroxyl group did not suppress the catalytic activity completely.

Subsequently, the effect of the different substituents on the phenylpyridines **35** was investigated. Thus, a range of diversely decorated phenylpyridines was probed in the ruthenium-catalyzed *meta*-selective tertiary C–H alkylation (Table 3.30).

Table 3.30: Scope of the ruthenium-catalyzed *meta*-selective C–H alkylation with phenylpyridines **35**.[a]

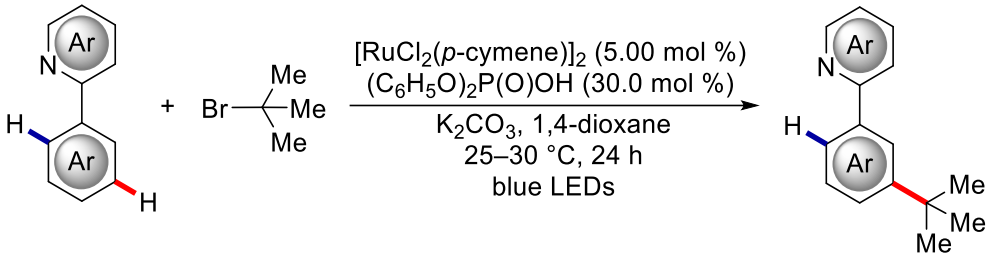

35 **95a** **96**

Entry	Phenylpyridine	Product	Yield [%]
1	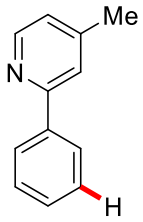 **35c**	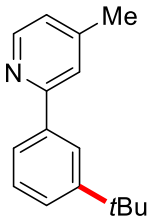 **96ca**	76
2	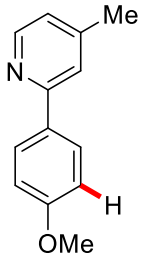 **35d**	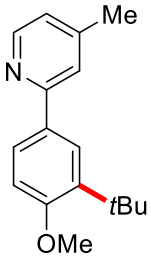 **96da**	72

Entry	Phenylpyridine	Product	Yield [%]
3	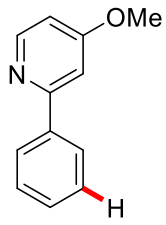 **35e**	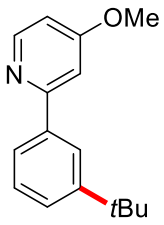 **96ea**	64
4	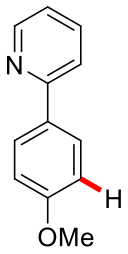 **35b**	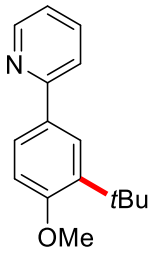 **96ba**	29
5	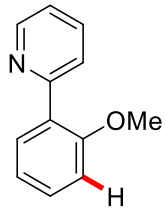 **35f**	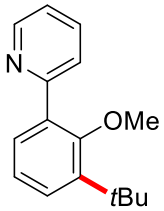 **96fa**	57
6	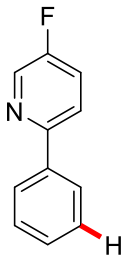 **35g**	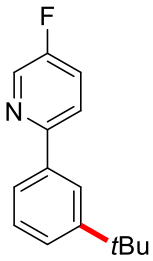 **96ga**	27
7	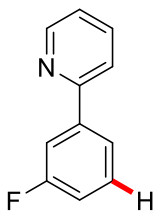 **35h**	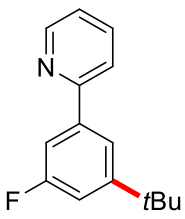 **96ha**	38

[a] Reaction conditions: **35** (0.40 mmol), **95a** (1.20 mmol), $[RuCl_2(p\text{-cymene})]_2$ (5.00 mol %), $(C_6H_5O)_2P(O)OH$ (30.0 mol %), K_2CO_3 (0.80 mmol), 1,4-dioxane (2.0 mL), 25–30 °C, 24 h, yield of isolated product.

Substituents in the C-4 position of the pyridine ring were well tolerated and gave the corresponding products in only slightly lower yields compared to the unsubstituted phenylpyridine **35a** (entries 1–3). Regarding the substituents on the phenyl ring, a significant influence of the position of the substituent was observed. While a methoxy group in the C-2 position of the phenyl ring was tolerated and the corresponding product was obtained in 57% yield (entry 5), the yield dropped drastically if a methoxy group was introduced in the C-4 position (entry 4). Electron-withdrawing substituents, such as fluorine led to significantly lowered yields when present on either the pyridine or phenylring (entries 6 and 7). Besides this observation, a clear trend could not be derived.

Simultaneously, the scope of the ruthenium-catalyzed *meta*-selective alkylation regarding secondary alkyl bromides **93** and *α*-bromoesters was investigated by Dr. P. Gandeepan. With prolonged reaction times, the corresponding products were obtained in good yields.[197a]

It is noteworthy that the reaction could be easily scaled to 2.00 mmol given that the reaction time was prolonged (Scheme 3.17).

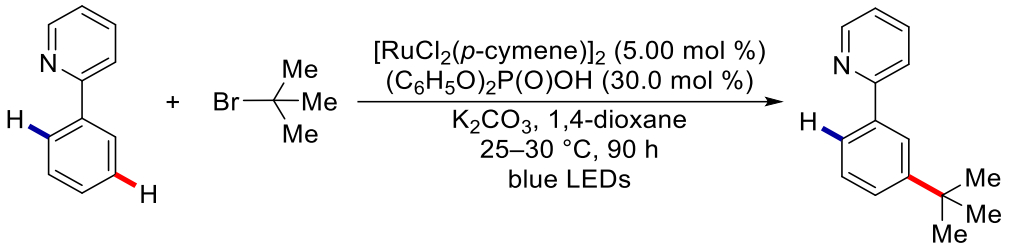

35a
2.00 mmol

95a

96aa: 88%

Scheme 3.17: Ruthenium-catalyzed *meta*-selective C–H alkylation on larger scale.

In addition to the benign scaling properties, the protocol proved suitable for further late-stage diversification. Thus, the pyridine product **96aa** could be readily converted into the corresponding piperidine **192** (Scheme 3.18). Given the high prevalence of the piperidine moiety in natural products[202] and pharmaceutical compounds,[203] this facile late-state diversification further highlights the importance of the developed methodology.

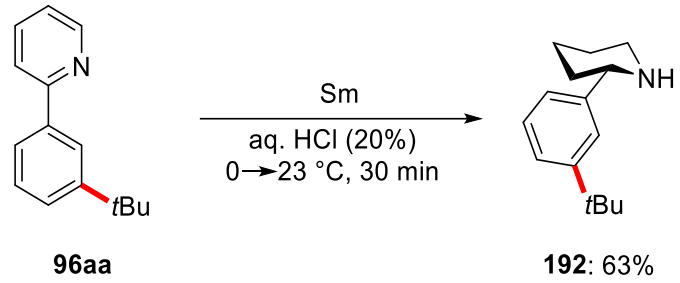

96aa **192**: 63%

Scheme 3.18: Reduction of phenylpyridine **96aa** to piperidine **192**.

3.4.2.3 Mechanistic Studies and Proposed Catalytic Cycle

After the substrate scope of the light-enabled ruthenium-catalyzed *meta*-selective alkylation had been established, the underlying mechanism of the transformation was investigated. To this end, a series of mechanistic experiments was conducted.

3.4.2.3.1 Reaction in the Presence of Radical Scavengers

To probe if the reaction proceeds under the involvement of a SET-type process several experiments in the presence of radical scavengers were performed (Table 3.31). The catalytic efficiency was completely diminished in the presence of either TEMPO or galvinoxyl (entries 2–3). In addition, BHT and 1,1-diphenylethylene also significantly reduced the obtained yield (entries 4–5). All these results are indicating that a SET-type process is involved in the product formation.

Table 3.31: *meta*-C–H Alkylation in the presence of typical radical scavengers.

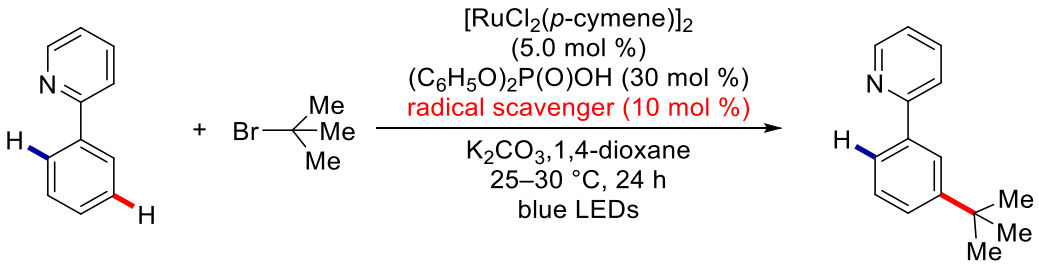

35a **95a** **96aa**

Entry	Radical scavenger (10.0 mol %)	Yield [%]
1	--	80
2	TEMPO	--
3	galvinoxyl free radical	--

Entry	Radical scavenger (10.0 mol %)	Yield [%]
4	BHT	48
5	1,1-diphenylethylene	17

[a]Reaction conditions: **35a** (0.40 mmol), **95a** (1.20 mmol), $[RuCl_2(p\text{-cymene})]_2$ (5.00 mol %), $(C_6H_5O)_2P(O)OH$ (30.0 mol %), radical scavenger (10.0 mol %) K_2CO_3 (0.80 mmol), 1,4-dioxane (2.0 mL), 25–30 °C, 24 h, yield of isolated product.

Yet, when 1,1-diphenylethylene was employed as radical scavenger, the corresponding product of the radical addition of the *tert*-butyl radical to the activated double bound could not be detected. However, when the reaction was conducted in the presence of TEMPO, the corresponding radical adduct **193** could be detected by ESI-HRMS (Figure 3.9). Furthermore, no product was detected in this measurement. This observation delivers further evidence for the formation of a *tert*-butyl radical during the *meta*-C–H alkylation reaction.

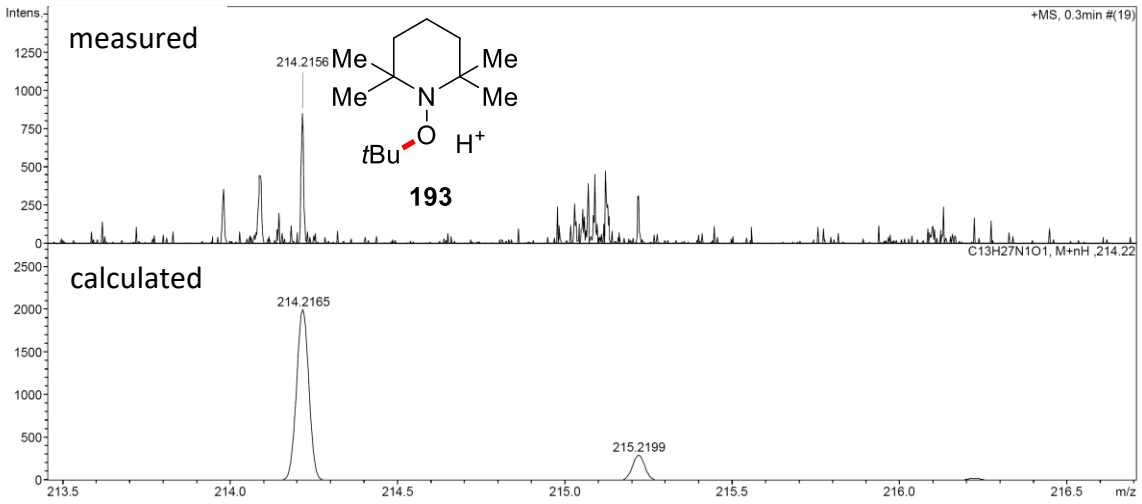

Figure 3.9: ESI-HRMS spectra of a sample taken from the reaction mixture, directly after irradiation.

3.4.2.3.2 Competition Experiments Between Alkyl Bromides

To investigate the influence of the nature of the alkyl bromide, a series of competition experiments was conducted.

First, a competition experiment employing *tert*-butyl bromide (**95a**) and cycloheptyl bromide (**93c**) was conducted (Scheme 3.19). After 24 h, the reaction was stopped, and the mixture was analyzed by ^{1}H-NMR spectroscopy. The experiment clearly showed that the tertiary alkyl bromide **95a** was converted preferentially. This indicates that the nucleophilic character of the intermediate radical has a significant influence on the C–H alkylation and suggest that a more nucleophilic character of the radical is beneficial.

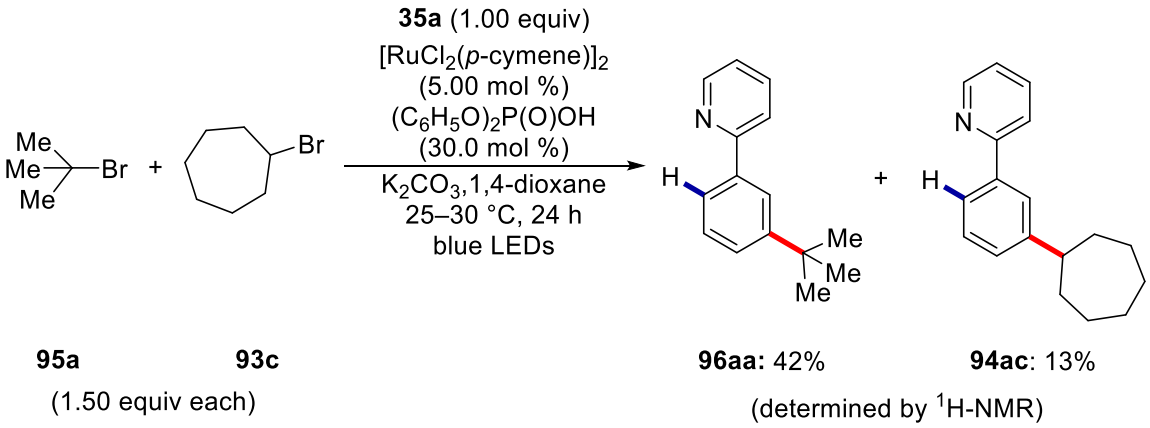

Scheme 3.19: Competition experiment between alkyl bromides **95a** and **93c**.

Interestingly, for competition experiments featuring *α*-bromoester **100** only trace amounts of the corresponding products **96aa** or **94ac** and **185a** could be detected (Scheme 3.20). Although the resulting products of a possible radical-radical coupling were not detected, these findings might be explained by the occurrence of such a coupling process between the nucleophilic alkyl radicals, generated from the secondary or tertiary alkyl bromides, and the electrophilic radical generated through the cleavage of the C–Br bond of the *α*-bromoester **100**.

*a) Competition experiment with tertiary alkyl bromide **95a** and ester **100***

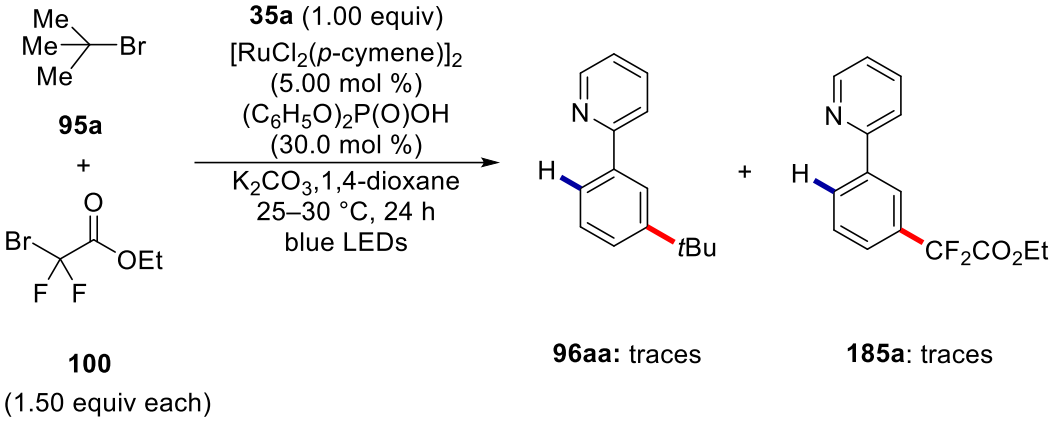

*b) Competition experiment with secondary alkyl bromide **93c** and ester **100***

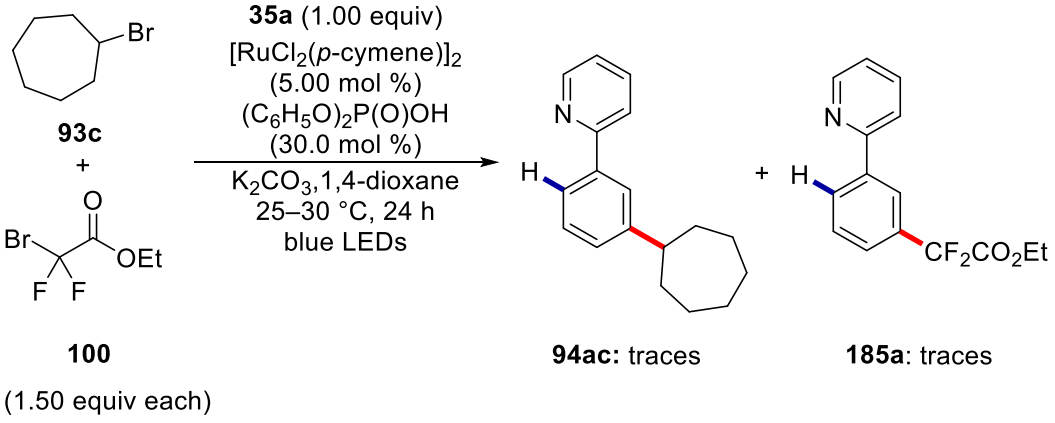

Scheme 3.20: Competition experiments with alkyl bromides **95a**/**93c** and *α*-bromoester **100**.

3.4.2.3.3 Effect of Visible-Light-Irradiation

In order to further investigate the influence of the light irradiation on the *meta*-C–H alkylation, the reaction progress was monitored during several cycles of irradiation and stirring in the dark. At each data point indicated in Figure 3.10, the yield was determined by ^{1}H-NMR spectroscopy. The obtained data clearly shows, that the transformation does not proceed in the absence of irradiation and thus further supports the light-dependent nature of the reaction.

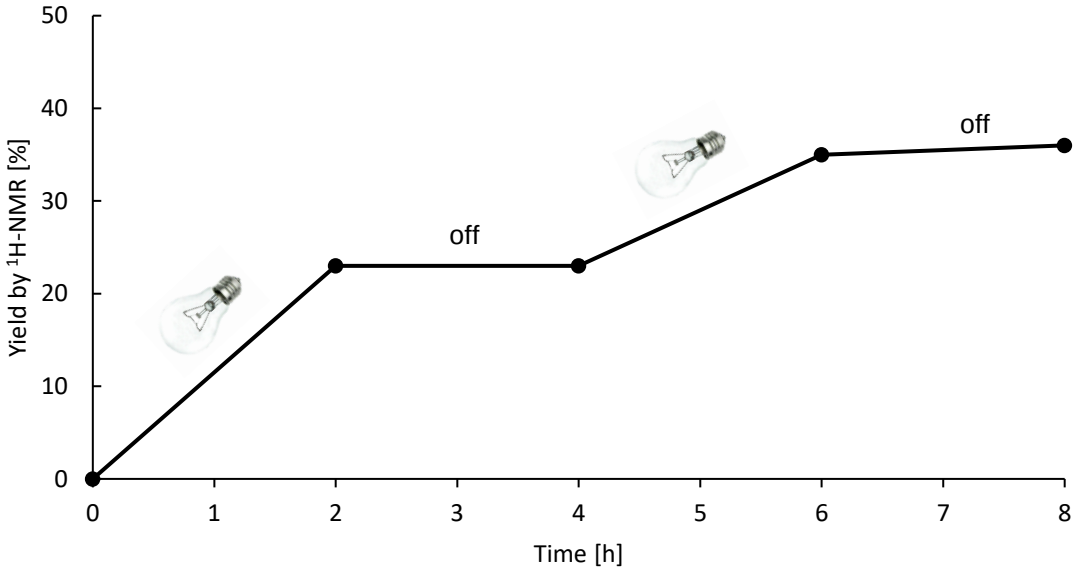

Figure 3.10: Effect of visible-light irradiation on the tertiary *meta*-C–H alkylation.

3.4.2.3.4 Reactions Using Well-Defined Ruthenium Complexes as Catalysts

To gain further insights into the underlying mechanism of the visible-light-enabled ruthenium-catalyzed *meta*-C–H alkylation, a series of experiments employing well-defined ruthenium complexes was conducted. First, the ruthenacycle **194** was employed as catalyst (Scheme 3.21).

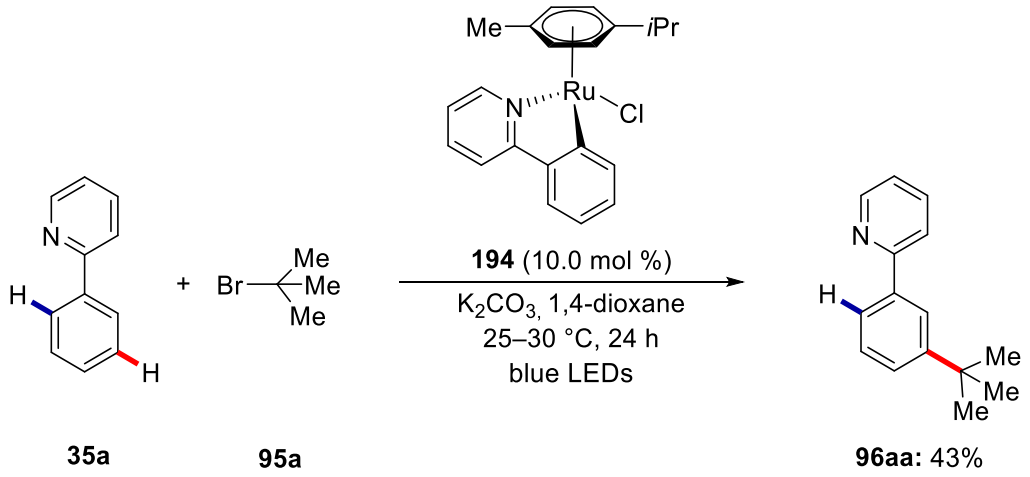

Scheme 3.21: *meta*-C–H alkylation using ruthenacycle **194** as catalyst.

The experiment showed that ruthenacycle **194** was catalytically competent even in the absence of the phosphate ligand, yet a significantly reduced yield was obtained. A similar

experiment with the phosphate ligand present was conducted by Dr. P. Gandeepan and a nearly quantitative yield was obtained if the diphenyl phosphate was present.[197a] In combination, these findings suggest that the phosphate ligand has a crucial role in the ruthenium-catalyzed *meta*-C–H alkylation.

Furthermore, experiments featuring the two cyclometalated ruthenium complexes **195** or **196** shown in Scheme 3.22 were conducted. Both ruthenacycles showed pronounced catalytic activity when employed as catalyst. However, reduced yields were obtained in comparison to the standard reaction conditions.

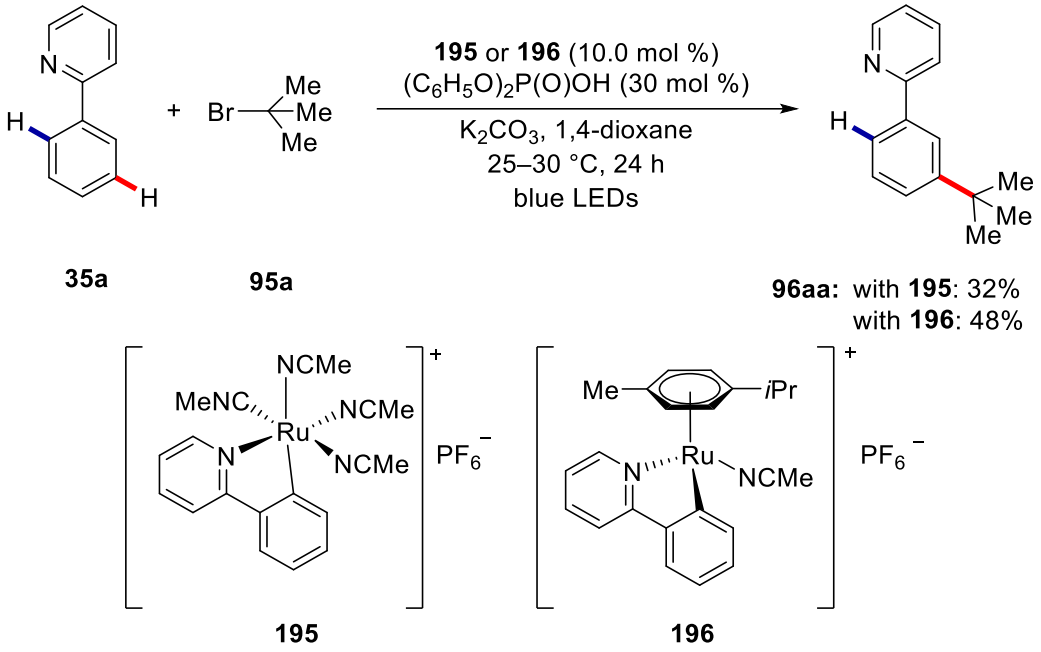

Scheme 3.22: *meta*-C–H alkylation using cyclometalated ruthenacycles **195** or **196** as catalyst.

3.4.2.3.5 Fluorescence-Quenching Experiments

Given the catalytic activity of the investigated ruthenium complexes, ruthenacycle **194** and **196** were selected for further investigations regarding their interaction with light and a possible SET-type process with the alkyl bromide. To this end, several fluorescence quenching experiments were conducted. Complex **196** did not display any fluorescence quenching when *tert*-butyl bromide (**95a**) was added (Figure 3.11). In addition, similar experiments conducted by Dr. P. Gandeepan revealed that neither the ruthenacycle **94**

nor the corresponding mesityl carboxylate-ruthenacycle did display any quenching effect.[197a]

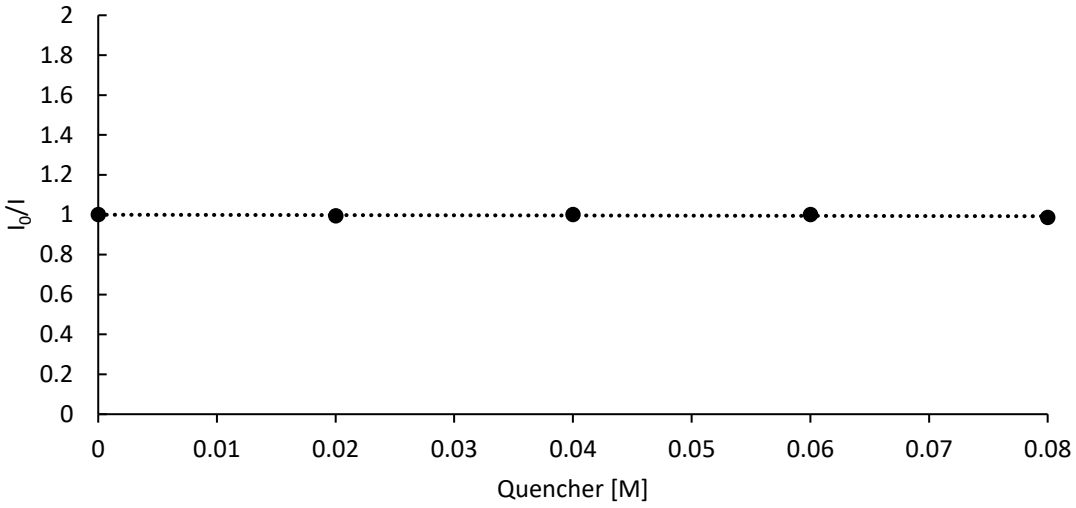

Figure 3.11: Fluorescence quenching of complex **196** with **95a**.

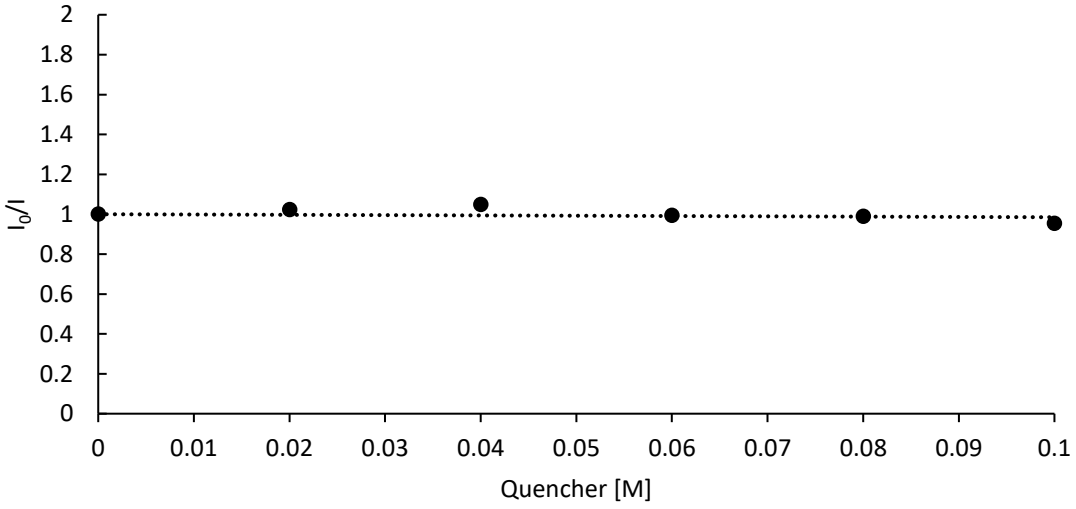

Figure 3.12: Fluorescence quenching of ruthenacycle **194** in the presence of substrate **35a** (10.0 equiv) with **95a**.

However, a quenching effect was observed in the case of the chloro-ruthenacycle **194**, when an excess of phenyl pyridine (**35a**) and sub-stoichiometric amounts of diphenyl phosphate were also present (Figure 3.13). In the absence of the ligand no quenching was detected in this case (Figure 3.12).

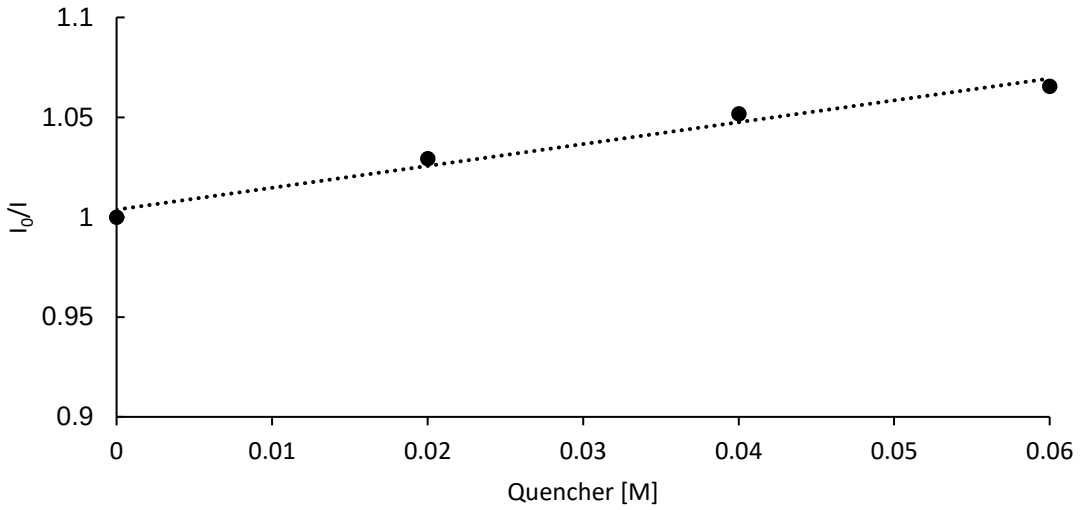

Figure 3.13: Fluorescence quenching of chloro-ruthenacycle **194** in the presence of substrate **35a** (10 equiv) and diphenyl phosphate (30 mol %).

Regarding the pronounced effect of the phosphate ligand observed in the reactions with the well-defined ruthenacycles, it is likely that an *in situ* formed cyclometalated ruthenium complex bearing a phosphate ligand is the photo-catalytically active species. Attempts to independently prepare such a complex failed and thus this hypothesis could not be further investigated.

3.4.2.4 Proposed Catalytic Cycle

Based on the conducted mechanistic studies and literature precedence, the following catalytic cycle is proposed (Scheme 3.23). A phosphate-assisted[34b,34c,197a] C–H ruthenation delivers the cyclometalated ruthenium complex **197**. As indicated by UV-Vis experiments this complex can undergo excitation by the absorption of visible light, thereby generating the excited species **197***.

The ensuing SET-process generates ruthenium(III) complex **198** and alkyl radical **199**. As previously presented,[113,196a] the subsequent radical attack is most favorable at the position *para* to ruthenium. Accordingly, intermediate **200** is generated through the attack of radical **199**. Next, an intramolecular SET and the successive rearomatization delivers ruthenacycle **202**. At last, protodemetalation yields the *meta*-alkylated product **96aa** and regenerates the catalytically active ruthenium(II) species **203**.

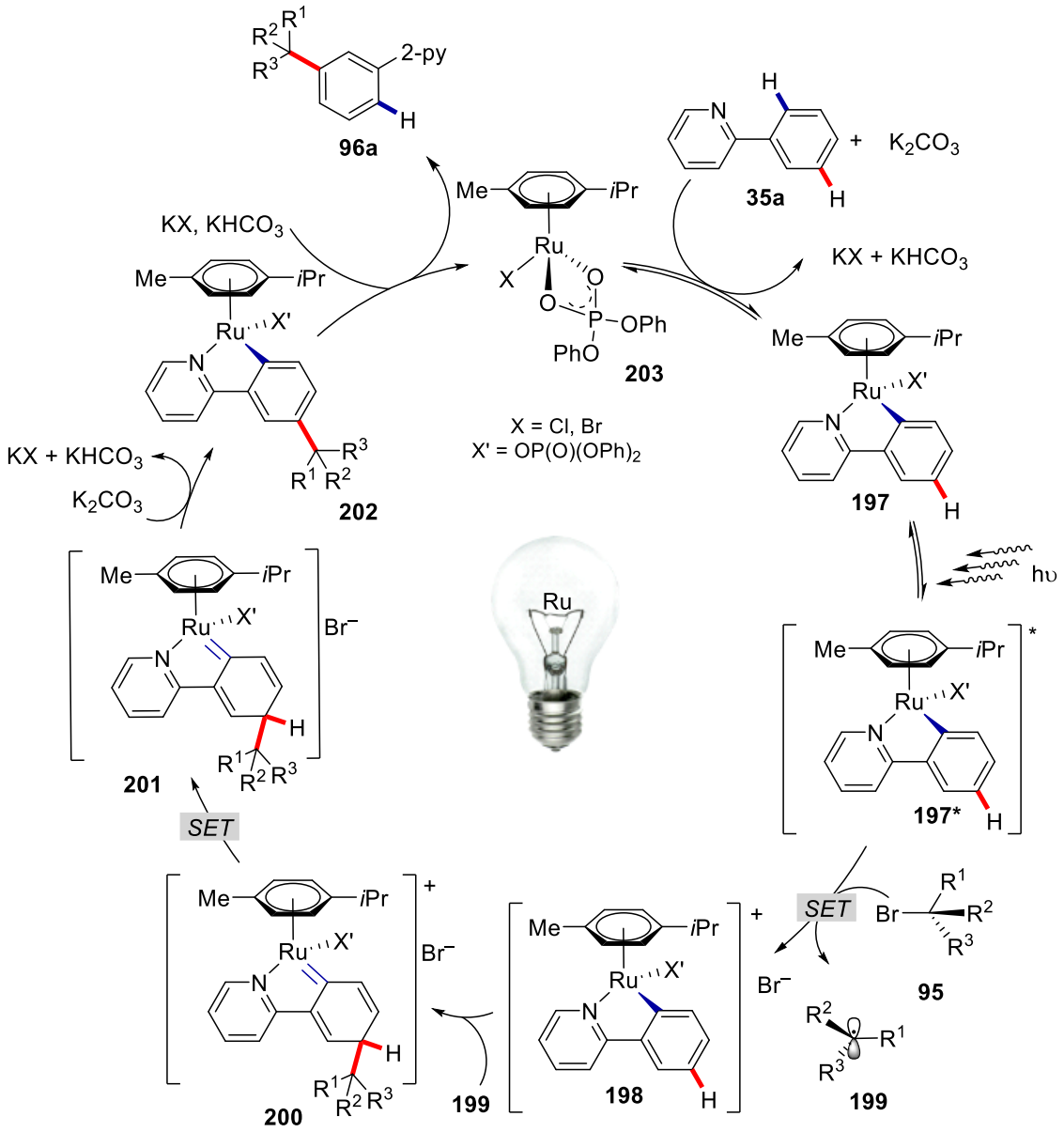

Scheme 3.23: Plausible catalytic cycle for the visible light-induced *meta*-C–H alkylation.

4 Summary and Outlook

During the last decades C–H activation has emerged as a sustainable and powerful tool for the cost-efficient synthesis of APIs, crop protection agents, and functional materials.[24] Its benign characteristics in comparison to cross-coupling chemistry had a significant contribution in addressing challenging issues connected to ecological impacts and the declining availability of resources. Furthermore, the combination of C–H activation with environmentally benign transition metals and photoredox catalysis is just beginning to show its full potential and may further reduce the ecological impact of chemical transformations.

In the first part of this thesis, the C-7 functionalization of indolines **133** by means of inexpensive and environmentally benign copper catalysis was investigated.[157] The developed catalytic system allowed for the facile chalcogenation of indolines **133** in the C-7 position. The versatility of the developed copper catalytic system was further demonstrated by the chalcogenation of indole substrates **134** in the C-2 position under otherwise identical conditions (Scheme 4.1).

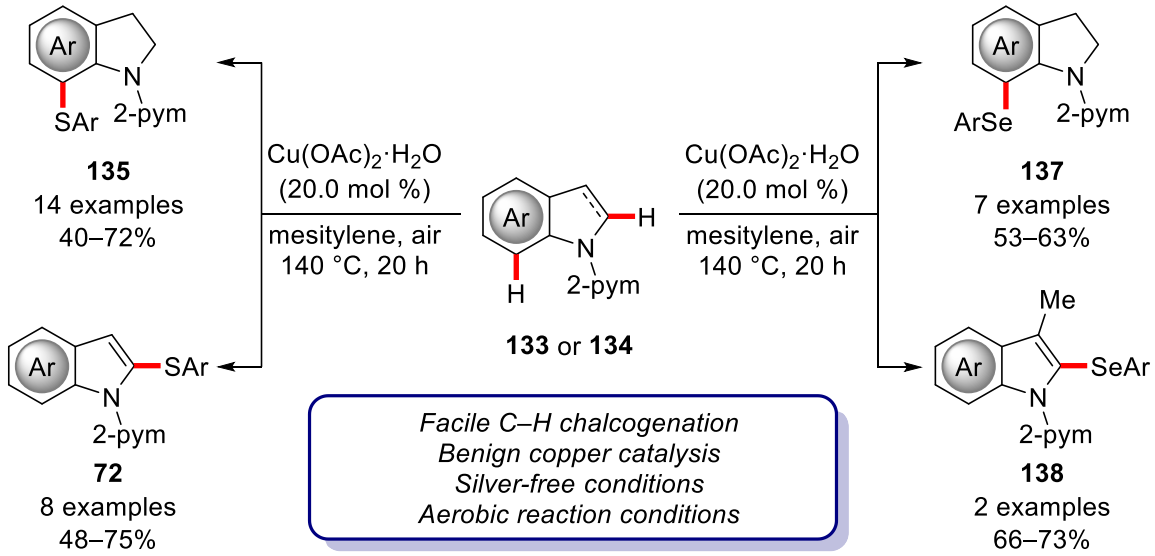

Scheme 4.1: Copper-catalyzed C–H chalcogenation of indoline **133** and indole derivatives **134**.

The protocol proved to be amenable to a broad range of indoline and indole substrates and the corresponding thiolation and selenylation products were obtained in good yields. The conducted mechanistic studies provided evidence for a reversible C–H activation step and the involvement of a SET-type process in the copper-catalyzed C–H chalcogenation.

Second, a dual cobalt photoredox system for the alkylation of azoles was devised and subsequently investigated. Although the protocol turned out to be limited to 1-adamantane carboxylic acid (**141**) as alkyl radical precursor, the transformation displayed a broad scope and high functional group tolerance of azoles **14** or **140** (Scheme 4.2).[175]

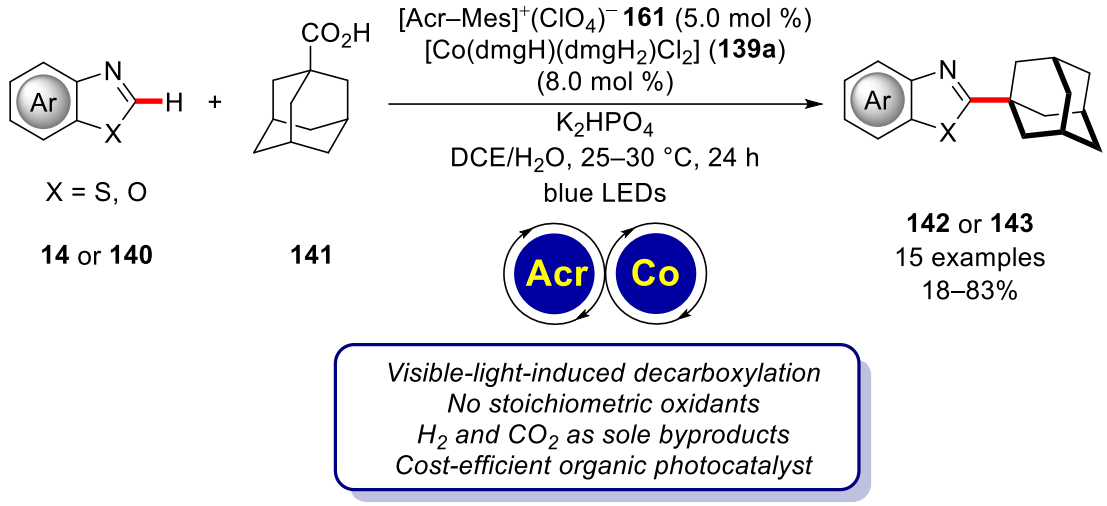

Scheme 4.2: Facile adamantylation by a dual cobalt photoredox catalytic system.

Albeit with reduced yields, the catalytic system also allowed the functionalization of xanthine alkaloids. Ensuing detailed mechanistic studies, including fluorescence quenching studies, clearly underlined the light-dependent nature of the transformation and shed light onto the action of the employed photocatalyst.

Considering the additional costs of external photocatalysts and the implications for the overall economy of the process in question, the development of protocols independent of additional photocatalysts is of great importance. To this end, in the course of this thesis the merger of C–H activation and photocatalysis was demonstrated with two unique and unprecedented applications.[189,197a] Previous copper-catalyzed C–H arylations as pioneered by Daugulis, Miura, and Ackermann required highly elevated temperatures and were therefore limited to some extent. By applying light irradiation an unprecedented mild copper-catalyzed C–H arylation could be realized.[189] Investigations regarding the scope of the protocol revealed its broad applicability, thus the methodology could be successfully applied to the synthesis of the natural product texamine (**146a**) and its derivatives (Scheme 4.3).

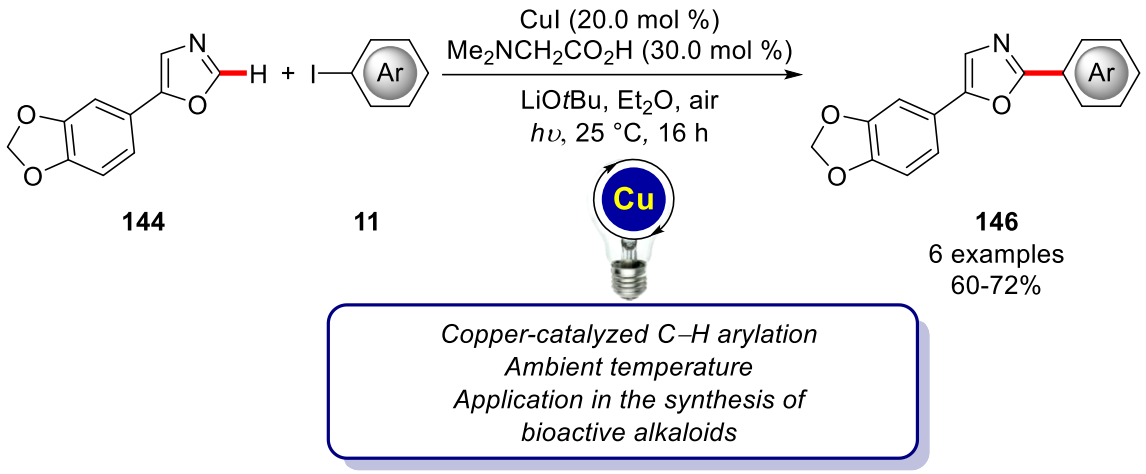

Scheme 4.3: Photo-induced copper-catalyzed arylation at ambient temperature.

Furthermore, it was probed whether the methodology could be extended to the use of visible light in the absence of any external photocatalyst. To this end, an extensive optimization delivered proof that the C–H arylation can indeed proceed under visible light irradiation, yet with reduced efficacy. The employment of additional photocatalysts did not deliver superior results in comparison to the reaction in the absence of an additional photocatalyst. Additionally, preliminary mechanistic studies were conducted to gain initial insights into to underlying mechanism.

Ackermann's proposal of a radical mechanism[109] being involved in ruthenium-catalyzed *meta*-selective C–H functionalization had revolutionized the mechanistic understanding of these transformations. It was this proposal, which sparked the idea to utilize visible light to induce the key SET process. At first, the ruthenium-catalyzed difluoroalkylation[112a] was chosen as a model system and was thoroughly investigated. The obtained initial results confirmed the hypothesis that visible light could be used to induce ruthenium-catalyzed *meta*-C–H functionalizations. Further investigations focused on the use of secondary and tertiary alkyl halides **93** and **95** and delivered suitable conditions, that allowed for facile *meta*-C–H alkylation to proceed at ambient temperature.[197a] A broad range of decorated phenylpyridines **35** and tertiary alkyl bromides **95** proved compatible and the corresponding products were usually obtained in good yields (Scheme 4.4).

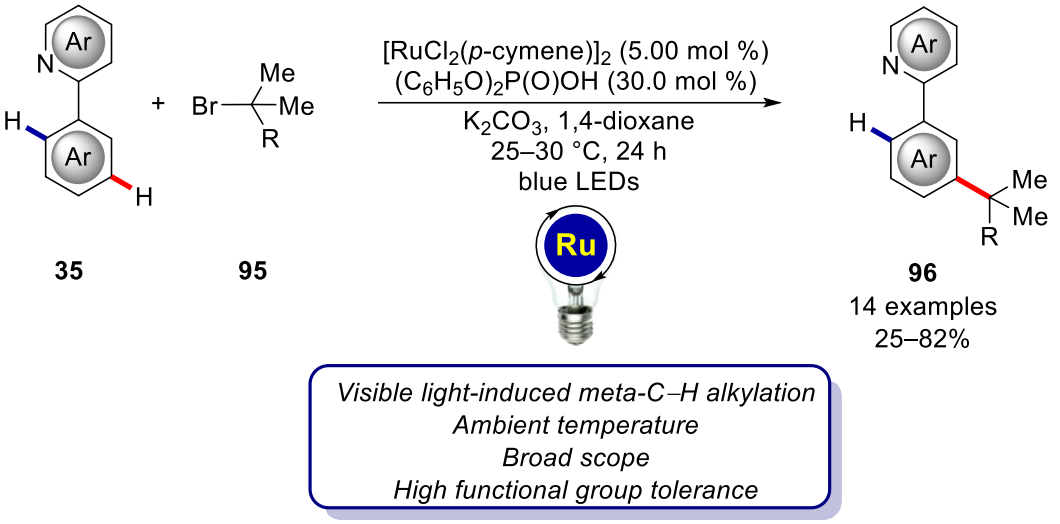

Scheme 4.4. Photo-induced ruthenium-catalyzed *meta*-selective C–H alkylation.

Furthermore, the developed protocol proved applicable to other valuable biaryl structures and could easily be scaled without the need for additional optimization. The high versatility was further demonstrated by a late-stage diversification which yielded the corresponding piperidine. The ensuing mechanistic investigations provided valuable insights into the underlying mechanism of the transformation. First, monitoring of the conversion profile in dependence of irradiation and fluorescence quenching experiments provided valuable insights regarding the effect of the visible-light-irradiation. Second, experiments with radical scavengers further delivered strong experimental evidence for an underlying SET type mechanism.

The displayed examples for the successful use of light to enable copper- and ruthenium-catalyzed C–H functionalizations under unprecedented mild conditions highlight the tremendous potential of this field and it can be expected that further research in this area will deliver fertile results.

5 Experimental Section

5.1 General Remarks

All reactions involving reagents or products sensitive to moisture or air were performed under an atmosphere of nitrogen using standard Schlenk techniques and pre-dried glassware. If not mentioned otherwise, yields refer to isolated compounds, estimated to be >95% pure as determined by ^{1}H-NMR. In case NMR yields are reported, they were determined using an internal standard.

Vacuum

The used Schlenk line was connected to a Vacuubrand® rotary vane pump. The following pressure was measured at the outlet of the used Schlenk line: 0.1 mbar. The values are not corrected.

Melting points

Melting points were measured using a Stuart Melting Point Apparatus SMP3 from BarloworldScientific. The given values are not corrected.

Chromatography

Thin layer chromatography (TLC) was performed on Merck, silica gel 60 F_{254} aluminum TLC plates. Visualization of the substances was achieved by exposure to UV light at 254 nm or by treatment of the plates with a chemical staining agent. Purification by column chromatography refers to flash column chromatography using Merck silica gel, grade 60 (40–63 µm, 230-400 mesh ASTM) and pre-distilled solvents.

Gas Chromatography

Sample analysis and reaction monitoring was performed *via* coupled gas chromatography-mass spectrometry on a 7890B GC System from Agilent Technologies coupled with either a 5977A or a 5977B mass detector from Agilent Technologies.

Nuclear Magnetic Resonance Spectroscopy (NMR)

NMR spectra were recorded on Varian VX 300, Bruker Avance 300, Bruker Avance 400 and 500 or Varian Inova 500 and 600 spectrometers in the solvent indicated. Chemical shifts are reported as δ values in ppm. ^{1}H- and ^{13}C-NMR spectra were referenced using the residual solvent signal.[204] The coupling constants *J* are reported in Hertz (Hz).

	^{1}H-NMR	^{13}C-NMR
$CDCl_3$	7.26	77.16

Abbreviations for the characterization of the signals are: s (singlet), d (doublet), t (triplet), q (quartet), dd (doublet of doublets), m (multiplet) and s_{br} (broad singlet) or analogous representations. For all spectra, a baseline and phase correction was performed. Mnova 10 from Mestrelab Research was used for the processing and analysis of the spectra.

Mass Spectrometry

Electrospray ionization (ESI) and high-resolution mass spectra (HR-MS) spectra were recorded on either a time-of-flight mass spectrometer micrOTOF (ESI-TOF-MS) or a quadrupole time-of-flight maXis (ESI-QTOF-MS) spectrometer, both from Bruker Daltonic.

Infrared Spectroscopy

Infrared (IR) spectra were recorded on a Bruker Alpha-P ATR spectrometer. Liquid samples were measured as a film and solid samples were measured neat. The spectra were recorded in the range from 4000 to 400 cm^{-1}. The analysis was performed using Opus 6 from Bruker. Reported are the most significant peaks and their respective wave numbers (cm^{-1}).

Photophysical measurements

UV-Vis absorption spectra were measured on a JASCO V-770 spectrophotometer. Fluorescence spectra were recorded on a JASCO FP-8500 spectrofluorometer. Fluorescence spectra were recorded, if not otherwise noted, at the absorption maximum of the analyte, which was determined beforehand by UV-Vis spectroscopy. The analyte solutions were degassed by sparging with N_2 prior to the measurements.

Solvents

Solvents used for column chromatography were purified by distillation under reduced pressure prior to use. Solvents used in reactions involving compounds sensitive to either air or moisture were dried, distilled and stored under inert atmosphere (argon or nitrogen) according to following standard procedures.[205]

Solvents purified by a solvent purification system (SPS-800) from M. Braun: dichloromethane, toluene, diethyl ether, tetrahydrofuran, and dimethylformamide.

Solvents dried and distilled over sodium with benzophenone as an indicator: toluene, xylenes, mesitylene, 1,4-dioxane, di-*n*-butyl ether, and dimethoxyethane.

Solvents dried and distilled over CaH_2: 1,2-dichloroethane, dimethylacetamide, dimethyl-formamide, dimethylsulfoxide.

Solvents dried over molecular sieves and degassed by freeze-pump-thaw cycles: acetonitrile (3 Å).

Water was degassed by sparging with N_2 and simultaneous sonification for 2 h.

Light sources and experimental setups

Reactions involving UV-light were performed in a Luzchem LZC-ICH2 photoreactor equipped with 16 UVC germicidal lamps (8 Watt, λ_{max} = 254 nm). The LZC-ICH2 photoreactor's temperature control unit ensured, that the reactions could be performed in a temperature range close to ambient temperature. Reactions using blue light

irradiation were performed, if not noted otherwise, with Kessil A360N lamps. To ensure sufficient cooling and temperature control of the reaction setup, additional fans were applied. To further exclude thermal reactions, the temperature of the reaction mixtures was monitored once with a temperature probe connected to a multimeter (Voltcraft VC-960). The temperature of the reaction solution was measured and recorded every 30 s during the reaction (Figure 5.1, Figure 5.2 and Figure 5.3).

Reagents

Chemicals obtained from commercial suppliers (with a purity >95%) were used without further purification. The following compounds have been previously reported and were synthesized according to previously described literature protocols:

N-Pyrimidyl indolines **133**,[206] *N*-pyrimidyl indoles **134**,[149a] carbazole **155a**,[78] disulfides **59**,[207] diselenide **63b**,[208] benzoxazoles **14**,[209] [Co(dmgH)(dmgH$_2$)Cl$_2$] (**139a**),[210] tetrabutylammonium adamantanecarboxylate (**167**),[178] triazole **27b**,[211] Ir-complex **177**,[212] Ir-complex **176**,[213] dap-ligand,[214] [Cu(dap)$_2$Cl],[215] phenyl pyridines **35**,[109a,216] alkyl bromides **95**,[217] [Ru$_2$Cl$_3$(*p*-cymene)][PF$_6$].[218]

The following chemicals were kindly supplied by the following coworkers:

Karsten Rauch:	[RuCl$_2$(*p*-cymene)]$_2$, [Cp*RhCl$_2$]$_2$, [Ru(O$_2$CMes)$_2$(*p*-cymene)], [Cp*IrCl$_2$]$_2$, [Ru(OAc)$_2$(*p*-cymene)], [Ru(O$_2$CAd)$_2$(*p*-cymene)]
Thomas Müller:	disulfide **56d**, purine derivative **163**
Nils Imse:	benzothiazoles **140b**-**140j**

5.2 General Procedures

5.2.1 General Procedure A: Copper-Catalyzed C–H Chalcogenation

To an oven-dried Schlenk tube were added indoline **133** or indole **134** (0.30 mmol, 1.00 equiv), disulfide **59** or diselenide **63** (0.30 mmol, 1.00 equiv), and $Cu(OAc)_2 \cdot H_2O$ (12.0 mg, 20.0 mol %) under ambient conditions. Mesitylene (1.5 mL) was added and the mixture was stirred for 20 h at 140 °C. After cooling to ambient temperature, the reaction mixture was diluted with Et_2O (10 mL) and filtered through a short pad of silica. The filtrate was concentrated, and the crude residue was purified by column chromatography on silica gel (*n*-pentane/Et_2O) affording the corresponding products **72**, **135**, **137** or **138**.

5.2.2 General Procedure B: Visible Light-Induced Decarboxylative C–H Adamantylation

To an oven-dried 10 mL vial were added the heteroarene **14**, **140**, **162** or **163** (0.40 mmol, 1.00 equiv), 1-adamantanecarboxylic acid (**141**) (216 mg, 1.20 mmol, 3.00 equiv), K_2HPO_4 (209 mg, 1.20 mmol, 3.00 equiv), 9-mesityl-10-methylacridinium perchlorate (**161**) (8.20 mg, 5.00 mol %) and [Co(dmgH)(dmgH_2)Cl_2] (**139a**) (11.6 mg, 8.00 mol %). After the vial was capped with a septum, it was evacuated and refilled with N_2 for three times before DCE (1.5 mL) and H_2O (0.5 mL) were added sequentially. If the heterocyclic substrate was a liquid, it was added at this point. The mixture was degassed and stirred for 24 h under visible light irradiation (*Kessil A360N*, Figure 5.1). After 24 h or 48 h, the mixture was diluted with CH_2Cl_2 (10 mL) and H_2O (10 mL) and the layers were separated. The aqueous layer was extracted with CH_2Cl_2 (2 x 10 mL), the combined organic layers were dried over Na_2SO_4 and the solvent was removed under reduced pressure. The residue was purified by column chromatography on silica gel (*n*-pentane/Et_2O) affording the corresponding products **142**, **143**, **164** or **165**.

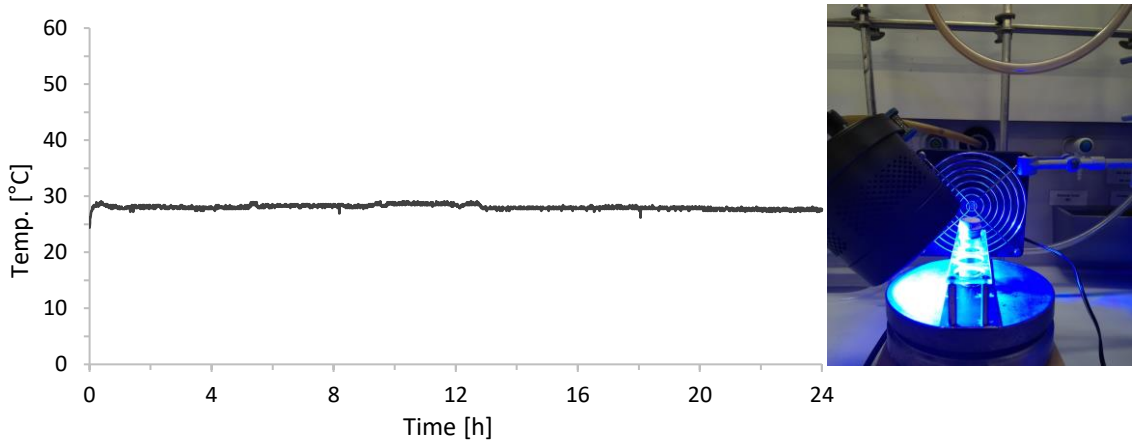

Figure 5.1: Internal temperature in the vial recorded during the reaction and experimental setup.

5.2.3 General Procedure C: Photo-Induced Copper-Catalyzed C–H Arylation

To an oven-dried 10 mL quartz tube heterocycle **14**, **140**, or **144** (0.25 mmol), iodoarene **11** (1.25 mmol), copper(I) iodide (9.50 mg, 20.0 mol %), dimethylglycine (7.70 mg, 30.0 mol %), LiO*t*Bu (60.0 mg, 0.75 mmol), and Et_2O (1.0 mL) were added under ambient atmosphere. The tube was capped with a septum and wrapped with Parafilm and stirred under 254 nm irradiation for 16 h (Luzchem LZC-ICH2 photoreactor, the temperature was maintained between 25 °C and 30 °C, Figure 5.2). After the indicated reaction time, the mixture was filtered over a short pad of silica (Et_2O) and the solvent was removed under reduced pressure. The residue was purified by column chromatography on silica gel (*n*-pentane/Et_2O) affording the corresponding products **15**, **145**, or **146**.

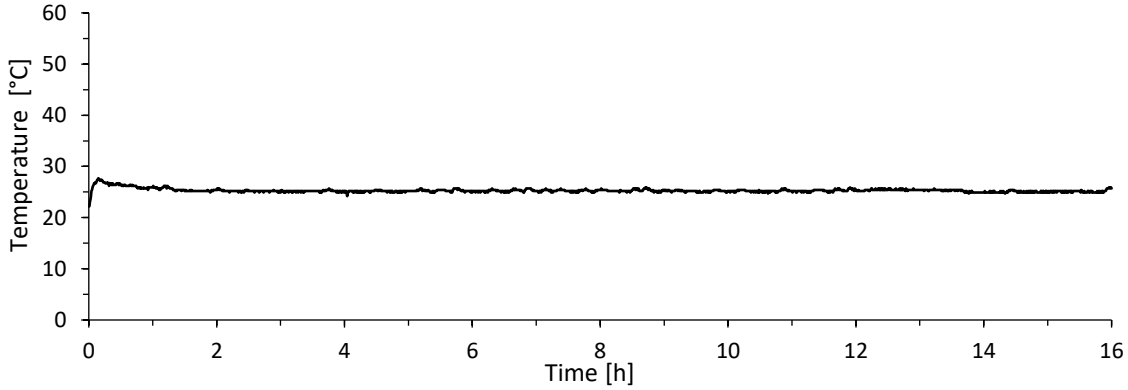

Figure 5.2: Internal temperature in the quartz tube recorded during the reaction.

5.2.4 General Procedure D: Visible Light-Enabled Ruthenium-Catalyzed *meta*-C–H Alkylation

To an oven-dried 10 mL vial were added $[RuCl_2(p\text{-cymene})]_2$ (12.2 mg, 5.00 mol %), diphenyl phosphate (30.0 mg, 30.0 mol %) and K_2CO_3 (111 mg, 0.80 mmol, 2.00 equiv). The vial was capped with a septum and wrapped with Parafilm. After the vial was evacuated and backfilled with N_2 three times, 1,4-dioxane (2.0 mL) was added *via* syringe. Substrate **35** (0.40 mmol, 1.00 equiv) and alkyl bromide **95** (1.20 mmol, 3.00 equiv) were added sequentially and the reaction mixture was degassed. Finally, the puncture hole in the septum was sealed with electric tape. The reaction mixture was stirred for 24 h under visible light irradiation (2 x Kessil A360N, temperature was maintained between 25 °C and 30 °C, Figure 5.3). After the indicated reaction time, the mixture was filtered over a short pad of silica (Et_2O) and the solvent was removed under reduced pressure. The residue was purified by column chromatography on silica gel (*n*-pentane/Et_2O) affording the corresponding products **96**.

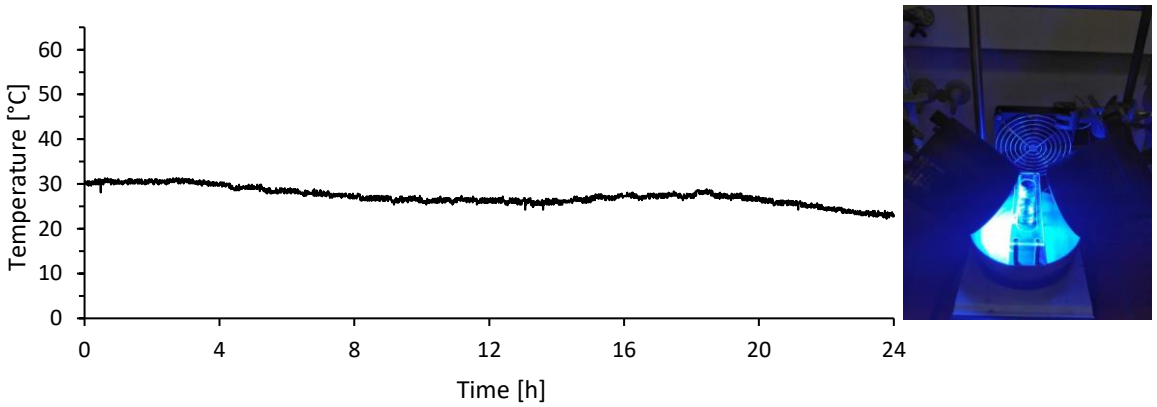

Figure 5.3: Internal temperature in the vial recorded during the reaction and experimental setup.

5.3 Copper-Catalyzed C–H Chalcogenation

5.3.1 Synthesis and Characterization of Starting Materials

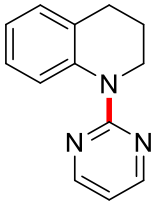

1-(Pyrimidin-2-yl)-1,2,3,4-tetrahydroquinoline (156a)

Tetrahydroquinoline **156a** was prepared according to a previously described procedure.[206] 1,2,3,4-Tetrahydroquinoline (666 mg, 5.00 mmol, 1.00 equiv) and 2-chloropyrimidine (573 mg, 5.00 mmol, 1.00 equiv) were dissolved in a mixture of EtOH and H_2O (4:1, 50 mL). At ambient temperature conc. HCl (1.0 mL) was added dropwise *via* syringe. After the addition, the solution was stirred for 16 h at 85 °C. The solution was concentrated under reduced pressure. To the residue H_2O (20 mL) was added and the mixture was extracted with CH_2Cl_2 (3 x 50 mL). The combined organic phases were dried over Na_2SO_4 and the solvent was removed under reduced pressure. Purification of the residue by column chromatography yielded the desired product **156a** (74.0 mg, 350 µmol, 7%) as a yellow oil.

^{1}H-NMR (300 MHz, $CDCl_3$): δ = 8.41 (d, *J* = 4.8 Hz, 2H), 7.74 (ddd, *J* = 8.2, 1.3, 0.5 Hz, 1H), 7.21–7.11 (m, 2H), 7.04–6.97 (m, 1H), 6.66 (t, *J* = 4.8 Hz, 1H), 4.03 (t, *J* = 6.3 Hz, 2H), 2.80 (t, *J* = 6.5 Hz, 2H), 2.02 (tt, *J* = 6.3, 6.5 Hz, 2H). **^{13}C-NMR** (76 MHz, $CDCl_3$): δ = 161.3 (C_q), 157.8 (CH), 139.6 (C_q), 131.1 (C_q), 128.7(CH), 125.6 (CH), 124.1 (CH), 123.4 (CH), 112.1 (CH), 45.5 (CH_2), 27.6 (CH_2), 24.2 (CH_2). **IR** (ATR): 1574, 1548, 1490, 1412, 1308, 1269, 1209, 1185, 796, 752 cm^{-1}. **MS** (ESI) *m/z* (relative intensity): 212 $[M+H]^+$ (100), 176 (20). **HR-MS** (ESI): *m/z* calcd for $C_{13}H_{14}N_3^+$ $[M+H]^+$ 212.1182, found 212.1175

5.3.2 Analytical Data

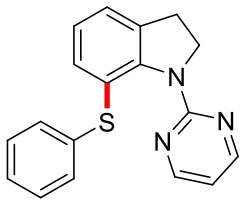

7-(Phenylthio)-1-(pyrimidin-2-yl)-1*H*-indole (135aa)

The general procedure **A** was followed using indoline **133a** (59.2 mg, 0.30 mmol) and disulfide **59a** (65.5 mg, 0.30 mmol). Purification by column chromatography on silica gel (*n*-pentane/Et_2O: 3/1) yielded **135aa** (61.0 mg, 200 µmol, 66%) as a pale yellow solid.

M. p.: 130–131 °C. **^{1}H-NMR** (500 MHz, $CDCl_3$): δ = 8.44 (d, *J* = 4.7 Hz, 2H), 7.29–7.02 (m, 7H), 6.90 (dd, *J* = 8.0, 7.1 Hz, 1H), 6.72 (t, *J* = 4.8 Hz, 1H), 4.46 (t, *J* = 7.9 Hz, 2H), 3.14 (t, *J* = 7.9 Hz, 2H). **^{13}C-NMR** (126 MHz, $CDCl_3$): δ = 160.9 (C_q), 157.4 (CH), 144.0 (C_q), 138.4 (C_q), 134.9 (C_q), 131.7 (CH), 131.3 (CH), 128.9 (CH), 126.7 (CH), 126.1 (C_q), 124.4 (CH), 123.2 (CH), 113.0 (CH), 52.5 (CH_2), 29.8 (CH_2). **IR** (ATR): 1574, 1551, 1452, 1423, 1379, 800, 771, 748, 724, 690 cm^{-1}. **MS** (ESI) *m/z* (relative intensity): 328 $[M+Na]^+$ (60) 306 $[M+H]^+$ (100), 197 $[M–SPh]^+$ (50). **HR-MS** (ESI): *m/z* calcd for $C_{18}H_{16}N_3S^+$ $[M+H]^+$ 306.1060, found 306.1059. The analytical data are in accordance with those reported in the literature.[206]

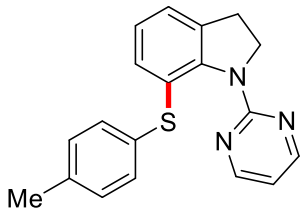

1-(Pyrimidin-2-yl)-7-(*p*-tolylthio)indoline (135ab)

The general procedure **A** was followed using indoline **135a** (59.2 mg, 0.30 mmol) and disulfide **59b** (73.9 mg, 0.30 mmol). Purification by column chromatography on silica gel (*n*-pentane/Et_2O: 3/1) yielded **135ab** (60.0 mg, 188 µmol, 63%) as a pale yellow solid.

M. p.: 117–119 °C. **^{1}H-NMR** (300 MHz, $CDCl_3$): δ = 8.46 (d, *J* = 4.7 Hz, 2H), 7.21 (d, *J* = 8.1 Hz, 2H), 7.10–7.00 (m, 4H), 6.88 (dd, *J* = 8.0, 7.2 Hz, 1H), 6.72 (t, *J* = 4.8 Hz, 1H),

4.47 (t, *J* = 7.9 Hz, 2H), 3.14 (t, *J* = 7.9 Hz, 2H), 2.30 (s, 3H). **^{13}C-NMR** (76 MHz, $CDCl_3$): δ = 160.9 (C_q), 157.4 (CH), 143.5 (C_q), 137.0 (C_q), 134.7 (C_q), 134.4 (C_q), 132.2 (CH), 131.0 (CH), 129.7 (CH), 127.2 (C_q), 124.3 (CH), 122.7 (CH), 112.9 (CH), 52.5 (CH_2), 29.8 (CH_2), 21.2 (CH_3). **IR** (ATR): 1574, 1549, 1418, 1278, 794, 768, 725, 615, 529, 488 cm^{-1}. **MS** (ESI) *m/z* (relative intensity): 320 $[M+H]^+$ (100), 197 $(M–STol]^+$ (46). **HR-MS** (ESI): *m/z* calcd for $C_{19}H_{18}N_3S^+$ $[M+H]^+$ 320.1216, found 320.1217. The analytical data are in accordance with those reported in the literature.[206]

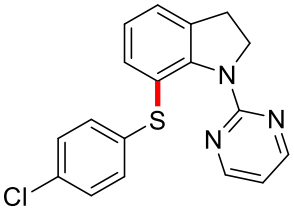

7-[(4-Chlorophenyl)thio]-1-(pyrimidin-2-yl)indoline (135ac)

The general procedure **A** was followed using indoline **133a** (59.2 mg, 0.30 mmol) and disulfide **59c** (86.2 mg, 0.30 mmol). Purification by column chromatography on silica gel (*n*-pentane/Et_2O: 3/1) yielded **135ac** (40.3 mg, 119 µmol, 40%) as a white solid.

M. p.: 123–124 °C. **^{1}H-NMR** (300 MHz, $CDCl_3$): δ = 8.43 (d, *J* = 4.8 Hz, 2H), 7.21–7.04 (m, 6H), 6.91 (dd, *J* = 8.0, 7.2 Hz, 1H), 6.73 (t, *J* = 4.8 Hz, 1H), 4.46 (t, *J* = 7.9 Hz, 2H), 3.15 (t, *J* = 7.9 Hz, 2H). **^{13}C-NMR** (76 MHz, $CDCl_3$): δ = 160.9 (C_q), 157.5 (CH), 144.2 (C_q), 137.3 (C_q), 135.0 (C_q), 132.6 (C_q), 132.4 (CH), 131.8 (CH), 129.0 (CH), 125.7 (C_q), 124.5 (CH), 123.5 (CH), 113.1 (CH), 52.4 (CH_2), 29.8 (CH_2). **IR** (ATR): 1574, 1551, 1420, 1090, 1011, 905, 816, 795, 770, 725 cm^{-1}. **MS** (ESI) *m/z* (relative intensity): 340 $[M+H]^+$ (100) (^{35}Cl), 197 $[M–SC_6H_4Cl]^+$ (51). **HR-MS** (ESI): *m/z* calcd for $C_{18}H_{15}N_3{}^{35}ClS^+$ $[M+H]^+$ 340.0670, found 340.0666. The analytical data are in accordance with those reported in the literature.[206]

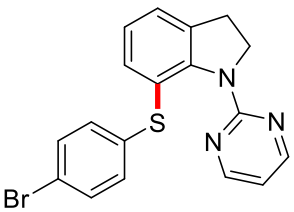

7-[(4-Bromophenyl)thio]-1-(pyrimidin-2-yl)indoline (135ad)

The general procedure **A** was followed using indoline **133a** (59.2 mg, 0.30 mmol) and disulfide **59d** (136 mg, 0.30 mmol). Purification by column chromatography on silica gel (*n*-pentane/Et_2O: 3/1) yielded **135ad** (59.1 mg, 154 µmol, 51%) as a pale yellow solid.

M. p.: 95–97 °C. **^{1}H-NMR** (300 MHz, $CDCl_3$): δ = 8.43 (d, *J* = 4.8 Hz, 2H), 7.36–7.27 (m, 2H), 7.17–7.04 (m, 4H), 6.92 (dd, *J* = 8.0, 7.2 Hz, 1H), 6.73 (t, *J* = 4.8 Hz, 1H), 4.46 (t, *J* = 7.9 Hz, 2H), 3.15 (t, *J* = 7.9 Hz, 2H). **^{13}C-NMR** (76 MHz, $CDCl_3$): δ = 160.9 (C_q), 157.5 (CH), 144.3 (C_q), 138.1 (C_q), 135.0 (C_q), 132.5 (CH), 131.9 (CH), 131.9 (CH), 125.4 (C_q), 124.5 (CH), 123.6 (CH), 120.5 (C_q), 113.1 (CH), 52.4 (CH_2), 29.8 (CH_2). **IR** (ATR): 1574, 1549, 1417, 1378, 1083, 1005, 810, 794, 768, 727 cm^{-1}. **MS** (ESI) *m/z* (relative intensity): 384 $[M+H]^+$ (100) (^{79}Br), 197 $[M–SC_6H_4Br]^+$ (54). **HR-MS** (ESI): *m/z* calcd for $C_{18}H_{15}N_3{}^{79}BrS^+$ $[M+H]^+$ 384.0165, found 384.0158. The analytical data are in accordance with those reported in the literature.[206]

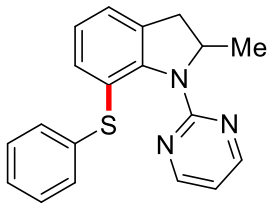

2-Methyl-7-(phenylthio)-1-(pyrimidin-2-yl)indoline (135ba)

The general procedure **A** was followed using indoline **133b** (63.4 mg, 0.30 mmol) and disulfide **59a** (65.5 mg, 0.30 mmol). Purification by column chromatography on silica gel (*n*-pentane/Et_2O: 3/1) yielded **135ba** (68.6 mg, 215 µmol, 72%) as an off-white solid.

M. p.: 123–124 °C. **^{1}H-NMR** (400 MHz, $CDCl_3$): δ = 8.42 (d, *J* = 4.8 Hz, 2H), 7.23–7.09 (m, 7H), 6.92 (dd, *J* = 7.9, 7.3 Hz, 1H), 6.70 (t, *J* = 4.8 Hz, 1H), 5.03–4.92 (m, 1H), 3.52 (dd, *J* = 15.2, 8.6 Hz, 1H), 2.58 (d, *J* = 15.2 Hz, 1H), 1.45 (d, *J* = 6.5 Hz, 3H). **^{13}C-NMR** (101 MHz, $CDCl_3$): δ = 160.5 (C_q), 157.4 (CH), 143.0 (C_q), 138.8 (C_q), 133.7 (C_q), 132.3 (CH), 131.0 (CH), 128.8 (CH), 126.5 (CH), 126.4 (C_q), 124.4 (CH), 124.0 (CH), 113.0 (CH), 59.9 (CH), 37.1 (CH_2), 21.5 (CH_3). **IR** (ATR): 1577, 1550, 1459, 1425, 794, 764, 742, 728, 701, 685 cm^{-1}. **MS** (ESI) *m/z* (relative intensity): 342 $[M+Na]^+$ (70), 320 $[M+H]^+$ (100) 211 [M–

SPh]$^+$ (28). **HR-MS** (ESI): *m/z* calcd for $C_{19}H_{17}N_3SNa^+$ [M+Na]$^+$ 342.1035, found 342.1036. The analytical data are in accordance with those reported in the literature.[206]

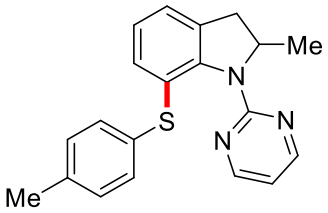

2-Methyl-1-(pyrimidin-2-yl)-7-(*p*-tolylthio)indoline (135bb)

The general procedure **A** was followed using indoline **133b** (63.4 mg, 0.30 mmol) and disulfide **59b** (73.9 mg, 0.30 mmol). Purification by column chromatography on silica gel (*n*-pentane/Et_2O: 3/1) yielded **135bb** (66.0 mg, 198 µmol, 66%) as a yellow oil.

^{1}H-NMR (400 MHz, $CDCl_3$): δ = 8.44 (d, *J* = 4.8 Hz, 2H), 7.15 (d, *J* = 8.1 Hz, 2H), 7.12–7.06 (m, 2H), 7.02 (d, *J* = 8.1 Hz, 2H), 6.89 (dd, *J* = 7.6, 7.6 Hz, 1H), 6.70 (t, *J* = 4.8 Hz, 1H), 5.03–4.93 (m, 1H), 3.52 (dd, *J* = 15.5, 8.6 Hz, 1H), 2.57 (d, *J* = 15.5 Hz, 1H), 2.29 (s, 3H), 1.45 (d, *J* = 6.5 Hz, 3H). **^{13}C-NMR** (101 MHz, $CDCl_3$): δ = 160.6 (C_q), 157.4 (CH), 142.4 (C_q), 136.7 (C_q), 134.8 (C_q), 133.5 (C_q), 131.9 (CH), 131.5 (CH), 129.7 (CH), 127.4 (C_q), 124.3 (CH), 123.5 (CH), 112.9 (CH), 59.8 (CH), 37.1 (CH_2), 21.5 (CH_3), 21.2 (CH_3). **IR** (ATR): 1576, 1549, 1453, 1421, 1346, 793, 763, 729, 709, 489 cm^{-1}. **MS** (ESI) *m/z* (relative intensity): 356 [M+Na]$^+$ (100), 334 [M+H]$^+$ (88) 211 [M–SC_6H_4Me]$^+$ (19). **HR-MS** (ESI): *m/z* calcd for $C_{20}H_{19}N_3SNa^+$ [M+Na]$^+$ 356.1192, found 356.1190.

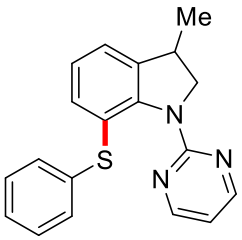

3-Methyl-7-(phenylthio)-1-(pyrimidin-2-yl)indoline (135ca)

The general procedure **A** was followed using indoline **133c** (63.4 mg, 0.30 mmol) and disulfide **59a** (65.5 mg, 0.30 mmol). Purification by column chromatography on silica gel (*n*-pentane/Et_2O: 3/1) yielded **135ca** (50.1 mg, 157 µmol, 52%) as a yellow oil.

^{1}H-NMR (400 MHz, $CDCl_3$): δ = 8.42 (d, *J* = 4.8 Hz, 2H), 7.27–7.22 (m, 2H), 7.21–7.11 (m, 3H), 7.08 (dt, *J* = 7.9, 1.0 Hz, 1H), 7.04 (dt, *J* = 7.3, 1.2 Hz, 1H), 6.91 (dd, *J* = 7.9, 7.3 Hz, 1H), 6.69 (t, *J* = 4.8 Hz, 1H), 4.62 (dd, *J* = 11.1, 8.2 Hz, 1H), 3.94 (dd, *J* = 11.1, 7.3 Hz, 1H), 3.50–3.39 (m, 1H), 1.30 (d, *J* = 6.9 Hz, 3H). **^{13}C-NMR** (101 MHz, $CDCl_3$): δ = 161.1 (C_q), 157.5 (CH), 143.6 (C_q), 140.1 (C_q), 138.3 (C_q), 131.7 (CH), 131.4 (CH), 128.9 (CH), 126.7 (CH), 126.1 (C_q), 124.5 (CH), 121.9 (CH), 112.9 (CH), 60.3 (CH_2), 36.5 (CH), 18.9 (CH_3). IR (ATR): 1574, 1550, 1419, 1377, 907, 796, 774, 732, 689, 619 cm^{-1}. **MS** (ESI) *m/z* (relative intensity): 342 $[M+Na]^+$ (100), 320 $[M+H]^+$ (66), 211 $[M–SPh]^+$ (22). **HR-MS** (ESI): *m/z* calcd for $C_{19}H_{17}N_3SNa^+$ $[M+Na]^+$ 342.1035, found 342.1036. The analytical data are in accordance with those reported in the literature.[206]

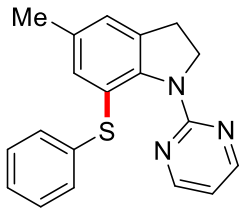

5-Methyl-7-(phenylthio)-1-(pyrimidin-2-yl)indoline (135da)

The general procedure **A** was followed using indoline **133d** (63.4 mg, 0.30 mmol) and disulfide **59a** (65.5 mg, 0.30 mmol). Purification by column chromatography on silica gel (*n*-pentane/Et_2O: 3/1) yielded **135da** (59.0 mg, 185 µmol, 62%) as a yellow solid.

M. p.: 135–137 °C. **^{1}H-NMR** (400 MHz, $CDCl_3$): δ = 8.41 (d, *J* = 4.8 Hz, 2H), 7.32–7.11 (m, 5H), 6.94 (d, *J* = 0.8 Hz, 2H), 6.69 (t, *J* = 4.8 Hz, 1H), 4.44 (t, *J* = 7.8 Hz, 2H), 3.10 (t, *J* = 7.8 Hz, 2H), 2.20 (s, 3H). **^{13}C-NMR** (126 MHz, $CDCl_3$): δ = 161.0 (C_q), 157.3 (CH), 142.0 (C_q), 138.6 (C_q), 135.0 (C_q), 134.1 (C_q), 132.0 (CH), 130.8 (CH), 128.7 (CH), 126.3 (CH), 125.4 (C_q), 124.3 (CH), 112.7 (CH), 52.6 (CH_2), 29.9 (CH_2), 21.0 (CH_3). **IR** (ATR): 1574, 1551, 1447, 1403, 1376, 799, 746, 723, 698, 688 cm^{-1}. **MS** (ESI) *m/z* (relative intensity): 342 $[M+Na]^+$ (88), 320 $[M+H]^+$ (100), 211 $[M–SPh]^+$ (22). **HR-MS** (ESI): *m/z* calcd for $C_{19}H_{17}N_3SNa^+$ $[M+Na]^+$

342.1035, found 342.1033. The analytical data are in accordance with those reported in the literature.[206]

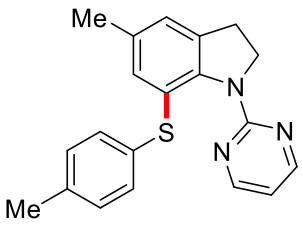

5-Methyl-1-(pyrimidin-2-yl)-7-(*p*-tolylthio)indoline (135db)

The general procedure **A** was followed using indoline **133d** (63.4 mg, 0.30 mmol) and disulfide **59a** (73.9 mg, 0.30 mmol). Purification by column chromatography on silica gel (*n*-pentane/Et_2O: 3/1) yielded **135db** (59.8 mg, 179 µmol, 60%) as a yellow solid.

M. p.: 138–140 °C. **^{1}H-NMR** (400 MHz, $CDCl_3$): δ = 8.43 (d, *J* = 4.8 Hz, 2H), 7.19 (d, *J* = 8.1 Hz, 2H), 7.03 (d, *J* = 8.1 Hz, 2H), 6.90 (s, 1H), 6.88 (s, 1H), 6.69 (t, *J* = 4.8 Hz, 1H), 4.45 (t, *J* = 7.8 Hz, 2H), 3.09 (t, *J* = 7.8 Hz, 2H), 2.30 (s, 3H), 2.18 (s, 3H). **^{13}C-NMR** (101 MHz, $CDCl_3$): δ = 161.2 (C_q), 157.4 (CH), 141.5 (C_q), 136.7 (C_q), 134.9 (C_q), 134.6 (C_q), 134.1 (C_q), 131.8 (CH), 131.3 (CH), 129.8 (CH), 126.5 (C_q), 123.9 (CH), 112.7 (CH), 52.6 (CH_2), 29.9 (CH_2), 21.2 (CH_3), 21.0 (CH_3). **IR** (ATR): 1574, 1552, 1426, 1302, 1222, 1198, 794, 724, 618, 486 cm^{-1}. **MS** (ESI) *m/z* (relative intensity): 356 $[M+Na]^+$ (95), 334 $[M+H]^+$ (100), 211 $[M–SC_6H_4Me]^+$ (35). **HR-MS** (ESI): *m/z* calcd for $C_{20}H_{19}N_3SNa^+$ $[M+Na]^+$ 356.1192, found 356.1188.

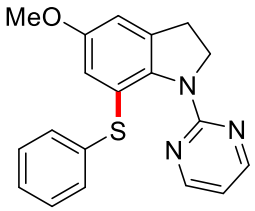

5-Methoxy-7-(phenylthio)-1-(pyrimidin-2-yl)indoline (135ea)

The general procedure **A** was followed using indoline **133e** (68.2 mg, 0.30 mmol) and disulfide **59a** (65.5 mg, 0.30 mmol). Purification by column chromatography on silica gel (*n*-pentane/Et_2O: 2.5/1) yielded **135ea** (62.8 mg, 187 µmol, 62%) as a yellow oil.

^{1}H-NMR (400 MHz, $CDCl_3$): δ = 8.42 (d, *J* = 4.8 Hz, 2H), 7.32–7.28 (m, 2H), 7.25–7.14 (m, 3H), 6.73–6.70 (m, 1H), 6.68 (t, *J* = 4.8 Hz, 1H), 6.61 (d, *J* = 2.6 Hz, 1H), 4.45 (t, *J* = 7.8 Hz, 2H), 3.62 (s, 3H), 3.09 (t, *J* = 7.8 Hz, 2H). **^{13}C-NMR** (101 MHz, $CDCl_3$): δ = 161.1 (C_q), 157.4 (CH), 156.8 (C_q), 137.9 (C_q), 137.7 (C_q), 136.3 (C_q), 131.6 (CH), 128.9 (CH), 127.1 (C_q), 126.9 (CH), 115.4 (CH), 112.5 (CH), 110.4 (CH), 55.8 (CH_3), 52.7 (CH_2), 30.3 (CH_2). **IR** (ATR): 1576, 1550, 1448, 1430, 1407, 906, 795, 724, 690, 645 cm^{-1}. **MS** (ESI) *m/z* (relative intensity): 358 $[M+Na]^+$ (100), 336 $[M+H]^+$ (90) 227 $[M–SPh]^+$ (22). **HR-MS** (ESI): *m/z* calcd for $C_{19}H_{17}N_3OSNa^+$ $[M+Na]^+$ 358.0985, found 358.0984. The analytical data are in accordance with those reported in the literature.[206]

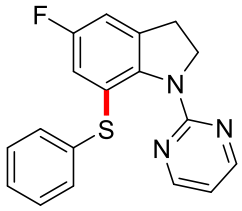

5-Fluoro-7-(phenylthio)-1-(pyrimidin-2-yl)indoline (135fa)

The general procedure **A** was followed using indoline **133f** (64.6 mg, 0.30 mmol) and disulfide **59a** (65.5 mg, 0.30 mmol). Purification by column chromatography on silica gel (*n*-pentane/Et_2O: 3/1) yielded **135fa** (67.0 mg, 207 µmol, 69%) as a pale yellow solid.

M. p.: 129–130 °C. **^{1}H-NMR** (400 MHz, $CDCl_3$): δ = 8.45 (d, *J* = 4.8 Hz, 2H), 7.35–7.30 (m, 2H), 7.29–7.20 (m, 3H), 6.82–6.78 (m, 1H), 6.75–6.70 (m, 2H), 4.49 (t, *J* = 7.9 Hz, 2H), 3.12 (t, *J* = 7.9 Hz, 2H). **^{13}C-NMR** (101 MHz, $CDCl_3$): δ = 161.0 (C_q), 159.6 (d, $^1J_{C\text{-}F}$ = 243.6 Hz, C_q), 157.5 (CH), 139.8 (d, $^4J_{C\text{-}F}$ = 2.1 Hz, C_q), 137.0 (C_q), 136.6 (d, $^3J_{C\text{-}F}$ = 8.9 Hz, C_q), 132.4 (CH), 129.2 (CH), 128.5 (d, $^3J_{C\text{-}F}$ = 8.4 Hz, C_q), 127.5 (CH), 116.6 (d, $^2J_{C\text{-}F}$ = 25.0 Hz, CH), 113.0 (CH), 110.6 (d, $^2J_{C\text{-}F}$ = 24.2 Hz, CH), 52.8 (CH_2), 30.1 (CH_2). **^{19}F{H}-NMR** (282 MHz, $CDCl_3$): δ = −119.2 (s). **IR** (ATR): 1575, 1549, 1452, 1427, 1405, 861, 796, 750, 699, 690 cm^{-1}. **MS** (ESI) *m/z* (relative intensity): 346 $[M+Na]^+$ (30), 324 $[M+H]^+$ (100). **HR-MS** (ESI): *m/z* calcd for $C_{18}H_{14}FN_3SNa^+$ $[M+Na]^+$ 346.0785, found 346.0796. The analytical data are in accordance with those reported in the literature.[206]

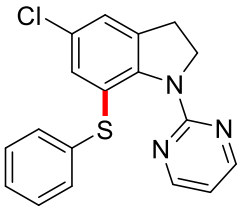

5-Chloro-7-(phenylthio)-1-(pyrimidin-2-yl)indoline (135ga)

The general procedure **A** was followed using indoline **133g** (69.5 mg, 0.30 mmol) and disulfide **59a** (65.5 mg, 0.30 mmol). Purification by column chromatography on silica gel (*n*-pentane/Et_2O: 3/1) yielded **135ga** (66.0 mg, 194 µmol, 65%) as a white solid.

M. p.: 142–144 °C. **^{1}H-NMR** (300 MHz, $CDCl_3$): δ = 8.44 (d, J = 4.8 Hz, 2H), 7.46–7.19 (m, 5H), 7.08–7.00 (m, 2H), 6.74 (t, J = 4.8 Hz, 1H), 4.46 (t, J = 7.9 Hz, 2H), 3.12 (t, J = 7.9 Hz, 2H). **^{13}C-NMR** (126 MHz, $CDCl_3$): δ = 160.6 (C_q), 157.4 (CH), 142.5 (C_q), 137.1 (C_q), 136.5 (C_q), 131.9 (CH), 130.3 (CH), 129.1 (CH), 128.9 (C_q), 128.0 (C_q), 127.3 (CH), 123.2 (CH), 113.2 (CH), 52.7 (CH_2), 29.8 (CH_2). IR (ATR): 1574, 1553, 1436, 1402, 854, 799, 759, 696, 635, 467 cm^{-1}. **MS** (ESI) *m/z* (relative intensity): 362 $[M+Na]^+$ (38), 340 $[M+H]^+$ (100), 231 $[M–SPh]^+$ (22). **HR-MS** (ESI): *m/z* calcd for $C_{18}H_{14}ClN_3SNa^+$ $[M+Na]^+$ 362.0489, found 362.0485. The analytical data are in accordance with those reported in the literature.[206]

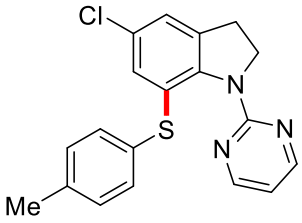

5-Chloro-1-(pyrimidin-2-yl)-7-(*p*-tolylthio)indoline (135gb)

The general procedure **A** was followed using indoline **133g** (69.5 mg, 0.30 mmol) and disulfide **59b** (73.9 mg, 0.30 mmol). Purification by column chromatography on silica gel (*n*-pentane/Et_2O: 3/1→2/1) yielded **135gb** (66.8 mg, 189 µmol, 63%) as a white solid.

M. p.: 93–95 °C. **^{1}H-NMR** (400 MHz, $CDCl_3$): δ = 8.46 (d, J = 4.8 Hz, 2H), 7.24 (d, J = 8.1 Hz, 2H), 7.08 (d, J = 8.1 Hz, 2H), 7.02 (d, J = 2.0 Hz, 1H), 6.95 (d, J = 2.0 Hz, 1H), 6.74 (t, J = 4.7 Hz, 1H), 4.46 (t, J = 7.9 Hz, 2H), 3.11 (t, J = 7.9 Hz, 2H), 2.32 (s, 3H). **^{13}C-NMR** (101 MHz, $CDCl_3$): δ = 160.9 (C_q), 157.5 (CH), 142.0 (C_q), 137.8 (C_q), 136.4 (C_q), 133.1 (C_q),

132.8 (CH), 130.1 (CH), 129.7 (CH), 129.1 (C_q), 129.0 (C_q), 122.8 (CH), 113.2 (CH), 52.7 (CH_2), 29.7 (CH_2), 21.3 (CH_3). **IR** (ATR): 1572, 1554, 1455, 1426, 1395, 859, 810, 797, 491, 460 cm^{-1}. **MS** (ESI) *m/z* (relative intensity): 376 $[M+Na]^+$ (84), 354 $[M+H]^+$ (100), 231 $[M–SC_6H_4Me]^+$ (35). **HR-MS** (ESI): *m/z* calcd for $C_{19}H_{16}{}^{35}ClN_3SNa^+$ $[M+Na]^+$ 376.0646, found 376.0632.

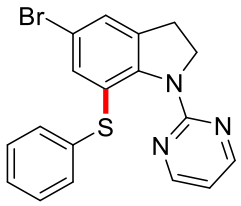

5-Bromo-7-(phenylthio)-1-(pyrimidin-2-yl)indoline (135ha)

The general procedure **A** was followed using indoline **133h** (82.8 mg, 0.30 mmol) and disulfide **59a** (65.5 mg, 0.30 mmol). Purification by column chromatography on silica gel (*n*-pentane/Et_2O: 3/1→2/1) yielded **135ha** (63.2 mg, 164 µmol, 55%) as an off-white solid.

M. p.: 160–161 °C. **^{1}H-NMR** (300 MHz, $CDCl_3$): δ = 8.45 (d, J = 4.8 Hz, 2H), 7.32–7.13 (m, 7H), 6.76 (t, J = 4.8 Hz, 1H), 4.46 (t, J = 8.0 Hz, 2H), 3.13 (t, J = 8.0 Hz, 2H). **^{13}C-NMR** (101 MHz, $CDCl_3$): δ = 160.8 (C_q), 157.5 (CH), 143.1 (C_q), 137.2 (C_q), 136.9 (C_q), 133.3 (CH), 131.8 (CH), 129.2 (CH), 128.5 (C_q), 127.4 (CH), 126.1 (CH), 116.4 (C_q), 113.3 (CH), 52.6 (CH_2), 29.6 (CH_2). **IR** (ATR): 1572, 1551, 1457, 1392, 798, 745, 724, 698, 687, 478 cm^{-1}. **MS** (ESI) *m/z* (relative intensity): 406 $[M+Na]^+$ (41) (^{79}Br), 384 $[M+H]^+$ (100) (^{79}Br), 275 $[M–SPh]^+$ (23). **HR-MS** (ESI): *m/z* calcd for $C_{18}H_{14}{}^{79}BrN_3SNa^+$ $[M+Na]^+$ 405.9984, found 405.9974. The analytical data are in accordance with those reported in the literature.[206]

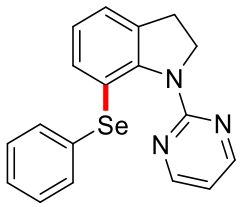

7-(Phenylselanyl)-1-(pyrimidin-2-yl)indoline (137aa)

The general procedure **A** was followed using indoline **133a** (59.2 mg, 0.30 mmol) and diselenide **63a** (93.6 mg, 0.30 mmol). Purification by column chromatography on silica gel (*n*-pentane/Et_2O: 3/1) yielded **137aa** (60.0 mg, 170 µmol, 57%) as a white solid.

M. p.: 153–155 °C. **^{1}H-NMR** (400 MHz, $CDCl_3$): δ = 8.46 (d, *J* = 4.8 Hz, 2H), 7.52–7.44 (m, 2H), 7.26–7.19 (m, 3H), 7.14 (dd, *J* = 7.9, 1.1 Hz, 1H), 7.08 (dd, *J* = 7.2, 1.1 Hz, 1H), 6.82 (dd, *J* = 7.9, 7.2 Hz, 1H), 6.72 (t, *J* = 4.8 Hz, 1H), 4.48 (t, *J* = 7.9 Hz, 2H), 4.48 (t, *J* = 7.9 Hz, 2H). **^{13}C-NMR** (101 MHz, $CDCl_3$): δ = 160.9 (C_q), 157.5 (CH), 144.3 (C_q), 134.9 (C_q), 134.4 (C_q), 134.2 (CH), 132.4 (CH), 129.1 (CH), 127.3 (CH), 124.4 (CH), 123.1 (CH), 122.9 (C_q), 112.8 (CH), 51.6 (CH_2), 29.6 (CH_2). **IR** (ATR): 1573, 1549, 1452, 1424, 1378, 801, 769, 738, 691, 466 cm^{-1}. **MS** (ESI) *m/z* (relative intensity): 354 $[M+H]^+$ (83) (^{80}Se), 197 $[M–SePh]^+$ (100). **HR-MS** (ESI): *m/z* calcd for $C_{18}H_{15}N_3{}^{80}SeNa^+$ $[M+Na]^+$ 376.0332, found 376.0324. The analytical data are in accordance with those reported in the literature.[206]

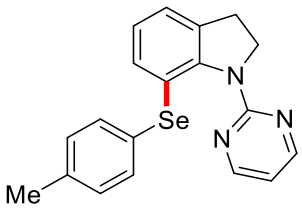

1-(Pyrimidin-2-yl)-7-(*p*-tolylselanyl)indoline (137ab)

The general procedure **A** was followed using indoline **133a** (59.2 mg, 0.30 mmol) and diselenide **63b** (102 mg, 0.30 mmol). Purification by column chromatography on silica gel (*n*-pentane/Et_2O: 3/1) yielded **137ab** (58.3 mg, 159 µmol, 53%) as a white solid.

M. p.: 137–139 °C. **^{1}H-NMR** (400 MHz, $CDCl_3$): δ = 8.46 (d, *J* = 4.7 Hz, 2H), 7.40 (d, *J* = 8.0 Hz, 2H), 7.09 (dd, *J* = 7.9, 1.1 Hz, 1H), 7.07–7.02 (m, 3H) 6.80 (dd, *J* = 7.9, 7.3 Hz, 1H), 6.72 (t, *J* = 4.8 Hz, 1H), 4.48 (t, *J* = 8.0 Hz, 2H), 3.14 (t, *J* = 8.0 Hz, 2H), 2.31 (s, 3H). **^{13}C-NMR** (101 MHz, $CDCl_3$): δ = 160.9 (C_q), 157.6 (CH), 144.0 (C_q), 137.5 (C_q), 134.8 (CH), 134.3 (C_q), 132.0 (CH), 130.9 (C_q), 130.0 (CH), 124.3 (CH), 123.5 (C_q), 122.8 (CH), 112.8 (CH), 51.6 (CH_2), 29.7 (CH_2), 21.3 (CH_3). **IR** (ATR): 1573, 1549, 1452, 1423, 1377, 804, 793, 767, 719, 486 cm^{-1}. **MS** (ESI) *m/z* (relative intensity): 390 $[M+Na]^+$ (100) (^{80}Se), 368 $[M+H]^+$ (19) (^{80}Se), 197 $[M–SePh]^+$ (70). **HR-MS** (ESI): *m/z* calcd for $C_{19}H_{17}N_3{}^{80}SeNa^+$ $[M+Na]^+$ 390.0481,

found 390.0479. The analytical data are in accordance with those reported in the literature.[206]

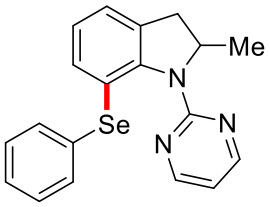

2-Methyl-7-(phenylselanyl)-1-(pyrimidin-2-yl)indoline (137ba)

The general procedure **A** was followed using indoline **133b** (63.4 mg, 0.30 mmol) and diselenide **63a** (93.6 mg, 0.30 mmol). Purification by column chromatography on silica gel (*n*-pentane/Et_2O: 3/1) yielded **137ba** (61.7 mg, 168 µmol, 56%) as a white solid.

M. p.: 138–140 °C. **^{1}H-NMR** (300 MHz, $CDCl_3$): δ = 8.44 (d, *J* = 4.8 Hz, 2H), 7.44 (dd, *J* = 6.6, 3.1 Hz, 2H), 7.25–7.14 (m, 4H), 7.09 (dd, *J* = 7.2, 1.0 Hz, 1H), 6.83 (dd, *J* = 7.9, 7.3 Hz, 1H), 6.71 (t, *J* = 4.8 Hz, 1H), 5.10–4.98 (m, 1H), 3.51 (dd, *J* = 15.6, 8.7 Hz, 1H), 2.60 (d, *J* = 15.6 Hz, 1H), 1.47 (d, *J* = 6.5 Hz, 3H). **^{13}C-NMR** (76 MHz, $CDCl_3$): δ = 160.5 (C_q), 157.6 (CH), 143.0 (C_q), 135.1 (C_q), 134.1 (CH), 133.1 (C_q), 132.7 (CH), 129.1 (CH), 127.2 (CH), 124.4 (CH), 123.7 (CH), 123.3 (C_q), 112.9 (CH), 58.9 (CH), 37.0 (CH_2), 21.4 (CH_3). **IR** (ATR): 1574, 1549, 1457, 1435, 1424, 1381, 1372, 793, 761, 688 cm^{-1}. **MS** (ESI) *m/z* (relative intensity): 390 $[M+Na]^+$ (27) (^{80}Se), 368 $[M+H]^+$ (100) (^{80}Se), 211 $[M–SePh]^+$ (73). **HR-MS** (ESI): *m/z* calcd for $C_{19}H_{17}N_3{}^{80}SeNa^+$ $[M+Na]^+$ 390.0481, found 390.0488.The analytical data are in accordance with those reported in the literature.[206]

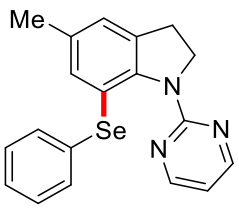

5-Methyl-7-(phenylselanyl)-1-(pyrimidin-2-yl)indoline (137da)

The general procedure **A** was followed using indoline **133d** (63.4 mg, 0.30 mmol) and diselenide **63a** (93.6 mg, 0.30 mmol). Purification by column chromatography on silica gel (*n*-pentane/Et_2O: 3/1) yielded **137da** (59.5 mg, 162 µmol, 54%) as a white solid.

M. p.: 155–157 °C. **^{1}H-NMR** (400 MHz, $CDCl_3$): δ = 8.43 (d, J = 4.8 Hz, 2H), 7.48–7.40 (m, 2H), 7.25–7.17 (m, 3H), 6.96 (dd, J = 1.6, 0.7 Hz, 1H), 6.92–6.90 (m, 1H), 6.69 (t, J = 4.8 Hz, 1H), 4.47 (t, J = 7.9 Hz, 2H), 3.10 (t, J = 7.9 Hz, 2H), 2.15 (s, 3H). **^{13}C-NMR** (101 MHz, $CDCl_3$): δ = 161.1 (C_q), 157.5 (CH), 142.2 (C_q), 135.0 (C_q), 134.5 (C_q), 134.2 (C_q), 133.9 (CH), 132.7 (CH), 129.1 (CH), 127.2 (CH), 124.2 (CH), 122.4 (C_q), 112.6 (CH), 51.7 (CH_2), 29.7 (CH_2), 20.9 (CH_3). **IR** (ATR): 1575, 1547, 1455, 1432, 1401, 1373, 793, 748, 737, 690 cm^{-1}. **MS** (ESI) *m/z* (relative intensity): 390 $[M+Na]^+$ (40) (^{80}Se), 368 $[M+H]^+$ (84) (^{80}Se), 211 $[M–SePh]^+$ (100). **HR-MS** (ESI): *m/z* calcd for $C_{19}H_{17}N_3{}^{80}SeNa^+$ $[M+Na]^+$ 390.0481, found 390.0486. The analytical data are in accordance with those reported in the literature.[206]

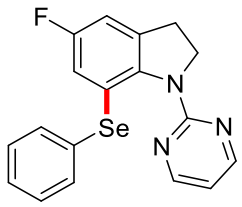

5-Fluoro-7-(phenylselanyl)-1-(pyrimidin-2-yl)indoline (137fa)

The general procedure **A** was followed using indoline **133f** (64.6 mg, 0.30 mmol) and diselenide **63a** (93.6 mg, 0.30 mmol). Purification by column chromatography on silica gel (*n*-pentane/Et_2O: 3/1) yielded **137fa** (68.4 mg, 185 µmol, 62%) as a pale yellow solid.

M. p.: 139–140 °C. **^{1}H-NMR** (400 MHz, $CDCl_3$): δ = 8.45 (d, J = 4.8 Hz, 2H), 7.55–7.50 (m, 2H), 7.31–7.23 (m, 3H), 6.81–6.76 (m, 2H), 6.73 (t, J = 4.8 Hz, 1H), 4.51 (t, J = 8.0 Hz, 2H), 3.12 (t, J = 8.0 Hz, 2H). **^{13}C-NMR** (101 MHz, $CDCl_3$): δ = 160.9 (C_q), 159.5 (d, $^1J_{C\text{-}F}$ = 244.3 Hz, C_q), 157.6 (CH), 140.3 (d, $^4J_{C\text{-}F}$ = 2.1 Hz, C_q), 136.1 (d, $^3J_{C\text{-}F}$ = 8.7 Hz, C_q), 134.9 (CH), 133.8 (C_q), 129.4 (CH), 128.0 (CH), 124.6 (d, $^3J_{C\text{-}F}$ = 7.8 Hz, C_q), 117.9 (d, $^2J_{C\text{-}F}$ = 24.8 Hz, CH), 112.9 (CH), 110.5 (d, $^2J_{C\text{-}F}$ = 24.0 Hz, CH), 51.9 (CH_2), 29.9 (CH_2). **^{19}F{H}-NMR** (282 MHz, $CDCl_3$): δ = −119.5 (s). IR (ATR): 1575, 1453, 1427, 1405, 864, 797, 739, 691, 546, 465 cm^{-1}. **MS** (ESI) *m/z* (relative intensity): 394 $[M+Na]^+$ (20) (^{80}Se), 372 $[M+H]^+$ (100) (^{80}Se), 215 [M–

SePh]$^+$ (72). **HR-MS** (ESI): *m/z* calcd for $C_{18}H_{14}FN_3{}^{80}SeNa^+$ [M+Na]$^+$ 394.0230, found 394.0237. The analytical data are in accordance with those reported in the literature.[206]

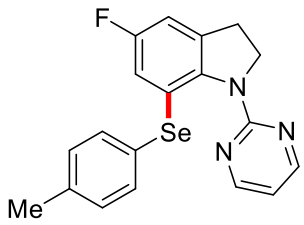

5-Fluoro-1-(pyrimidin-2-yl)-7-(*p*-tolylselanyl)indoline (137fb)

The general procedure **A** was followed using indoline **133f** (64.6 mg, 0.30 mmol) and diselenide **63b** (102 mg, 0.30 mmol). Purification by column chromatography on silica gel (*n*-pentane/Et_2O: 3/1) yielded **137fb** (72.8 mg, 189 µmol, 63%) as a white solid.

M. p.: 133–134 °C. **^{1}H-NMR** (400 MHz, $CDCl_3$): δ = 8.45 (d, J = 4.8 Hz, 2H), 7.43 (d, J = 8.0 Hz, 2H), 7.08 (d, J = 8.0 Hz, 2H), 6.80–6.69 (m, 3H), 4.50 (t, J = 8.0 Hz, 2H), 3.11 (t, J = 8.0 Hz, 2H), 2.33 (s, 3H). **^{13}C-NMR** (101 MHz, $CDCl_3$): δ = 160.8 (C_q), 159.5 (d, $^1J_{C\text{-}F}$ = 244.0 Hz, C_q), 157.6 (CH), 140.0 (d, $^4J_{C\text{-}F}$ = 2.1 Hz, C_q), 138.2 (C_q), 136.0 (d, $^3J_{C\text{-}F}$ = 8.5 Hz, C_q), 135.3 (CH), 130.2 (CH), 129.8 (C_q), 125.1 (d, $^3J_{C\text{-}F}$ = 7.7 Hz, C_q), 117.5 (d, $^2J_{C\text{-}F}$ = 24.9 Hz, CH), 112.8 (CH), 110.2 (d, $^2J_{C\text{-}F}$ = 24.1 Hz, CH) 51.9 (CH_2), 29.9 (CH_2), 21.3 (CH_3). **^{19}F{H}-NMR** (282 MHz, $CDCl_3$): δ = −119.6 (s). IR (ATR): 1578, 1551, 1429, 1406, 906, 856, 793, 727, 546, 488 cm^{-1}. **MS** (ESI) *m/z* (relative intensity): 408 [M+Na]$^+$ (100) (^{80}Se), 215 [M–SeC_6H_4Me]$^+$ (65). **HR-MS** (ESI): *m/z* calcd for $C_{19}H_{16}FN_3{}^{80}SeNa^+$ [M+Na]$^+$ 408.0386, found 408.0384.

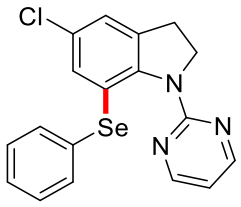

5-Chloro-7-(phenylselanyl)-1-(pyrimidin-2-yl)indoline (137ga)

The general procedure **A** was followed using indoline **133g** (69.5 mg, 0.30 mmol) and diselenide **63a** (93.6 mg, 0.30 mmol). Purification by column chromatography on silica gel (*n*-pentane/Et_2O: 3/1) yielded **137ga** (61.0 mg, 158 µmol, 53%) as a white solid.

M. p.: 154–156 °C. **^{1}H-NMR** (400 MHz, $CDCl_3$): δ = 8.46 (d, *J* = 4.8 Hz, 2H), 7.53–7.45 (m, 2H), 7.31–7.22 (m, 3H), 7.07–7.05 (m, 1H), 7.04–7.02 (m, 1H), 6.75 (t, *J* = 4.8 Hz, 1H), 4.48 (t, *J* = 8.0 Hz, 2H), 3.12 (t, *J* = 8.0 Hz, 2H). **^{13}C-NMR** (101 MHz, $CDCl_3$): δ = 160.7 (C_q), 157.6 (CH), 143.0 (C_q), 136.0 (C_q), 134.6 (CH), 133.9 (C_q), 131.3(CH), 129.4 (CH), 129.0 (C_q), 127.9 (CH), 124.4 (C_q), 123.2 (CH), 113.1 (CH), 51.8 (CH_2), 29.5 (CH_2). **IR** (ATR): 1574, 1552, 1470, 1443, 1401, 857, 799, 750, 695, 636 cm^{-1}. **MS** (ESI) *m/z* (relative intensity): 388 $[M+H]^+$ (100) (^{80}Se), 231 $[M–SePh]^+$ (63). **HR-MS** (ESI): *m/z* calcd for $C_{18}H_{14}ClN_3{}^{80}SeNa^+$ $[M+Na]^+$ 409.9932, found 409.9938. The analytical data are in accordance with those reported in the literature.[206]

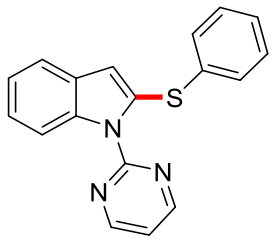

2-(Phenylthio)-1-(pyrimidin-2-yl)-1*H*-indole (72aa)

The general procedure **A** was followed using indole **134a** (58.6 mg, 0.30 mmol) and disulfide **59a** (65.5 mg, 0.30 mmol). Purification by column chromatography on silica gel (*n*-pentane/Et_2O: 7/1) yielded **72aa** (56.4 mg, 186 µmol, 62%) as a white solid.

M. p.: 80–82 °C. **^{1}H-NMR** (400 MHz, $CDCl_3$): δ = 8.80 (d, *J* = 4.8 Hz, 2H), 8.43–8.39 (m, 1H), 7.59–7.53 (m, 2H), 7.42 (ddd, *J* = 7.7, 1.4, 0.7 Hz, 1H) 7.39–7.31 (m, 3H), 7.26 (ddd, *J* = 8.5, 7.2, 1.4 Hz, 1H), 7.19 (ddd, *J* = 7.6, 7.2, 1.1 Hz, 1H), 7.13 (t, *J* = 4.8 Hz, 1H), 6.25 (d, *J* = 0.8 Hz, 1H). **^{13}C-NMR** (101 MHz, $CDCl_3$): δ = 158.0 (CH), 157.6 (C_q), 137.4 (C_q), 135.6 (C_q), 135.2 (C_q), 133.1 (CH), 129.5 (C_q), 129.4 (CH), 128.3 (CH), 123.1 (CH), 122.4 (CH), 119.5 (CH), 117.2 (CH), 114.3 (CH), 109.8 (CH). **IR** (ATR): 1562, 1446, 1423, 1345, 1303, 1207, 741, 702, 691, 613 cm^{-1}. **MS** (ESI) *m/z* (relative intensity): 326 $[M+Na]^+$ (100), 304 $[M+H]^+$

(45). **HR-MS** (ESI): *m/z* calcd for $C_{18}H_{13}N_3SNa^+$ $[M+Na]^+$ 326.0722, found 326.0726. The analytical data are in accordance with those reported in the literature.[219]

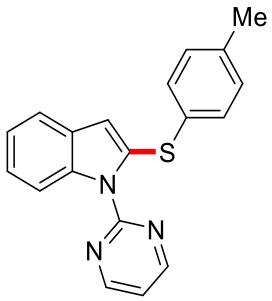

1-(Pyrimidin-2-yl)-2-(*p*-tolylthio)-1*H*-indole (72ab)

The general procedure **A** was followed using indole **134a** (58.6 mg, 0.30 mmol) and disulfide **59b** (73.9 mg, 0.30 mmol). Purification by column chromatography on silica gel (*n*-pentane/Et_2O: 7/1) yielded **72ab** (64.7 mg, 204 µmol, 68%) as a white solid.

M. p.: 91–93 °C. **^{1}H-NMR** (400 MHz, $CDCl_3$): δ = 8.81 (d, *J* = 4.8 Hz, 2H), 8.47–8.42 (m, 1H), 7.53–7.48 (m, 2H), 7.38 (ddd, *J* = 7.6, 1.5, 0.7 Hz, 1H), 7.26–7.15 (m, 4H), 7.14 (t, *J* = 4.8 Hz, 1H), 6.12 (d, *J* = 0.7 Hz, 1H), 2.39 (s, 3H). **^{13}C-NMR** (101 MHz, $CDCl_3$): δ = 157.9 (CH), 157.6 (C_q), 138.8 (C_q), 137.3 (C_q), 137.0 (C_q), 133.9 (CH), 131.1 (C_q), 130.3 (CH), 129.7 (C_q), 122.8 (CH), 122.3 (CH), 119.3 (CH), 117.1 (CH), 114.4 (CH), 108.6 (CH), 21.4 (CH_3). **IR** (ATR): 1561, 1422, 1345, 1300, 1204, 797, 740, 612, 503, 399 cm^{-1}. **MS** (ESI) *m/z* (relative intensity): 340 $[M+Na]^+$ (100), 318 $[M+H]^+$ (63), 195 $[M–SPh]^+$ (53). **HR-MS** (ESI): *m/z* calcd for $C_{19}H_{15}N_3SNa^+$ $[M+Na]^+$ 340.0879, found 340.0874. The analytical data are in accordance with those reported in the literature.[219]

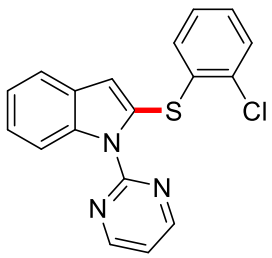

2-[(2-Chlorophenyl)thio]-1-(pyrimidin-2-yl)-*1H*-indole (72af)

The general procedure **A** was followed using indole **134a** (58.6 mg, 0.30 mmol) and disulfide **59f** (86.2 mg, 0.30 mmol). Purification by column chromatography on silica gel (*n*-pentane/Et_2O: 7/1) yielded **72af** (25.2 mg, 74.6 µmol, 25%) as a colorless oil.

^{1}H-NMR (400 MHz, $CDCl_3$): δ = 8.78 (d, *J* = 4.8 Hz, 2H), 8.37 (dd, *J* = 8.3, 0.9 Hz, 1H), 7.48 (ddd, *J* = 7.8, 1.4, 0.7 Hz, 1H), 7.41 (ddd, *J* = 8.0, 8.0, 1.8 Hz, 2H), 7.33–7.10 (m, 5H), 6.43 (d, *J* = 0.7 Hz, 1H). **^{13}C-NMR** (101 MHz, $CDCl_3$): δ = 158.1 (CH), 157.4 (C_q), 137.7 (C_q), 135.5 (C_q), 135.5 (C_q), 133.5 (CH), 131.8 (C_q), 130.1 (CH), 129.3 (C_q), 128.9 (CH), 127.5 (CH), 123.8 (CH), 122.4 (CH), 120.0 (CH), 117.4 (CH), 114.3 (CH), 112.3 (CH). **IR** (ATR): 1561, 1418, 1343, 1303, 1204, 1031, 792, 741, 612, 429 cm^{-1}. **MS** (ESI) *m/z* (relative intensity): 360 $[M+Na]^+$ (35) (^{35}Cl), 338 $[M+H]^+$ (100) (^{35}Cl), 258 $[M–Pym]^+$ (95). **HR-MS** (ESI): *m/z* calcd for $C_{18}H_{13}N_3S^{35}Cl^+$ $[M+H]^+$ 338.0513, found 338.0507. The analytical data are in accordance with those reported in the literature.[219]

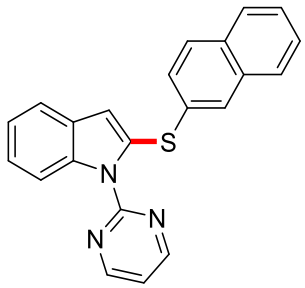

2-(Naphthalen-2-ylthio)-1-(pyrimidin-2-yl)-1*H*-indole (72ag)

The general procedure **A** was followed using indole **134a** (58.6 mg, 0.30 mmol) and disulfide **59g** (95.5 mg, 0.30 mmol). Purification by column chromatography on silica gel (*n*-pentane/Et_2O: 5/1) yielded **72ag** (63.5 mg, 180 µmol, 60%) as an off-white solid.

M. p.: 143–146 °C. **^{1}H-NMR** (400 MHz, $CDCl_3$): δ = 8.81 (d, *J* = 4.8 Hz, 2H), 8.45 (dd, *J* = 8.3, 0.9 Hz, 1H), 8.10 (d, *J* = 1.2 Hz, 1H), 7.88–7.78 (m, 3H), 7.58 (dd, *J* = 8.6, 1.8 Hz, 1H), 7.55–7.49 (m, 2H), 7.39 (ddd, *J* = 7.7, 1.3, 0.7 Hz, 1H), 7.31–7.23 (m, 1H), 7.22–7.16 (m, 1H), 7.14 (t, *J* = 4.8 Hz, 1H), 6.26 (d, *J* = 0.7 Hz, 1H). **^{13}C-NMR** (126 MHz, $CDCl_3$): δ = 157.9 (CH), 157.5 (C_q), 137.3 (C_q), 135.6 (C_q), 133.8 (C_q), 132.9 (C_q), 132.4 (C_q), 132.2 (CH), 130.2 (CH), 129.5 (C_q), 129.1 (CH), 127.8 (CH), 127.8 (CH), 126.7 (CH), 126.6 (CH), 123.1 (CH), 122.4 (CH), 119.5 (CH), 117.1 (CH), 114.3 (CH), 109.9 (CH). **IR** (ATR): 1440, 1424, 1345, 815, 801, 790,

780, 742, 610, 478 cm^{-1}. **MS** (ESI) *m/z* (relative intensity): 376 $[M+Na]^+$ (76), 354 $[M+H]^+$ (100), 169 (79). **HR-MS** (ESI): *m/z* calcd for $C_{22}H_{15}N_3SNa^+$ $[M+Na]^+$ 376.0879, found 376.0887. The analytical data are in accordance with those reported in the literature.[219]

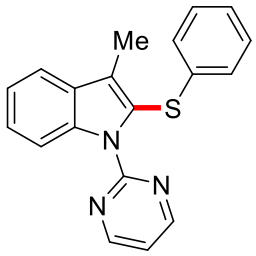

3-Methyl-2-(phenylthio)-1-(pyrimidin-2-yl)-1*H*-indole (72ba)

The general procedure **A** was followed using indole **134b** (62.8 mg, 0.30 mmol) and disulfide **59a** (65.5 mg, 0.30 mmol). Purification by column chromatography on silica gel (*n*-pentane/Et_2O: 7/1) yielded **72ba** (70.7 mg, 225 µmol, 75%) as a slightly yellow solid.

M. p.: 102–104 °C. **^{1}H-NMR** (400 MHz, $CDCl_3$): δ = 8.75 (d, *J* = 4.8 Hz, 2H), 8.15–8.12 (m, 1H), 7.64 (ddd, *J* = 7.8, 1.3, 0.8 Hz, 1H), 7.38 (ddd, *J* = 8.4, 7.2, 1.3 Hz, 1H), 7.29 (ddd, *J* = 7.8, 7.1, 1.1 Hz, 1H), 7.19–7.13 (m, 2H), 7.11 (t, *J* = 4.8 Hz, 1H), 7.09–7.04 (m, 3H), 2.38 (s, 3H). **^{13}C-NMR** (126 MHz, $CDCl_3$): δ = 158.1 (CH), 157.3 (C_q), 138.1 (C_q), 137.7 (C_q), 129.3 (C_q), 128.8 (CH), 126.7 (CH), 125.4 (CH), 125.3(C_q), 125.0 (C_q), 125.0 (CH) 121.8 (CH), 119.3 (CH), 117.6 (CH), 113.1 (CH), 10.3 (CH_3). **IR** (ATR): 1559, 1442, 1419, 1339, 1308, 1196, 742, 691 631, 474 cm^{-1}. **MS** (ESI) *m/z* (relative intensity): 340 $[M+Na]^+$ (100), 318 $[M+H]^+$ (93), 209 $[M–SPh]^+$ (53). **HR-MS** (ESI): *m/z* calcd for $C_{19}H_{15}N_3SNa^+$ $[M+Na]^+$ 340.0879, found 340.0873. The analytical data are in accordance with those reported in the literature.[219]

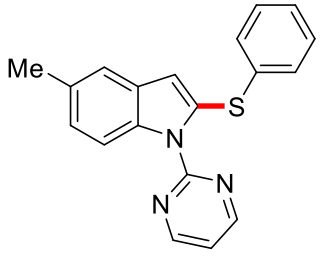

5-Methyl-2-(phenylthio)-1-(pyrimidin-2-yl)-1*H*-indole (72ca)

The general procedure **A** was followed using indole **134c** (62.8 mg, 0.30 mmol) and disulfide **59a** (65.5 mg, 0.30 mmol). Purification by column chromatography on silica gel (*n*-pentane/Et_2O: 7/1) yielded **72ca** (59.7 mg, 188 µmol, 63%) as a yellow oil.

^{1}H-NMR (400 MHz, $CDCl_3$): δ = 8.78 (d, *J* = 4.8 Hz, 2H), 8.30 (d, *J* = 8.4 Hz, 1H), 7.58–7.52 (m, 2H), 7.39–7.30 (m, 3H), 7.21–7.19 (m, 1H), 7.11 (t, *J* = 4.8 Hz, 1H), 7.07 (ddd, *J* = 8.5, 1.8, 0.8 Hz, 1H), 6.17 (d, *J* = 0.8 Hz, 1H), 2.42 (s, 3H). **^{13}C-NMR** (126 MHz, $CDCl_3$): δ = 157.8 (CH), 157.5 (C_q), 135.6 (C_q), 135.3 (C_q), 135.3 (C_q), 132.9 (CH), 131.7 (C_q), 129.6 (C_q), 129.3 (CH), 128.1 (CH), 124.5 (CH), 119.3 (CH), 116.9 (CH), 114.1 (CH), 109.7 (CH), 21.5 (CH_3). **IR** (ATR): 1573, 1560, 1451, 1419, 1156, 798, 738, 726, 689, 630 cm^{-1}. **MS** (ESI) *m/z* (relative intensity): 340 $[M+Na]^+$ (100), 318 $[M+H]^+$ (76), 209 $[M–SPh]^+$ (30). **HR-MS** (ESI): *m/z* calcd for $C_{19}H_{15}N_3SNa^+$ $[M+Na]^+$ 340.0879, found 340.0874.

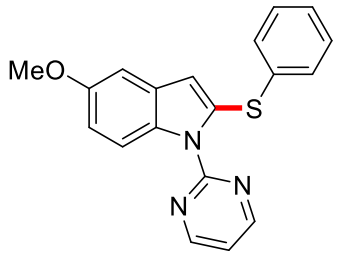

5-Methoxy-2-(phenylthio)-1-(pyrimidin-2-yl)-1*H*-indole (72da)

The general procedure **A** was followed using indole **134d** (67.6 mg, 0.30 mmol) and disulfide **59a** (65.5 mg, 0.30 mmol). Purification by column chromatography on silica gel (*n*-pentane/Et_2O: 5/1) yielded **72da** (48.0 mg, 144 µmol, 48%) as a yellow oil.

^{1}H-NMR (400 MHz, $CDCl_3$): δ = 8.77 (d, *J* = 4.8 Hz, 2H), 8.35 (dd, *J* = 9.8, 0.8 Hz, 1H), 7.59–7.56 (m, 2H), 7.40–7.34 (m, 3H), 7.12 (t, *J* = 4.8 Hz, 1H), 6.88–6.83 (m, 2H), 6.08 (d, *J* = 0.8 Hz, 1H), 3.82 (s, 3H). **^{13}C-NMR** (101 MHz, $CDCl_3$): δ = 157.9 (CH), 157.6 (C_q), 155.7 (C_q), 136.5 (C_q), 135.0 (C_q), 133.5 (CH), 132.3 (C_q), 130.3 (C_q), 129.5 (CH), 128.5 (CH), 116.9 (CH), 115.5 (CH), 112.0 (CH), 109.1 (CH), 101.7 (CH), 55.8 (CH_3). **IR** (ATR): 1463, 1426, 1323, 1158, 826, 797, 753, 727, 962, 491 cm^{-1}. **MS** (ESI) *m/z* (relative intensity): 356 $[M+Na]^+$ (70), 334 $[M+H]^+$ (100), 234 $[M–SPh]^+$ (56). **HR-MS** (ESI): *m/z* calcd for $C_{19}H_{16}N_3OS^+$ $[M+H]^+$

334.1009, found 334.1002. The analytical data are in accordance with those reported in the literature.[219]

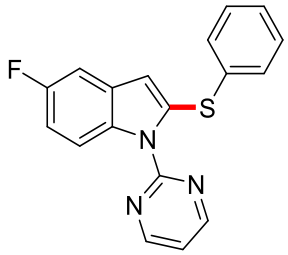

5-Fluoro-2-(phenylthio)-1-(pyrimidin-2-yl)-1*H*-indole (72ea)

The general procedure **A** was followed using indole **134e** (64.0 mg, 0.30 mmol) and disulfide **59a** (65.5 mg, 0.30 mmol). Purification by column chromatography on silica gel (*n*-pentane/Et_2O: 9/1) yielded **72ea** (55.0 mg, 171 µmol, 57%) as a colorless oil.

^{1}H-NMR (400 MHz, $CDCl_3$): δ = 8.79 (d, J = 4.9 Hz, 2H), 8.41 (dd, J = 9.1, 4.7 Hz, 1H), 7.63–7.57 (m, 2H), 7.43–7.36 (m, 3H), 7.15 (t, J = 4.8 Hz, 1H), 7.02 (ddd, J = 9.0, 2.6, 0.8 Hz, 1H), 6.98–6.91 (m, 1H), 6.04 (d, J = 0.8 Hz, 1H). **^{13}C-NMR** (101 MHz, $CDCl_3$): δ = 159.2 (d, $^1J_{C\text{-}F}$ = 238.1 Hz, C_q), 158.0 (CH), 157.4 (C_q), 138.5 (C_q), 134.4 (C_q), 133.9 (CH), 133.7 (C_q), 130.4 (d, $^3J_{C\text{-}F}$ = 10.3 Hz, C_q), 129.6 (CH), 128.8 (CH), 117.2 (CH), 115.6 (d, $^3J_{C\text{-}F}$ = 9.1 Hz, CH), 110.5 (d, $^2J_{C\text{-}F}$ = 25.0 Hz, CH), 108.2 (d, $^4J_{C\text{-}F}$ = 4.1 Hz, CH), 104.5 (d, $^2J_{C\text{-}F}$ = 23.9 Hz, CH). **^{19}F{H}-NMR** (282 MHz, $CDCl_3$): δ = −121.57 (s). **IR** (ATR): 1563, 1421, 1154, 1108, 797, 777, 749, 689, 561, 492 cm^{-1}. **MS** (ESI) *m/z* (relative intensity): 360 $[M+K]^+$ (76), 344 $[M+Na]^+$ (100), 322 $[M+H]^+$ (76), 213 $[M–SPh]^+$ (28). **HR-MS** (ESI): *m/z* calcd for $C_{18}H_{12}N_3FSNa^+$ $[M+Na]^+$ 344.0628, found 344.0618.

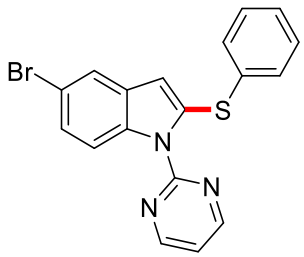

5-Bromo-2-(phenylthio)-1-(pyrimidin-2-yl)-1H-indole (72fa)

The general procedure **A** was followed using indole **134f** (82.2 mg, 0.30 mmol) and disulfide **59a** (65.5 mg, 0.30 mmol). Purification by column chromatography on silica gel (*n*-pentane/Et_2O: 7/1) yielded **72fa** (58.3 mg, 152 µmol, 51%) as a white solid.

M. p.: 129–130 °C. **^{1}H-NMR** (400 MHz, $CDCl_3$): δ = 8.80 (d, *J* = 4.8 Hz, 2H), 8.32 (d, *J* = 8.9 Hz, 1H), 7.61–7.55 (m, 2H), 7.50–7.47 (m, 1H), 7.43–7.35 (m, 3H), 7.29 (dd, *J* = 8.9, 2.0 Hz, 1H), 7.17 (t, *J* = 4.8 Hz, 1H), 6.02 (d, *J* = 0.7 Hz, 1H). **^{13}C-NMR** (101 MHz, $CDCl_3$): δ = 158.0 (CH), 157.4 (C_q), 138.3 (C_q), 135.9 (C_q), 134.3 (C_q), 133.9 (CH), 131.3 (C_q), 129.8 (CH), 128.9 (CH), 125.5 (CH), 121.8 (CH), 117.4 (CH), 116.1 (CH), 115.7 (C_q), 107.7 (CH). **IR** (ATR): 1574, 1429, 1302, 1198, 794, 780, 747, 692, 628, 425 cm^{-1}. **MS** (ESI) *m/z* (relative intensity): 404 $[M+Na]^+$ (49) (^{79}Br), 382 $[M+H]^+$ (100) (^{79}Br). **HR-MS** (ESI): *m/z* calcd for $C_{18}H_{12}N_3{}^{79}BrSNa^+$ $[M+Na]^+$ 403.9828, found 403.9818. The analytical data are in accordance with those reported in the literature.[219]

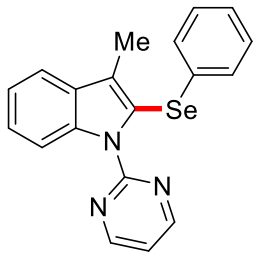

3-Methyl-2-(phenylselanyl)-1-(pyrimidin-2-yl)-1*H*-indole (138ba)

The general procedure **A** was followed using indole **134b** (62.8 mg, 0.30 mmol) and diselenide **63a** (93.6 mg, 0.30 mmol). Purification by column chromatography on silica gel (*n*-pentane/Et_2O: 7/1) yielded **138ba** (71.9 mg, 197 µmol, 66%) as a colorless oil.

^{1}H-NMR (400 MHz, $CDCl_3$): δ = 8.78 (d, *J* = 4.8 Hz, 2H), 8.35–8.31 (m, 1H), 7.57 (ddd, *J* = 7.7, 1.3, 0.7 Hz, 1H), 7.35 (ddd, *J* = 8.4, 7.2, 1.3 Hz, 1H), 7.31–7.23 (m, 3H), 7.20–7.14 (m, 3H), 7.12 (t, *J* = 4.8 Hz, 1H), 2.18 (s, 3H). **^{13}C-NMR** (101 MHz, $CDCl_3$): δ = 157.9 (CH), 157.7 (C_q), 137.9 (C_q), 133.7 (C_q), 130.4 (C_q), 130.4 (CH) 129.1 (CH), 126.4 (CH), 124.4 (CH), 123.7 (C_q), 123.6 (C_q), 121.9 (CH), 118.8 (CH), 117.1 (CH), 113.4 (CH), 11.3 (CH_3). **IR** (ATR): 1559, 1419, 1345, 1304, 1188, 732, 703, 688, 627, 615 cm^{-1}. **MS** (ESI) *m/z* (relative intensity): 388 $[M+Na]^+$ (74) (^{80}Se), 209 $[M–SePh]^+$ (100). **HR-MS** (ESI): *m/z* calcd for $C_{19}H_{15}N_3{}^{80}SeNa^+$

$[M+Na]^+$ 388.0324, found 388.0314. The analytical data are in accordance with those reported in the literature.[219]

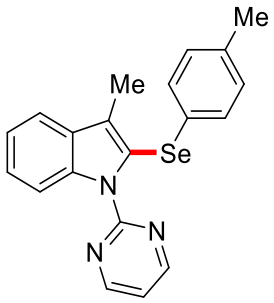

3-Methyl-1-(pyrimidin-2-yl)-2-(*p*-tolylselanyl)-1*H*-indole (138bb)

The general procedure **A** was followed using indole **134b** (62.8 mg, 0.30 mmol) and diselenide **63b** (102 mg, 0.30 mmol). Purification by column chromatography on silica gel (*n*-pentane/Et_2O: 8/1) yielded **138bb** (82.8 mg, 219 µmol, 73%) as a colorless oil.

^{1}H-NMR (400 MHz, $CDCl_3$): δ = 8.78 (d, J = 4.8 Hz, 2H), 8.35–8.31 (m, 1H), 7.56 (ddd, J = 7.7, 1.4, 0.7 Hz, 1H), 7.34 (ddd, J = 8.3, 7.1, 1.4 Hz, 1H), 7.29–7.24 (m, 1H), 7.23–7.19 (m, 2H), 7.12 (t, J = 4.8 Hz, 1H), 7.01–6.97 (m, 2H), 2.28 (s, 3H), 2.15 (s, 3H). **^{13}C-NMR** (101 MHz, $CDCl_3$): δ = 157.8 (CH), 157.7 (C_q), 137.8 (C_q), 136.3 (C_q), 130.8 (CH), 130.5 (C_q), 129.9 (CH), 129.8 (C_q), 124.2 (CH), 124.1 (C_q), 123.3 (C_q), 121.8 (CH), 118.6 (CH), 117.1 (CH), 113.3 (CH), 21.1 (CH_3), 11.2 (CH_3). **IR** (ATR): 1560, 1421, 1346, 1305, 1181, 1014, 800, 742, 628, 487 cm^{-1}. **MS** (ESI) *m/z* (relative intensity): 402 $[M+Na]^+$ (18) (^{80}Se), 380 $[M+H]^+$ (32) (^{80}Se), 209 $[M–SeC_6H_4Me]^+$ (100). **HR-MS** (ESI): *m/z* calcd for $C_{20}H_{18}N_3{}^{80}Se^+$ $[M+H]^+$ 380.0661, found 380.0647.

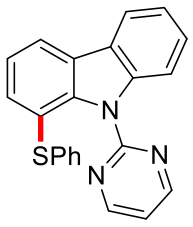

1-(Phenylthio)-9-(pyrimidin-2-yl)-*9H*-carbazole (70aa)

The general procedure **A** was followed using carbazole **155a** (73.6 mg, 0.30 mmol) and disulfide **59a** (65.5 mg, 0.30 mmol). Purification by column chromatography on silica gel (*n*-pentane/Et_2O: 3/1) yielded **70aa** (20.9 mg, 59.0 µmol, 20%) as a colorless oil.

^{1}H-NMR (300 MHz, $CDCl_3$): δ = 8.78 (d, *J* = 4.8 Hz, 2H), 8.13–8.01 (m, 3H), 7.50–7.42 (m, 2H), 7.39–7.04 (m, 8H). **^{13}C-NMR** (126 MHz, $CDCl_3$): δ = 158.7 (C_q), 158.4 (CH), 141.3 (C_q), 140.3 (C_q) 137.8 (C_q), 133.1 (CH), 129.8 (CH), 128.9 (CH), 127.1 (C_q), 127.0 (CH), 126.4 (CH), 125.0 (C_q), 122.8 (CH), 122.3 (CH), 120.5 (C_q), 120.1 (CH), 119.7 (CH), 118.3 (CH), 112.6 (CH). **IR** (ATR): 1562, 1449, 1413, 1335, 1211, 904, 723, 688, 647, 633 cm^{-1}. **MS** (ESI) *m/z* (relative intensity): 376 $[M+Na]^+$ (92), 354 $[M+H]^+$ (100), 245 $[M–SPh]^+$ (47). **HR-MS** (ESI): *m/z* calcd for $C_{22}H_{15}N_3SNa^+$ $[M+Na]^+$ 376.0879, found 376.0867. The analytical data are in accordance with those reported in the literature.[78]

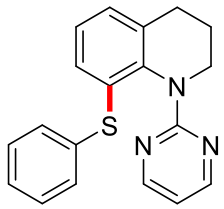

8-(Phenylthio)-1-(pyrimidin-2-yl)-1,2,3,4-tetrahydroquinoline (157aa)

The general procedure **A** was followed using tetrahydroquinoline **156a** (63.4 mg, 0.30 mmol) and disulfide **59a** (65.5 mg, 0.30 mmol). Purification by column chromatography on silica gel (*n*-pentane/Et_2O: 3/1) yielded **157aa** (16.2 mg, 50.7 µmol, 17%) as a colorless oil.

^{1}H-NMR (300 MHz, $CDCl_3$): δ = 8.38 (d, *J* = 4.8 Hz, 2H), 7.27–6.96 (m, 8H), 6.64 (t, *J* = 4.8 Hz, 1H), 4.02 (t, *J* = 6.9 Hz, 2H), 2.77 (t, *J* = 6.9 Hz, 2H), 2.03 (tt, *J* = 6.9, 6.9 Hz, 2H). **^{13}C-NMR** (76 MHz, $CDCl_3$): δ = 161.6 (C_q), 157.6 (CH), 141.0 (C_q), 138.0 (C_q), 134.9 (C_q), 133.0 (C_q), 131.5 (CH), 130.6 (CH), 128.8 (CH), 127.7 (CH), 126.3 (CH), 125.3 (CH), 112.0 (CH), 45.3 (CH_2), 27.1 (CH_2), 24.5 (CH_2). **IR** (ATR): 1577, 1550, 1413, 1299, 1187, 795, 777, 734, 689, 637 cm^{-1}. **MS** (ESI): *m/z* (relative intensity): 320 $[M+H]^+$ (100), 210 $[M–SPh]^+$ (22). **HR-MS** (ESI) *m/z* calcd for $C_{19}H_{18}N_3S^+$ $[M+H]^+$ 320.1216, found 320.1213.

5.3.3 Mechanistic Studies

5.3.3.1 Reaction in the Presence of Radical Scavengers

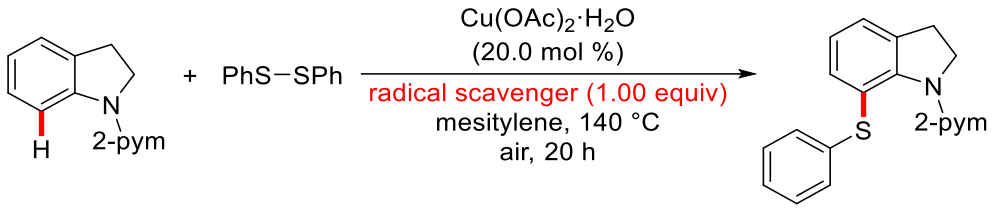

133a **59a** **135aa**

To an oven-dried 25 mL Schlenk tube were added disulfide **59a** (65.5 mg, 0.30 mmol, 1.00 equiv), $Cu(OAc)_2 \cdot H_2O$ (12.0 mg, 0.06 mmol, 20.0 mol %) and radical scavenger (0.30 mmol, 1.00 equiv). A solution of indoline **133a** (59.2 mg, 0.30 mmol, 1.00 equiv) in mesitylene (1.5 mL) was added *via* syringe and the resulting mixture was stirred under ambient air for 20 h at 140 °C. After cooling to ambient temperature, the reaction mixture was diluted with Et_2O (10 mL) and filtered through a short pad of silica. The filtrate was concentrated, and the crude residue was purified by column chromatography (*n*-pentane/Et_2O: 5/1).

Table 5.1: Effect of Radical Scavengers on the reaction.[a]

Entry	Radical scavenger (1.00 equiv)	Yield [%]
1	--	66
2	TEMPO	23
3	Galvinoxyl free radical	--
4	BHT	--

[a] Reaction conditions: **133a** (0.30 mmol), **59a** (0.30 mmol), $Cu(OAc)_2 \cdot H_2O$ (0.06 mmol, 20.0 mol %), mesitylene (1.5 mL), radical scavenger (1.00 equiv), 140 °C, 20 h, yields of isolated products.

5.3.3.2 H/D Exchange Experiments

5.3.3.2.1 In the Absence of Disulfide 59a

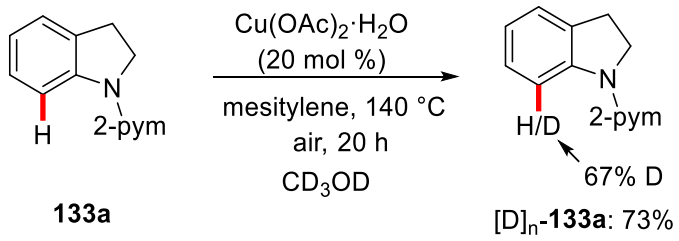

133a

[D]$_n$-**133a**: 73%

To an oven-dried 25 mL Schlenk tube was added $Cu(OAc)_2 \cdot H_2O$ (12.0 mg, 0.06 mmol, 20.0 mol %). A solution of indoline **133a** (59.2 mg, 0.30 mmol, 1.00 equiv) in mesitylene (1.3 mL) and CD_3OD (0.2 mL) were added *via* syringe and the resulting mixture was stirred under ambient air for 20 h at 140 °C. After cooling to ambient temperature, the reaction mixture was diluted with Et_2O (10 mL) and filtered through a short pad of silica. The filtrate was concentrated and the crude residue was purified by column chromatography on silica gel (*n*-pentane/Et_2O: 3/1) yielding [D]$_n$-**133a** (43.0 mg, 73%).

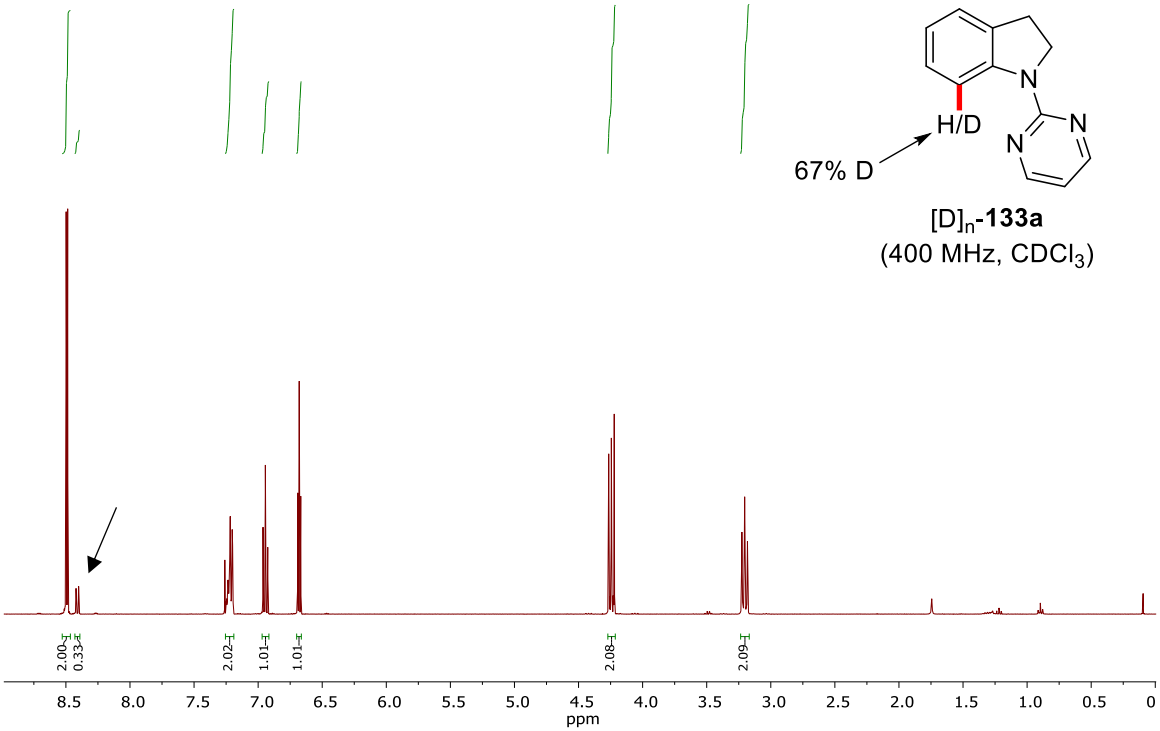

Figure 5.4: ^{1}H-NMR spectra of reisolated **133a**.

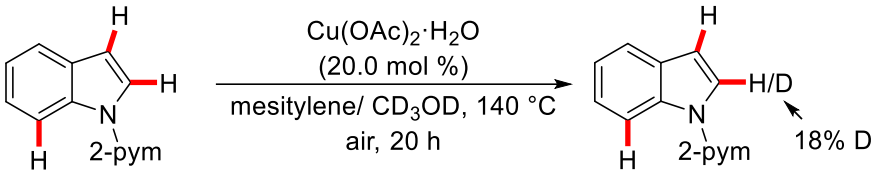

134a

[D]$_n$-**134a**: 73%

To an oven-dried 25 mL Schlenk tube were added indole **134a** (58.6 mg, 0.30 mmol) and $Cu(OAc)_2 \cdot H_2O$ (12.0 mg, 0.06 mmol, 20 mol %). Mesitylene (1.3 mL) and CD_3OD (0.2 mL) were added *via* syringe and the resulting mixture was stirred under ambient air for 20 h at 140 °C. After cooling to ambient temperature, the reaction mixture was diluted with Et_2O (10 mL) and filtered through a short pad of silica. The filtrate was concentrated and the crude residue was purified by column chromatography on silica gel (*n*-pentane/Et_2O: 5/1) yielding [D]$_n$-**134a** (42.8 mg, 73%).

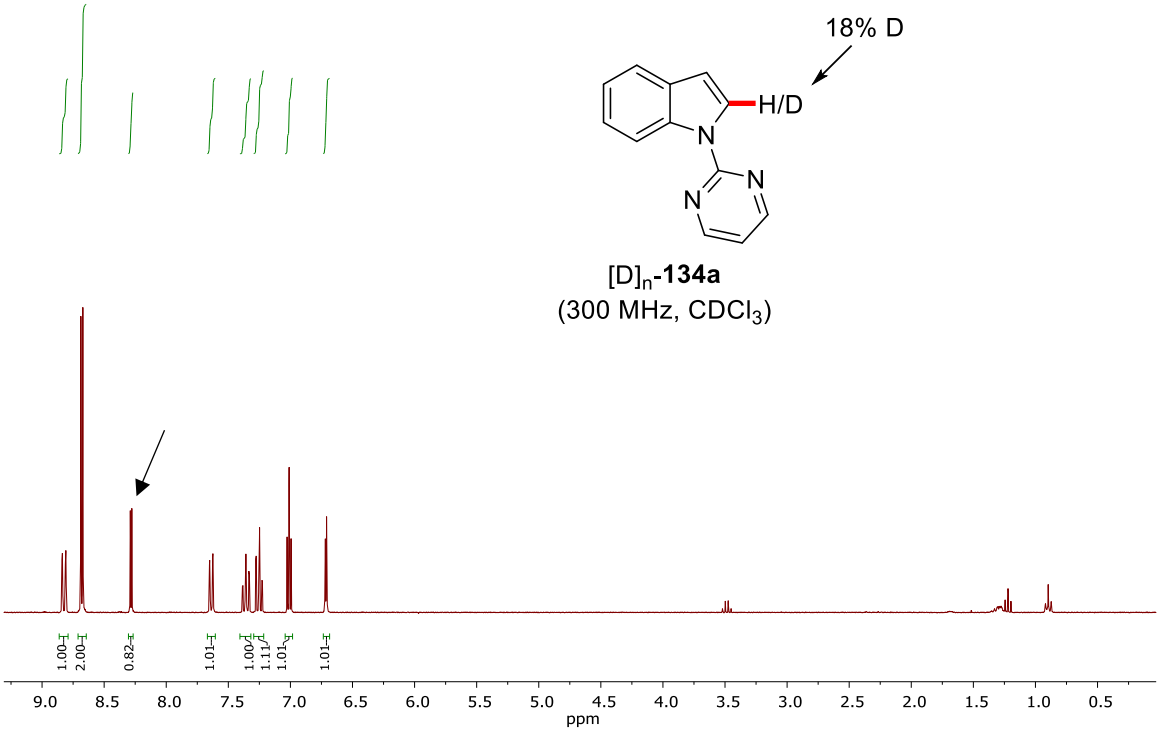

Figure 5.5: ^{1}H-NMR spectra of reisolated [D]$_n$-**134a**.

5.3.3.2.2 In the Presence of Disulfide 59a

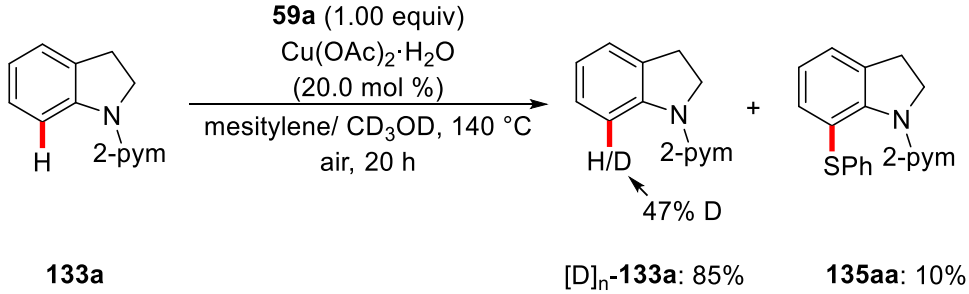

133a [D]$_n$-**133a**: 85% **135aa**: 10%

To an oven-dried 25 mL Schlenk tube was added disulfide **59a** (65.5 mg, 0.30 mmol, 1.00 equiv) and $Cu(OAc)_2 \cdot H_2O$ (12.0 mg, 20 mol %). A solution of indoline **133a** (59.2 mg, 0.30 mmol, 1.00 equiv) in mesitylene (1.3 mL) and CD_3OD (0.2 mL) were added *via* syringe and the resulting mixture was stirred under ambient air for 20 h at 140 °C. After cooling to ambient temperature, the reaction mixture was diluted with Et_2O (10 mL) and filtered through a short pad of silica. The filtrate was concentrated, and the crude residue was purified by column chromatography on silica gel (*n*-pentane/Et_2O: 3/1) yielding the product **135aa** (9.0 mg, 10%) and reisolated [D]$_n$-**133a** (50.0 mg, 85%).

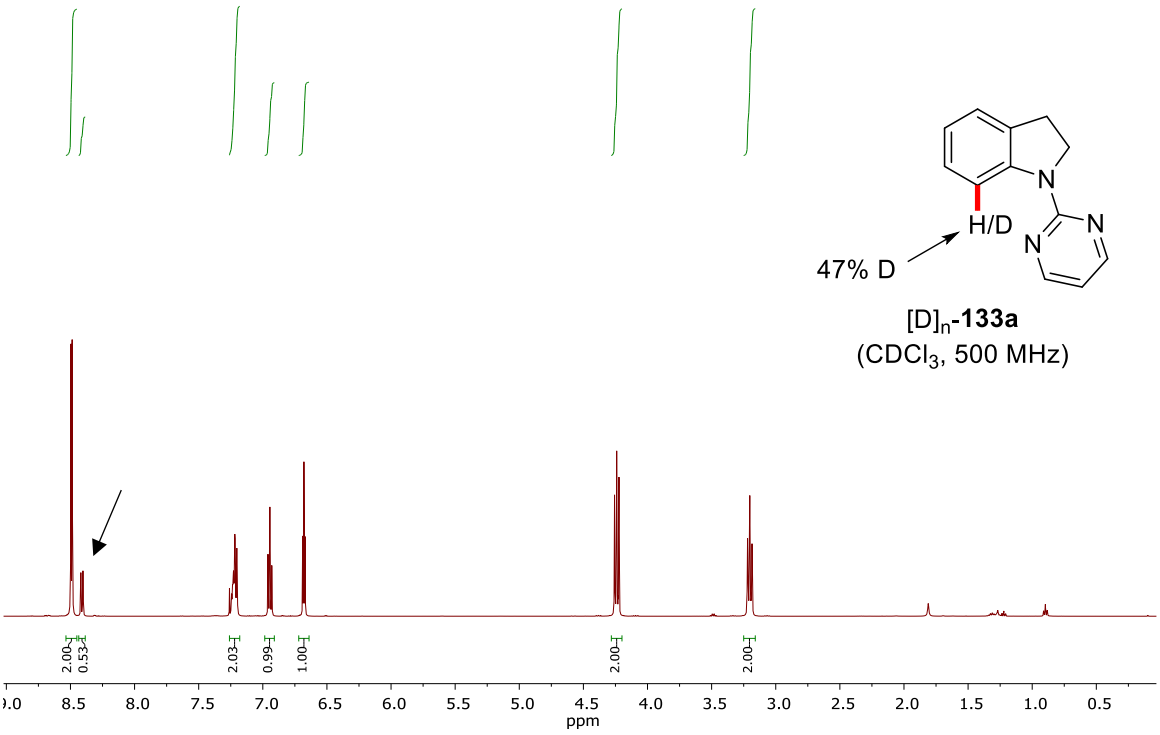

Figure 5.6: ^{1}H-NMR spectra of reisolated [D]$_n$-**133a**.

5.4 Visible Light-Induced Decarboxylative C–H Adamantylation

5.4.1 Synthesis and Characterization of Starting Materials

The following benzothiazoles **140b**-**140j** have been prepared in the course of the bachelor thesis of N. Imse.[190] They were prepared according a previously described procedure starting from 2-aminobenzothiazoles.[220] For compounds that had not been reported before, the analytical data is given below.

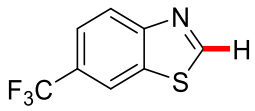

6-(Trifluoromethyl)benzo[*d*]thiazole (140d)

M. p.: 36–40 °C. **^{1}H-NMR** (300 MHz, $CDCl_3$): δ = 9.16 (s, 1H), 8.29–8.27 (m, 1H), 8.26–8.22 (m, 1H), 7.78–7.75 (m, 1H). **^{13}C-NMR** (126 MHz, $CDCl_3$): δ = 156.7 (CH), 155.0 (C_q), 133.8 (C_q), 127.8 (q, $^2J_{C\text{-}F}$ = 32.7 Hz, C_q), 124.1 (CH), 124.0 (q, $^1J_{C\text{-}F}$ = 272 Hz, C_q), 123.1 (q, $^3J_{C\text{-}F}$ = 3.0 Hz, CH), 119.6 (q, $^3J_{C\text{-}F}$ = 4.1 Hz, CH). **^{19}F-NMR** (282 MHz, $CDCl_3$): δ = -61.5 (s). **IR** (ATR): 1315, 1293, 1160, 1102, 1077, 1046, 886, 843, 818, 718 cm^{-1}. **MS** (ESI) *m/z* (relative intensity): 373 (100), 204 $[M+H]^+$ (45). **HR-MS** (ESI): *m/z* calcd for $C_8H_5F_3NS^+$ $[M+H]^+$ 204.0089, found 204.0092.

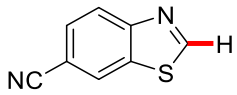

Benzo[*d*]thiazole-6-carbonitrile (140j)

M. p.: 136–137 °C. **^{1}H-NMR** (300 MHz, $CDCl_3$): δ = 9.19 (s, 1H), 8.30 (s, 1H), 8.20 (d, *J* = 8.5 Hz, 1H), 7.75 (dd, *J* = 8.5, 1.2 Hz, 1H). **^{13}C-NMR** (126 MHz, $CDCl_3$): δ = 157.9 (CH), 155.4 (C_q), 134.3 (C_q), 129.2 (CH), 126.9 (CH), 124.5 (CH), 118.5 (C_q), 109.3 (C_q). **IR** (ATR): 1469, 1401, 1290, 1261, 897, 851, 833, 821, 772, 610 cm^{-1}. **MS** (ESI) *m/z* (relative intensity): 161 $[M+H]^+$ (100). **HR-MS** (ESI): *m/z* calcd for $C_8H_5N_2S^+$ $[M+H]^+$ 161.0168, found 161.0169.

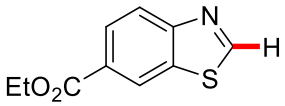

Ethyl benzo[*d*]thiazole-6-carboxylate (140h)

M. p.: 59–62 °C. **^{1}H-NMR** (300 MHz, $CDCl_3$): δ = 9.12 (s, 1H), 8.68 (s, 1H), 8.19-8.12 (m, 2H), 4.40 (q, *J* = 7.2 Hz, 2H), 1.41 (t, *J* = 7.2 Hz, 3H). **^{13}C-NMR** (126 MHz, $CDCl_3$): δ = 165.9 (C_q), 157.0 (CH), 155.8 (C_q), 133.6 (C_q), 127.7 (C_q), 127.2 (CH), 124.0 (CH), 123.3 (CH), 61.3 (CH_2), 14.4 (CH_3). **IR** (ATR): 1702, 1279, 1246, 1130, 1101, 1019, 856, 767, 746, 727 cm^{-1}. **MS** (ESI) *m/z* (relative intensity): 208 $[M+H]^+$ (100). **HR-MS** (ESI): *m/z* calcd for $C_{10}H_{10}NO_2S^+$ $[M+H]^+$ 208.0427, found 208.0431.

The following compound was prepared according to a modified literature procedure.[221]

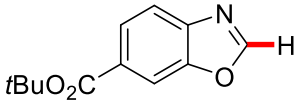

***tert*-Butyl benzo[*d*]oxazole-6-carboxylate (14f)**

To a solution of benzo[*d*]oxazole-6-carboxylic acid (510 mg, 3.13 mmol, 1.00 equiv) in CH_2Cl_2 (15 mL) DMF (0.1 mL) was added and the solution was cooled to 0 °C. Oxalyl chloride (597 mg, 4.70 mmol, 1.50 equiv) was added dropwise at 0 °C. The solution was allowed to warm to ambient temperature and was stirred for 1.5 h. A mixture of *tert*-butanol and pyridine (1:1, 6 mL) was added dropwise and the solution was stirred for 20 h. The solvent was removed under reduced pressure and H_2O (20 mL) and EtOAc (20 mL) were added. The phases were separated, and the aqueous phase was extracted with EtOAc (2 x 20 mL). The combined organic layers were washed with brine and dried over Na_2SO_4. The solvent was removed under reduced pressure yielding the crude product as a brown oil. Purification of the residue by column chromatography on silica gel (*n*-pentane/Et_2O: 10/1→6/1) yielded **14f** (360 mg, 1.64 mmol, 52%) as a white solid.

M. p.: 70–72 °C. **^{1}H-NMR** (300 MHz, $CDCl_3$): δ = 8.20 (dd, *J* = 1.5, 0.6 Hz, 1H), 8.18 (s, 1H), 8.03 (dd, *J* = 8.4, 1.5 Hz, 1H), 7.77 (dd, *J* = 8.4, 0.6 Hz, 1H), 1.60 (s, 9H). **^{13}C NMR** (76 MHz,

$CDCl_3$): δ = 165.0 (C_q), 154.6 (CH), 149.6 (C_q), 143.4 (C_q), 129.8 (C_q), 126.1 (CH), 120.0 (CH), 112.5 (CH), 81.5 (C_q), 28.2 (CH_3). **IR** (ATR): 1700, 1316, 1299, 1166, 1114, 1066, 844, 771, 748, 424 cm^{-1}. **MS** (ESI) *m/z* (relative intensity): 337 (100), 242 $[M+Na]^+$ (58), 220 $[M+H]^+$ (3). **HR-MS** (ESI): *m/z* calcd for $C_{12}H_{14}NO_3^+$ $[M+H]^+$ 220.0968, found 220.0961.

5.4.2 Analytical Data

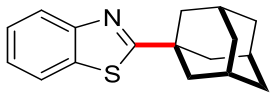

2-[(3*R*,5*R*,7*R*)-Adamantan-1-yl]benzo[*d*]thiazole (142a)

The general procedure **B** was followed using benzothiazole **140a** (54.1 mg, 0.40 mmol) and 1-adamantanecarboxylic acid (**141**) (216 mg, 1.20 mmol) for 24 h. Purification by column chromatography on silica gel (*n*-pentane/Et_2O: 30/1) yielded **142a**. (89.3 mg, 331 µmol, 83%) as a white solid.

M. p.: 103–104 °C. **^{1}H-NMR** (400 MHz, $CDCl_3$): δ = 8.00 (ddd, *J* = 8.2, 1.2, 0.7 Hz, 1H), 7.86 (ddd, *J* = 7.2, 1.2, 0.7 Hz, 1H), 7.44 (ddd, *J* = 8.2, 7.2, 1.2 Hz, 1H), 7.32 (ddd, *J* = 8.2, 7.2, 1.2 Hz, 1H), 2.18–2.12 (m, 9H), 1.86–1.81 (m, 6H). **^{13}C NMR** (101 MHz, $CDCl_3$): δ = 182.3 (C_q), 153.3 (C_q), 134.5 (C_q), 125.8 (CH), 124.5 (CH), 122.8 (CH), 121.7 (CH), 43.1 (CH_2), 40.3 (C_q), 36.7 (CH_2), 28.7 (CH). **IR** (ATR): 2898, 2845, 1506, 1434, 1168, 999, 963, 754, 725, 680 cm^{-1}. **MS** (ESI) *m/z* (relative intensity): 270 $[M+H]^+$ (100). **HR-MS** (ESI): *m/z* calcd for $C_{17}H_{20}NS^+$ $[M+H]^+$ 270.1311, found 270.1313. The analytical data are in accordance with those reported in the literature.[171a]

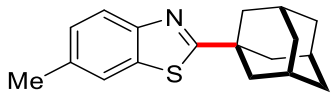

2-[(3R,5*R*,7*R*)-Adamantan-1-yl]-6-methylbenzo[*d*]thiazole (142b)

The general procedure **B** was followed using benzothiazole **140b** (59.7 mg, 0.40 mmol) and 1-adamantanecarboxylic acid (**141**) (216 mg, 1.20 mmol) for 24 h. After aqueous

workup, purification by column chromatography on silica gel (*n*-pentane/Et_2O: 30/1) yielded **142b** (60.6 mg, 214 µmol, 53%) as a white solid.

M. p.: 132–133 °C. **^{1}H-NMR** (400 MHz, $CDCl_3$): δ = 7.87 (d, J = 8.3 Hz, 1H), 7.65–7.62 (m, 1H), 7.24 (ddd, J = 8.2, 1.7, 0.6 Hz, 1H), 2.46 (s, 3H), 2.16–2.11 (m, 9H), 1.83–1.80 (m, 6H). **^{13}C-NMR** (101 MHz, $CDCl_3$): δ = 181.2 (C_q), 151.4 (C_q), 134.6 (C_q), 134.5 (C_q), 127.3 (CH), 122.2 (CH), 121.4 (CH), 43.1 (CH_2), 40.2 (C_q), 36.7 (CH_2), 28.7 (CH), 21.6 (CH_3). **IR** (ATR): 2899, 2845, 1510, 1449, 1164, 1000, 835, 812, 679, 569 cm^{-1}. **MS** (ESI) *m/z* (relative intensity): 284 $[M+H]^+$ (100). **HR-MS** (ESI): *m/z* calcd for $C_{18}H_{22}NS^+$ $[M+H]^+$ 284.1467, found 284.1471. The analytical data are in accordance with those reported in the literature.[222]

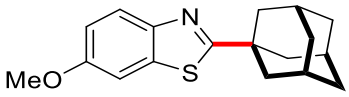

2-[(3*R*,5*R*,7*R*)-Adamantan-1-yl]-6-methoxylbenzo[*d*]thiazole (142c)

The general procedure **B** was followed using benzothiazole **140c** (66.1 mg, 0.40 mmol) and 1-adamantanecarboxylic acid (**141**) (216 mg, 1.20 mmol) for 24 h. Purification by column chromatography on silica gel (*n*-pentane/Et_2O: 25/1) yielded **142c** (70.2 mg, 234 µmol, 59%) as a white solid.

M. p.: 118–119 °C. **^{1}H-NMR** (400 MHz, $CDCl_3$): δ = 7.87 (dd, J = 8.9, 0.4 Hz, 1H), 7.31 (d, J = 2.5 Hz, 1H), 7.03 (dd, J = 8.9, 2.5 Hz, 1H), 3.85 (s, 3H), 2.15–2.11 (m, 9H), 1.82-1.79 (m, 6H). **^{13}C-NMR** (101 MHz, $CDCl_3$) δ = 179.8 (C_q), 157.3 (C_q), 147.8 (C_q), 135.7 (C_q), 123.2 (CH), 114.9 (CH), 104.4 (CH), 55.9 (CH_3), 43.1 (CH_2), 40.1 (C_q), 36.7 (CH_2), 28.7 (CH). **IR** (ATR): 2904, 1467, 1450, 1435, 1261, 1223, 1028, 1000, 834, 827 cm^{-1}. **MS** (ESI) *m/z* (relative intensity): 300 $[M+H]^+$ (100). **HR-MS** (ESI): *m/z* calcd for $C_{18}H_{22}NOS^+$ $[M+H]^+$ 300.1417, found 300.1419. The analytical data are in accordance with those reported in the literature.[222]

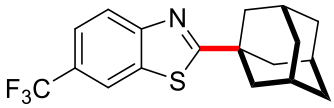

2-[(3*R*,5*R*,7*R*)-Adamantan-1-yl]-6-(trifluoromethyl)benzo[*d*]thiazole (142d)

The general procedure **B** was followed using benzothiazole **140d** (81.3 mg, 0.40 mmol) and 1-adamantanecarboxylic acid (**141**) (216 mg, 1.20 mmol) for 48 h. Purification by column chromatography on silica gel (*n*-pentane/Et_2O: 30/1) yielded **142d**. (96.3 mg, 285 µmol, 71%) as a white solid.

M. p.: 183–184 °C. **^{1}H-NMR** (400 MHz, $CDCl_3$): δ = 8.15 (dq, J = 1.8, 0.7 Hz, 1H), 8.07 (dt, J = 8.6, 0.7 Hz, 1H), 7.68 (ddd, J = 8.6, 1.8, 0.7 Hz, 1H), 2.19–2.14 (m, 9H), 1.87–1.80 (m, 6H). **^{13}C-NMR** (101 MHz, $CDCl_3$): δ = 185.7 (C_q), 155.4 (C_q), 134.7 (C_q), 126.8 (q, $^2J_{C\text{-}F}$ = 32.7 Hz, C_q), 124.4 (q, $^1J_{C\text{-}F}$ = 272 Hz, C_q) 123.1 (CH), 122.8 (q, $^3J_{C\text{-}F}$ = 3.5 Hz, CH), 119.2 (q, $^3J_{C\text{-}F}$ = 4.2 Hz, CH) 43.1 (CH_2), 40.7 (C_q), 36.6 (CH_2), 28.7 (CH). **^{19}F{H}-NMR** (376 MHz, $CDCl_3$): δ = –61.3 (s). **IR** (ATR): 2911, 1317, 1278, 1163, 1112, 1085, 1001, 880, 829, 681 cm^{-1}. **MS** (ESI) *m/z* (relative intensity): 338 $[M+H]^+$ (13), 300 (100). **HR-MS** (ESI): *m/z* calcd for $C_{18}H_{19}F_3NS^+$ $[M+H]^+$ 338.1185, found 338.1188.

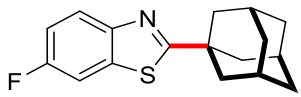

2-[(3*R*,5*R*,7*R*)-Adamantan-1-yl]-6-fluorobenzo[*d*]thiazole (142e)

The general procedure **B** was followed using benzothiazole **140e** (61.3 mg, 0.40 mmol) and 1-adamantanecarboxylic acid (**141**) (216 mg, 1.20 mmol) for 24 h. Purification by column chromatography on silica gel (*n*-pentane/Et_2O: 30/1) yielded **142e** (62.1 mg, 216 µmol, 54%) as a white solid.

M. p.: 107–108 °C. **^{1}H-NMR** (400 MHz, $CDCl_3$): δ = 7.91 (ddd, J = 8.9, 4.8, 0.4 Hz, 1H), 7.52 (ddd, J = 8.2, 2.6, 0.4 Hz, 1H), 7.16 (ddd, J = 8.9, 8.2, 2.6 Hz, 1H), 2.16–2.12 (m, 9H), 1.83–1.79 (m, 6H). **^{13}C-NMR** (101 MHz, $CDCl_3$): δ = 182.0 (d, $^5J_{C\text{-}F}$ = 3.1 Hz, C_q), 160.2 (d, $^1J_{C\text{-}F}$ = 244.2 Hz, C_q), 149.9 (d, $^4J_{C\text{-}F}$ = 1.6 Hz, C_q), 135.5 (d, $^3J_{C\text{-}F}$ = 11.2 Hz, C_q), 123.6 (d, $^3J_{C\text{-}F}$ = 9.4 Hz, CH), 114.3 (d, $^2J_{C\text{-}F}$ = 24.6 Hz, CH), 107.8 (d, $^3J_{C\text{-}F}$ = 26.4 Hz, CH), 43.1 (CH_2), 40.4 (C_q), 36.6 (CH_2), 28.7 (CH). **^{19}F{H}-NMR** (376 MHz, $CDCl_3$): δ = –117.4 (s). **IR** (ATR): 2911, 2889, 1454, 1245, 1161, 1001, 915, 836, 800, 791 cm^{-1}. **MS** (ESI) *m/z* (relative intensity):

288 [M+H]$^{+}$ (100). **HR-MS** (ESI): *m/z* calcd for $C_{17}H_{19}NSF^{+}$ [M+H]$^{+}$ 288.1217, found 288.1219.

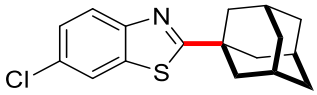

2-[(3*R*,5*R*,7*R*)-Adamantan-1-yl]-6-chlorobenzo[*d*]thiazole (142f)

The general procedure **B** was followed using benzothiazole **140f** (67.9 mg, 0.40 mmol) and 1-adamantanecarboxylic acid (**141**) (216 mg, 1.20 mmol) for 24 h. Purification by column chromatography on silica gel (*n*-pentane/Et_2O: 30/1) yielded **142f** (71.8 mg, 236 µmol, 59%) as a white solid.

M. p.: 145–146 °C. **^{1}H-NMR** (400 MHz, $CDCl_3$): δ = 7.88 (dd, *J* = 8.7, 0.4 Hz, 1H), 7.81 (dd, *J* = 2.1, 0.4 Hz, 1H), 7.38 (dd, *J* = 8.7, 2.1 Hz, 1H), 2.16–2.11 (m, 9H), 1.84–1.79 (m, 6H). **^{13}C-NMR** (101 MHz, $CDCl_3$): δ = 182.8 (C_q), 151.9 (C_q), 135.8 (C_q), 130.4 (C_q), 126.6 (CH), 123.5 (CH), 121.3 (CH), 43.1 (CH_2), 40.4 (C_q), 36.6 (CH_2), 28.7 (CH). **IR** (ATR): 2898, 2844, 1514, 1435, 1259, 1097, 999, 802, 768, 680 cm^{-1}. **MS** (ESI) *m/z* (relative intensity): 304 [M+H]$^{+}$ (100). **HR-MS** (ESI): *m/z* calcd for $C_{17}H_{19}{}^{35}ClNS^{+}$ [M+H]$^{+}$ 304.0921, found 304.0924. The analytical data are in accordance with those reported in the literature.[222]

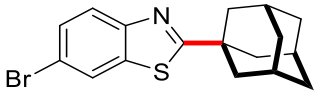

2-[(3*R*,5*R*,7*R*)-Adamantan-1-yl]-6-bromobenzo[*d*]thiazole (142g)

The general procedure **B** was followed using benzothiazole **140g** (85.6 mg, 0.40 mmol) and 1-adamantanecarboxylic acid (**141**) (216 mg, 1.20 mmol) for 24 h. Purification by column chromatography on silica gel (*n*-pentane/Et_2O: 30/1) yielded **142g** (75.1 mg, 216 µmol, 54%) as a white solid.

M. p.: 182–183 °C. **^{1}H-NMR** (400 MHz, $CDCl_3$): δ = 7.97 (dd, *J* = 2.0, 0.4 Hz, 1H), 7.82 (dd, *J* = 8.7, 0.4 Hz, 1H), 7.52 (dd, *J* = 8.7, 2.0 Hz, 1H), 2.16– 2.11 (m, 9H), 1.83–1.78 (m, 6H). **^{13}C-NMR** (76 MHz, $CDCl_3$): δ = 182.9 (C_q), 152.2 (C_q), 136.3 (C_q), 129.2 (CH), 124.2 (CH),

123.9 (CH), 118.0 (C_q), 43.0 (CH_2), 40.4 (C_q), 36.6 (CH_2), 28.6 (CH). **IR** (ATR): 2907, 2847, 1438, 1269, 1086, 1000, 860, 814, 804, 682 cm^{-1}. **MS** (ESI) *m/z* (relative intensity): 348 $[M+H]^+$ (100) (^{79}Br). **HR-MS** (ESI): *m/z* calcd for $C_{17}H_{19}{}^{79}BrNS^+$ $[M+H]^+$ 348.0416, found 348.0420.

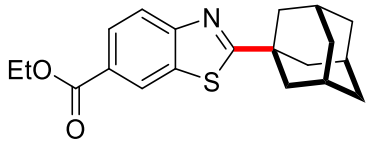

Ethyl 2-[(3*R*,5*R*,7*R*)-adamantan-1-yl]benzo[*d*]thiazole-6-carboxylate (142h)

The general procedure **B** was followed using benzothiazole **140h** (82.9 mg, 0.40 mmol) and 1-adamantanecarboxylic acid (**141**) (216 mg, 1.20 mmol) for 48 h. Purification by column chromatography on silica gel (*n*-pentane/Et_2O: 15/1) yielded **142h** (60.0 mg, 176 µmol, 44%) as a white solid.

M. p.: 131–133 °C. **^{1}H-NMR** (400 MHz, $CDCl_3$): δ = 8.58 (dd, *J* = 1.7, 0.6 Hz, 1H), 8.12 (dd, *J* = 8.6, 1.7 Hz, 1H), 8.00 (dd, *J* = 8.6, 0.6 Hz, 1H), 4.41 (q, *J* = 7.1 Hz, 2H), 2.16–2.12 (m, 9H), 1.84–1.80 (m, 6H), 1.41 (t, *J* = 7.1 Hz, 3H). **^{13}C-NMR** (101 MHz, $CDCl_3$): δ = 186.0 (C_q), 166.4 (C_q), 156.3 (C_q), 134.4 (C_q), 127.1 (CH), 126.7 (C_q), 123.9 (CH), 122.4 (CH), 61.3 (CH_2), 43.0 (CH_2), 40.7 (C_q), 36.6 (CH_2), 28.6 (CH), 14.5 (CH_3). **IR** (ATR): 2899, 1707, 1272, 1231, 1106, 1001, 850, 772, 730, 681 cm^{-1}. **MS** (ESI) *m/z* (relative intensity): 342 $[M+H]^+$ (100). **HR-MS** (ESI): *m/z* calcd for $C_{20}H_{24}NO_2S^+$ $[M+H]^+$ 342.1522, found 342.1524.

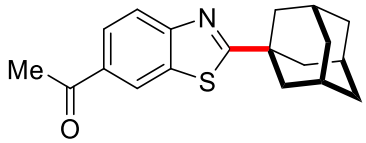

1-{2-[(3*R*,5*R*,7*R*)-adamantan-1-yl]benzo[*d*]thiazol-6-yl}ethan-1-one (142i)

The general procedure **B** was followed using benzothiazole **140i** (70.9 mg, 0.40 mmol) and 1-adamantanecarboxylic acid (**141**) (216 mg, 1.20 mmol) for 48 h. Purification by column chromatography on silica gel (*n*-pentane/Et_2O: 5/1) yielded **142i** (40.3 mg, 129 µmol, 32%) as a white solid.

M. p.: 121–122 °C. **^{1}H-NMR** (400 MHz, $CDCl_3$): δ = 8.50 (dd, *J* = 1.6, 0.8 Hz, 1H), 8.04 (dd, *J* = 8.6, 1.6 Hz, 1H), 8.01 (dd, *J* = 8.6, 0.8 Hz, 1H), 2.67 (s, 3H), 2.18–2.12 (m, 9H), 1.84–1.80 (m, 6H). **^{13}C-NMR** (101 MHz, $CDCl_3$): δ = 197.4 (C_q), 186.6 (C_q), 156.4 (C_q), 134.9 (C_q), 133.5 (C_q), 126.1 (CH), 122.7 (CH), 122.6 (CH), 43.0 (CH_2), 40.8 (C_q), 36.6 (CH_2), 28.6 (CH), 27.0 (CH_3). **IR** (ATR): 2916, 2878, 1676, 1451, 1348, 1267, 1236, 1004, 824, 586 cm^{-1}. **MS** (ESI) *m/z* (relative intensity): 312 $[M+H]^+$ (100). **HR-MS** (ESI): *m/z* calcd for $C_{19}H_{22}NOS^+$ $[M+H]^+$ 312.1417, found 312.1419.

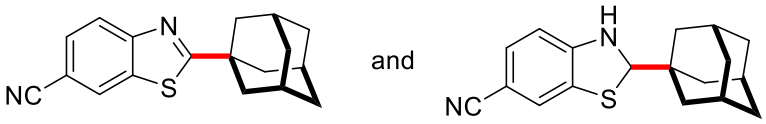

2-[(3*R*,5*R*,7*R*)-Adamantan-1-yl]benzo[*d*]thiazole-6-carbonitrile (142j) and 2-[(1*S*,3*S*)-Adamantan-1-yl]-2,3-dihydrobenzo[*d*]thiazole-6-carbonitrile (142j')

The general procedure **B** was followed using benzothiazole **140j** (64.1 mg, 0.40 mmol) and 1-adamantanecarboxylic acid (**141**) (180 mg, 0.90 mmol) for 24 h. Purification by column chromatography on silica gel (n-pentane/Et_2O: 10/1→5/1) yielded benzothiazole **142j** (21.0 mg, 71.3 µmol, 18%) and the dihydrobenzothiazole **142j'** (35.0 mg, 118 µmol, 30%) as white solids.

2-[(3*R*,5*R*,7*R*)-Adamantan-1-yl]benzo[*d*]thiazole-6-carbonitrile (142j)

M. p.: 172-173 °C. **^{1}H-NMR** (400 MHz, $CDCl_3$): δ = 8.19 (dd, *J* = 1.6, 0.7 Hz, 1H), 8.04 (dd, *J* = 8.5, 0.6 Hz, 1H), 7.68 (dd, *J* = 8.5, 1.6 Hz, 1H), 2.15 (s, 9H), 1.83 (s, 6H). **^{13}C-NMR** (101 MHz, $CDCl_3$): δ = 187.0 (C_q), 155.8 (C_q), 135.1 (C_q), 129.1 (CH), 126.6 (CH), 123.6 (CH), 119.1 (C_q), 108.0 (C_q), 43.0 (CH_2), 40.9 (C_q), 36.5 (CH_2), 28.6 (CH). **IR** (ATR): 2898, 2855, 2230, 1506, 1448, 1156, 996, 871, 817, 595 cm^{-1}. **MS** (ESI) *m/z* (relative intensity): 474 (100), 318 (90), 317 $[M+Na]^+$ (79), 295 $[M+H]^+$ (72). **HR-MS** (ESI): *m/z* calcd for $C_{18}H_{18}N_2SNa^+$ $[M+Na]^+$ 317.1083, found 317.1080. The analytical data are in accordance with those reported in the literature.[222]

2-[(1*S*,3*S*)-Adamantan-1-yl]-2,3-dihydrobenzo[*d*]thiazole-6-carbonitrile (142j')

M. p.: 56-58 °C. **^{1}H-NMR** (400 MHz, $CDCl_3$): δ = 7.20–7.09 (m, 2H), 6.45 (d, *J* = 8.1 Hz, 1H), 5.08 (d, *J* = 2.1 Hz, 1H), 4.79 (s, 1H), 2.03 (t, *J* = 3.2 Hz, 3H), 1.76–1.68 (m, 3H), 1.67–1.56 (m, 6H), 1.53–1.46 (m, 3H). **^{13}C-NMR** (101 MHz, $CDCl_3$): δ = 151.2 (C_q), 130.8 (CH), 127.1 (C_q), 124.1 (CH), 120.2 (C_q), 106.9 (CH), 100.8 (C_q), 78.6 (CH), 38.8 (C_q), 37.8 (CH_2), 36.9 (CH_2), 28.1 (CH). **IR** (ATR): 3348, 2900, 2846, 2209, 1586, 1489, 1448, 1192, 811, 585 cm^{-1}. **MS** (ESI) *m/z* (relative intensity): 319 $[M+Na]^+$ (42), 297 $[M+H]^+$ (81), 231 (100). **HR-MS** (ESI): *m/z* calcd for $C_{18}H_{20}N_2SNa^+$ $[M+Na]^+$ 319.1239, found 319.1236.

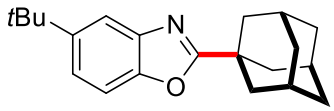

2-[(3*R*,5*R*,7*R*)-Adamantan-1-yl]-5-(*tert*-butyl)benzo[*d*]oxazole (143b)

The general procedure **B** was followed using benzoxazole **14b** (66.1 mg, 0.40 mmol) and 1-adamantanecarboxylic acid (**141**) (216 mg, 1.20 mmol) for 48 h. Purification by column chromatography on silica gel (*n*-pentane/Et_2O: 20/1) yielded **143b** (56.0 mg, 182 µmol, 45%) as a white solid.

M. p.: 159–160 °C. **^{1}H-NMR** (600 MHz, $CDCl_3$): δ = 7.74 (dd, *J* = 2.0, 0.6 Hz, 1H), 7.39 (dd, *J* = 8.6, 0.6 Hz, 1H), 7.34 (dd, *J* = 8.6, 2.0 Hz, 1H), 2.15–2.13 (m, 6H), 2.12–2.10 (m, 3H), 1.81 (t, *J* = 2.9 Hz, 6H), 1.36 (s, 9H). **^{13}C-NMR** (126 MHz, $CDCl_3$): δ = 173.2 (C_q), 148.5 (C_q), 147.5 (C_q), 141.2 (C_q), 121.9 (CH), 116.4 (CH), 109.5 (CH), 40.5 (CH_2), 36.7 (CH_2), 36.3 (C_q), 35.0 (C_q), 32.0 (CH_3), 28.2 (CH). **IR** (ATR): 2906, 2849, 1561, 1480, 1452, 1272, 1041, 924, 800 cm^{-1}. **MS** (ESI) *m/z* (relative intensity): 332 $[M+Na]^+$ (2), 310 $[M+H]^+$ (100). **HR-MS** (ESI): *m/z* calcd for $C_{21}H_{28}NO$ $[M+H]^+$ 310.2165, found 310.2168.

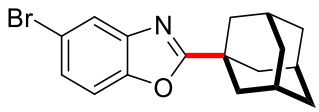

2-[(3*R*,5*R*,7*R*)-Adamantan-1-yl]-5-bromobenzo[*d*]oxazole (143c)

The general procedure **B** was followed using benzoxazole **14c** (79.2 mg, 0.40 mmol) and 1-adamantanecarboxylic acid (**141**) (216 mg, 1.20 mmol) for 48 h. Purification by column

chromatography on silica gel (*n*-pentane/Et_2O: 20/1) yielded **143c** (56.1 mg, 169 µmol, 42%) as a white solid.

M. p.:135–136 °C. **^{1}H-NMR** (600 MHz, $CDCl_3$): δ = 7.80 (d, *J* = 1.9 Hz, 1H), 7.38 (dd, *J* = 8.4, 1.9 Hz, 1H), 7.34 (d, *J* = 8.4 Hz, 1H), 2.14–2.11 (m, 9H), 1.84–1.77 (m, 6H). **^{13}C-NMR** (126 MHz, $CDCl_3$): δ = 174.2 (C_q), 150.0 (C_q), 143.0 (C_q), 127.3 (CH), 122.8 (CH), 116.7 (C_q), 111.6 (CH), 40.3 (CH_2), 36.6 (CH_2), 36.4 (C_q), 28.1 (CH). **IR** (ATR): 2905, 2849, 1555, 1444, 1253, 1040, 907, 871, 798, 682 cm^{-1}. **MS** (ESI) *m/z* (relative intensity): 334 $[M+H]^+$ (97) (^{81}Br), 332 $[M+H]^+$ (100) (^{79}Br). **HR-MS** (ESI): *m/z* calcd for $C_{17}H_{19}{}^{79}BrNO^+$ $[M+H]^+$ 332.0645, found 332.0648.

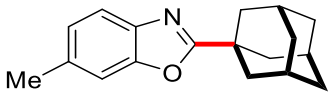

2-[(3*R*,5*R*,7*R*)-Adamantan-1-yl]-6-methylbenzo[*d*]oxazole (143d)

The general procedure **B** was followed using benzoxazole **14d** (53.3 mg, 0.40 mmol) and 1-adamantanecarboxylic acid (**141**) (216 mg, 1.20 mmol) for 48 h. Purification by column chromatography on silica gel (*n*-pentane/Et_2O: 20/1) yielded **143d** (53.0 mg, 198 µmol, 50%) as a white solid.

M. p.: 112–114 °C. **^{1}H-NMR** (400 MHz, $CDCl_3$): δ = 7.55 (d, *J* = 8.1 Hz, 1H), 7.29–7.27 (m, 1H), 7.11–7.08 (m, 1H), 2.46 (s, 3H), 2.16–2.10 (m, 9H), 1.83–1.79 (m, 6H). **^{13}C-NMR** (101 MHz, $CDCl_3$): δ = 172.6 (C_q), 150.9 (C_q), 139.1 (C_q), 134.7 (C_q), 125.2 (CH), 119.1 (CH), 110.7 (CH), 40.4 (CH_2), 36.6 (CH_2), 36.2 (C_q), 28.1 (CH), 21.8 (CH_3). **IR** (ATR): 2908, 2849, 1566, 1451, 1263, 1234, 1040, 919, 809, 602 cm^{-1}. **MS** (ESI) *m/z* (relative intensity): 290 $[M+Na]^+$ (9), 268 $[M+H]^+$ (100). **HR-MS** (ESI): *m/z* calcd for $C_{18}H_{22}NO$ $[M+H]^+$ 268.1696, found 268.1697.

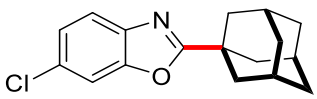

2-[(3*R*,5*R*,7*R*)-Adamantan-1-yl]-6-chlorobenzo[*d*]oxazole (143e)

The general procedure **B** was followed using benzoxazole **14e** (50.2 mg, 0.40 mmol) and 1-adamantanecarboxylic acid (**141**) (216 mg, 1.20 mmol) for 48 h. Purification by column chromatography on silica gel (*n*-pentane/Et_2O: 10/1) yielded **143e** (52.5 mg, 182 µmol, 46%) as a white solid.

M. p.: 150–152 °C. **^{1}H-NMR** (400 MHz, $CDCl_3$): δ = 7.58 (dd, *J* = 8.5, 0.4 Hz, 1H), 7.50–7.46 (m, 1H), 7.26 (dd, *J* = 8.5, 2.0 Hz, 1H), 2.16–2.10 (m, 9H), 1.84–1.78 (m, 6H). **^{13}C-NMR** (101 MHz, $CDCl_3$): δ = 173.8 (C_q), 150.9 (C_q), 140.2 (C_q), 130.0 (C_q), 124.7 (CH), 120.3 (CH), 111.2 (CH), 40.3 (CH_2), 36.6 (CH_2), 36.3 (C_q), 28.0 (CH). **IR** (ATR): 2915, 2851, 1609, 1564, 1460, 1039, 819, 800, 702, 599 cm^{-1}. **MS** (ESI) *m/z* (relative intensity): 288 $[M+H]^+$ (60). **HR-MS** (ESI): *m/z* calcd for $C_{17}H_{19}NO^{35}Cl$ $[M+H]^+$ 288.1150, found 288.1153.

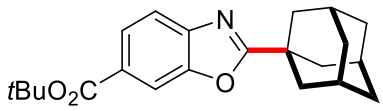

***tert*-Butyl 2-[(3*R*,5*R*,7*R*)-adamantan-1-yl]benzo[*d*]oxazole-6-carboxylate (143f)**

The general procedure **B** was followed using benzoxazole **14f** (87.7 mg, 0.40 mmol) and 1-adamantanecarboxylic acid (**141**) (216 mg, 1.20 mmol) for 48 h. Purification by column chromatography on silica gel (*n*-pentane/Et_2O: 10/1) yielded **143f** (52.8 mg, 161 µmol, 40%) as a white solid.

M. p.: 116–118 °C. **^{1}H-NMR** (400 MHz, $CDCl_3$): δ = 8.12 (dd, *J* = 1.5, 0.6 Hz, 1H), 7.98 (dd, *J* = 8.3, 1.5 Hz, 1H), 7.67 (dd, *J* = 8.3, 0.6 Hz, 1H), 2.17–2.10 (m, 9H), 1.83–1.79 (m, 6H), 1.60 (s, 9H). **^{13}C-NMR** (101 MHz, $CDCl_3$): δ = 175.6 (C_q), 165.5 (C_q), 150.3 (C_q), 145.0 (C_q), 128.6 (C_q), 125.8 (CH), 119.1 (CH), 112.0 (CH), 81.3 (C_q), 40.2 (CH_2), 36.5 (CH_2), 36.5 (C_q), 28.4 (CH_3), 28.0 (CH). **IR** (ATR): 2904, 1710, 1291, 1268, 1244, 1154, 1044, 943, 777 cm^{-1}. **MS** (ESI) *m/z* (relative intensity): 354 $[M+H]^+$ (100), 298 (14). **HR-MS** (ESI): *m/z* calcd for $C_{22}H_{28}NO_3$ $[M+H]^+$ 354.2064, found 354.2064.

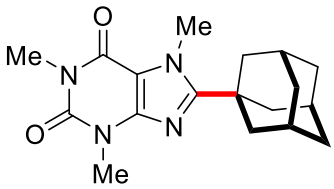

8-[(3*R*,5*R*,7*R*)-Adamantan-1-yl]-1,3,7-trimethyl-3,7-dihydro-1*H*-purine-2,6-dione (164)

The general procedure **B** was followed using caffeine **162** (77.6 mg, 0.40 mmol) and 1-adamantanecarboxylic acid (**141**) (180 mg, 1.20 mmol) for 48 h. Purification by column chromatography on silica gel (*n*-pentane/Et_2O: 1/1) yielded **164** (80.4 mg, 245 µmol, 61%) as a white solid.

M. p.: 263–264 °C. **^{1}H-NMR** (400 MHz, $CDCl_3$): δ = 4.15 (s, 3H), 3.54 (s, 3H), 3.37 (s, 3H), 2.16–2.08 (m, 9H), 1.81–1.74 (m, 6H). **^{13}C-NMR** (101 MHz, $CDCl_3$): δ = 159.6 (C_q), 155.8 (C_q), 151.9 (C_q), 147.2 (C_q), 108.2 (C_q), 40.0 (CH_2), 36.9 (C_q), 36.6 (CH_2), 34.5 (CH_3), 29.7 (CH_3), 28.3 (CH), 28.0 (CH_3). **IR** (ATR): 2895, 1700, 1660, 1539, 1426, 1361, 1223, 982, 743 cm^{-1}. **MS** (ESI) *m/z* (relative intensity): 329 $[M+H]^+$ (100). **HR-MS** (ESI): *m/z* calcd for $C_{18}H_{25}N_4O_2^+$ $[M+H]^+$ 329.1972, found 329.1969.

The analytical data are in accordance with those reported in the literature.[145c]

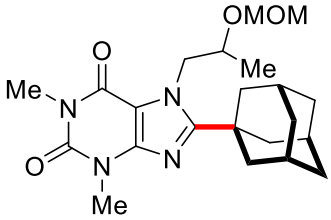

8-[(3*R*,5*R*,7*R*)-Adamantan-1-yl]-7-[2-(methoxymethoxy)propyl]-1,3-dimethyl-3,7-dihydro-*1H*-purine-2,6-dione (165)

The general procedure **B** was followed using substrate **163** (85.0 mg, 0.30 mmol) and 1-adamantanecarboxylic acid (**141**) (162 mg, 0.90 mmol) for 48 h. Purification by column chromatography on silica gel (*n*-pentane/Et_2O: 10/1) yielded **165** (53.5 mg, 129 µmol, 43%) as a white solid.

M. p.: 147–148 °C. **^{1}H-NMR** (400 MHz, $CDCl_3$): δ = 4.55–4.46 (m, 2H), 4.41 (dd, *J* = 14.0, 3.6 Hz, 1H), 4.28–4.22 (m, 2H), 3.56 (s, 3H), 3.38 (s, 3H), 3.01 (s, 3H), 2.25–2.06 (m, 9H),

1.80–1.75 (m, 6H), 1.27 (d, *J* = 6.3 Hz, 3H). **^{13}C-NMR** (101 MHz, $CDCl_3$): δ = 160.8 (C_q), 155.4 (C_q), 151.9 (C_q), 147.8 (C_q), 107.6 (C_q), 95.3 (CH_2), 73.1 (CH), 55.2 (CH_3), 52.4 (CH_2), 41.4 (CH_2), 37.6 (C_q), 36.6 (CH_2), 29.7 (CH_3), 28.5 (CH), 28.1 (CH_3), 18.4 (CH_3). **IR** (ATR): 2890, 1165, 1536, 1426, 1382, 1137, 1105, 1035, 743 cm^{-1}. **MS** (ESI) *m/z* (relative intensity): 439 $[M+Na]^+$ (100), 417 $[M+H]^+$ (99). **HR-MS** (ESI): *m/z* calcd for $C_{22}H_{32}N_4O_4Na^+$ $[M+Na]^+$ 439.2316, found 439.2319.

5.4.3 Mechanistic Studies

5.4.3.1 Reaction in the Presence of Radical Scavengers

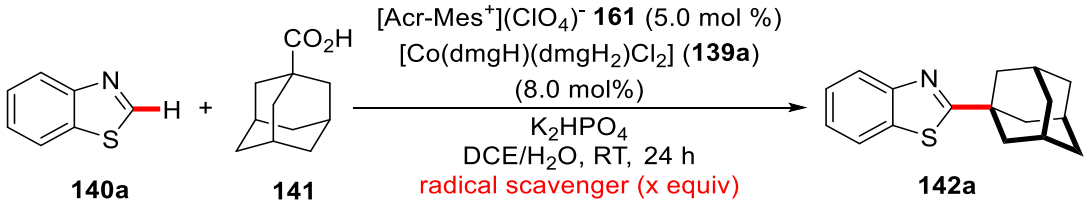

To an oven-dried 10 mL vial were added benzothiazole **140a** (0.40 mmol, 1.00 equiv), 1-adamantanecarboxylic acid (**141**) (1.20 mmol, 3.00 equiv), K_2HPO_4 (209 mg, 1.20 mmol, 3.00 equiv), 9-mesityl-10-methylacridinium perchlorate (8.2 mg, 5.00 mol %), $Co(dmgH)_2Cl_2$ (11.6 mg, 8.00 mol %), and radical scavenger (0.40 mmol, 1.00 equiv). After the vial was capped with a septum it was evacuated and refilled with N_2 for three times before DCE (1.5 mL) and H_2O (0.5 mL) were added sequentially. The mixture was degassed and stirred for 24 h under visible light irradiation. After 24 h the mixture was diluted with CH_2Cl_2 (10 mL) and H_2O (10 mL) and the phases were separated. The aqueous layer was extracted with CH_2Cl_2 (2 x 10 mL), the combined organic phases were dried over Na_2SO_4 and the solvent was removed under reduced pressure. The residue was purified by column chromatography on silica gel (*n*-pentane or *n*-hexane/Et_2O = 10/1) affording the corresponding product **142a**.

Table 5.2: Effect of Radical Scavengers on the reaction.[a]

Entry	Radical scavenger (1.0 equiv)	Yield [%]
1	--	84
2	TEMPO	34
3	Galvinoxyl free radical	--
4	BHT	53
5	BHT (3.0 equiv)	36

[a]TEMPO = (2,2,6,6-Tetramethylpiperidin-1-yl)oxidanyl. BHT = 2,6-Di-*tert*-butyl-4-methylphenol, yield of isolated product.

5.4.3.2 Competition Experiment Between Benzothiazoles 140

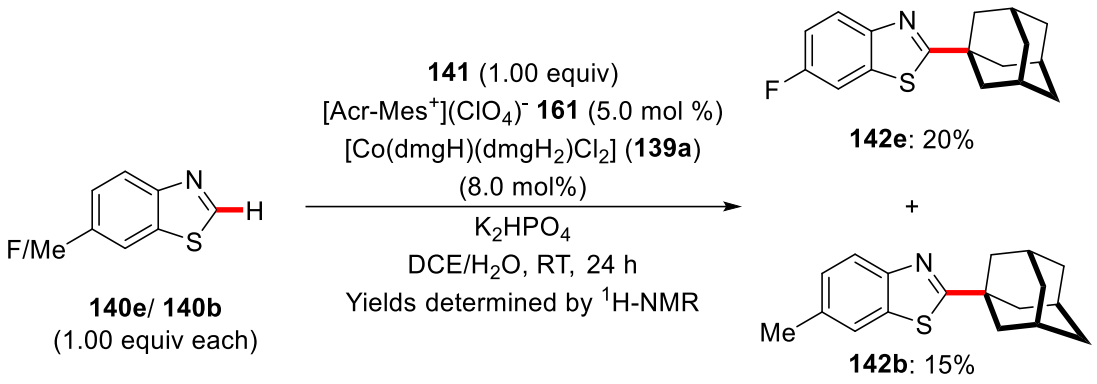

The general procedure **B** was followed using benzothiazole **140e** (61.3 mg, 0.40 mmol) and **140b** (-Me, 59.7 mg, 0.40 mmol) as well as 1-adamantanecarboxylic acid (**141**) (72.0 mg, 0.40 mmol). After aqueous workup and removal of remaining solvent, the crude mixture was analyzed by $^{1}H/^{19}F$-NMR spectroscopy (Figure 5.7 and Figure 5.8) using 4-fluoroanisole as internal standard (14.5 mg, 0.115 mmol).

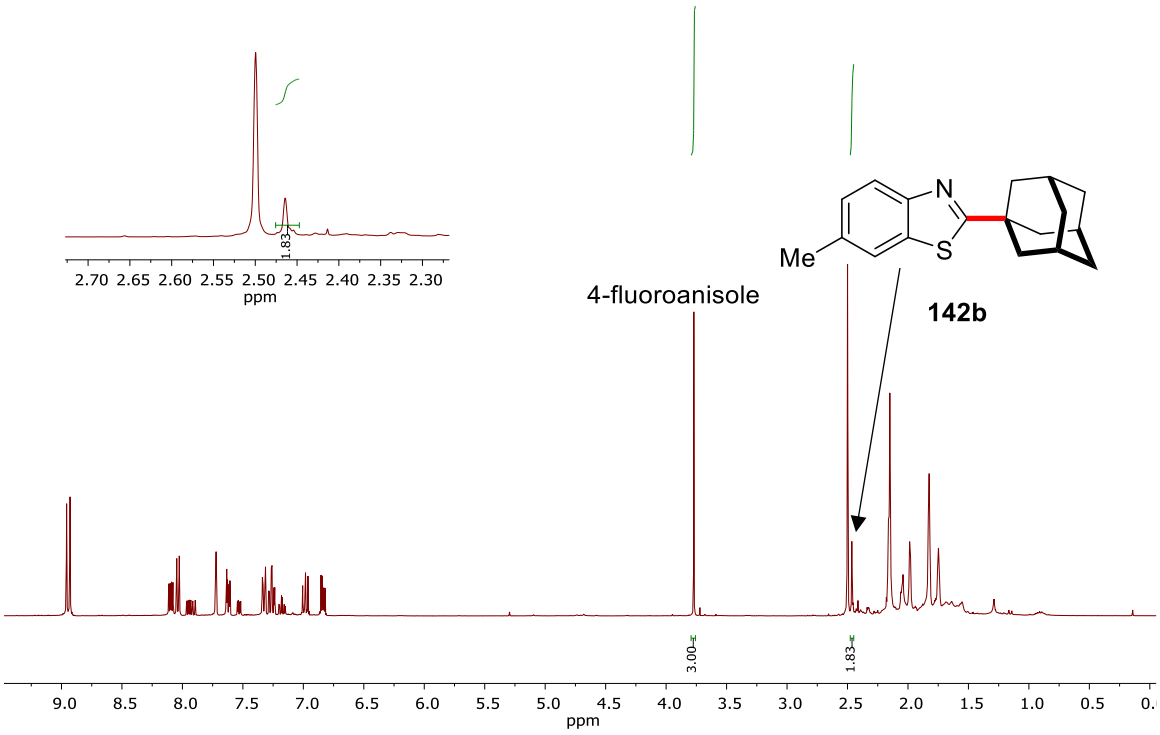

Figure 5.7: ^{1}H-NMR spectra of the reaction mixture after aqueous workup.

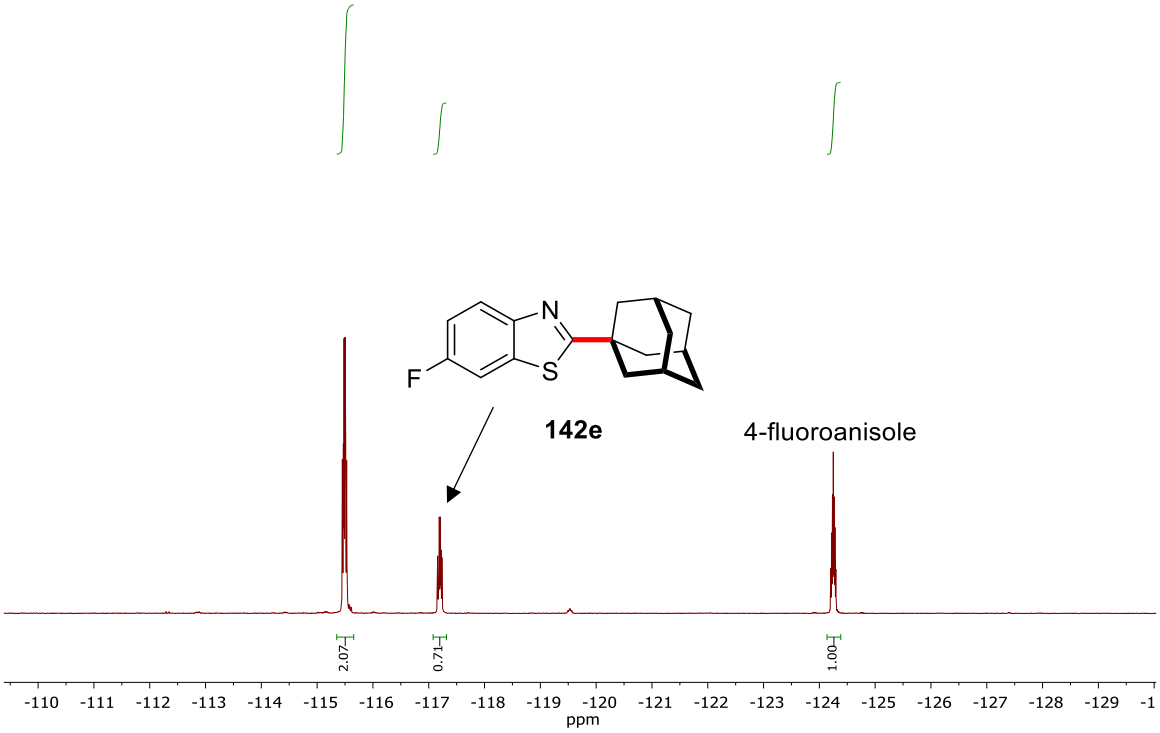

Figure 5.8: ^{19}F-NMR spectra of the reaction mixture after aqueous workup.

5.4.3.3 Effect of Light: On/Off Plot

According to the general procedure **B**, five independent reaction were set up and placed in front of the LEDs. The reactions were sequentially stirred under visible light irradiation and in the absence of light. Every two hours a reaction was removed from the setup and workup was performed according to the general procedure. After a total of ten hours the obtained isolated yields were plotted against the reaction time.

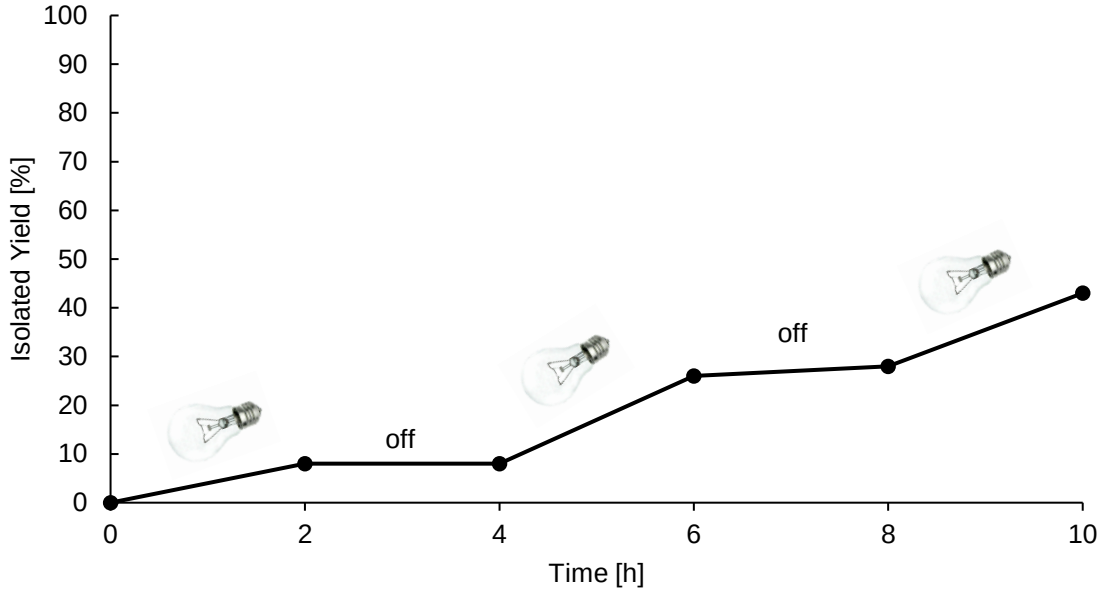

Figure 5.9: Effect of visible light irradiation.

5.4.3.4 Fluorescence quenching experiments

Sample solutions were prepared in DCE with c([Acr-Mes]$^{+}$(ClO)$_4^{-}$ = 1.6 x 10^{-7} M and varying concentrations of the respective quencher, added to each sample from a stock solution. Stern-Volmer experiments were conducted with a fixed excitation wavelength of 430 nm and detection at 518 nm (emission maximum). Plotting of the I_0/I value against the concentration of the potential quencher yielded the following graphs.

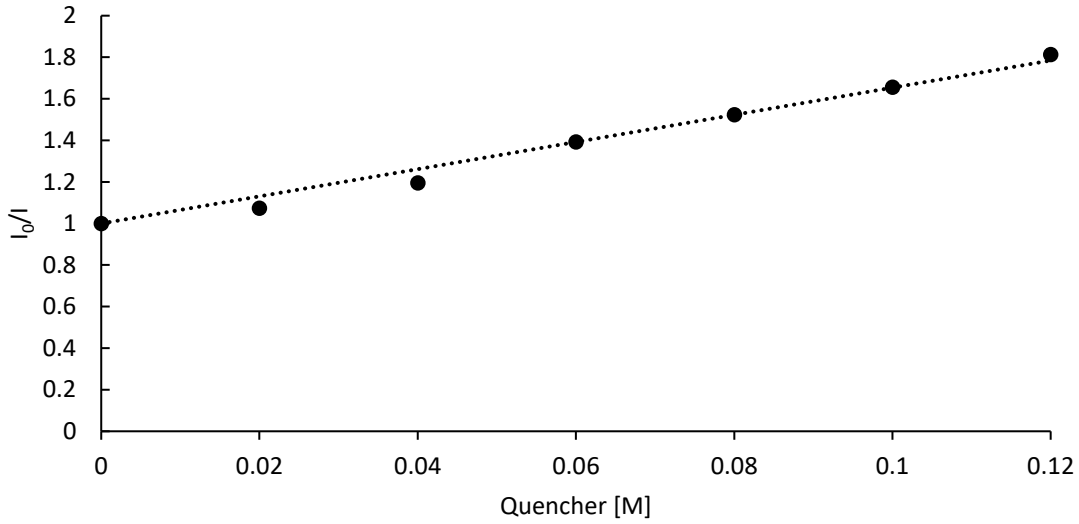

Figure 5.10: Fluorescence quenching of **161** with **140a**.

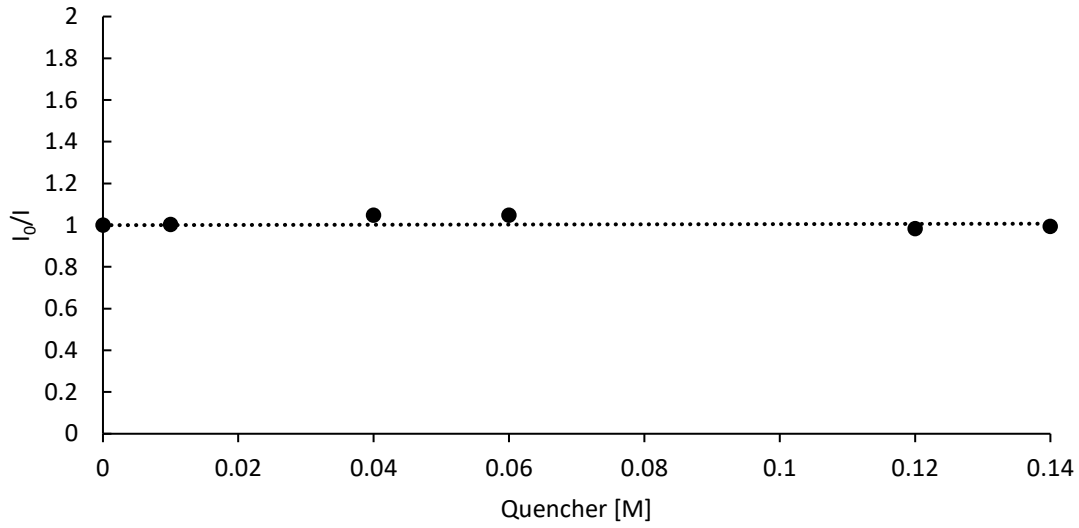

Figure 5.11: Fluorescence quenching of **161** with 1-adamantanecarboxylic acid (**141**).

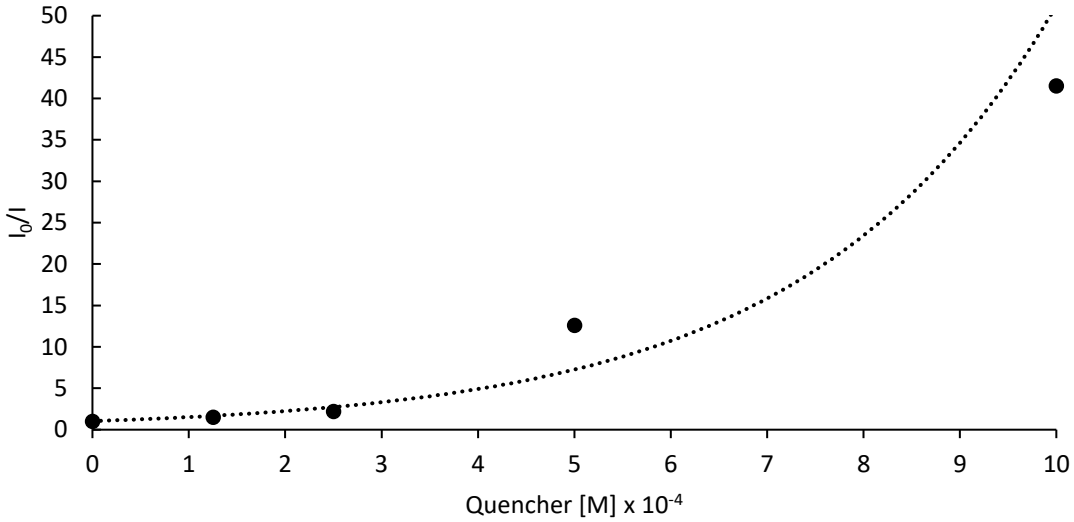

Figure 5.12: Fluorescence quenching of **161** with the carboxylate **167**.

5.5 Photo-Induced Copper-Catalyzed C–H Arylation

5.5.1 Photo-Induced Copper-Catalyzed C–H Arylation using UV Irradiation

5.5.1.1 Analytical Data

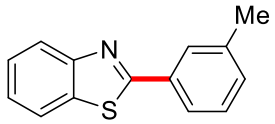

2-(*m*-Tolyl)benzo[*d*]thiazole (145ac)

The general procedure **C** was followed using benzo[*d*]thiazole (**140a**) (33.8 mg, 0.25 mmol) and 1-iodo-3-methylbenzene (**11c**) (273 mg, 1.25 mmol). Purification by column chromatography on silica gel (*n*-pentane/Et_2O: 30/1→20/1) yielded **145ac** (39.5 mg, 211 µmol,70%) as a slightly yellow liquid.

^{1}H-NMR (400 MHz, $CDCl_3$): δ = 8.08 (ddd, *J* = 8.2, 1.2, 0.7 Hz, 1H), 7.96–7.94 (m, 1H), 7.90 (ddd, *J* = 8.0, 1.3, 0.7 Hz, 1H), 7.89–7.85 (m, 1H), 7.50 (ddd, *J* = 8.3, 7.2, 1.3 Hz, 1H), 7.39 (ddd, *J* = 8.1, 7.2, 1.0 Hz, 2H), 7.33–7.29 (m, 1H), 2.46 (s, 3H). **^{13}C-NMR** (101 MHz, $CDCl_3$): δ = 168.5 (C_q), 154.3 (C_q), 139.0 (C_q), 135.2 (C_q), 133.7 (C_q), 131.9 (CH), 129.1 (CH), 128.1 (CH), 126.4 (CH), 125.2 (CH), 125.0 (CH), 123.3 (CH), 121.7 (CH), 21.5 (CH_3). **IR** (ATR): 1503, 1483, 1471, 1456, 1434, 1312, 1255, 785, 757, 728 cm^{-1}. **MS** (EI) *m/z* (relative intensity): 226 $[M+H]^+$ (100). **HR-MS** (ESI): *m/z* calcd for $C_{14}H_{12}NS$, $[M+H]^+$ 226.0685, found 226.0686. The analytical data are in accordance with those reported in the literature.[223]

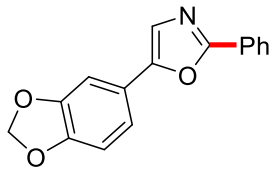

5-(Benzo[*d*][1,3]dioxol-5-yl)-2-phenyloxazole (**146a**)

The general procedure **C** was followed using 5-(benzo[*d*][1,3]dioxol-5-yl)oxazole (**144**) (47.3 mg, 0.25 mmol) and iodobenzene (**11a**) (255 mg, 1.25 mmol). Purification by column chromatography (*n*-pentane/Et_2O: 5/1) yielded **146a** (41.1 mg, 155 µmol, 62%) as a pale yellow solid.

M. p.: 136–138 °C. **^{1}H-NMR** (400 MHz, $CDCl_3$): δ = 8.10–8.06 (m, 2H), 7.51–7.41 (m, 3H), 7.31 (s, 1H), 7.24 (dd, *J* = 8.1, 1.7 Hz, 1H), 7.17 (d, *J* = 1.5 Hz, 1H), 6.88 (d, *J* = 8.1 Hz, 1H), 6.01 (s, 2H). **^{13}C-NMR** (101 MHz, $CDCl_3$): δ = 160.8 (C_q), 151.3 (C_q), 148.4 (C_q), 148.0 (C_q), 130.3 (CH), 128.9 (CH), 127.6 (C_q), 126.3 (CH), 122.5 (CH), 122.4 (C_q), 118.5 (CH), 109.0 (CH), 105.0 (CH), 101.5 (CH_2). **IR** (ATR): 1484, 1242, 1032, 928, 873, 817, 802, 705, 696, 680 cm^{-1}. **MS** (ESI): *m/z* (relative intensity): 288 $[M+Na]^+$ (100), 266 $[M+H]^+$ (71). **HR-MS** (ESI): *m/z* calcd for $C_{16}H_{12}NO_3^+$ $[M+H]^+$ 266.0812, found 266.0813. The analytical data are in accordance with those reported in the literature.[224]

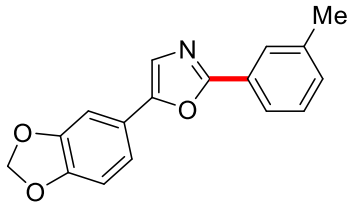

5-(Benzo[*d*][1,3]dioxol-5-yl)-2-(*m*-tolyl)oxazole (**146c**)

The general procedure **C** was followed using 5-(benzo[*d*][1,3]dioxol-5-yl)oxazole (**144**) (47.3 mg, 0.25 mmol) and 1-iodo-3-methylbenzene (**11c**) (273 mg, 1.25 mmol). Purification by column chromatography (*n*-pentane/Et_2O: 5/1) yielded **146c** (41.8 mg, 150 µmol, 60%) as a pale yellow solid.

M. p.: 86–88 °C. **^{1}H-NMR** (400 MHz, $CDCl_3$): δ = 7.92–7.86 (m, 2H), 7.36 (dd, *J* = 7.7, 7.7 Hz, 1H), 7.29 (s, 1H), 7.28–7.21 (m, 2H), 7.17 (dd, *J* = 1.7, 0.4 Hz, 1H), 6.87 (dd, *J* = 8.1, 0.4 Hz, 1H), 6.00 (s, 2H), 2.43 (s, 3H). **^{13}C-NMR** (101 MHz, $CDCl_3$): δ = 160.9 (C_q), 151.2 (C_q), 148.3 (C_q), 148.0 (C_q), 138.7 (C_q), 131.1 (CH), 128.8 (CH), 127.5 (C_q), 126.9 (CH), 123.5 (CH), 122.4 (CH), 122.4 (C_q), 118.5 (CH), 109.0 (CH), 104.9 (CH), 101.5 (CH_2), 21.5 (CH_3). **IR** (ATR): 1482, 1449, 1225, 1037, 963, 931, 800, 786, 719, 685 cm^{-1}. **MS** (ESI): *m/z* (relative intensity): 302 $[M+Na]^+$ (100), 280 $[M+H]^+$ (51). **HR-MS** (ESI): *m/z* calcd for $C_{17}H_{14}NO_3^+$ $[M+H]^+$ 280.0968, found 280.0969.

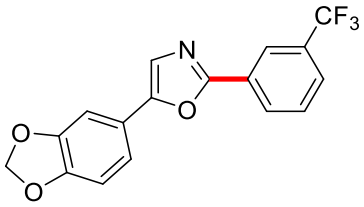

5-(Benzo[*d*][1,3]dioxol-5-yl)-2-(3-(trifluoromethyl)phenyl)oxazole (**146d**)

The general procedure **C** was followed using 5-(benzo[*d*][1,3]dioxol-5-yl)oxazole (**144**) (47.3 mg, 0.25 mmol) and 1-iodo-3-(trifluoromethyl)benzene (**11d**) (340 mg, 1.25 mmol). Purification by column chromatography (*n*-pentane/Et_2O: 5/1) yielded **146d** (53.2 mg, 160 µmol, 64%) as a pale yellow solid.

M. p.: 152–153 °C. **^{1}H-NMR** (400 MHz, $CDCl_3$): δ = 8.35–8.30 (m, 1H), 8.27–8.22 (m, 1H), 7.71–7.67 (m, 1H), 7.62–7.56 (m, 1H), 7.32 (s, 1H), 7.24 (dd, *J* = 8.1, 1.7 Hz, 1H), 7.16 (dd, *J* = 1.7, 0.4 Hz, 1H), 6.88 (dd, *J* = 8.1, 0.4 Hz, 1H), 6.01 (s, 2H). **^{13}C-NMR** (101 MHz, $CDCl_3$): δ = 159.3 (C_q), 152.0 (C_q), 148.4 (C_q), 148.3 (C_q), 131.6 (q, $^2J_{C-F}$ = 33.2 Hz, C_q), 129.5 (CH), 129.3 (CH), 128.3 (C_q), 126.7 (q, $^3J_{C-F}$ = 4.1 Hz, CH), 123.9 (q, $^1J_{C-F}$ = 273.0 Hz, C_q), 123.1 (q, $^3J_{C-F}$ = 4.0 Hz, CH), 122.7 (CH), 121.9 (C_q), 118.7 (CH), 109.0 (CH), 105.0 (CH), 101.6 (CH_2). **^{19}F{H}-NMR** (282 MHz, $CDCl_3$): δ = −62.9 (s). **IR** (ATR): 1481, 1264, 1118, 1105, 1035, 935, 861, 808, 726, 692 cm^{-1}. **MS** (ESI) *m/z* (relative intensity): 356 $[M+Na]^+$ (30), 334 $[M+H]^+$ (100). **HR-MS** (ESI): *m/z* calcd for $C_{17}H_{11}NO_3F_3^+$ $[M+H]^+$ 334.0686, found 334.0681.

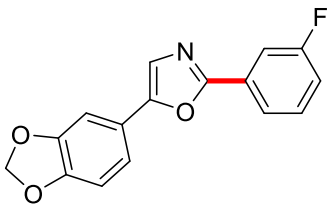

5-(Benzo[*d*][1,3]dioxol-5-yl)-2-(3-fluorophenyl)oxazole (**146e**)

The general procedure **C** was followed using 5-(benzo[*d*][1,3]dioxol-5-yl)oxazole (**144**) (47.3 mg, 0.25 mmol) and 1-fluoro-3-iodobenzene (**11e**) (278 mg, 1.25 mmol). Purification by column chromatography (*n*-pentane/Et_2O: 5/1) yielded **146e** (50.1 mg, 177 µmol, 71%) as a pale yellow solid.

M. p.: 131–133 °C. **^{1}H-NMR** (400 MHz, $CDCl_3$): δ = 7.85 (ddd, *J* = 7.8, 1.5, 1.0 Hz, 1H), 7.75 (ddd, *J* = 9.6, 2.3, 1.4 Hz, 1H), 7.43 (ddd, *J* = 8.0, 5.7 Hz, 1H), 7.30 (s, 1H), 7.22 (dd, *J* = 8.1, 1.7 Hz, 1H), 7.18–7.08 (m, 2H), 6.87 (dd, *J* = 8.1, 0.4 Hz, 1H), 6.01 (s, 2H). **^{13}C-NMR** (101 MHz, $CDCl_3$): δ = 163.1 (d, $^1J_{C\text{-}F}$ = 246.0 Hz, C_q), 159.6 (d, $^4J_{C\text{-}F}$ = 4.0 Hz, C_q), 151.7 (C_q), 148.4 (C_q), 148.2 (C_q), 130.6 (d, $^3J_{C\text{-}F}$ = 8.3 Hz, CH), 129.5 (d, $^3J_{C\text{-}F}$ = 8.7 Hz, C_q), 122.6 (CH), 122.1 (C_q), 122.0 (d, $^4J_{C\text{-}F}$ = 3.1 Hz, CH), 118.6 (CH), 117.2 (d, $J_{C\text{-}F}$ = 21.4 Hz, CH), 113.2 (d, $^2J_{C\text{-}F}$ = 24.0 Hz, CH), 109.0 (CH), 105.0 (CH), 101.6 (CH_2). **^{19}F{H}-NMR** (282 MHz, $CDCl_3$): δ = −112.1 (s). **IR** (ATR): 1502, 1446, 1237, 1034, 933, 856, 802, 787, 724, 675 cm^{-1}. **MS** (ESI) *m/z* (relative intensity): 306 $[M+Na]^+$ (62), 284 $[M+H]^+$ (100), 242 (60). **HR-MS** (ESI): *m/z* calcd for $C_{16}H_{11}NO_3F^+$ $[M+H]^+$ 284.0717, found 284.0719.

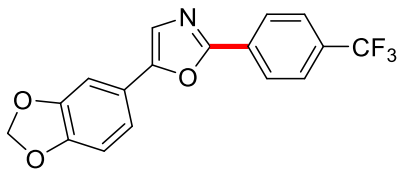

5-(Benzo[*d*][1,3]dioxol-5-yl)-2-(4-(trifluoromethyl)phenyl)oxazole (**146f**)

The general procedure **C** was followed using 5-(benzo[*d*][1,3]dioxol-5-yl)oxazole (**144**) (47.3 mg, 0.25 mmol) and 1-iodo-4-(trifluoromethyl)benzene (**11f**) (340 mg, 1.25 mmol). Purification by column chromatography (*n*-pentane/Et_2O: 5/1) yielded **146f** (60.3 mg, 181 µmol, 72%) as a colorless solid.

M. p.: 152–153 °C. **^{1}H-NMR** (400 MHz, $CDCl_3$): δ = 8.17 (dd, *J* = 8.9, 0.8 Hz, 2H), 7.72 (dd, *J* = 8.9, 0.7 Hz, 2H), 7.33 (s, 1H), 7.23 (dd, *J* = 8.1, 1.7 Hz, 1H), 7.16 (dd, *J* = 1.8, 0.4 Hz, 1H), 6.88 (dd, *J* = 8.1, 0.4 Hz, 1H), 6.02 (s, 2H). **^{13}C-NMR** (101 MHz, $CDCl_3$): δ = 159.3 (C_q), 152.1 (C_q), 148.4 (C_q), 148.4 (C_q), 131.8 (q, $^2J_{C\text{-}F}$ = 33.2 Hz, C_q), 130.3 (C_q), 126.5 (CH), 126.0 (q, $^3J_{C\text{-}F}$ = 4.1 Hz, CH), 124.0 (q, $^1J_{C\text{-}F}$ = 272.0 Hz, C_q), 122.8 (CH), 121.9 (C_q), 118.8 (CH), 109.1 (CH), 105.0 (CH), 101.6 (CH_2). **^{19}F{H}-NMR** (282 MHz, $CDCl_3$): δ = −62.8 (s). **IR** (ATR): 1480, 1321, 1231, 1102, 1077, 1038, 1016, 846, 811, 704 cm^{-1}. **MS** (ESI) *m/z* (relative intensity): 334 $[M+H]^+$ (97). **HR-MS** (ESI): *m/z* calcd for $C_{17}H_{11}NO_3F_3^+$ $[M+H]^+$ 334.0686, found 334.0675.

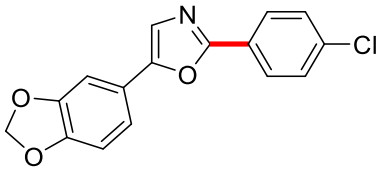

5-(Benzo[*d*][1,3]dioxol-5-yl)-2-(4-chlorophenyl)oxazole (**146g**)

The general procedure **C** was followed using 5-(benzo[*d*][1,3]dioxol-5-yl)oxazole (**144**) (47.3 mg, 0.25 mmol) and 1-chloro-4-iodobenzene (**11g**) (298 mg, 1.25 mmol). Purification by column chromatography (*n*-pentane/Et_2O: 5/1) yielded **146g** (52.1 mg, 174 µmol, 69%) as a colorless solid.

M. p.: 160–161 °C. **^{1}H-NMR** (400 MHz, $CDCl_3$): δ = 8.01–7.96 (m, 2H), 7.45–7.40 (m, 2H), 7.28 (s, 1H), 7.20 (dd, *J* = 8.1, 1.7 Hz, 1H), 7.13 (d, *J* = 1.7 Hz, 1H), 6.86 (d, *J* = 8.1 Hz, 1H), 6.00 (s, 2H). **^{13}C-NMR** (101 MHz, $CDCl_3$): δ = 159.8 (C_q), 151.5 (C_q), 148.4 (C_q), 148.1 (C_q), 136.3 (C_q), 129.2 (CH), 127.5 (CH), 126.1 (C_q), 122.6 (C_q), 122.1 (CH), 118.5 (CH), 109.0 (CH), 104.9 (CH), 101.6 (CH_2). **IR** (ATR): 1488, 1451, 1238, 1092, 1031, 1010, 930, 830, 800, 729 cm^{-1}. **MS** (ESI): *m/z* (relative intensity): 322 $[M+Na]^+$ (100), 300 $[M+H]^+$ (76). **HR-MS** (ESI) *m/z* calcd for $C_{16}H_{10}NO_3{}^{35}ClNa^+$ $[M+Na]^+$ 322.0241, found 322.0246.

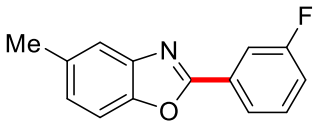

2-(3-Fluorophenyl)-5-methylbenzo[*d*]oxazole (**15ge**)

The general procedure **C** was followed using 5-methylbenzo[*d*]oxazole (**14g**) (33.3 mg, 0.25 mmol) and 1-fluoro-3-iodobenzene (**11e**) (278 mg, 1.25 mmol). Purification by column chromatography (*n*-pentane/Et_2O: 15/1) yielded **15ge** (38.3 mg, 169 µmol, 67%) as a colorless solid.

M. p.: 87–89 °C. **^{1}H-NMR** (400 MHz, $CDCl_3$): δ = 8.02 (ddd, *J* = 7.8, 1.6, 1.0 Hz, 1H), 7.92 (ddd, *J* = 9.5, 2.6, 1.5 Hz, 1H), 7.56–7.54 (m, 1H), 7.51–7.42 (m, 2H), 7.24–7.15 (m, 2H), 2.49 (s, 3H). **^{13}C-NMR** (101 MHz, $CDCl_3$): δ = 163.1 (d, $^1J_{C\text{-}F}$ = 247.0 Hz, C_q), 162.0 (d, $^4J_{C\text{-}F}$ = 3.5 Hz, C_q), 149.2 (C_q), 142.3 (C_q), 134.8 (C_q), 130.7 (d, $^3J_{C\text{-}F}$ = 8 Hz, CH), 129.5 (d, $^3J_{C\text{-}F}$ = 9.0 Hz, C_q), 126.8 (CH), 123.4 (d, $^4J_{C\text{-}F}$ = 3.2 Hz, CH), 120.2 (CH), 118.5 (d, $^2J_{C\text{-}F}$ = 21.4

Hz, CH), 114.6 (d, $^{2}J_{C\text{-}F}$ = 24.0 Hz, CH), 110.2 (CH), 21.7 (CH_3). **^{19}F{H}-NMR** (282 MHz, $CDCl_3$): δ = −111.9 (s). **IR** (ATR): 1557, 1471, 1448, 1262, 1211, 876, 789, 724, 676, 598 cm^{-1}. **MS** (ESI) *m/z* (relative intensity): 228 $[M+H]^+$ (100). **HR-MS** (ESI): *m/z* calcd for $C_{14}H_{11}NOF^+$ $[M+H]^+$ 228.0819, found 228.0824.

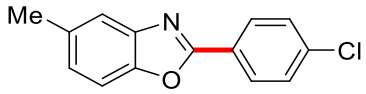

2-(4-Chlorophenyl)-5-methylbenzo[*d*]oxazole (**15gg**)

The representative procedure **C** was followed using 5-methylbenzo[*d*]oxazole (**14g**) (33.3 mg, 0.25 mmol) and 1-chloro-4-iodobenzene (**11g**) (298 mg, 1.25 mmol). Purification by column chromatography (*n*-pentane/Et_2O: 15/1) yielded **15gg** (43.8 mg, 179 µmol, 72%) as a colorless solid.

M. p.: 145–147 °C. **^{1}H-NMR** (400 MHz, $CDCl_3$): δ = 8.17–8.13 (m, 2H), 7.55–7.53 (m, 1H), 7.50–7.45 (m, 2H), 7.43 (dd, *J* = 8.3, 0.6 Hz, 1H), 7.18–7.14 (m, 1H), 2.48 (s, 3H). **^{13}C-NMR** (101 MHz, $CDCl_3$): δ = 162.2 (C_q), 149.1 (C_q), 142.3 (C_q), 137.7 (C_q), 134.7 (C_q), 129.3 (CH), 128.9 (CH), 126.6 (CH), 126.0 (C_q), 120.1 (CH), 110.1 (CH), 21.7 (CH_3). **IR** (ATR): 1477, 1403, 1089, 1052, 1008, 839, 827, 795, 729, 502 cm^{-1}. **MS** (ESI) *m/z* (relative intensity): 244 $[M+H]^+$ (100). **HR-MS** (ESI): *m/z* calcd for $C_{14}H_{11}NO^{35}Cl^+$ $[M+H]^+$ 244.0524, found 244.0522. The analytical data are in accordance with those reported in the literature.[225]

The following benzothiazoles **145bc** to **145hc** were synthesized by N. Imse during the course of his bachelor thesis:[190]

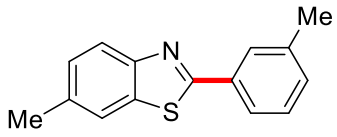

6-Methyl-2-(*m*-tolyl)benzo[*d*]thiazole (145bc)

The general procedure **C** was followed using benzo[*d*]thiazole **140b** (37.8 mg, 0.25 mmol) and iodobenzene **11c** (273 mg, 1.25 mmol). Purification by column chromatography (*n*-pentane/Et_2O: 60:1→20:1) yielded **145bc** (34.2 mg, 143 µmol, 57%) as an orange solid.

M. p.: 84–86 °C. **^{1}H-NMR** (300 MHz, $CDCl_3$): δ = 7.94 (d, *J* = 8.4 Hz, 1H), 7.92–7.90 (m, 1H), 7.85–7.81 (m, 1H), 7.66–7.65 (m, 1H), 7.35 (dd, *J* = 7.6, 7.6 Hz, 1H), 7.30–7.25 (m, 2H), 2.47 (s, 3H), 2.43 (s, 3H). **^{13}C-NMR** (126 MHz, $CDCl_3$): δ = 167.2 (C_q), 152.3 (C_q), 138.8 (C_q), 135.3 (C_q), 135.3 (C_q), 133.7 (C_q), 131.6 (CH), 128.9 (CH), 127.9 (CH), 127.9 (CH) 124.8 (CH), 122.7 (CH), 121.4 (CH), 21.7 (CH_3), 21.5 (CH_3). **IR** (ATR): 1448, 1258, 1165, 831, 814, 795, 779, 686, 651, 572 cm^{-1}. **MS** (ESI) *m/z* (relative intensity): 240 $[M+H]^+$ (100). **HR-MS** (ESI): *m/z* calcd for $C_{15}H_{14}NS^+$ $[M+H]^+$ 240.0841, found 240.0840.

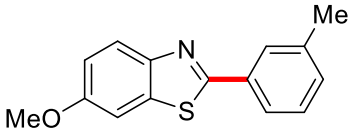

6-Methoxy-2-(*m*-tolyl)benzo[*d*]thiazole (145cc)

The general procedure **C** was followed using benzo[*d*]thiazole **140c** (41.2 mg, 0.25 mmol) and iodobenzene **11c** (273 mg, 1.25 mmol). Purification by column chromatography (*n*-pentane/Et_2O: 60:1→20:1) yielded **145cc** (29.6 mg, 116 µmol, 46%) as an orange solid.

M. p.: 103 °C. **^{1}H-NMR** (300 MHz, $CDCl_3$): δ = 7.93 (dd, *J* = 8.9, 0.5 Hz, 1H), 7.88-7.86 (m, 1H), 7.81–7.77 (m, 1H), 7.34–7.31 (m, 2H), 7.27–7.23 (m, 1H), 7.07 (dd, *J* = 9.0, 2.6 Hz, 1H), 3.86 (s, 3H), 2.42 (s, 3H). **^{13}C-NMR** (126 MHz, $CDCl_3$): δ = 165.8 (C_q), 157.8 (C_q), 148.7 (C_q), 138.8 (C_q), 136.4 (C_q), 133.7 (C_q), 131.4 (CH), 128.9 (CH), 127.7 (CH), 124.6 (CH), 123.7 (CH), 115.6 (CH), 104.3 (CH), 56.0 (CH_3), 21.6 (CH_3). **IR** (ATR): 1600, 1457, 1428, 1263, 1225, 1026, 830, 820, 789, 688 cm^{-1}. **MS** (ESI) *m/z* (relative intensity): 256 $[M+H]^+$ (100). **HR-MS** (ESI) *m/z* calcd for $C_{15}H_{14}NOS^+$ $[M+H]^+$ 256.0791, found 256.0788.

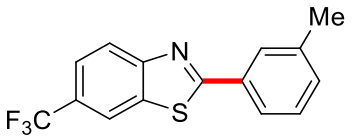

2-(*m*-Tolyl)-6-(trifluoromethyl)benzo[*d*]thiazole (145dc)

The general procedure **C** was followed using benzo[*d*]thiazole **140d** (50.8 mg, 0.25 mmol) and iodobenzene **11c** (273 mg, 1.25 mmol). Purification by column chromatography (*n*-pentane/Et_2O: 60:1→20:1) yielded **145dc** (43.2 mg, 147 µmol, 55%) as an orange solid.

M. p.: 110 °C. **^{1}H-NMR** (400 MHz, $CDCl_3$): δ = 8.17–8.16 (m, 1H), 8.12 (dd, J = 8.6, 0.6 Hz, 1H), 7.93–7.91 (m, 1H), 7.86 (dd, J = 7.6, 1.8 Hz, 1H), 7.70 (dd, J = 8.6, 1.8 Hz, 1H), 7.40–7.31 (m, 2H), 2.44 (s, 3H). **^{13}C-NMR** (101 MHz, $CDCl_3$): δ = 171.5 (C_q), 156.2 (C_q), 139.2 (C_q), 135.2 (C_q), 133.1 (C_q), 132.7 (CH), 129.2 (CH), 128.4 (CH), 127.4 (q, $^2J_{C\text{-}F}$ = 32.6 Hz, C_q), 125.2 (CH), 124.4 (q, $^1J_{C\text{-}F}$= 272.2 Hz, C_q), 123.5 (CH), 123.5 (q, $^3J_{C\text{-}F}$= 3.4 Hz, CH), 119.4 (q, $^3J_{C\text{-}F}$ = 4.2 Hz, CH), 21.5 (CH_3). **^{19}F{H}-NMR** (282 MHz, $CDCl_3$): δ = −61.4 (s). **IR** (ATR): 1319, 1251, 1159, 1139, 1110, 1086, 1054, 834, 789, 686 cm^{-1}. **MS** (ESI) *m/z* (relative intensity): 294 $[M+H]^+$ (100). **HR-MS** (ESI): *m/z* calcd for $C_{15}H_{11}F_3NS^+$ $[M+H]^+$ 294.0559, found 294.0562.

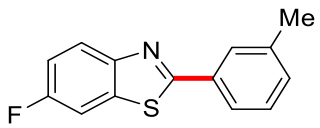

6-Fluoro-2-(*m*-tolyl)benzo[*d*]thiazole (145ec)

The general procedure **C** was followed using benzo[*d*]thiazole **140e** (38.6 mg, 0.25 mmol) and iodobenzene **11c** (273 mg, 1.25 mmol). Purification by column chromatography (*n*-pentane/Et_2O: 35:1→20:1) yielded **145ec** (24.1 mg, 99.1 µmol, 39%) as an orange solid.

M. p.: 78–80 °C. **^{1}H-NMR** (400 MHz, $CDCl_3$): δ = 7.98 (dd, J = 8.8, 4.7 Hz, 1H), 7.88–7.87 (m, 1H), 7.82–7.79 (m, 1H), 7.57–7.54 (m, 1H), 7.36 (dd, J = 7.6, 7.6 Hz, 1H), 7.30–7.27 (m, 1H), 7.23–7.17 (m, 1H), 2.43 (s, 3H). **^{13}C-NMR** (101 MHz, $CDCl_3$): δ = 168.2 (d, $^4J_{C\text{-}F}$ = 3.5 Hz, C_q), 160.6 (d, $^1J_{C\text{-}F}$ = 245.0 Hz, C_q), 150.9 (d, $^4J_{C\text{-}F}$ = 1.8 Hz, C_q), 139.1 (C_q), 136.2 (d, $^3J_{C\text{-}F}$ = 11.2 Hz, C_q), 133.4 (C_q), 132.0 (CH), 129.1 (CH), 128.0 (CH), 124.8 (CH), 124.2 (d, $^3J_{C\text{-}F}$ = 9.4 Hz, CH), 115.0 (d, $^2J_{C\text{-}F}$ = 24.7 Hz, CH), 108.0 (d, $^2J_{C\text{-}F}$ = 26.9 Hz, CH), 21.5 (CH_3). **^{19}F{H}-NMR** (282 MHz, $CDCl_3$): δ = −116.0 (s). **IR** (ATR): 1451, 1307, 1247, 1191, 1167, 840, 807, 775, 686, 583 cm^{-1}. **MS** (ESI) *m/z* (relative intensity): 244 $[M+H]^+$ (100). **HR-MS** (ESI): *m/z* calcd for $C_{14}H_{11}FNS^+$ $[M+H]^+$ 244.0591, found 244.0596.

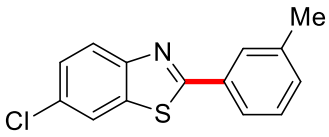

6-Chloro-2-(*m*-tolyl)benzo[*d*]thiazole (145fc)

The general procedure **C** was followed using benzo[*d*]thiazole **140f** (41.0 mg, 0.25 mmol) and iodobenzene **11c** (273 mg, 1.25 mmol). Purification by column chromatography (*n*-pentane/Et_2O: 60:1→20:1) yielded **145fc** (27.5 mg, 106 µmol, 44%) as an orange solid.

M. p.: 125–128 °C. **^{1}H-NMR** (400 MHz, $CDCl_3$): δ = 7.94 (dd, *J* = 8.7, 0.4 Hz, 1H), 7.88–7.87 (m, 1H), 7.84 (dd, *J* = 2.1, 0.4 Hz, 1H), 7.82–7.80 (m, 1H), 7.42 (dd, *J* = 8.7, 2.1 Hz, 1H), 7.36 (dd, *J* = 7.6, 7.6 Hz, 1H), 7.31–7.28 (m, 1H), 2.43 (s, 3H). **^{13}C-NMR** (101 MHz, $CDCl_3$): δ = 168.9 (C_q), 152.8 (C_q), 139.1 (C_q), 136.3 (C_q), 133.3 (C_q), 132.3 (CH), 131.2 (C_q) 129.1 (CH), 128.1 (CH), 127.2 (CH), 125.0 (CH), 124.0 (CH), 121.3 (CH), 21.5 (CH_3). **IR** (ATR): 1305, 1248, 1169, 1095, 1023, 852, 816, 804, 771, 759 cm^{-1}. **MS** (ESI) *m/z* (relative intensity): 260 $[M+H]^+$ (100). **HR-MS** (ESI): *m/z* calcd for $C_{14}H_{11}{}^{35}ClNS^+$ $[M+H]^+$ 260.0295, found 260.0296.

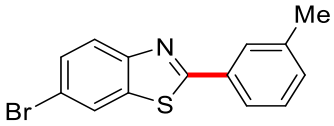

6-Bromo-2-(*m*-tolyl)benzo[*d*]thiazole (145gc)

The general procedure **C** was followed using benzo[*d*]thiazole **140gc** (53.5 mg, 0.25 mmol) and iodobenzene **11c** (273 mg, 1.25 mmol). Purification by column chromatography (*n*-pentane/Et_2O: 60:1→20:1) yielded **145gc** (15.6 mg, 51.2 µmol, 21%) as an orange solid.

M. p.: 117–122 °C. **^{1}H-NMR** (400 MHz, $CDCl_3$): δ = 8.00 (dd, *J* = 2.0, 0.5 Hz, 1H), 7.89–7.88 (m, 2H), 7.83–7.80 (m, 1H), 7.56 (dd, 8.7, 2.0 Hz, 1H), 7.36 (dd, *J* = 7.6, 7.6 Hz, 1H), 7.31–7.28 (m, 1H), 2.43 (s, 3H). **^{13}C-NMR** (101 MHz, $CDCl_3$): δ = 169.0 (C_q), 153.1 (C_q), 139.1 (C_q), 136.8 (C_q), 133.2 (C_q), 132.3 (CH), 129.9 (CH), 129.1 (CH), 128.1 (CH), 125.0 (CH), 124.4 (CH), 124.3 (CH), 118.8 (C_q), 21.5 (CH_3). **IR** (ATR): 1435, 1248, 1168, 1088, 853, 814, 800,

771, 684, 699 cm^{-1}. **MS** (ESI) *m/z* (relative intensity): 304 $[M+H]^+$ (51), 236 (100). **HR-MS** (ESI): *m/z* calcd for $C_{14}H_{11}{}^{79}BrNS^+$ $[M+H]^+$: 303.9790, found 303.9793.

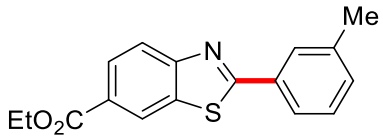

Ethyl 2-(*m*-tolyl)benzo[*d*]thiazole-6-carboxylate (145hc)

The general procedure **C** was followed using benzo[*d*]thiazole **140h** (51.8 mg, 0.25 mmol) and iodobenzene **11c** (273 mg, 1.25 mmol). Purification by column chromatography (*n*-pentane/Et_2O: 60:1→20:1) yielded **145hc** (16.8 mg, 56.5 µmol, 23%) as an orange solid.

M. p.: 99–101 °C. **^{1}H-NMR** (400 MHz, $CDCl_3$): δ = 8.60 (dd, *J* = 1.7, 0.6 Hz, 1H), 8.15 (dd, *J* = 8.6, 1.7 Hz, 1H), 8.05 (dd, *J* = 8.5, 0.6 Hz, 1H), 7.93–7.92 (m, 1H), 7.88–7.85 (m, 1H), 7.37 (dd, *J* = 7.6, 7.6 Hz, 1H), 7.33–7.30 (m, 1H), 4.41 (q, *J* = 7.1 Hz, 2H), 2.44 (s, 3H), 1.42 (t, *J* = 7.1 Hz, 3H). **^{13}C-NMR** (101 MHz, $CDCl_3$): δ = 171.9 (C_q), 166.3 (C_q), 157.1 (C_q), 139.2 (C_q), 135.1 (C_q), 133.3 (C_q), 132.6 (CH), 129.2 (CH), 128.4 (CH), 127.7 (CH), 127.4 (C_q), 125.2 (CH), 123.9 (CH), 122.9 (CH), 61.4 (CH_2), 21.5 (CH_3), 14.5 (CH_3).**IR** (ATR): 1709, 1265, 1246, 1224, 1109, 1026, 783, 767, 725, 684 cm^{-1}. **MS** (ESI) *m/z* (relative intensity): 298 $[M+H]^+$ (100). **HR-MS** (ESI): *m/z* calcd for $C_{17}H_{16}NO_2S^+$ $[M+H]^+$ 298.0896, found 298.0897.

5.5.2 Photo-Induced Copper-catalyzed C–H Arylation Using Visible Light

5.5.2.1 Analytical Data

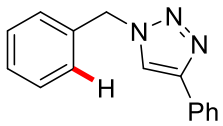

1-Benzyl-4-phenyl-1*H*-1,2,3-triazole (175)

To an oven-dried 10 mL vial triazole **27b** (90.0 mg, 0.25 mmol, 1.00 equiv), copper(I) iodide (9.5 mg, 20 mol %), Li*O*t*Bu (60 mg, 0.75 mmol, 3.00 equiv), and DMF (1.0 mL) were added. The tube was capped with a septum and wrapped with Parafilm and stirred under

254 nm irradiation for 16 h (Luzchem LZC-ICH2 photoreactor, the temperature was maintained between 25 °C and 30 °C, Figure 5.2). After the indicated reaction time, the mixture was filtered over a short pad of silica (Et_2O) and the solvent was removed under reduced pressure. The residue was purified by column chromatography on silica gel (*n*-pentane/Et_2O: 2/1) affording the corresponding triazole **175** (27.5 mg, 117 µmol, 47%) as an off-white solid.

M. p.: 129–130 °C. **^{1}H-NMR** (400 MHz, $CDCl_3$): δ 7.82–7.78 (m, 2H), 7.66 (s, 1H), 7.42–7.36 (m, 5H), 7.34–7.28 (m, 3H), 5.57 (s, 2H). **^{13}C-NMR** (101 MHz, $CDCl_3$): δ = 148.3 (C_q), 134.8 (C_q), 130.7 (C_q), 129.3 (CH), 128.9 (CH), 128.9 (CH), 128.3 (CH), 128.2 (CH), 125.8 (CH), 119.6 (CH), 54.3 (CH_2). **IR** (ATR): 1450, 1223, 1045, 971, 767, 727, 694, 588, 506, 480 cm^{-1}. **MS** (ESI) *m/z* (relative intensity): 258 $[M+Na]^+$ (12), 236 $[M+H]^+$ (100). **HR-MS** (ESI): *m/z* calcd for $C_{15}H_{14}N_3^+$ $[M+H]^+$ 236.1182, found 236.1184. The analytical data are in accordance with those reported in the literature.[226]

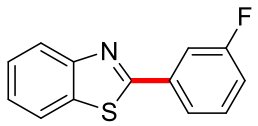

2-(3-Fluorophenyl)benzo[*d*]thiazole (145ae)

To an oven-dried 10 mL vial were added copper(I) chloride (5.0 mg, 20 mol %) and LiO*t*Bu (60 mg, 0.75 mmol, 3.00 equiv). The vial was capped with a septum and wrapped with Parafilm and Et_2O (1.0 mL) was added. Benzo[*d*]thiazole (**140a**) (33.8 mg, 0.25 mmol), and iodobenzene **11e** (278 mg, 1.25 mmol) were sequentially added *via* syringe. The mixture was irradiated for 16 h using a Kessil A-360N blue LED. The mixture was filtered over a short pad of silica (Et_2O) and the solvent was removed under reduced pressure. Purification of the residue by column chromatography (*n*-pentane/Et_2O: 25:1→20:1) yielded **145ae** (31.0 mg, 135 µmol, 54%) as a slightly orange solid.

M. p.: 85–86 °C. **^{1}H-NMR** (400 MHz, $CDCl_3$): δ = 8.09 (d, *J* = 8.1 Hz, 1H), 7.91 (ddd, *J* = 8.0, 1.3, 0.7 Hz, 1H), 7.88–7.79 (m, 2H), 7.54–7.36 (m, 3H), 7.18 (ddd, *J* = 8.0, 7.5, 1.9 Hz, 1H). **^{13}C-NMR** (101 MHz, $CDCl_3$): δ = 166.5 (d, $^4J_{C\text{-}F}$ = 3.2 Hz, C_q), 163.1 (d, $^1J_{C\text{-}F}$ = 247.2 Hz, C_q), 154.1 (C_q), 135.8 (d, $^3J_{C\text{-}F}$ = 8.1 Hz, C_q), 135.2 (C_q), 130.7 (d, $^3J_{C\text{-}F}$ = 8.2 Hz, CH), 126.7 (CH),

125.6 (CH), 123.6 (CH), 123.4 (d, $^{4}J_{C\text{-}F}$ = 3.0 Hz, CH), 121.8 (CH), 117.9 (d, $^{2}J_{C\text{-}F}$ = 21.4 Hz, CH), 114.4 (d, $^{2}J_{C\text{-}F}$ = 23.5 Hz, CH). **^{19}F-NMR** (378 MHz, $CDCl_3$): δ = (−112.0)–(−112.1) (m). **IR** (ATR): 1443, 1259, 878, 810, 779, 751, 728, 676, 520, 449 cm^{-1}. **MS** (ESI) *m/z* (relative intensity): 230 $[M+H]^+$ (100). **HR-MS** (ESI): *m/z* calcd for $C_{13}H_9FNS^+$, $[M+H]^+$ 230.0434, found 230.0436. The analytical data are in accordance with those reported in the literature.[227]

5.5.2.2 Mechanistic Studies

5.5.2.2.1 Fluorescence Quenching Studies

Sample solutions were prepared in MeCN with c($Ir(ppy)_3$) = 1.6 x 10^{-8} M and varying concentrations of the respective quencher. The experiments were conducted with a fixed excitation wavelength of 430 nm and detection at 520 nm (emission maximum). Plotting of the I_0/I value against the concentration of the potential quencher yielded the following graphs.

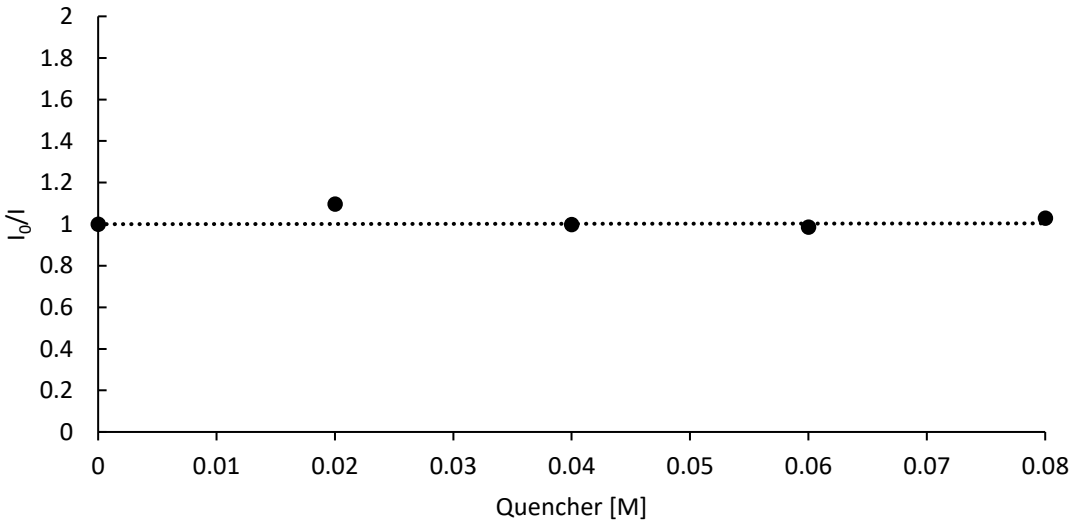

Figure 5.13: Fluorescence quenching of $Ir(ppy)_3$ with 3-iodotoluene (**11c**).

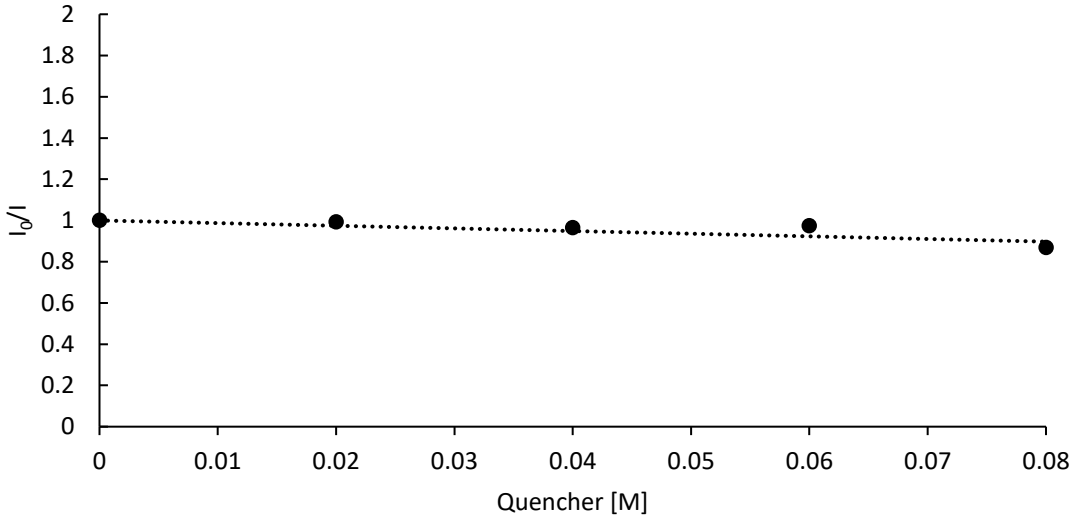

Figure 5.14: Fluorescence quenching of $Ir(ppy)_3$ with benzothiazole (**140a**).

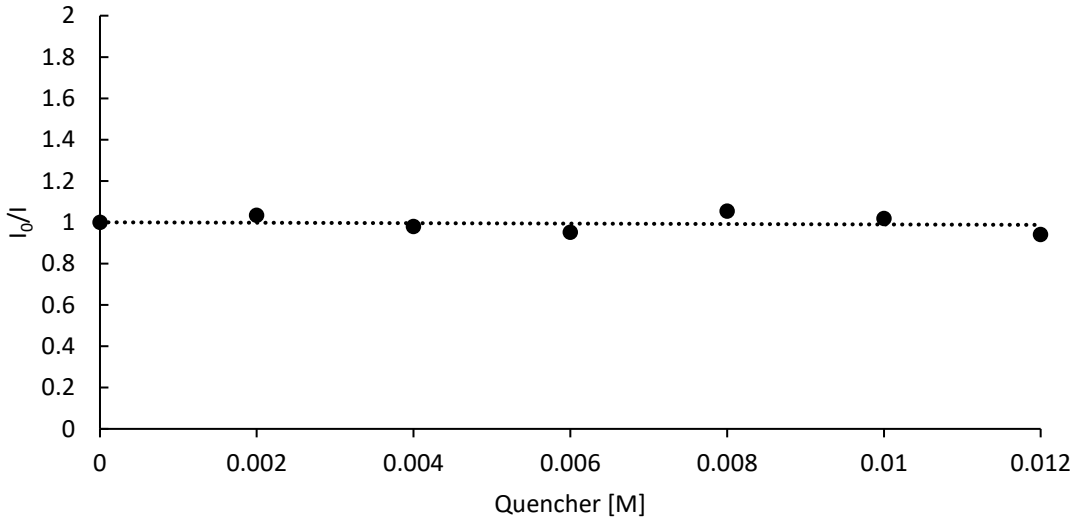

Figure 5.15: Fluorescence quenching of $Ir(ppy)_3$ with CuI.

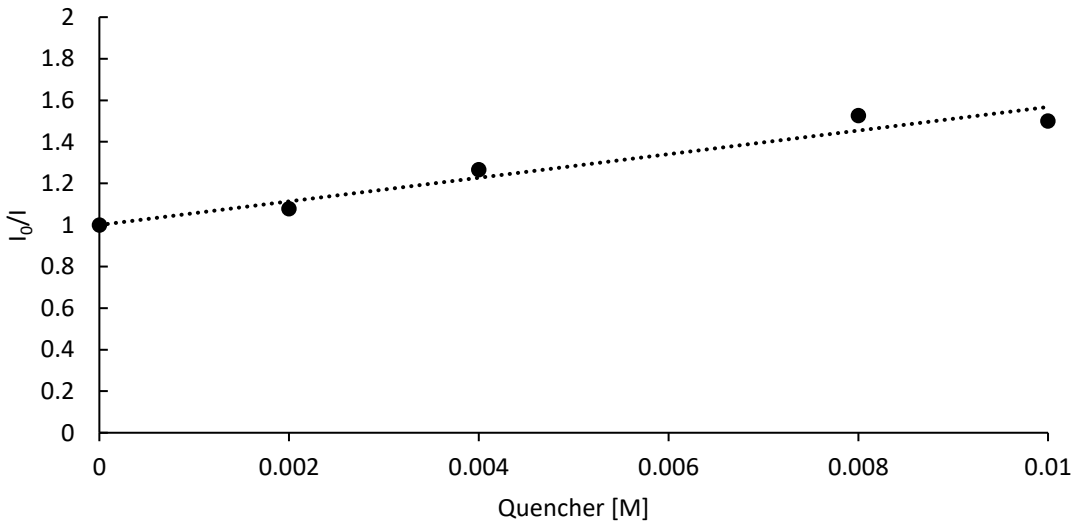

Figure 5.16: Fluorescence quenching of $Ir(ppy)_3$ with CuI (in DMSO).

5.6 Visible Light-Induced Ruthenium-Catalyzed *meta*-C–H Functionalizations

5.6.1 Visible Light-Induced Ruthenium-Catalyzed *meta*-C–H Difluoromethylation

5.6.1.1 Analytical Data

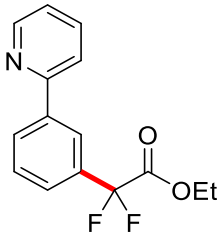

Ethyl 2,2-difluoro-2-[3-(pyridin-2-yl)phenyl]acetate (185a)

The general procedure **D** was followed using 2-phenylpyridine (**35a**) (46.6 mg, 0.30 mmol) and ester **100** (183 mg, 0.90 mmol). Purification by column chromatography on silica gel (*n*-pentane/Et_2O: 10/1) yielded **185a** (29.8 mg, 107 µmol, 36%) as colorless oil. **^{1}H-NMR** (400 MHz, $CDCl_3$): δ = 8.69 (dd, *J* = 4.8, 1.6 Hz, 1H), 8.22 (ddd, *J* = 1.8, 0.9, 0.9 Hz, 1H), 8.15–8.12 (m, 1H), 7.79–7.71 (m, 2H), 7.66–7.62 (m, 1H), 7.55 (ddd, *J* = 7.8, 7.8, 0.6 Hz, 1H), 7.25 (ddd, *J* = 6.7, 4.8, 2.0 Hz, 1H), 4.29 (q, *J* = 7.1 Hz, 2H), 1.29 (t, *J* = 7.1 Hz, 3H). **^{13}C-NMR** (101 MHz, $CDCl_3$): δ = 164.1 (t, $^2J_{C\text{-}F}$ = 35.1 Hz, C_q), 156.2 (C_q), 149.8 (CH), 140.0 (C_q), 136.9 (CH), 133.4 (t, $^2J_{C\text{-}F}$ = 25.6 Hz, C_q), 129.4 (t, $^4J_{C\text{-}F}$ = 1.7 Hz, CH), 129.1 (CH), 125.9 (t, $^3J_{C\text{-}F}$ = 6.1 Hz, CH), 123.9 (t, $^3J_{C\text{-}F}$ = 6.3 Hz, CH), 122.6 (CH), 120.6 (CH), 114.6 (t, $^1J_{C\text{-}F}$ = 252.0, C_q), 63.2 (CH_2), 13.9 (CH_3). **^{19}F-NMR** (282 MHz, $CDCl_3$): δ = −103.74. **IR** (ATR): 2984, 1761, 1584, 1462, 1291, 1228, 1102, 1018, 778, 745 cm^{-1}. **MS** (ESI) *m/z* (relative intensity): 278 $[M+H]^+$ (100). **HR-MS** (ESI): *m/z* calcd for $C_{15}H_{14}F_2NO_2^+$ $[M+H]^+$ 278.0987, found 278.0988. The analytical data are in accordance with those reported in the literature.[112a]

5.6.1.2 Mechanistic Studies

5.6.1.2.1 Fluorescence Quenching Experiments

Sample solutions were prepared in 1,4-dioxane with c($Ir(ppy)_3$) = 1.6 x 10^{-8} M and varying concentrations of the respective quencher, added to each sample from a stock solution. Stern-Volmer experiments were conducted with a fixed excitation wavelength of 430 nm and detection at 520 nm (emission maximum). Plotting of the I_0/I value against the concentration of the potential quencher yielded the following graphs.

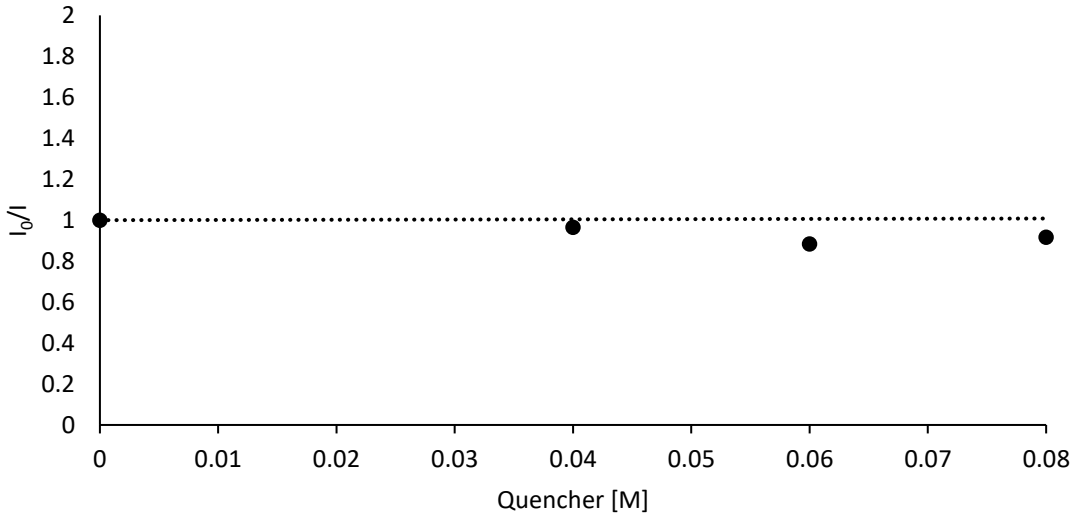

Figure 5.17: Fluorescence quenching of $Ir(ppy)_3$ with 2-phenylpyridine (**35a**).

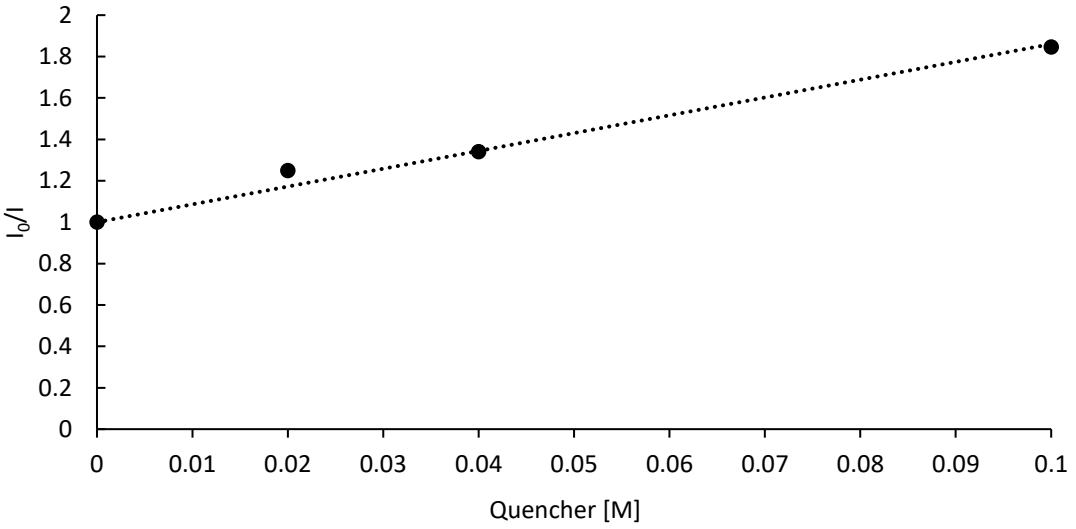

Figure 5.18: Fluorescence quenching of $Ir(ppy)_3$ with **100**.

5.6.2 Visible Light-Enabled Ruthenium-catalyzed *meta*-C–H Tertiary Alkylation

5.6.2.1 Analytical Data

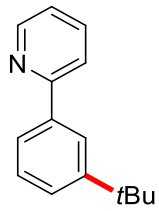

2-[3-(*tert*-Butyl)phenyl]pyridine (96aa)

The general procedure **D** was followed using 2-phenylpyridine (**35a**) (62.1 mg, 0.40 mmol) and alkyl bromide **95a** (164 mg, 1.20 mmol) for 24 h. Purification by column chromatography on silica gel (*n*-pentane/Et_2O: 5/1) yielded **96aa** (67.7 mg, 320 µmol, 80%) as a colorless oil.

^{1}H-NMR (400 MHz, $CDCl_3$): δ = 8.72 (ddd, *J* = 4.8, 1.3, 1.3 Hz, 1H), 8.07 (dd, *J* = 1.9, 1.9 Hz, 1H), 7.78 (ddd, *J* = 7.4, 1.5, 1.5 Hz, 1H), 7.75–7.70 (m, 2H), 7.50–7.40 (m, 2H), 7.25–7.19 (m, 1H), 1.41 (s, 9H). **^{13}C-NMR** (101 MHz, $CDCl_3$): δ = 158.2 (C_q), 151.7 (C_q), 149.7 (CH), 139.3 (C_q), 136.7 (CH), 128.6 (CH), 126.2 (CH), 124.3 (CH), 124.1 (CH), 122.0 (CH), 120.8 (CH), 35.0 (C_q), 31.5 (CH_3). **IR** (ATR): 2962, 1584, 1565, 1461, 1431, 1252, 771, 740, 699, 613 cm^{-1}. **MS** (ESI) *m/z* (relative intensity): 212 $[M+H]^+$ (100). **HR-MS** (ESI): *m/z* calcd for $C_{15}H_{18}N^+$ $[M+H]^+$ 212.1434, found 212.1437. The analytical data are in accordance with those reported in the literature.[109a]

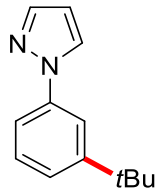

1-[3-(*tert*-Butyl)phenyl]-1*H*-pyrazole (189a)

The general procedure **D** was followed using 1-phenylpyrazole (57.7 mg, 0.40 mmol) and alkyl bromide **95a** (164 mg, 1.20 mmol) for 24 h at 60 °C. Purification by column chromatography on silica gel (*n*-pentane/Et_2O: 5/1) yielded **189a** (51.3 mg, 256 µmol, 64%) as colorless oil. **^{1}H-NMR** (400 MHz, $CDCl_3$): δ = 7.92 (dd, *J* = 2.5, 0.7 Hz, 1H), 7.80–

7.71 (m, 2H), 7.45 (ddd, *J* = 7.7, 2.2, 1.4 Hz, 1H), 7.40–7.31 (m, 2H), 6.46 (dd, *J* = 2.5, 1.8 Hz, 1H), 1.38 (s, 9H). **^{13}C-NMR** (101 MHz, $CDCl_3$): δ = 153.1 (C_q), 141.0 (CH), 140.2 (C_q), 129.1 (CH), 127.1 (CH), 123.8 (CH), 117.0 (CH), 116.6 (CH), 107.5 (CH), 35.1 (C_q), 31.4 (CH_3). **IR** (ATR): 2962, 1608, 1589, 1518, 1391, 1044, 947, 787, 746, 698 cm^{-1}. **MS** (ESI) *m/z* (relative intensity): 201 $[M+H]^+$ (100). **HR-MS** (ESI): *m/z* calcd for $C_{13}H_{17}N_2^+$ $[M+H]^+$ 201.1386, found 201.1390. The analytical data are in accordance with those reported in the literature.[113]

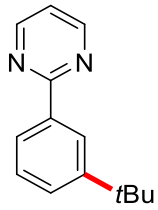

2-[3-(*tert*-Butyl)phenyl]pyrimidine (191a)

The general procedure **D** was followed using 1-phenylpyrimidine (62.5 mg, 0.40 mmol) and alkyl bromide **95a** (164 mg, 1.20 mmol) for 24 h at 60 °C. Purification by column chromatography on silica gel (*n*-pentane/Et_2O: 2/1) yielded **191a** (13.5 mg, 63.6 µmol, 16%) as colorless oil.

^{1}H-NMR (500 MHz, $CDCl_3$): δ = 8.81 (d, *J* = 4.8 Hz, 2H), 8.51 (dd, *J* = 1.9, 1.9 Hz, 1H), 8.26 (ddd, *J* = 7.7, 1.7, 1.2 Hz, 1H), 7.54 (ddd, *J* = 7.8, 2.1, 1.2 Hz, 1H), 7.44 (dd, *J* = 7.7, 7.7 Hz, 1H), 7.17 (t, *J* = 4.8 Hz, 1H), 1.41 (s, 9H). **^{13}C-NMR** (126 MHz, $CDCl_3$): δ = 165.3 (C_q), 157.3 (CH), 151.7 (C_q), 137.4 (C_q) 128.5 (CH), 128.1 (CH), 125.6 (CH), 125.2 (CH), 119.1 (CH), 35.0 (C_q), 31.6 (CH_3). **IR** (ATR): 2961, 1567, 1554, 1420, 1404, 1260, 786, 700, 648, 635 cm^{-1}. **MS** (ESI) *m/z* (relative intensity): 213 $[M+H]^+$ (100). **HR-MS** (ESI): *m/z* calcd for $C_{14}H_{17}N_2^+$ $[M+H]^+$ 213.1386, found 213.1391. The analytical data are in accordance with those reported in the literature.[113]

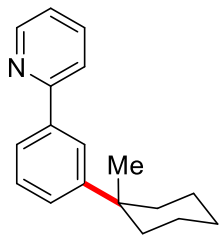

2-[3-(1-Methylcyclohexyl)phenyl]pyridine (96ab)

The general procedure **D** was followed using 2-phenylpyridine (**35a**) (62.1 mg, 0.40 mmol) and alkyl bromide **95b** (213 mg, 1.20 mmol) for 24 h. Purification by column chromatography on silica gel (*n*-pentane/Et_2O: 5/1) yielded **96ab** (63.3 mg, 252 µmol, 63%) as a colorless oil.

^{1}H-NMR (300 MHz, $CDCl_3$): δ = 8.71 (ddd, *J* = 4.8, 1.4, 1.4 Hz, 1H), 8.04 (dd, *J* = 2.0, 0.8 Hz, 1H), 7.81–7.69 (m, 3H), 7.50–7.40 (m, 2H), 7.21 (ddd, *J* = 5.6, 4.9, 2.9 Hz, 1H), 2.24–1.98 (m, 2H), 1.73–1.38 (m, 8H), 1.26 (s, 3H). **^{13}C-NMR** (101 MHz, $CDCl_3$): δ = 158.3 (C_q), 150.8 (C_q), 149.8 (CH), 139.5 (C_q), 136.7 (CH), 128.7 (CH), 126.8 (CH), 124.8 (CH), 124.1 (CH), 122.0 (CH), 120.9 (CH), 38.2 (C_q), 38.1 (CH_2), 30.4 (CH_3), 26.5 (CH_2), 22.8 (CH_2). **IR** (ATR): 2926, 2856, 1584, 1462, 1431, 907, 772, 729, 701, 613 cm^{-1}. **MS** (ESI) *m/z* (relative intensity): 252 $[M+H]^+$ (100). **HR-MS** (ESI): *m/z* calcd for $C_{18}H_{22}N^+$ $[M+H]^+$ 252.1747, found 252.1749.

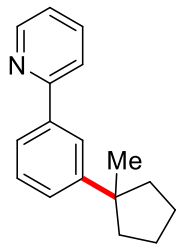

2-[3-(1-Methylcyclopentyl)phenyl]pyridine (96ac)

The general procedure **D** was followed using 2-phenylpyridine (**35a**) (62.1 mg, 0.40 mmol) and alkyl bromide **95c** (196 mg, 1.20 mmol) for 24 h. Purification by column chromatography on silica gel (*n*-pentane/Et_2O: 5/1) yielded **96ac** (63.3 mg, 329 µmol, 82%) as a colorless oil.

^{1}H-NMR (400 MHz, $CDCl_3$): δ = 8.71 (ddd, *J* = 4.8, 1.5, 1.5 Hz, 1H), 8.00 (ddd, *J* = 1.7, 1.0, 1.0 Hz, 1H), 7.80–7.75 (m, 1H), 7.75–7.71 (m, 2H), 7.46–7.36 (m, 2H), 7.25–7.18 (m, 1H), 2.06– 1.96 (m, 2H), 1.94–1.72 (m, 6H), 1.33 (s, 3H). **^{13}C-NMR** (101 MHz, $CDCl_3$): δ = 158.2 (C_q), 152.1 (C_q), 149.7 (CH), 139.3 (C_q), 136.7 (CH), 128.5 (CH), 127.0 (CH), 124.8 (CH), 124.2 (CH), 122.0 (CH), 120.8 (CH), 47.4 (C_q), 39.8 (CH_2), 29.6 (CH_3), 23.9 (CH_2). **IR** (ATR): 2956, 1585, 1565,1462, 1432, 907,772, 428, 701, 644 cm^{-1}. **MS** (ESI) *m/z* (relative intensity): 238 $[M+H]^+$ (100). **HR-MS** (ESI): *m/z* calcd for $C_{17}H_{20}N^+$ $[M+H]^+$ 238.1590, found 238.1595.

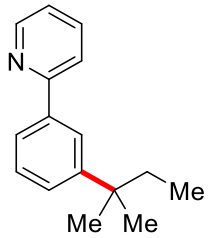

2-[3-(*tert*-Pentyl)phenyl]pyridine (96ad)

The general procedure **D** was followed using 2-phenylpyridine (**35a**) (62.1 mg, 0.40 mmol) and alkyl bromide **95d** (181 mg, 1.20 mmol) for 24 h. Purification by column chromatography on silica gel (*n*-pentane/Et_2O: 5/1) yielded **96ad** (63.3 mg, 284 µmol, 71%) as a colorless oil.

^{1}H-NMR (600 MHz, $CDCl_3$): δ = 8.71 (ddd, *J* = 4.8, 1.2, 1.2 Hz, 1H), 8.00 (ddd, *J* = 2.3, 1.0, 1.0 Hz, 1H), 7.81–7.76 (m, 1H), 7.75–7.70 (m, 2H), 7.44–7.38 (m, 2H), 7.21 (dddd, *J* = 5.7, 4.8, 2.6, 0.6 Hz, 1H), 1.73 (q, *J* = 7.4 Hz, 2H), 1.37 (s, 6H), 0.73 (t, *J* = 7.4 Hz, 3H). **^{13}C-NMR** (126 MHz, $CDCl_3$): δ = 158.1 (C_q), 150.0 (C_q), 149.6 (CH), 139.2 (C_q), 136.6 (CH), 128.4 (CH), 126.8 (CH), 124.7 (CH), 124.1 (CH), 121.9 (CH), 120.8 (CH), 38.3 (C_q), 37.1 (CH_2), 28.7 (CH_3), 9.4 (CH_3). **IR** (ATR): 2964, 1585, 1565, 1462, 1431, 907, 773, 729, 701, 644 cm^{-1}. **MS** (ESI) *m/z* (relative intensity): 248 $[M+Na]^+$ (26), 226 $[M+H]^+$ (100). **HR-MS** (ESI): *m/z* calcd for $C_{16}H_{20}N^+$ $[M+H]^+$ 226.1590, found 226.1592.

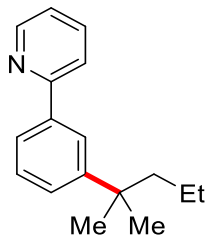

2-[3-(2-Methylpentan-2-yl)phenyl]pyridine (96ae)

The general procedure **D** was followed using 2-phenylpyridine (**35a**) (62.1 mg, 0.40 mmol) and alkyl bromide **95e** (198 mg, 1.20 mmol) for 24 h. Purification by column chromatography on silica gel (*n*-pentane/Et_2O: 5/1) yielded **96ae** (78.4 mg, 328 µmol, 82%) as a colorless oil.

^{1}H-NMR (400 MHz, $CDCl_3$): δ = 8.71 (ddd, *J* = 4.8, 1.5, 1.5 Hz, 1H), 8.00 (ddd, *J* = 1.7, 1.7, 1.0 Hz, 1H), 7.81–7.75 (m, 1H), 7.75–7.71 (m, 2H), 7.44–7.39 (m, 2H), 7.24–7.18 (m, 1H), 1.69–1.62 (m, 2H), 1.38 (s, 6H), 1.20–1.08 (m, 2H), 0.84 (t, *J* = 7.3 Hz, 3H). **^{13}C-NMR** (101 MHz, $CDCl_3$): δ = 158.2 (C_q), 150.5 (C_q), 149.7 (CH), 139.2 (C_q), 136.7 (CH), 128.5 (CH), 126.7 (CH), 124.6 (CH), 124.2 (CH), 122.0 (CH), 120.8 (CH), 47.3 (CH_2), 38.1 (C_q), 29.1 (CH_3), 18.1 (CH_2), 14.9 (CH_3). **IR** (ATR): 2957, 1585, 1565, 1462, 1432, 907, 772, 729, 700, 644 cm^{-1}. **MS** (ESI) *m/z* (relative intensity): 240 $[M+H]^+$ (100). **HR-MS** (ESI): *m/z* calcd for $C_{17}H_{22}N^+$ $[M+H]^+$ 240.1747, found 240.1741.

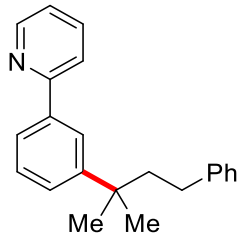

2-[3-(2-Methylpentan-2-yl)phenyl]pyridine (96af)

The general procedure **D** was followed using 2-phenylpyridine (**35a**) (62.1 mg, 0.40 mmol) and alkyl bromide **95f** (273 mg, 1.20 mmol) for 24 h. Purification by column chromatography on silica gel (*n*-pentane/Et_2O: 6/1) yielded **96af** (96.0 mg, 319 µmol, 80%) as a colorless oil.

^{1}H-NMR (400 MHz, $CDCl_3$): δ = 8.75 (ddd, *J* = 4.9, 1.4, 1.4 Hz, 1H), 8.08 (d, *J* = 2.4 Hz, 1H), 7.86–7.74 (m, 3H), 7.53–7.45 (m, 2H), 7.30–7.23 (m, 3H), 7.20–7.11 (m, 3H), 2.48–2.41 (m, 2H), 2.07–2.00 (m, 2H), 1.49 (s, 6H). **^{13}C-NMR** (101 MHz, $CDCl_3$): δ = 158.2 (C_q), 149.8 (CH), 149.8 (C_q), 143.2 (C_q), 139.5 (C_q), 136.8 (CH), 128.7 (CH), 128.4 (CH), 128.4 (CH), 126.8 (CH), 125.7 (CH), 124.7 (CH), 124.5 (CH), 122.1 (CH), 120.9 (CH), 46.8 (CH_2), 38.3 (C_q), 31.5 (CH_2), 29.2 (CH_3). **IR** (ATR): 2961, 1584, 1565, 1461, 1431, 908, 773, 732, 697, 613 cm^{-1}. **MS** (ESI) *m/z* (relative intensity): 302 $[M+H]^+$ (100). **HR-MS** (ESI): *m/z* calcd for $C_{22}H_{24}N^+$ $[M+H]^+$ 302.1903, found 302.1907.

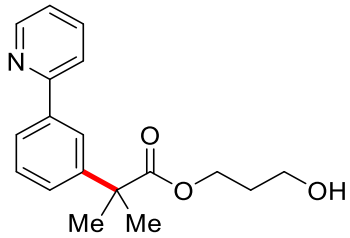

3-Hydroxypropyl 2-methyl-2-[3-(pyridin-2-yl)phenyl]propanoate (96ag)

The general procedure **D** was followed using phenyl pyridine **35a** (62.1 mg, 0.40 mmol) and alkyl bromide **95g** (270 mg, 1.20 mmol) for 48 h. Purification by column chromatography on silica gel (*n*-pentane/Et_2O: 2/1) yielded **96ag** (30.5 mg, 102 µmol, 25%) as colorless oil.

^{1}H-NMR (400 MHz, $CDCl_3$): δ = 8.64 (ddd, *J* = 4.9, 1.8, 0.9 Hz, 1H), 7.92 (d, *J* = 1.1 Hz, 1H), 7.79–7.66 (m, 3H), 7.47–7.39 (m, 2H), 7.25 (ddd, *J* = 7.4, 4.9, 1.4 Hz, 1H), 4.28 (t, *J* = 6.0 Hz, 2H), 3.51 (s_{br}, 1H), 3.46 (t, *J* = 6.0 Hz, 2H), 1.79 (tt, *J* = 6.0, 6.0 Hz, 2H), 1.63 (s, 6H). **^{13}C-NMR** (101 MHz, $CDCl_3$): δ = 177.1 (C_q), 157.7 (C_q), 149.6 (CH), 145.8 (C_q), 139.7 (C_q), 137.2 (CH), 128.9 (CH), 126.0 (CH), 125.5 (CH), 125.2 (CH), 122.4 (CH), 121.4 (CH), 61.5 (CH_2), 58.1 (CH_2), 47.1 (C_q), 31.2 (CH_2), 26.8 (CH_3). **IR** (ATR): 3350, 2971, 1722, 1463, 1253, 1146, 1050, 770, 744, 699 cm^{-1}. **MS** (ESI) *m/z* (relative intensity): 322 $[M+Na]^+$ (65), 300 $[M+H]^+$ (100). **HR-MS** (ESI): *m/z* calcd for $C_{18}H_{22}NO_3^+$ $[M+H]^+$ 300.1594, found 300.1597.

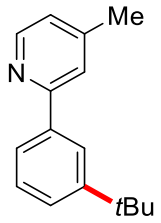

2-[3-(*tert*-Butyl)phenyl]-4-methylpyridine (96ca)

The general procedure **D** was followed using phenyl pyridine **35c** (67.7 mg, 0.40 mmol) and alkyl bromide **95a** (164 mg, 1.20 mmol) for 24 h. Purification by column chromatography on silica gel (*n*-pentane/Et_2O: 5/1) yielded **96ca** (68.1 mg, 302 µmol, 76%) as a colorless oil.

^{1}H-NMR (400 MHz, $CDCl_3$): δ = 8.57 (dd, *J* = 5.0, 0.8 Hz, 1H), 8.04 (ddd, *J* = 1.9, 1.9, 0.5 Hz, 1H), 7.76 (ddd, *J* = 7.4, 1.8, 1.3 Hz, 1H), 7.54 (ddd, *J* = 1.6, 0.8, 0.8 Hz, 1H), 7.46 (ddd, *J* = 7.8, 2.0, 1.3 Hz, 1H), 7.44–7.38 (m, 1H), 7.05 (ddd, *J* = 5.0, 1.6, 0.7 Hz, 1H), 2.41 (s, 3H), 1.41 (s,

9H). **^{13}C-NMR** (101 MHz, $CDCl_3$): δ = 158.1 (C_q), 151.6 (C_q), 149.5 (CH), 147.7 (C_q), 139.5 (C_q), 128.5 (CH), 126.0 (CH), 124.3 (CH), 124.1 (CH), 123.1 (CH), 121.8 (CH), 35.0 (C_q), 31.5 (CH_3), 21.3 (CH_3). **IR** (ATR): 2963, 1599, 1468, 1257, 907, 826, 797, 727, 701, 644 cm^{-1}. **MS** (ESI) *m/z* (relative intensity): 226 $[M+H]^+$ (100). **HR-MS** (ESI): *m/z* calcd for $C_{16}H_{20}N^+$ $[M+H]^+$ 226.1590, found 226.1595.

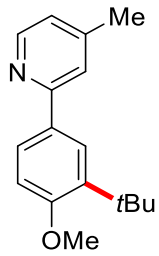

2-[3-(*tert*-Butyl)-4-methoxyphenyl]-4-methylpyridine (96da)

The general procedure **D** was followed using phenyl pyridine **35d** (79.7 mg, 0.40 mmol) and alkyl bromide **95a** (164 mg, 1.20 mmol) for 24 h. Purification by column chromatography on silica gel (*n*-pentane/Et_2O: 3/1) yielded **96da** (74.0 mg, 290 µmol, 72%) as a colorless oil.

^{1}H-NMR (400 MHz, $CDCl_3$): δ = 8.52 (dd, *J* = 5.0, 0.8 Hz, 1H), 7.95 (d, *J* = 2.3 Hz, 1H), 7.79 (dd, *J* = 8.5, 2.3 Hz, 1H), 7.48 (ddd, *J* = 1.6, 0.8, 0.8 Hz, 1H), 6.99 (ddd, *J* = 5.0, 1.6, 0.8 Hz, 1H), 6.96 (d, *J* = 8.5 Hz, 1H), 3.89 (s, 3H), 2.39 (s, 3H), 1.46 (s, 9H). **^{13}C-NMR** (101 MHz, $CDCl_3$): δ = 159.5 (C_q), 157.9 (C_q), 149.4 (CH), 147.5 (C_q), 138.5 (C_q), 131.7 (C_q), 125.8 (CH), 125.6 (CH), 122.4 (CH), 121.0 (CH), 111.7 (CH), 55.2 (CH_3), 35.1 (C_q), 29.9 (CH_3), 21.3 (CH_3). **IR** (ATR): 2956, 1603, 1454, 1279, 1235, 1179, 1029, 907, 811, 727 cm^{-1}. **MS** (ESI) *m/z* (relative intensity): 256 $[M+H]^+$ (100). **HR-MS** (ESI): *m/z* calcd for $C_{17}H_{22}NO^+$ $[M+H]^+$ 256.1696, found 256.1699. The analytical data are in accordance with those reported in the literature.[109a]

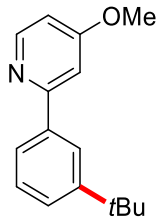

2-[3-(*tert*-Butyl)phenyl]-4-methoxypyridine (96ea)

The general procedure **D** was followed using phenyl pyridine **35e** (74.1 mg, 0.40 mmol) and alkyl bromide **95a** (164 mg, 1.20 mmol) for 24 h. Purification by column chromatography on silica gel (*n*-pentane/Et_2O: 3/1→2:1) yielded **96ea** (61.5 mg, 255 µmol, 64%) as a colorless oil.

^{1}H-NMR (400 MHz, $CDCl_3$): δ = 8.53 (dd, *J* = 5.7, 0.5 Hz, 1H), 8.02 (ddd, *J* = 1.9 1.9, 0.5 Hz, 1H), 7.73 (ddd, *J* = 7.5, 1.8, 1.3 Hz, 1H), 7.47 (ddd, *J* = 7.8, 2.0, 1.3 Hz, 1H), 7.43–7.38 (m, 1H), 7.23 (dd, *J* = 2.5, 0.5 Hz, 1H), 6.77 (dd, *J* = 5.7, 2.4 Hz, 1H), 3.90 (s, 3H), 1.40 (s, 9H). **^{13}C-NMR** (101 MHz, $CDCl_3$): δ = 166.4 (C_q), 160.0 (C_q), 151.7 (C_q), 151.0 (CH), 139.4 (C_q), 128.5 (CH), 126.2 (CH), 124.3 (CH), 124.2 (CH), 107.9 (CH), 107.3 (CH), 55.3 (CH_3), 35.0 (C_q), 31.5 (CH_3). **IR** (ATR): 2962, 1590, 1472, 1211, 1036, 908, 798, 729, 701 cm^{-1}. **MS** (ESI) *m/z* (relative intensity): 242 $[M+H]^+$ (100). **HR-MS** (ESI): *m/z* calcd for $C_{16}H_{20}NO^+$ $[M+H]^+$ 242.1539, found 242.1539.

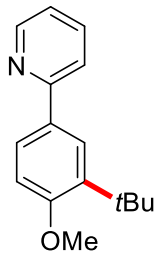

2-[3-(*tert*-Butyl)-4-methoxyphenyl]pyridine (**96ba**)

The general procedure **D** was followed using phenyl pyridine **35b** (74.0 mg, 0.40 mmol) and alkyl bromide **95a** (164 mg, 1.20 mmol) for 24 h. Purification by column chromatography on silica gel (*n*-pentane/Et_2O: 3/1) yielded **96ba** (28.0 mg, 116 µmol, 29%) as pale-yellow oil.

^{1}H-NMR (500 MHz, $CDCl_3$): δ = 8.66 (ddd, *J* = 4.8, 1.8, 1.0 Hz, 1H), 7.96 (d, *J* = 2.3 Hz, 1H), 7.80 (dd, *J* = 8.4, 2.3 Hz, 1H), 7.72–7.64 (m, 2H), 7.16 (ddd, *J* = 7.1, 4.8, 1.4 Hz, 1H), 6.97 (d, *J* = 8.5 Hz, 1H), 3.90 (s, 3H), 1.45 (s, 9H). **^{13}C-NMR** (126 MHz, $CDCl_3$): δ = 160.0 (C_q), 158.0(C_q), 149.6 (CH), 138.5 (C_q), 136.6 (CH), 131.6 (C_q), 125.8 (CH), 125.6 (CH), 121.3 (CH), 120.1 (CH), 111.7 (CH), 55.3 (CH_3), 35.2 (C_q), 29.8 (CH_3). **IR** (ATR): 1586, 1463, 1439, 1429,

1271, 1235, 1180, 1092, 1027, 779 cm^{-1}. **MS** (ESI) *m/z* (relative intensity): 242 $[M+H]^+$ (100). **HR-MS** (ESI): *m/z* calcd for $C_{16}H_{20}NO^+$ $[M+H]^+$ 242.1539, found 242.1541. The analytical data are in accordance with those reported in the literature.[109a]

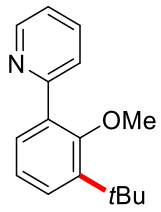

2-[3-(*tert*-Butyl)-2-methoxyphenyl]pyridine (96fa)

The general procedure **D** was followed using phenyl pyridine **35f** (74.1 mg, 0.40 mmol) and alkyl bromide **95a** (164 mg, 1.20 mmol) for 24 h. Purification by column chromatography on silica gel (*n*-pentane/Et_2O: 3/1) yielded **96fa** (54.6 mg, 226 µmol, 57%) as colorless oil.

^{1}H-NMR (400 MHz, $CDCl_3$): δ = 8.73 (ddd, *J* = 4.9, 1.8, 1.0 Hz, 1H), 7.78–7.67 (m, 2H), 7.47 (dd, *J* = 7.6, 1.8 Hz, 1H), 7.36 (dd, *J* = 7.9, 1.8 Hz, 1H), 7.22 (ddd, *J* = 7.2, 4.9, 1.5 Hz, 1H), 7.14–7.08 (m, 1H), 3.33 (s, 3H), 1.44 (s, 9H).**^{13}C-NMR** (101 MHz, $CDCl_3$): δ = 158.0 (C_q), 149.9 (CH), 149.8 (C_q), 143.0 (C_q), 136.2 (CH), 134.3 (C_q), 130.0 (CH), 127.5 (CH), 124.7 (CH), 123.5 (CH), 121.8 (CH), 61.4 (CH_3), 35.3 (C_q), 31.0 (CH_3). **IR** (ATR): 1588, 1428, 1409, 1224, 1088, 1006, 778, 746, 674, 615 cm^{-1}. **MS** (ESI) *m/z* (relative intensity): 242 $[M+H]^+$ (100). **HR-MS** (ESI): *m/z* calcd for $C_{16}H_{20}NO^+$ $[M+H]^+$ 242.1539, found 242.1539.

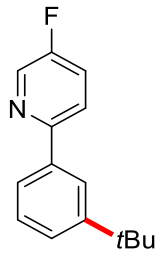

2-[3-(*tert*-Butyl)phenyl]-5-fluoropyridine (96ga)

The general procedure **D** was followed using phenyl pyridine **35g** (69.3 mg, 0.40 mmol) and alkyl bromide **95a** (164 mg, 1.20 mmol) for 24 h. Purification by column

chromatography on silica gel (*n*-pentane/Et_2O: 9/1) yielded **96fa** (25.0 mg, 109 µmol, 27%) as colorless oil.

^{1}H-NMR (400 MHz, $CDCl_3$): δ = 8.55 (d, *J* = 2.9 Hz, 1H), 7.99 (dd, *J* = 1.9, 1.9 Hz, 1H), 7.74–7.68 (m, 2H), 7.50–7.37 (m, 3H), 1.40 (s, 9H). **^{13}C-NMR** (101 MHz, $CDCl_3$): δ = 158.9 (d, $^1J_{C-F}$ = 256.0 Hz, C_q), 154.5 (d, $^1J_{C-F}$ = 3.9 Hz, C_q), 151.9 (C_q), 138.4 (C_q), 137.8 (d, $^2J_{C-F}$ = 23.4 Hz, CH), 128.8 (CH), 126.2 (CH), 124.2 (CH), 124.0 (CH), 123.6 (d, $^2J_{C-F}$ = 18.5 Hz, CH), 121.6 (d, $^3J_{C-F}$ = 4.2 Hz, CH), 35.0 (C_q), 31.5 (CH_3). **^{19}F-NMR** (378 MHz, $CDCl_3$): δ = −130.2 (dd, *J* = 8.1, 4.3 Hz). **IR** (ATR): 2963, 1469, 1421, 1254, 1237, 1224, 835, 796, 700, 569 cm^{-1}. **MS** (ESI) *m/z* (relative intensity): 252 $[M+Na]^+$ (10), 230 $[M+H]^+$ (100). **HR-MS** (ESI): *m/z* calcd for $C_{15}H_{17}NF^+$ $[M+H]^+$ 230.1340, found 230.1334. The analytical data are in accordance with those reported in the literature.[109a]

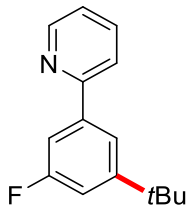

2-[3-(*tert*-Butyl)-5-fluorophenyl]pyridine (96ha)

The general procedure **D** was followed using phenyl pyridine **35h** (69.3 mg, 0.40 mmol) and alkyl bromide **95a** (164 mg, 1.20 mmol) for 24 h. Purification by column chromatography on silica gel (*n*-pentane/Et_2O: 9/1) yielded **96ha** (35.2 mg, 153 µmol, 38%) as colorless oil.

^{1}H-NMR (400 MHz, $CDCl_3$): δ = 8.70 (ddd, *J* = 4.8, 1.8, 1.0 Hz, 1H), 7.81 (dd, *J* = 1.6, 1.6 Hz, 1H), 7.75 (ddd, *J* = 8.0, 7.3, 1.8 Hz, 1H), 7.69 (ddd, *J* = 8.0, 1.2, 1.2 Hz, 1H), 7.50 (ddd, *J* = 9.7, 2.5, 1.5 Hz, 1H), 7.24 (ddd, *J* = 7.3, 4.7, 1.2 Hz, 1H), 7.14 (ddd, *J* = 10.6, 2.4, 1.7 Hz, 1H), 1.38 (s, 9H). **^{13}C-NMR** (126 MHz, $CDCl_3$): δ = 163.7 (d, $^1J_{C-F}$ = 244.2 Hz, C_q), 157.1 (d, $^4J_{C-F}$ = 3.0 Hz, C_q), 154.7 (d, $^3J_{C-F}$ = 6.8 Hz, C_q), 150.1 (CH), 141.5 (d, $^3J_{C-F}$ = 8.0 Hz, C_q), 137.2 (CH), 122.8 (CH), 121.1 (CH), 120.0 (d, $^4J_{C-F}$ = 2.3 Hz, CH), 113.5 (d, $^2J_{C-F}$ = 21.8 Hz, CH), 111.4 (d, $^2J_{C-F}$ = 22.9 Hz, CH), 35.5 (d, $^4J_{C-F}$ = 1.7 Hz, C_q), 31.8 (CH_3). **^{19}F-NMR** (282 MHz, $CDCl_3$): δ = −113.8 (dd, *J* = 10.2, 10.2 Hz). **IR** (ATR): 2965, 1586, 1567, 1429, 1412, 942, 866, 781, 733,

697 cm^{-1}. **MS** (ESI) *m/z* (relative intensity): 230 $[M+H]^+$ (100). **HR-MS** (ESI): *m/z* calcd for $C_{15}H_{17}NF^+$ $[M+H]^+$ 230.1340, found 230.1341.

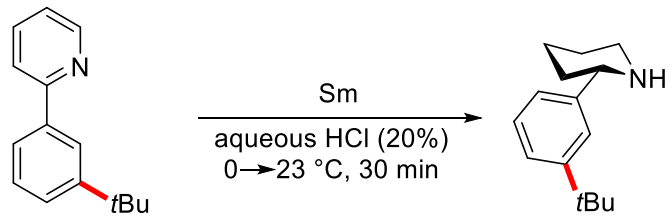

96aa **192**: 63%

2-[3-(*tert*-Butyl)phenyl]piperidine (192)

Following a modified literature procedure,[228] to an oven-dried 10 mL Schlenk flask was added 2-[3-(*tert*-butyl)phenyl]pyridine (**96aa**) (21.1 mg, 100 µmol, 1.00 equiv) and aqueous HCl (20%, 2.0 mL). The resulting solution was cooled in an ice bath and Sm (180 mg, 1.20 mmol, 12.0 equiv) was added portion wise over a period of 10 min. The reaction mixture was allowed to warm to ambient temperature and was then stirred for additional 20 min. The mixture was again put in an ice bath and the pH value was adjusted to pH = 8 by addition of aqueous NaOH solution (2 M). The aqueous layer was extracted with CH_2Cl_2 (3 x 20 mL). The combined organic layers were washed with H_2O (20 mL) and dried over Na_2SO_4. Removal of the solvent yielded the crude product, which was purified by column chromatography on silica gel (CH_2Cl_2/MeOH: 98/2 to 95/5) to yield the product **192** (13.6 mg, 62.6 µmol, 63%) as a pale yellow oil.

^{1}H-NMR (600 MHz, CD_2Cl_2): δ = 7.37 (dd, *J* = 1.9, 1.9 Hz, 1H), 7.25 (ddd, *J* = 7.8, 2.1, 1.4 Hz, 1H), 7.22 (dd, *J* = 7.6 Hz, 1H), 7.15 (ddd, *J* = 7.2, 1.8, 1.8 Hz, 1H), 3.56 (dd, *J* = 10.5, 2.7 Hz, 1H), 3.16–3.11 (m, 1H), 2.76 (ddd, *J* = 11.6, 11.6, 2.9 Hz, 1H), 1.90–1.83 (m, 1H), 1.83 (s_{br}, 1H), 1.77–1.70 (m, 1H), 1.65–1.58 (m, 1H), 1.53–1.42 (m, 3H), 1.30 (s, 9H). **^{13}C-NMR** (101 MHz, $CDCl_3$): δ =151.3 (C_q), 145.3 (C_q), 128.2 (CH), 124.1 (CH), 123.9 (CH), 123.8 (CH), 63.0 (CH), 48.0 (CH_2), 35.2 (CH_2), 34.9 (C_q), 31.6 (CH_3), 26.0 (CH_2), 25.7 (CH_2). **IR** (ATR): 2931, 2853, 1440, 1364, 1324, 1108, 792, 758, 706, 537 cm^{-1}. **MS** (ESI) *m/z* (relative intensity): 218 $[M+H]^+$ (100). **HR-MS** (ESI): *m/z* calcd for $C_{15}H_{24}N^+$ 218.1903 $[M+H]^+$, found 218.1906.

5.6.2.2 Mechanistic Studies

5.6.2.2.1 *meta*-C–H Alkylation in the Presence of Typical Radical Scavengers

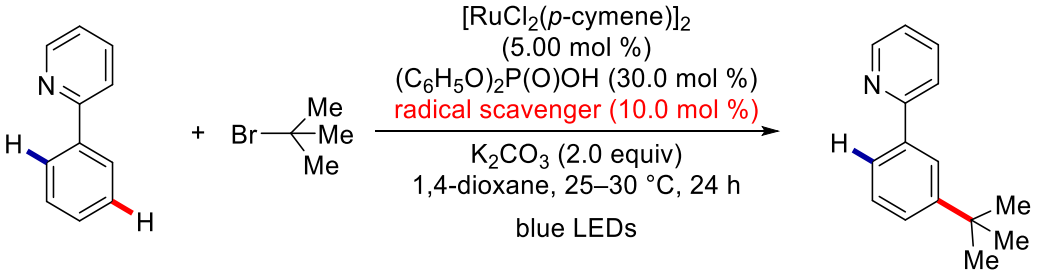

35a **95a** **96aa**

To an oven-dried 10 mL vial were added $[RuCl_2(p\text{-cymene})]_2$ (12.2 mg, 5.0 mol %), diphenyl phosphate (30.0 mg, 30.0 mol %), and K_2CO_3 (111 mg, 0.80 mmol, 2.0 equiv) and, in case the radical scavenger was a solid, the radical scavenger (10 mol %). The vial was capped with a septum and wrapped with Parafilm. After the vial was evacuated and backfilled with N_2 three times, 1,4-dioxane (2.0 mL) was added *via* syringe. 2-Phenylpyridine (**35a**) (62.1 mg, 0.40 mmol, 1.00 equiv) and *tert*-butyl bromide (**95a**) (164 mg, 1.20 mmol, 3.00 equiv) were added sequentially - in case the radical scavenger was a liquid, it was added now - and the reaction mixture was degassed. Finally, the puncture hole in the septum was sealed with electrical tape. The reaction mixture was stirred for 24 h under visible light irradiation. After 24 h the mixture was filtered over a short pad of silica (Et_2O) and the solvent was removed under reduced pressure. The residue was purified by column chromatography on silica gel (*n*-pentane/Et_2O = 5/1) affording product **96aa**.

Table 5.3: Effect of typical radical scavengers on the reaction.[a]

Entry	Radical scavenger (10 mol %)	Yield [%]
1	--	80
2	TEMPO	--
3	Galvinoxyl free radical	--
4	BHT	48
5	1,1-Diphenylethylene	17

[a] Yield of isolated product.

5.6.2.2.2 Competition Experiments Between Alkyl Halides

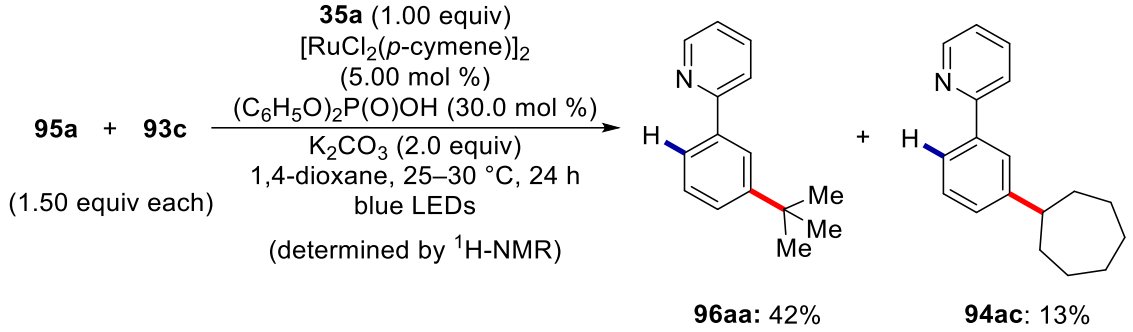

The general procedure was followed using 2-phenylpyridine (**35a**) (62.1 mg, 0.40 mmol) and alkyl bromides **95a** (82.2 mg, 0.60 mmol, 1.50 equiv) and **93c** (106 mg, 0.60 mmol, 1.50 equiv). After 24 h of irradiation, the mixture was filtered over a short pad of silica (Et_2O) and the solvent was removed under reduced pressure. The crude mixture was analyzed by ^{1}H-NMR spectroscopy using CH_2Br_2 as internal standard (17.6 mg, 0.101 mmol).

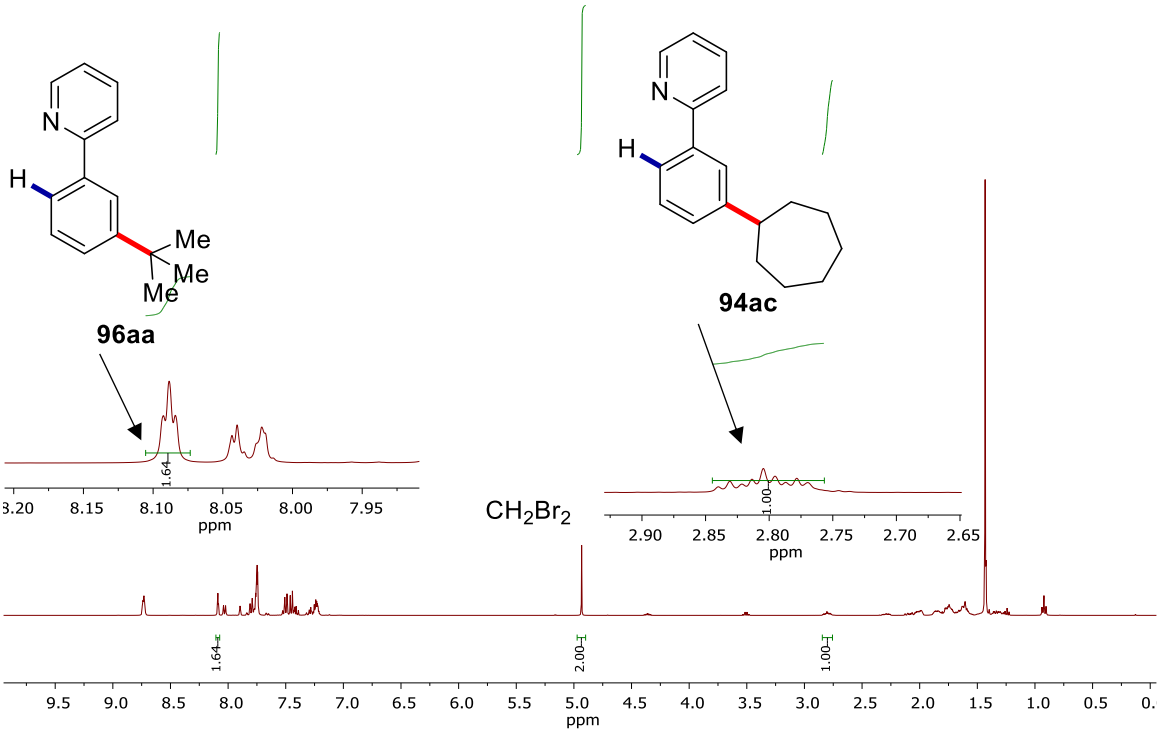

Figure 5.19: ^{1}H-NMR spectra of the crude reaction mixture.

5.6.2.2.3 Effect of Light: On/Off Plot

According to the general procedure, a reaction containing mesitylene as internal standard was set up and placed in front of the LEDs. The reaction was sequentially stirred under visible light irradiation and in the absence of light. Every two hours an aliquot of 50 µL was removed *via* syringe and analyzed by ^{1}H-NMR spectroscopy. After a total of 8 h the determined yields were plotted against the reaction time.

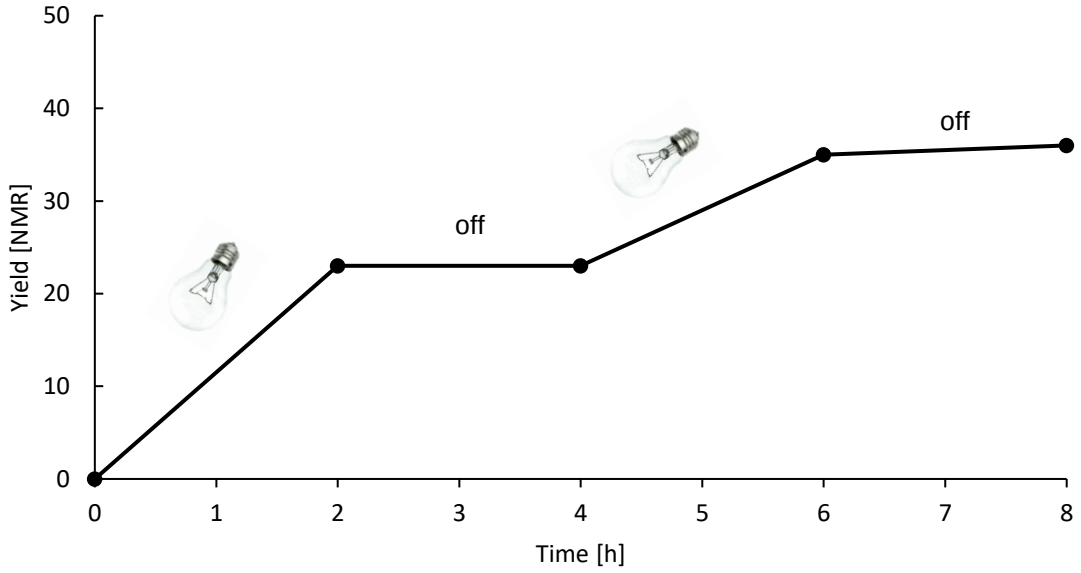

Figure 5.20: Effect of visible light irradiation.

5.6.2.2.4 Fluorescence Quenching Experiments

Sample solutions were prepared in 1,4-dioxane with $c_{(Ru)}$ = 1.6 x 10^{-6} M and varying concentrations of *tert*-butyl bromide (**95a**), added to each sample from a stock solution. The experiments were conducted with a fixed excitation wavelength of 430 nm and detection at 493 nm (emission maximum). Plotting of the I_0/I value against the concentration of the potential quencher yielded the following graphs.

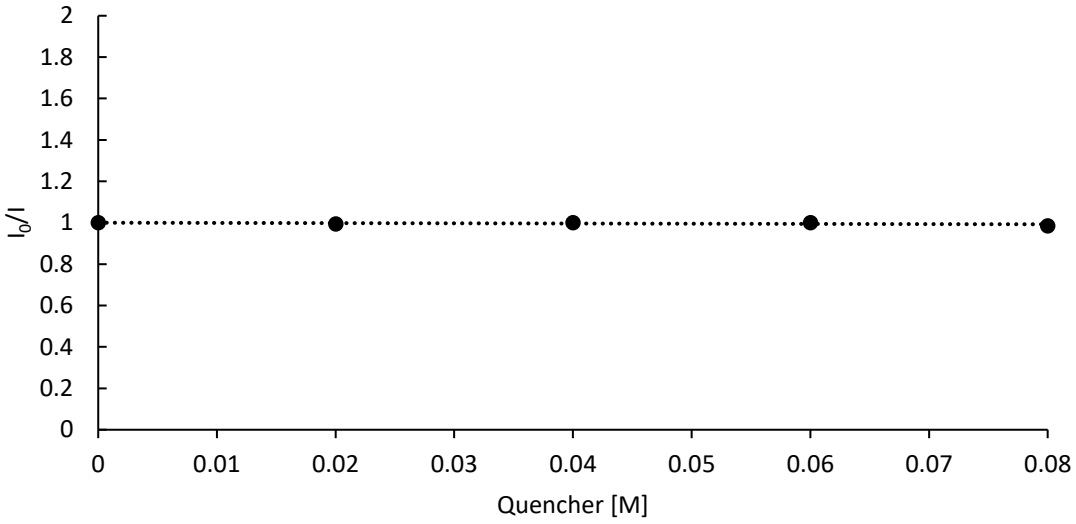

Figure 5.21: Fluorescence quenching of **196** with complex with **95a**.

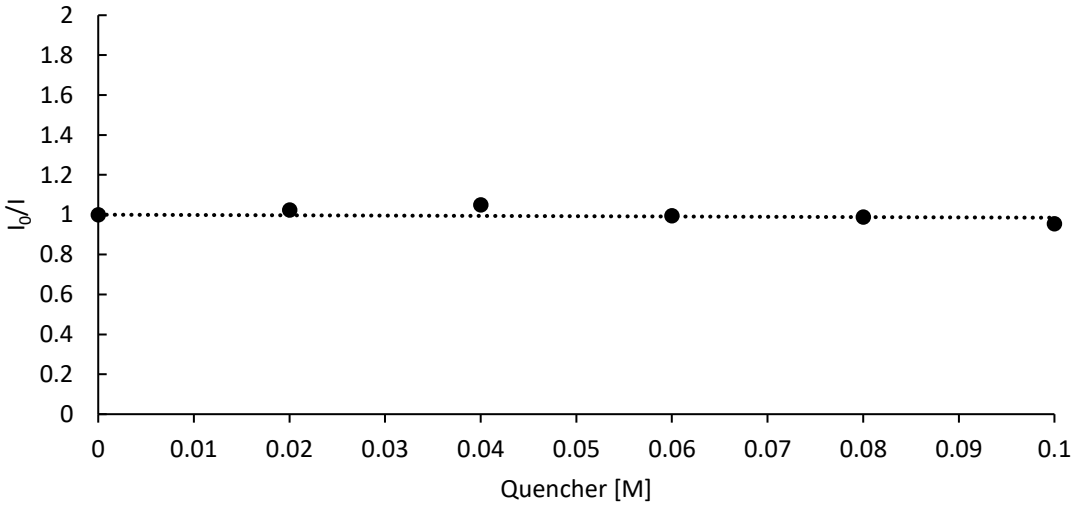

Figure 5.22: Fluorescence quenching of chloro-ruthenacycle **194** in the presence of 10.0 equiv. of substrate **35a** with **95a**.

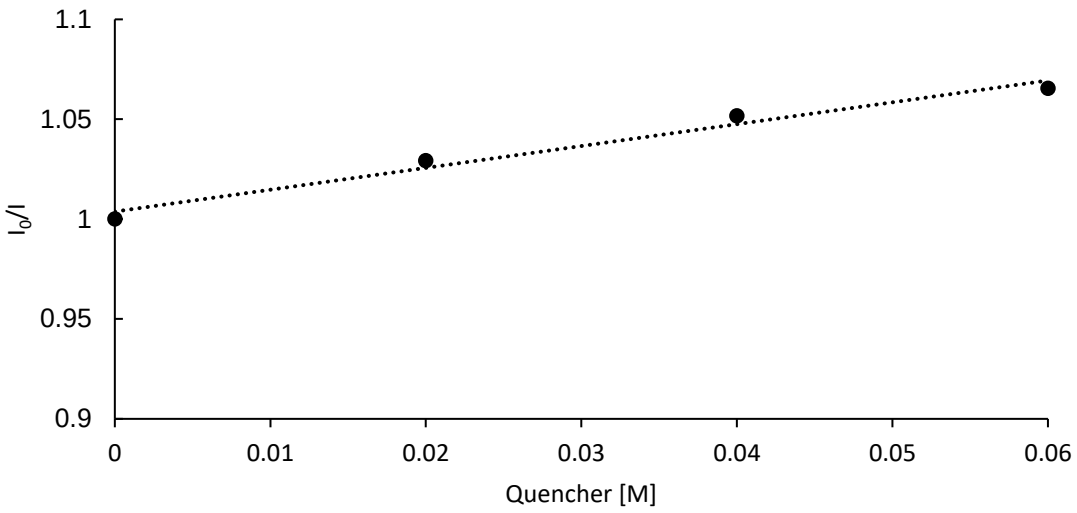

Figure 5.23: Fluorescence quenching of chloro-ruthenacycle **194** in the presence of 10.0 equiv. of substrate **35a** and 30.0 mol % diphenyl phosphate with **95a**.

6 References

[1] V. Smil, *Nature* **1999**, *400*, 415–415.

[2] J. W. Erisman, M. A. Sutton, J. Galloway, Z. Klimont, W. Winiwarter, *Nat. Geosci.* **2008**, *1*, 636–639.

[3] The Nobel Prize in Chemistry 1918, Nobel Media AB, www.nobelprize.org/prizes/chemistry/1918/summary/, accessed on Thu. 23 May 2019.

[4] The Nobel Prize in Chemistry 1931, Nobel Media AB, www.nobelprize.org/prizes/chemistry/1931/summary/, accessed on Thu. 23 May 2019.

[5] R. A. Sheldon, *Green Chem.* **2016**, *18*, 3180–3183.

[6] B. M. Trost, *Science* **1991**, *254*, 1471–1477.

[7] a) R. A. Sheldon, in *Pure Appl. Chem., Vol. 72*, **2000**, p. 1233; b) B. M. Trost, *Angew. Chem. Int. Ed.* **1995**, *34*, 259–281.

[8] P. T. Anastas, J. C. Warner, *Green Chemistry: Theory and Practice*, Oxford University Press, Oxford, UK, **1998**.

[9] W. S. Knowles, *Adv. Synth. Catal.* **2003**, *345*, 3–13.

[10] R. Noyori, *Angew. Chem. Int. Ed.* **2002**, *41*, 2008–2022.

[11] K. B. Sharpless, *Angew. Chem. Int. Ed.* **2002**, *41*, 2024–2032.

[12] The Nobel Prize in Chemistry 2001, Nobel Media AB, www.nobelprize.org/prizes/chemistry/2001/summary, accessed on Fri. 24 May 2019.

[13] Y. Chauvin, *Angew. Chem. Int. Ed.* **2006**, *45*, 3740–3747.

[14] R. H. Grubbs, *Angew. Chem. Int. Ed.* **2006**, *45*, 3760–3765.

[15] R. R. Schrock, *Angew. Chem. Int. Ed.* **2006**, *45*, 3748–3759.

[16] The Nobel Prize in Chemistry 2005, Nobel Media AB, www.nobelprize.org/prizes/chemistry/2005/summary, accessed on Fri. 24 May 2019.

[17] E.-i. Negishi, *Angew. Chem. Int. Ed.* **2011**, *50*, 6738–6764.

[18] A. Suzuki, *Angew. Chem. Int. Ed.* **2011**, *50*, 6722–6737.

[19] The Nobel Prize in Chemistry 2010, Nobel Media AB, www.nobelprize.org/prizes/chemistry/2010/summary/, accessed on Fri. 24 May 2019.

[20] G. Ertl, *Angew. Chem. Int. Ed.* **2008**, *47*, 3524–3535.

[21] The Nobel Prize in Chemistry 2007, Nobel Media AB, https://www.nobelprize.org/prizes/chemistry/2007/summary/, accessed on Thu. 12 September 2019.

[22] a) C. Torborg, M. Beller, *Adv. Synth. Catal.* **2009**, *351*, 3027–3043; b) M. Beller, A. Zapf, W. Magerlein, *Chem. Eng. Technol.* **2001**, *24*, 575–582.

[23] P. A. Wender, V. A. Verma, T. J. Paxton, T. H. Pillow, *Acc. Chem. Res.* **2008**, *41*, 40–49.

[24] L. Ackermann, R. Vicente, A. R. Kapdi, *Angew. Chem. Int. Ed.* **2009**, *48*, 9792–9826.

[25] P. Gandeepan, T. Müller, D. Zell, G. Cera, S. Warratz, L. Ackermann, *Chem. Rev.* **2019**, *119*, 2192–2452.

[26] T. H. Meyer, L. H. Finger, P. Gandeepan, L. Ackermann, *Trends Chem.* **2019**, *1*, 63–76.

[27] R. G. Bergman, *Nature* **2007**, *446*, 391–393.

[28] X. S. Xue, P. Ji, B. Zhou, J. P. Cheng, *Chem. Rev.* **2017**, *117*, 8622–8648.

[29] a) W. Ma, P. Gandeepan, J. Li, L. Ackermann, *Org. Chem. Front.* **2017**, *4*, 1435–1467; b) Z. K. Chen, B. J. Wang, J. T. Zhang, W. L. Yu, Z. X. Liu, Y. H. Zhang, *Org. Chem. Front.* **2015**, *2*, 1107–1295; c) L. Ackermann, in *Directed Metallation* (Ed.: N. Chatani), Springer-Verlag Berlin Heidelberg, Berlin, Heidelberg, **2007**, pp. 35–60.

[30] M. Zhang, Y. F. Zhang, X. M. Jie, H. Q. Zhao, G. Li, W. P. Su, *Org. Chem. Front.* **2014**, *1*, 843–895.

[31] W. Wang, M. M. Lorion, J. Shah, A. R. Kapdi, L. Ackermann, *Angew. Chem. Int. Ed.* **2018**, *57*, 14700–14717.

[32] J. Wencel-Delord, F. Glorius, *Nat. Chem.* **2013**, *5*, 369–375.

[33] K. Godula, D. Sames, *Science* **2006**, *312*, 67–72.

[34] a) C. Shan, L. Zhu, L. B. Qu, R. Bai, Y. Lan, *Chem. Soc. Rev.* **2018**, *47*, 7552–7576; b) D. L. Davies, S. A. Macgregor, C. L. McMullin, *Chem. Rev.* **2017**, *117*, 8649–8709; c) L. Ackermann, *Chem. Rev.* **2011**, *111*, 1315–1345; d) D. Balcells, E. Clot, O. Eisenstein, *Chem. Rev.* **2010**, *110*, 749–823; e) Y. Boutadla, D. L. Davies, S. A. Macgregor, A. I. Poblador-Bahamonde, *Dalton Trans.* **2009**, 5820–5831; f) J. A. Labinger, J. E. Bercaw, *Nature* **2002**, *417*, 507–514; g) B. Biswas, M. Sugimoto, S. Sakaki, *Organometallics* **2000**, *19*, 3895–3908.

[35] a) A. P. Walsh, W. D. Jones, *Organometallics* **2015**, *34*, 3400–3407; b) S. Potavathri, K. C. Pereira, S. I. Gorelsky, A. Pike, A. P. LeBris, B. DeBoef, *J. Am. Chem. Soc.* **2010**, *132*, 14676–14681; c) D. Lapointe, K. Fagnou, *Chem. Lett.* **2010**, *39*, 1118–1126; d) S. I. Gorelsky, D. Lapointe, K. Fagnou, *J. Am. Chem. Soc.* **2008**, *130*, 10848–10849; e) D. Garcia-Cuadrado, A. A. Braga, F. Maseras, A. M. Echavarren, *J. Am. Chem. Soc.* **2006**, *128*, 1066–1067.

[36] D. L. Davies, S. M. Donald, S. A. Macgregor, *J. Am. Chem. Soc.* **2005**, *127*, 13754–13755.

[37] a) W. Liu, S. C. Richter, Y. Zhang, L. Ackermann, *Angew. Chem. Int. Ed.* **2016**, *55*, 7747–7750; b) W. Ma, R. Mei, G. Tenti, L. Ackermann, *Chem. Eur. J.* **2014**, *20*, 15248–15251.

[38] J. Oxgaard, W. J. Tenn, R. J. Nielsen, R. A. Periana, W. A. Goddard, *Organometallics* **2007**, *26*, 1565–1567.

[39] a) Y. Yang, J. Lan, J. You, *Chem. Rev.* **2017**, *117*, 8787–8863; b) J. He, M. Wasa, K. S. L. Chan, Q. Shao, J. Q. Yu, *Chem. Rev.* **2017**, *117*, 8754–8786; c) N. Della Ca, M. Fontana, E. Motti, M. Catellani, *Acc. Chem. Res.* **2016**, *49*, 1389–1400; d) S. R. Neufeldt, M. S. Sanford, *Acc. Chem. Res.* **2012**, *45*, 936–946; e) X. Chen, K. M. Engle, D. H. Wang, J. Q. Yu, *Angew. Chem. Int. Ed.* **2009**, *48*, 5094–5115.

[40] a) S. G. Pan, T. Shibata, *ACS Catal.* **2013**, *3*, 704–712; b) J. Choi, A. S. Goldman, in *Iridium Catalysis* (Ed.: P. G. Andersson), Springer-Verlag Berlin Heidelberg, Berlin, Heidelberg, **2011**, pp. 139–167; c) I. A. Mkhalid, J. H. Barnard, T. B. Marder, J. M. Murphy, J. F. Hartwig, *Chem. Rev.* **2010**, *110*, 890–931.

[41] a) S. S. Li, L. Qin, L. Dong, *Org. Biomol. Chem.* **2016**, *14*, 4554–4570; b) G. Song, F. Wang, X. Li, *Chem. Soc. Rev.* **2012**, *41*, 3651–3678; c) D. A. Colby, A. S. Tsai, R. G. Bergman, J. A. Ellman, *Acc. Chem. Res.* **2012**, *45*, 814–825; d) D. A. Colby, R. G. Bergman, J. A. Ellman, *Chem. Rev.* **2010**, *110*, 624–655.

[42] C. A. Flemming, J. T. Trevors, *Water Air Soil Pollut.* **1989**, *44*, 143–158.

[43] S. E. Allen, R. R. Walvoord, R. Padilla-Salinas, M. C. Kozlowski, *Chem. Rev.* **2013**, *113*, 6234–6458.

[44] a) W. H. Rao, B. F. Shi, *Org. Chem. Front.* **2016**, *3*, 1028–1047; b) W. Hao, Y. Liu, *Beilstein J. Org. Chem.* **2015**, *11*, 2132–2144; c) X. X. Guo, D. W. Gu, Z. Wu, W. Zhang, *Chem. Rev.* **2015**, *115*, 1622–1651; d) J. P. Wan, Y. Jing, *Beilstein J. Org. Chem.* **2015**, *11*, 2209–2222; e) C. Sambiagio, S. P. Marsden, A. J. Blacker, P. C. McGowan, *Chem. Soc. Rev.* **2014**, *43*, 3525–3550; f) G. Evano, N. Blanchard, *Copper-Mediated Cross-Coupling Reactions*, John Wiley & Sons, Hoboken, **2013**; g) I. P. Beletskaya, A. V. Cheprakov, *Coord. Chem. Rev.* **2004**, *248*, 2337–2364.

[45] a) L. Ackermann, *Modern Arylation Methods*, Wiley-VCH, Weinheim, **2009**; b) I. Goldberg, *Ber. Dtsch. Chem. Ges.* **1906**, *39*, 1691–1692; c) F. Ullmann, P. Sponagel, *Ber. Dtsch. Chem. Ges.* **1905**, *38*, 2211–2212; d) F. Ullmann, *Ber. Dtsch. Chem. Ges.* **1903**, *36*, 2382–2384; e) F. Ullmann, J. Bielecki, *Ber. Dtsch. Chem. Ges.* **1901**, *34*, 2174–2185.

[46] W. R. H. Hurtley, *J. Chem. Soc.* **1929**, 1870–1873.

[47] E. Sperotto, G. P. van Klink, G. van Koten, J. G. de Vries, *Dalton Trans.* **2010**, *39*, 10338–10351.
[48] A. J. Paine, *J. Am. Chem. Soc.* **1987**, *109*, 1496–1502.
[49] a) M. Mansour, R. Giacovazzi, A. Ouali, M. Taillefer, A. Jutand, *Chem. Commun.* **2008**, 6051–6053; b) A. Ouali, M. Taillefer, J. F. Spindler, A. Jutand, *Organometallics* **2007**, *26*, 65–74.
[50] C. Björklund, M. Nilsson, T. Olson, T. Norin, *Acta Chem. Scand.* **1968**, *22*, 2338–2346.
[51] H. Ljusberg, R. Wahren, *Acta Chem. Scand.* **1973**, *27*, 2717–2721.
[52] S. Pivsa-Art, T. Satoh, Y. Kawamura, M. Miura, M. Nomura, *Bull. Chem. Soc. Jpn.* **1998**, *71*, 467–473.
[53] a) S. Pivsa-Art, Y. Fukui, M. Miura, M. Nomura, *Bull. Chem. Soc. Jpn.* **1996**, *69*, 2039–2042; b) J. Lindley, *Tetrahedron* **1984**, *40*, 1433–1456.
[54] H. Q. Do, O. Daugulis, *J. Am. Chem. Soc.* **2007**, *129*, 12404–12405.
[55] H. Q. Do, O. Daugulis, *J. Am. Chem. Soc.* **2008**, *130*, 1128–1129.
[56] H. Q. Do, R. M. Khan, O. Daugulis, *J. Am. Chem. Soc.* **2008**, *130*, 15185–15192.
[57] T. Yoshizumi, H. Tsurugi, T. Satoh, M. Miura, *Tetrahedron Lett.* **2008**, *49*, 1598–1600.
[58] L. Ackermann, H. K. Potukuchi, D. Landsberg, R. Vicente, *Org. Lett.* **2008**, *10*, 3081–3084.
[59] a) D. P. Khambhati, K. A. N. Sachinthani, A. L. Rheingold, T. L. Nelson, *Chem. Commun.* **2017**, *53*, 5107–5109; b) J. Wu, Q. You, J. Lan, Q. Guo, X. Li, Y. Xue, J. You, *Org. Biomol. Chem.* **2015**, *13*, 5372–5375; c) Y.-T. Song, P.-H. Lin, C.-Y. Liu, *Adv. Synth. Catal.* **2014**, *356*, 3761–3768; d) C. Cheng, Y. C. Shih, H. T. Chen, T. C. Chien, *Tetrahedron* **2013**, *69*, 1387–1396; e) D. Zhao, W. Wang, F. Yang, J. Lan, L. Yang, G. Gao, J. You, *Angew. Chem. Int. Ed.* **2009**, *48*, 3296–3300; f) S. Yotphan, R. G. Bergman, J. A. Ellman, *Org. Lett.* **2009**, *11*, 1511–1514.
[60] S. Zhang, D. Zhang, L. S. Liebeskind, *J. Org. Chem.* **1997**, *62*, 2312–2313.
[61] a) F. Y. Kwong, S. L. Buchwald, *Org. Lett.* **2003**, *5*, 793–796; b) F. Y. Kwong, A. Klapars, S. L. Buchwald, *Org. Lett.* **2002**, *4*, 581–584; c) A. Kiyomori, J. F. Marcoux, S. L. Buchwald, *Tetrahedron Lett.* **1999**, *40*, 2657–2660; d) J. F. Marcoux, S. Doye, S. L. Buchwald, *J. Am. Chem. Soc.* **1997**, *119*, 10539–10540.
[62] a) H. J. Cristau, P. P. Cellier, J. F. Spindler, M. Taillefer, *Chem. Eur. J.* **2004**, *10*, 5607–5622; b) H. J. Cristau, P. P. Cellier, S. Hamada, J. F. Spindler, M. Taillefer, *Org. Lett.* **2004**, *6*, 913–916.
[63] a) S. Xia, L. Gan, K. Wang, Z. Li, D. Ma, *J. Am. Chem. Soc.* **2016**, *138*, 13493–13496; b) M. Fan, W. Zhou, Y. Jiang, D. Ma, *Angew. Chem. Int. Ed.* **2016**, *55*, 6211–6215; c) W. Zhou, M. Fan, J. Yin, Y. Jiang, D. Ma, *J. Am. Chem. Soc.* **2015**, *137*, 11942–11945.
[64] a) X. Chen, X. S. Hao, C. E. Goodhue, J. Q. Yu, *J. Am. Chem. Soc.* **2006**, *128*, 6790–6791; b) T. Uemura, S. Imoto, N. Chatani, *Chem. Lett.* **2006**, *35*, 842–843.
[65] Q. Wang, S. L. Schreiber, *Org. Lett.* **2009**, *11*, 5178–5180.
[66] L. D. Tran, J. Roane, O. Daugulis, *Angew. Chem. Int. Ed.* **2013**, *52*, 6043–6046.
[67] a) M. Shang, S. Z. Sun, H. X. Dai, J. Q. Yu, *J. Am. Chem. Soc.* **2014**, *136*, 3354–3357; b) A. M. Martinez, N. Rodriguez, R. G. Arrayas, J. C. Carretero, *Chem. Commun.* **2014**, *50*, 2801–2803; c) Q. Li, S. Y. Zhang, G. He, Z. Ai, W. A. Nack, G. Chen, *Org. Lett.* **2014**, *16*, 1764–1767.
[68] A. E. Wendlandt, A. M. Suess, S. S. Stahl, *Angew. Chem. Int. Ed.* **2011**, *50*, 11062–11087.
[69] X. Ribas, D. A. Jackson, B. Donnadieu, J. Mahia, T. Parella, R. Xifra, B. Hedman, K. O. Hodgson, A. Llobet, T. D. P. Stack, *Angew. Chem. Int. Ed.* **2002**, *41*, 2991–2994.
[70] a) A. M. Suess, M. Z. Ertem, C. J. Cramer, S. S. Stahl, *J. Am. Chem. Soc.* **2013**, *135*, 9797–9804; b) A. E. King, L. M. Huffman, A. Casitas, M. Costas, X. Ribas, S. S. Stahl, *J. Am. Chem.*

Soc. **2010**, *132*, 12068–12073; c) L. M. Huffman, S. S. Stahl, *J. Am. Chem. Soc.* **2008**, *130*, 9196–9197.

[71] J. Roane, O. Daugulis, *Org. Lett.* **2013**, *15*, 5842–5845.

[72] S. Fukuzawa, E. Shimizu, Y. Atsuumi, M. Haga, K. Ogata, *Tetrahedron Lett.* **2009**, *50*, 2374–2376.

[73] S. Zhang, P. Qian, M. Zhang, M. Hu, J. Cheng, *J. Org. Chem.* **2010**, *75*, 6732–6735.

[74] L. Chu, X. Yue, F. L. Qing, *Org. Lett.* **2010**, *12*, 1644–1647.

[75] T. J. Wallace, *J. Am. Chem. Soc.* **1964**, *86*, 2018–2021.

[76] L. D. Tran, I. Popov, O. Daugulis, *J. Am. Chem. Soc.* **2012**, *134*, 18237–18240.

[77] G. Cera, L. Ackermann, *Chem. Eur. J.* **2016**, *22*, 8475–8478.

[78] L. Z. Zhu, X. Cao, R. H. Qiu, T. Iwasaki, V. P. Reddy, X. H. Xu, S. F. Yin, N. Kambe, *RSC Adv.* **2015**, *5*, 39358–39365.

[79] a) T. W. Lyons, M. S. Sanford, *Chem. Rev.* **2010**, *110*, 1147–1169; b) E. M. Beck, M. J. Gaunt, in *C-H Activation* (Eds.: J.-Q. Yu, Z. Shi), Springer-Verlag Berlin Heidelberg, Berlin, Heidelberg, **2010**, pp. 85–121; c) L. C. Campeau, K. Fagnou, *Chem. Commun.* **2006**, 1253–1264.

[80] J. Bouffard, K. Itami, in *C-H Activation* (Eds.: J.-Q. Yu, Z. Shi), Springer-Verlag Berlin Heidelberg, Berlin, Heidelberg, **2010**, pp. 231–280.

[81] P. B. Arockiam, C. Bruneau, P. H. Dixneuf, *Chem. Rev.* **2012**, *112*, 5879–5918.

[82] S. Murai, F. Kakiuchi, S. Sekine, Y. Tanaka, A. Kamatani, M. Sonoda, N. Chatani, *Nature* **1993**, *366*, 529–531.

[83] a) S. Oi, Y. Ogino, S. Fukita, Y. Inoue, *Org. Lett.* **2002**, *4*, 1783–1785; b) S. Oi, S. Fukita, N. Hirata, N. Watanuki, S. Miyano, Y. Inoue, *Org. Lett.* **2001**, *3*, 2579–2581.

[84] L. N. Lewis, J. F. Smith, *J. Am. Chem. Soc.* **1986**, *108*, 2728–2735.

[85] a) G. Duarah, P. P. Kaishap, T. Begum, S. Gogoi, *Adv. Synth. Catal.* **2019**, *361*, 654–672; b) P. Nareddy, F. Jordan, M. Szostak, *ACS Catal.* **2017**, *7*, 5721–5745; c) L. Ackermann, *Acc. Chem. Res.* **2014**, *47*, 281–295.

[86] S. G. Ouellet, A. Roy, C. Molinaro, R. Angelaud, J.-F. Marcoux, P. D. O'Shea, I. W. Davies, *J. Org. Chem.* **2011**, *76*, 1436–1439.

[87] L. Ackermann, R. Vicente, A. Althammer, *Org. Lett.* **2008**, *10*, 2299–2302.

[88] L. Ackermann, R. Vicente, H. K. Potukuchi, V. Pirovano, *Org. Lett.* **2010**, *12*, 5032–5035.

[89] J. Li, S. De Sarkar, L. Ackermann, *Top. Organomet. Chem.* **2016**, *55*, 217–258.

[90] a) S. Mochida, K. Hirano, T. Satoh, M. Miura, *J. Org. Chem.* **2011**, *76*, 3024–3033; b) S. Mochida, K. Hirano, T. Satoh, M. Miura, *Org. Lett.* **2010**, *12*, 5776–5779.

[91] N. Y. Kumar, A. Bechtoldt, K. Raghuvanshi, L. Ackermann, *Angew. Chem. Int. Ed.* **2016**, *55*, 6929–6932.

[92] a) T. Ishiyama, J. Takagi, J. F. Hartwig, N. Miyaura, *Angew. Chem. Int. Ed.* **2002**, *41*, 3056–3058; b) T. Ishiyama, J. Takagi, K. Ishida, N. Miyaura, N. R. Anastasi, J. F. Hartwig, *J. Am. Chem. Soc.* **2002**, *124*, 390–391; c) J. Y. Cho, M. K. Tse, D. Holmes, R. E. Maleczka, M. R. Smith, *Science* **2002**, *295*, 305–308.

[93] C. Cheng, J. F. Hartwig, *Science* **2014**, *343*, 853–857.

[94] a) M. Catellani, F. Frignani, A. Rangoni, *Angew. Chem. Int. Ed. Engl.* **1997**, *36*, 119–122; b) M. Catellani, G. P. Chiusoli, S. Ricotti, *J. Organomet. Chem.* **1985**, *296*, 11–15.

[95] M. Catellani, E. Motti, N. Della Ca, *Acc. Chem. Res.* **2008**, *41*, 1512–1522.

[96] T. Wilhelm, M. Lautens, *Org. Lett.* **2005**, *7*, 4053–4056.

[97] Z. Dong, J. Wang, G. Dong, *J. Am. Chem. Soc.* **2015**, *137*, 5887–5890.

[98] a) Q. Ding, S. Ye, G. Cheng, P. Wang, M. E. Farmer, J. Q. Yu, *J. Am. Chem. Soc.* **2017**, *139*, 417–425; b) P. Wang, M. E. Farmer, X. Huo, P. Jain, P. X. Shen, M. Ishoey, J. E. Bradner, S. R. Wisniewski, M. D. Eastgate, J. Q. Yu, *J. Am. Chem. Soc.* **2016**, *138*, 9269–9276.

[99] a) L. Chu, M. Shang, K. Tanaka, Q. Chen, N. Pissarnitski, E. Streckfuss, J. Q. Yu, *ACS Cent Sci* **2015**, *1*, 394–399; b) R. Y. Tang, G. Li, J. Q. Yu, *Nature* **2014**, *507*, 215–220; c) D. Leow, G. Li, T. S. Mei, J. Q. Yu, *Nature* **2012**, *486*, 518–522.

[100] Y. Kuninobu, H. Ida, M. Nishi, M. Kanai, *Nat. Chem.* **2015**, *7*, 712–717.

[101] J. A. Leitch, C. G. Frost, *Chem. Soc. Rev.* **2017**, *46*, 7145–7153.

[102] G. R. Clark, C. E. L. Headford, W. R. Roper, L. J. Wright, V. P. D. Yap, *Inorg. Chim. Acta* **1994**, *220*, 261–272.

[103] J.-P. Sutter, D. M. Grove, M. Beley, J.-P. Collin, N. Veldman, A. L. Spek, J.-P. Sauvage, G. van Koten, *Angew. Chem. Int. Ed. Engl.* **1994**, *33*, 1282–1285.

[104] C. Coudret, S. Fraysse, J. P. Launay, *Chem. Commun.* **1998**, 663–664.

[105] A. M. Clark, C. E. F. Rickard, W. R. Roper, L. J. Wright, *Organometallics* **1999**, *18*, 2813–2820.

[106] L. Ackermann, N. Hofmann, R. Vicente, *Org. Lett.* **2011**, *13*, 1875–1877.

[107] O. Saidi, J. Marafie, A. E. Ledger, P. M. Liu, M. F. Mahon, G. Kociok-Kohn, M. K. Whittlesey, C. G. Frost, *J. Am. Chem. Soc.* **2011**, *133*, 19298–19301.

[108] N. Hofmann, L. Ackermann, *J. Am. Chem. Soc.* **2013**, *135*, 5877–5884.

[109] a) J. Li, S. Warratz, D. Zell, S. De Sarkar, E. E. Ishikawa, L. Ackermann, *J. Am. Chem. Soc.* **2015**, *137*, 13894–13901; b) A. J. Paterson, S. St John-Campbell, M. F. Mahon, N. J. Press, C. G. Frost, *Chem. Commun.* **2015**, *51*, 12807–12810.

[110] a) Q. Yu, L. Hu, Y. Wang, S. Zheng, J. Huang, *Angew. Chem. Int. Ed.* **2015**, *54*, 15284–15288; b) C. J. Teskey, A. Y. Lui, M. F. Greaney, *Angew. Chem. Int. Ed.* **2015**, *54*, 11677–11680.

[111] S. Warratz, D. J. Burns, C. Zhu, K. Korvorapun, T. Rogge, J. Scholz, C. Jooss, D. Gelman, L. Ackermann, *Angew. Chem. Int. Ed.* **2017**, *56*, 1557–1560.

[112] a) Z. Ruan, S. K. Zhang, C. Zhu, P. N. Ruth, D. Stalke, L. Ackermann, *Angew. Chem. Int. Ed.* **2017**, *56*, 2045–2049; b) Z. Y. Li, L. Li, Q. L. Li, K. Jing, H. Xu, G. W. Wang, *Chem. Eur. J.* **2017**, *23*, 3285–3290.

[113] F. Fumagalli, S. Warratz, S. K. Zhang, T. Rogge, C. Zhu, A. C. Stückl, L. Ackermann, *Chem. Eur. J.* **2018**, *24*, 3984–3988.

[114] Z. Fan, J. Ni, A. Zhang, *J. Am. Chem. Soc.* **2016**, *138*, 8470–8475.

[115] J. M. Narayanam, C. R. Stephenson, *Chem. Soc. Rev.* **2011**, *40*, 102–113.

[116] G. Ciamician, *Science* **1912**, *36*, 385–394.

[117] G. O. Schenck, K. Ziegler, *Die Naturwissenschaften* **1944**, *32*, 157–157.

[118] G. O. Schenck, *Angew. Chem.* **1952**, *64*, 12–23.

[119] a) I. Ghosh, L. Marzo, A. Das, R. Shaikh, B. Konig, *Acc. Chem. Res.* **2016**, *49*, 1566–1577; b) K. L. Skubi, T. R. Blum, T. P. Yoon, *Chem. Rev.* **2016**, *116*, 10035–10074; c) N. A. Romero, D. A. Nicewicz, *Chem. Rev.* **2016**, *116*, 10075–10166; d) C. K. Prier, D. A. Rankic, D. W. MacMillan, *Chem. Rev.* **2013**, *113*, 5322–5363.

[120] J. Twilton, C. Le, P. Zhang, M. H. Shaw, R. W. Evans, D. W. C. MacMillan, *Nat. Rev. Chem.* **2017**, *1*, 1–18.

[121] M. Osawa, H. Nagai, M. Akita, *Dalton Trans.* **2007**, 827–829.

[122] D. Kalyani, K. B. McMurtrey, S. R. Neufeldt, M. S. Sanford, *J. Am. Chem. Soc.* **2011**, *133*, 18566–18569.

[123] D. A. Nagib, M. E. Scott, D. W. MacMillan, *J. Am. Chem. Soc.* **2009**, *131*, 10875–10877.

[124] Y. Ye, M. S. Sanford, *J. Am. Chem. Soc.* **2012**, *134*, 9034–9037.

[125] S. E. Creutz, K. J. Lotito, G. C. Fu, J. C. Peters, *Science* **2012**, *338*, 647–651.

[126] D. T. Ziegler, J. Choi, J. M. Munoz-Molina, A. C. Bissember, J. C. Peters, G. C. Fu, *J. Am. Chem. Soc.* **2013**, *135*, 13107–13112.

[127] a) Q. M. Kainz, C. D. Matier, A. Bartoszewicz, S. L. Zultanski, J. C. Peters, G. C. Fu, *Science* **2016**, *351*, 681–684; b) A. C. Bissember, R. J. Lundgren, S. E. Creutz, J. C. Peters, G. C. Fu, *Angew. Chem. Int. Ed.* **2013**, *52*, 5129–5133.

[128] Y. C. Tan, J. M. Munoz-Molina, G. C. Fu, J. C. Peters, *Chem. Sci.* **2014**, *5*, 2831–2835.

[129] W. J. Yoo, T. Tsukamoto, S. Kobayashi, *Angew. Chem. Int. Ed.* **2015**, *54*, 6587–6590.

[130] W. J. Yoo, T. Tsukamoto, S. Kobayashi, *Org. Lett.* **2015**, *17*, 3640–3642.

[131] D. C. Fabry, M. Rueping, *Acc. Chem. Res.* **2016**, *49*, 1969–1979.

[132] a) D. C. Fabry, M. A. Ronge, J. Zoller, M. Rueping, *Angew. Chem. Int. Ed.* **2015**, *54*, 2801–2805; b) D. C. Fabry, J. Zoller, S. Raja, M. Rueping, *Angew. Chem. Int. Ed.* **2014**, *53*, 10228–10231.

[133] S. I. Kozhushkov, L. Ackermann, *Chem. Sci.* **2013**, *4*, 886–896.

[134] a) J. A. Milligan, J. P. Phelan, S. O. Badir, G. A. Molander, *Angew. Chem. Int. Ed.* **2019**, *58*, 6152–6163; b) J. C. Tellis, C. B. Kelly, D. N. Primer, M. Jouffroy, N. R. Patel, G. A. Molander, *Acc. Chem. Res.* **2016**, *49*, 1429–1439.

[135] J. C. Tellis, D. N. Primer, G. A. Molander, *Science* **2014**, *345*, 433–436.

[136] Z. Zuo, D. T. Ahneman, L. Chu, J. A. Terrett, A. G. Doyle, D. W. MacMillan, *Science* **2014**, *345*, 437–440.

[137] O. Gutierrez, J. C. Tellis, D. N. Primer, G. A. Molander, M. C. Kozlowski, *J. Am. Chem. Soc.* **2015**, *137*, 4896–4899.

[138] E. R. Welin, C. Le, D. M. Arias-Rotondo, J. K. McCusker, D. W. MacMillan, *Science* **2017**, *355*, 380–385.

[139] M. Rueping, R. M. Koenigs, K. Poscharny, D. C. Fabry, D. Leonori, C. Vila, *Chem. Eur. J.* **2012**, *18*, 5170–5174.

[140] a) N. Sauermann, T. H. Meyer, Y. Qiu, L. Ackermann, *ACS Catal.* **2018**, *8*, 7086–7103; b) N. Sauermann, T. H. Meyer, L. Ackermann, *Chem. Eur. J.* **2018**, *24*, 16209–16217.

[141] D. A. Nicewicz, T. M. Nguyen, *ACS Catal.* **2014**, *4*, 355–360.

[142] S. Fukuzumi, H. Kotani, K. Ohkubo, S. Ogo, N. V. Tkachenko, H. Lemmetyinen, *J. Am. Chem. Soc.* **2004**, *126*, 1600–1601.

[143] A. Joshi-Pangu, F. Levesque, H. G. Roth, S. F. Oliver, L. C. Campeau, D. Nicewicz, D. A. DiRocco, *J. Org. Chem.* **2016**, *81*, 7244–7249.

[144] a) L. Niu, J. Liu, H. Yi, S. Wang, X.-A. Liang, A. K. Singh, C.-W. Chiang, A. Lei, *ACS Catal.* **2017**, *7*, 7412–7416; b) L. B. Niu, H. Yi, S. C. Wang, T. Y. Liu, J. M. Liu, A. W. Lei, *Nat. Commun.* **2017**, *8*, 14226.

[145] a) W. J. Zhou, G. M. Cao, G. Shen, X. Y. Zhu, Y. Y. Gui, J. H. Ye, L. Sun, L. L. Liao, J. Li, D. G. Yu, *Angew. Chem. Int. Ed.* **2017**, *56*, 15683–15687; b) R. A. Garza-Sanchez, A. Tlahuext-Aca, G. Tavakoli, F. Glorius, *ACS Catal.* **2017**, *7*, 4057–4061; c) T. McCallum, L. Barriault, *Chem. Sci.* **2016**, *7*, 4754–4758.

[146] D. A. Horton, G. T. Bourne, M. L. Smythe, *Chem. Rev.* **2003**, *103*, 893–930.

[147] a) M. Ishikura, T. Abe, T. Choshi, S. Hibino, *Nat. Prod. Rep.* **2013**, *30*, 694–752; b) T. C. Barden, in *Heterocyclic Scaffolds II:* (Ed.: G. W. Gribble), Springer-Verlag Berlin Heidelberg, Berlin, Heidelberg, **2010**, pp. 31–46; c) A. J. Kochanowska-Karamyan, M. T. Hamann, *Chem. Rev.* **2010**, *110*, 4489–4497; d) V. Sharma, P. Kumar, D. Pathak, *J. Heterocycl. Chem.* **2010**, *47*, 491–502; e) L. Ackermann, *Synlett* **2007**, 507–526.

[148] a) L. Ping, D. S. Chung, J. Bouffard, S. G. Lee, *Chem. Soc. Rev.* **2017**, *46*, 4299–4328; b) J. A. Leitch, Y. Bhonoah, C. G. Frost, *ACS Catal.* **2017**, *7*, 5618–5627; c) A. H. Sandtorv, *Adv. Synth. Catal.* **2015**, *357*, 2403–2435.

[149] a) L. Ackermann, A. V. Lygin, *Org. Lett.* **2011**, *13*, 3332–3335; b) L. Ackermann, M. Dell'Acqua, S. Fenner, R. Vicente, R. Sandmann, *Org. Lett.* **2011**, *13*, 2358–2360; c) L. Ackermann, S. Barfüßer, *Synlett* **2009**, 808–812; d) N. Lebrasseur, I. Larrosa, *J. Am. Chem. Soc.* **2008**, *130*, 2926–2927; e) X. Wang, D. V. Gribkov, D. Sames, *J. Org. Chem.* **2007**, *72*, 1476–1479; f) N. R. Deprez, D. Kalyani, A. Krause, M. S. Sanford, *J. Am. Chem. Soc.* **2006**, *128*, 4972–4973; g) X. Wang, B. S. Lane, D. Sames, *J. Am. Chem. Soc.* **2005**, *127*, 4996–4997; h) B. S. Lane, M. A. Brown, D. Sames, *J. Am. Chem. Soc.* **2005**, *127*, 8050–8057.

[150] a) J. Li, L. Ackermann, *Angew. Chem. Int. Ed.* **2015**, *54*, 3635–3638; b) M. Chaitanya, P. Anbarasan, *J. Org. Chem.* **2015**, *80*, 3695–3700; c) D. G. Yu, T. Gensch, F. de Azambuja, S. Vasquez-Cespedes, F. Glorius, *J. Am. Chem. Soc.* **2014**, *136*, 17722–17725; d) G. Yan, C. Kuang, Y. Zhang, J. Wang, *Org. Lett.* **2010**, *12*, 1052–1055.

[151] a) D. Zell, U. Dhawa, V. Müller, M. Bursch, S. Grimme, L. Ackermann, *ACS Catal.* **2017**, *7*, 4209–4213; b) M. Moselage, N. Sauermann, S. C. Richter, L. Ackermann, *Angew. Chem. Int. Ed.* **2015**, *54*, 6352–6355; c) A. Garcia-Rubia, R. Gomez Arrayas, J. C. Carretero, *Angew. Chem. Int. Ed.* **2009**, *48*, 6511–6515; d) N. P. Grimster, C. Gauntlett, C. R. Godfrey, M. J. Gaunt, *Angew. Chem. Int. Ed.* **2005**, *44*, 3125–3129; e) E. Capito, J. M. Brown, A. Ricci, *Chem. Commun.* **2005**, 1854–1856.

[152] a) L. Xu, C. Zhang, Y. He, L. Tan, D. Ma, *Angew. Chem. Int. Ed.* **2016**, *55*, 321–325; b) L. Xu, L. Tan, D. Ma, *J. Org. Chem.* **2016**, *81*, 10476–10483; c) Y. Yang, X. Qiu, Y. Zhao, Y. Mu, Z. Shi, *J. Am. Chem. Soc.* **2016**, *138*, 495–498.

[153] a) C. Premi, A. Dixit, N. Jain, *Org. Lett.* **2015**, *17*, 2598–2601; b) L. Y. Jiao, P. Smirnov, M. Oestreich, *Org. Lett.* **2014**, *16*, 6020–6023.

[154] a) T. Zhou, Y. Wang, B. Li, B. Wang, *Org. Lett.* **2016**, *18*, 5066–5069; b) X. F. Yang, X. H. Hu, T. P. Loh, *Org. Lett.* **2015**, *17*, 1481–1484.

[155] a) H. Kim, G. Park, J. Park, S. Chang, *ACS Catal.* **2016**, *6*, 5922–5929; b) Y. Wu, Y. Yang, B. Zhou, Y. Li, *J. Org. Chem.* **2015**, *80*, 1946–1951.

[156] a) H. Jo, J. Park, N. K. Mishra, M. Jeon, S. Sharma, H. Oh, S.-Y. Lee, Y. H. Jung, I. S. Kim, *Tetrahedron* **2017**, *73*, 1725–1732; b) H. Jo, J. Park, M. Choi, S. Sharma, M. Jeon, N. K. Mishra, T. Jeong, S. Han, I. S. Kim, *Adv. Synth. Catal.* **2016**, *358*, 2714–2720; c) C. Pan, A. Abdukader, J. Han, Y. Cheng, C. Zhu, *Chem. Eur. J.* **2014**, *20*, 3606–3609; d) N. Chatani, S. Yorimitsu, T. Asaumi, F. Kakiuchi, S. Murai, *J. Org. Chem.* **2002**, *67*, 7557–7560.

[157] P. Gandeepan, J. Koeller, L. Ackermann, *ACS Catal.* **2017**, *7*, 1030–1034.

[158] A. Gavriilidis, A. Constantinou, K. Hellgardt, K. K. Hii, G. J. Hutchings, G. L. Brett, S. Kuhn, S. P. Marsden, *React. Chem. Eng.* **2016**, *1*, 595–612.

[159] P. M. Osterberg, J. K. Niemeier, C. J. Welch, J. M. Hawkins, J. R. Martinelli, T. E. Johnson, T. W. Root, S. S. Stahl, *Org. Process Res. Dev.* **2015**, *19*, 1537–1543.

[160] a) P. Sharma, S. Rohilla, N. Jain, *J. Org. Chem.* **2015**, *80*, 4116–4122; b) C. M. Yu, C. L. Zhang, X. J. Shi, *Eur. J. Org. Chem.* **2012**, 1953–1959.

[161] a) D. Bartolini, L. Sancineto, A. Fabro de Bem, K. D. Tew, C. Santi, R. Radi, P. Toquato, F. Galli, in *Advances in Cancer Research, Vol. 136* (Eds.: K. D. Tew, F. Galli), Academic Press, **2017**, pp. 259–302; b) C. W. Nogueira, G. Zeni, J. B. Rocha, *Chem. Rev.* **2004**, *104*, 6255–6285; c) G. Mugesh, W. W. du Mont, H. Sies, *Chem. Rev.* **2001**, *101*, 2125–2179.

[162] J. C. Pleasants, W. Guo, D. L. Rabenstein, *J. Am. Chem. Soc.* **1989**, *111*, 6553–6558.

[163] S. K. Bhunia, P. Das, R. Jana, *Org. Biomol. Chem.* **2018**, *16*, 9243–9250.

[164] P. T. Beurskens, J. A. Cras, J. J. Steggerda, *Inorg. Chem.* **1968**, *7*, 810–813.

[165] J. L. García Ruano, A. Parra, J. Alemán, *Green Chem.* **2008**, *10*, 706–711.

[166] S. Landa, V. Macháček, *Collect. Czech. Chem. Commun.* **1933**, *5*, 1–5.

[167] V. Prelog, R. Seiwerth, *Ber. Dtsch. Chem. Ges.* **1941**, *74*, 1644–1648.

[168] P. von R. Schleyer, *J. Am. Chem. Soc.* **1957**, *79*, 3292–3292.
[169] L. Wanka, K. Iqbal, P. R. Schreiner, *Chem. Rev.* **2013**, *113*, 3516–3604.
[170] a) S. Aiello, G. Wells, E. L. Stone, H. Kadri, R. Bazzi, D. R. Bell, M. F. Stevens, C. S. Matthews, T. D. Bradshaw, A. D. Westwell, *J. Med. Chem.* **2008**, *51*, 5135–5139; b) S. M. Sondhi, N. Singh, A. Kumar, O. Lozach, L. Meijer, *Bioorg. Med. Chem.* **2006**, *14*, 3758–3765; c) B. Gong, F. Hong, C. Kohm, L. Bonham, P. Klein, *Bioorg. Med. Chem. Lett.* **2004**, *14*, 1455–1459.
[171] a) X. Wu, J. W. See, K. Xu, H. Hirao, J. Roger, J. C. Hierso, J. S. Zhou, *Angew. Chem. Int. Ed.* **2014**, *53*, 13573–13577; b) P. Ren, I. Salihu, R. Scopelliti, X. Hu, *Org. Lett.* **2012**, *14*, 1748–1751; c) T. Yao, K. Hirano, T. Satoh, M. Miura, *Angew. Chem. Int. Ed.* **2012**, *51*, 775–779; d) L. Ackermann, B. Punji, W. F. Song, *Adv. Synth. Catal.* **2011**, *353*, 3325–3329.
[172] a) J. Tauber, D. Imbri, T. Opatz, *Molecules* **2014**, *19*, 16190–16222; b) M. A. J. Duncton, *Medchemcomm* **2011**, *2*, 1135–1161; c) F. Minisci, F. Fontana, E. Vismara, *J. Heterocycl. Chem.* **1990**, *27*, 79–96.
[173] F. Minisci, R. Bernardi, F. Bertini, R. Galli, M. Perchinummo, *Tetrahedron* **1971**, *27*, 3575–3579.
[174] J. Dong, X. Lyu, Z. Wang, X. Wang, H. Song, Y. Liu, Q. Wang, *Chem. Sci.* **2019**, *10*, 976–982.
[175] J. Koeller, P. Gandeepan, L. Ackermann, *Synthesis* **2018**, *51*, 1284–1292.
[176] L. K. Fraiji, D. M. Hayes, T. C. Werner, *J. Chem. Educ.* **1992**, *69*, 424–428.
[177] K. A. Margrey, J. B. McManus, S. Bonazzi, F. Zecri, D. A. Nicewicz, *J. Am. Chem. Soc.* **2017**, *139*, 11288–11299.
[178] M. Galicia, F. J. Gonzalez, *J. Electrochem. Soc.* **2002**, *149*, 46–50.
[179] H. Yi, L. Niu, C. Song, Y. Li, B. Dou, A. K. Singh, A. Lei, *Angew. Chem. Int. Ed.* **2017**, *56*, 1120–1124.
[180] S. Fukuzumi, K. Ohkubo, T. Suenobu, *Acc. Chem. Res.* **2014**, *47*, 1455–1464.
[181] N. P. Ramirez, J. C. Gonzalez-Gomez, *Eur. J. Org. Chem.* **2017**, 2154–2163.
[182] a) B. Wang, P. Li, T. Miao, L. Zou, L. Wang, *Org. Biomol. Chem.* **2018**, *17*, 115–121; b) J. D. Griffin, M. A. Zeller, D. A. Nicewicz, *J. Am. Chem. Soc.* **2015**, *137*, 11340–11348.
[183] F. De Vleeschouwer, V. Van Speybroeck, M. Waroquier, P. Geerlings, F. De Proft, *Org. Lett.* **2007**, *9*, 2721–2724.
[184] a) M. Ohno, K. Ishizaki, S. Eguchi, *J. Org. Chem.* **1988**, *53*, 1285–1288; b) L. Testaferri, M. Tiecco, M. Tingoli, M. Fiorentino, L. Troisi, *J. Chem. Soc., Chem. Commun.* **1978**, 93–94.
[185] G. Yan, N. R. Brinkmann, H. F. Schaefer, *J. Phys. Chem. A* **2003**, *107*, 9479–9485.
[186] J. Liu, G. Chen, Z. Tan, *Adv. Synth. Catal.* **2016**, *358*, 1174–1194.
[187] T. Yoshizumi, T. Satoh, K. Hirano, D. Matsuo, A. Orita, J. Otera, M. Miura, *Tetrahedron Lett.* **2009**, *50*, 3273–3276.
[188] R. Jeyachandran, H. K. Potukuchi, L. Ackermann, *Beilstein J. Org. Chem.* **2012**, *8*, 1771–1777.
[189] F. Yang, J. Koeller, L. Ackermann, *Angew. Chem. Int. Ed.* **2016**, *55*, 4759–4762.
[190] Synthese von Benzothiazol- und Benzoxazolderivaten und deren Untersuchung in der lichtinduzierten C-H Aktivierung, N. Imse, Bachelor Thesis, Georg-August-Universität Göttingen (Göttingen), **2017**.
[191] J. R. Ochola, M. O. Wolf, *Org. Biomol. Chem.* **2016**, *14*, 9088–9092.
[192] T. M. Arkhireeva, B. M. Bulychev, A. I. Sizov, T. A. Sokolova, V. K. Belsky, G. L. Soloveichik, *Inorg. Chim. Acta* **1990**, *169*, 109–118.
[193] G. H. Zhang, H. Yi, J. Xin, Y. Deng, R. P. Bai, Z. L. Huang, J. T. Miller, A. J. Kropf, E. E. Bunel, X. T. Qi, Y. Lan, A. W. Lei, *Org. Chem. Front.* **2016**, *3*, 975–978.

[194] H. Yi, G. Zhang, J. Xin, Y. Deng, J. T. Miller, A. J. Kropf, E. E. Bunel, X. Qi, Y. Lan, J. F. Lee, A. Lei, *Chem. Commun.* **2016**, *52*, 6914–6917.
[195] a) C. Sambiagio, D. Schonbauer, R. Blieck, T. Dao-Huy, G. Pototschnig, P. Schaaf, T. Wiesinger, M. F. Zia, J. Wencel-Delord, T. Besset, B. U. W. Maes, M. Schnurch, *Chem. Soc. Rev.* **2018**, *47*, 6603–6743; b) P. Gandeepan, L. Ackermann, *Chem* **2018**, *4*, 199–222; c) Y. Park, Y. Kim, S. Chang, *Chem. Rev.* **2017**, *117*, 9247–9301.
[196] a) K. Korvorapun, N. Kaplaneris, T. Rogge, S. Warratz, A. C. Stückl, L. Ackermann, *ACS Catal.* **2018**, *8*, 886–892; b) J. Li, K. Korvorapun, S. De Sarkar, T. Rogge, D. J. Burns, S. Warratz, L. Ackermann, *Nat. Commun.* **2017**, *8*, 15430.
[197] a) P. Gandeepan, J. Koeller, K. Korvorapun, J. Mohr, L. Ackermann, *Angew. Chem. Int. Ed.* **2019**, *58*, 9820–9825; b) A. Sagadevan, M. F. Greaney, *Angew. Chem. Int. Ed.* **2019**, *58*, 9826–9830.
[198] Y. Boutadla, O. Al-Duaij, D. L. Davies, G. A. Griffith, K. Singh, *Organometallics* **2009**, *28*, 433–440.
[199] a) C. J. Wallentin, J. D. Nguyen, P. Finkbeiner, C. R. Stephenson, *J. Am. Chem. Soc.* **2012**, *134*, 8875–8884; b) J. D. Nguyen, J. W. Tucker, M. D. Konieczynska, C. R. Stephenson, *J. Am. Chem. Soc.* **2011**, *133*, 4160–4163.
[200] J. J. Devery Iii, J. J. Douglas, J. D. Nguyen, K. P. Cole, R. A. Flowers Ii, C. R. J. Stephenson, *Chem. Sci.* **2015**, *6*, 537–541.
[201] H. Wang, I. Choi, T. Rogge, N. Kaplaneris, L. Ackermann, *Nat. Catal.* **2018**, *1*, 993–1001.
[202] Q. B. Chen, J. Gao, G. A. Zou, X. L. Xin, H. A. Aisa, *J. Nat. Prod.* **2018**, *81*, 1474–1482.
[203] a) P. Goel, O. Alam, M. J. Naim, F. Nawaz, M. Iqbal, M. I. Alam, *Eur. J. Med. Chem.* **2018**, *157*, 480–502; b) M. Baumann, I. R. Baxendale, *Beilstein J. Org. Chem.* **2013**, *9*, 2265–2319.
[204] G. R. Fulmer, A. J. M. Miller, N. H. Sherden, H. E. Gottlieb, A. Nudelman, B. M. Stoltz, J. E. Bercaw, K. I. Goldberg, *Organometallics* **2010**, *29*, 2176–2179.
[205] W. L. F. Armarego, C. Chai, *Purification of Laboratory Chemicals (Seventh Edition)*, Butterworth-Heinemann, Boston, **2013**.
[206] W. Xie, B. Li, B. Wang, *J. Org. Chem.* **2016**, *81*, 396–403.
[207] M. Kirihara, Y. Asai, S. Ogawa, T. Noguchi, A. Hatano, Y. Hirai, *Synthesis* **2007**, 3286–3289.
[208] Z. Li, F. Ke, H. Deng, H. Xu, H. Xiang, X. Zhou, *Org. Biomol. Chem.* **2013**, *11*, 2943–2946.
[209] D. Yu, L. Lu, Q. Shen, *Org. Lett.* **2013**, *15*, 940–943.
[210] S. Hou, H. Yang, B. Cheng, H. Zhai, Y. Li, *Chem. Commun.* **2017**, *53*, 6926–6929.
[211] K. Kacprzak, *Synlett* **2005**, 943–946.
[212] W. G. Zhu, C. Z. Liu, L. J. Su, W. Yang, M. Yuan, Y. Cao, *J. Mater. Chem.* **2003**, *13*, 50–55.
[213] A. B. Tamayo, B. D. Alleyne, P. I. Djurovich, S. Lamansky, I. Tsyba, N. N. Ho, R. Bau, M. E. Thompson, *J. Am. Chem. Soc.* **2003**, *125*, 7377–7387.
[214] J. Frey, T. Kraus, V. Heitz, J. P. Sauvage, *Chem. Eur. J.* **2007**, *13*, 7584–7594.
[215] M. Pirtsch, S. Paria, T. Matsuno, H. Isobe, O. Reiser, *Chem. Eur. J.* **2012**, *18*, 7336–7340.
[216] J. Y. Kim, S. H. Park, J. Ryu, S. H. Cho, S. H. Kim, S. Chang, *J. Am. Chem. Soc.* **2012**, *134*, 9110–9113.
[217] X. Wang, S. Wang, W. Xue, H. Gong, *J. Am. Chem. Soc.* **2015**, *137*, 11562–11565.
[218] L. Ackermann, A. V. Lygin, *Org. Lett.* **2012**, *14*, 764–767.
[219] T. Gensch, F. J. Klauck, F. Glorius, *Angew. Chem. Int. Ed.* **2016**, *55*, 11287–11291.
[220] M. Yu, B. Wang, P. Zhou, X. Jia, Y. Yuan, *ChemistrySelect* **2016**, *1*, 6217–6220.
[221] T. Yamamoto, K. Muto, M. Komiyama, J. Canivet, J. Yamaguchi, K. Itami, *Chem. Eur. J.* **2011**, *17*, 10113–10122.
[222] M. Fiorentino, L. Testaferri, M. Tiecco, L. Troisi, *Perkin Trans.* **1977**, 1679–1683.
[223] S. Hara, T. Fukuhara, C. Hasegawa, *Synthesis* **2007**, 1528–1534.

[224] F. Besselievre, F. Mahuteau-Betzer, D. S. Grierson, S. Piguel, *J. Org. Chem.* **2008**, *73*, 3278–3280.
[225] M. M. Guru, M. A. Ali, T. Punniyamurthy, *Org. Lett.* **2011**, *13*, 1194–1197.
[226] R. Chung, A. Vo, V. V. Fokin, J. E. Hein, *ACS Catal.* **2018**, *8*, 7889–7897.
[227] Q. Song, Q. Feng, M. Zhou, *Org. Lett.* **2013**, *15*, 5990–5993.
[228] Y. Kamochi, T. Kudo, *Chem. Pharm. Bull.* **1995**, *43*, 1422–1424.

7 Spectra of Compounds

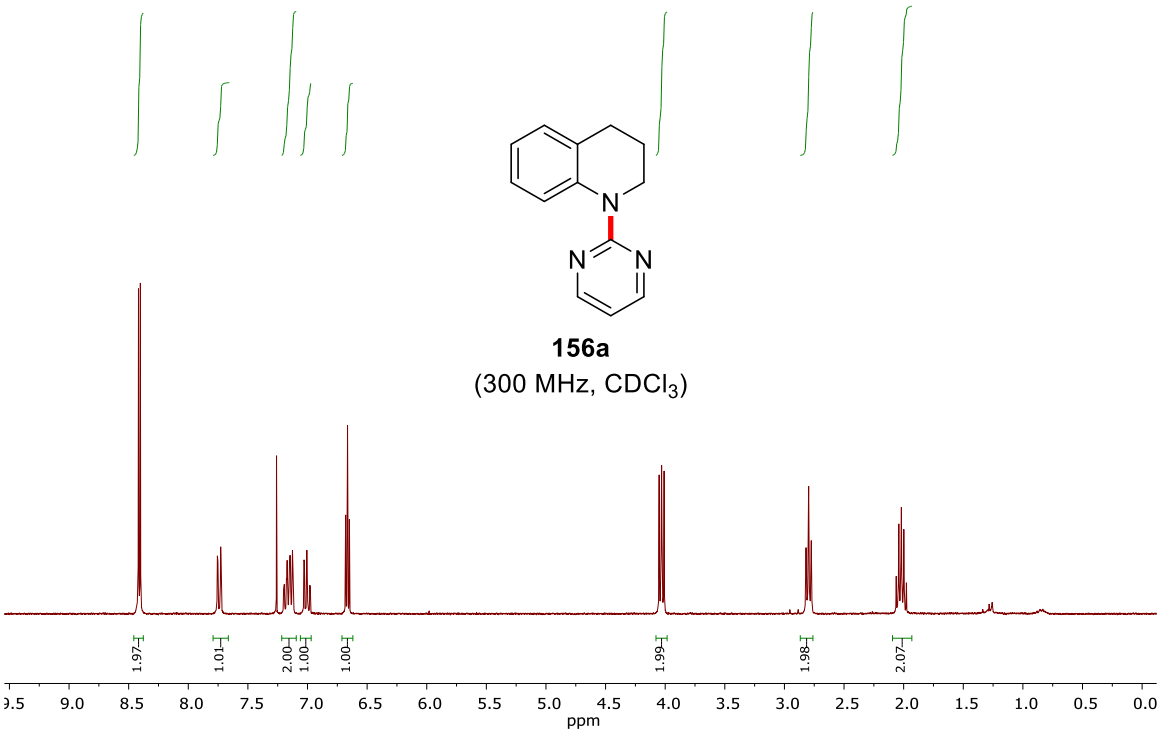

156a
(300 MHz, $CDCl_3$)

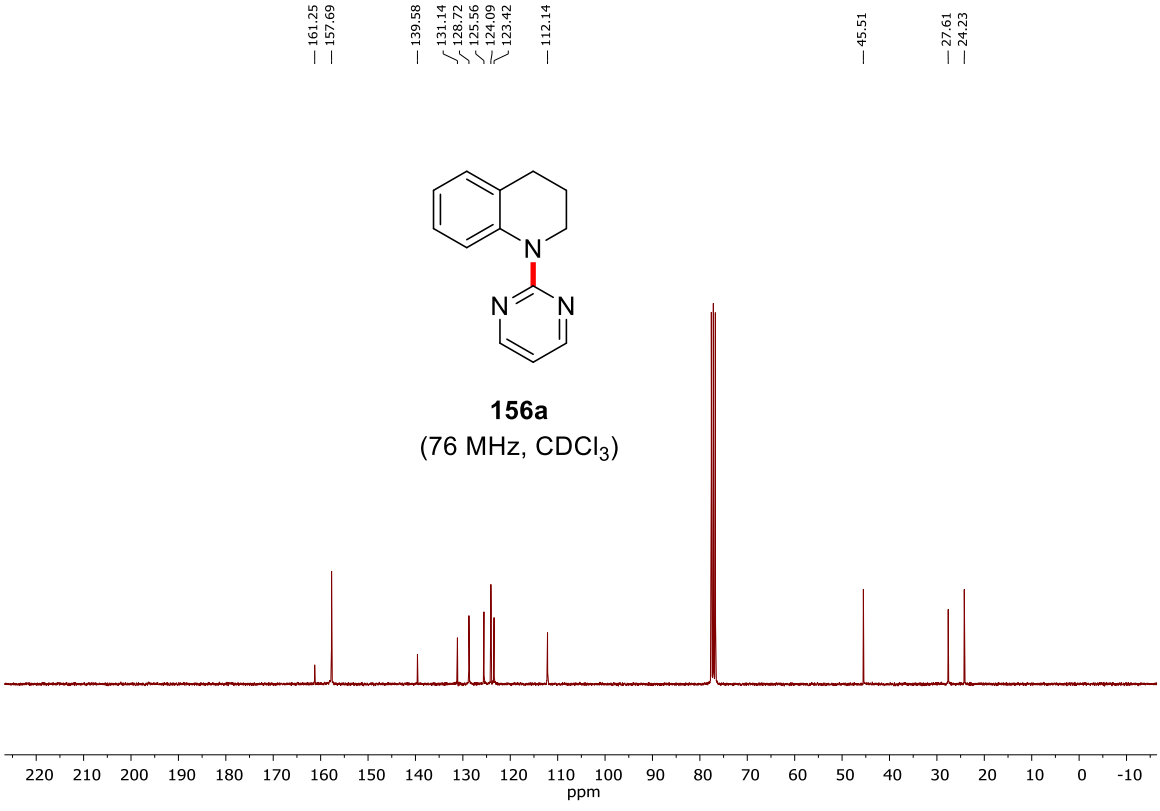

156a
(76 MHz, $CDCl_3$)

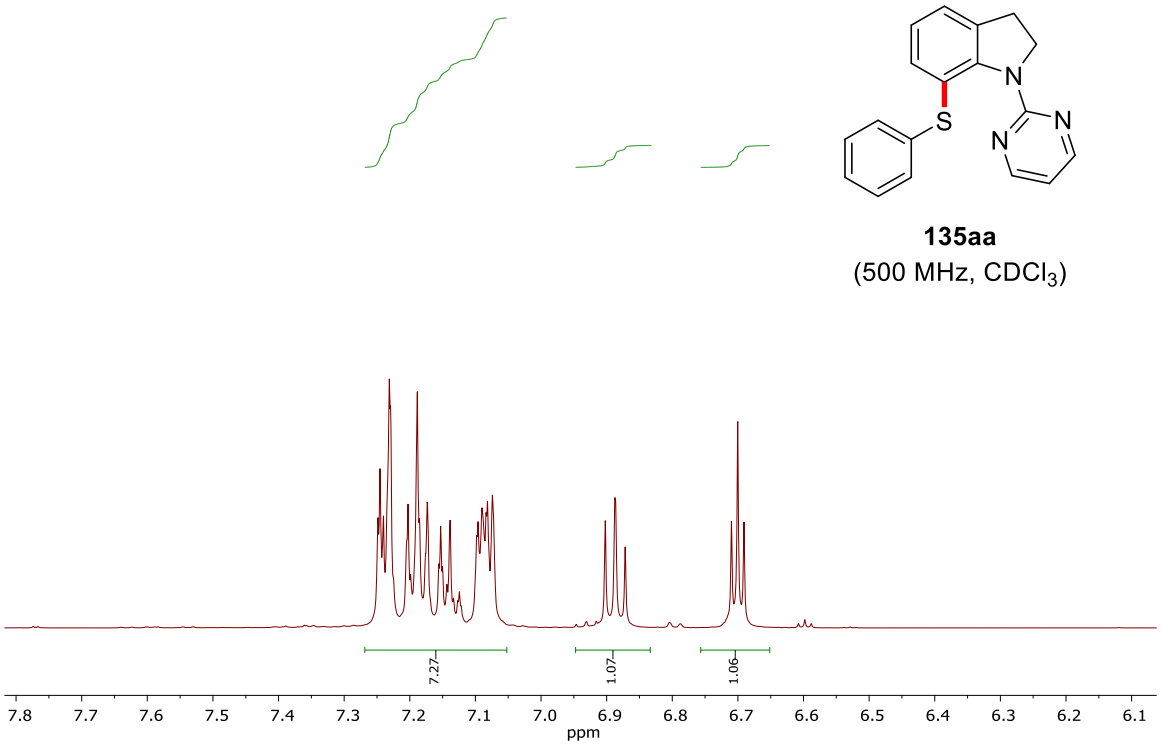

135aa
(500 MHz, $CDCl_3$)

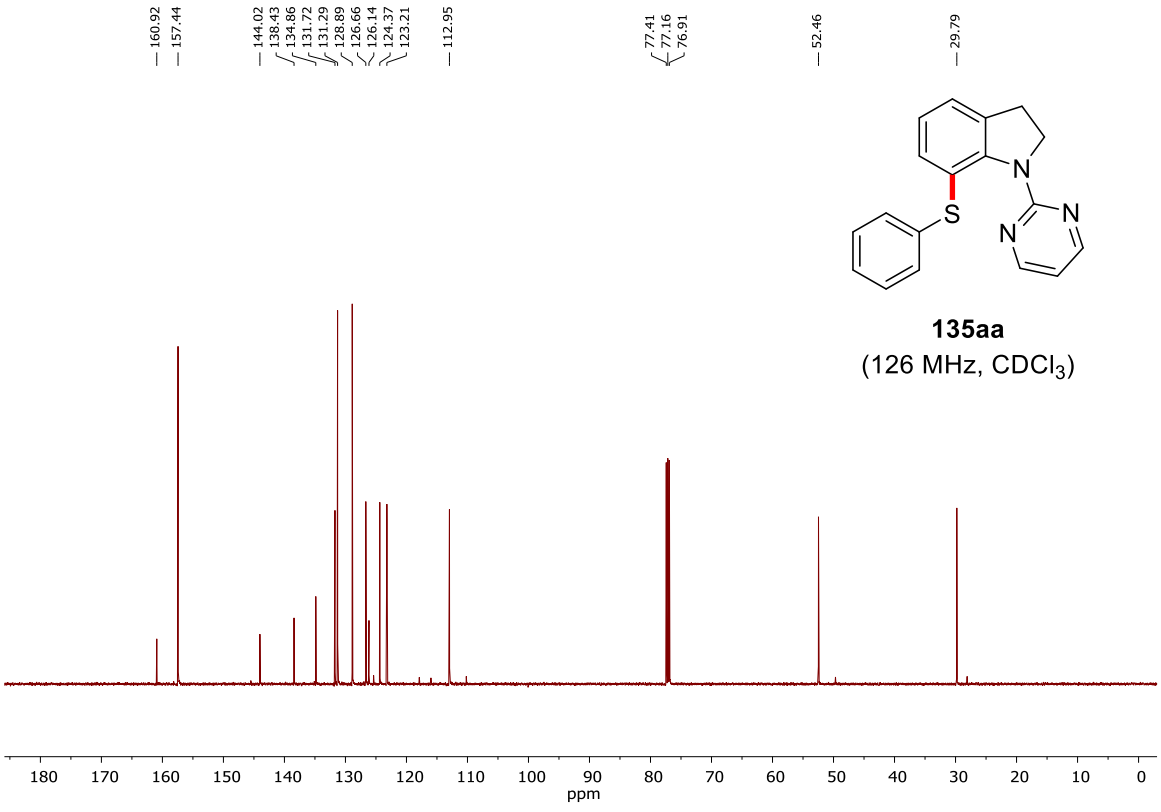

135aa
(126 MHz, $CDCl_3$)

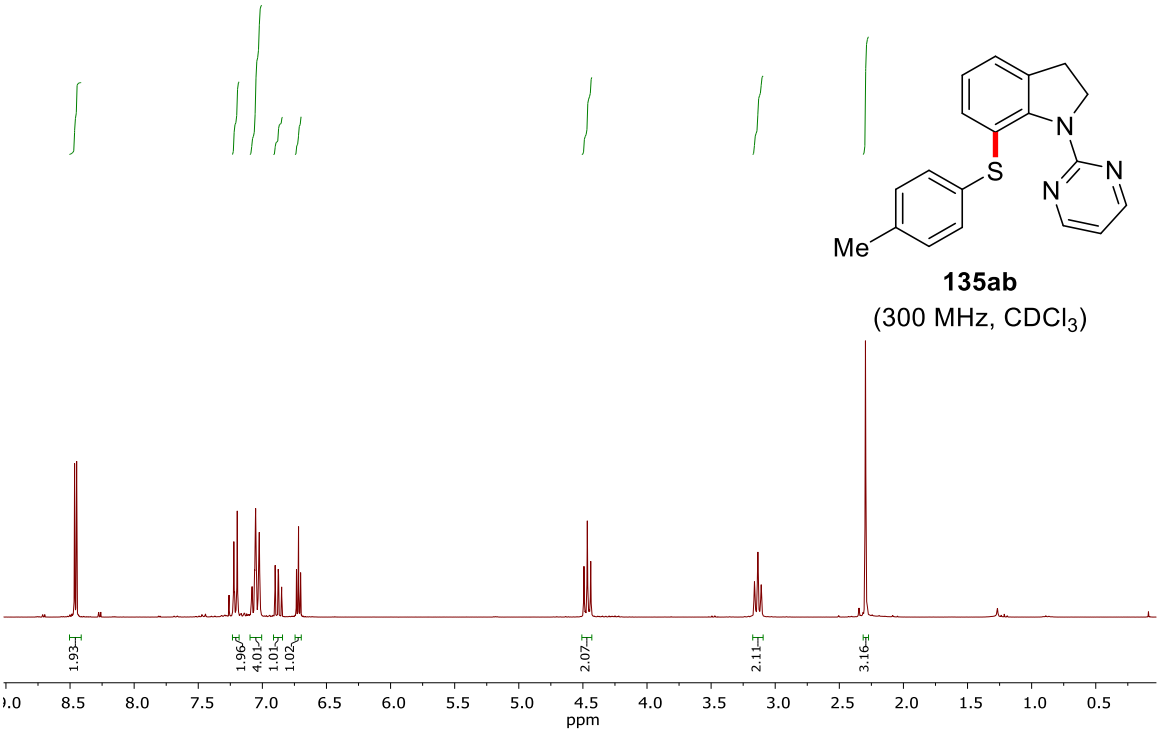

135ab

(300 MHz, $CDCl_3$)

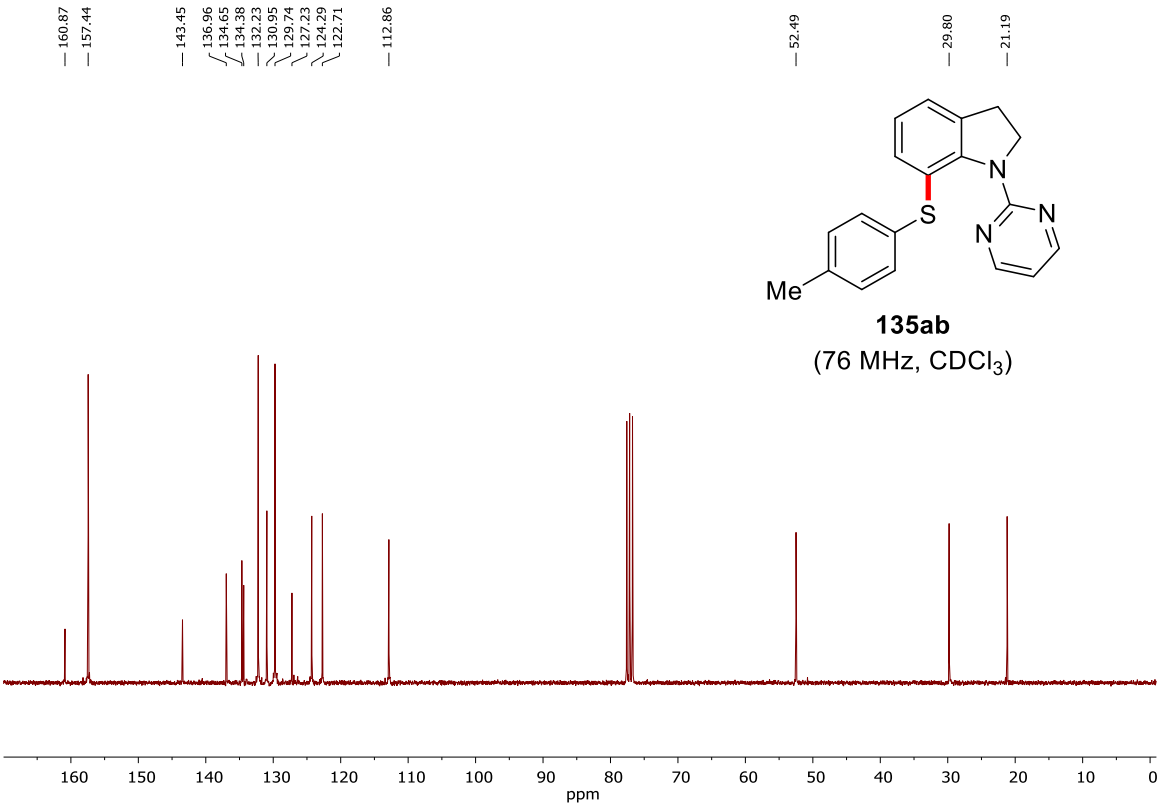

135ab

(76 MHz, $CDCl_3$)

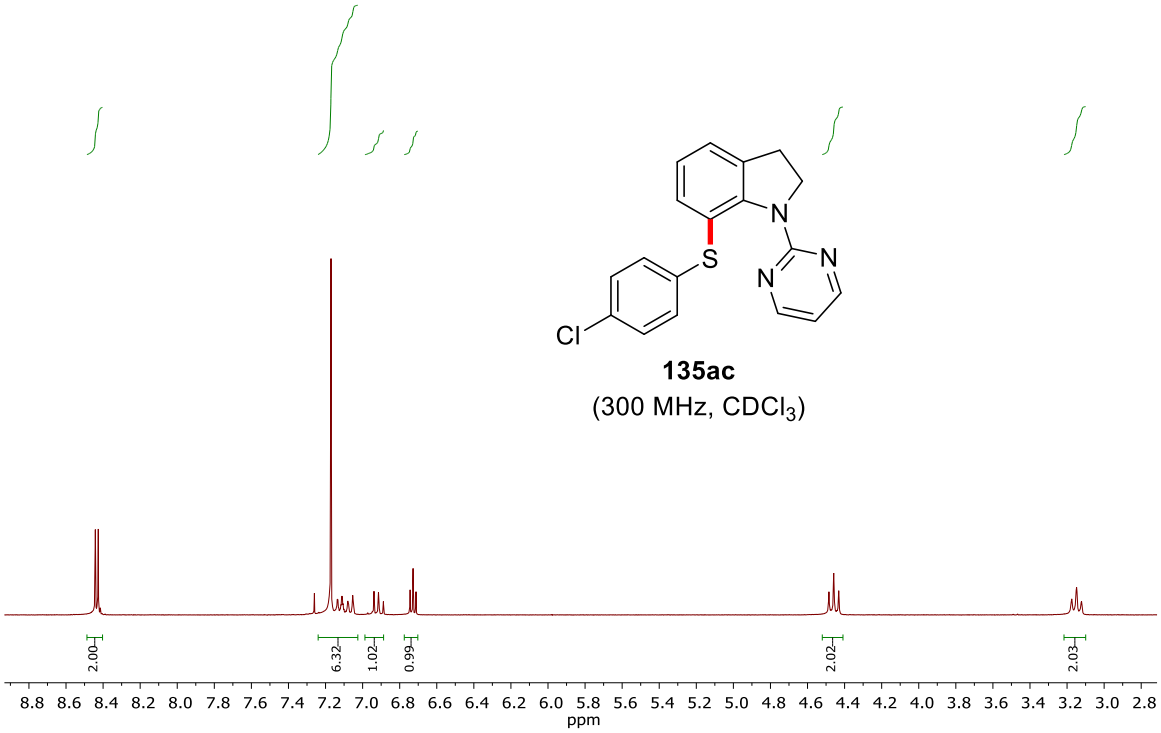

135ac

(300 MHz, $CDCl_3$)

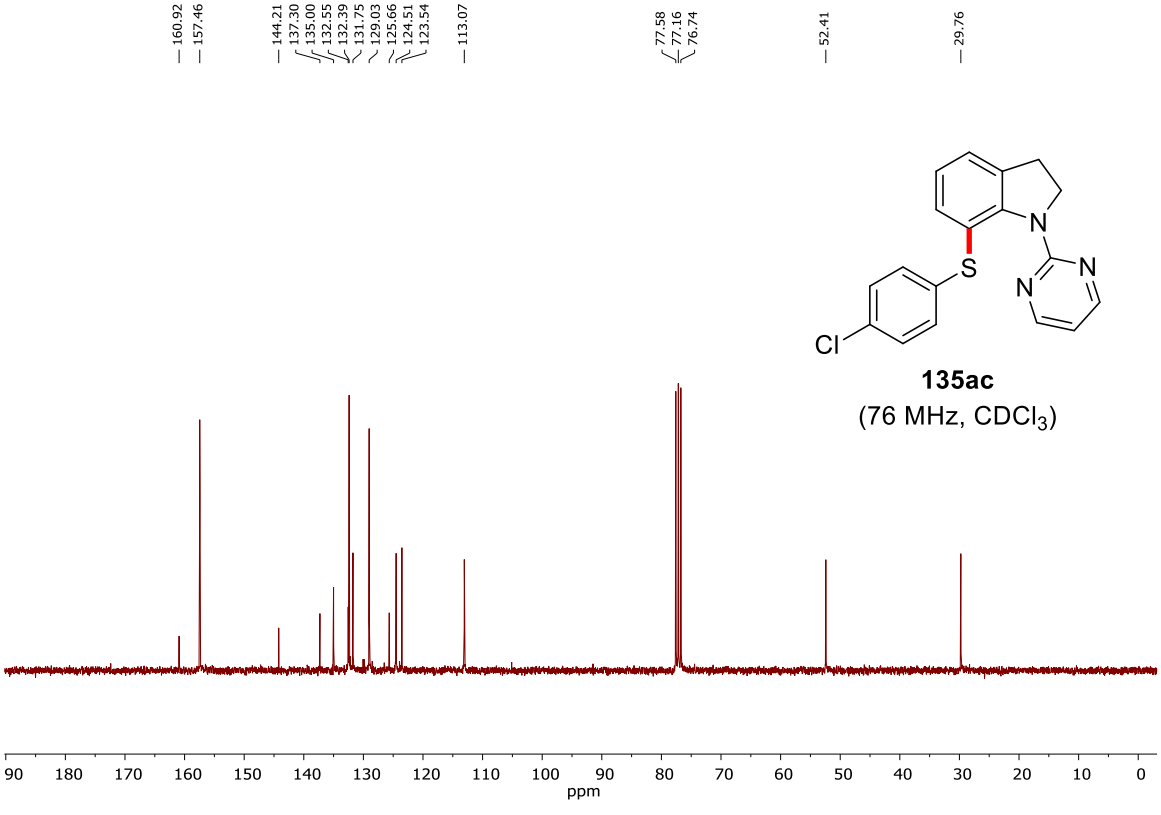

135ac

(76 MHz, $CDCl_3$)

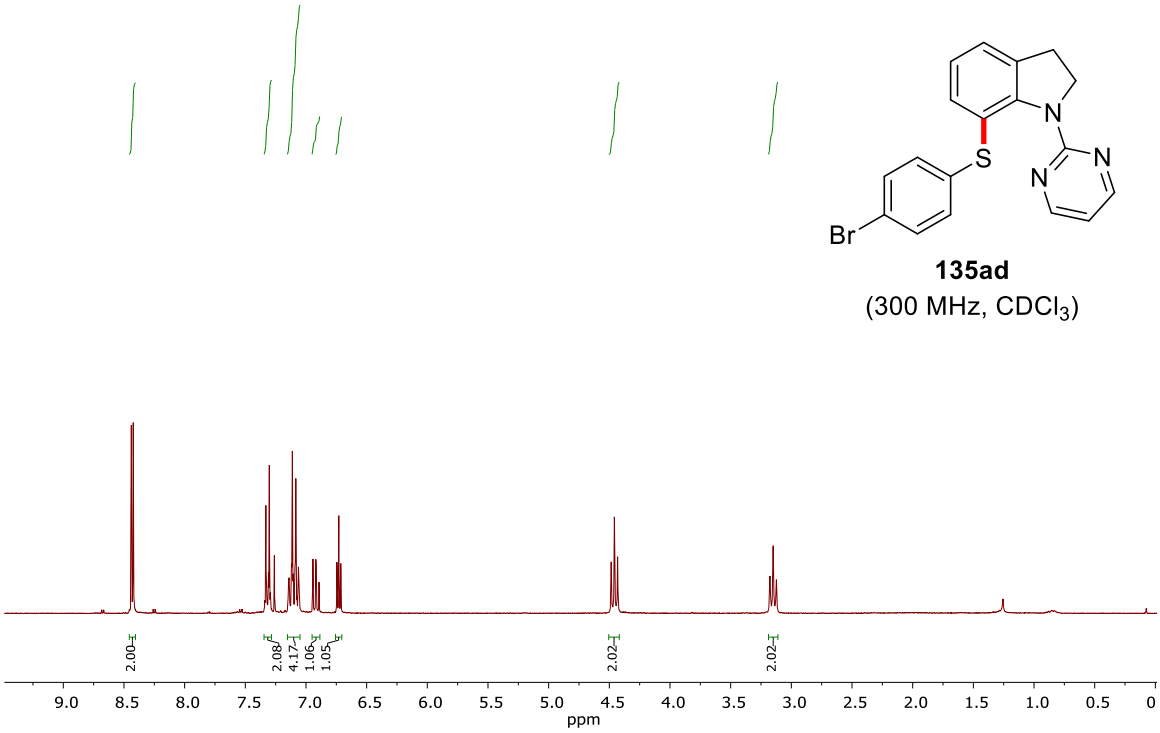

135ad
(300 MHz, $CDCl_3$)

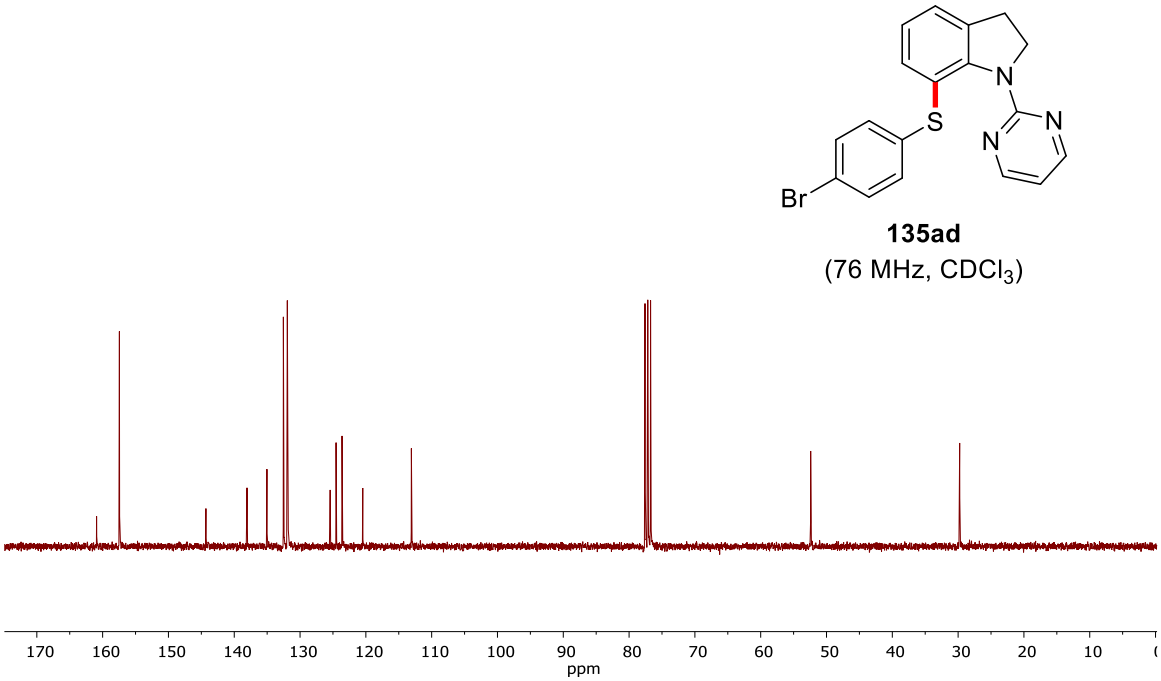

135ad
(76 MHz, $CDCl_3$)

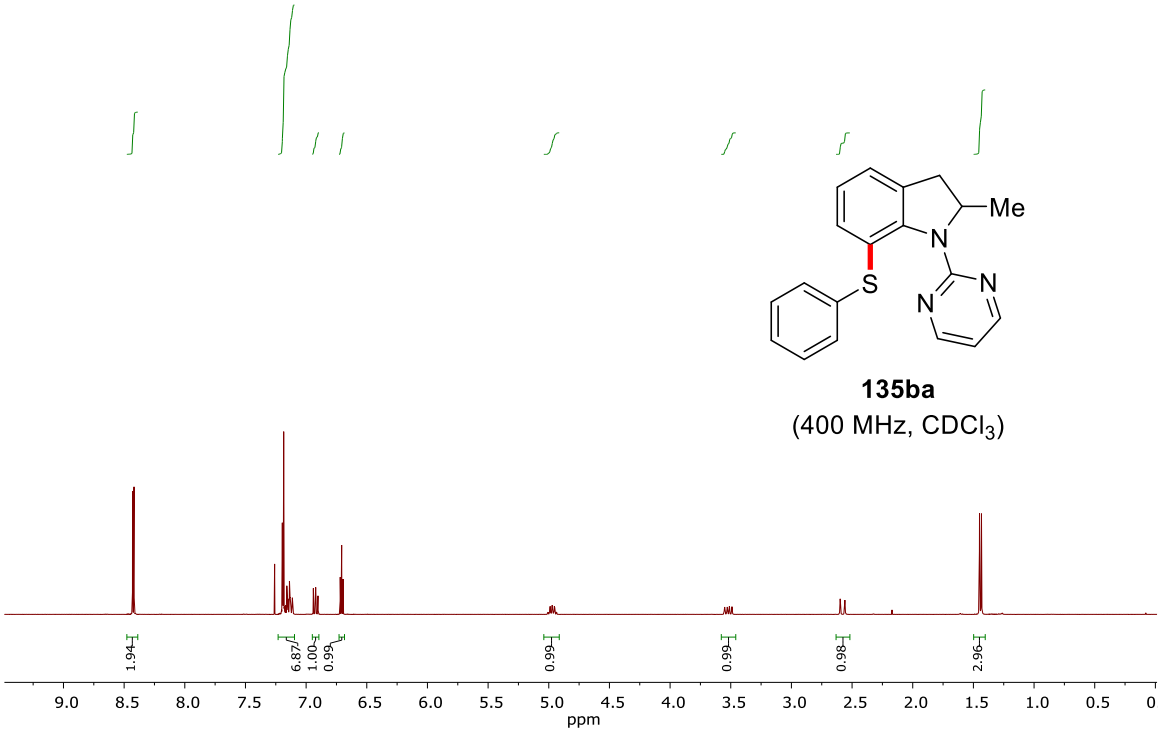

135ba
(400 MHz, $CDCl_3$)

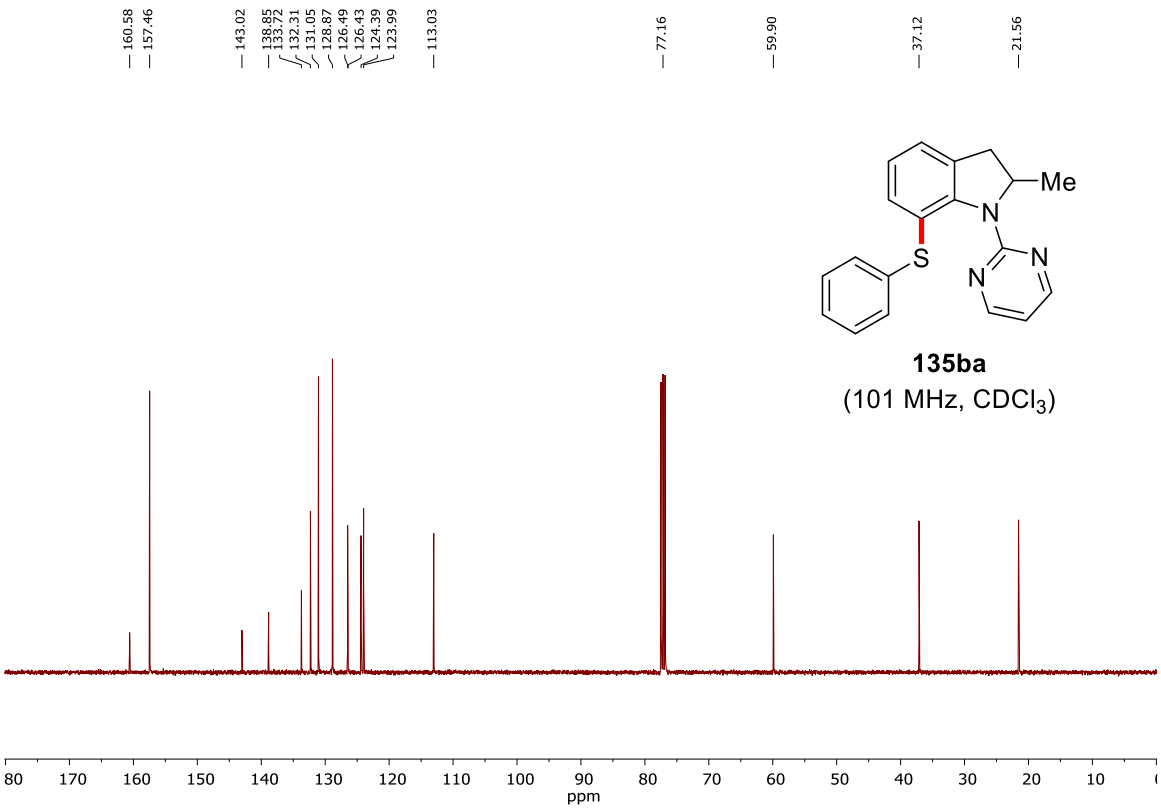

135ba
(101 MHz, $CDCl_3$)

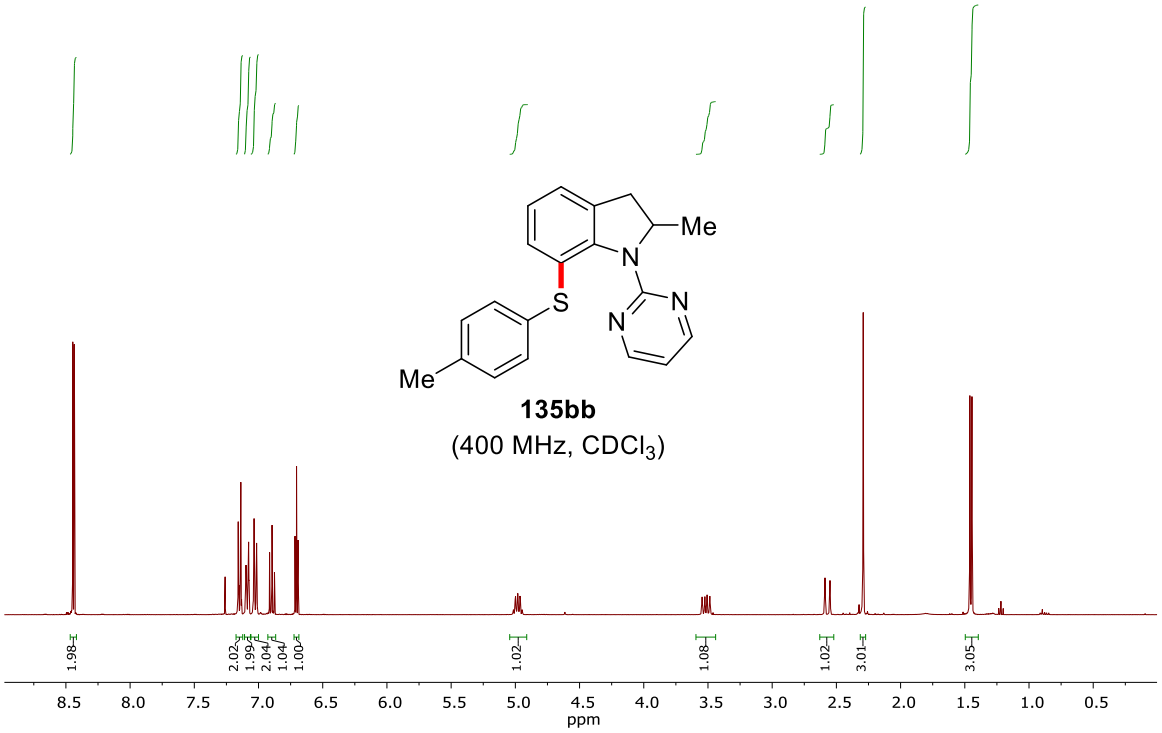

135bb

(400 MHz, $CDCl_3$)

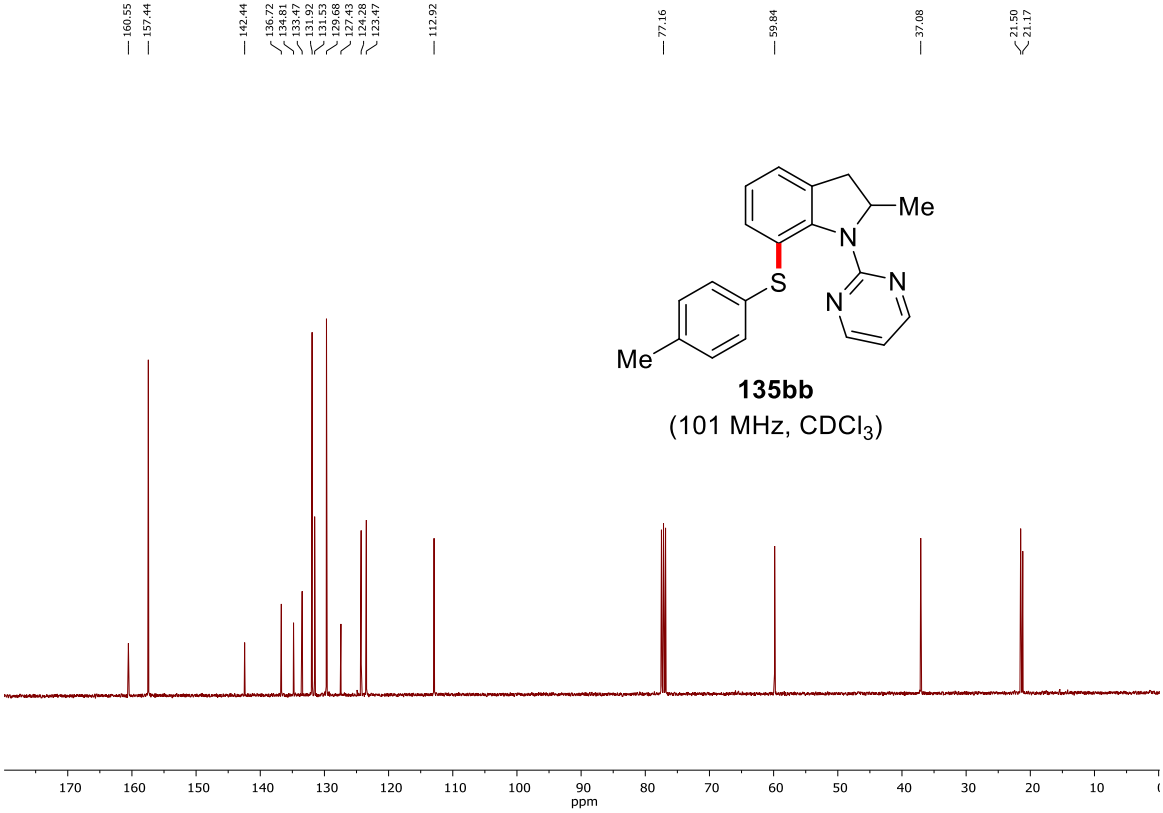

135bb

(101 MHz, $CDCl_3$)

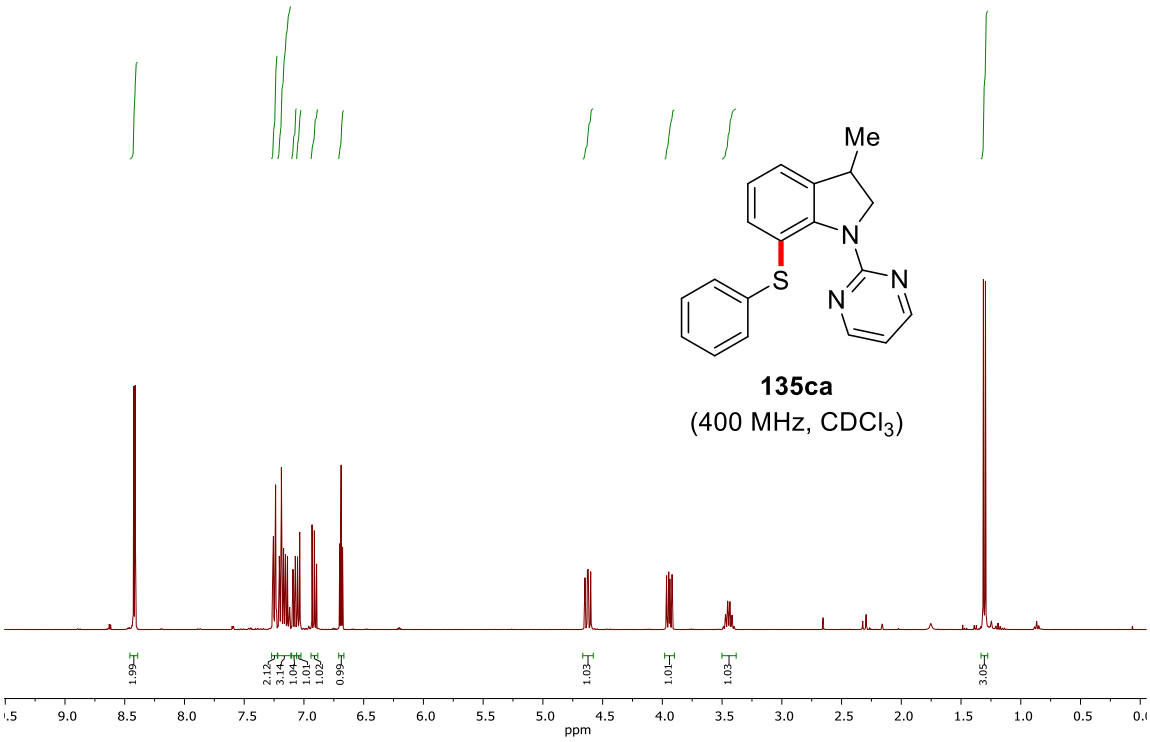

135ca
(400 MHz, $CDCl_3$)

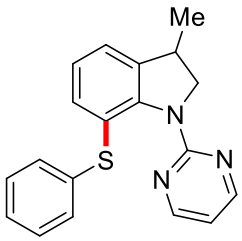

135ca
(101 MHz, $CDCl_3$)

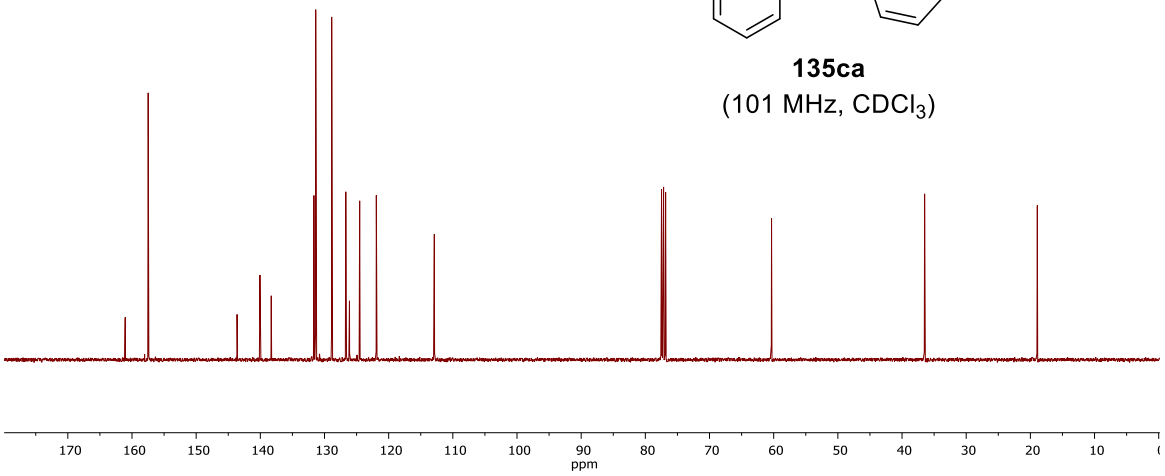

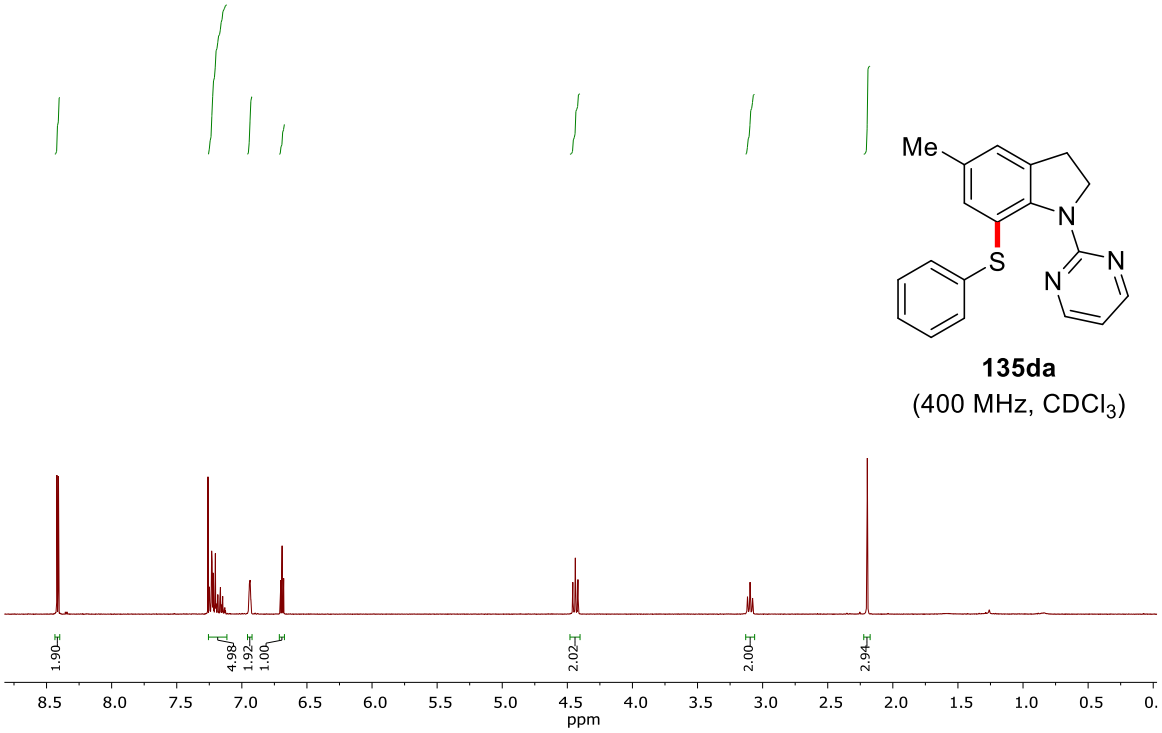
Me
N
S
N
N
135da
(400 MHz, CDCl3)
1.90
4.98
1.92
1.00
2.02
2.00
2.94
8.5 8.0 7.5 7.0 6.5 6.0 5.5 5.0 4.5 4.0 3.5 3.0 2.5 2.0 1.5 1.0 0.5 0.
ppm

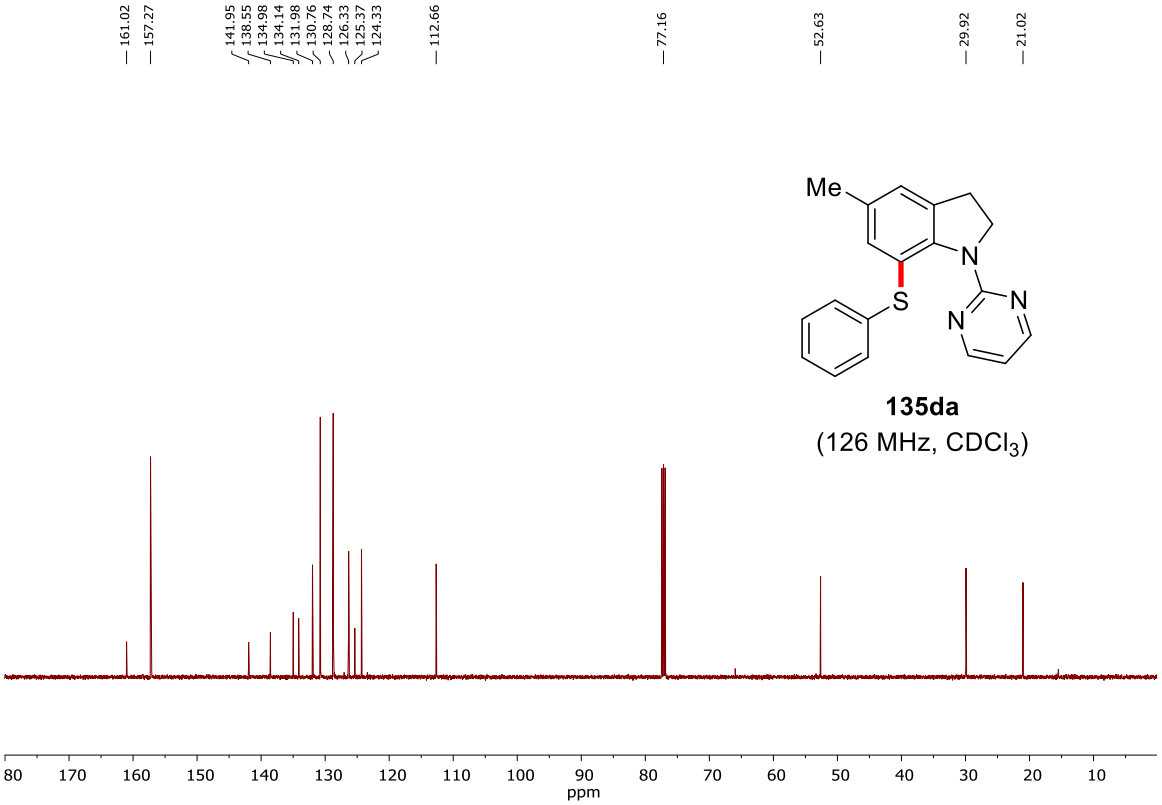
161.02
157.27
141.95
138.55
134.98
134.14
131.98
130.76
128.74
126.33
125.37
124.33
112.66
77.16
52.63
29.92
21.02
Me
N
S
N
N
135da
(126 MHz, CDCl3)
80 170 160 150 140 130 120 110 100 90 80 70 60 50 40 30 20 10
ppm

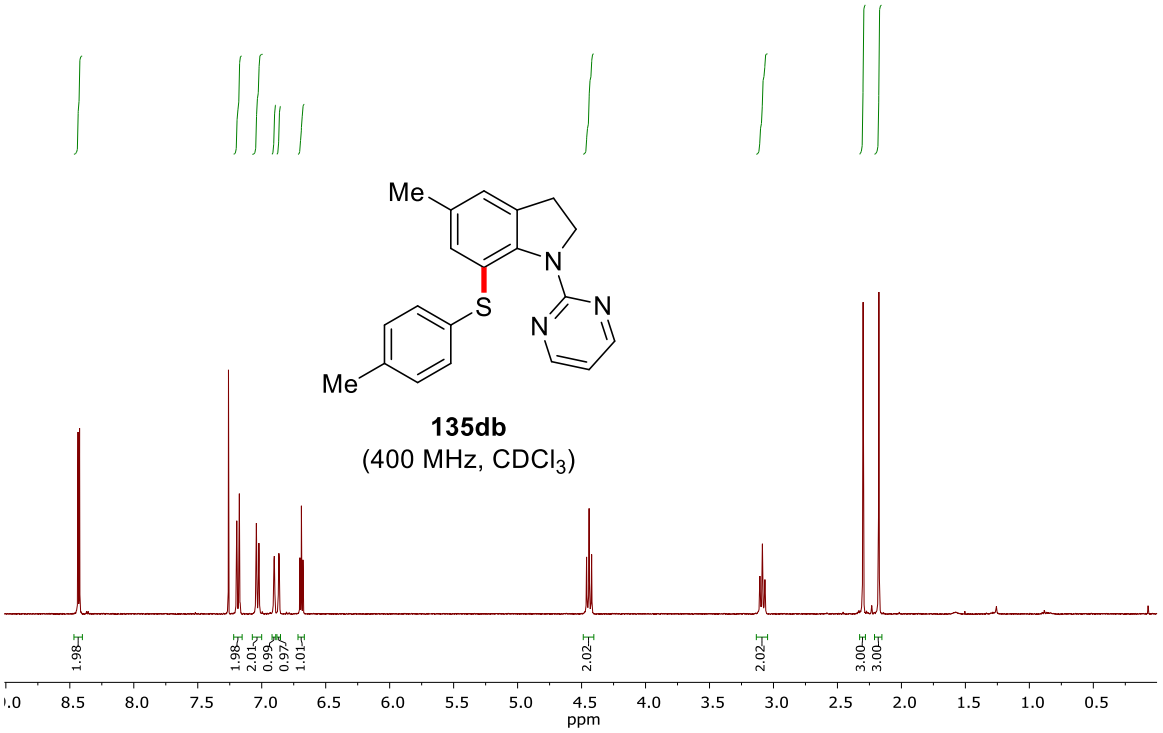

135db
(400 MHz, $CDCl_3$)

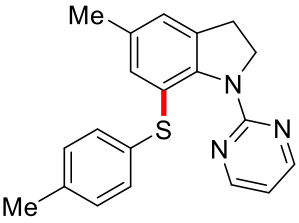

135db
(101 MHz, $CDCl_3$)

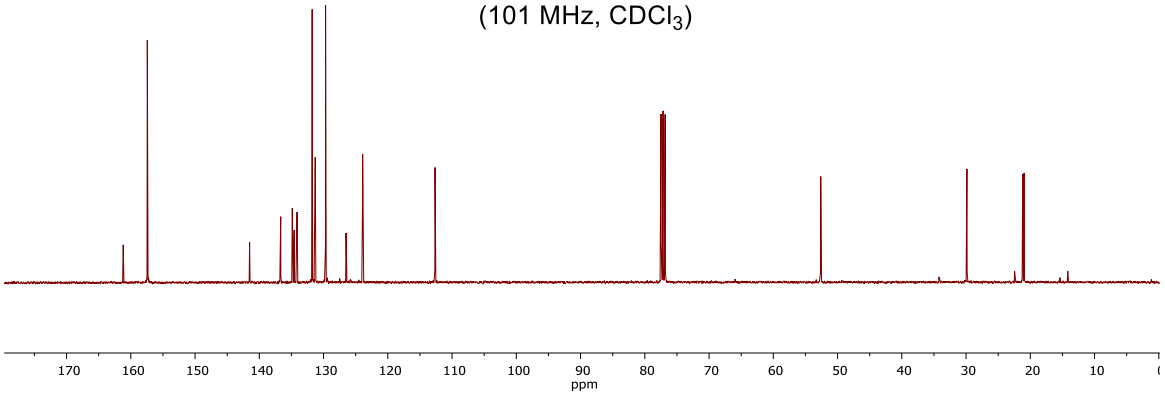

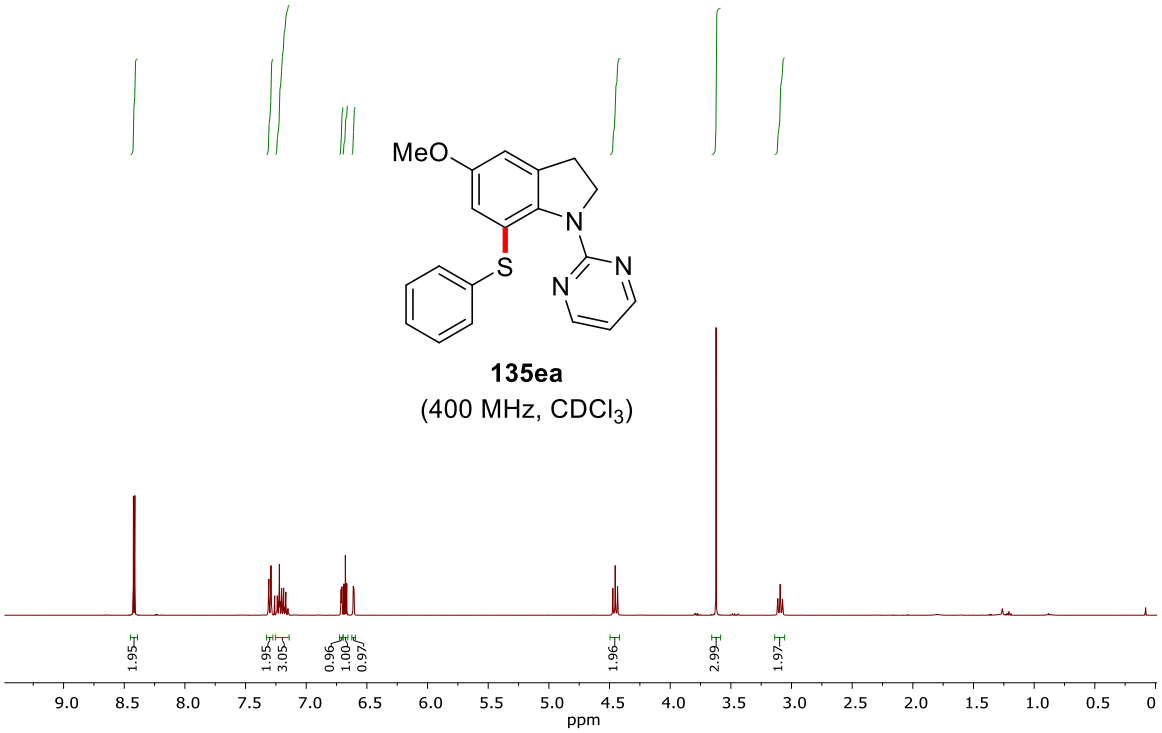
MeO
N
S
N
N
135ea
(400 MHz, CDCl3)
1.95
1.95
3.05
0.96
1.00
0.97
1.96
2.99
1.97
9.0
8.5
8.0
7.5
7.0
6.5
6.0
5.5
5.0
4.5
4.0
3.5
3.0
2.5
2.0
1.5
1.0
0.5
0
ppm
161.13
157.43
156.82
137.86
137.72
136.33
131.59
128.93
127.09
126.87
115.41
112.52
110.46
77.16
55.79
52.66
30.25

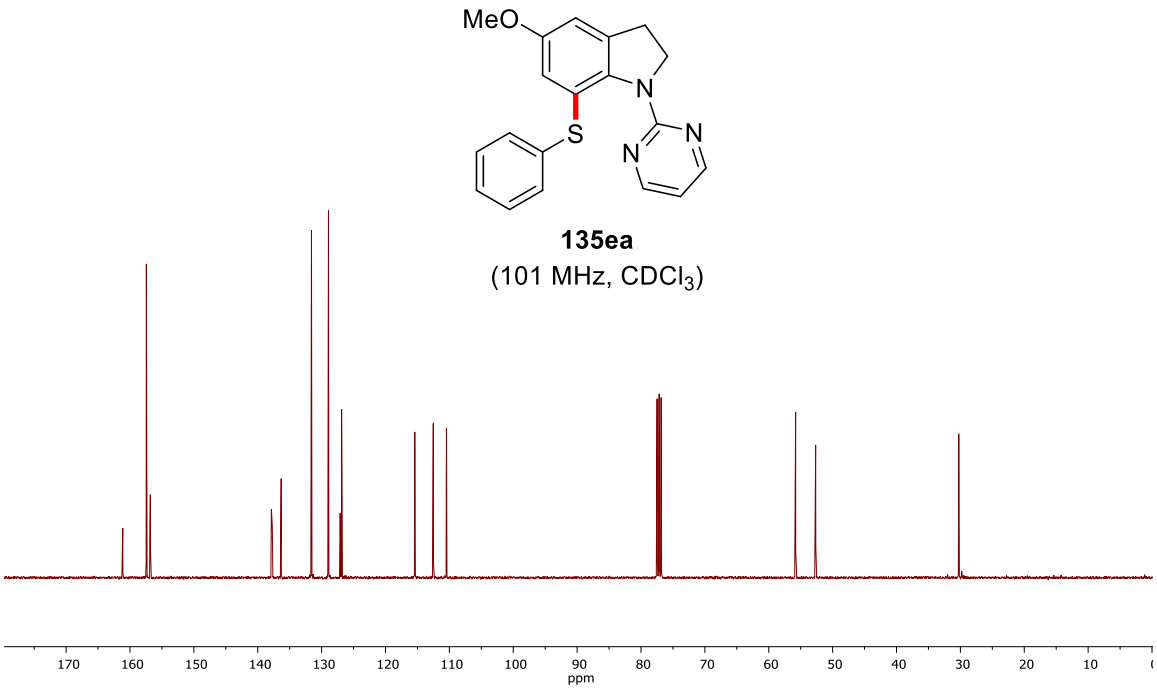
MeO
N
S
N
N
135ea
(101 MHz, CDCl3)
170
160
150
140
130
120
110
100
90
80
70
60
50
40
30
20
10
ppm

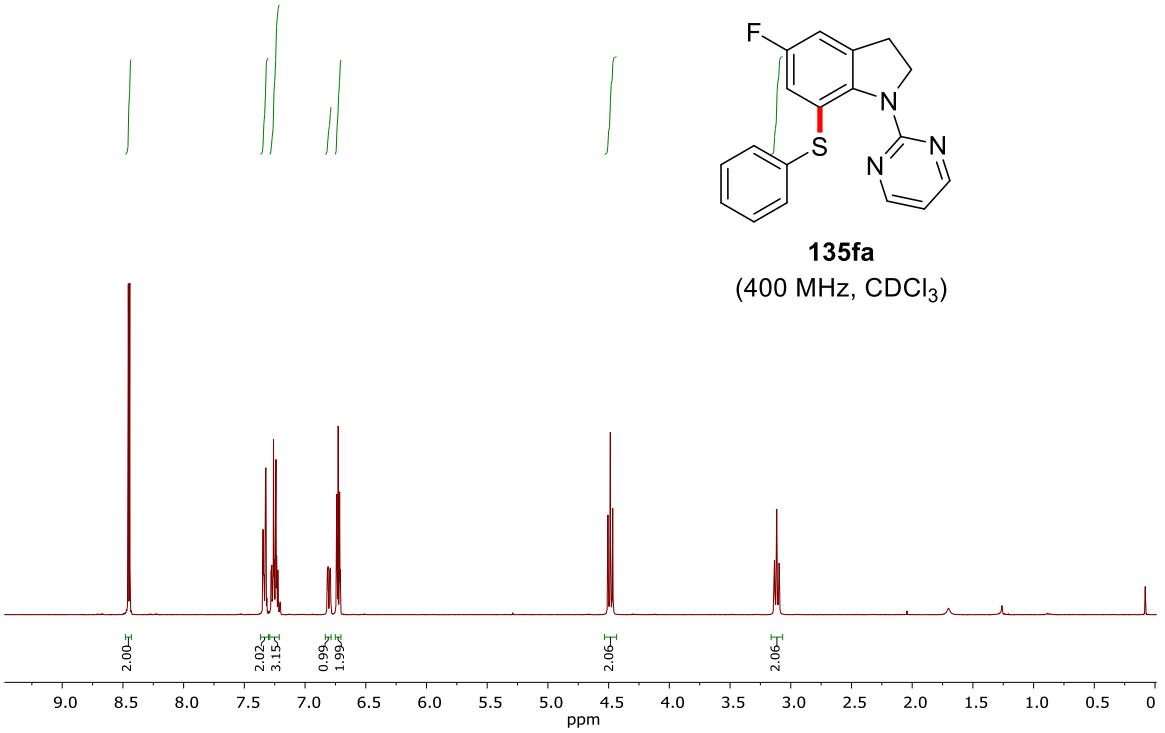

135fa
(400 MHz, $CDCl_3$)

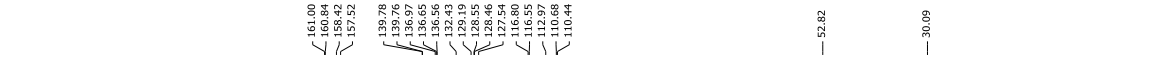

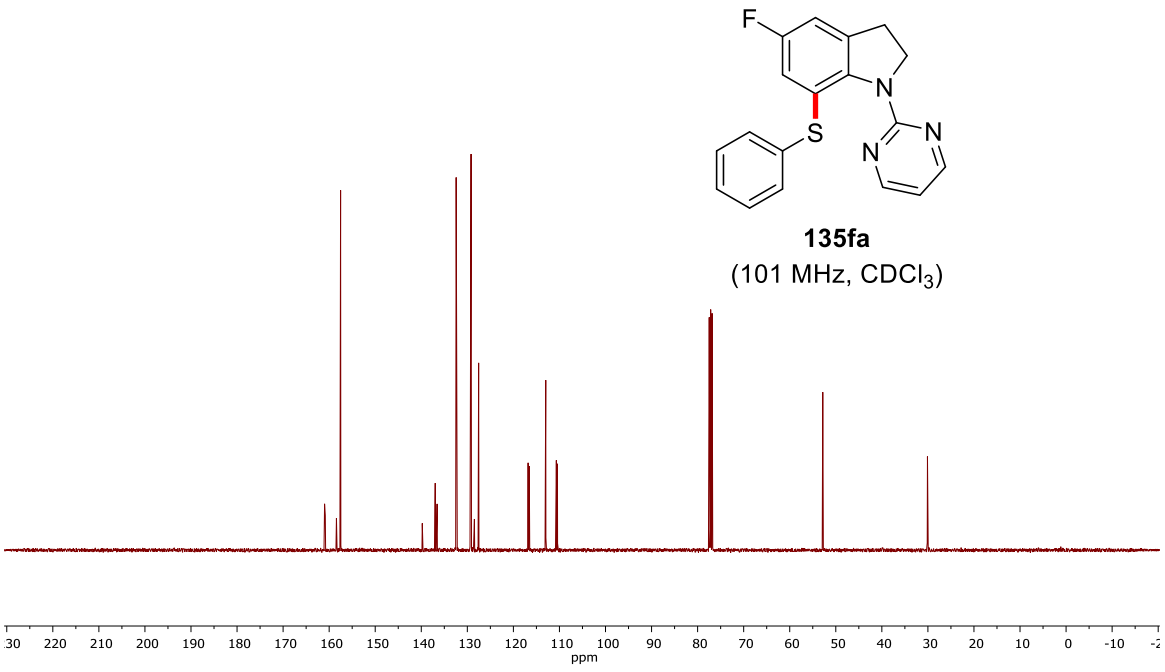

135fa
(101 MHz, $CDCl_3$)

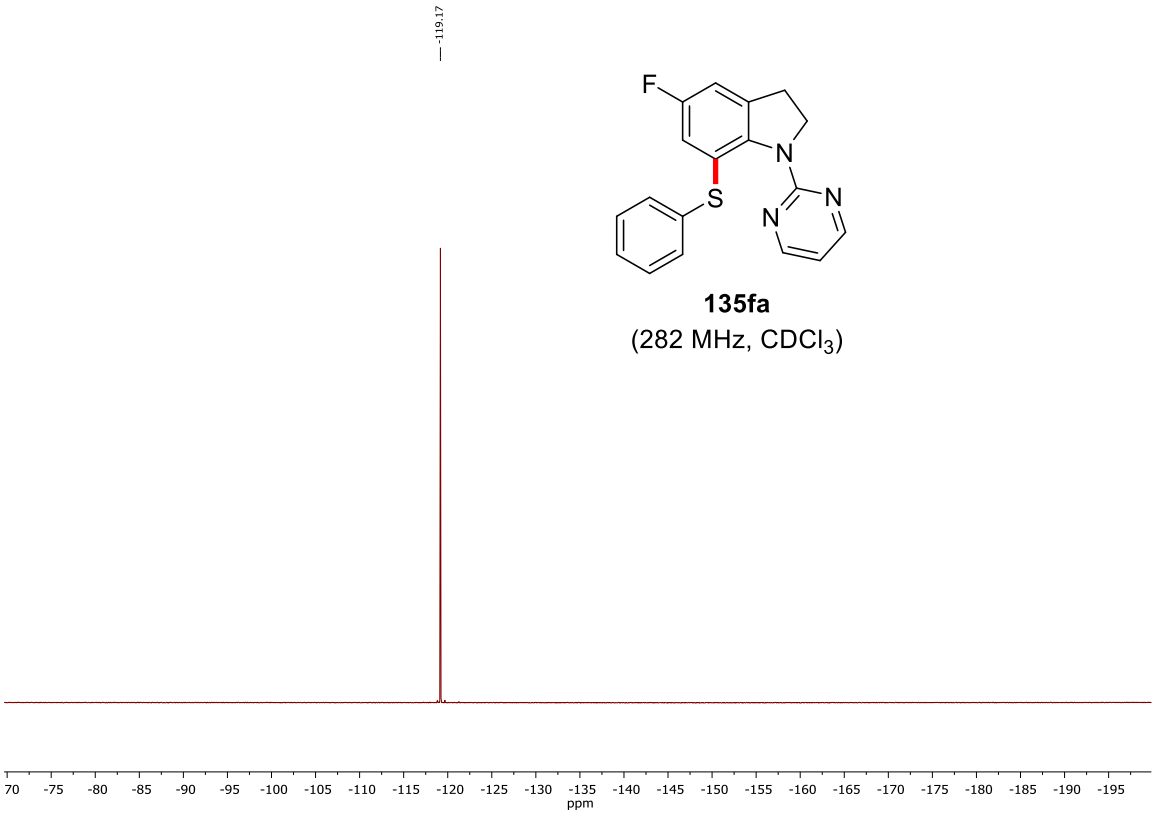

135fa

(282 MHz, $CDCl_3$)

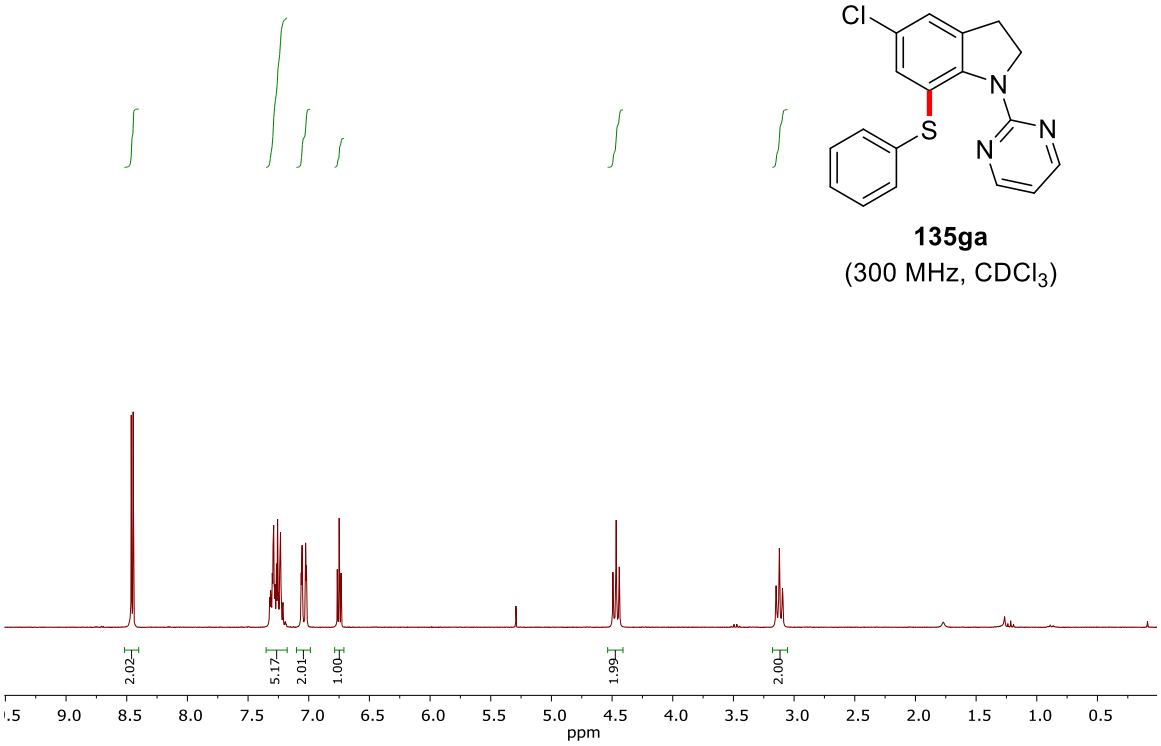

135ga
(300 MHz, $CDCl_3$)

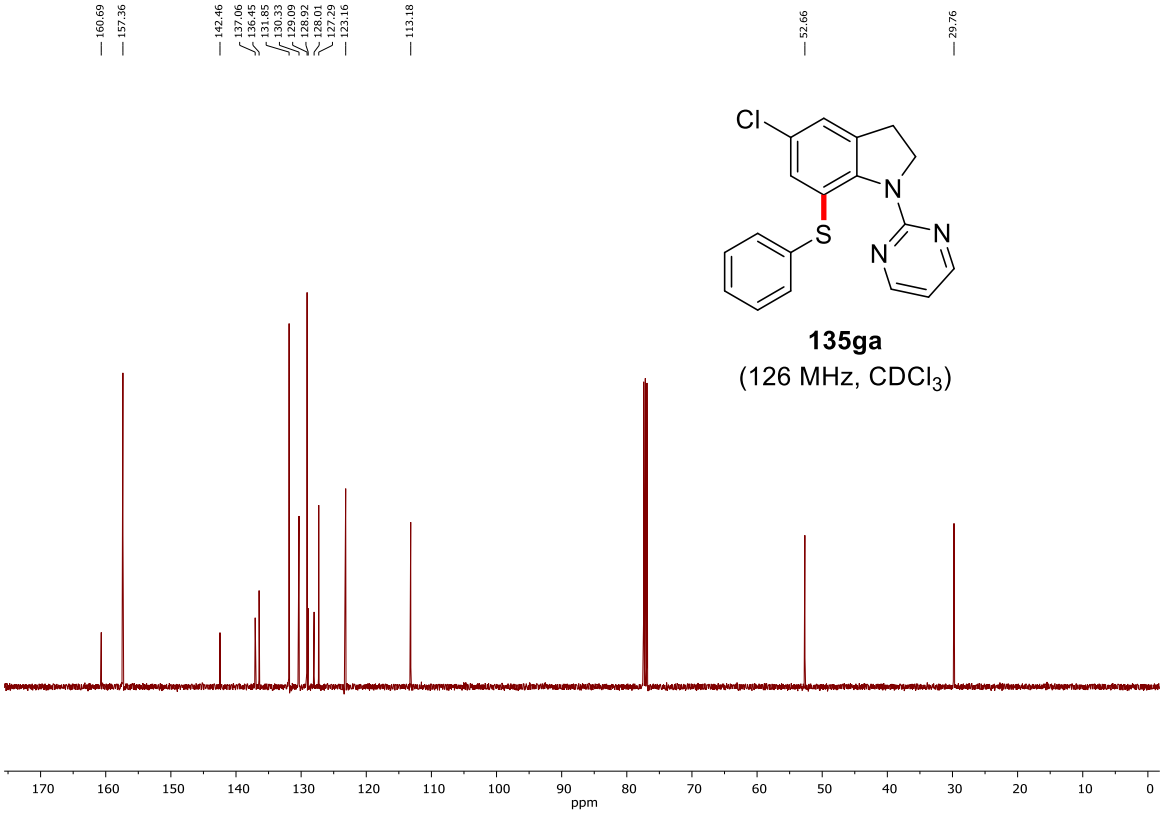

135ga
(126 MHz, $CDCl_3$)

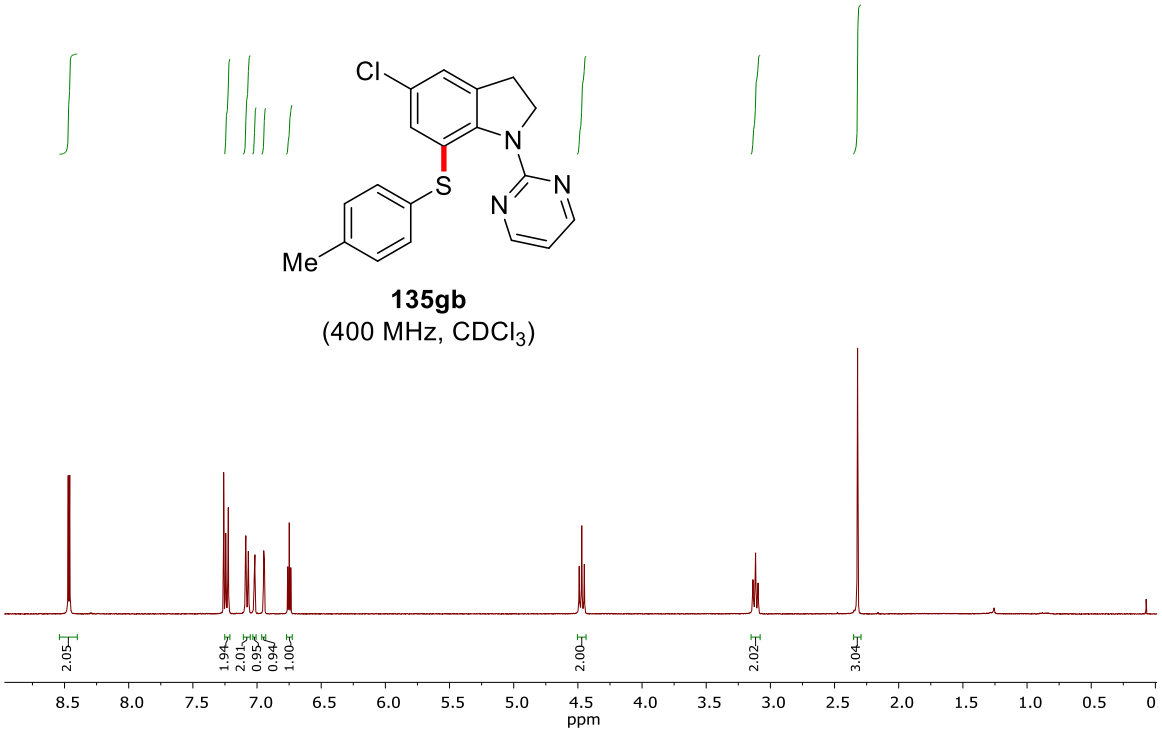
Cl
N
S
N
N
Me
135gb
(400 MHz, CDCl3)
2.05
1.94
2.01
0.95
0.94
1.00
2.00
2.02
3.04
8.5 8.0 7.5 7.0 6.5 6.0 5.5 5.0 4.5 4.0 3.5 3.0 2.5 2.0 1.5 1.0 0.5 0
ppm

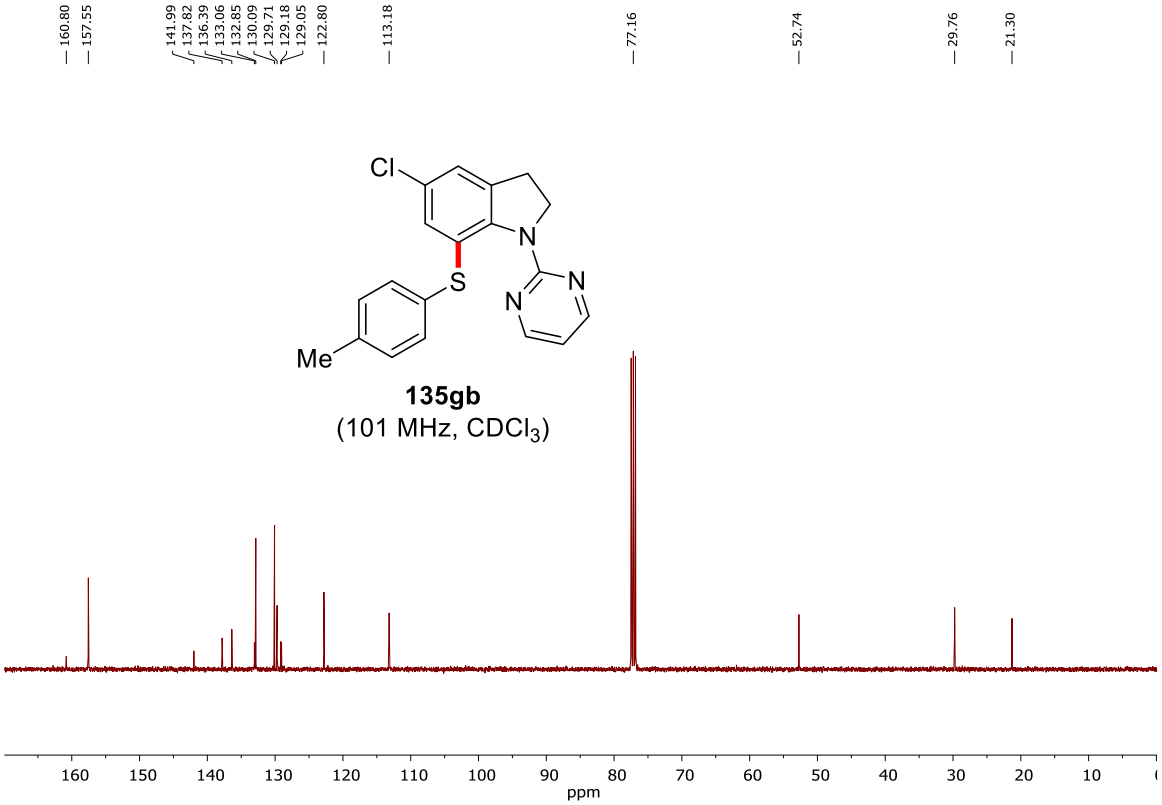
160.80
157.55
141.99
137.82
136.39
133.06
132.85
130.09
129.71
129.18
129.05
122.80
113.18
77.16
52.74
29.76
21.30
Cl
N
S
N
N
Me
135gb
(101 MHz, CDCl3)
160 150 140 130 120 110 100 90 80 70 60 50 40 30 20 10
ppm

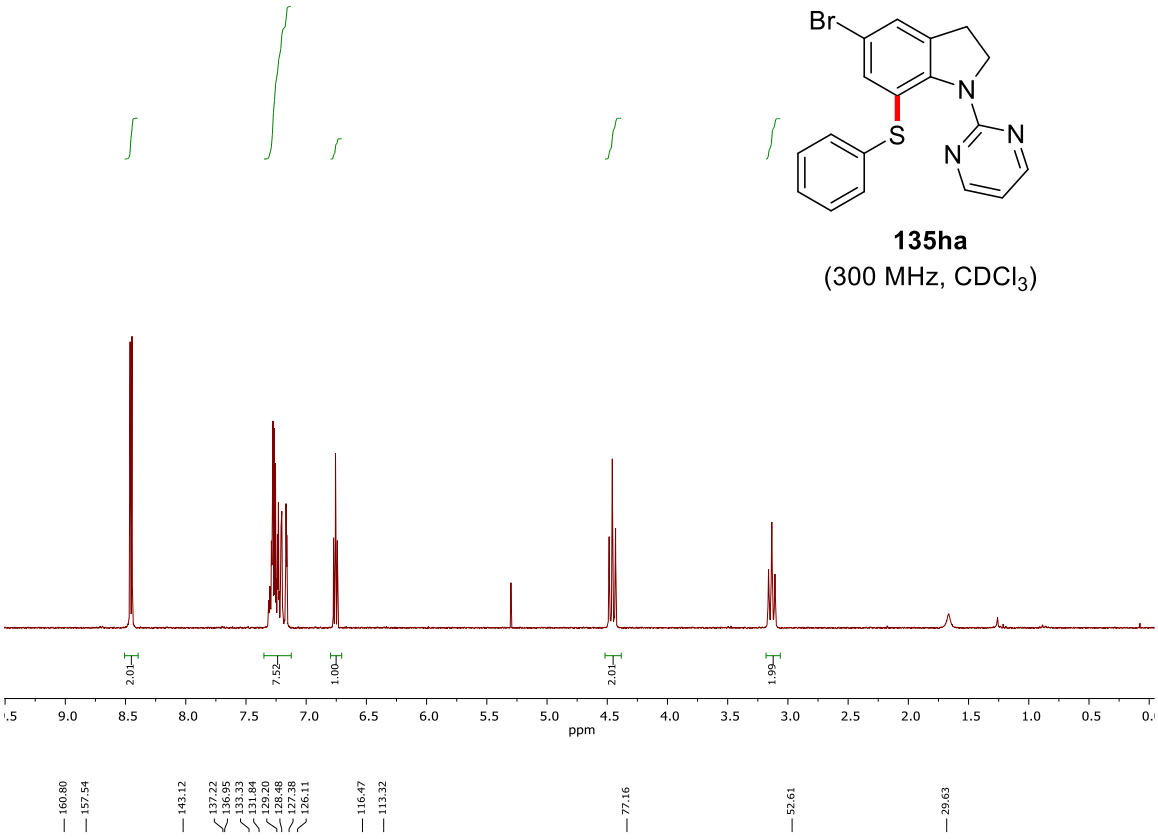

135ha
(300 MHz, $CDCl_3$)

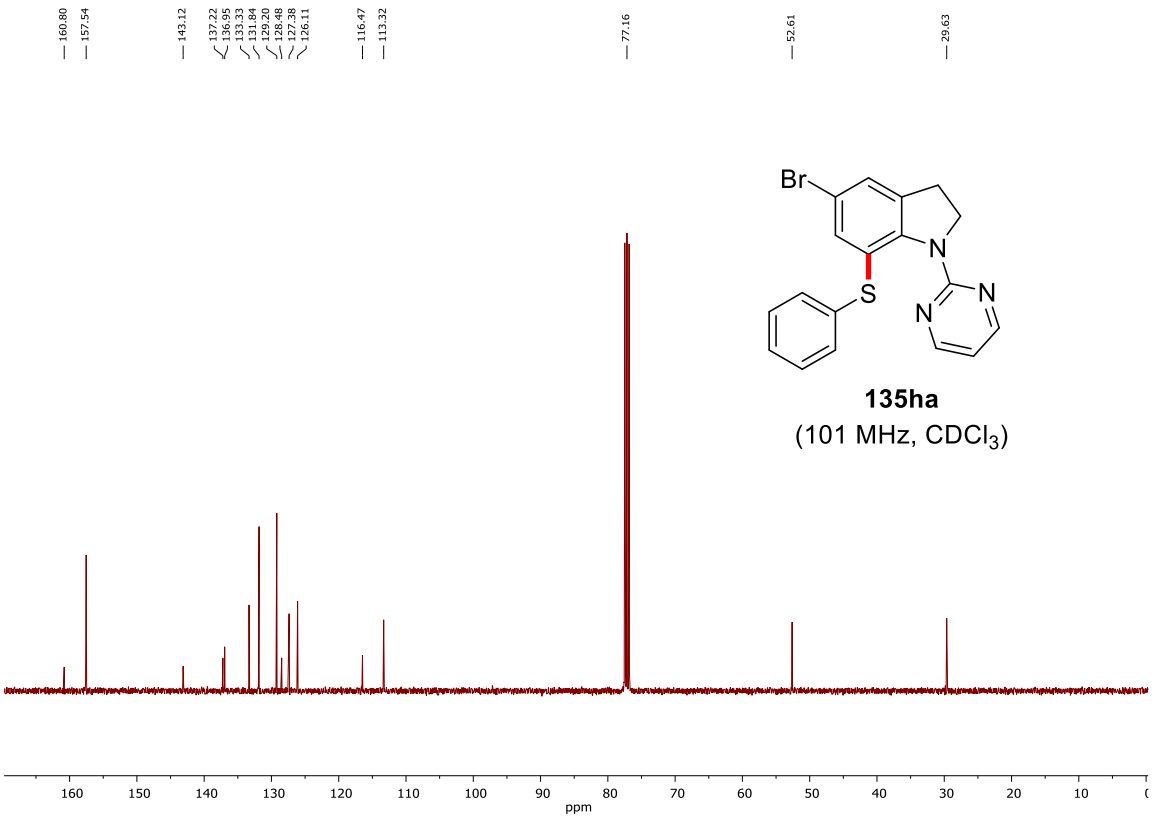

135ha
(101 MHz, $CDCl_3$)

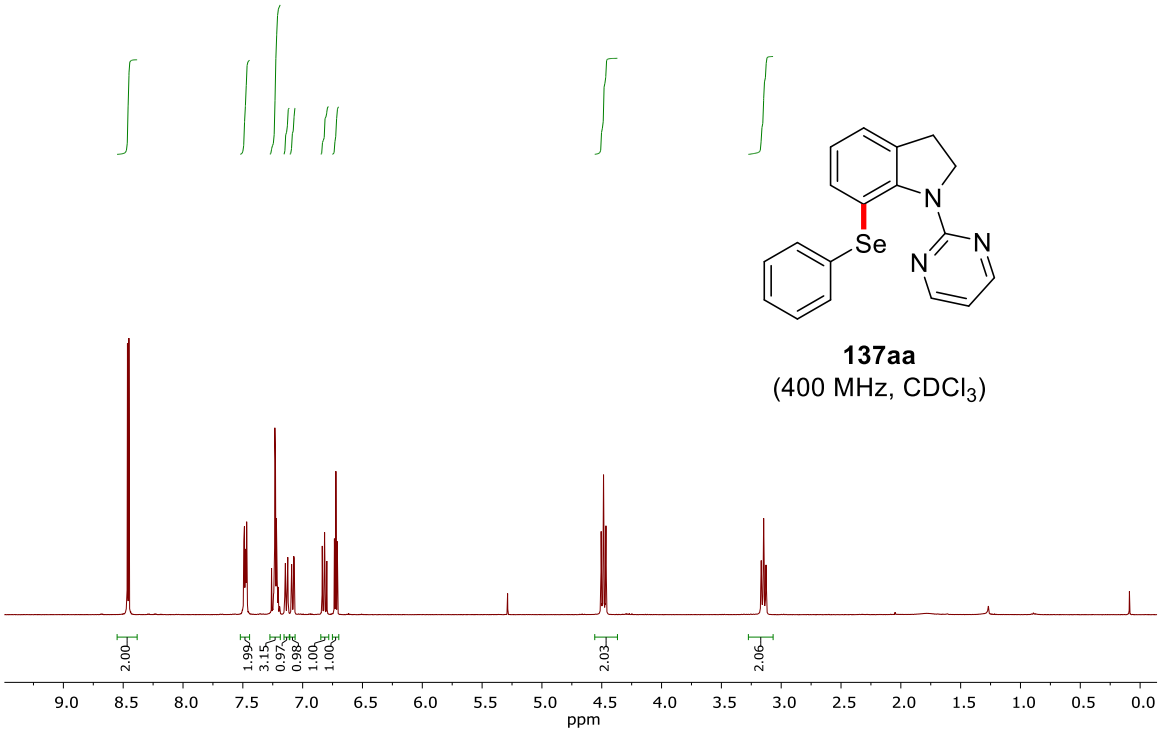

137aa
(400 MHz, $CDCl_3$)

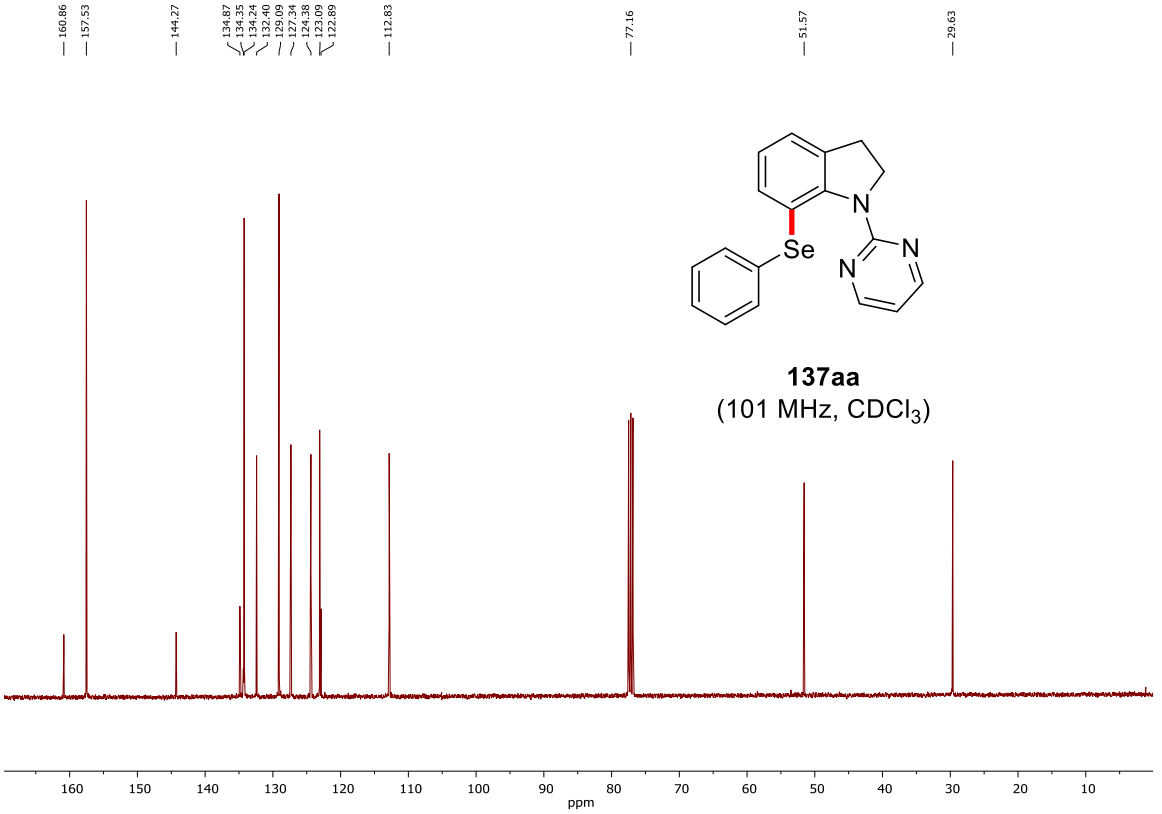

137aa
(101 MHz, $CDCl_3$)

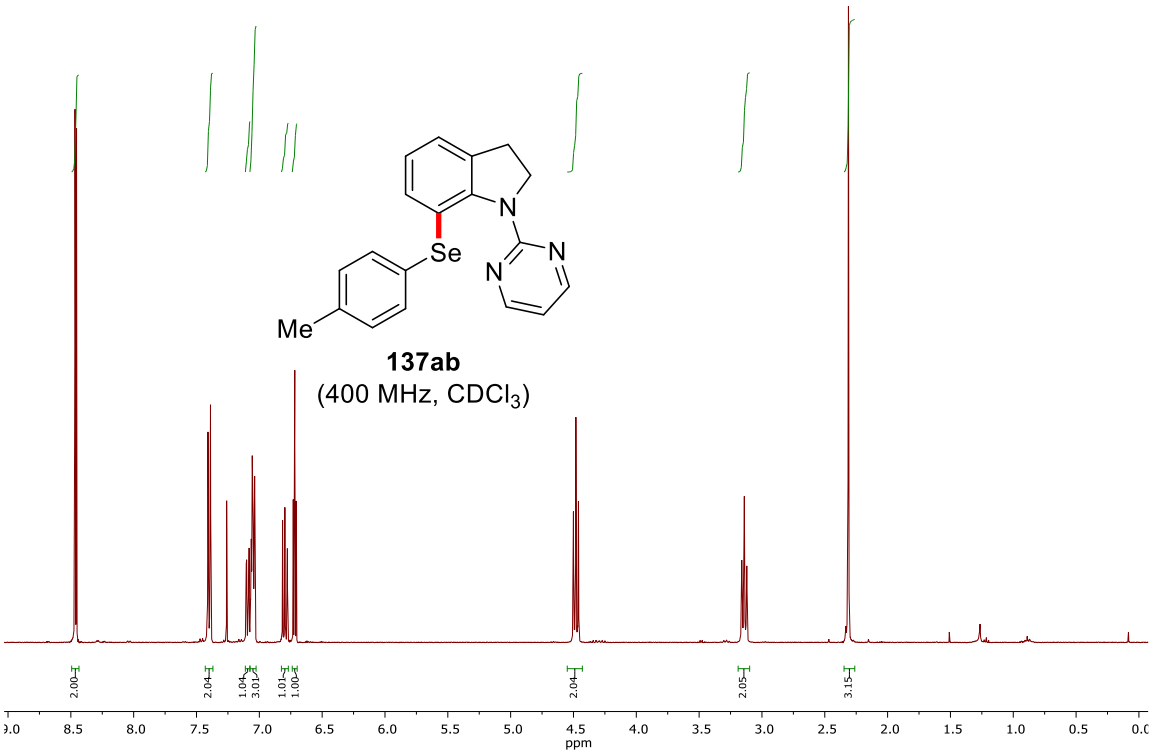

137ab
(400 MHz, $CDCl_3$)

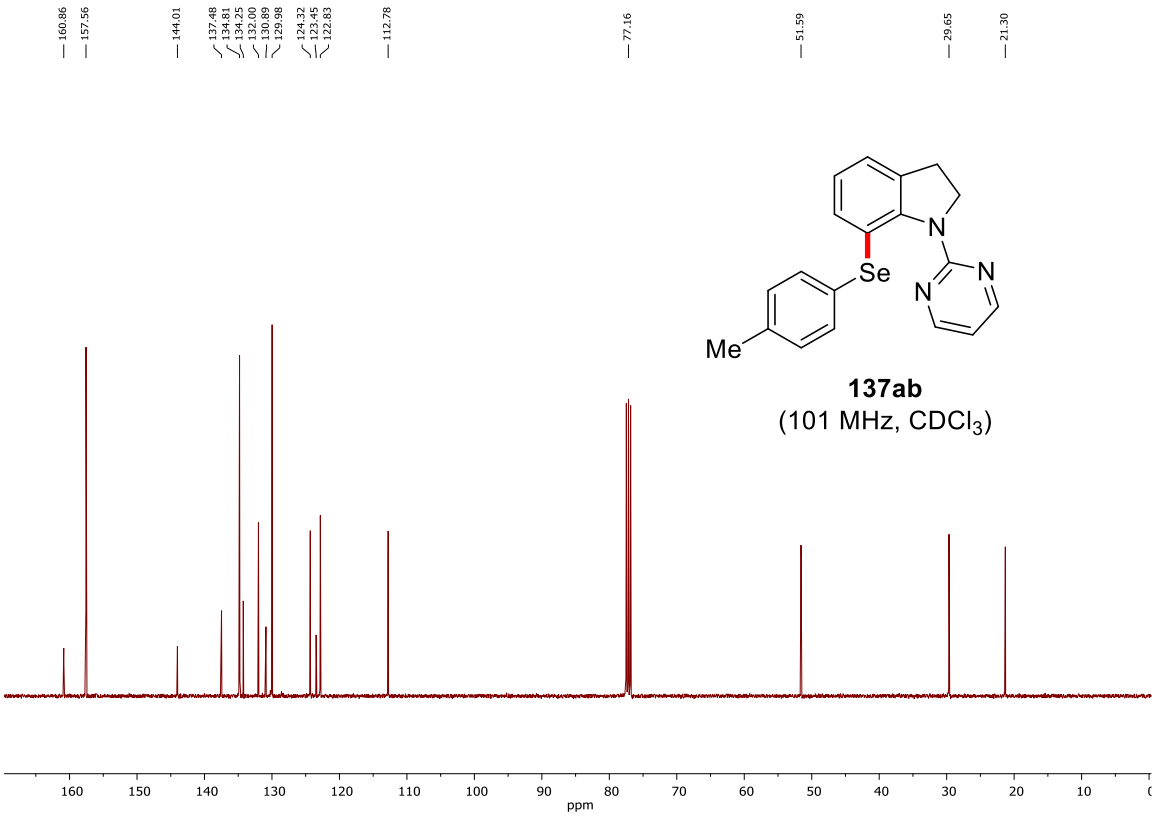

137ab
(101 MHz, $CDCl_3$)

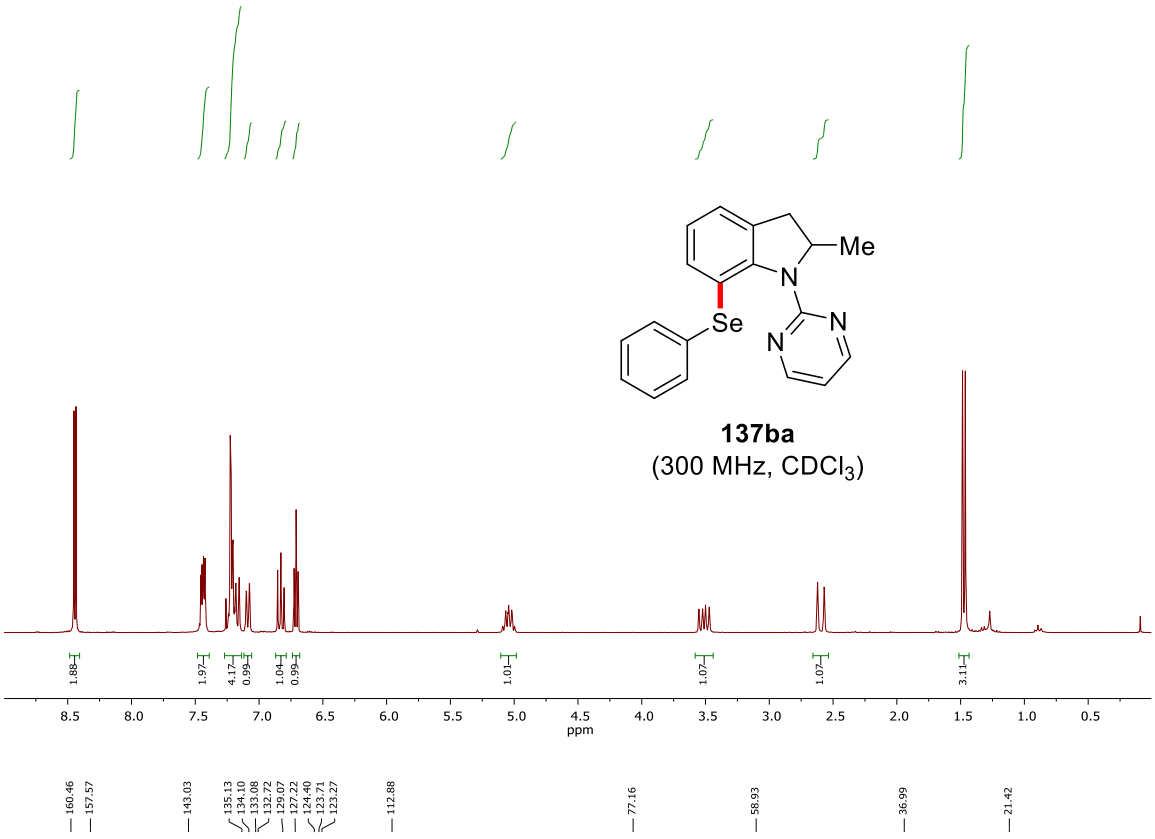
Me
N
Se
N
N
137ba
(300 MHz, CDCl3)
1.88
1.97
4.17
0.99
1.04
0.99
1.01
1.07
1.07
3.11
8.5
8.0
7.5
7.0
6.5
6.0
5.5
5.0
4.5
4.0
3.5
3.0
2.5
2.0
1.5
1.0
0.5
ppm
160.46
157.57
143.03
135.13
134.10
133.08
132.72
129.07
127.22
124.40
123.71
123.27
112.88
77.16
58.93
36.99
21.42

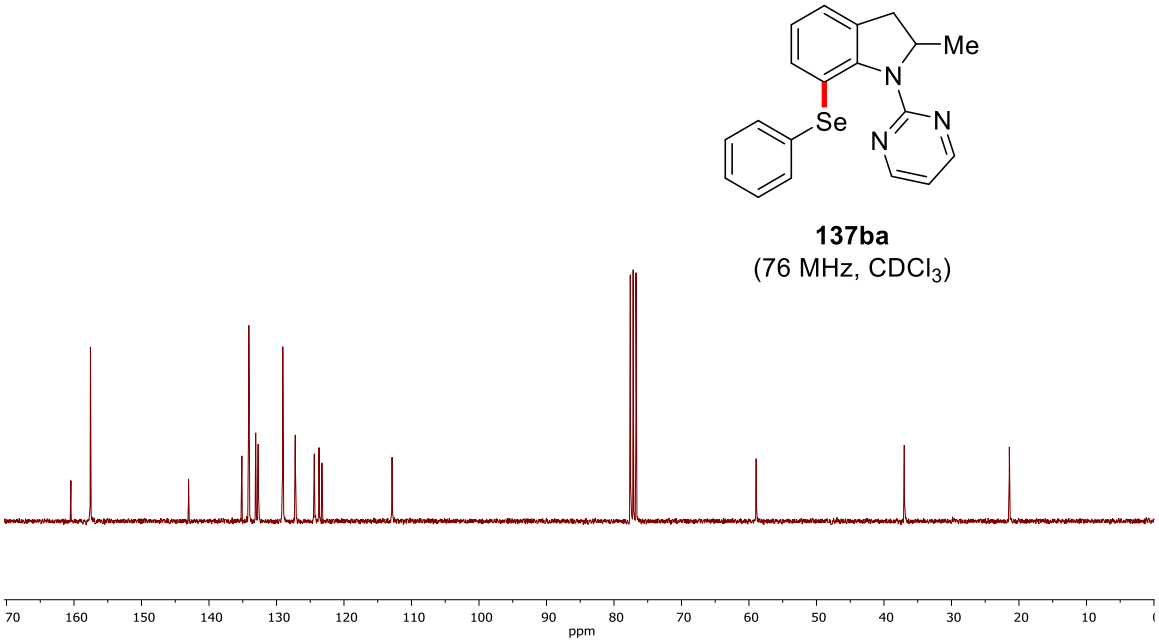
Me
N
Se
N
N
137ba
(76 MHz, CDCl3)
70
160
150
140
130
120
110
100
90
80
70
60
50
40
30
20
10
ppm

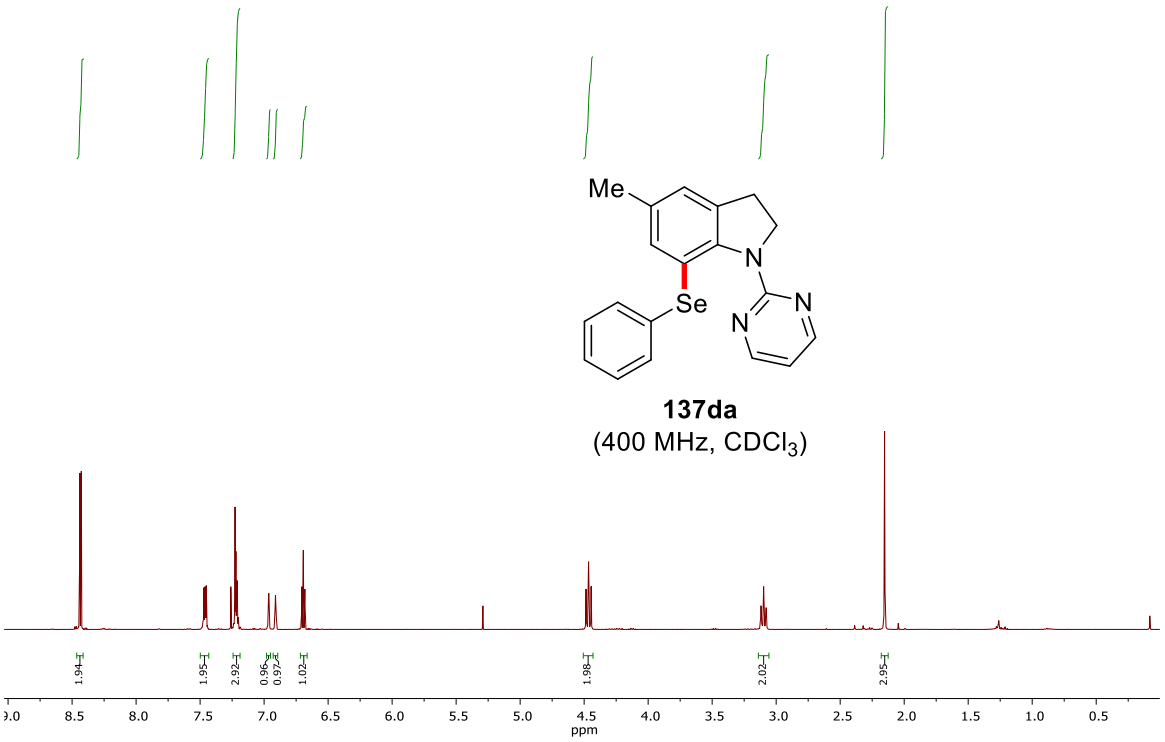

137da
(400 MHz, $CDCl_3$)

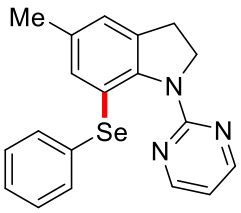

137da
(101 MHz, $CDCl_3$)

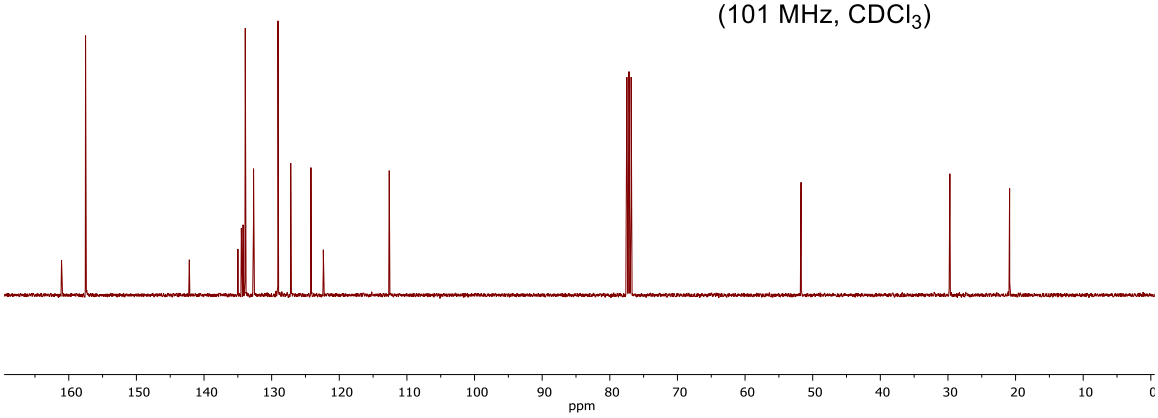

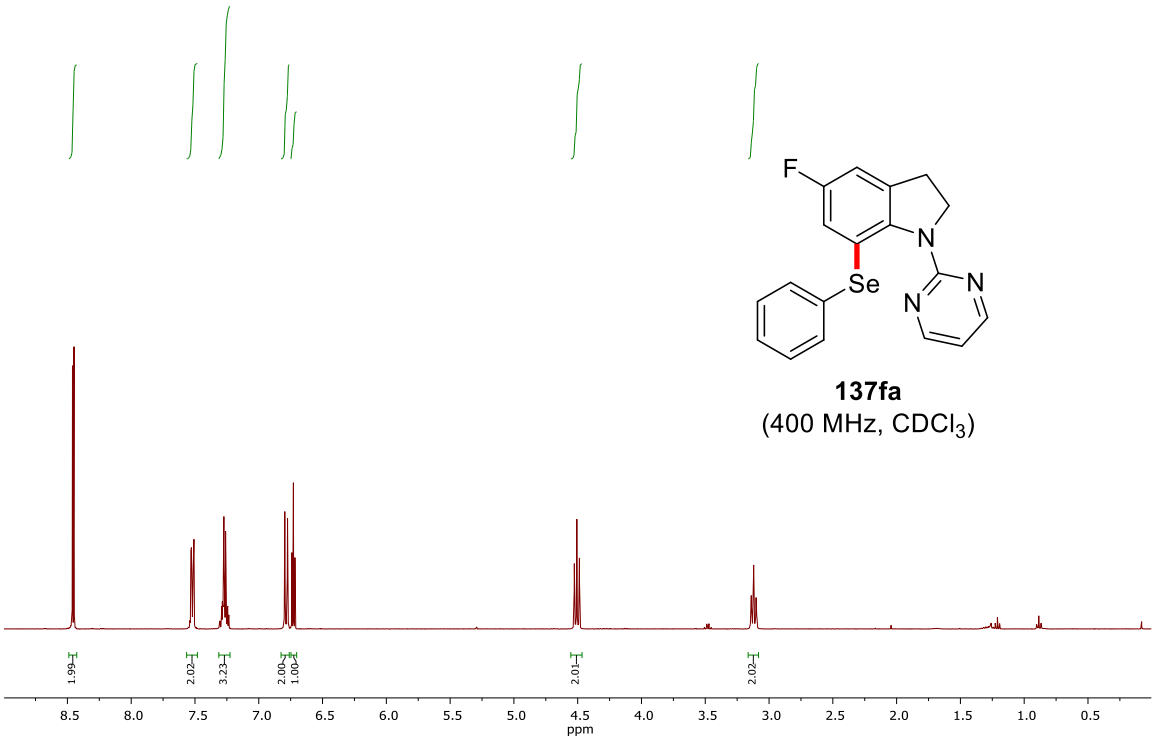

137fa
(400 MHz, $CDCl_3$)

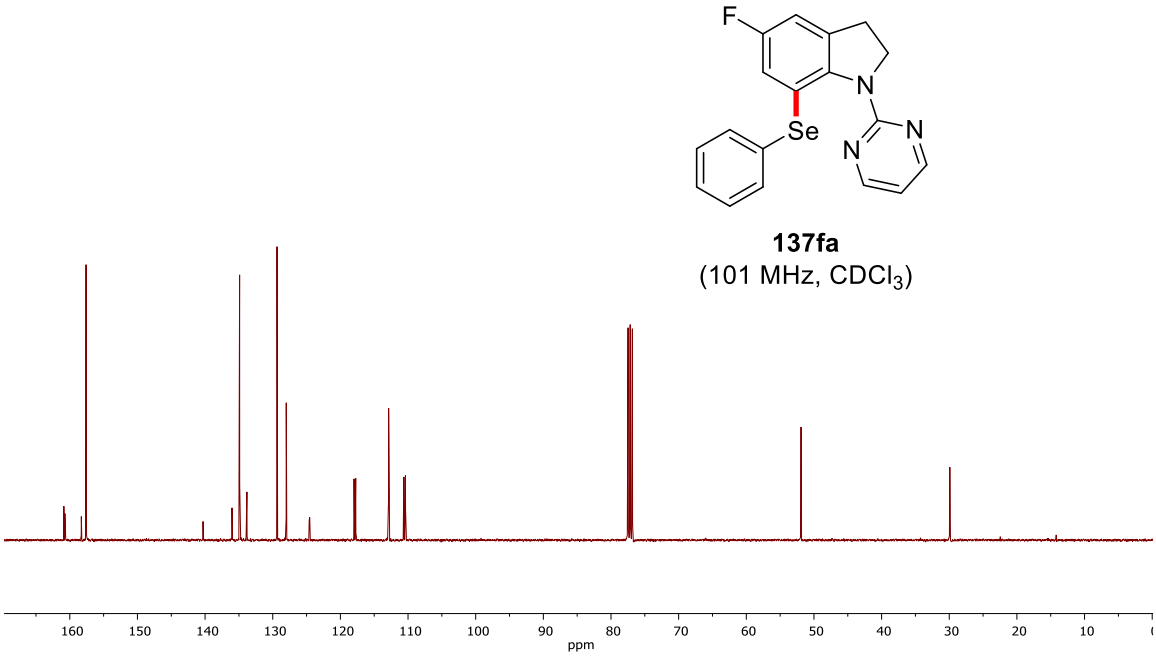

137fa
(101 MHz, $CDCl_3$)

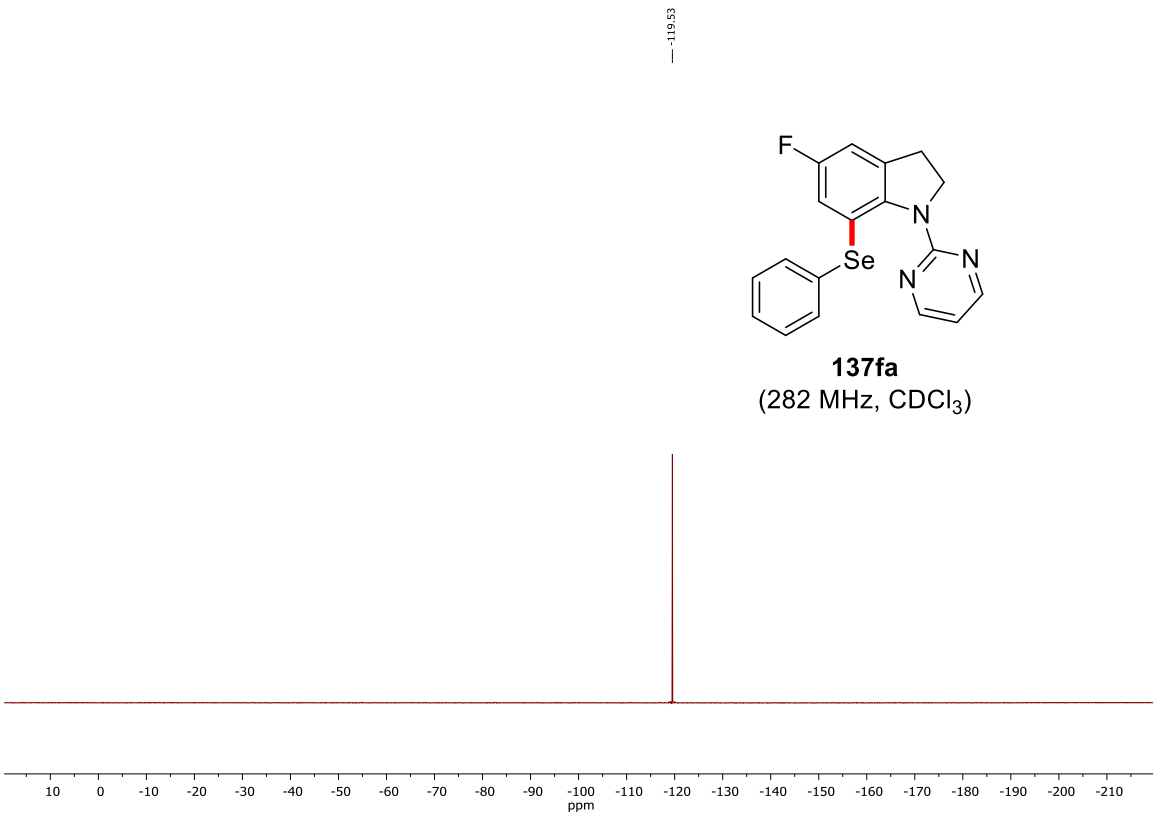

137fa
(282 MHz, $CDCl_3$)

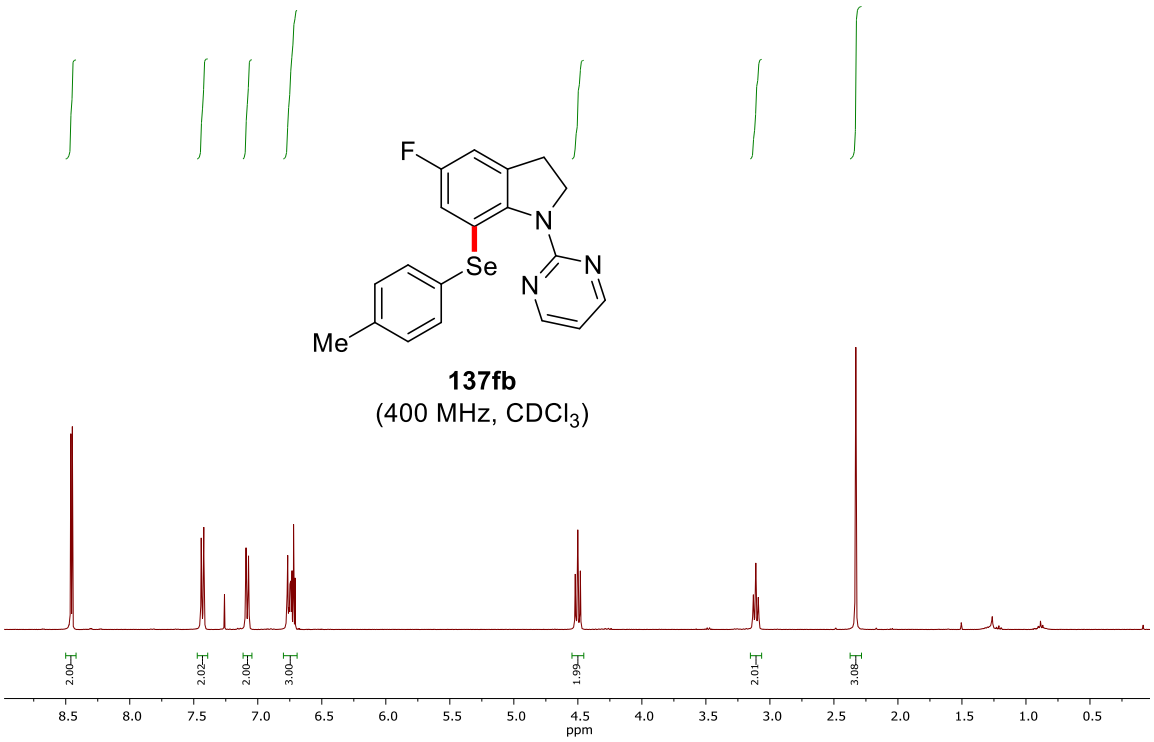

137fb
(400 MHz, $CDCl_3$)

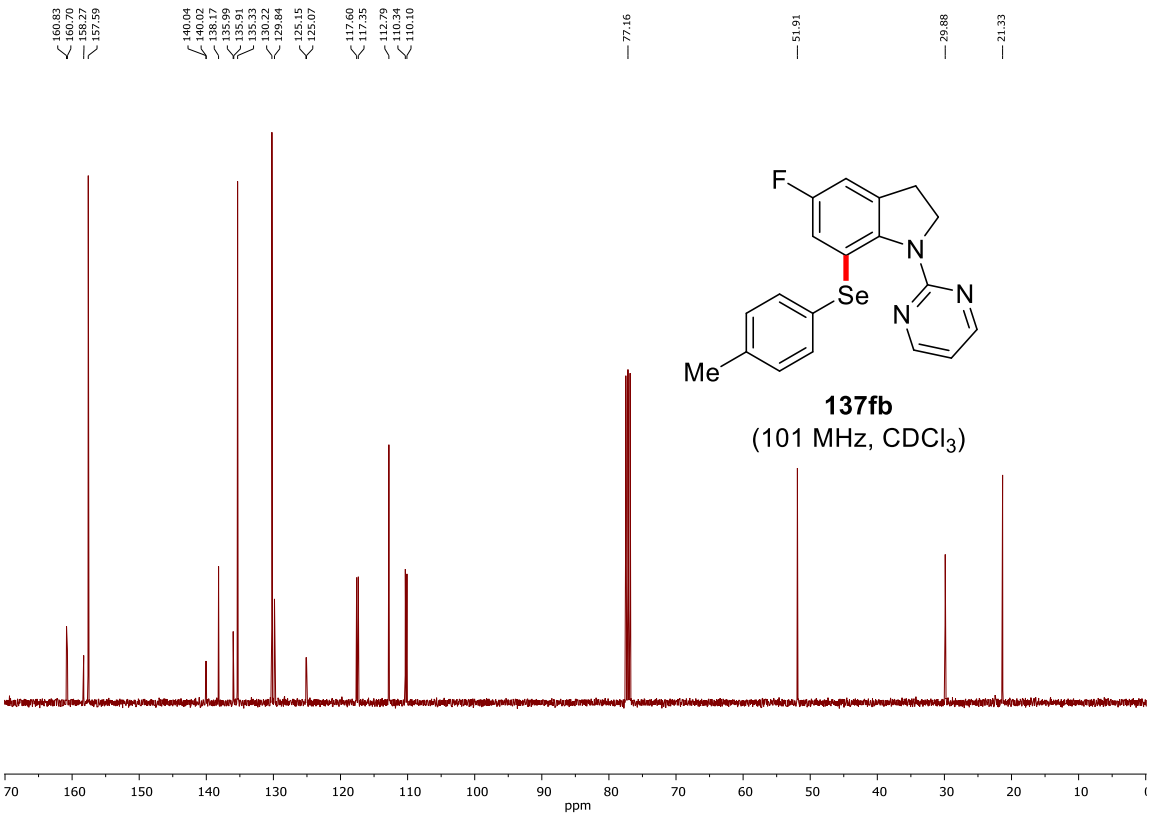

137fb
(101 MHz, $CDCl_3$)

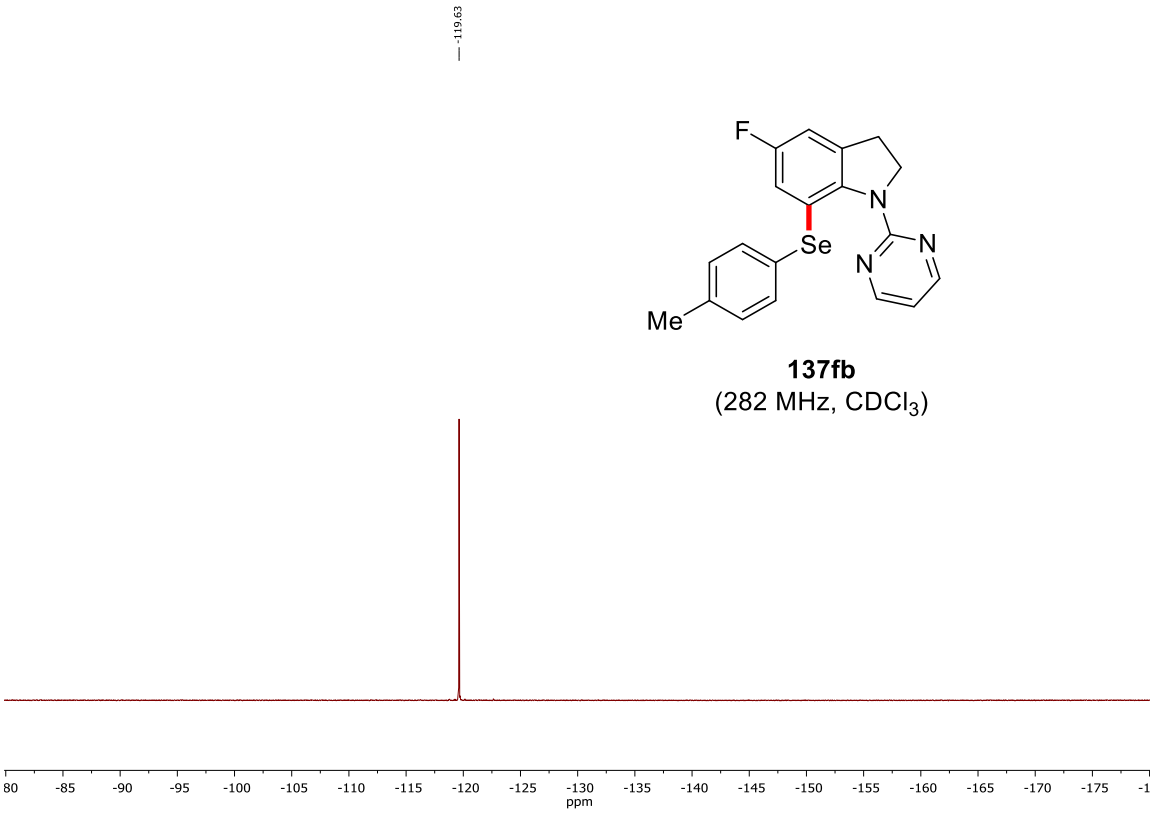

137fb
(282 MHz, $CDCl_3$)

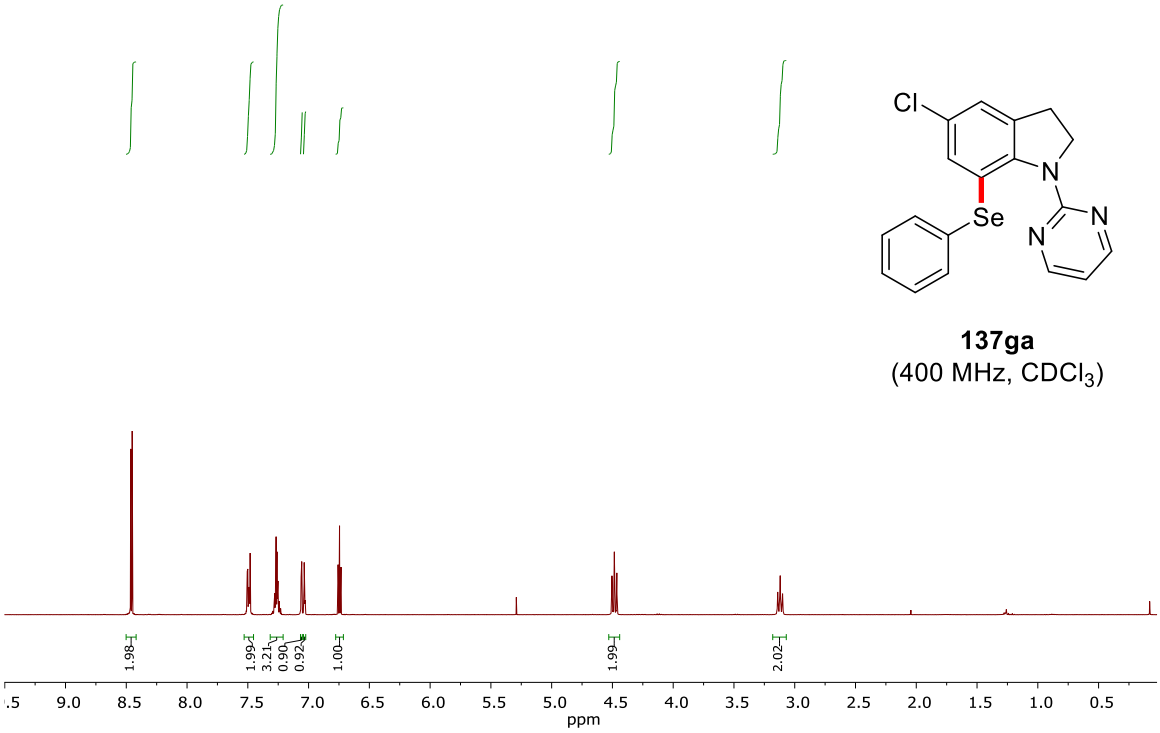

137ga
(400 MHz, $CDCl_3$)

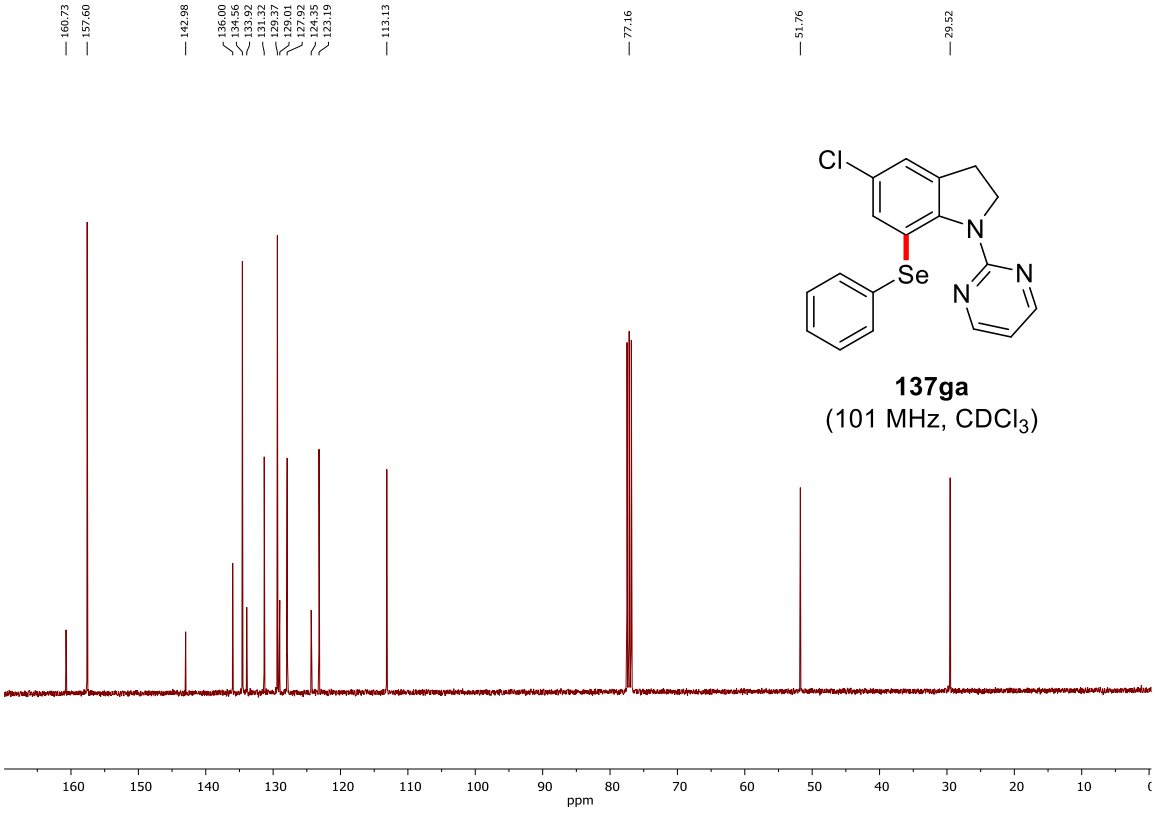

137ga
(101 MHz, $CDCl_3$)

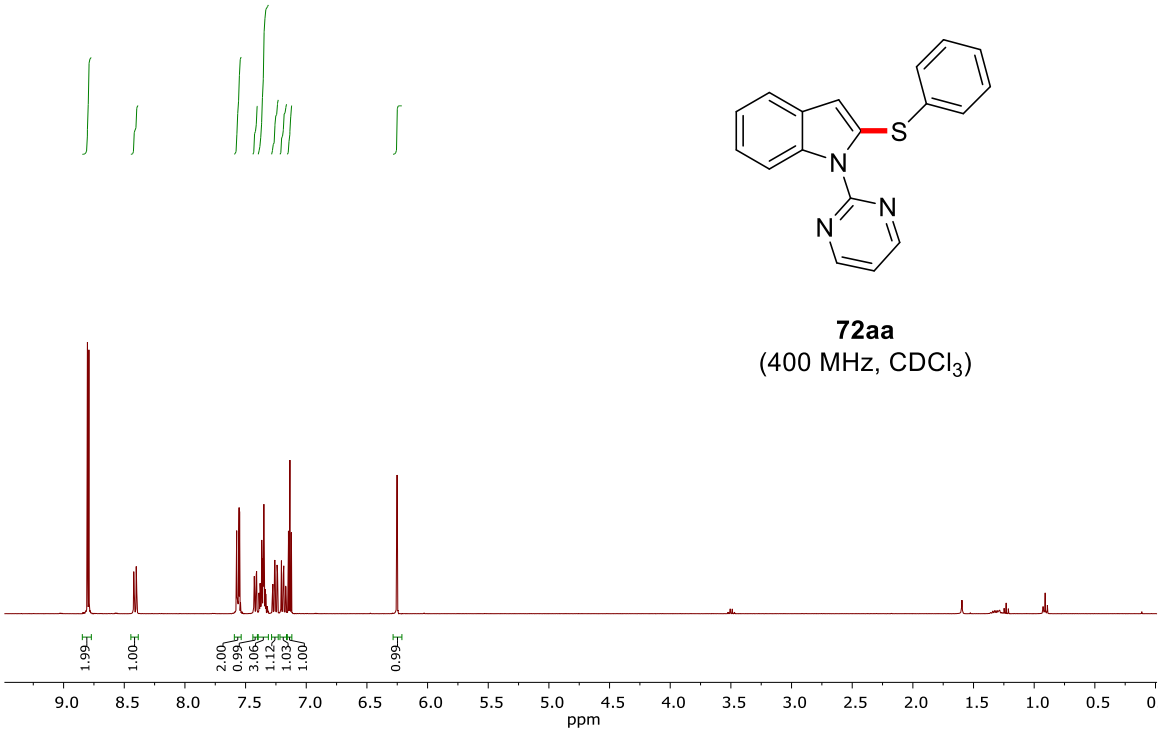

72aa
(400 MHz, $CDCl_3$)

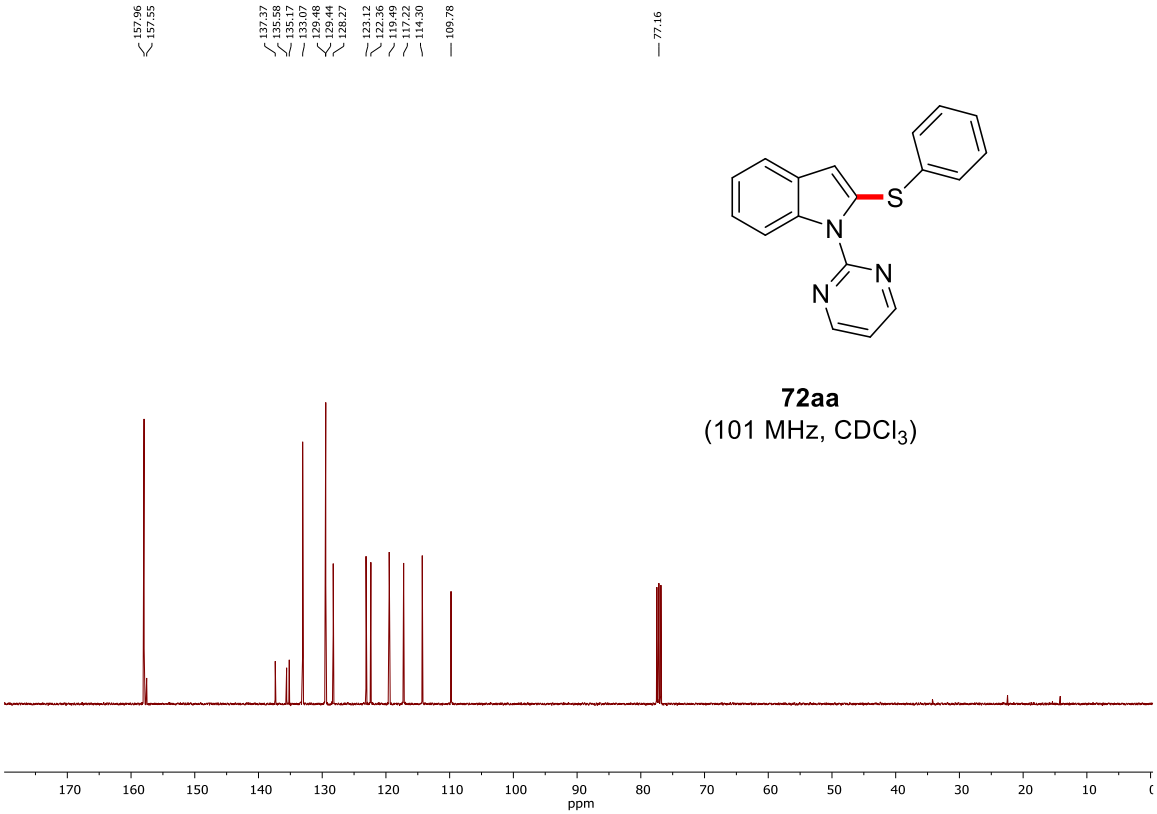

72aa
(101 MHz, $CDCl_3$)

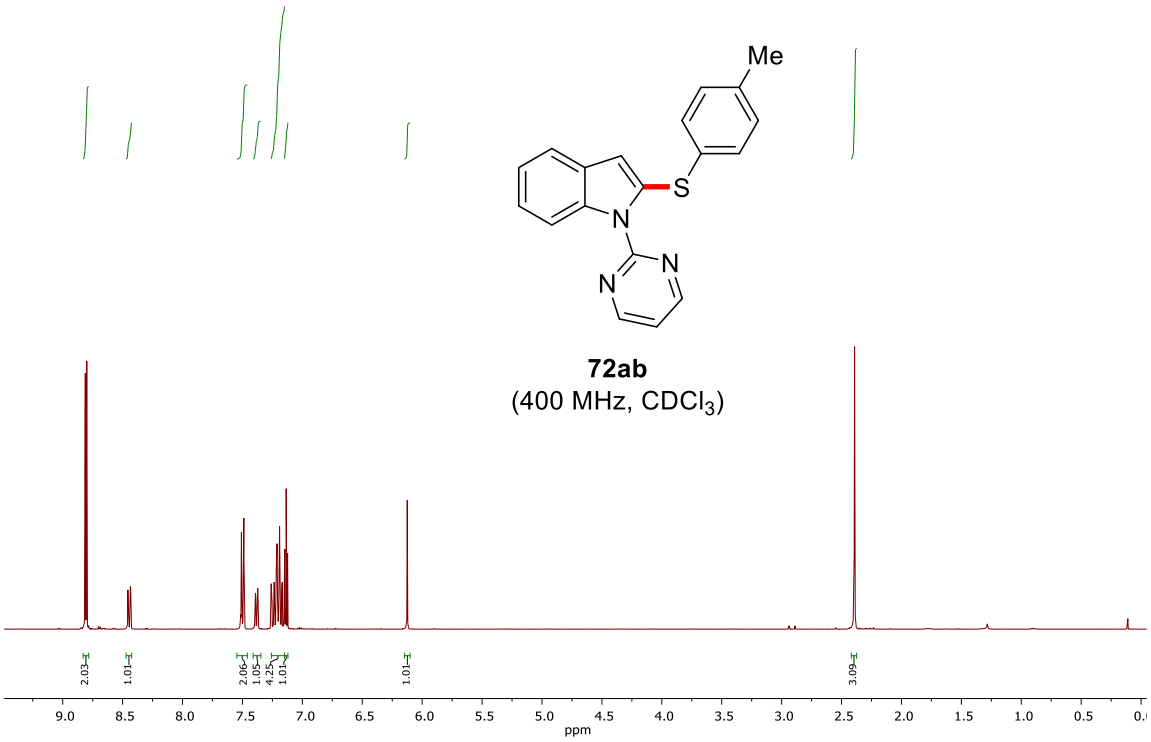

72ab
(400 MHz, $CDCl_3$)

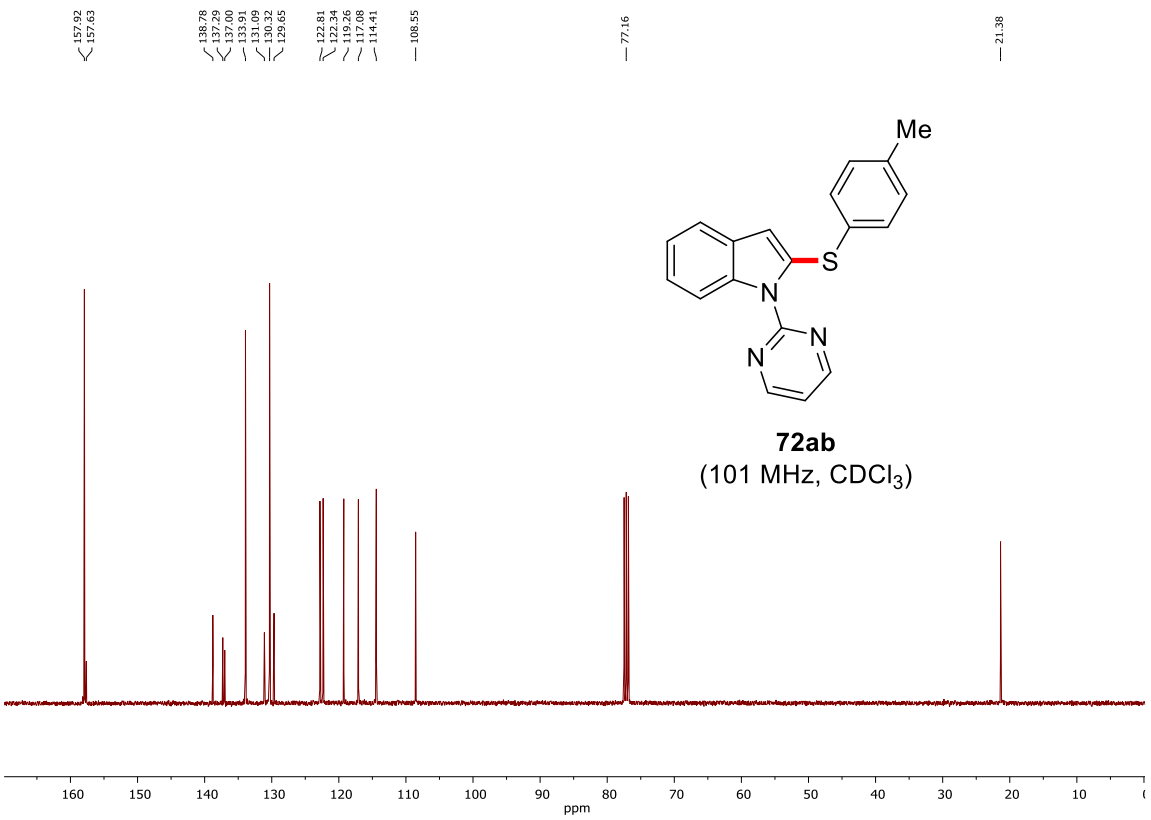

72ab
(101 MHz, $CDCl_3$)

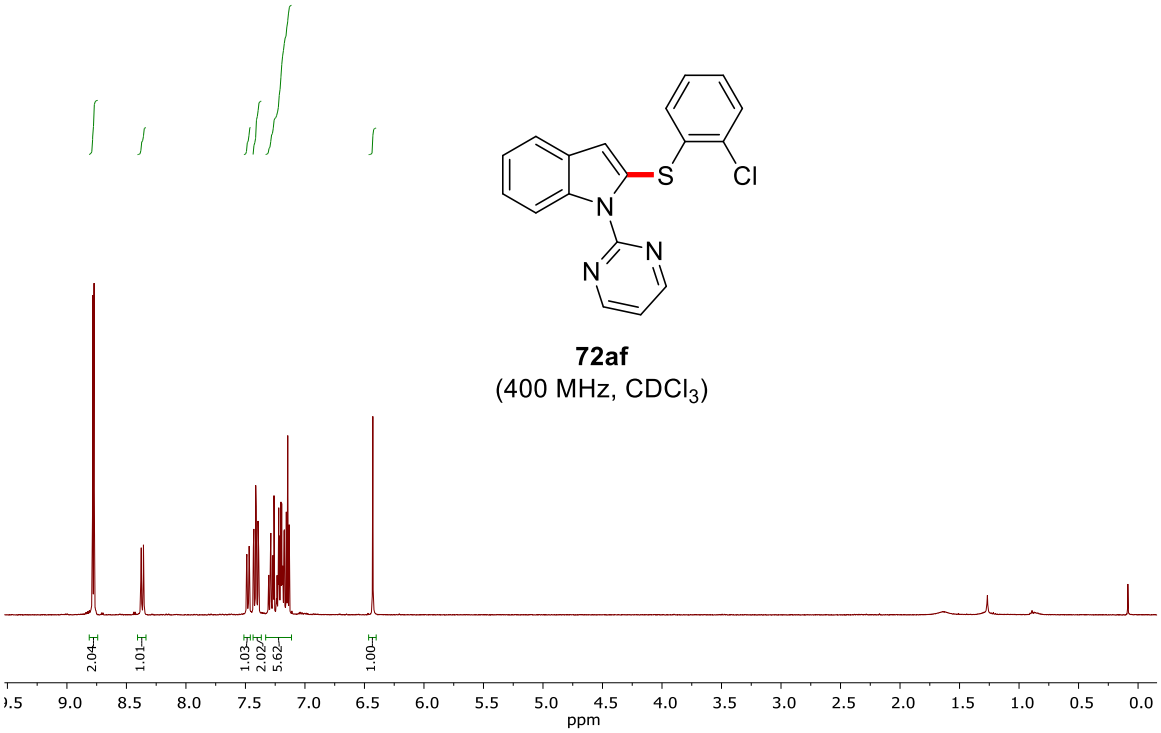

72af
(400 MHz, $CDCl_3$)

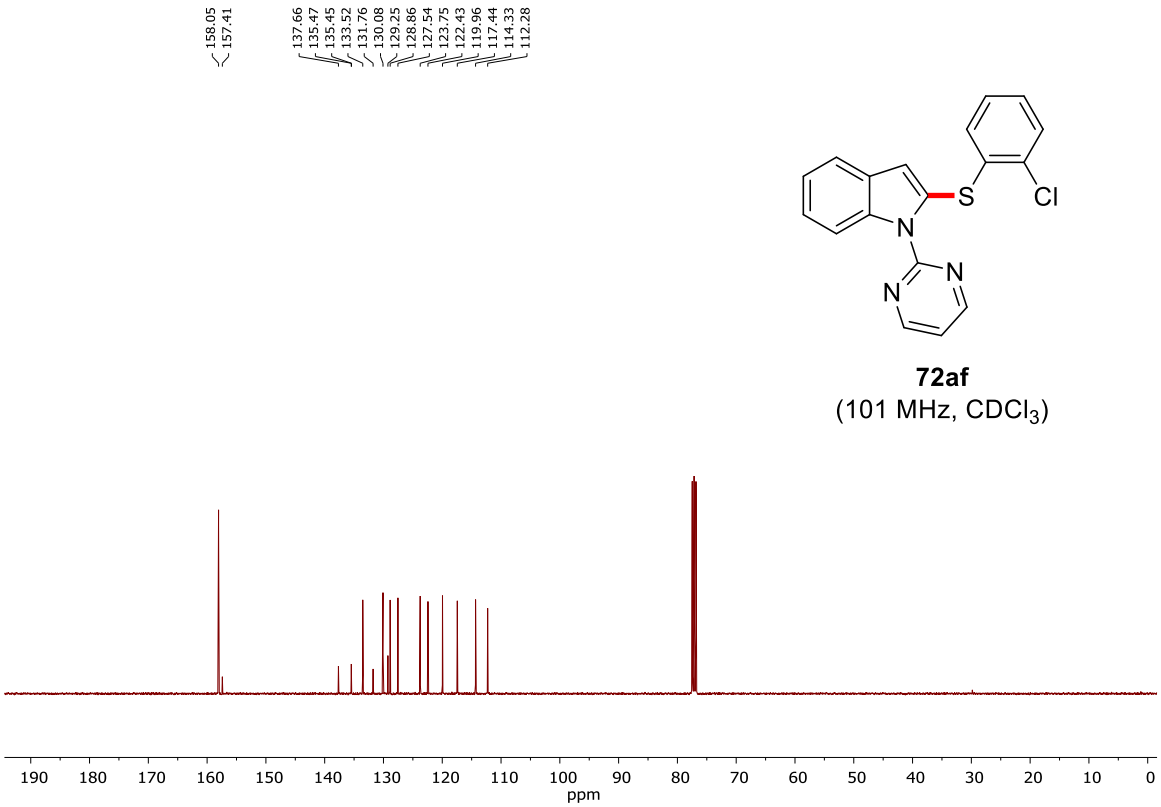

72af
(101 MHz, $CDCl_3$)

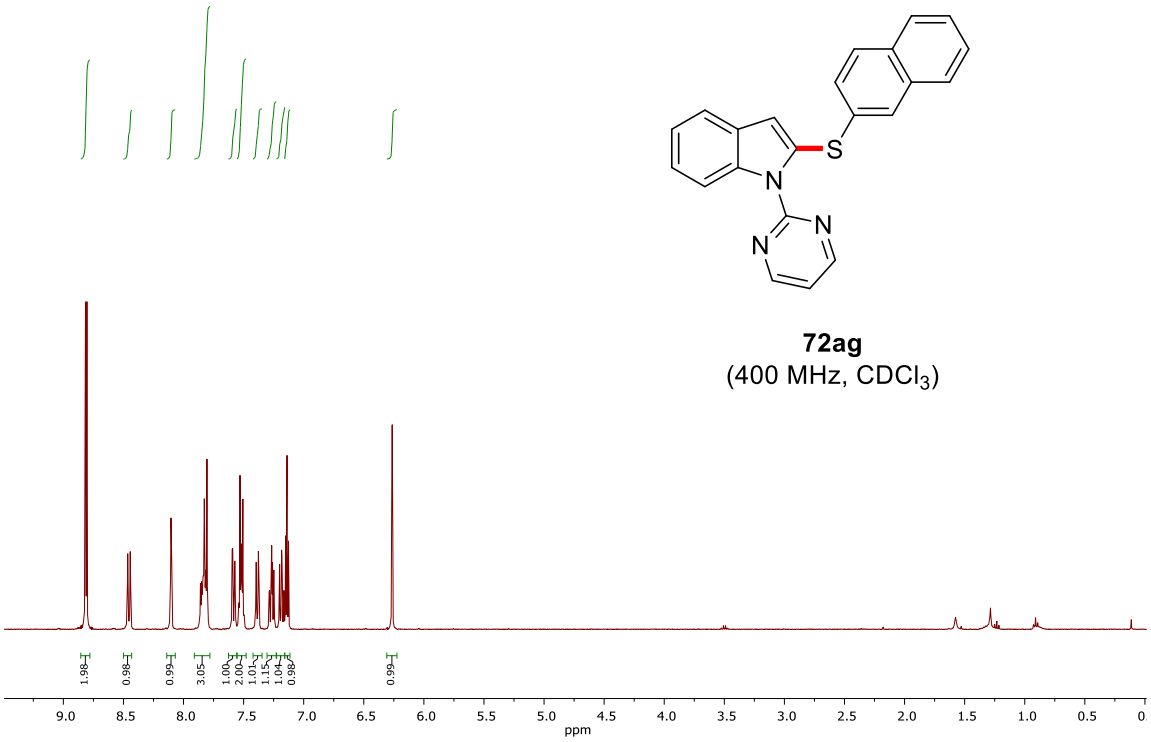

72ag
(400 MHz, $CDCl_3$)

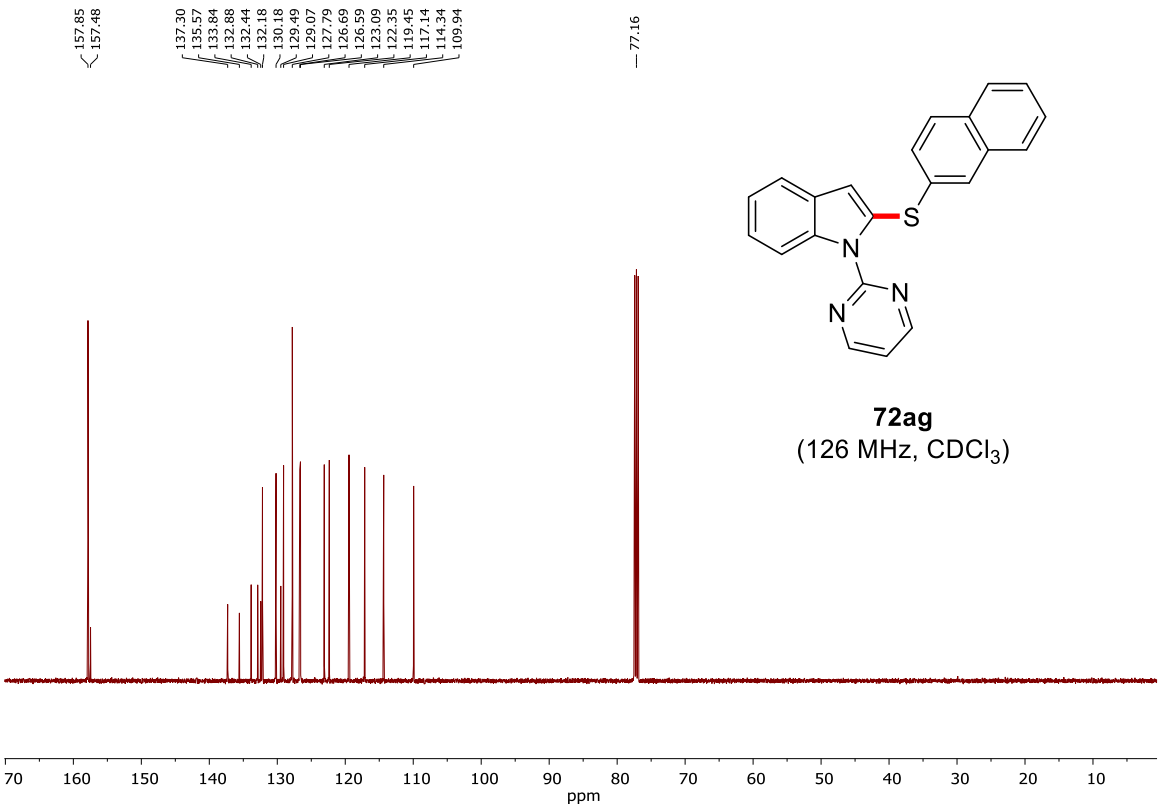

72ag
(126 MHz, $CDCl_3$)

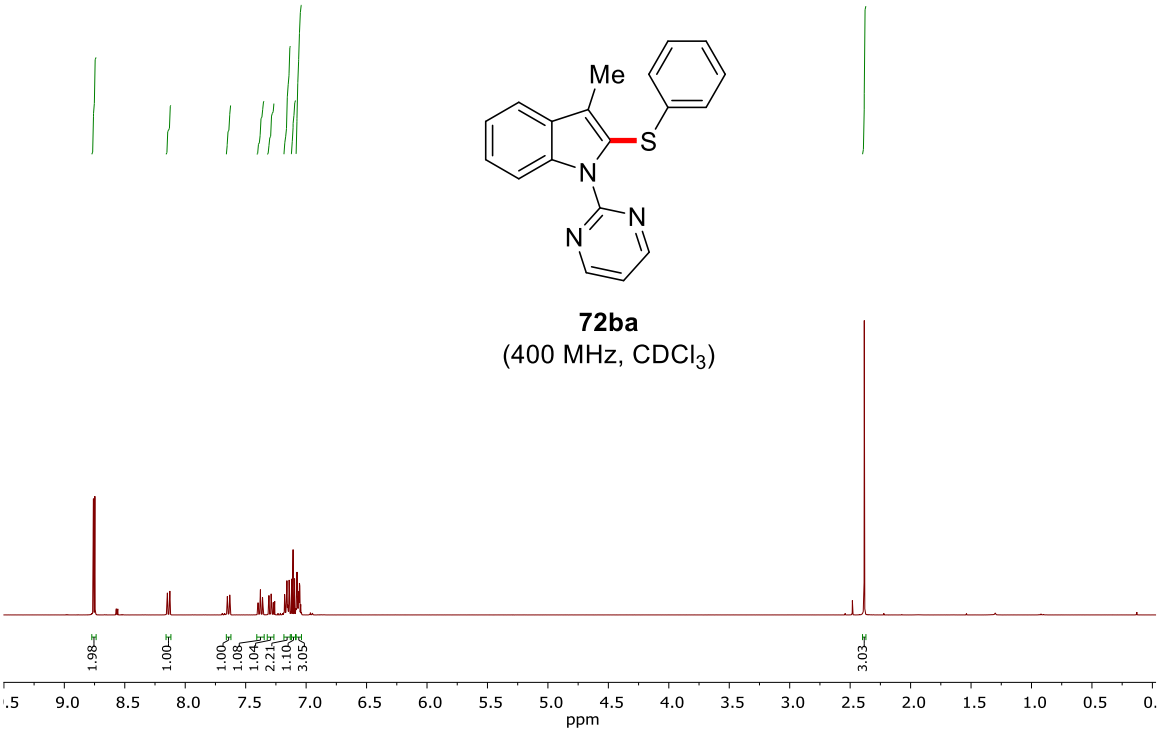

72ba
(400 MHz, $CDCl_3$)

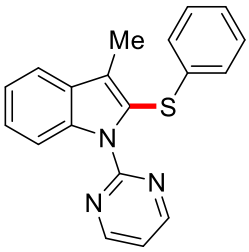

72ba
(126 MHz, $CDCl_3$)

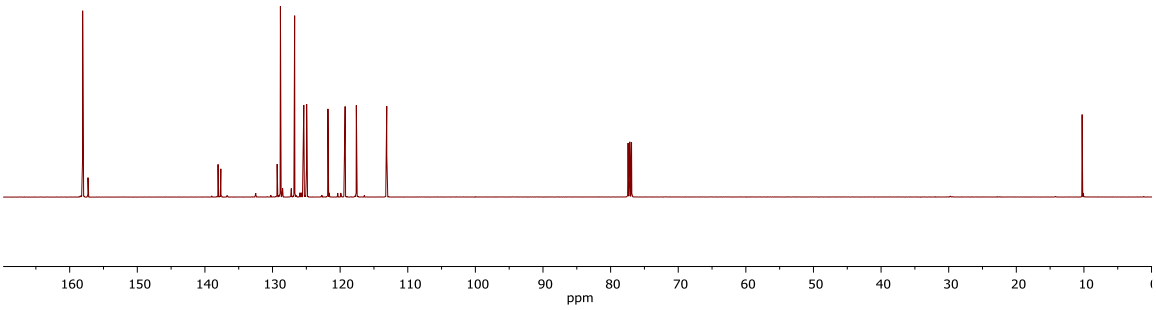

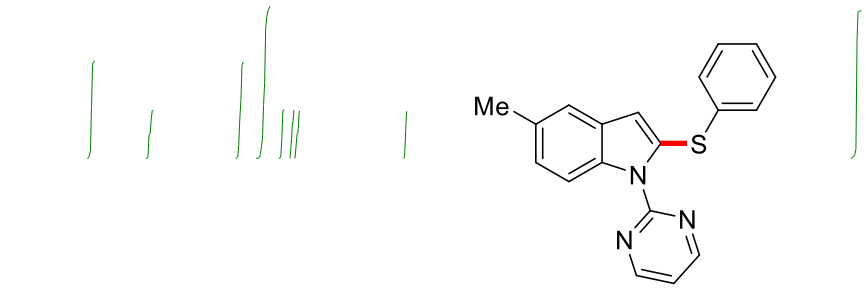

72ca
(400 MHz, $CDCl_3$)

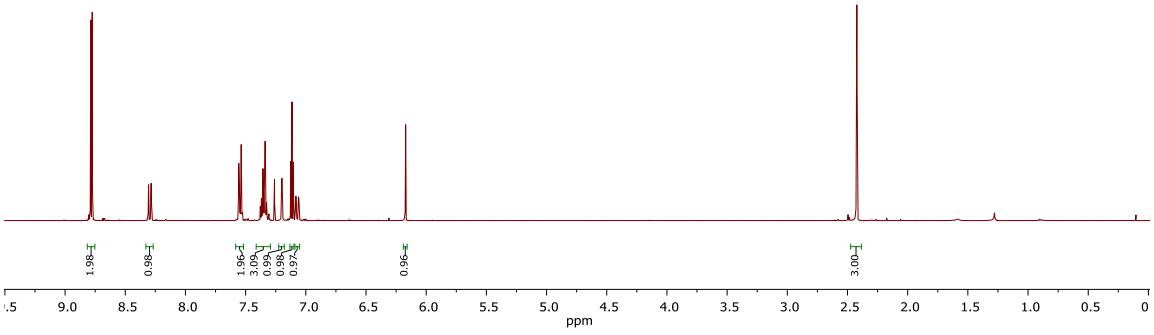

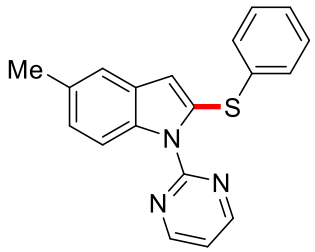

72ca
(126 MHz, $CDCl_3$)

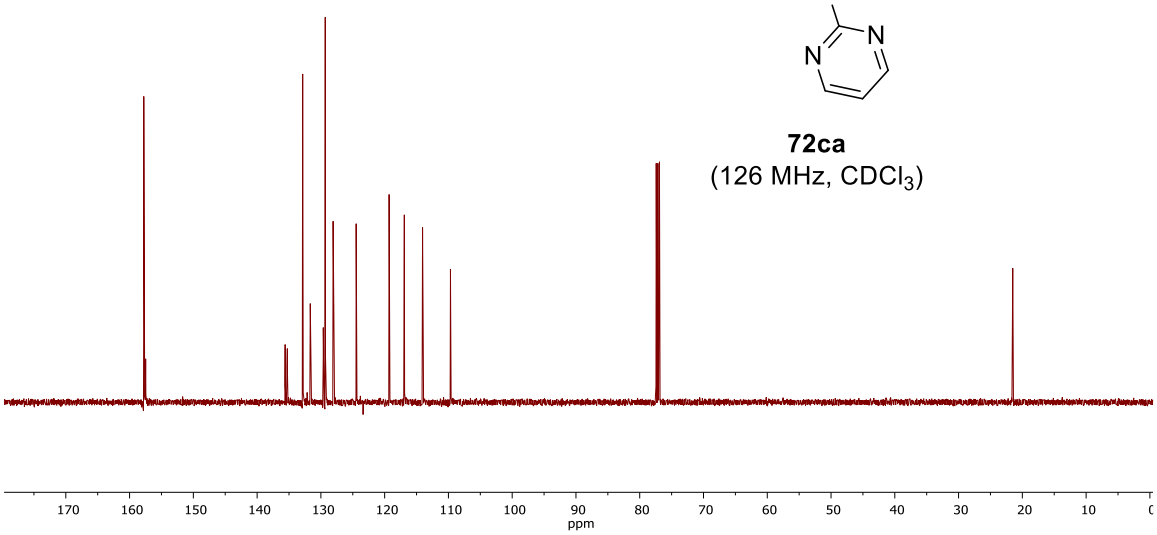

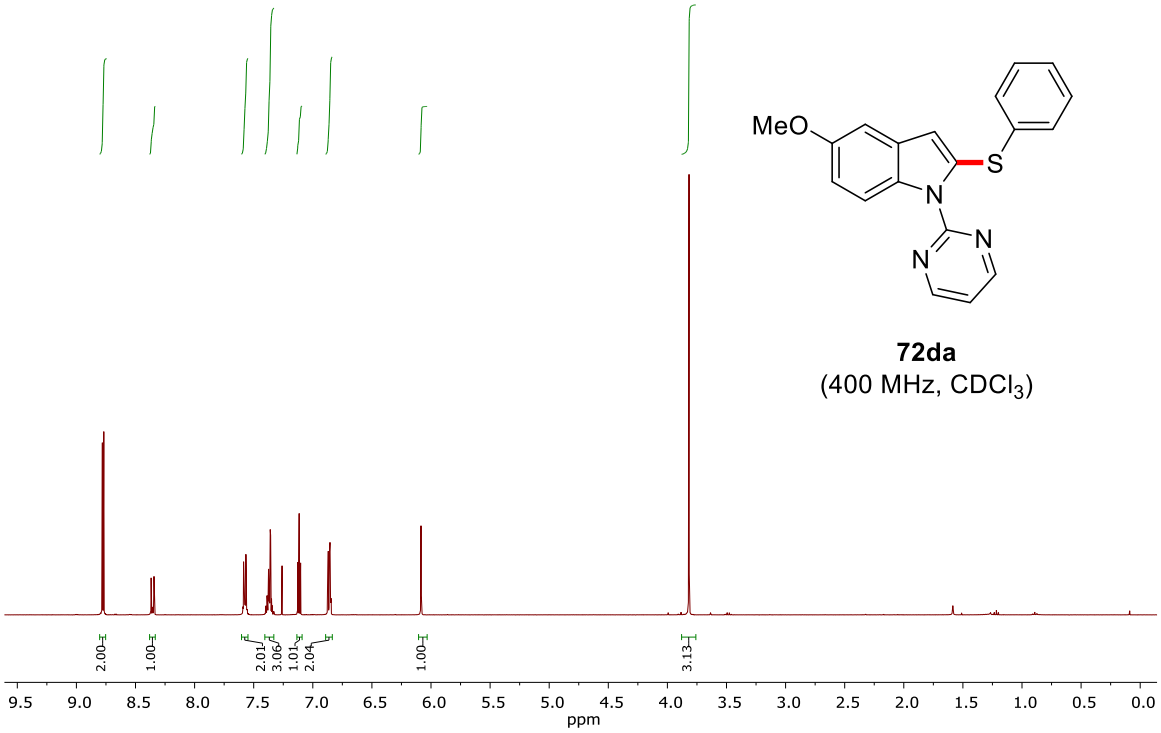

72da
(400 MHz, $CDCl_3$)

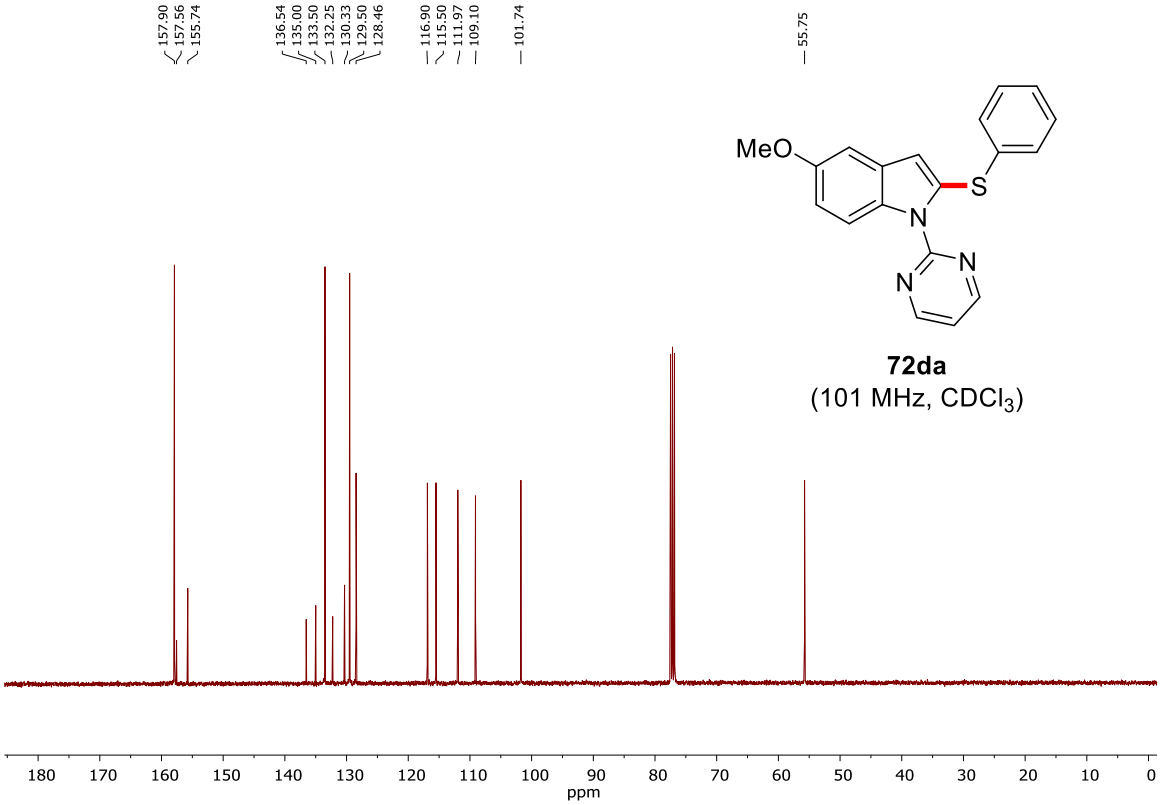

72da
(101 MHz, $CDCl_3$)

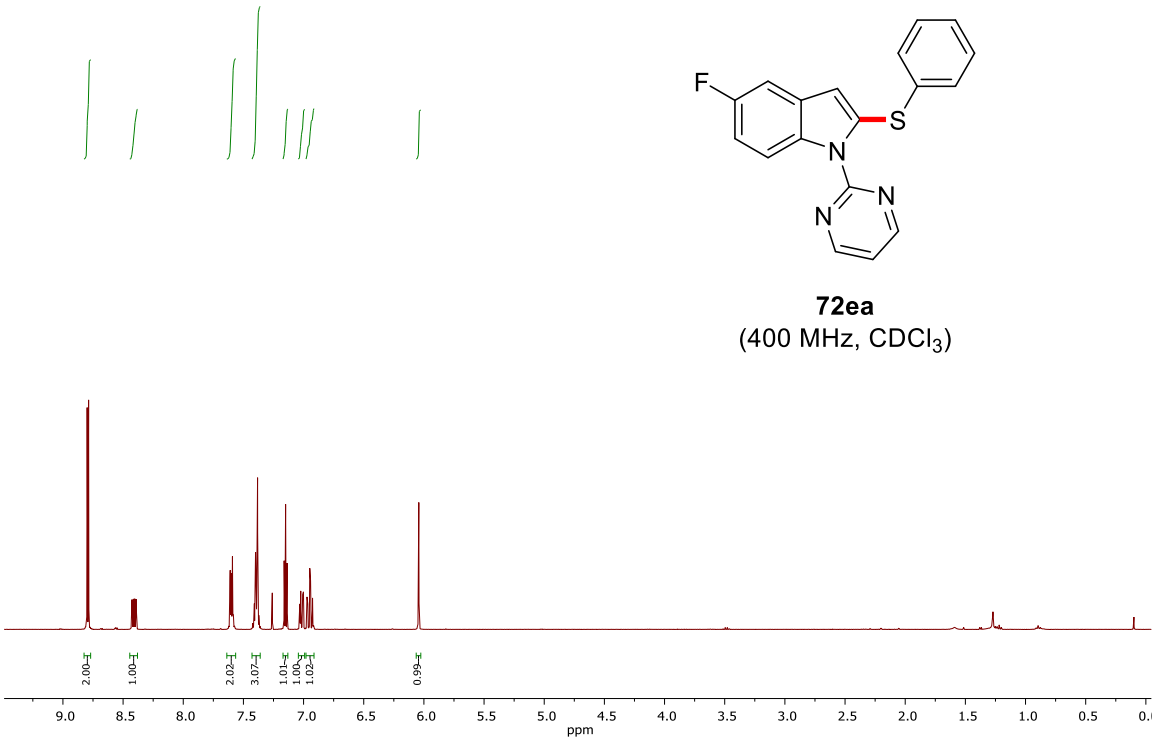

72ea
(400 MHz, $CDCl_3$)

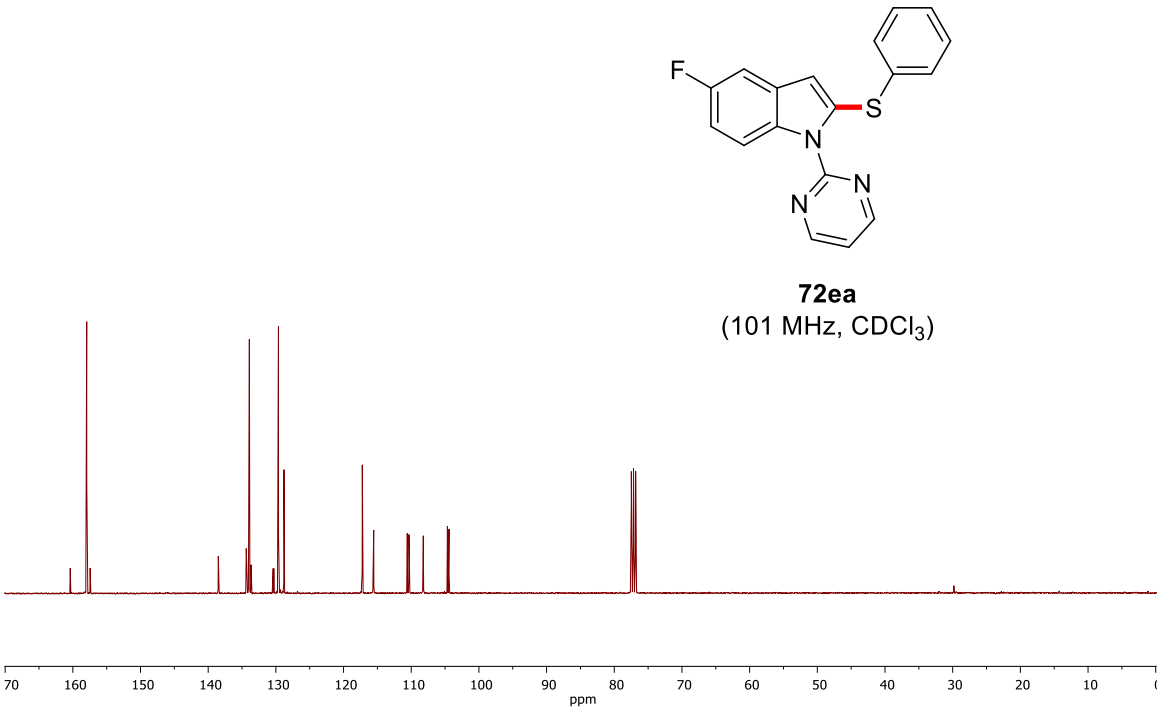

72ea
(101 MHz, $CDCl_3$)

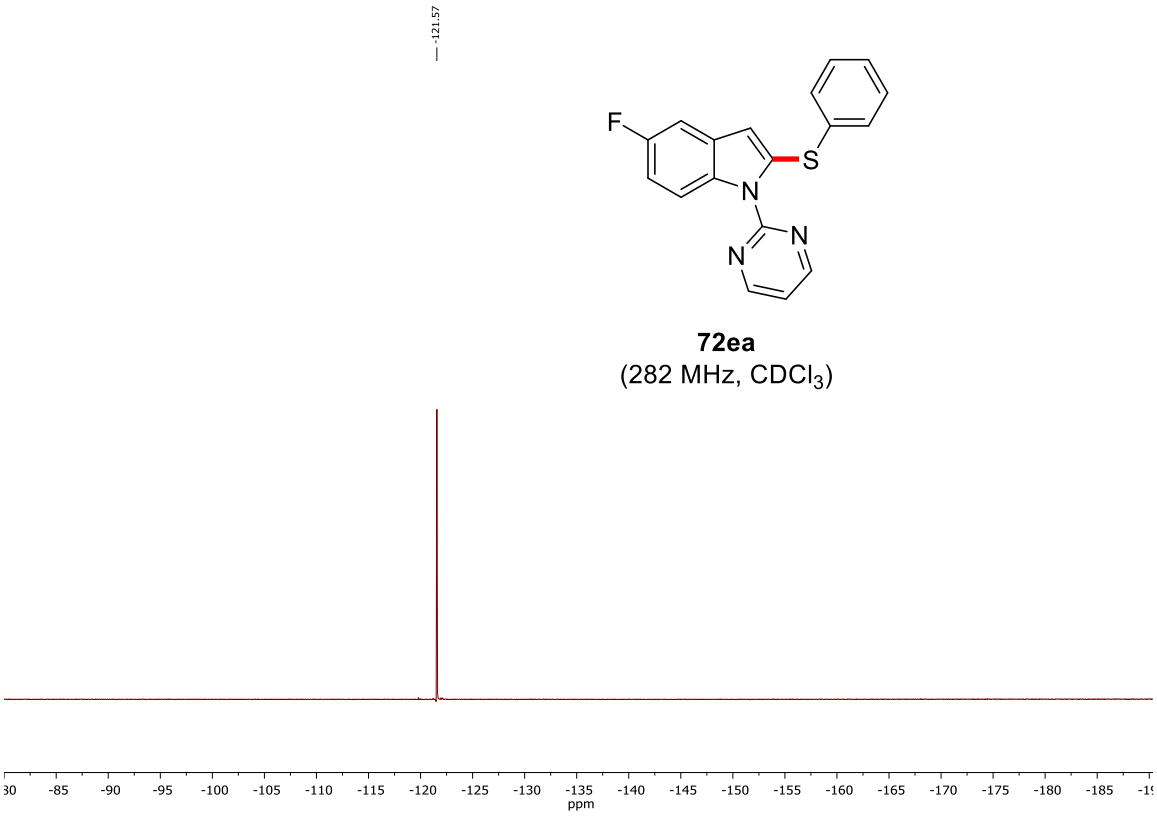

72ea
(282 MHz, $CDCl_3$)

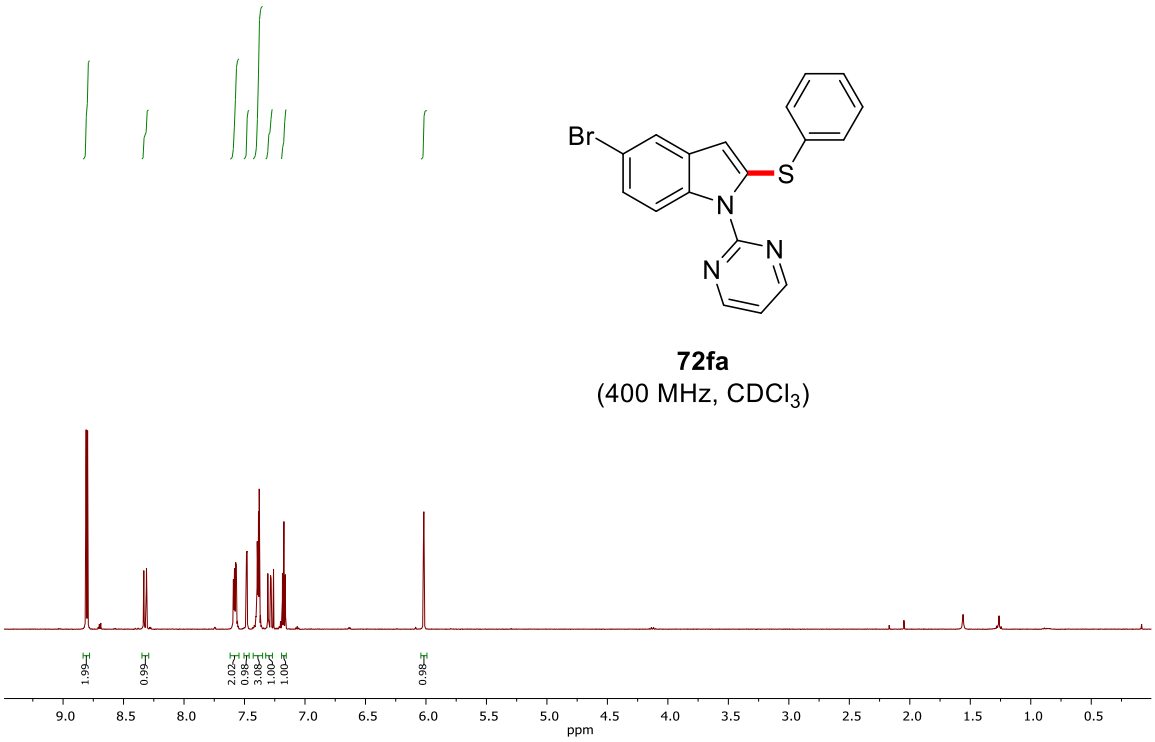

72fa
(400 MHz, $CDCl_3$)

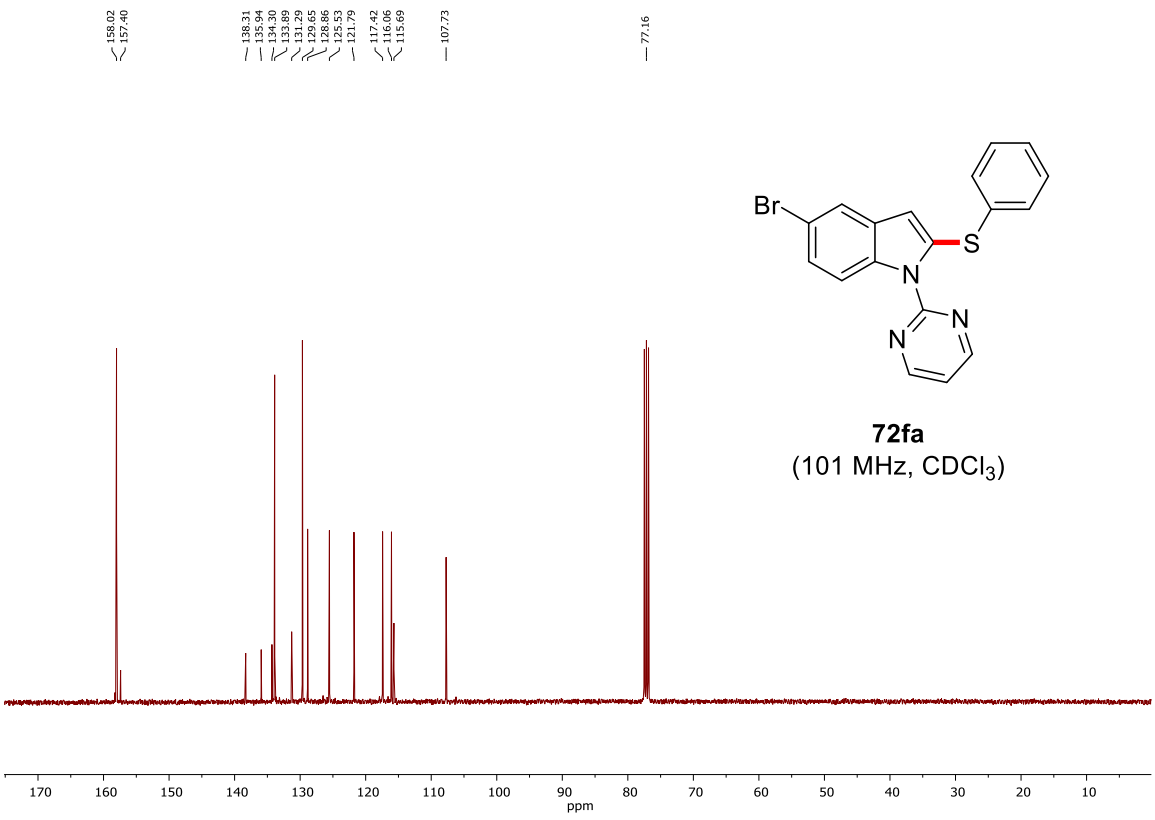

72fa
(101 MHz, $CDCl_3$)

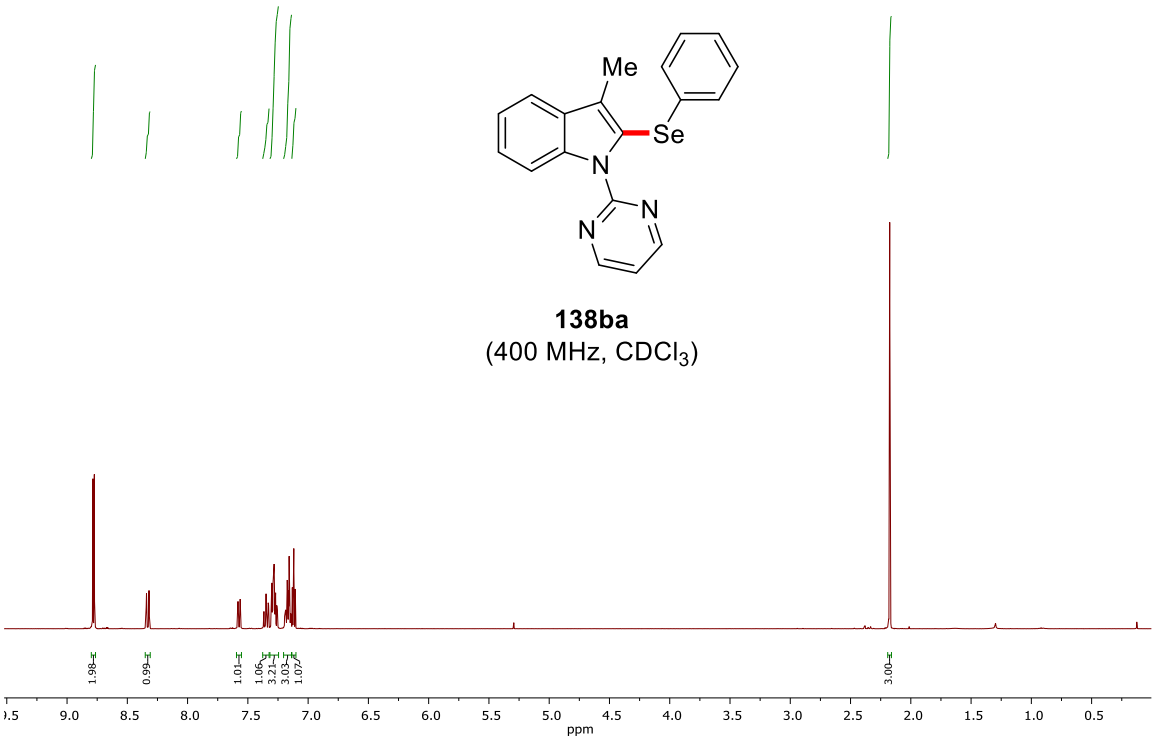

138ba
(400 MHz, $CDCl_3$)

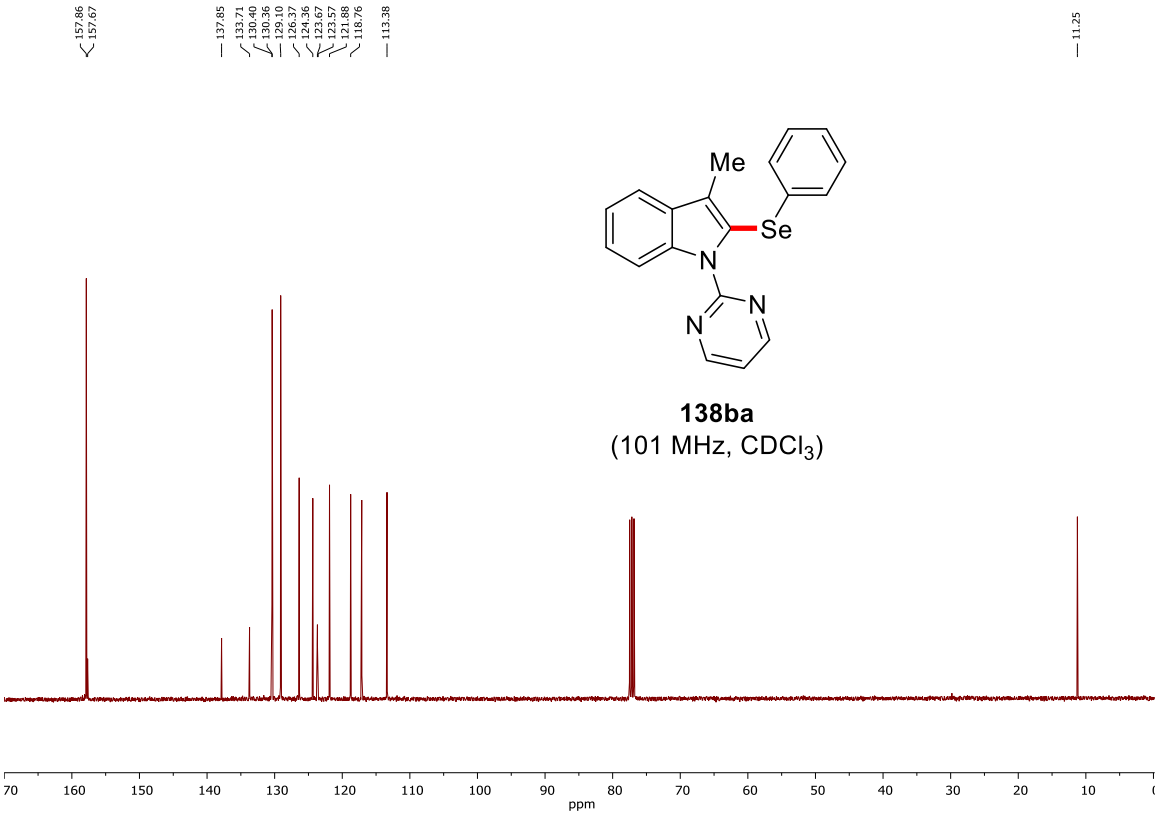

138ba
(101 MHz, $CDCl_3$)

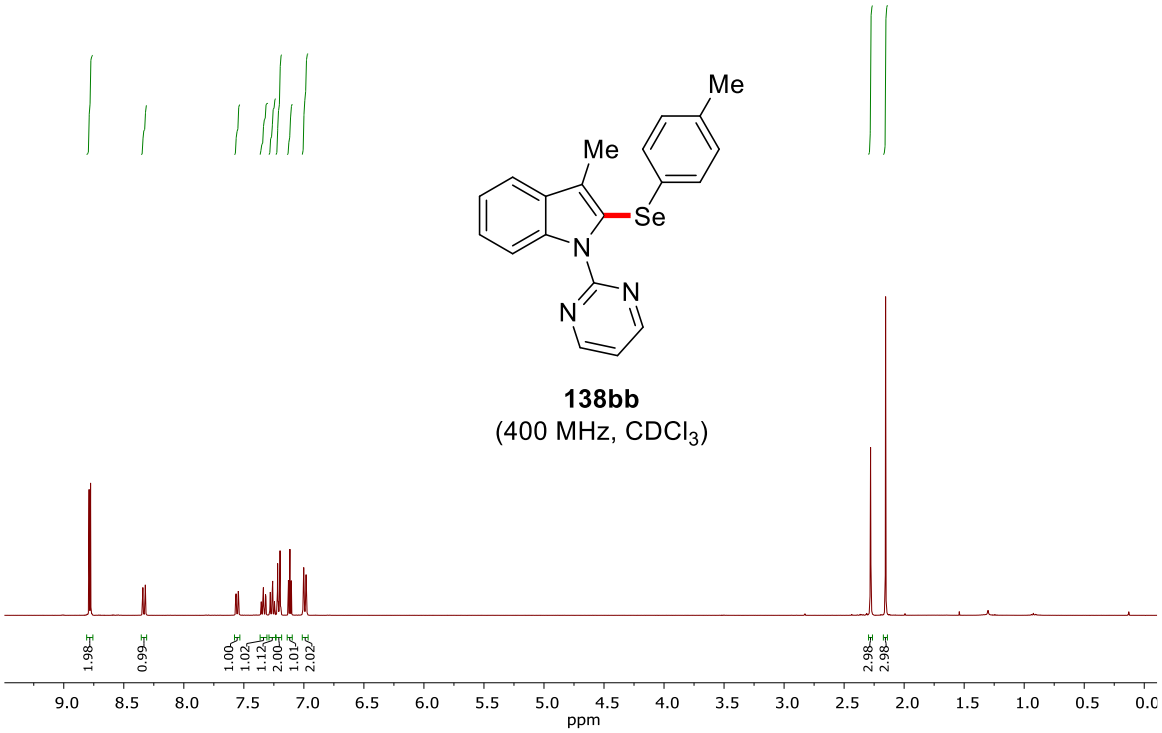

138bb
(400 MHz, $CDCl_3$)

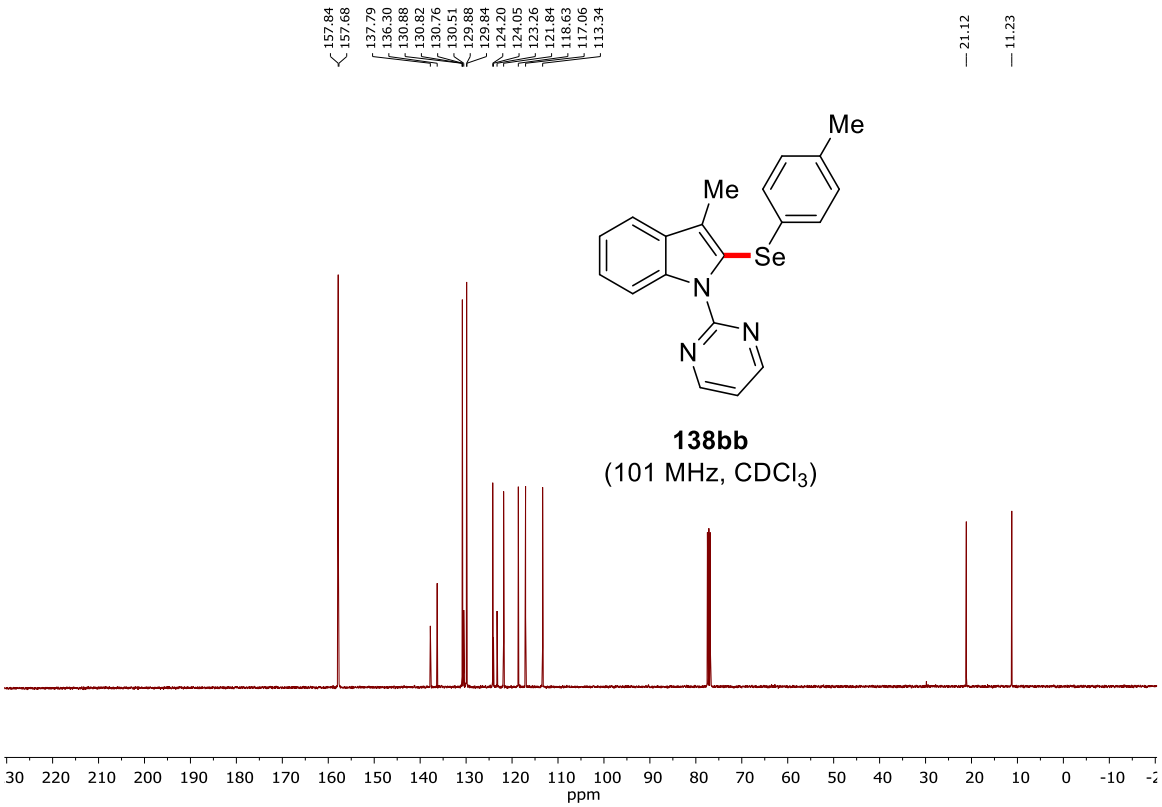

138bb
(101 MHz, $CDCl_3$)

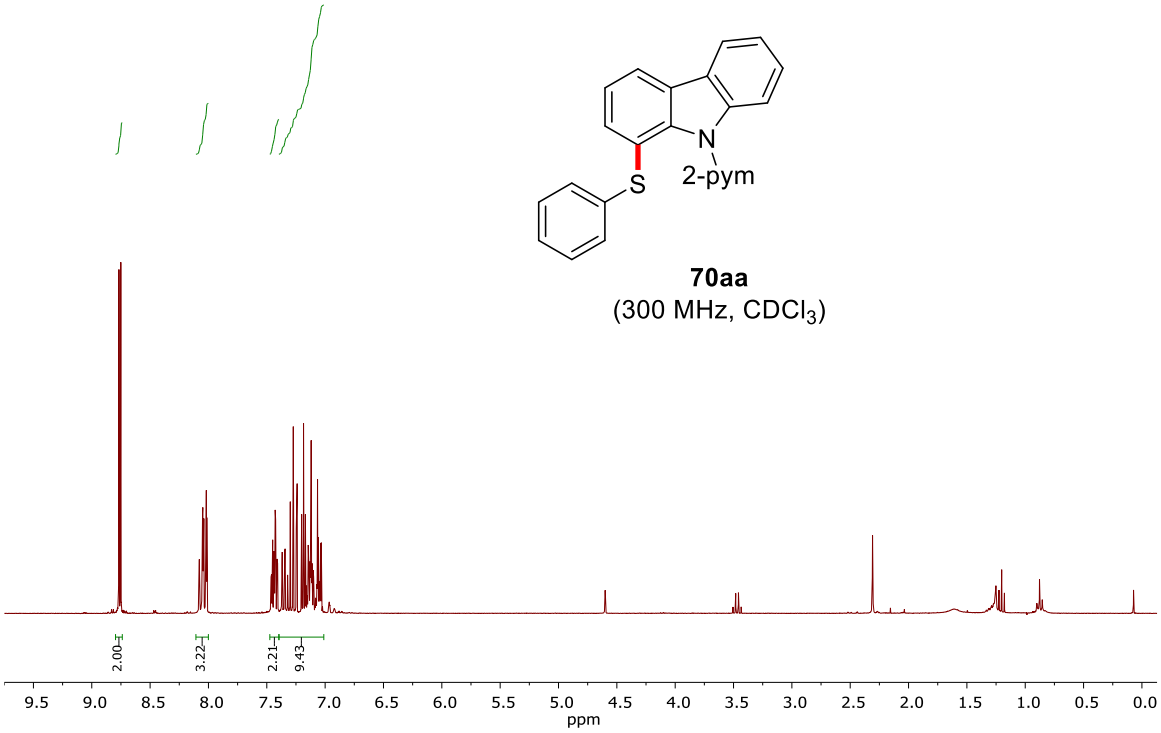

70aa
(300 MHz, $CDCl_3$)

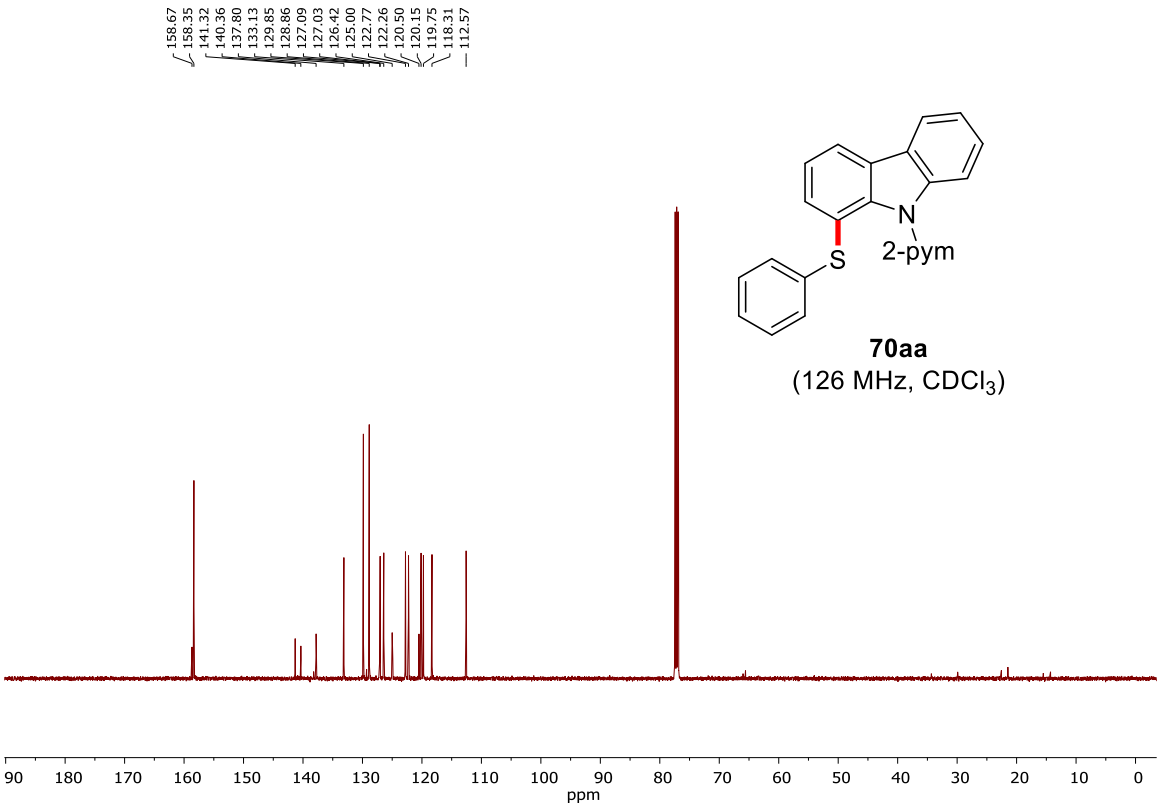

70aa
(126 MHz, $CDCl_3$)

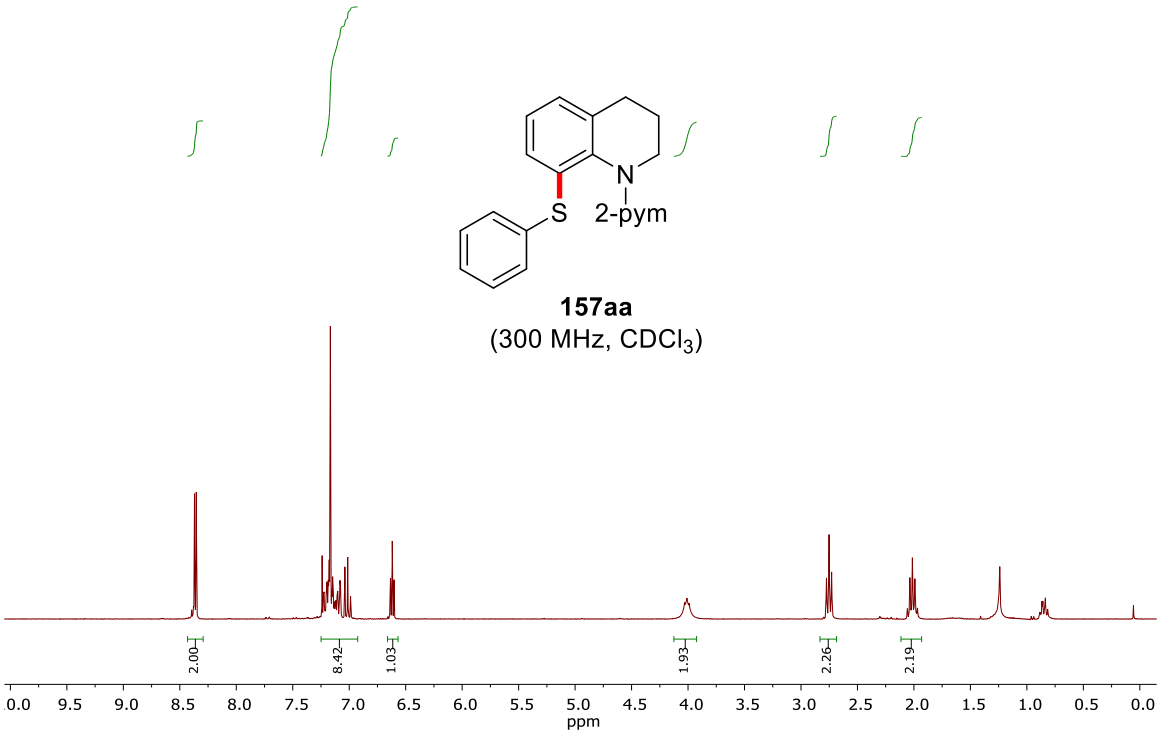

157aa
(300 MHz, $CDCl_3$)

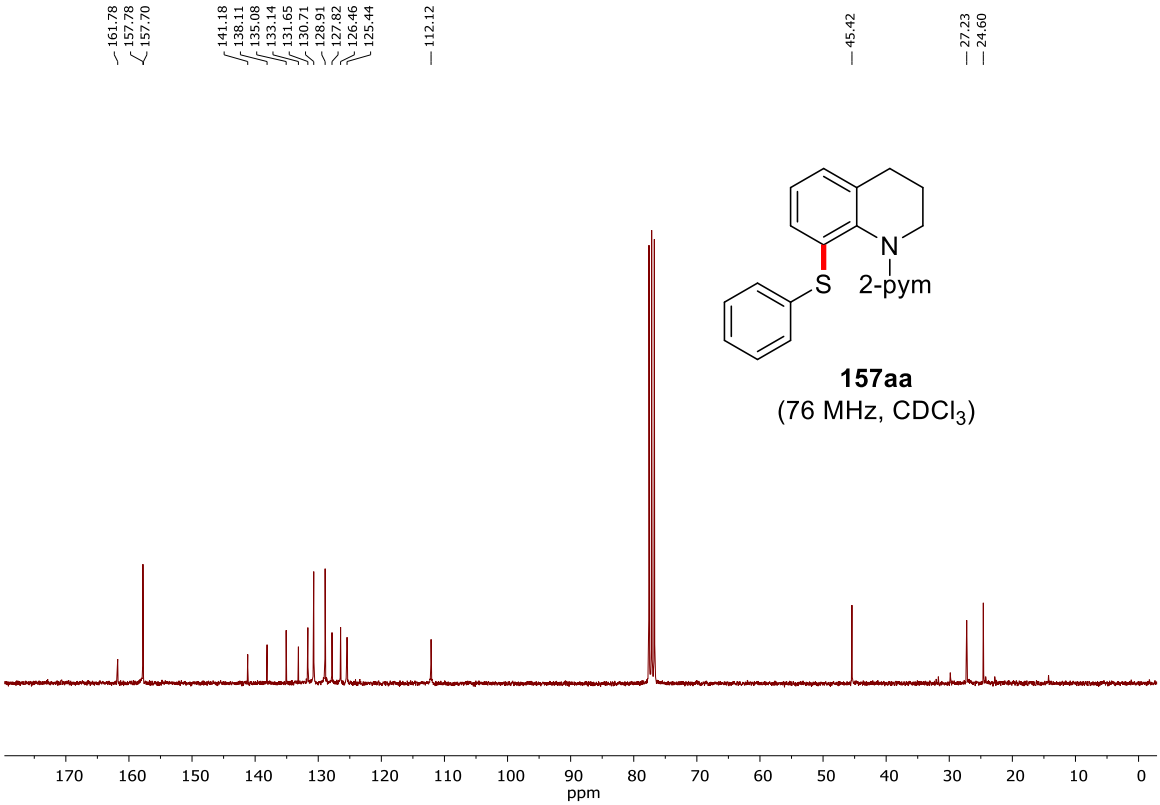

157aa
(76 MHz, $CDCl_3$)

The following benzothiazoles **140d** to **140h** were prepared and characterized by N. Imse.

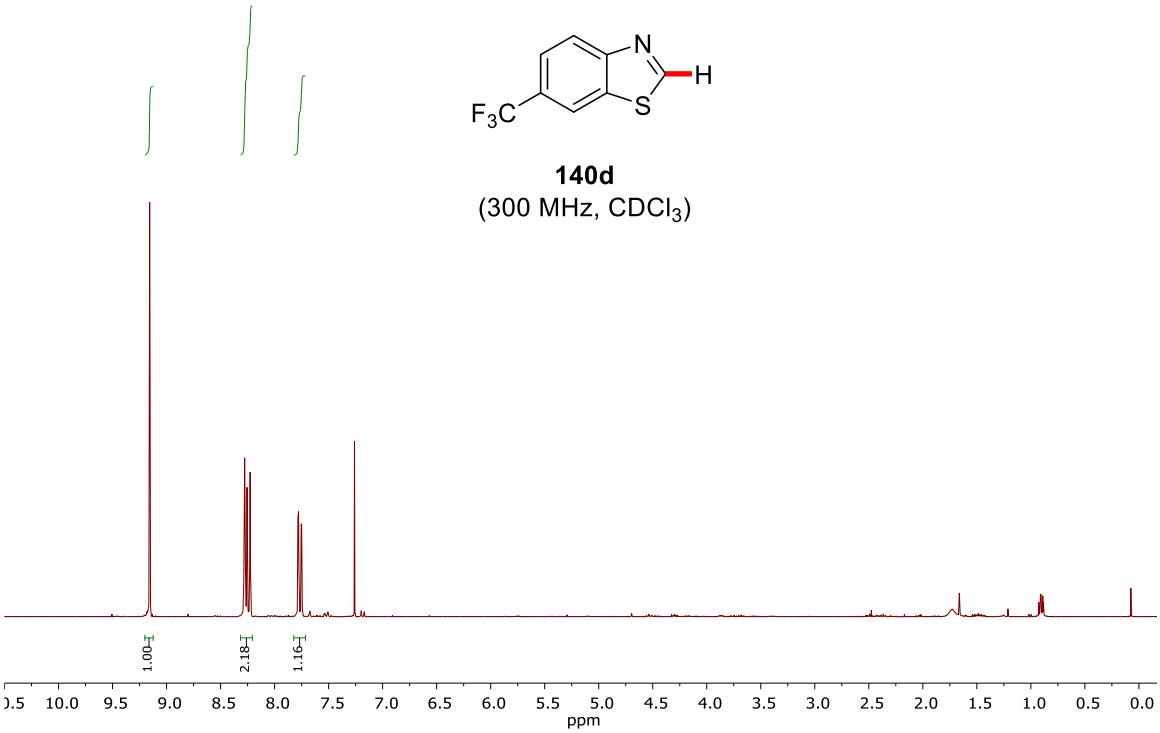

140d
(300 MHz, $CDCl_3$)

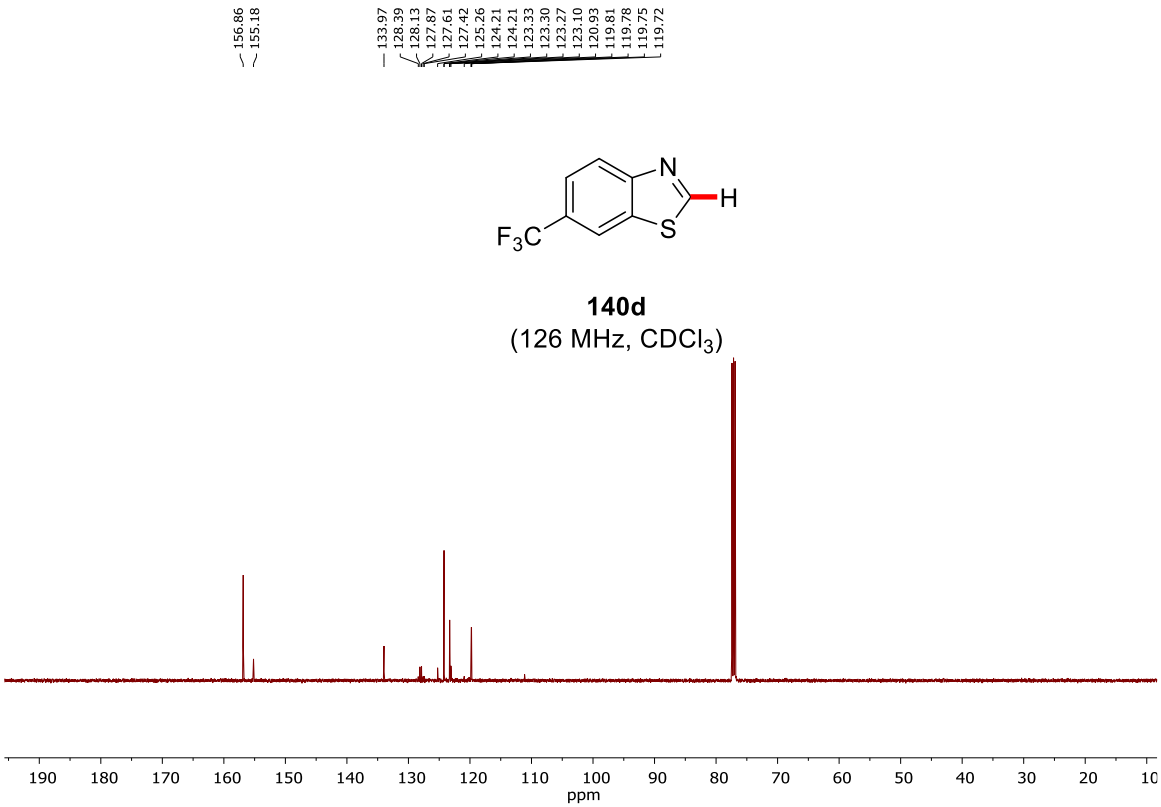

140d
(126 MHz, $CDCl_3$)

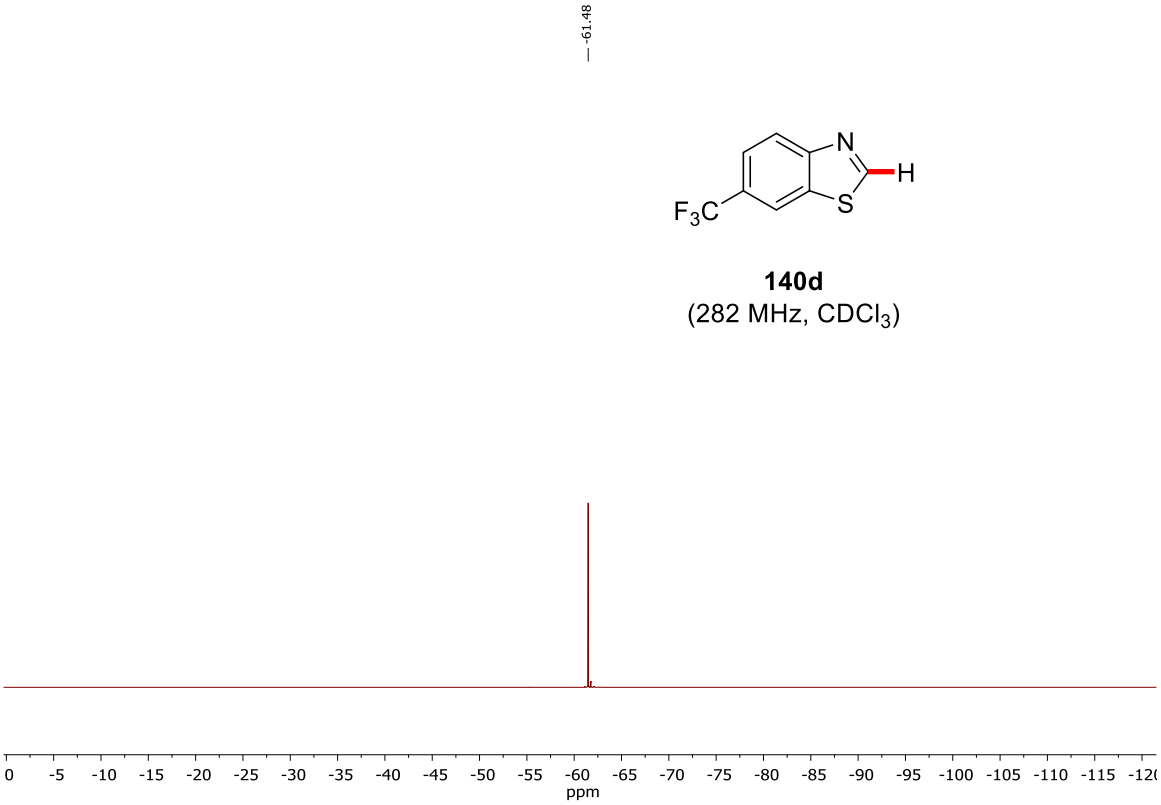

140d
(282 MHz, $CDCl_3$)

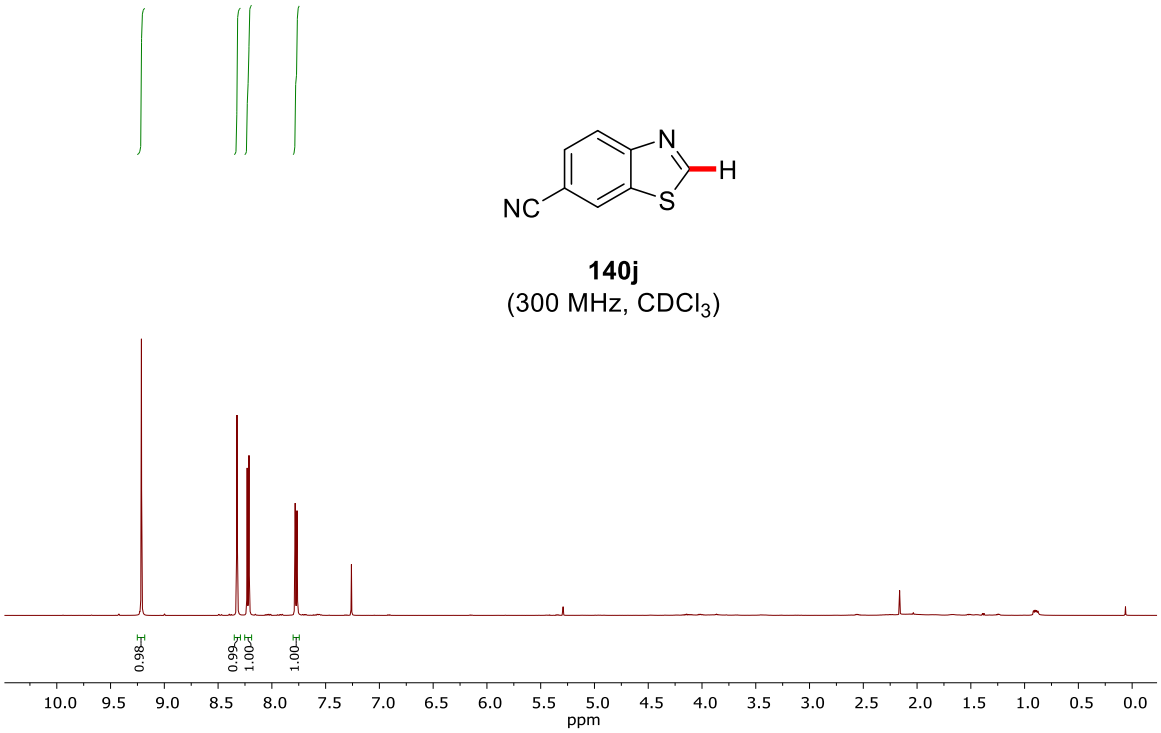

140j
(300 MHz, $CDCl_3$)

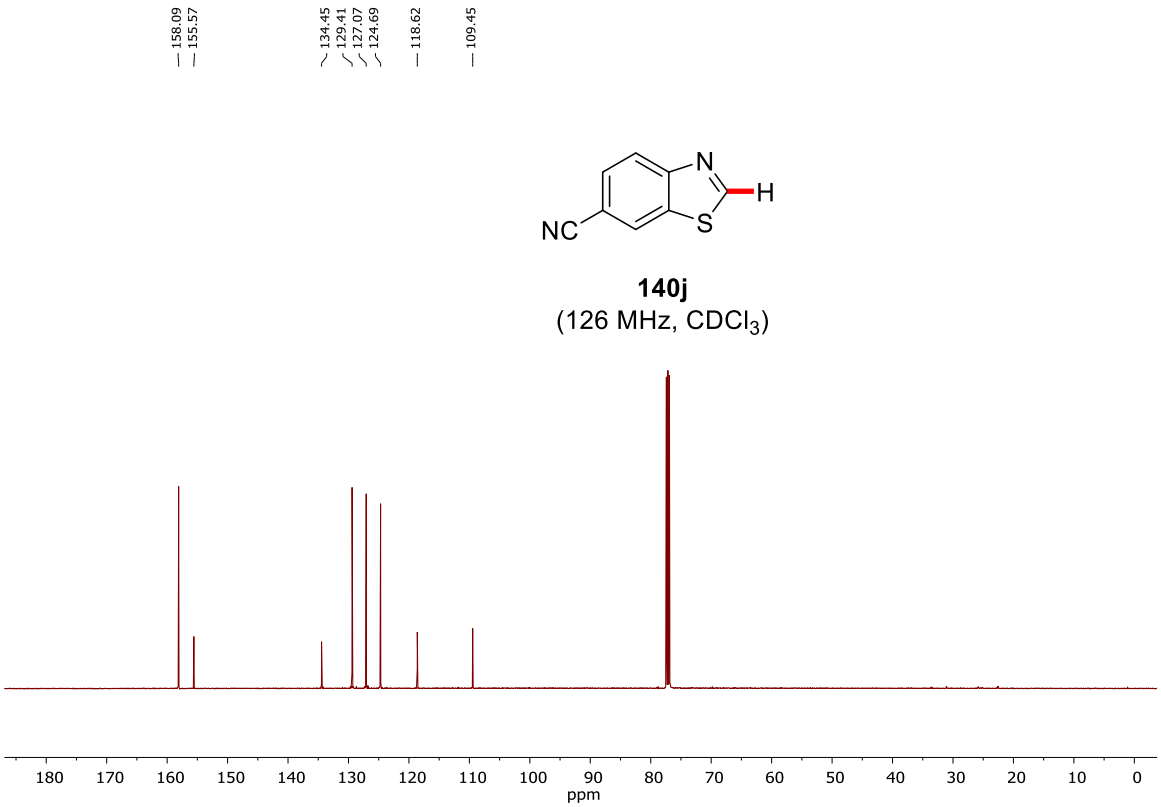

140j
(126 MHz, $CDCl_3$)

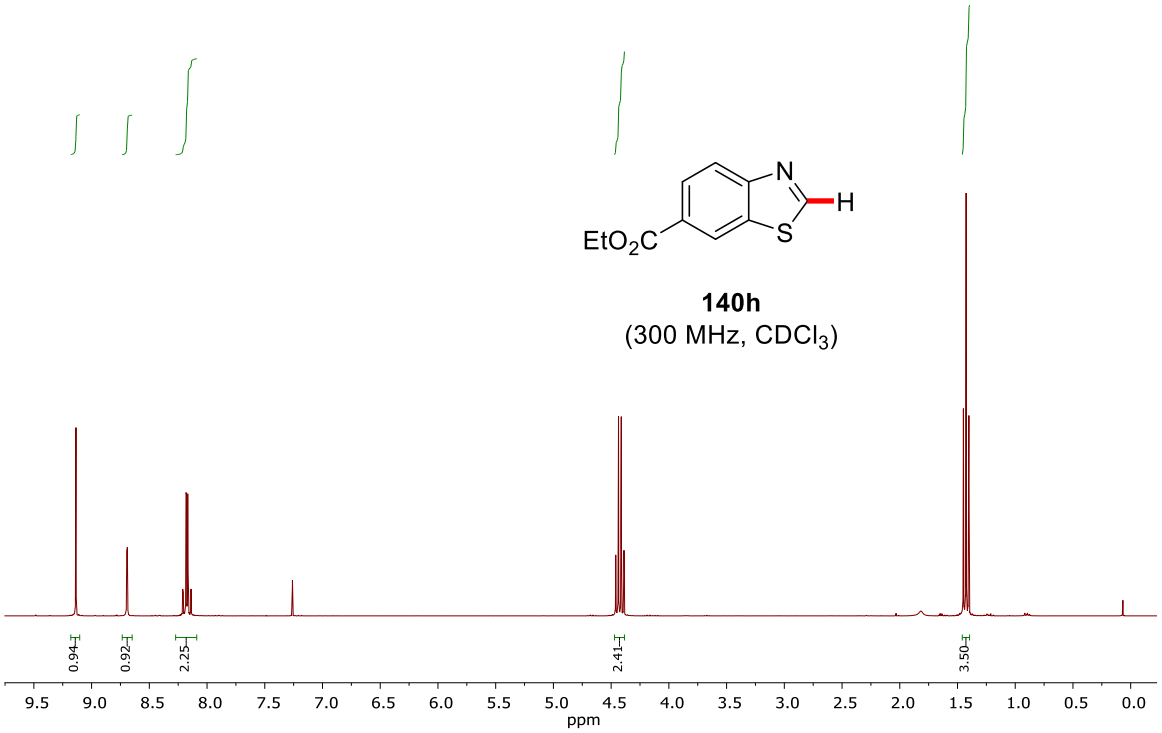
N
H
S
EtO2C
140h
(300 MHz, CDCl3)
0.94
0.92
2.25
2.41
3.50
9.5 9.0 8.5 8.0 7.5 7.0 6.5 6.0 5.5 5.0 4.5 4.0 3.5 3.0 2.5 2.0 1.5 1.0 0.5 0.0
ppm

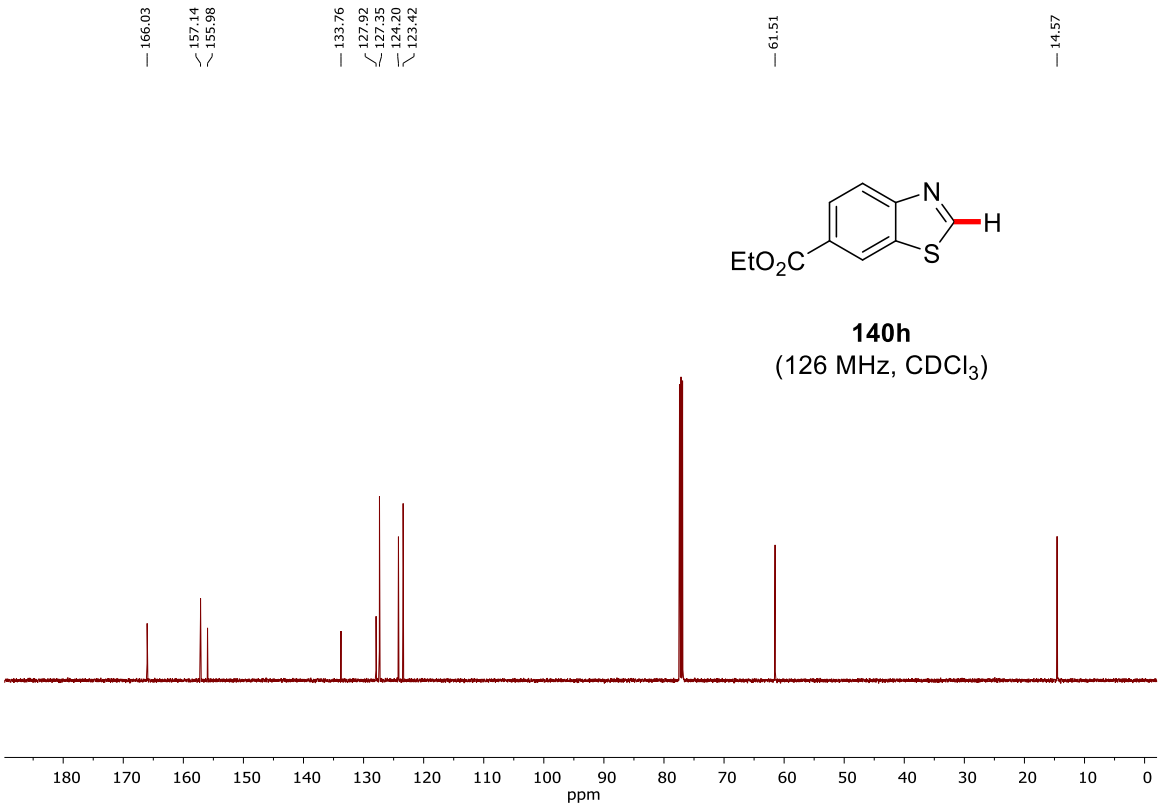
166.03
157.14
155.98
133.76
127.92
127.35
124.20
123.42
61.51
14.57
N
H
S
EtO2C
140h
(126 MHz, CDCl3)
180 170 160 150 140 130 120 110 100 90 80 70 60 50 40 30 20 10 0
ppm

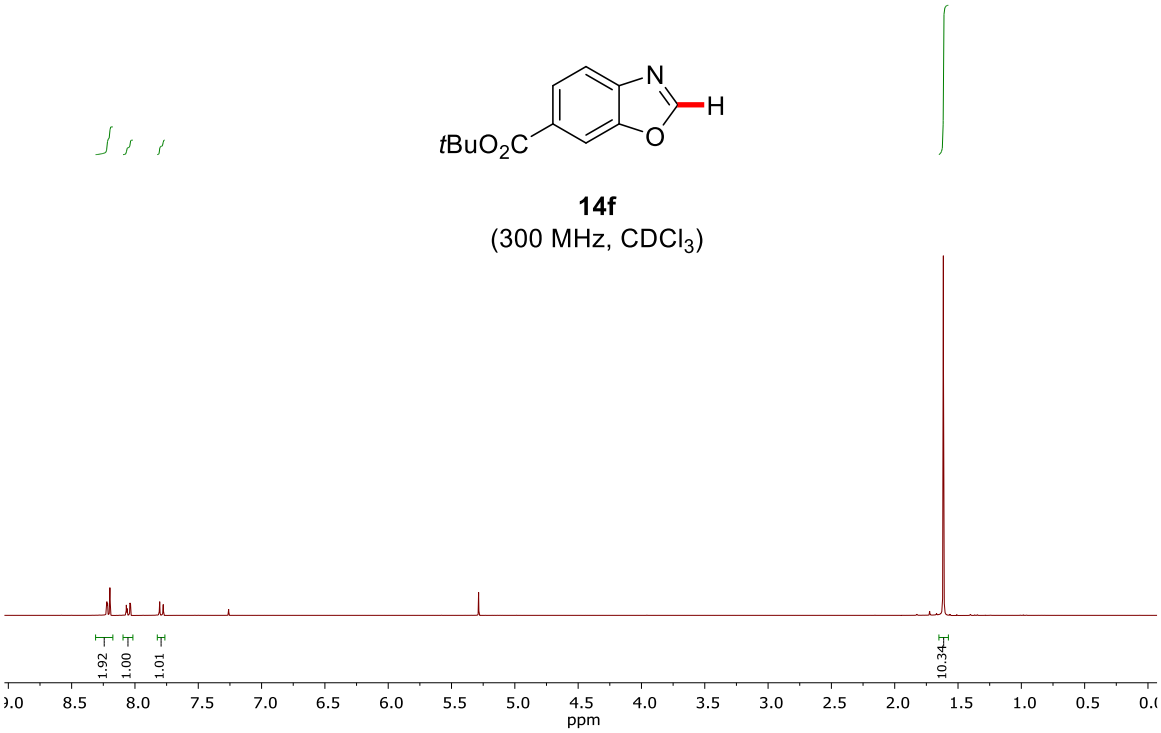

14f
(300 MHz, $CDCl_3$)

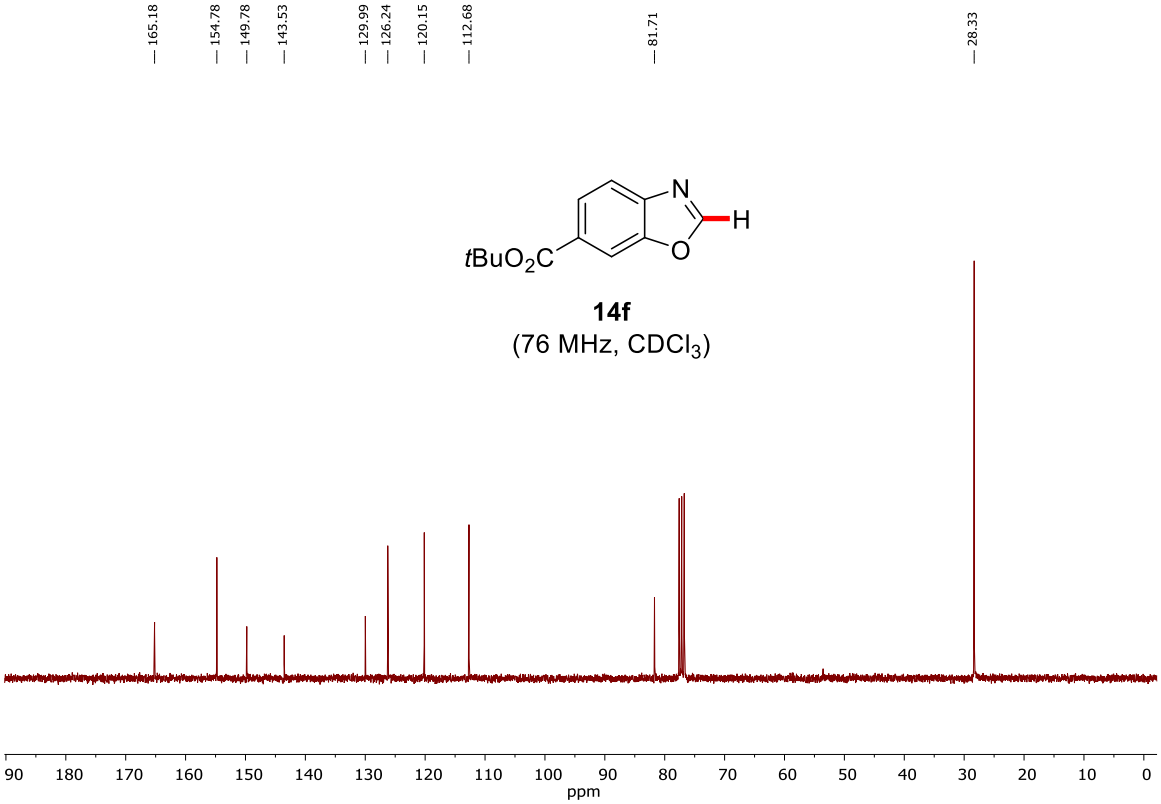

14f
(76 MHz, $CDCl_3$)

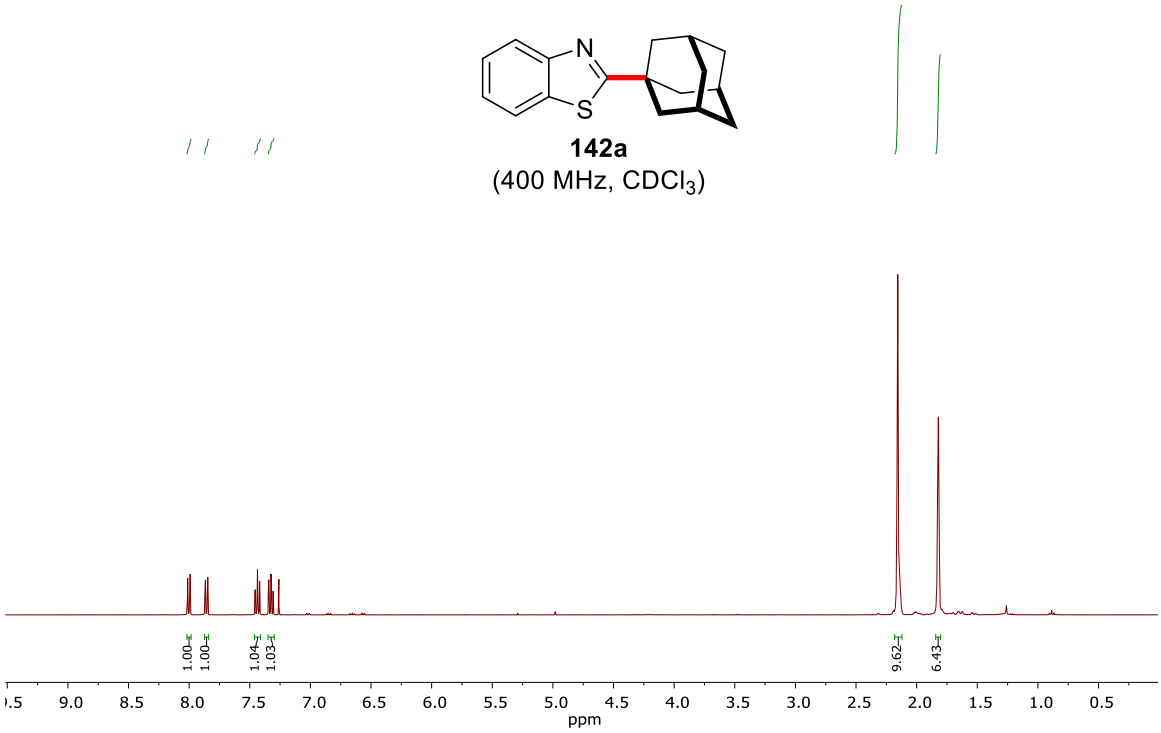
N
S
142a
(400 MHz, CDCl3)
1.00
1.00
1.04
1.03
9.62
6.43
ppm

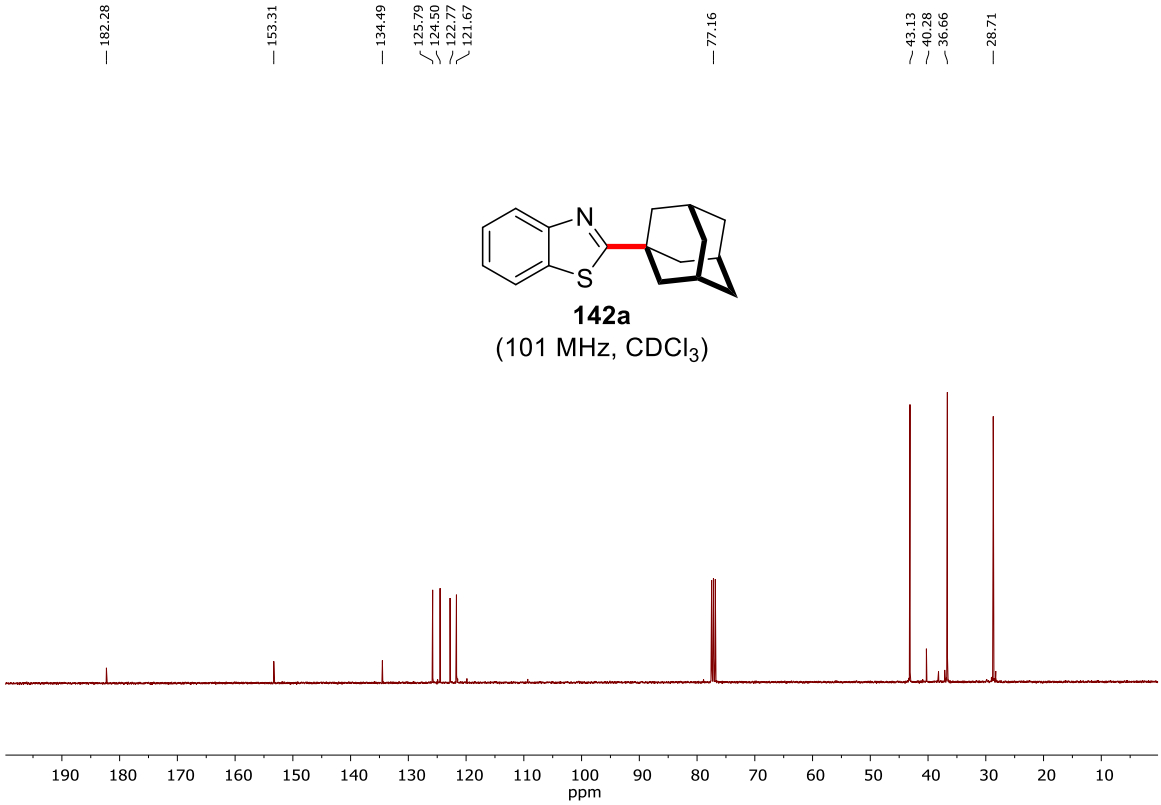
182.28
153.31
134.49
125.79
124.50
122.77
121.67
77.16
43.13
40.28
36.66
28.71
N
S
142a
(101 MHz, CDCl3)
ppm

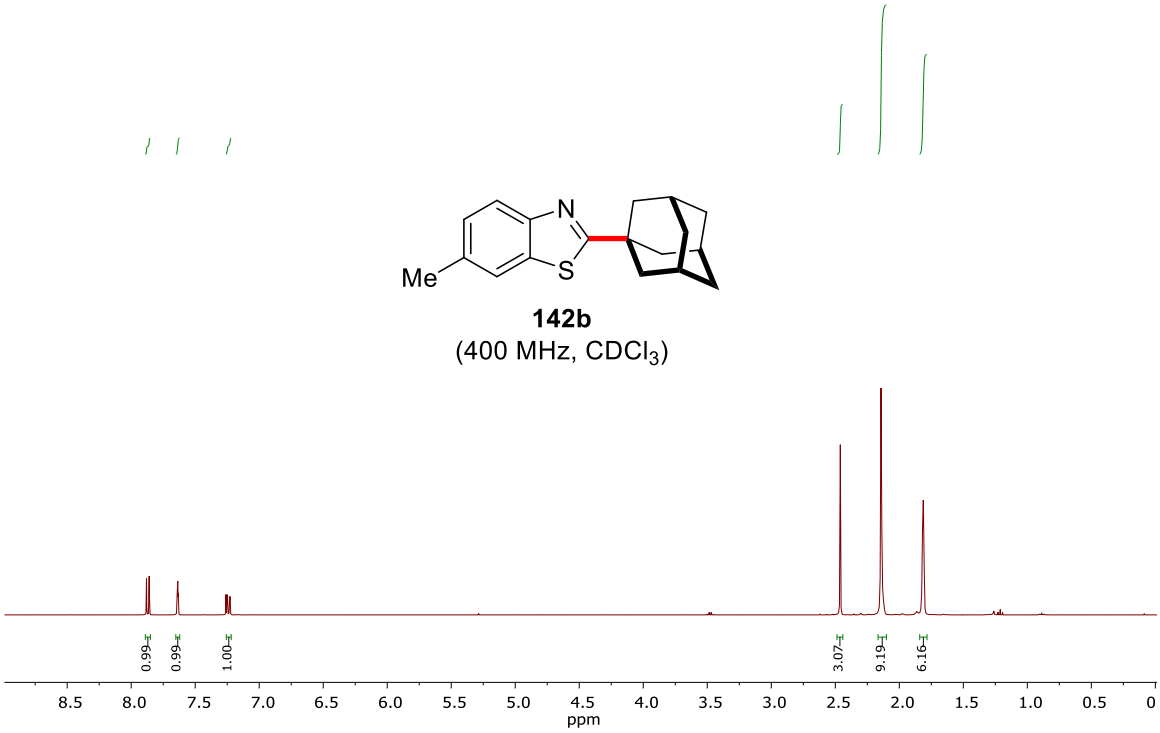
Me
N
S
142b
(400 MHz, CDCl3)
0.99
0.99
1.00
3.07
9.19
6.16
8.5 8.0 7.5 7.0 6.5 6.0 5.5 5.0 4.5 4.0 3.5 3.0 2.5 2.0 1.5 1.0 0.5 0
ppm

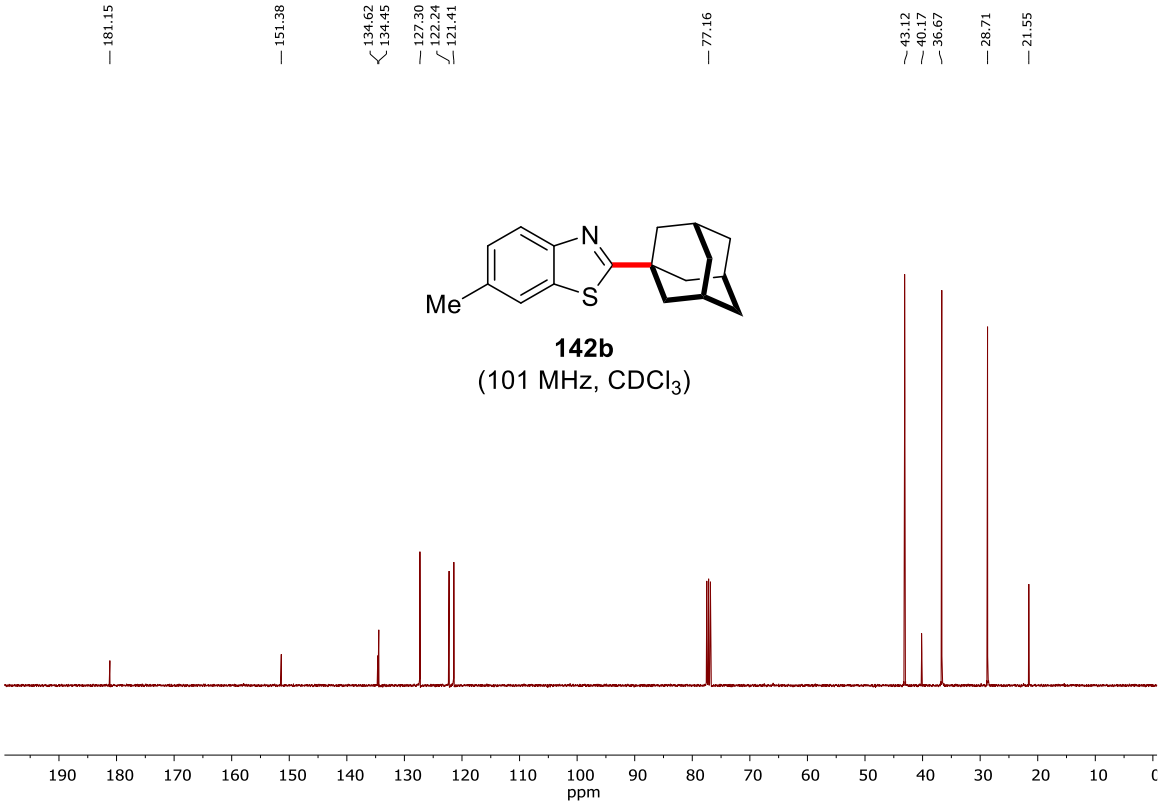
181.15
151.38
134.62
134.45
127.30
122.24
121.41
77.16
43.12
40.17
36.67
28.71
21.55
Me
N
S
142b
(101 MHz, CDCl3)
190 180 170 160 150 140 130 120 110 100 90 80 70 60 50 40 30 20 10
ppm

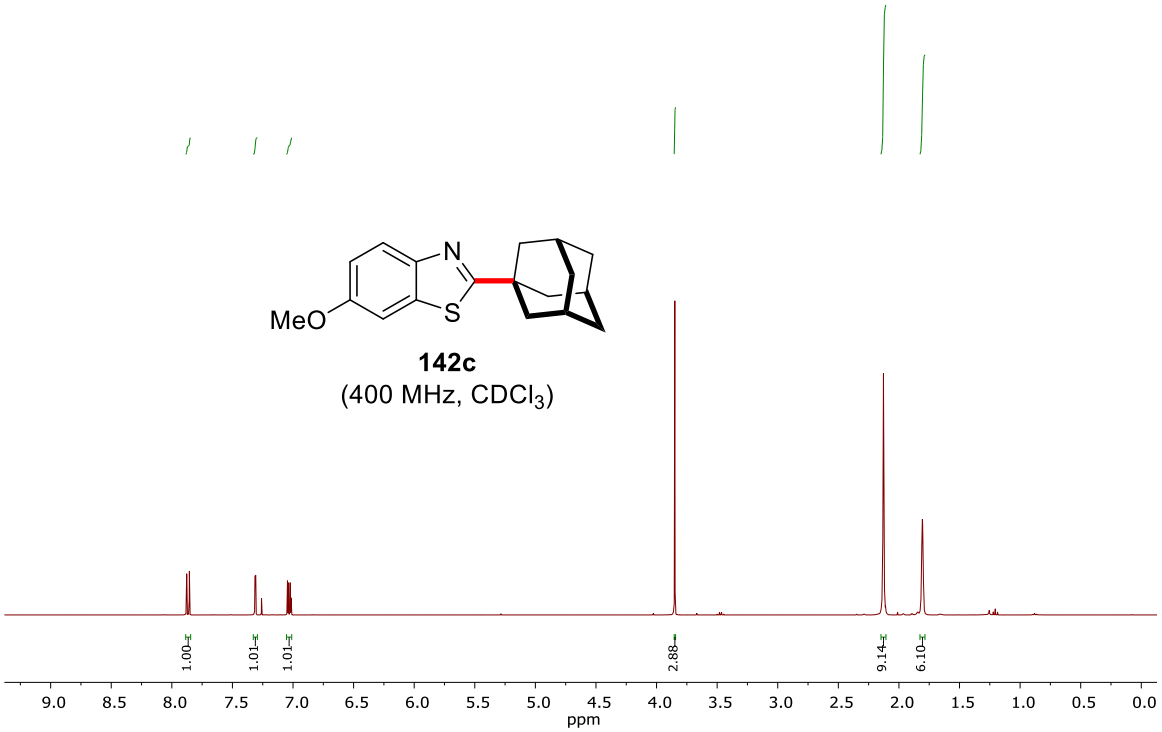

142c
(400 MHz, $CDCl_3$)

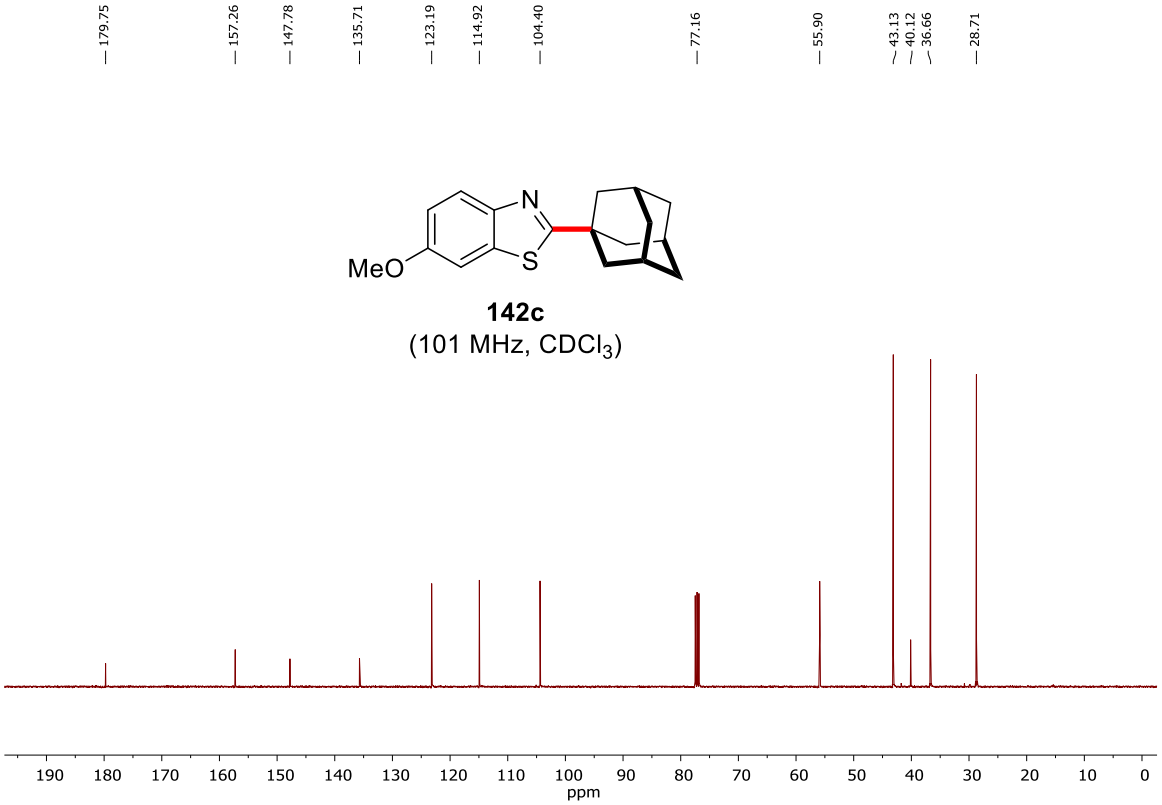

142c
(101 MHz, $CDCl_3$)

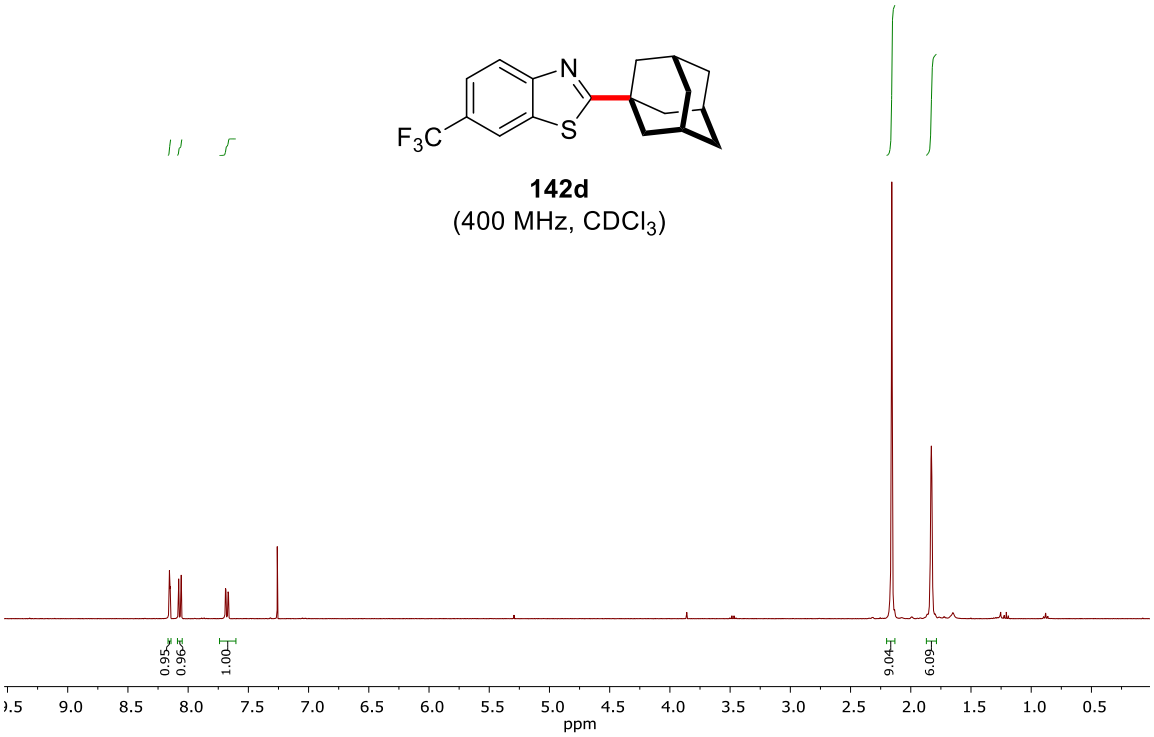
F3C
N
S
142d
(400 MHz, CDCl3)
0.95
0.96
1.00
9.04
6.09
ppm

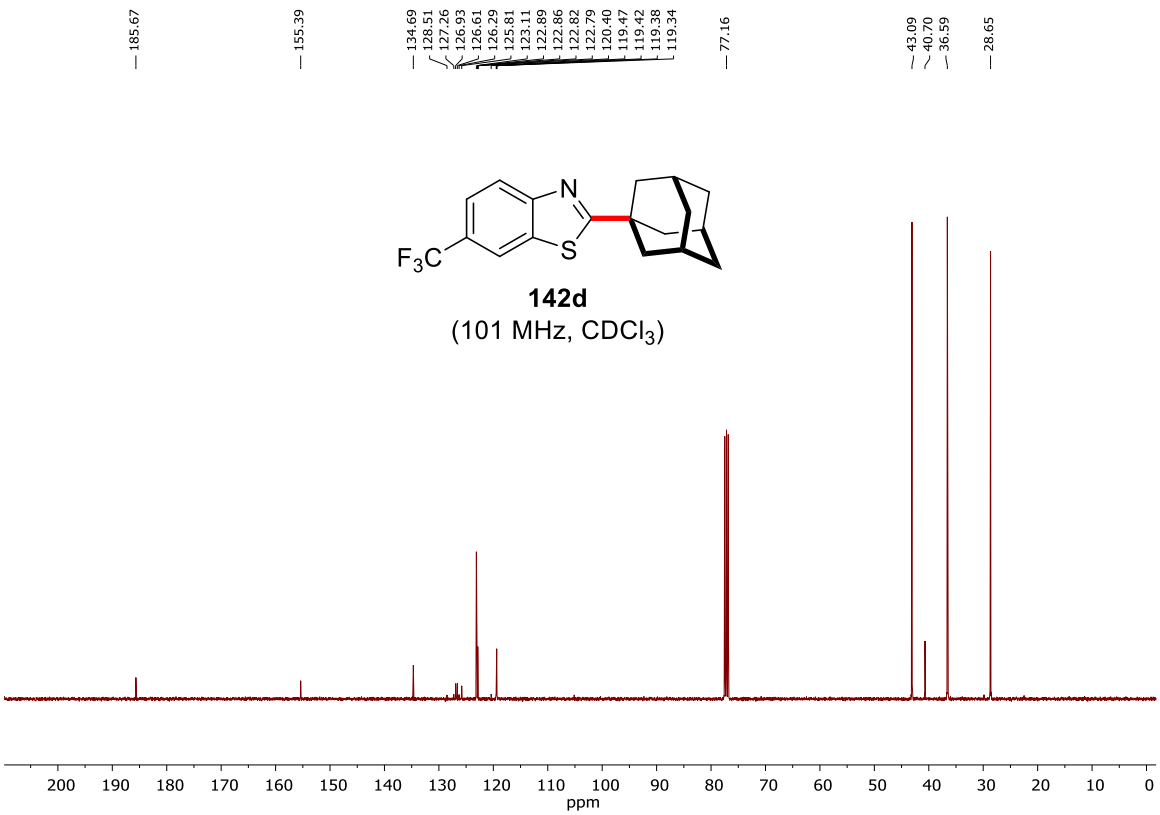
F3C
N
S
142d
(101 MHz, CDCl3)
ppm

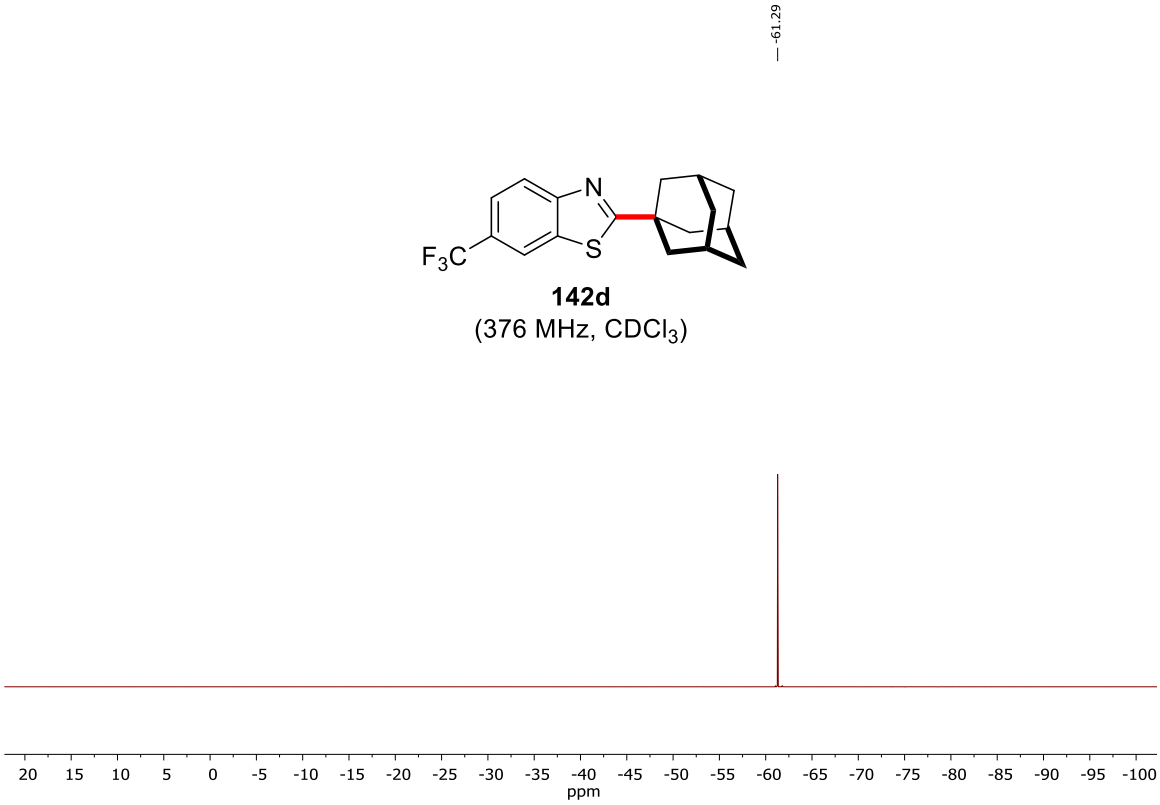

142d

(376 MHz, $CDCl_3$)

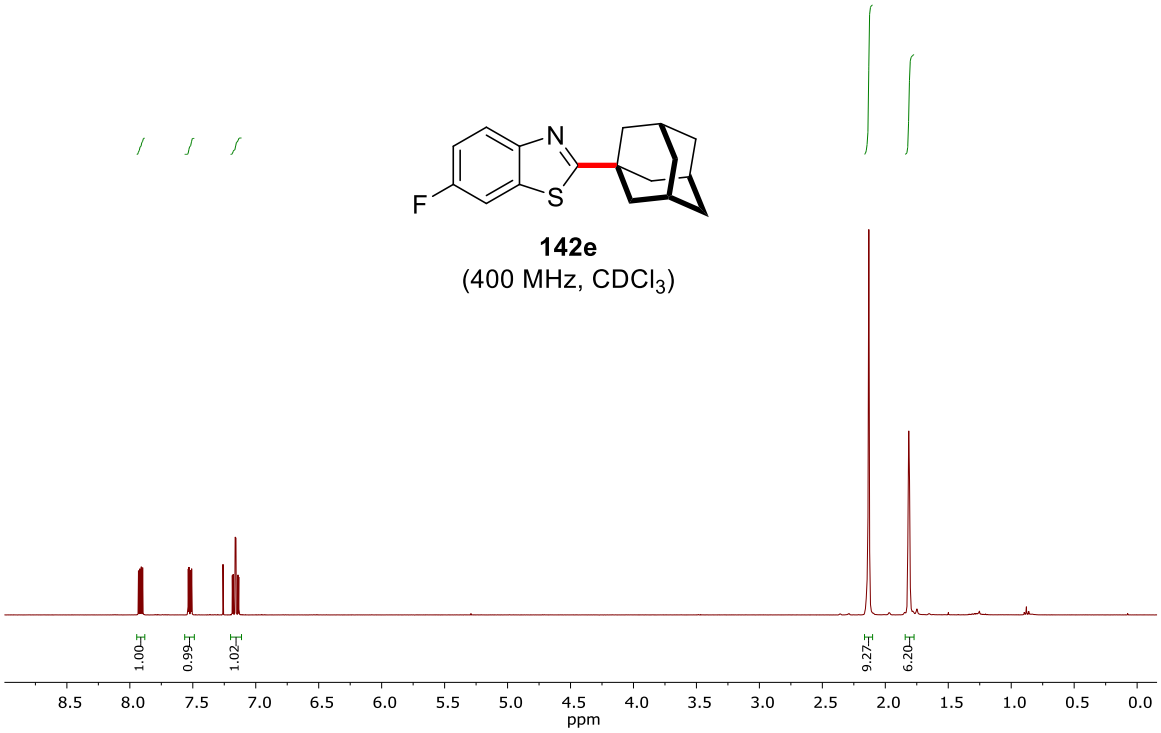

142e
(400 MHz, $CDCl_3$)

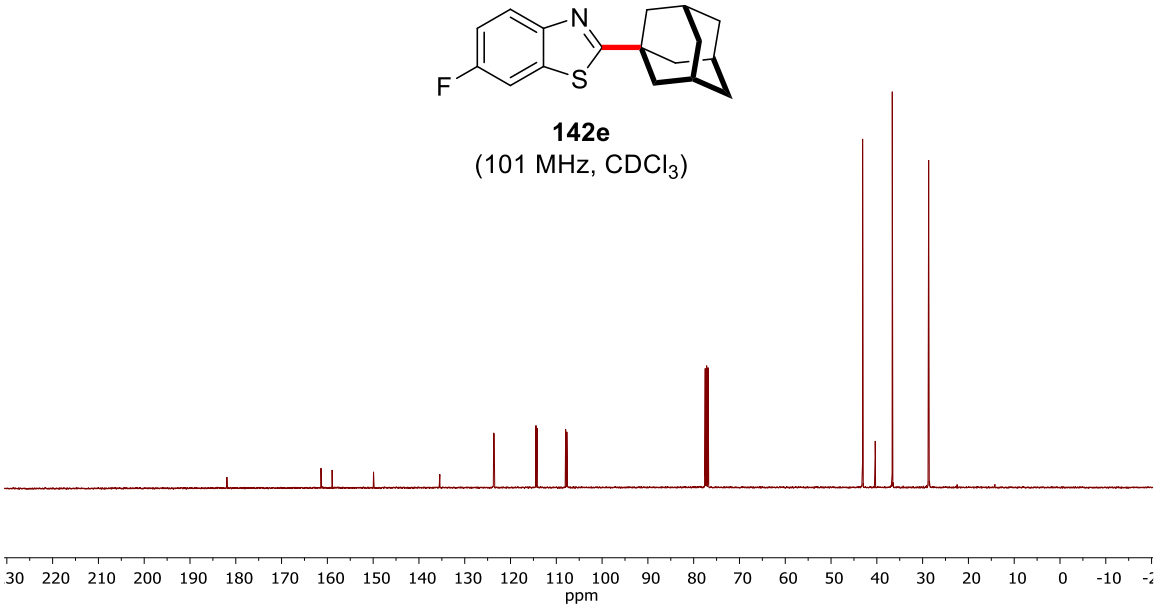

142e
(101 MHz, $CDCl_3$)

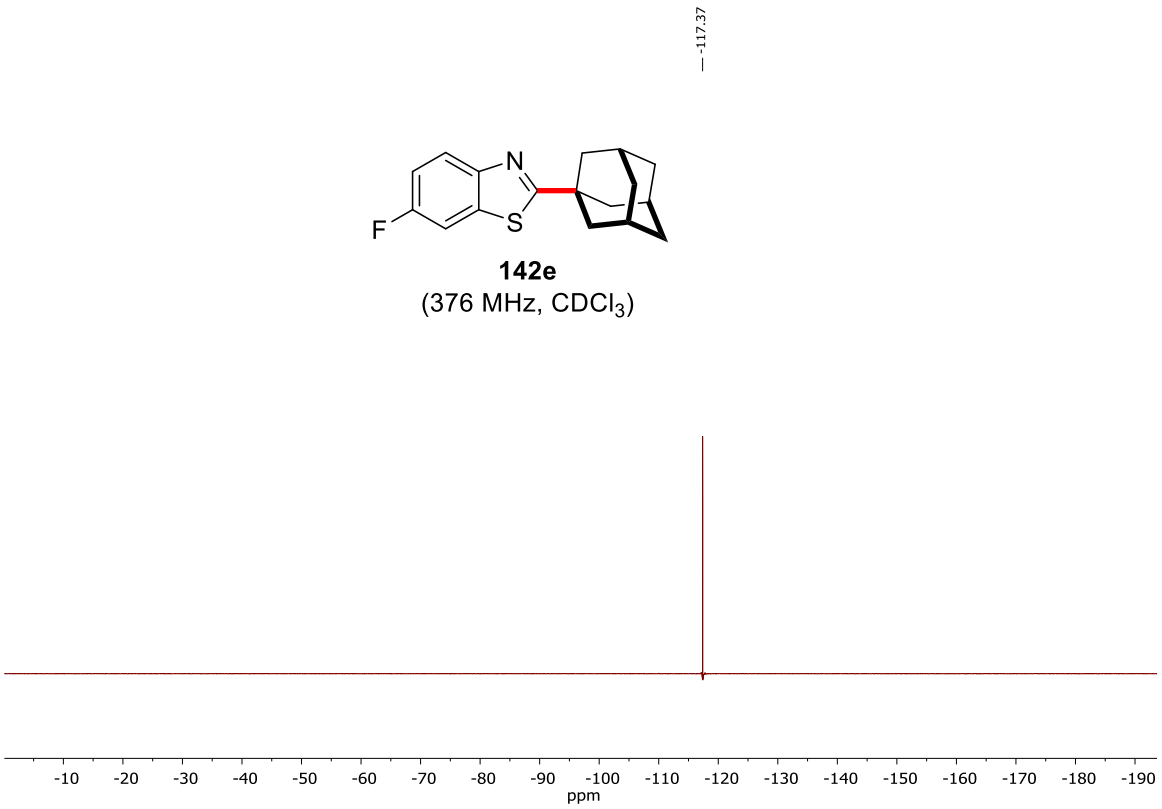

142e
(376 MHz, $CDCl_3$)

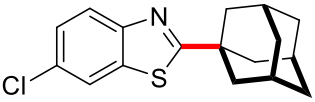

142f
(400 MHz, $CDCl_3$)

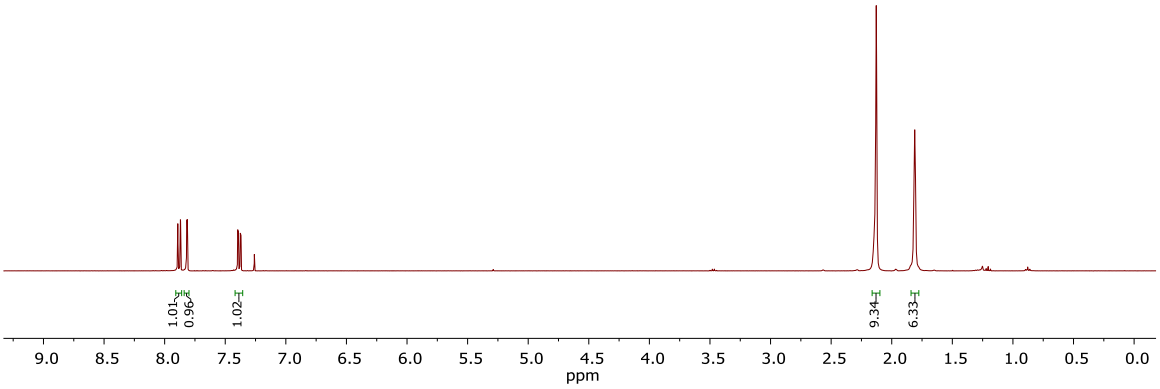

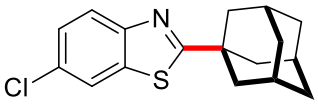

142f
(101 MHz, $CDCl_3$)

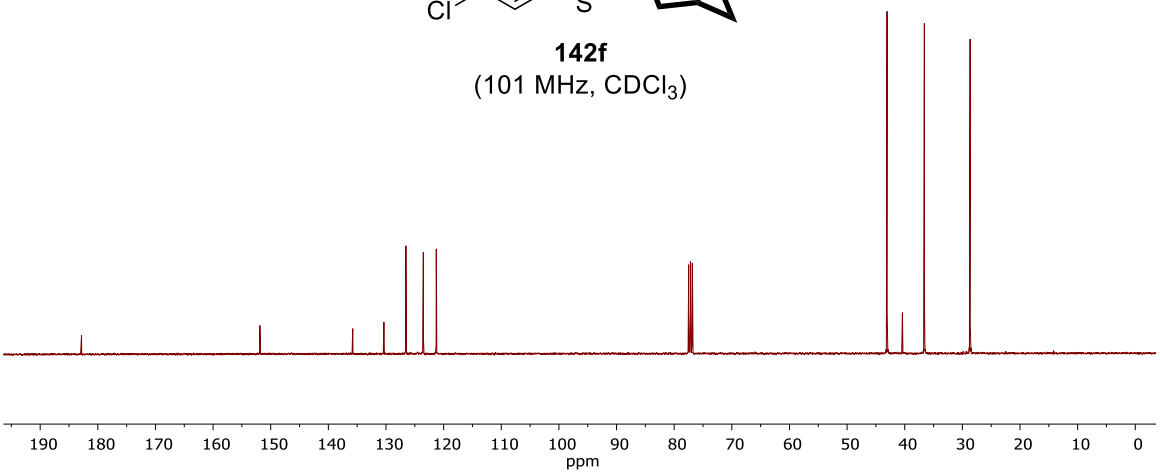

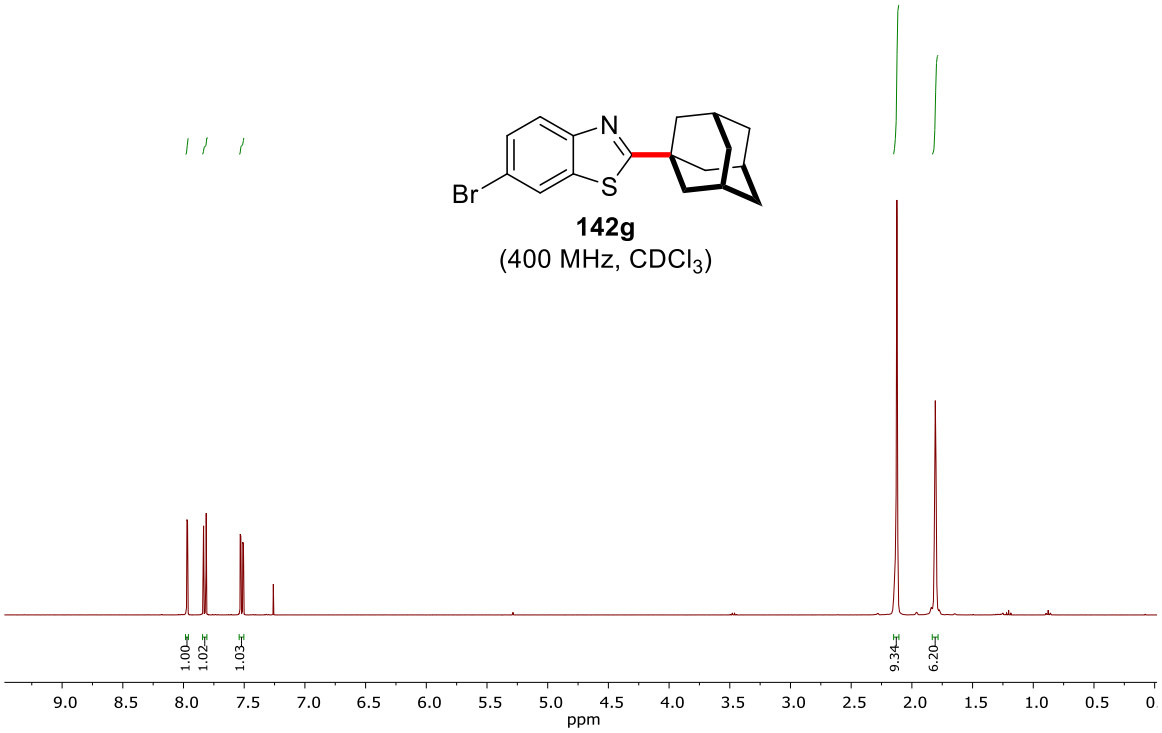
Br
N
S
142g
(400 MHz, CDCl3)
1.00
1.02
1.03
9.34
6.20
ppm

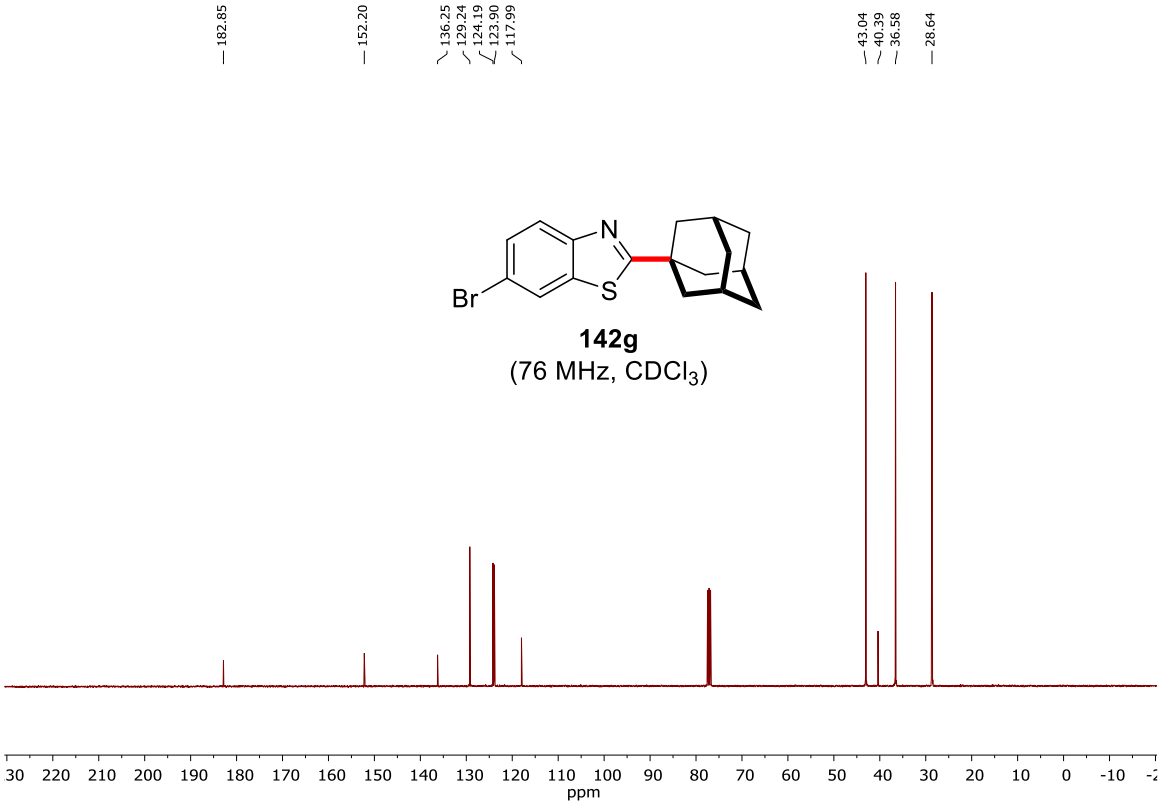
182.85
152.20
136.25
129.24
124.19
123.90
117.99
43.04
40.39
36.58
28.64
Br
N
S
142g
(76 MHz, CDCl3)
ppm

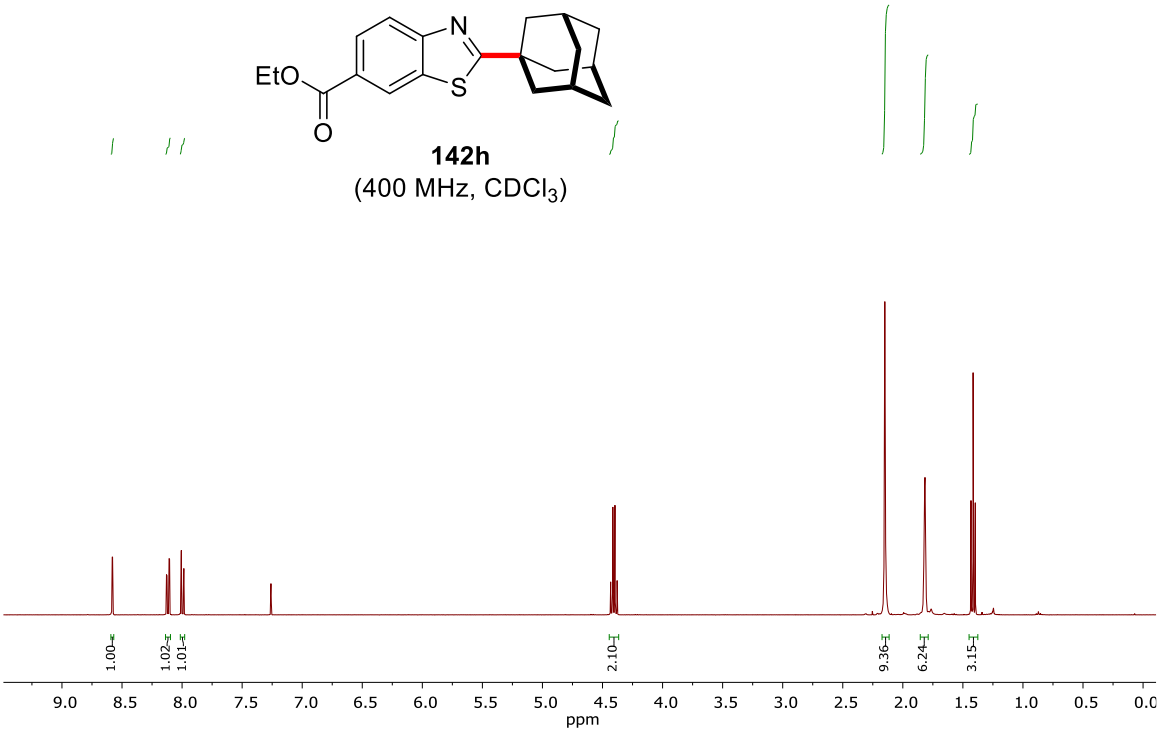
EtO
O
N
S
142h
(400 MHz, CDCl3)
1.00
1.02
1.01
2.10
9.36
6.24
3.15
ppm


186.03
166.43
156.28
134.44
127.07
126.69
123.88
122.40
77.16
61.27
43.02
40.67
36.57
28.63
14.48

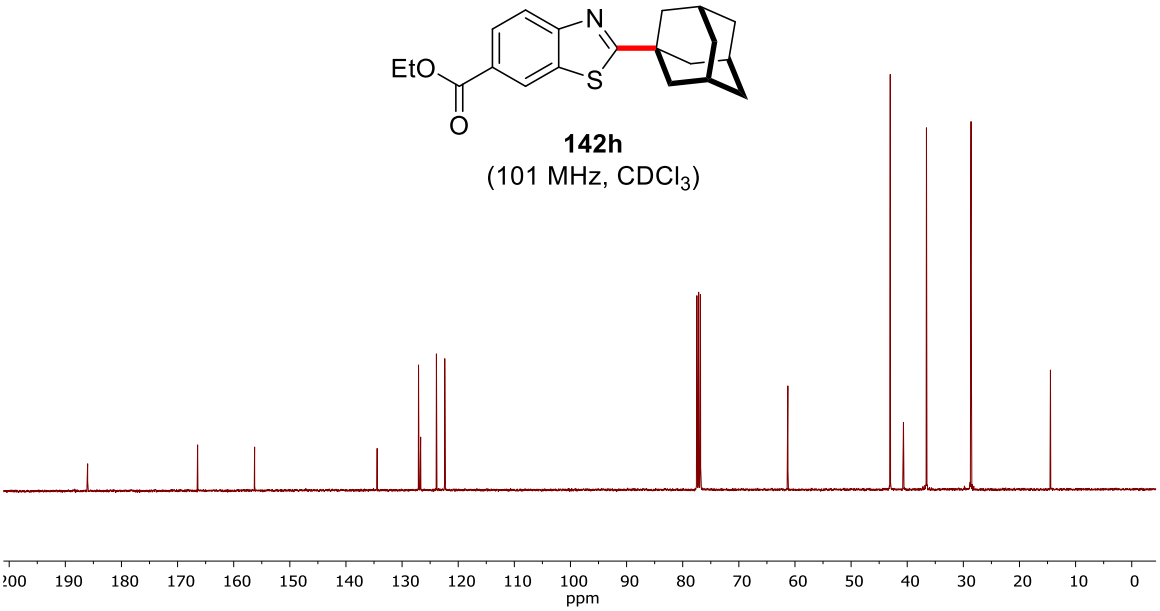
EtO
O
N
S
142h
(101 MHz, CDCl3)
ppm

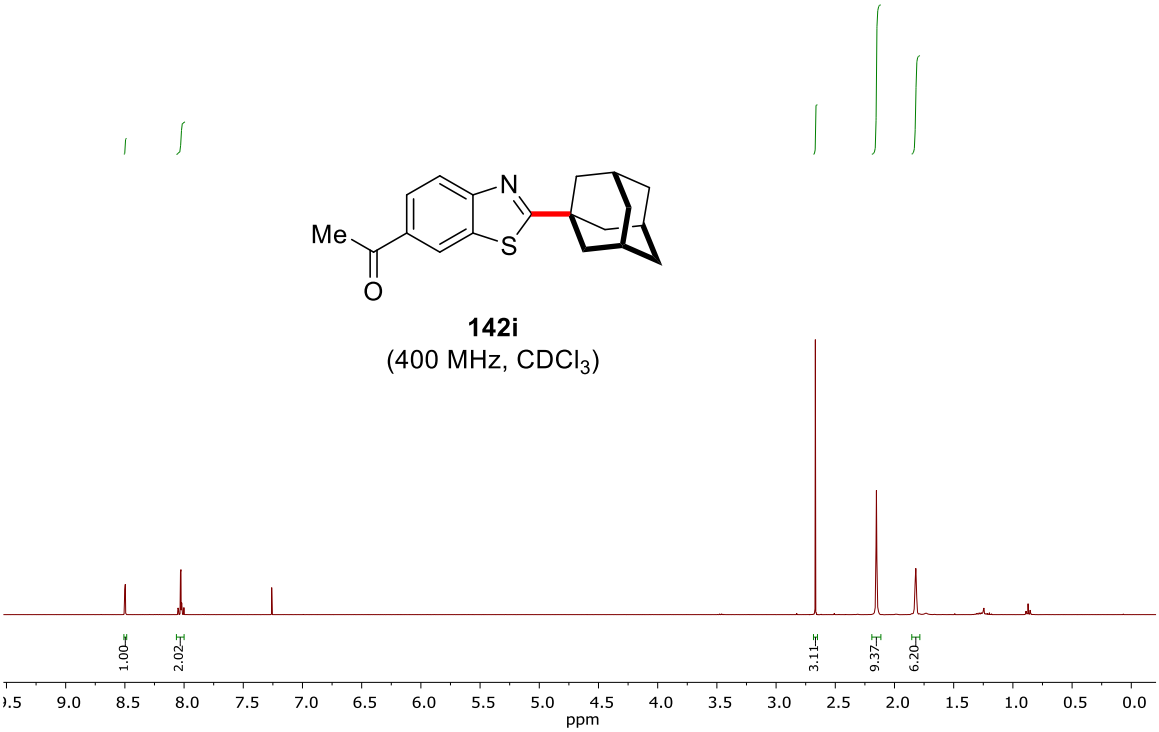
Me
O
N
S
142i
(400 MHz, CDCl3)
1.00
2.02
3.11
9.37
6.20
ppm

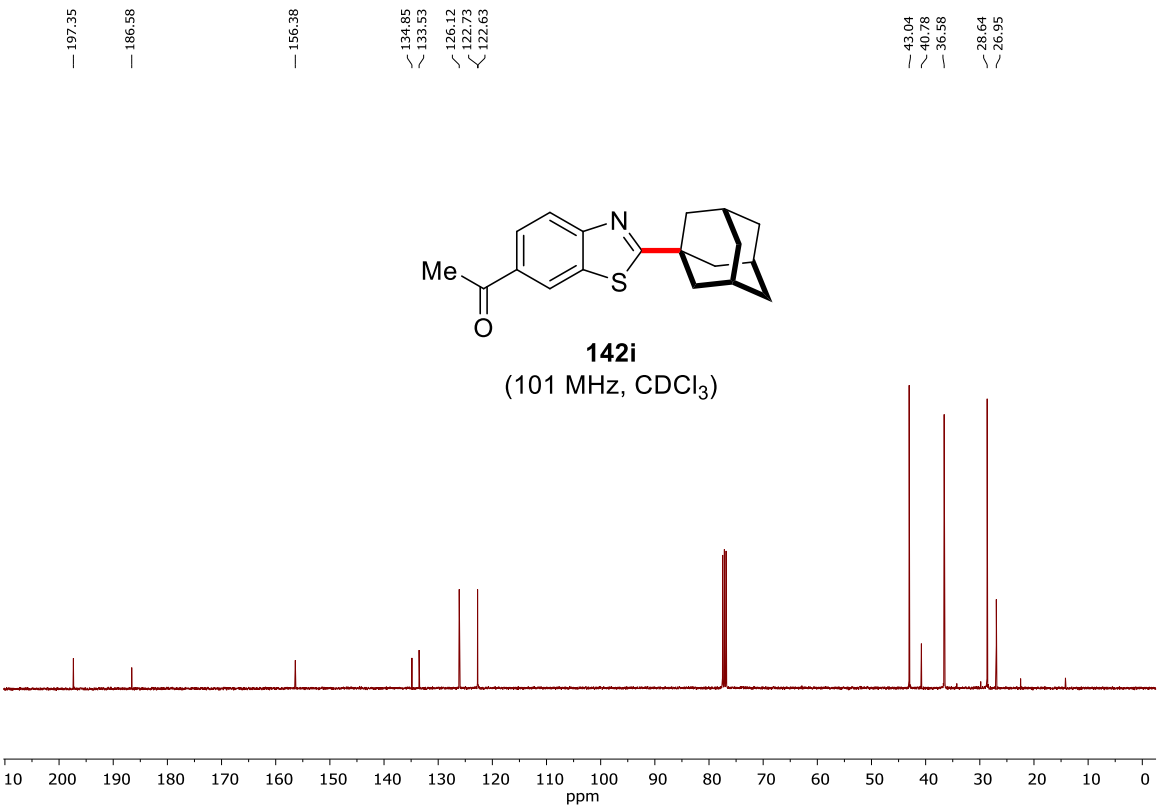
Me
O
N
S
142i
(101 MHz, CDCl3)
197.35
186.58
156.38
134.85
133.53
126.12
122.73
122.63
43.04
40.78
36.58
28.64
26.95
ppm

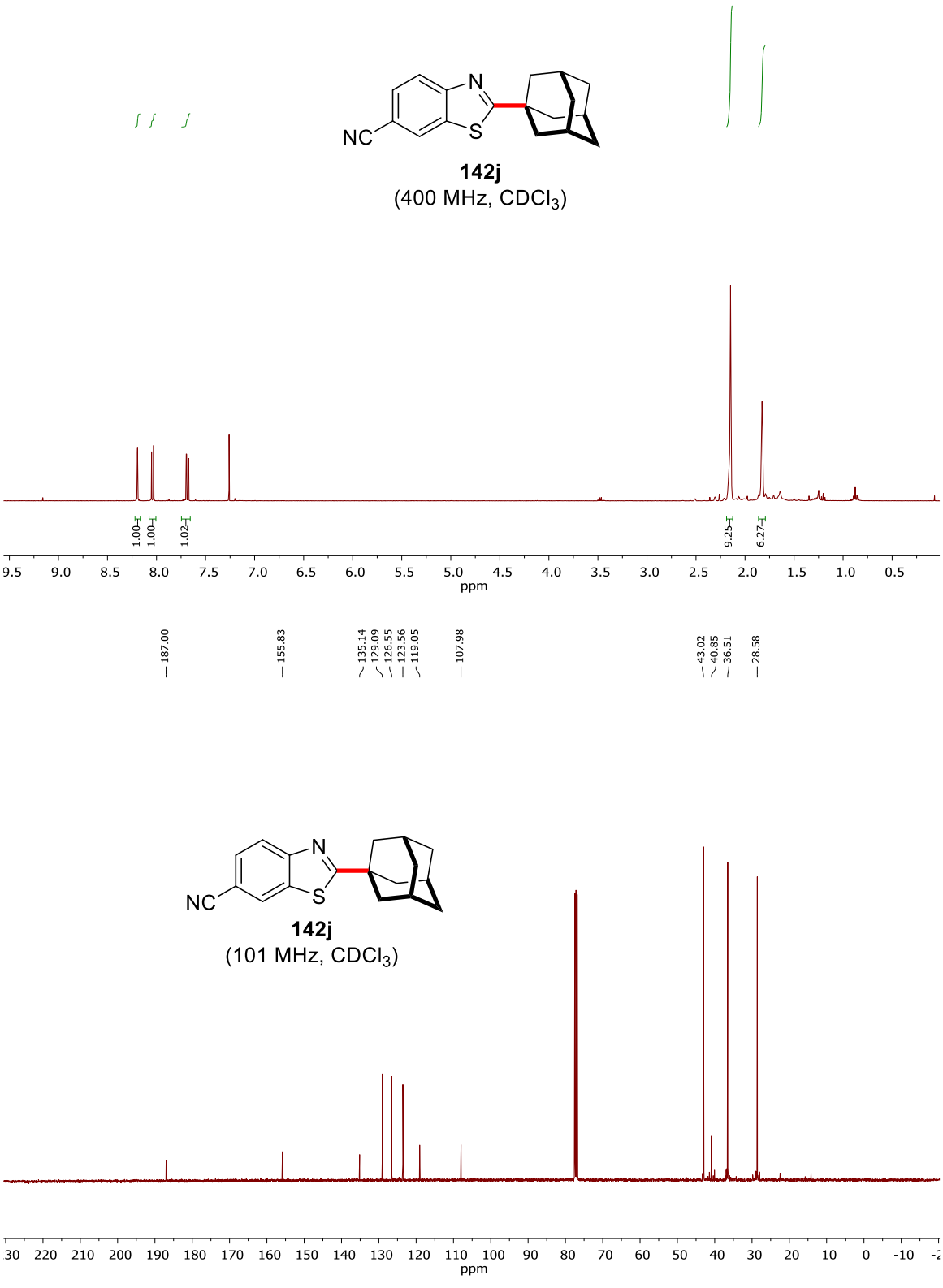
NC
N
S
142j
(400 MHz, CDCl3)
1.00
1.00
1.02
9.25
6.27
9.5 9.0 8.5 8.0 7.5 7.0 6.5 6.0 5.5 5.0 4.5 4.0 3.5 3.0 2.5 2.0 1.5 1.0 0.5
ppm
187.00
155.83
135.14
129.09
126.55
123.56
119.05
107.98
43.02
40.85
36.51
28.58
NC
N
S
142j
(101 MHz, CDCl3)
30 220 210 200 190 180 170 160 150 140 130 120 110 100 90 80 70 60 50 40 30 20 10 0 -10
ppm

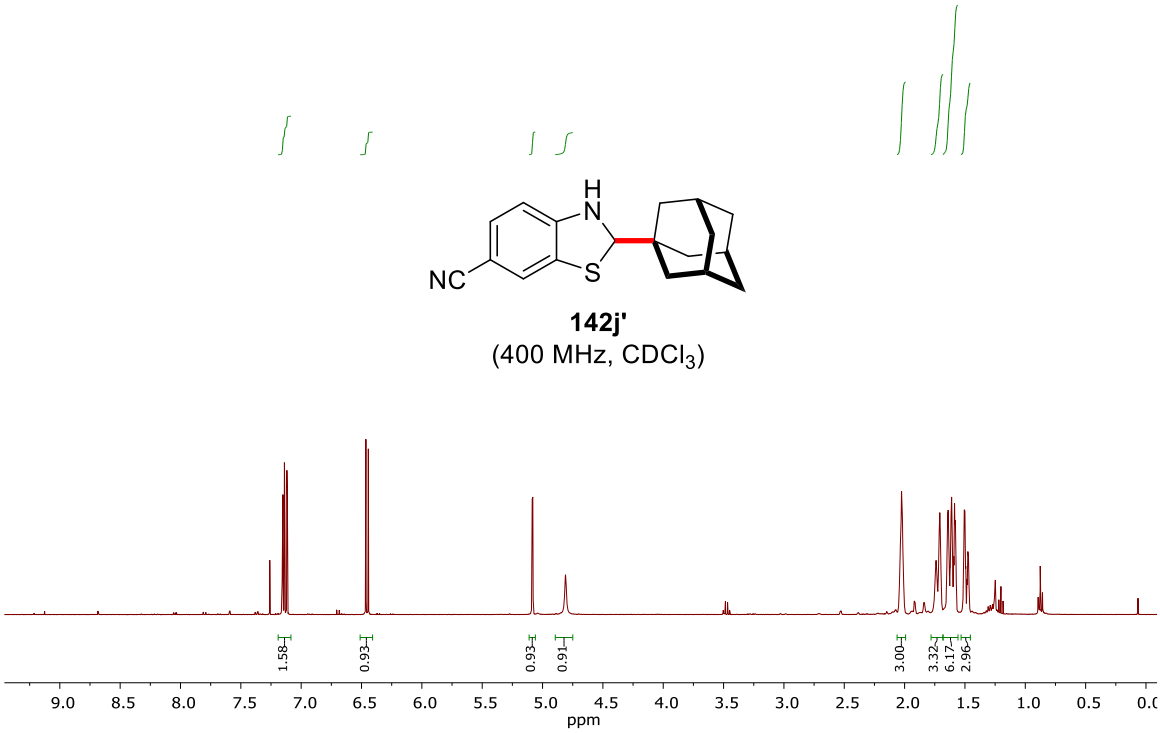

142j'
(400 MHz, $CDCl_3$)

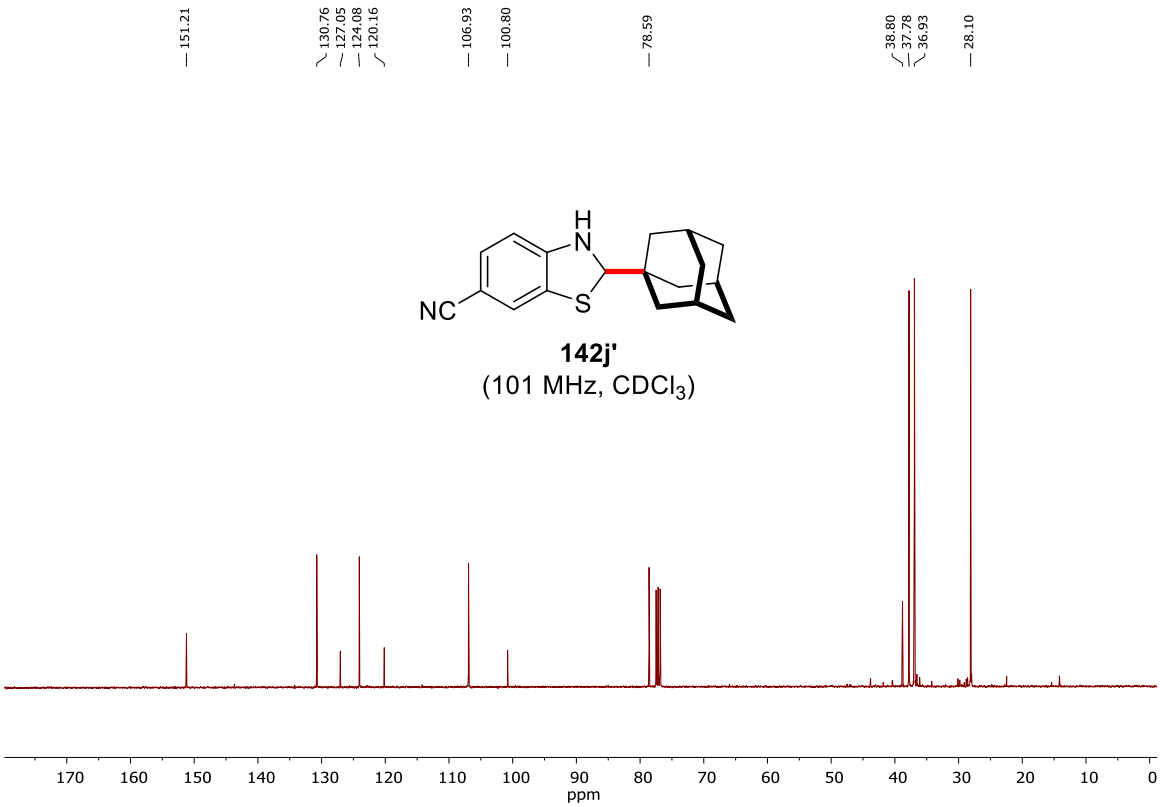

142j'
(101 MHz, $CDCl_3$)

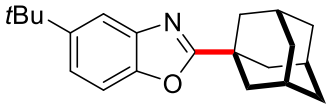

143b
(600 MHz, $CDCl_3$)

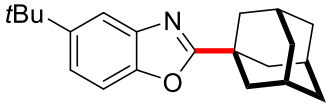

143b
(126 MHz, $CDCl_3$)

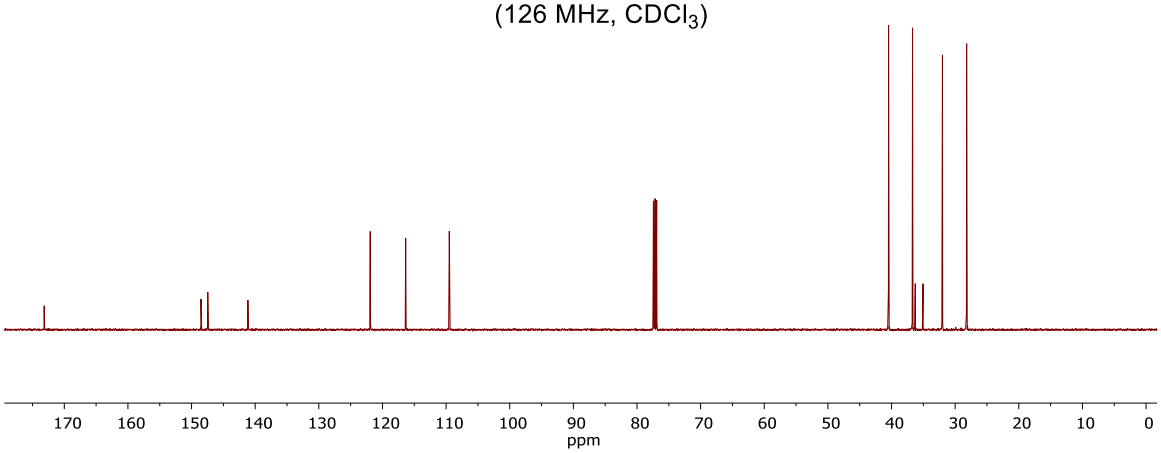

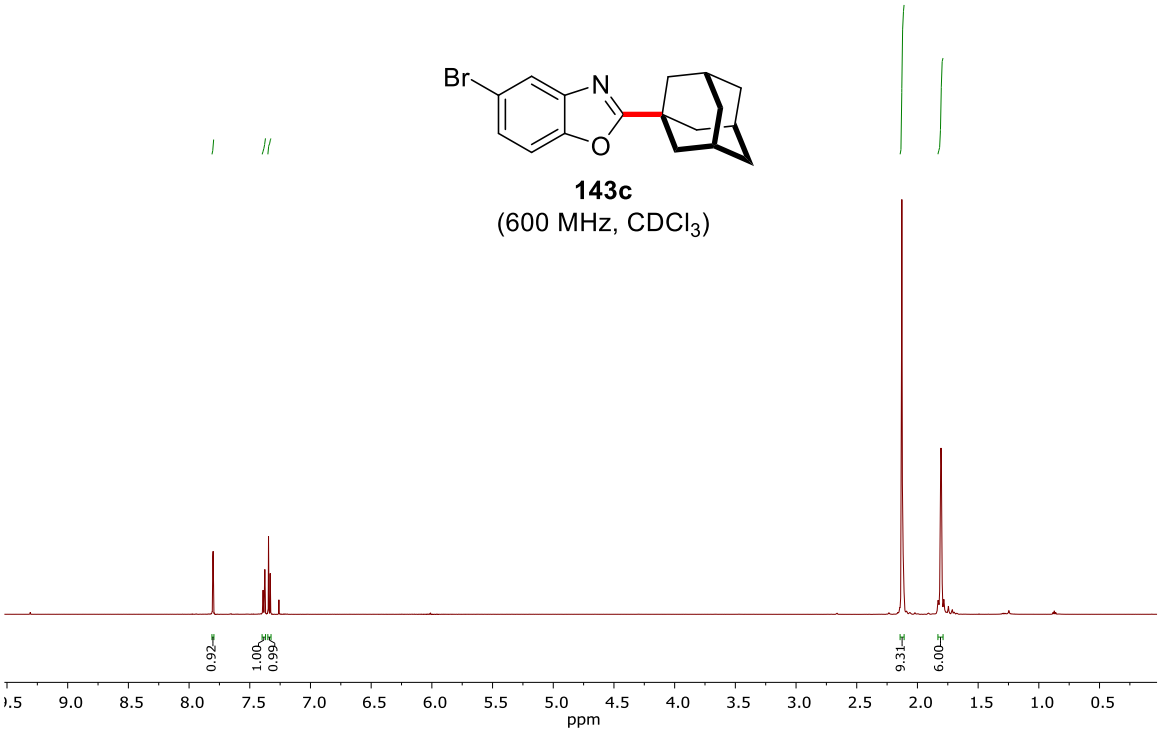
Br
N
O
143c
(600 MHz, CDCl3)
0.92
1.00
0.99
9.31
6.00
ppm

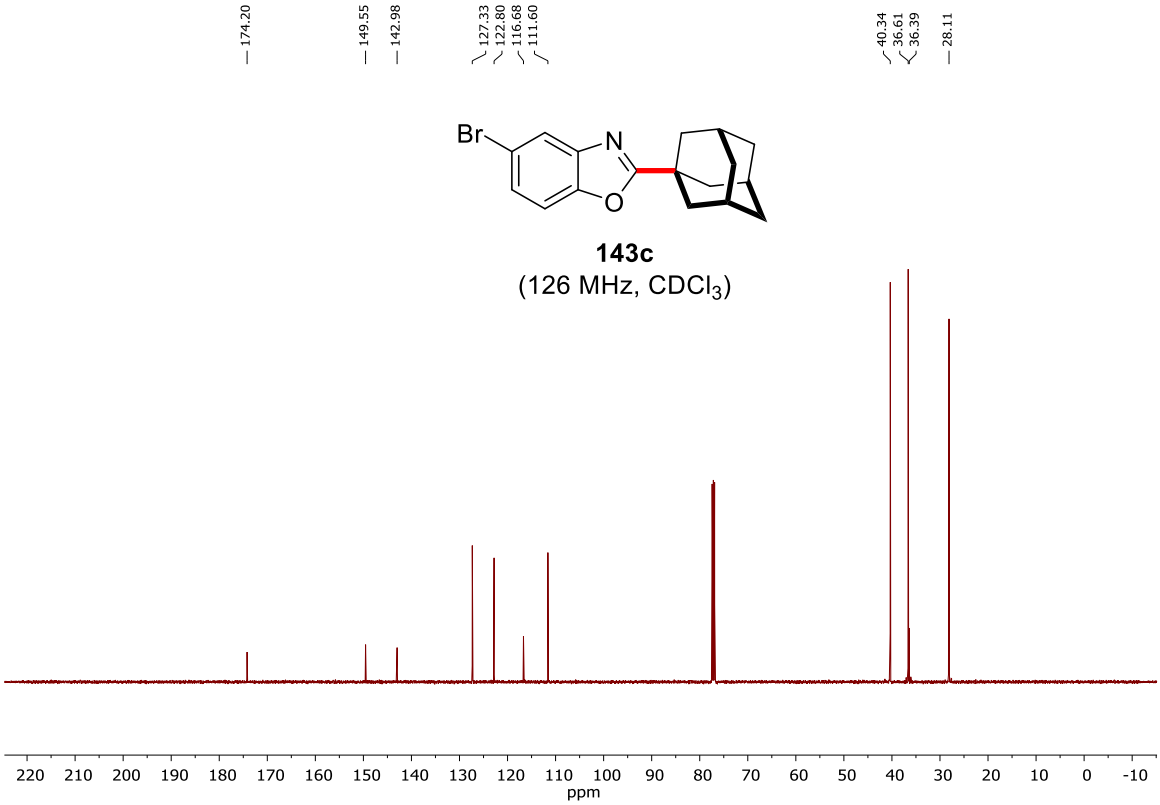
174.20
149.55
142.98
127.33
122.80
116.68
111.60
40.34
36.61
36.39
28.11
Br
N
O
143c
(126 MHz, CDCl3)
ppm

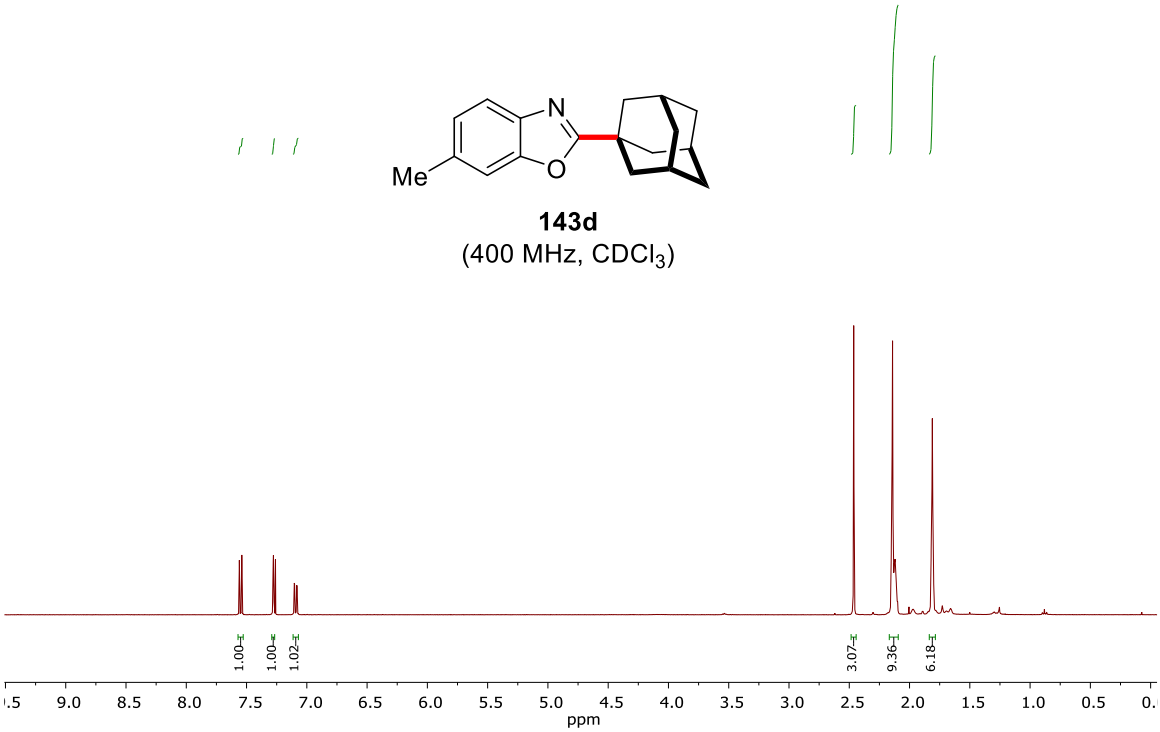
Me
N
O
143d
(400 MHz, CDCl3)
1.00
1.00
1.02
3.07
9.36
6.18
ppm

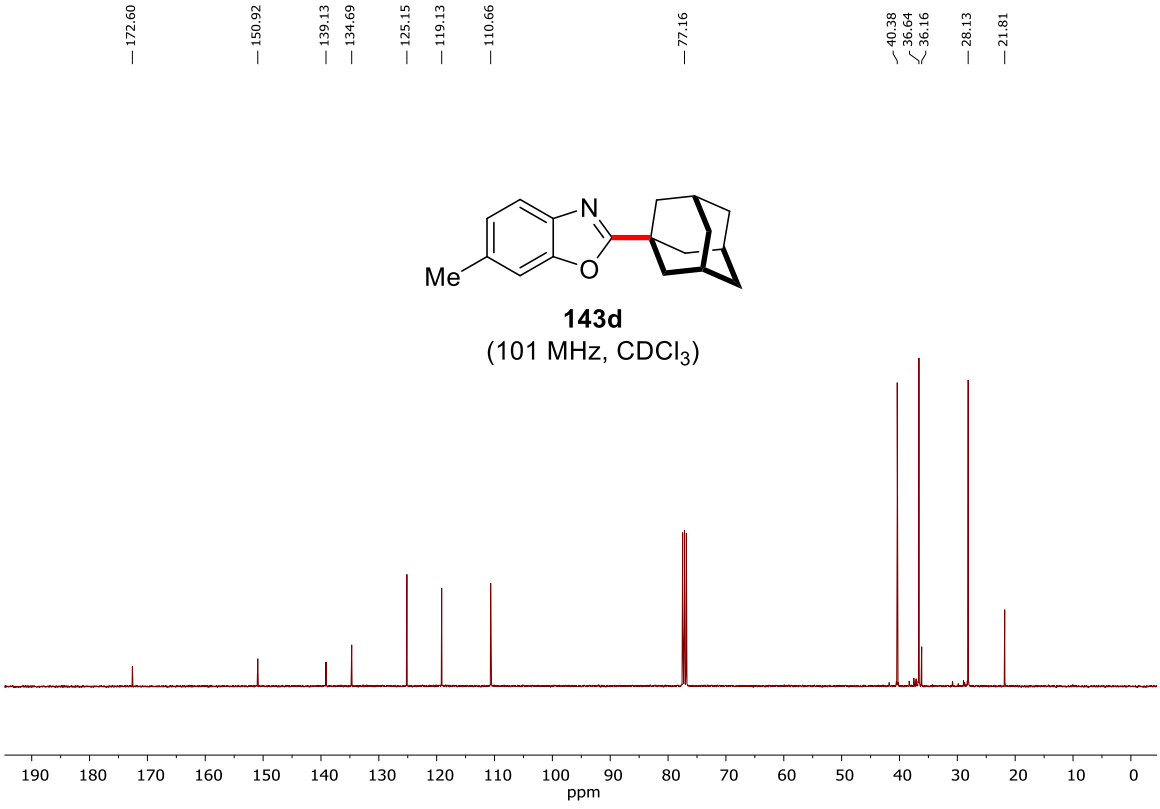
172.60
150.92
139.13
134.69
125.15
119.13
110.66
77.16
40.38
36.64
36.16
28.13
21.81
Me
N
O
143d
(101 MHz, CDCl3)
ppm

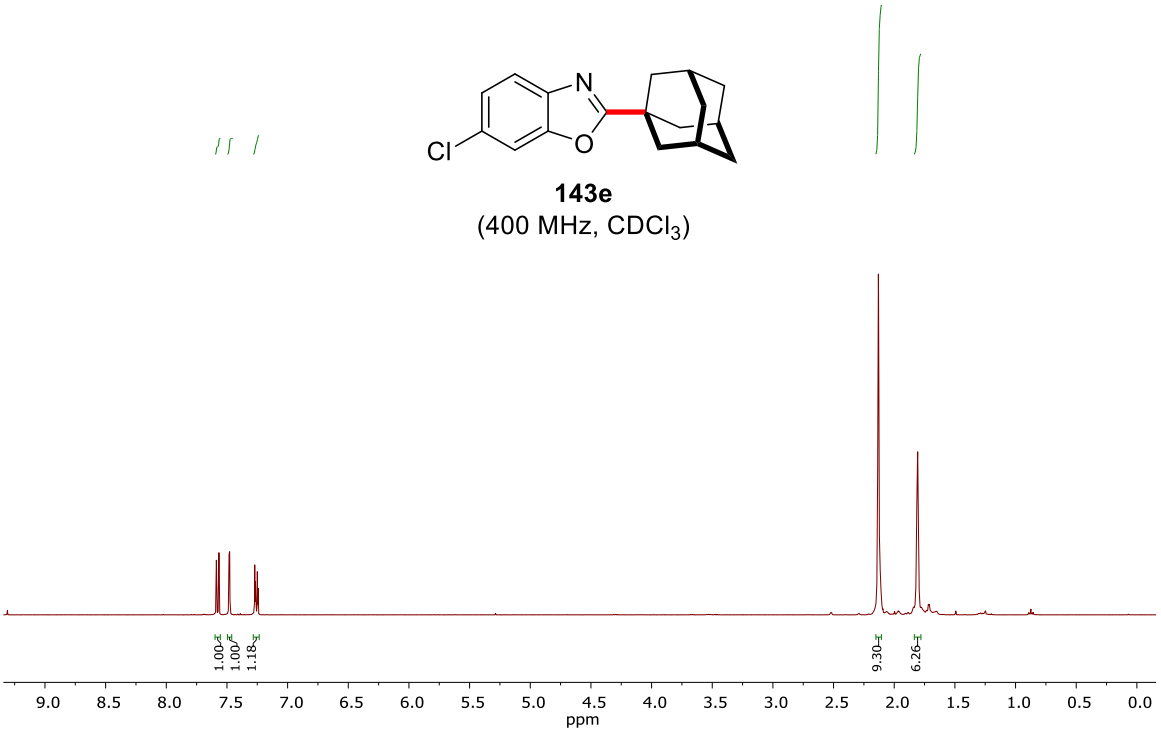
Cl
N
O
143e
(400 MHz, CDCl3)
1.00
1.00
1.18
9.30
6.26
9.0 8.5 8.0 7.5 7.0 6.5 6.0 5.5 5.0 4.5 4.0 3.5 3.0 2.5 2.0 1.5 1.0 0.5 0.0
ppm
173.81
150.85
140.15
130.04
124.67
120.28
111.15
77.16
40.28
36.55
36.29
28.03
Cl
N
O
143e
(101 MHz, CDCl3)
180 170 160 150 140 130 120 110 100 90 80 70 60 50 40 30 20 10
ppm

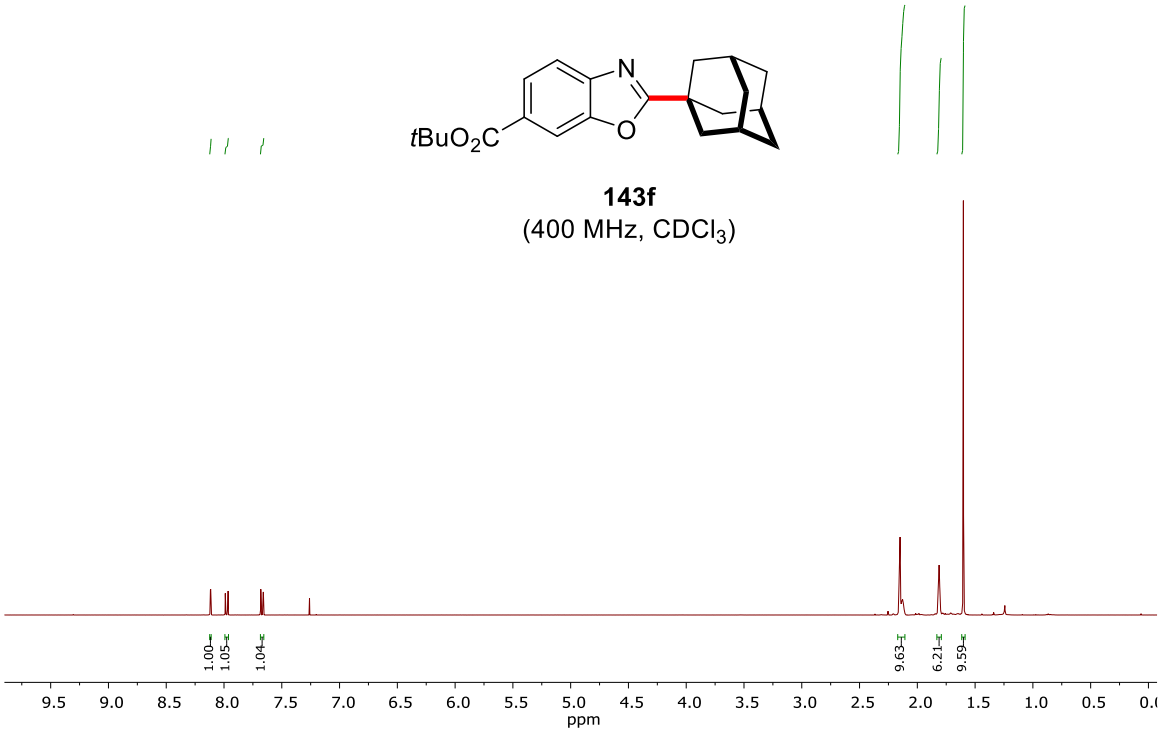

143f
(400 MHz, $CDCl_3$)

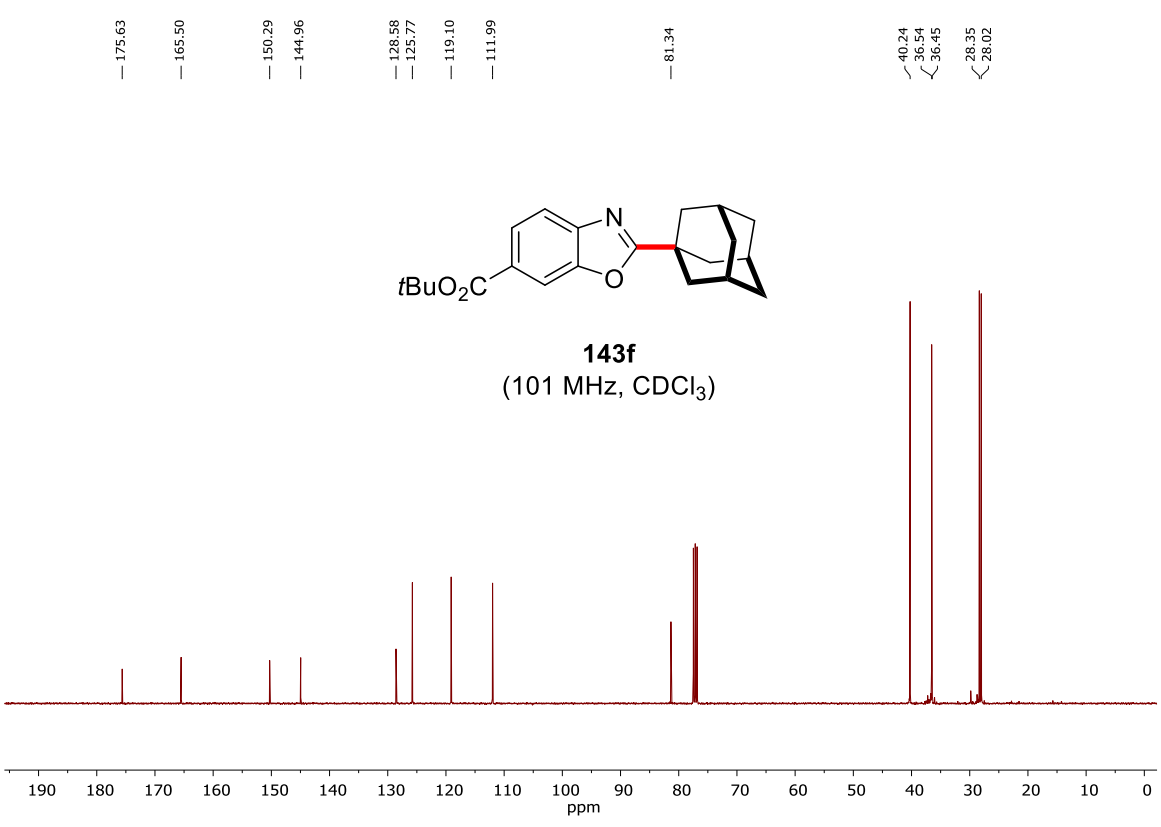

143f
(101 MHz, $CDCl_3$)

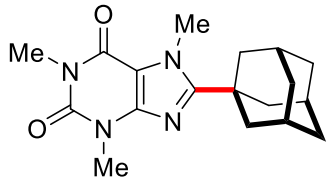

164
(400 MHz, $CDCl_3$)

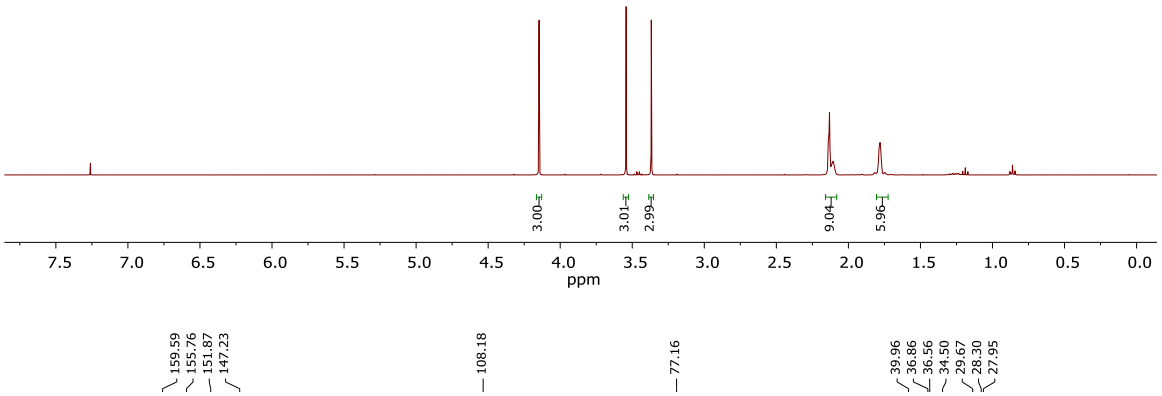

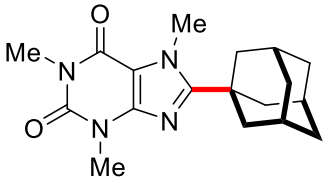

164
(101 MHz, $CDCl_3$)

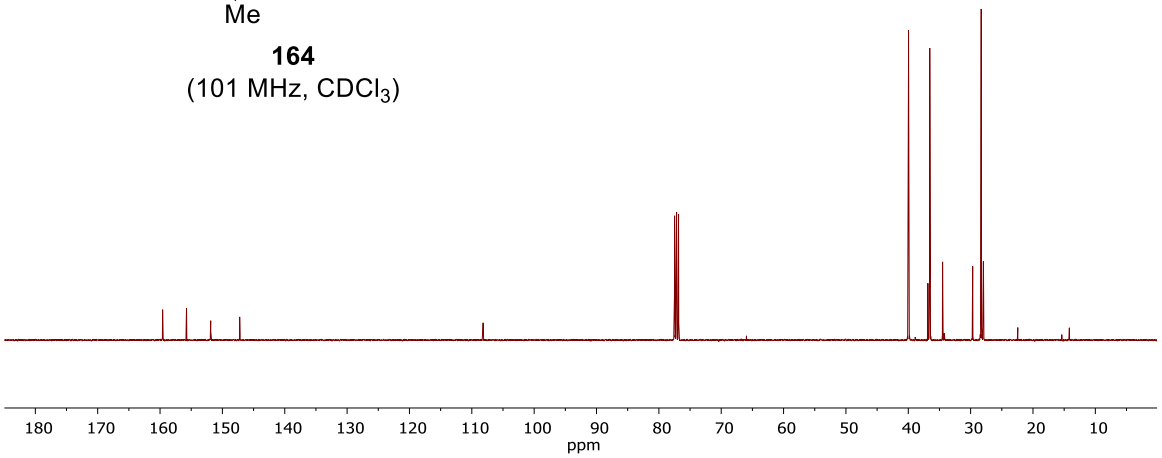

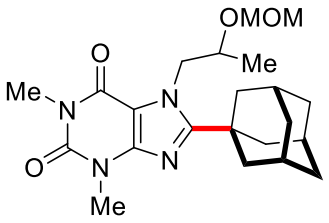

165
(400 MHz, $CDCl_3$)

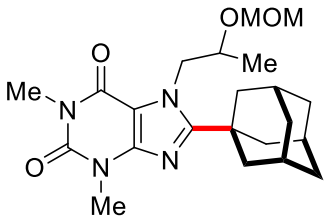

165
(101 MHz, $CDCl_3$)

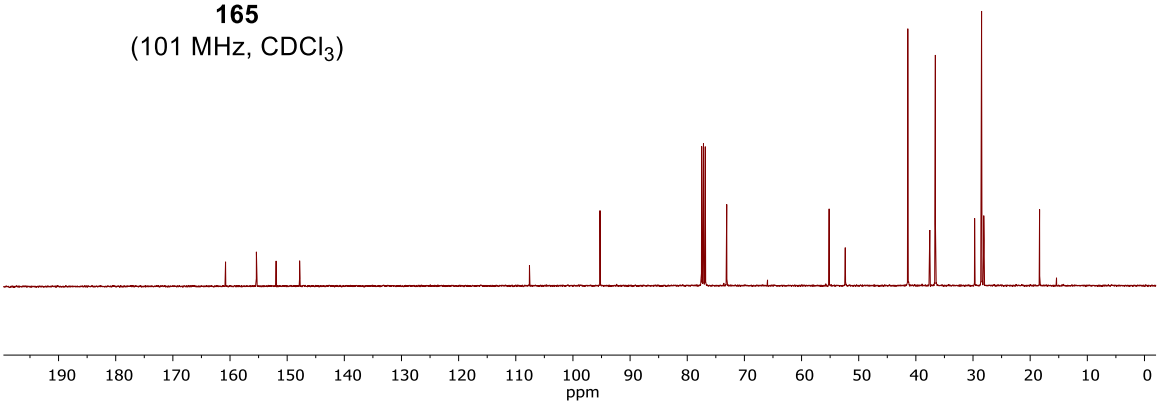

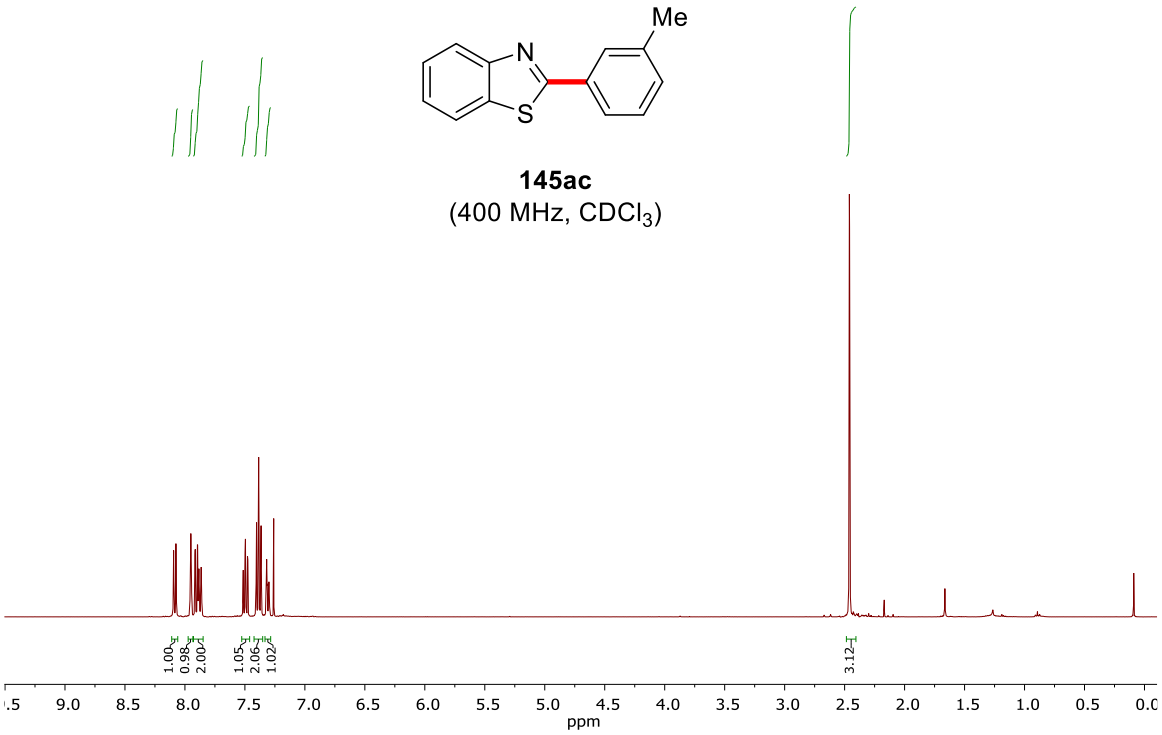
Me
N
S
145ac
(400 MHz, CDCl3)
1.00
0.98
2.00
1.05
2.06
1.02
3.12
ppm

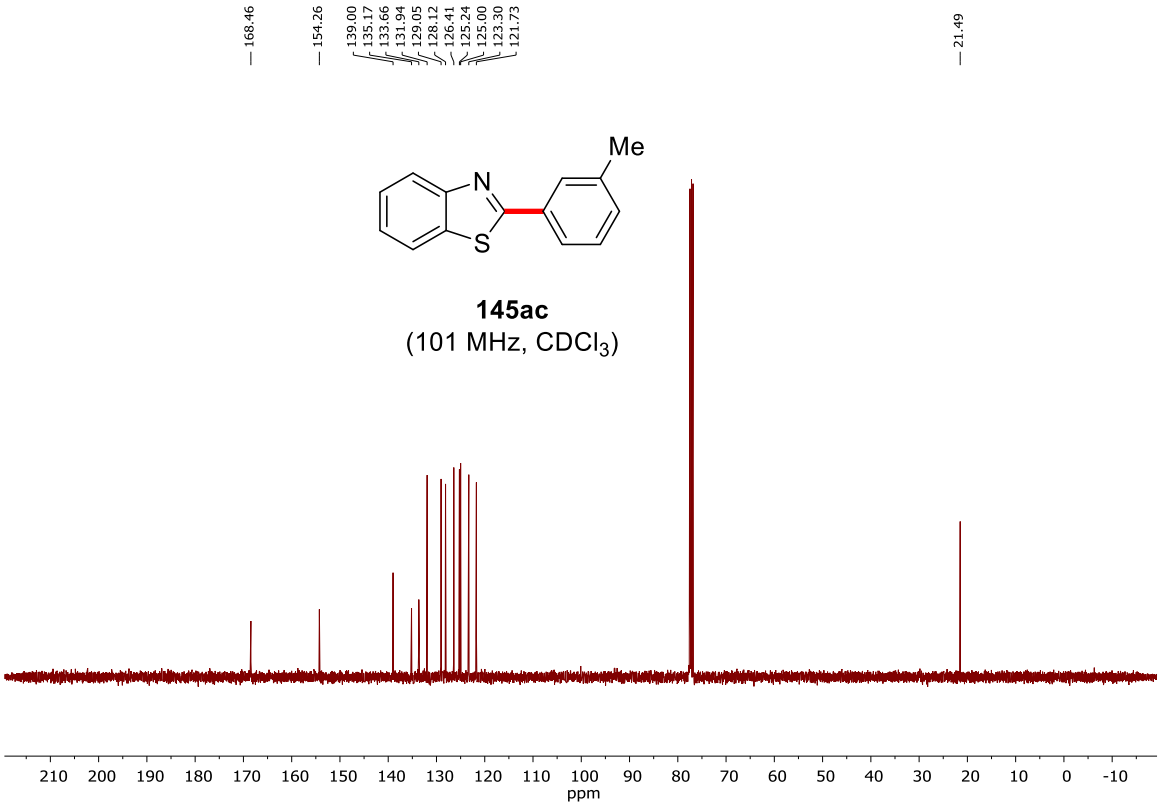
168.46
154.26
139.00
135.17
133.66
131.94
129.05
128.12
126.41
125.24
125.00
123.30
121.73
21.49
Me
N
S
145ac
(101 MHz, CDCl3)
ppm

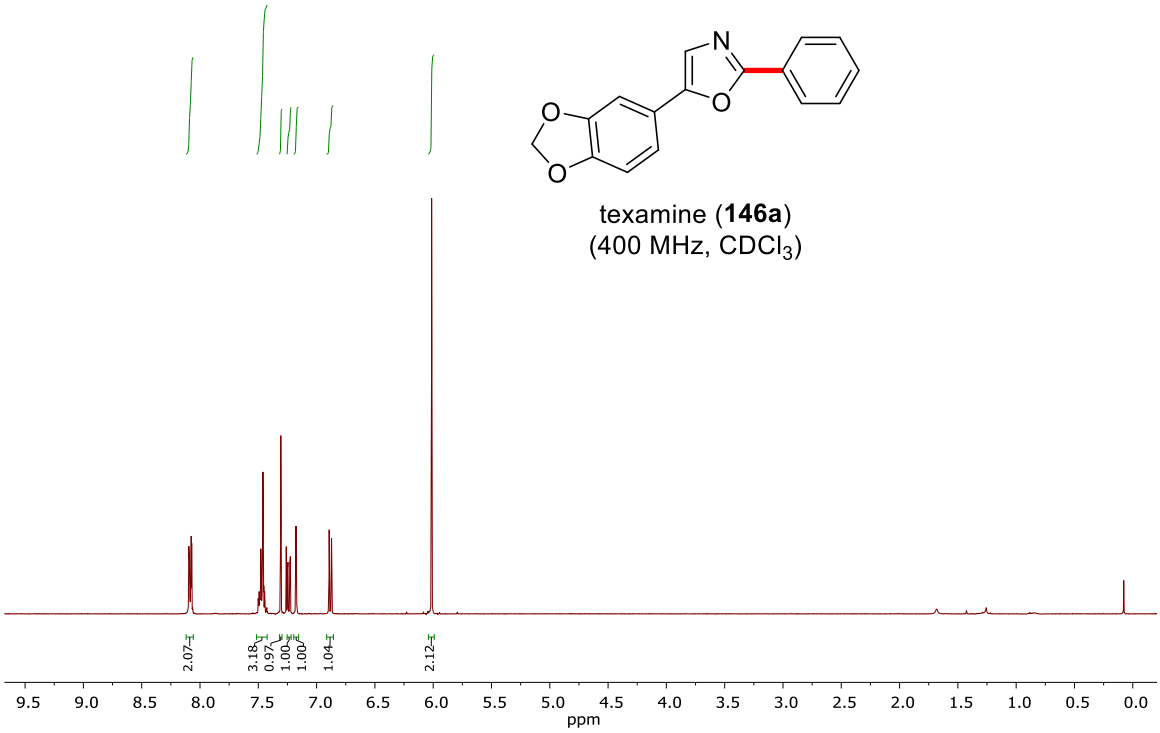
texamine (146a)
(400 MHz, CDCl3)
2.07
3.18
0.97
1.00
1.00
1.04
2.12
9.5 9.0 8.5 8.0 7.5 7.0 6.5 6.0 5.5 5.0 4.5 4.0 3.5 3.0 2.5 2.0 1.5 1.0 0.5 0.0
ppm

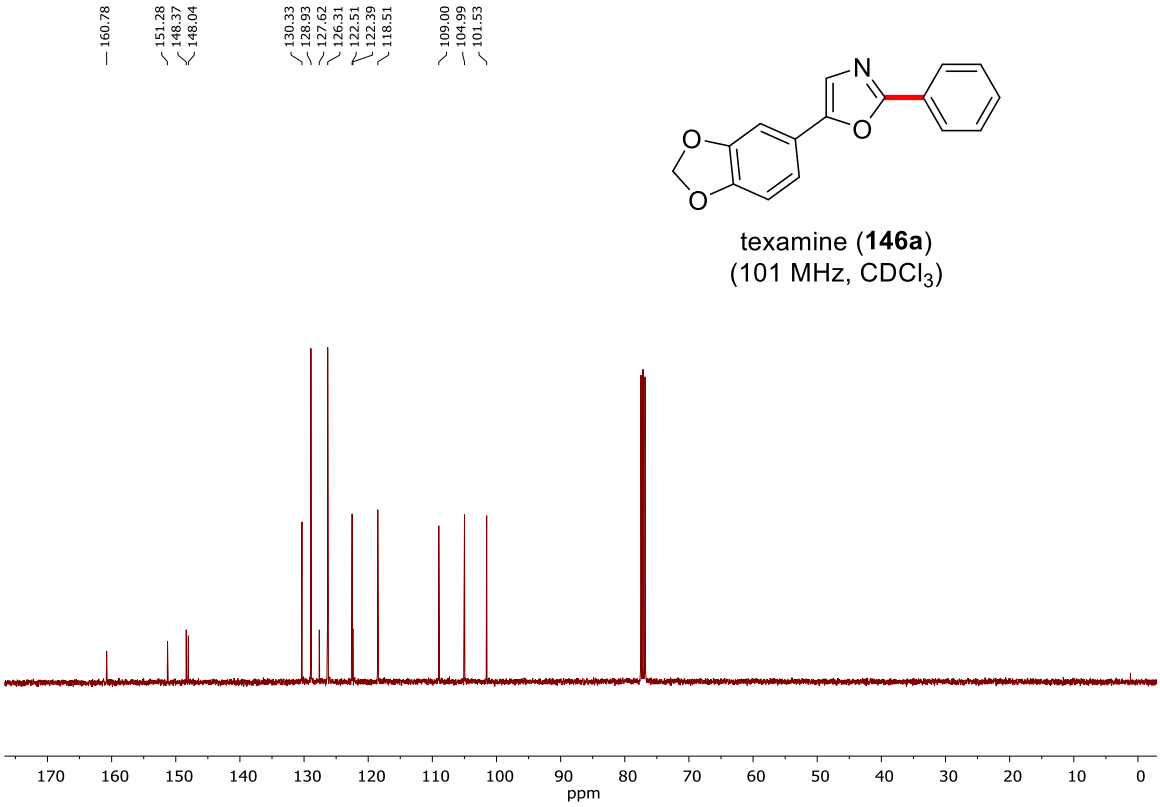
160.78
151.28
148.37
148.04
130.33
128.93
127.62
126.31
122.51
122.39
118.51
109.00
104.99
101.53
texamine (146a)
(101 MHz, CDCl3)
170 160 150 140 130 120 110 100 90 80 70 60 50 40 30 20 10 0
ppm

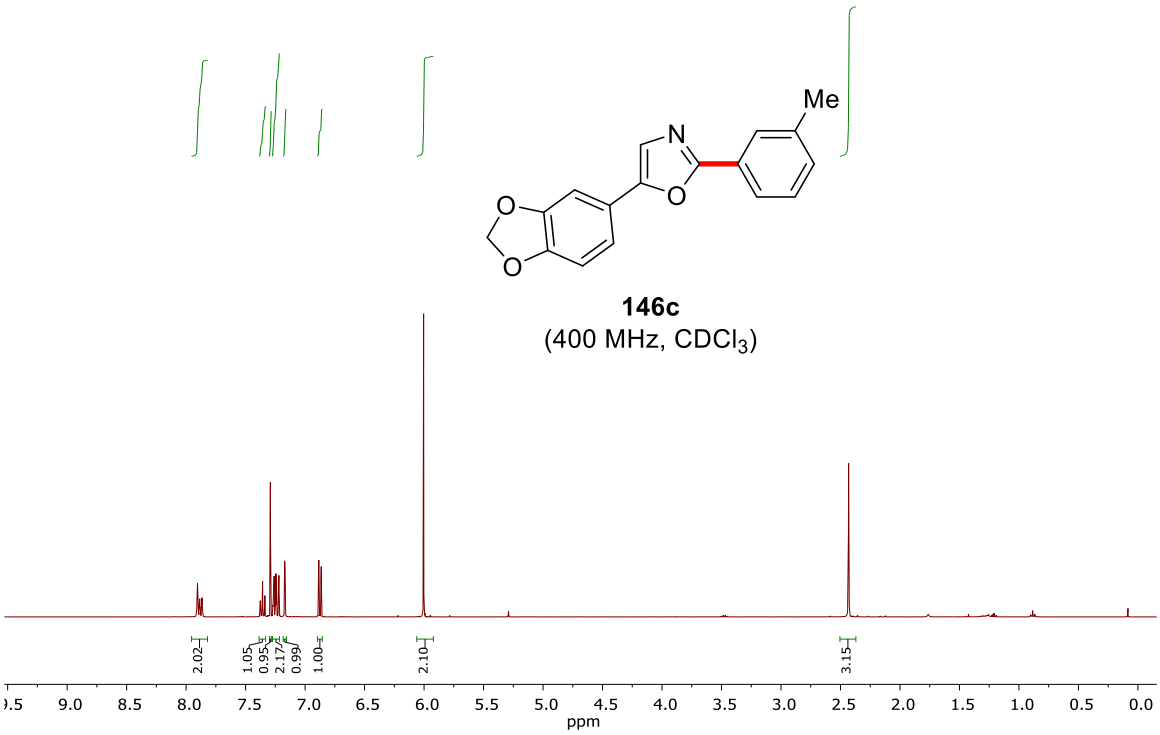
Me
N
O
O
O
146c
(400 MHz, CDCl3)
2.02
1.05
0.95
2.17
0.99
1.00
2.10
3.15
ppm

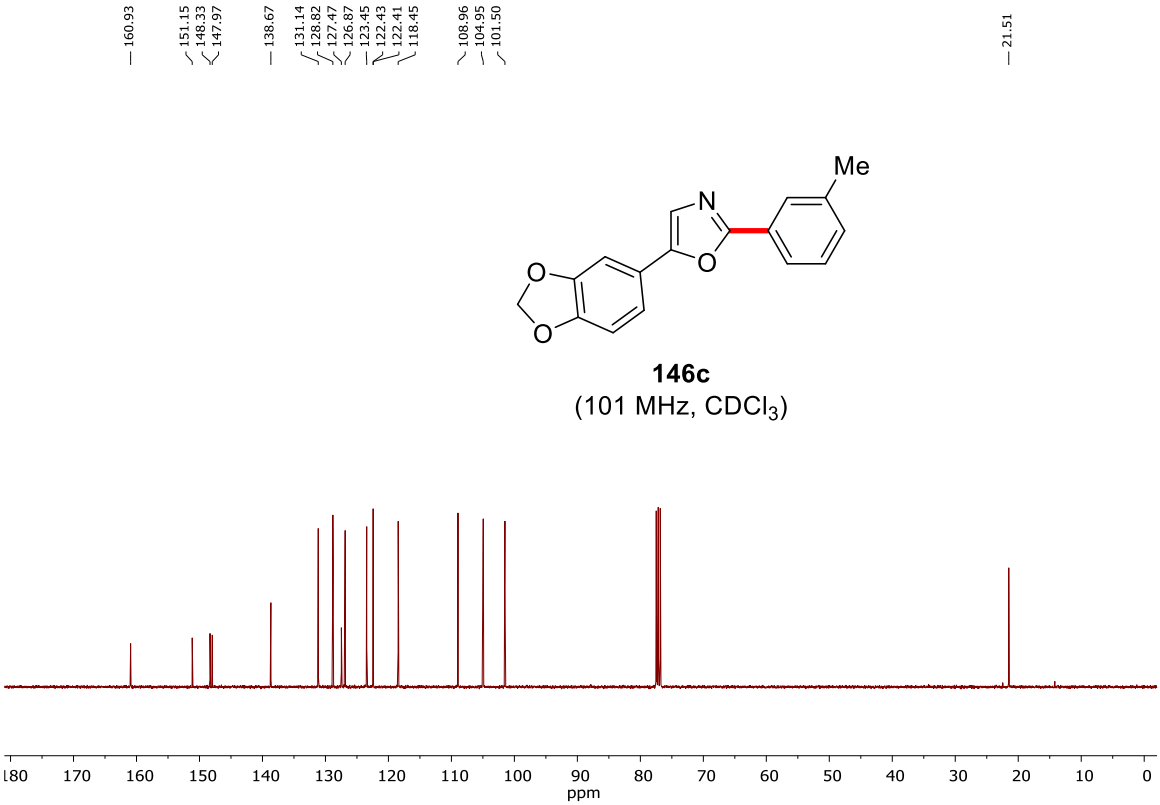
160.93
151.15
148.33
147.97
138.67
131.14
128.82
127.47
126.87
123.45
122.43
122.41
118.45
108.96
104.95
101.50
21.51
Me
N
O
O
O
146c
(101 MHz, CDCl3)
ppm

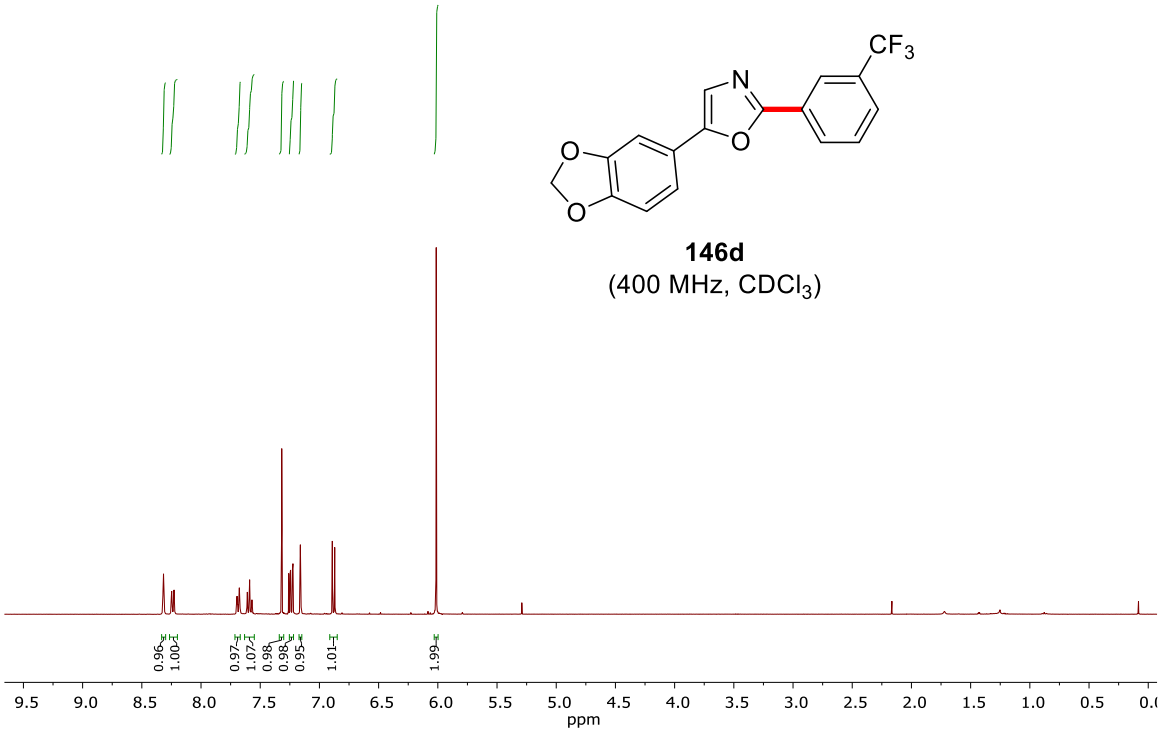

146d
(400 MHz, $CDCl_3$)

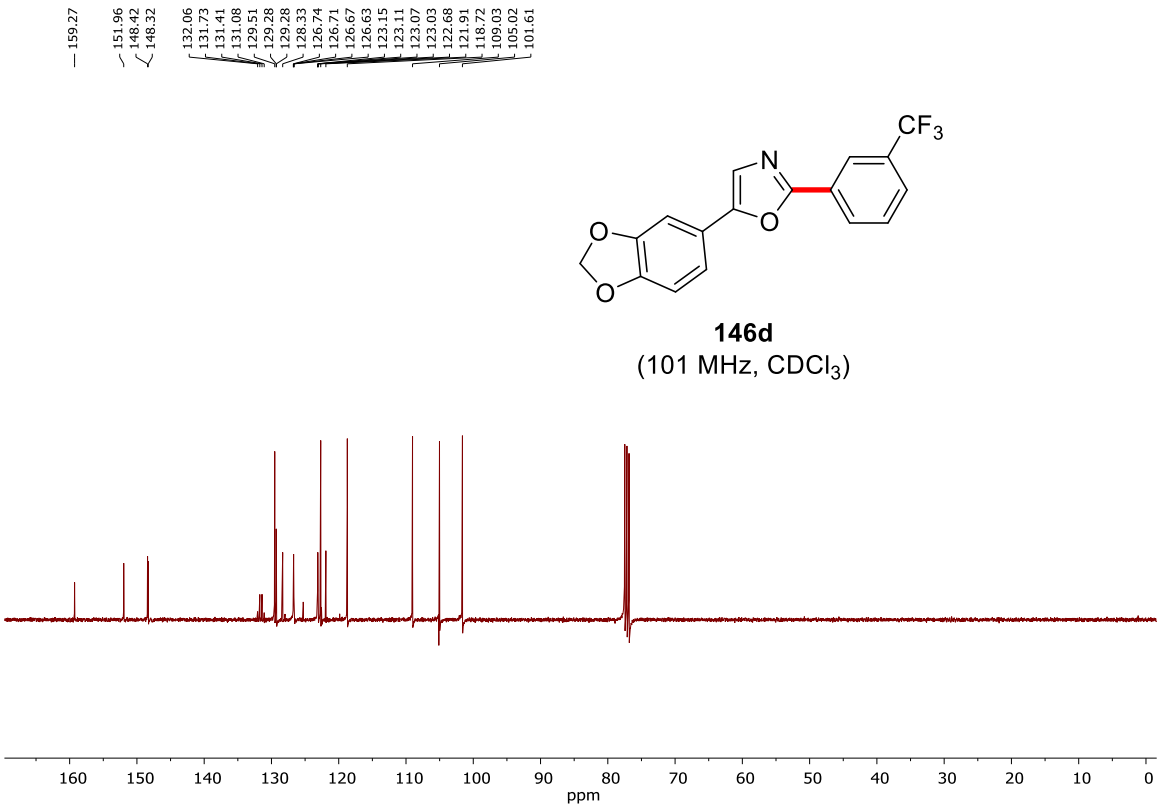

146d
(101 MHz, $CDCl_3$)

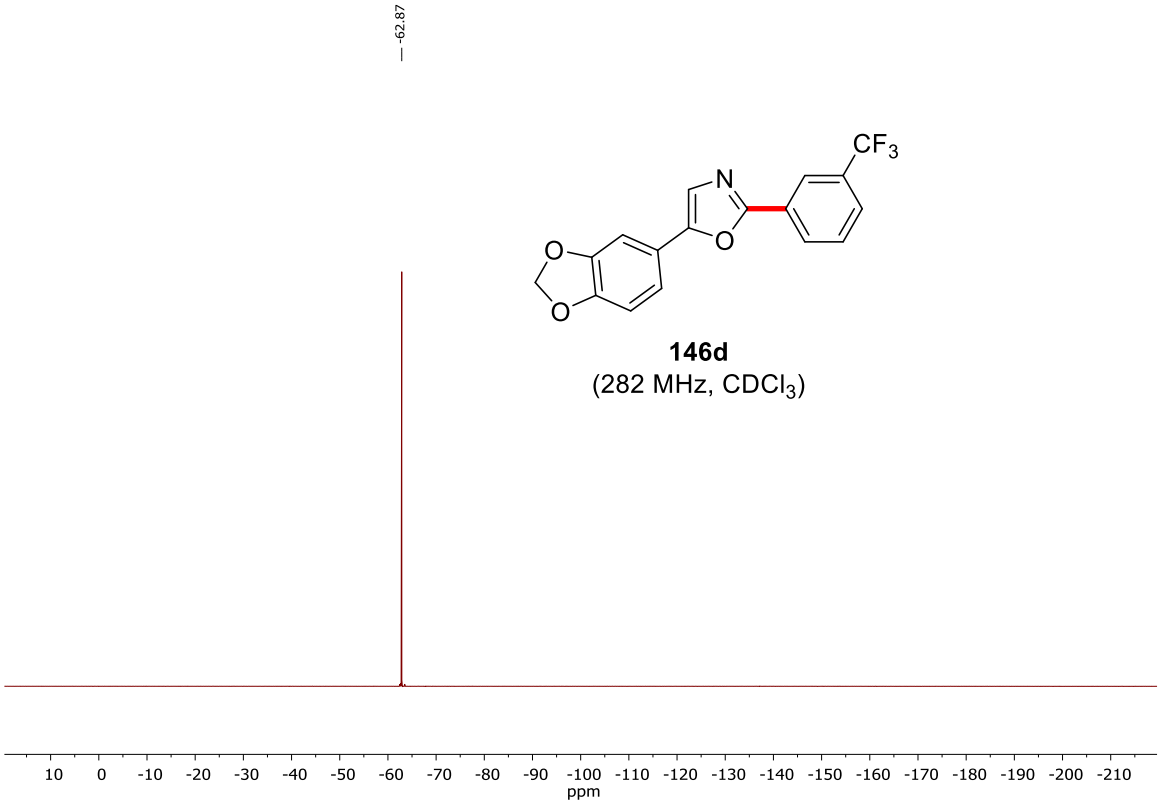

146d
(282 MHz, $CDCl_3$)

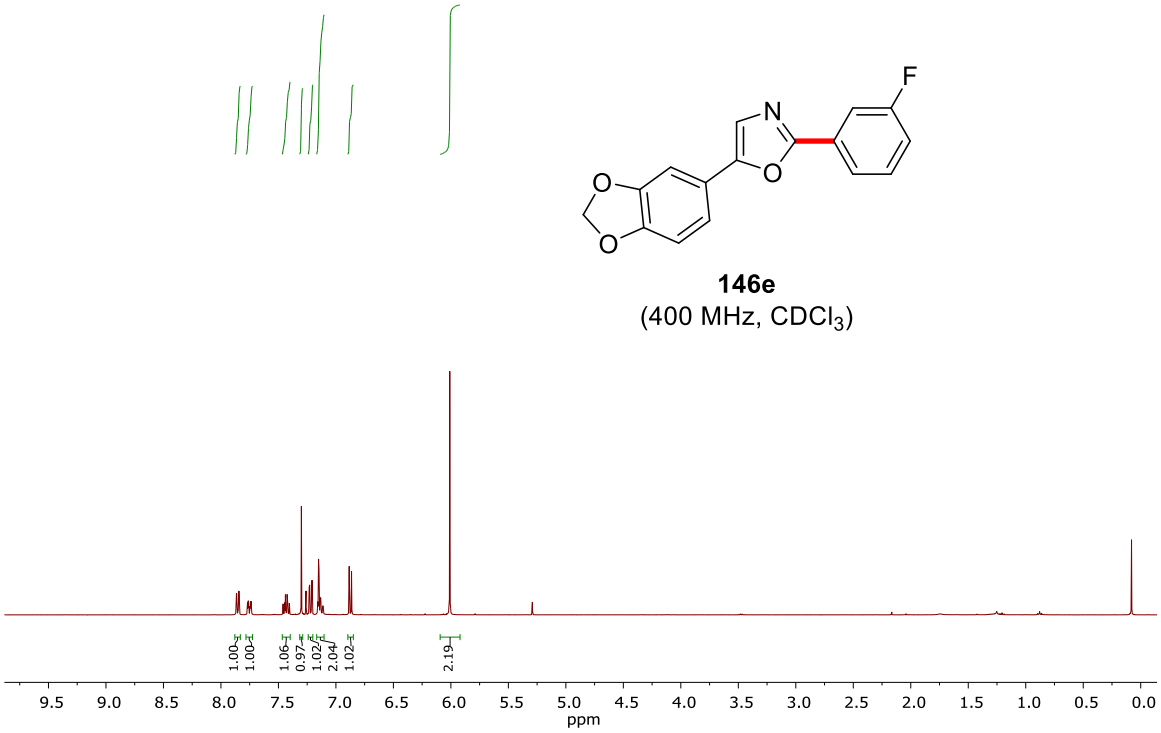

146e
(400 MHz, $CDCl_3$)

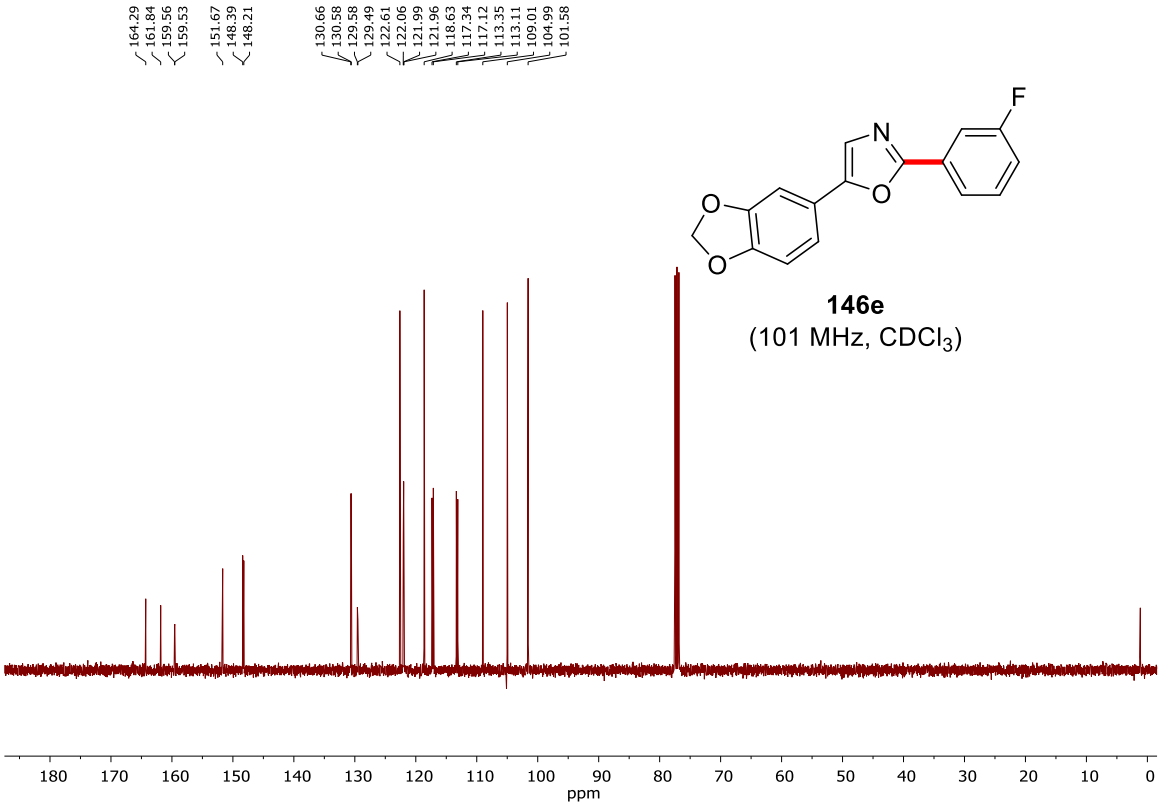

146e
(101 MHz, $CDCl_3$)

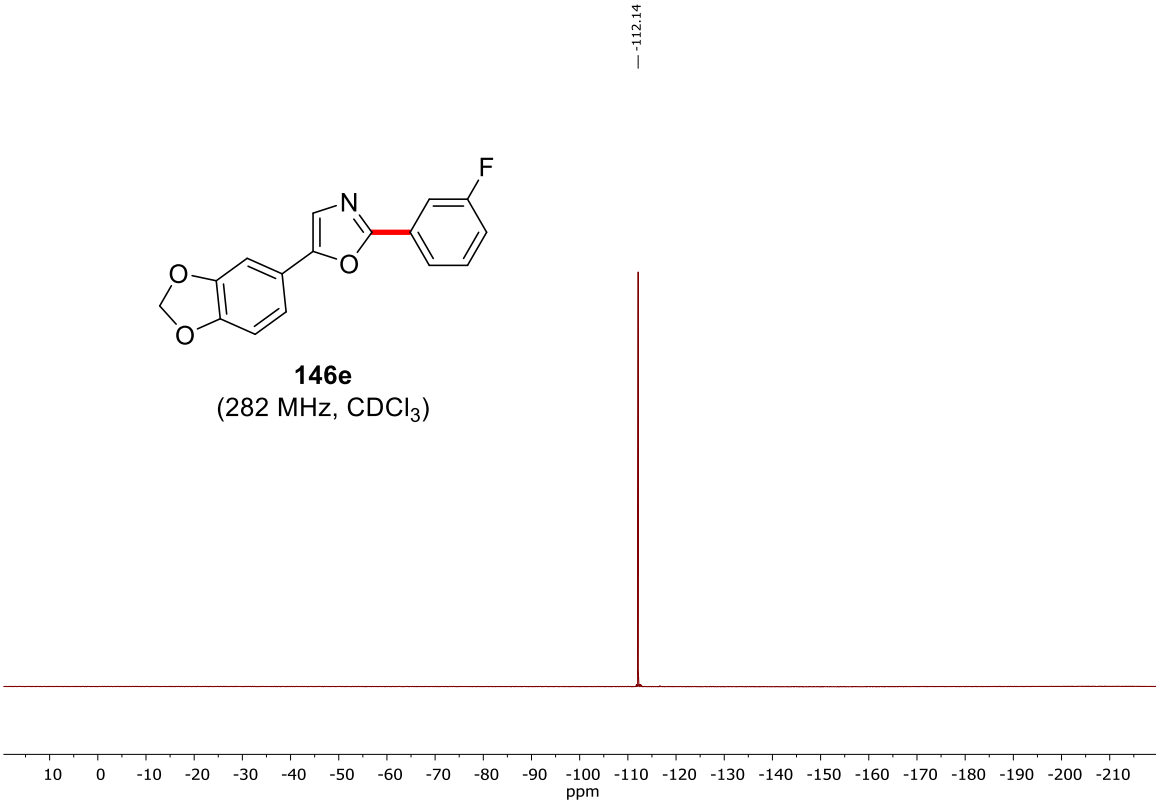
-112.14
F
N
O
O
O
146e
(282 MHz, CDCl3)
10 0 -10 -20 -30 -40 -50 -60 -70 -80 -90 -100 -110 -120 -130 -140 -150 -160 -170 -180 -190 -200 -210
ppm

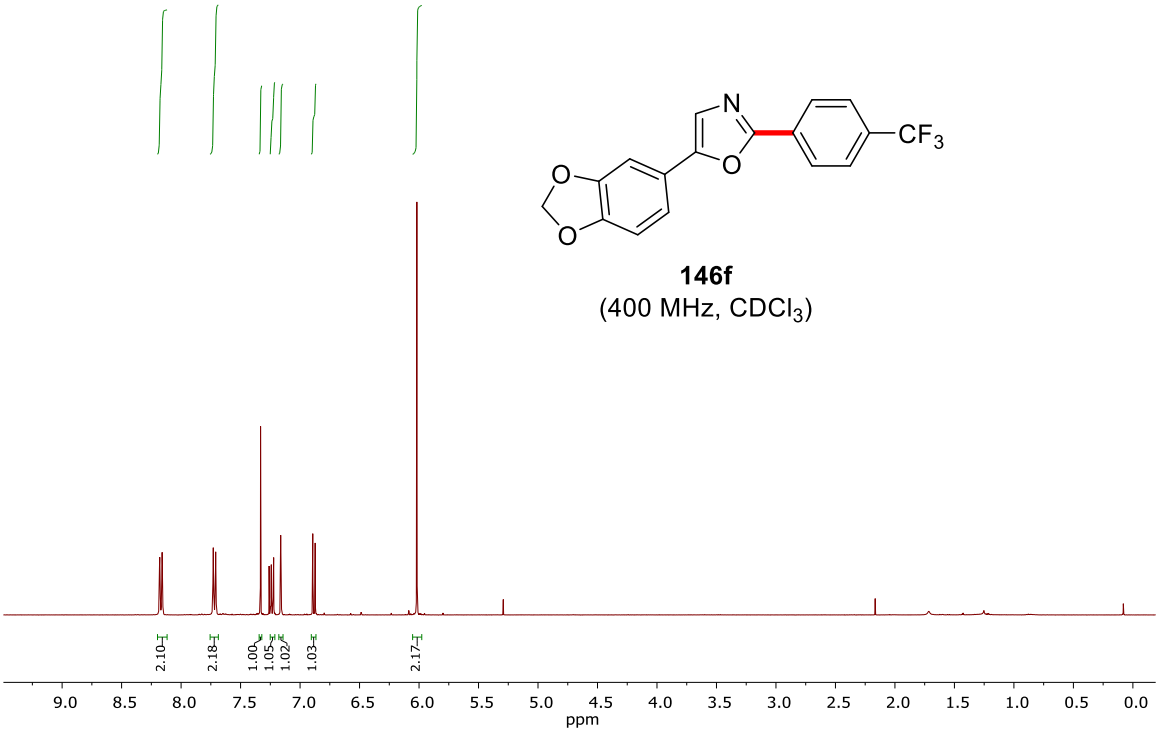

146f
(400 MHz, $CDCl_3$)

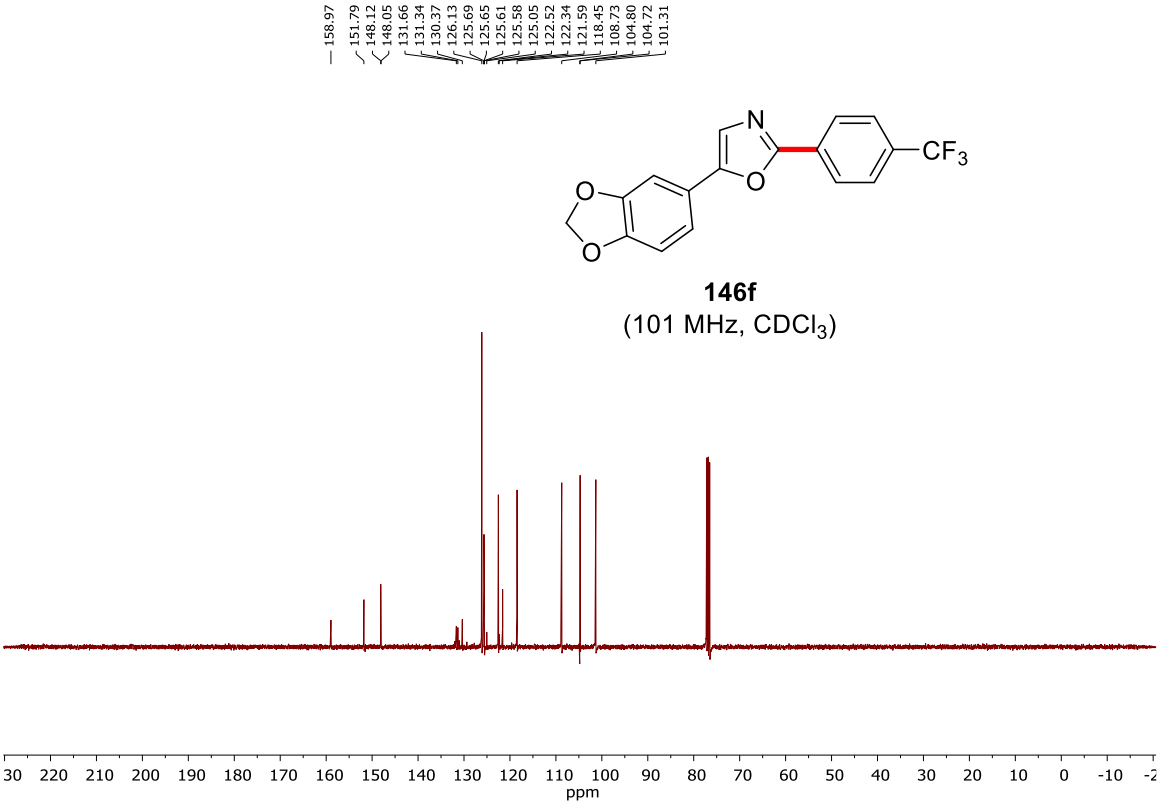

146f
(101 MHz, $CDCl_3$)

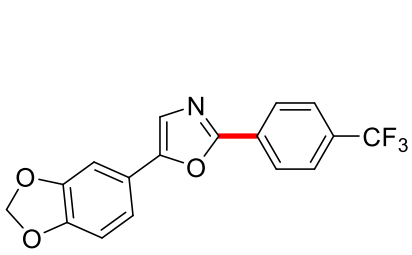

146f
(282 MHz, $CDCl_3$)

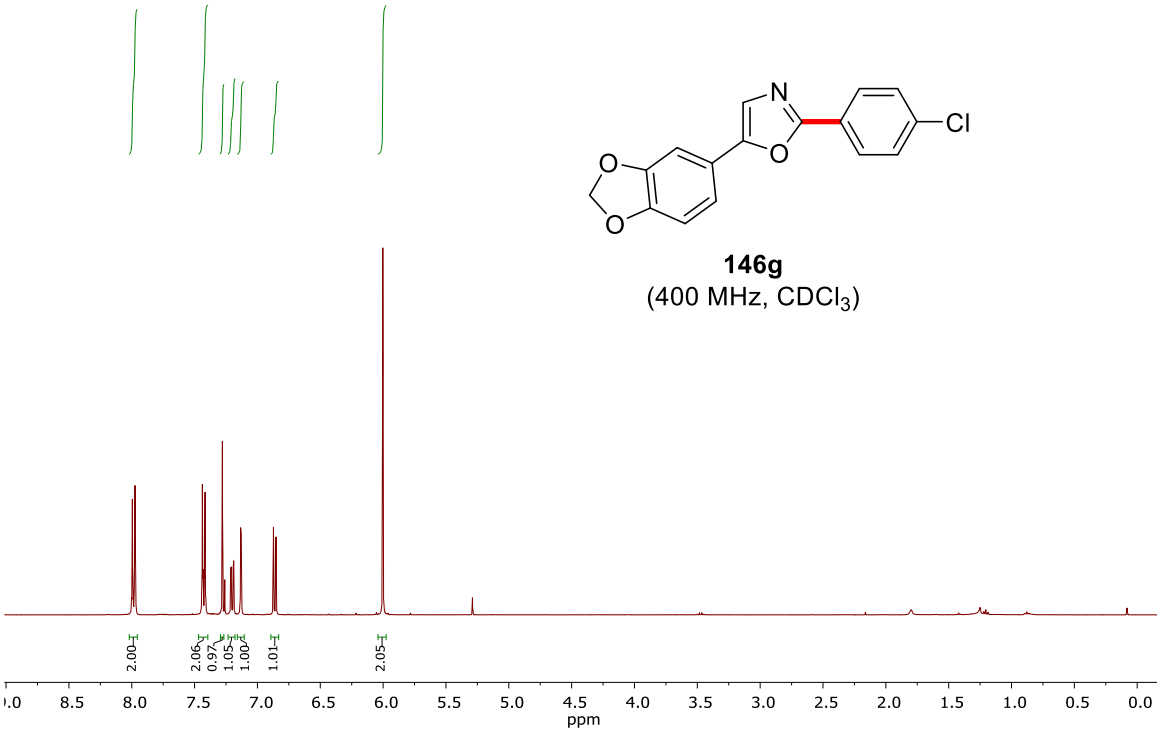

146g
(400 MHz, $CDCl_3$)

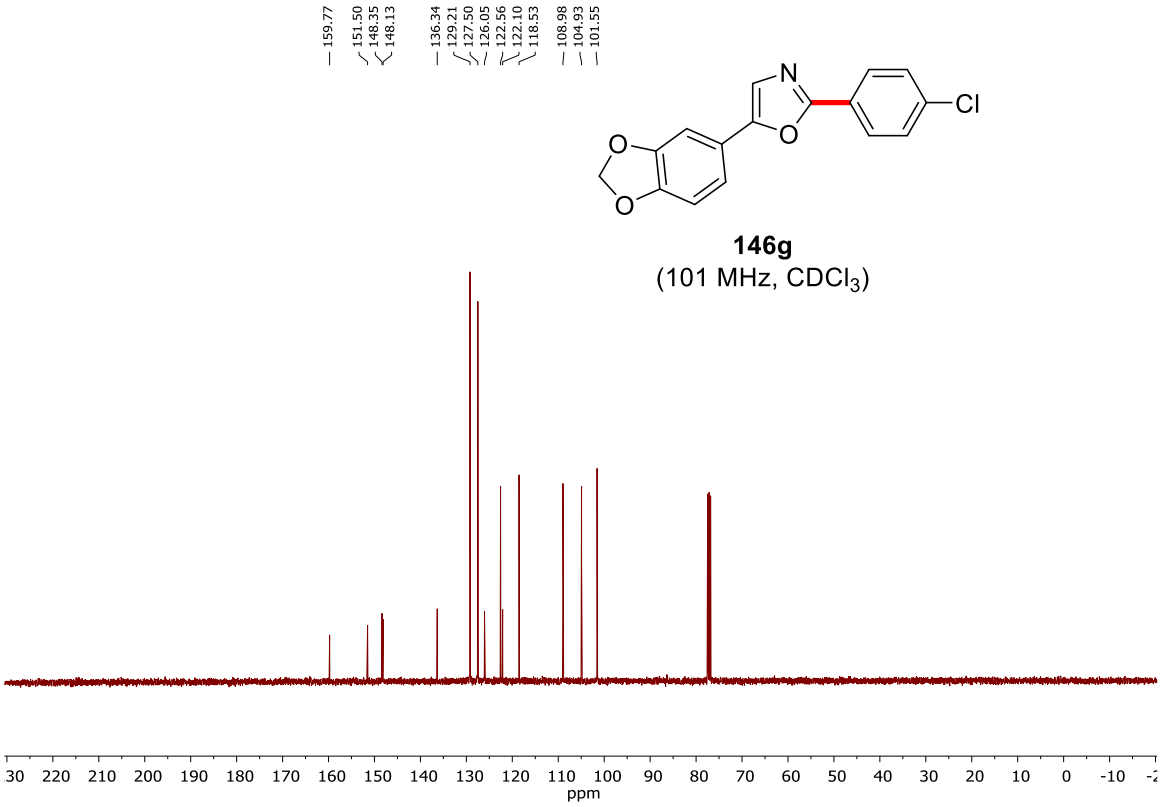

146g
(101 MHz, $CDCl_3$)

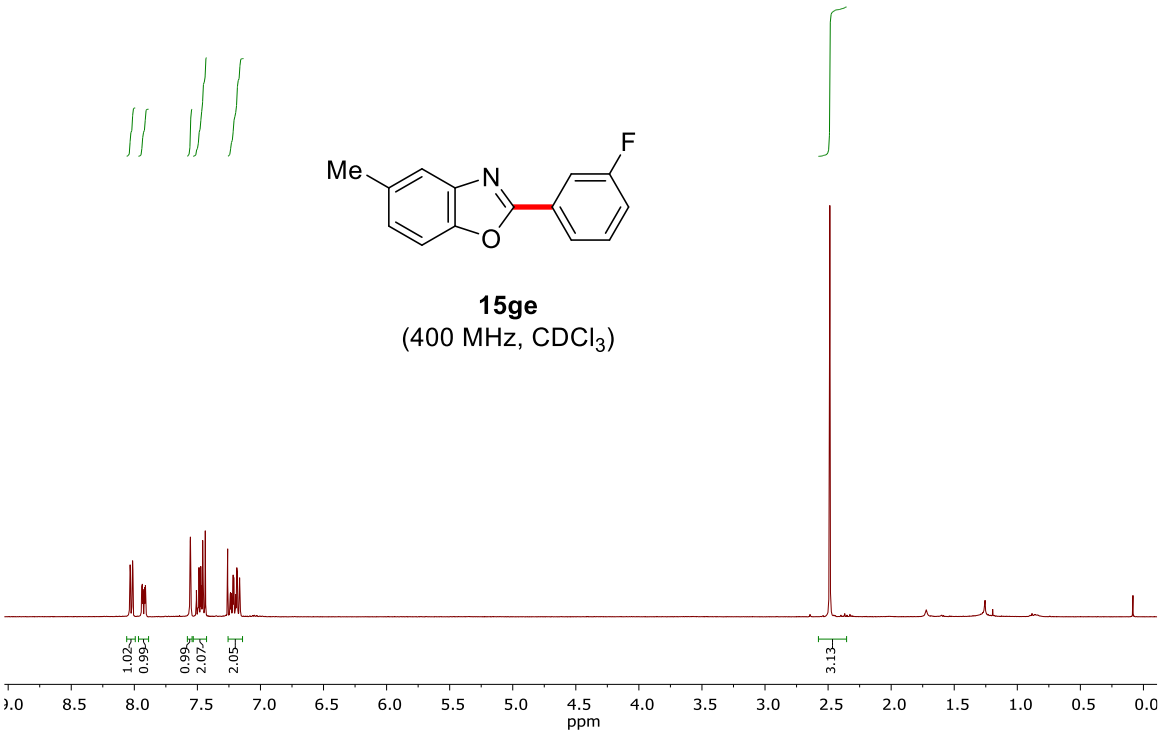

15ge
(400 MHz, $CDCl_3$)

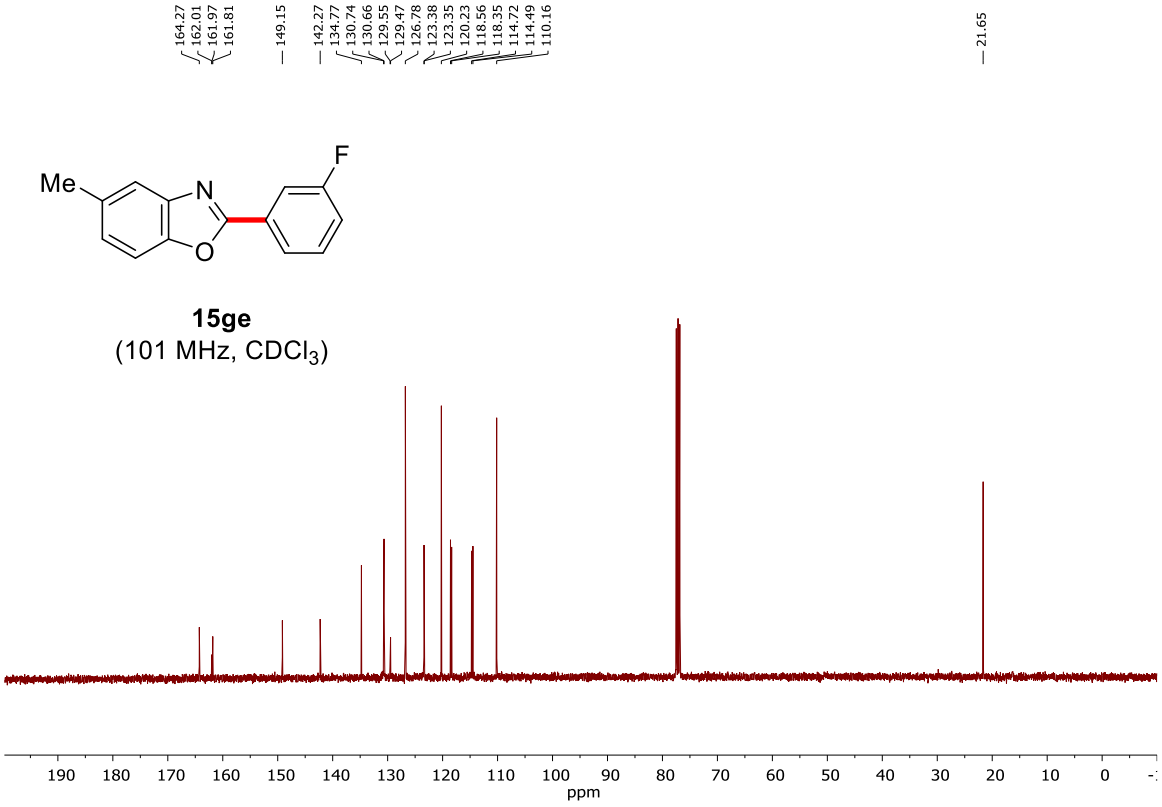

15ge
(101 MHz, $CDCl_3$)

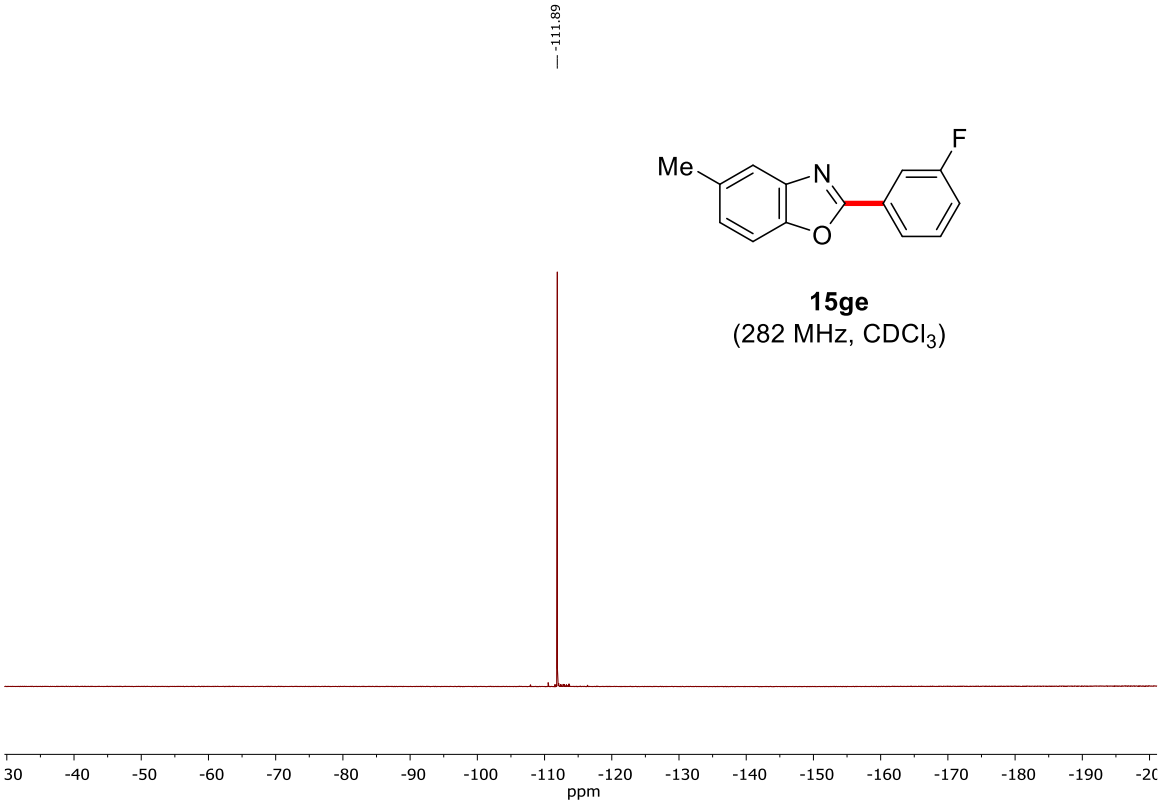

15ge
(282 MHz, $CDCl_3$)

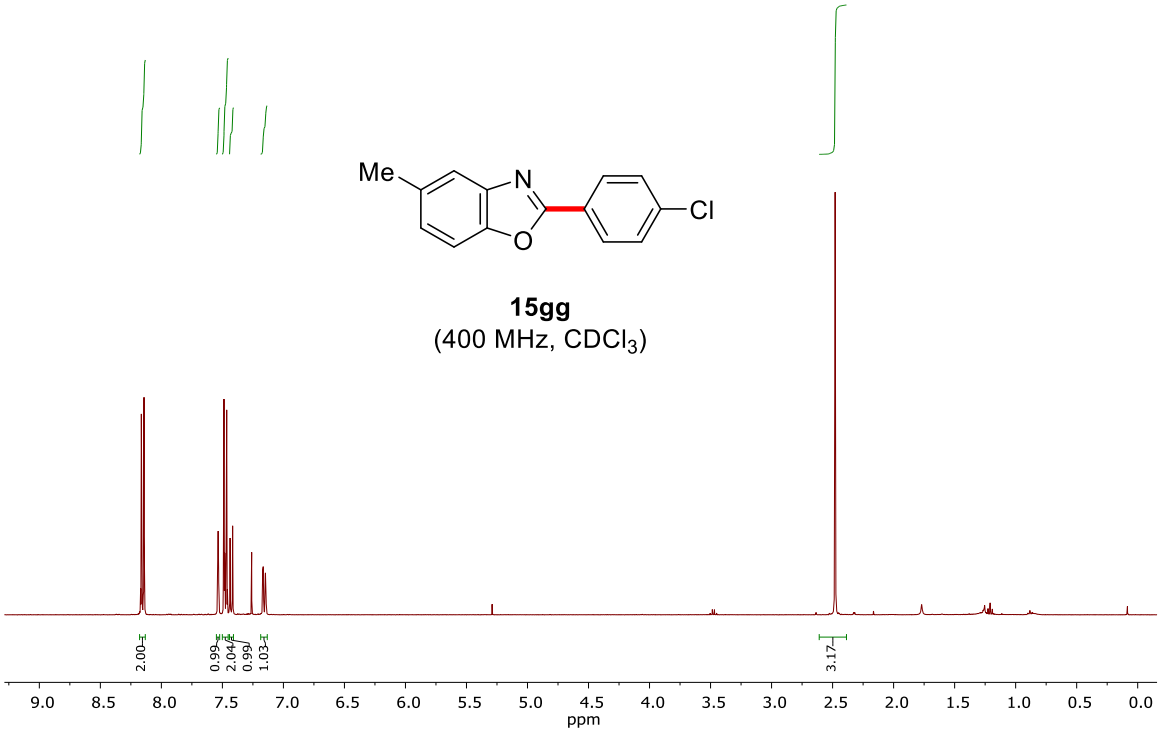

15gg
(400 MHz, $CDCl_3$)

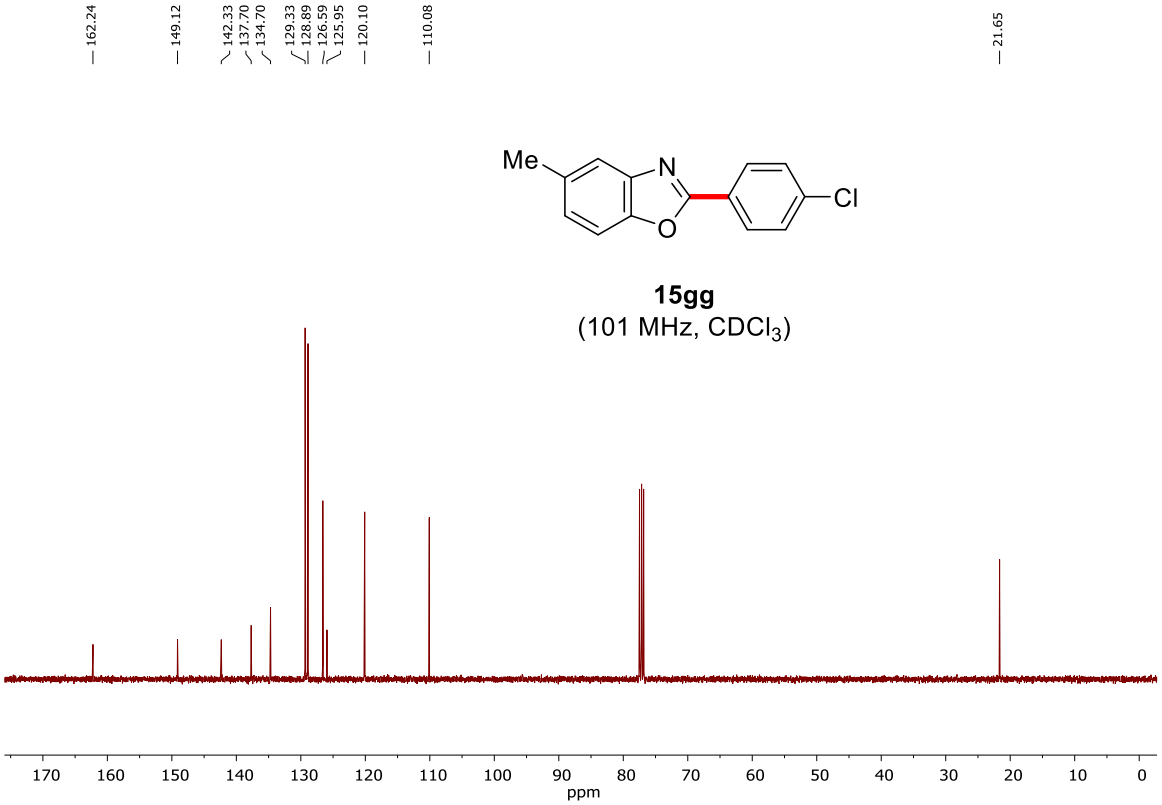

15gg
(101 MHz, $CDCl_3$)

Compounds **145bc** to **145hc** were prepared and characterized by N. Imse:

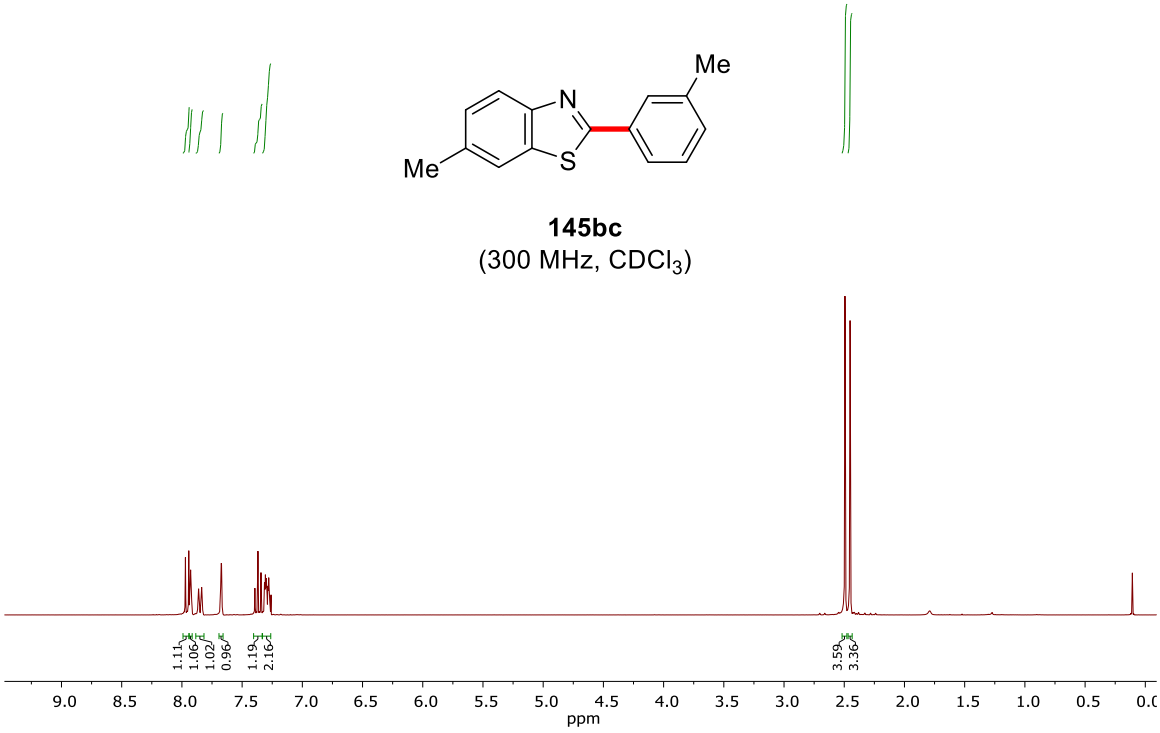

145bc
(300 MHz, $CDCl_3$)

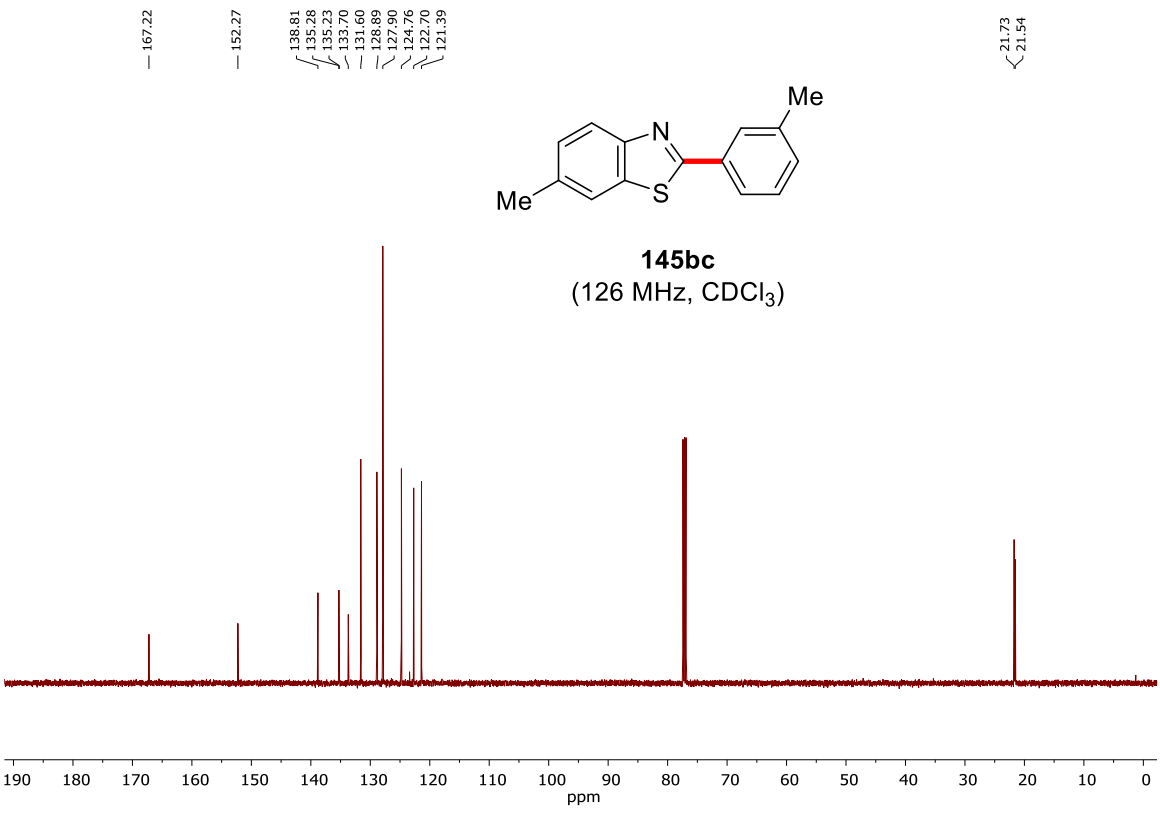

145bc
(126 MHz, $CDCl_3$)

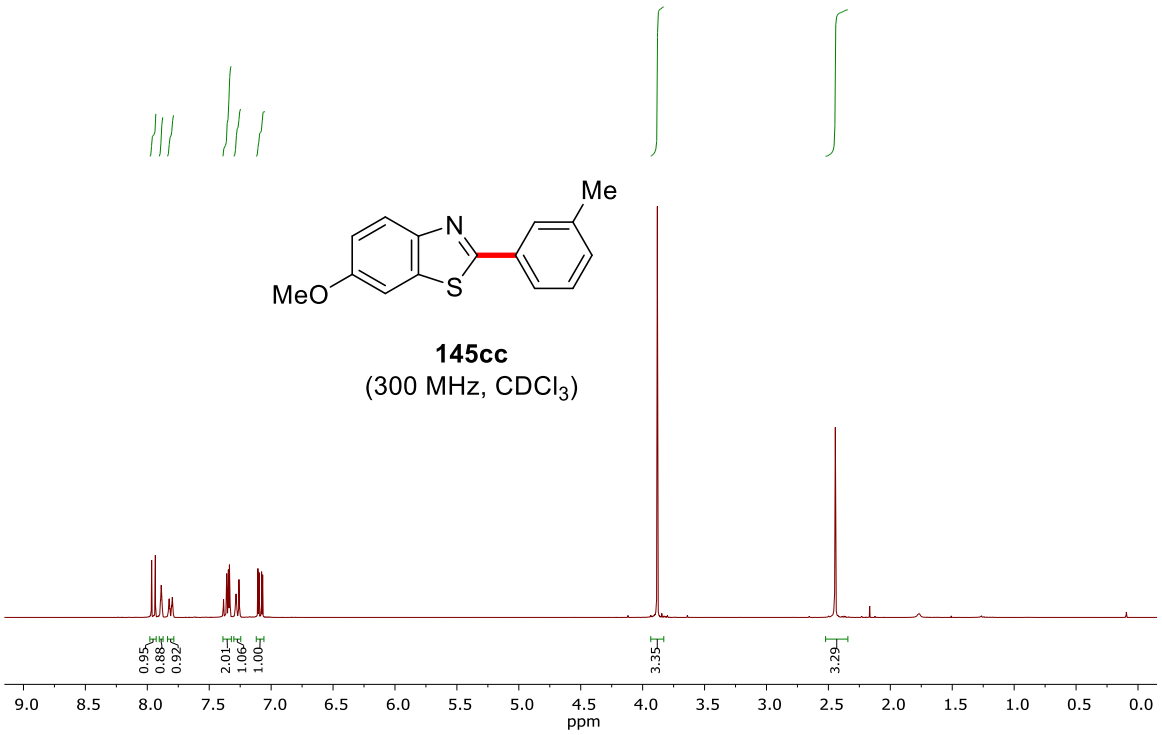

145cc
(300 MHz, $CDCl_3$)

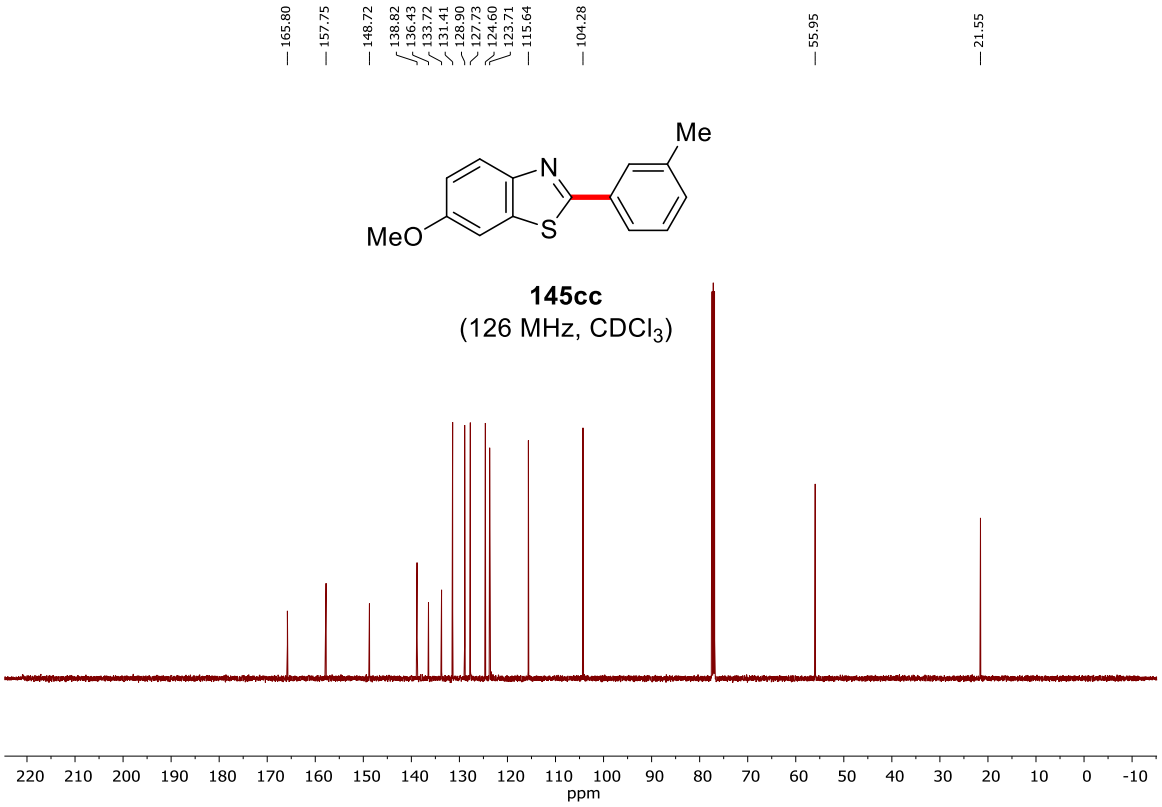

145cc
(126 MHz, $CDCl_3$)

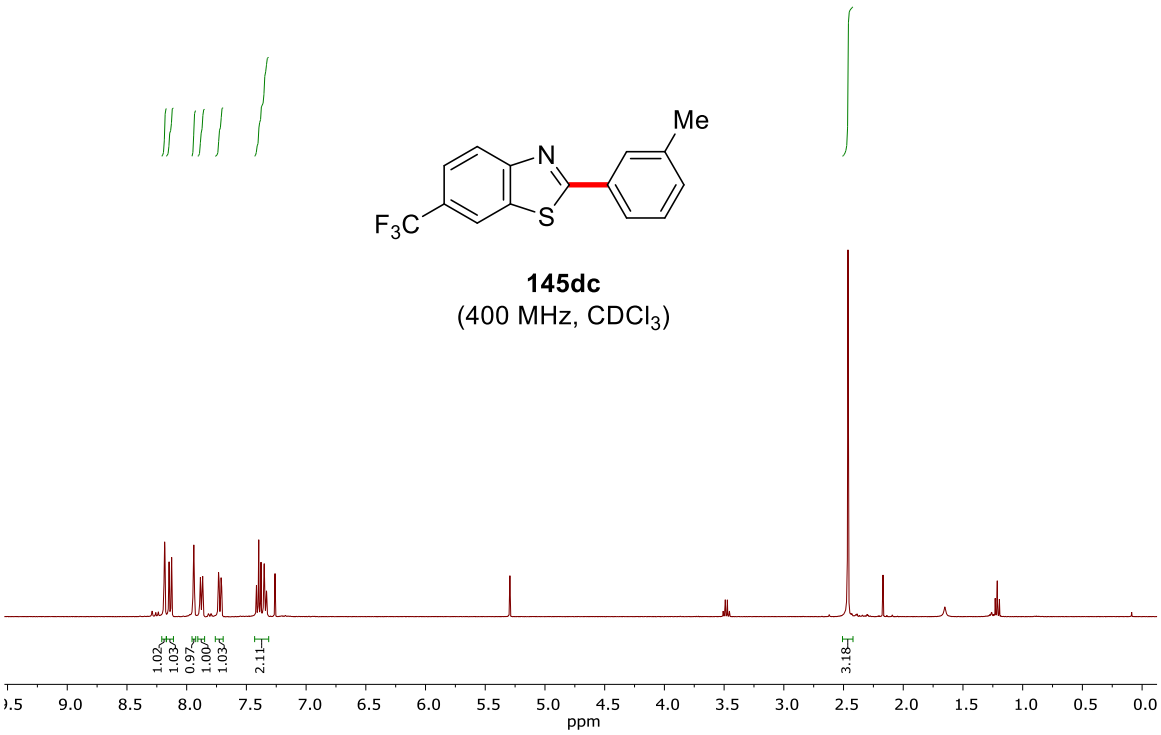

145dc
(400 MHz, $CDCl_3$)

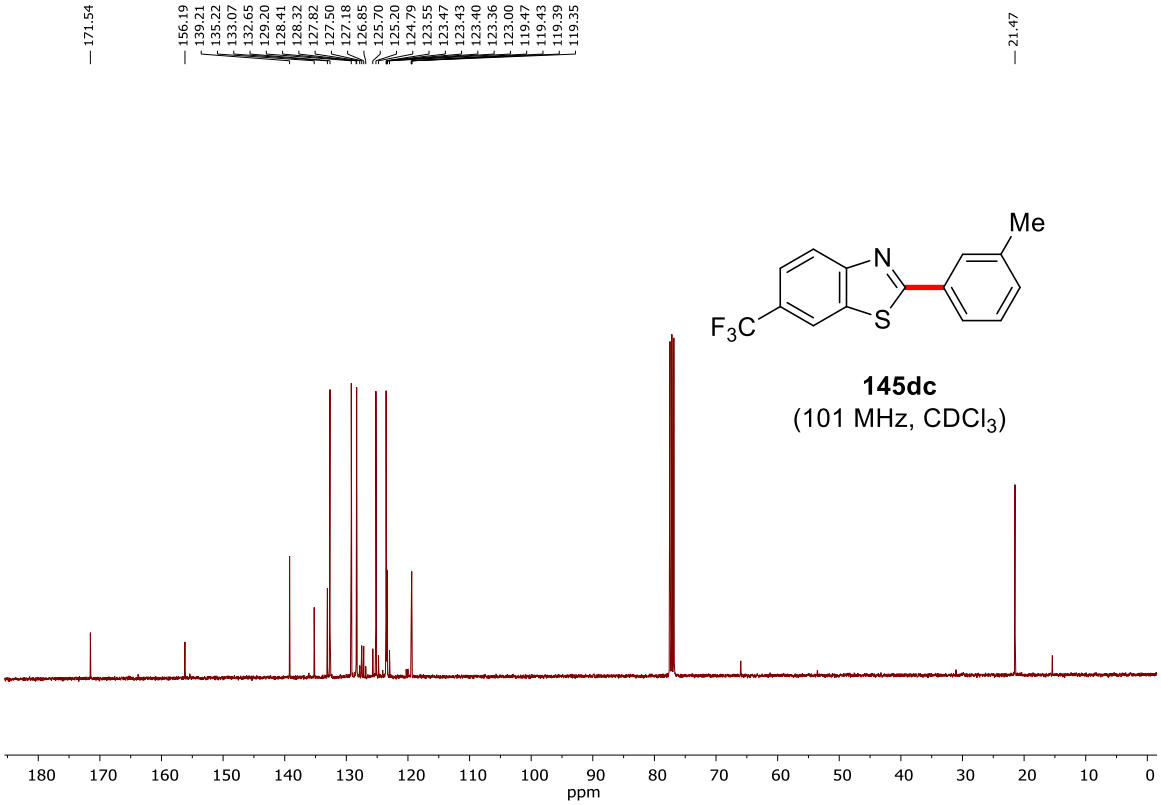

145dc
(101 MHz, $CDCl_3$)

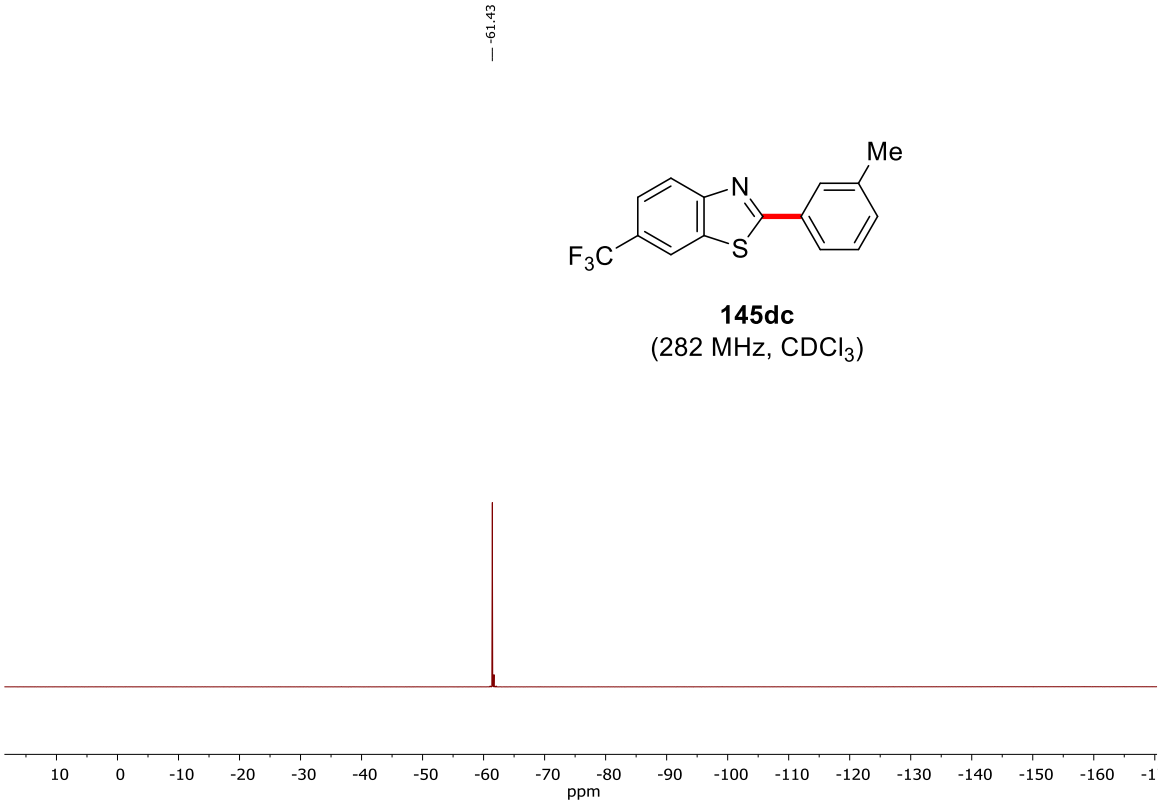

145dc
(282 MHz, $CDCl_3$)

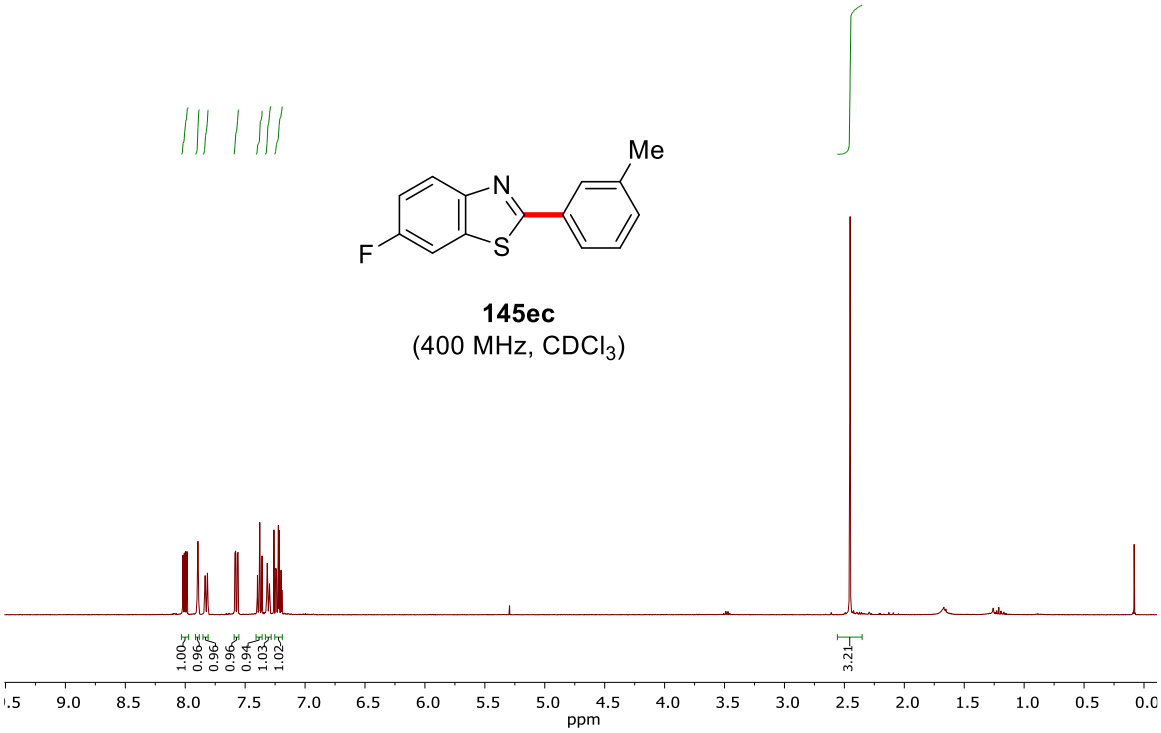

145ec
(400 MHz, $CDCl_3$)

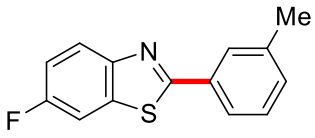

145ec
(101 MHz, $CDCl_3$)

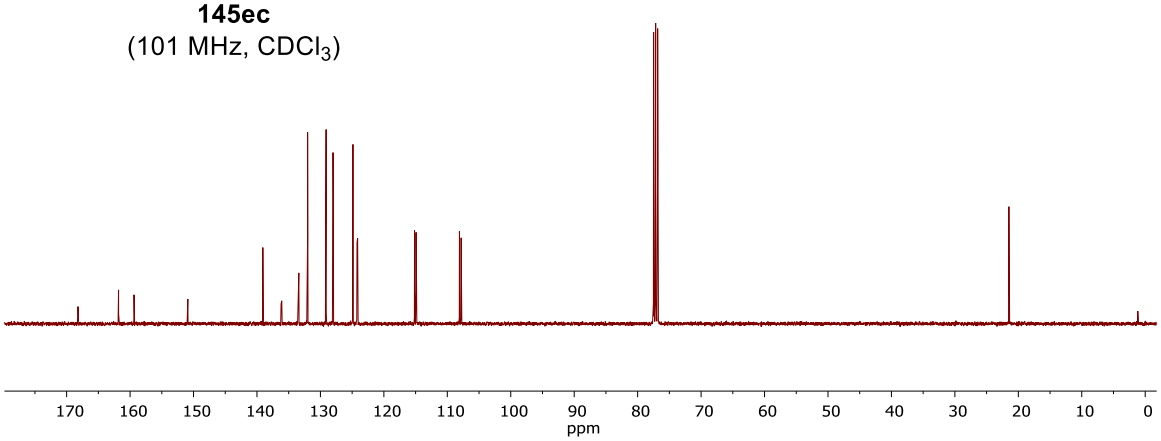

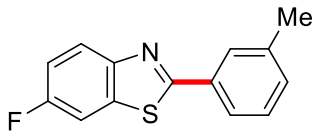

145ec
(282 MHz, $CDCl_3$)

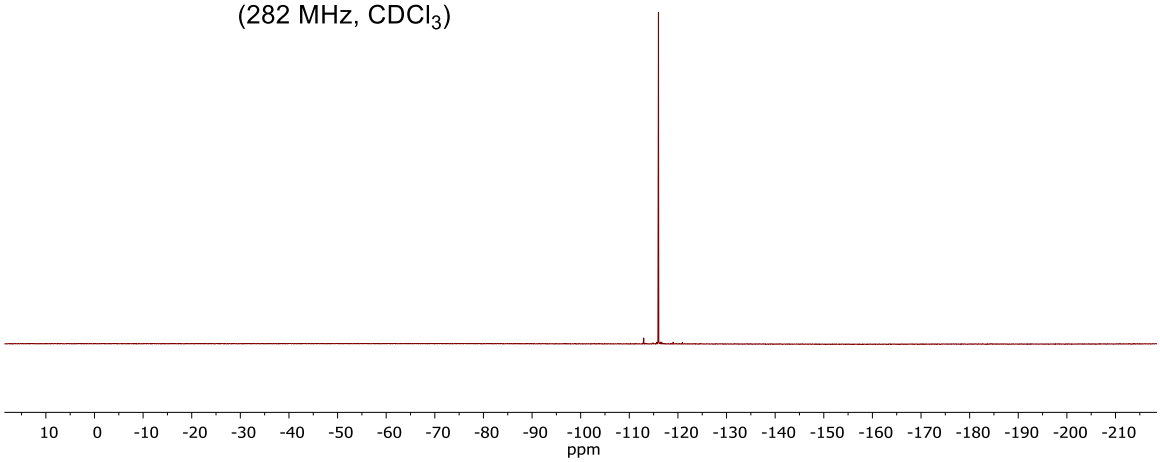

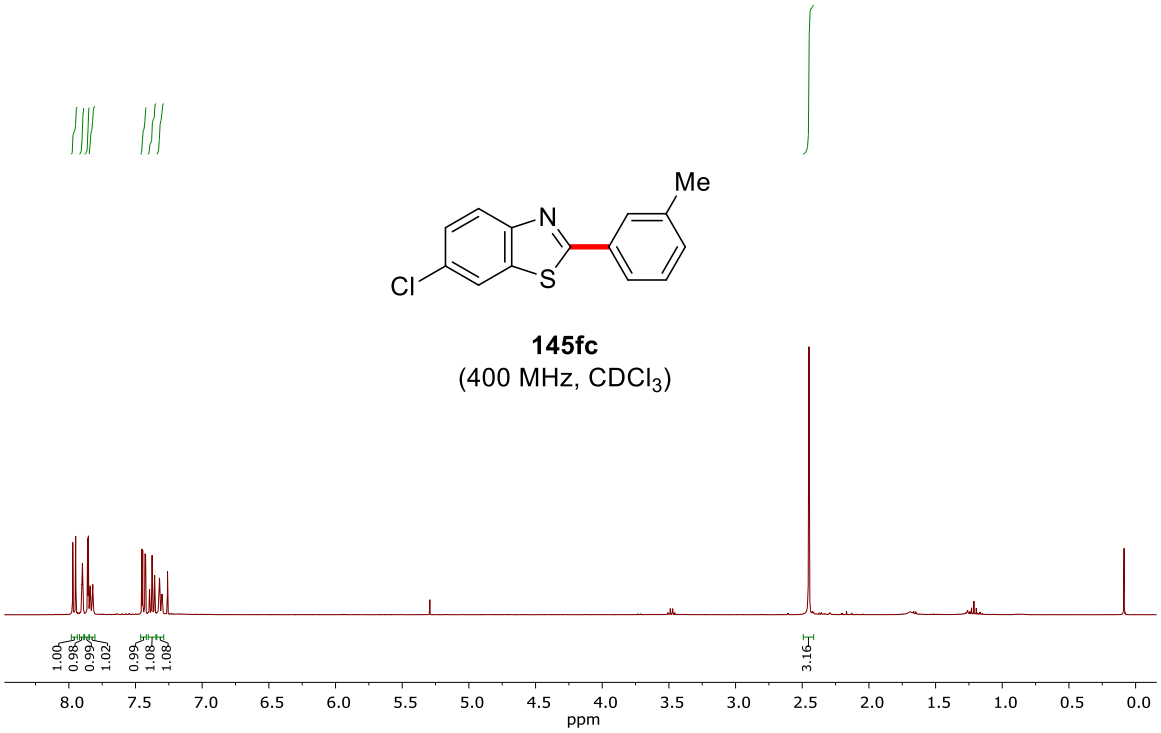

145fc
(400 MHz, $CDCl_3$)

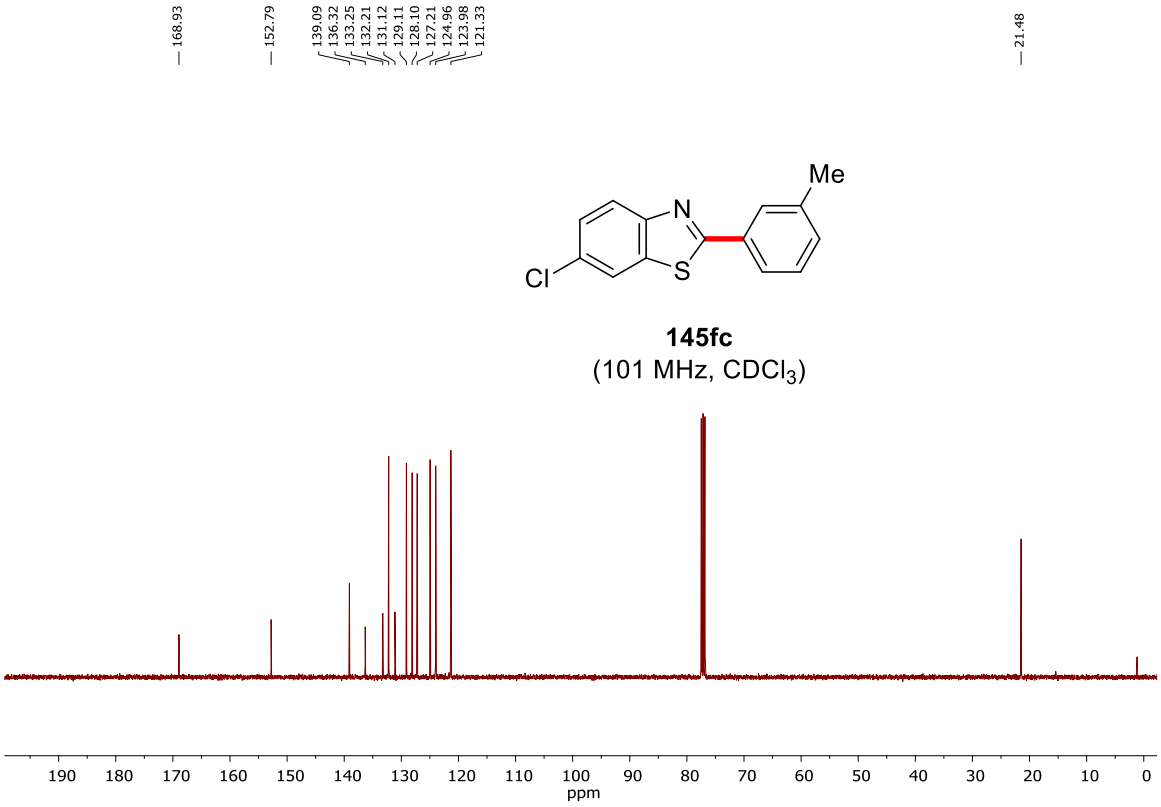

145fc
(101 MHz, $CDCl_3$)

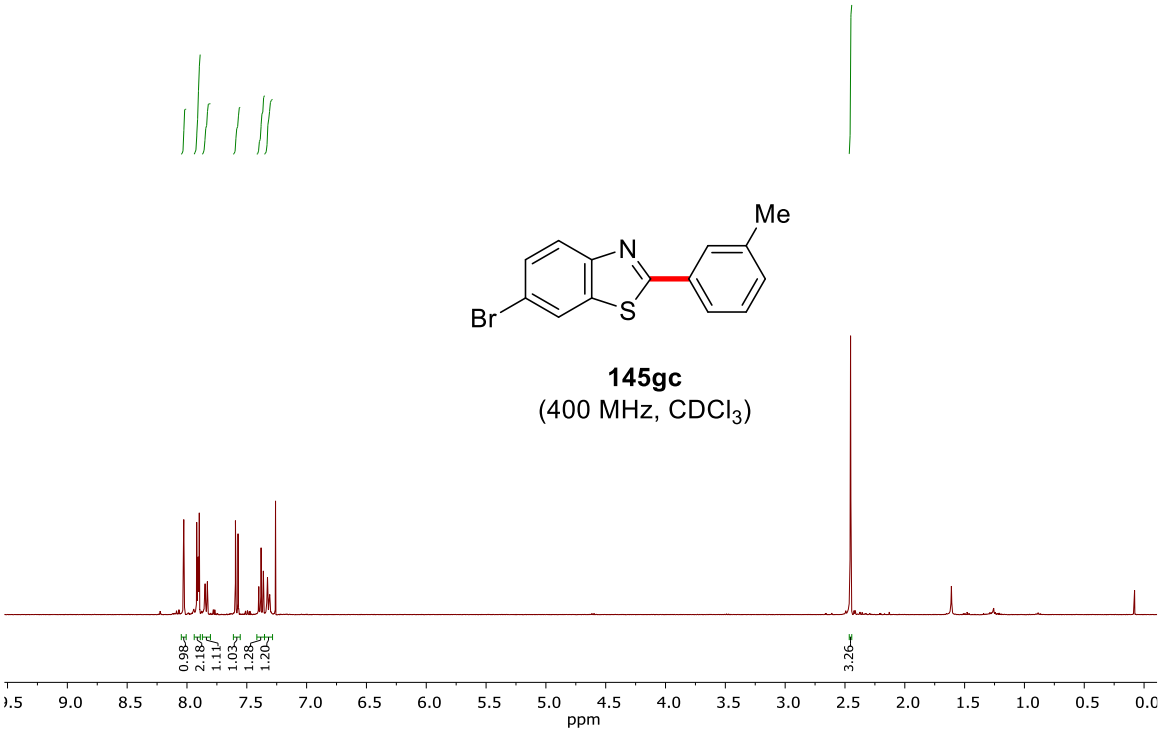

145gc
(400 MHz, $CDCl_3$)

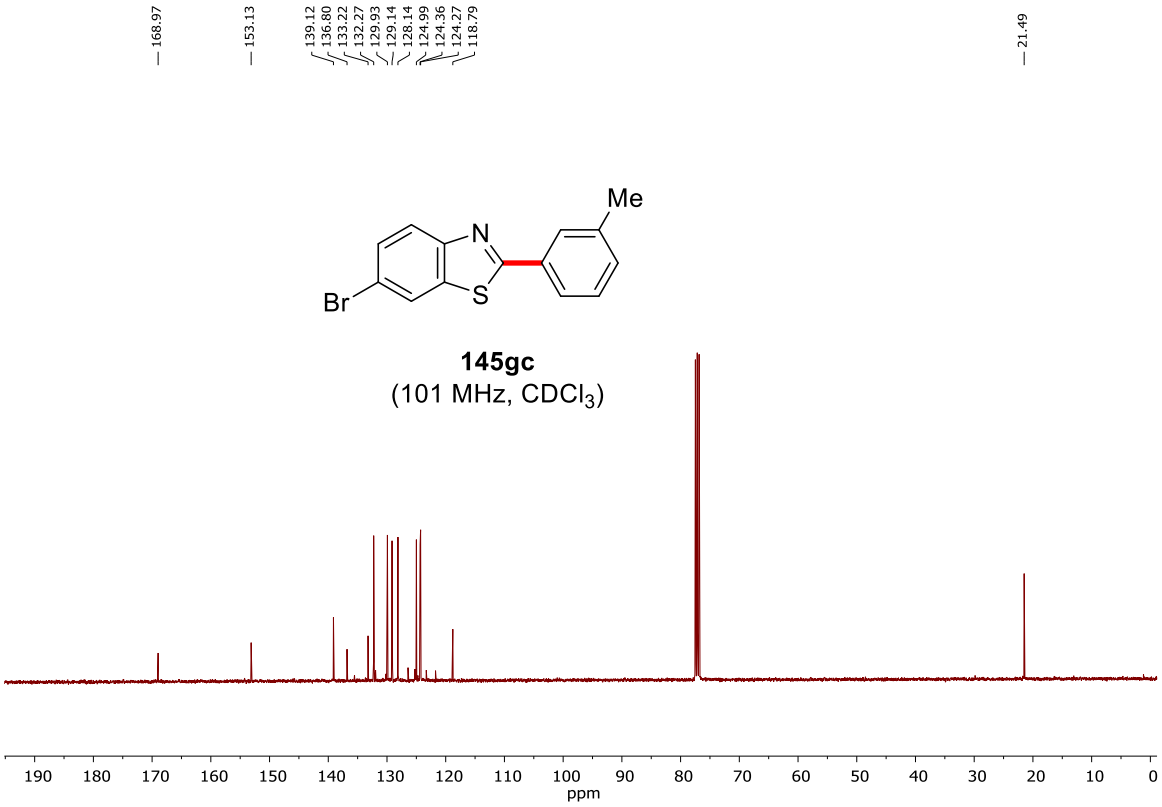

145gc
(101 MHz, $CDCl_3$)

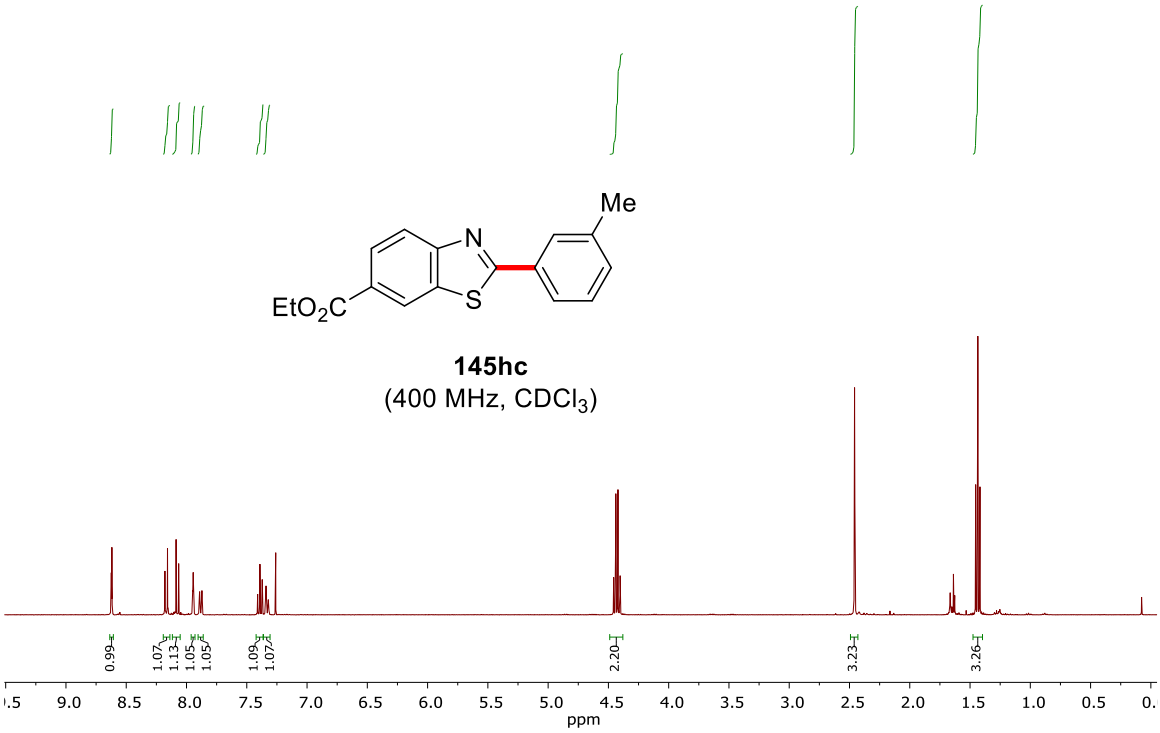

145hc
(400 MHz, $CDCl_3$)

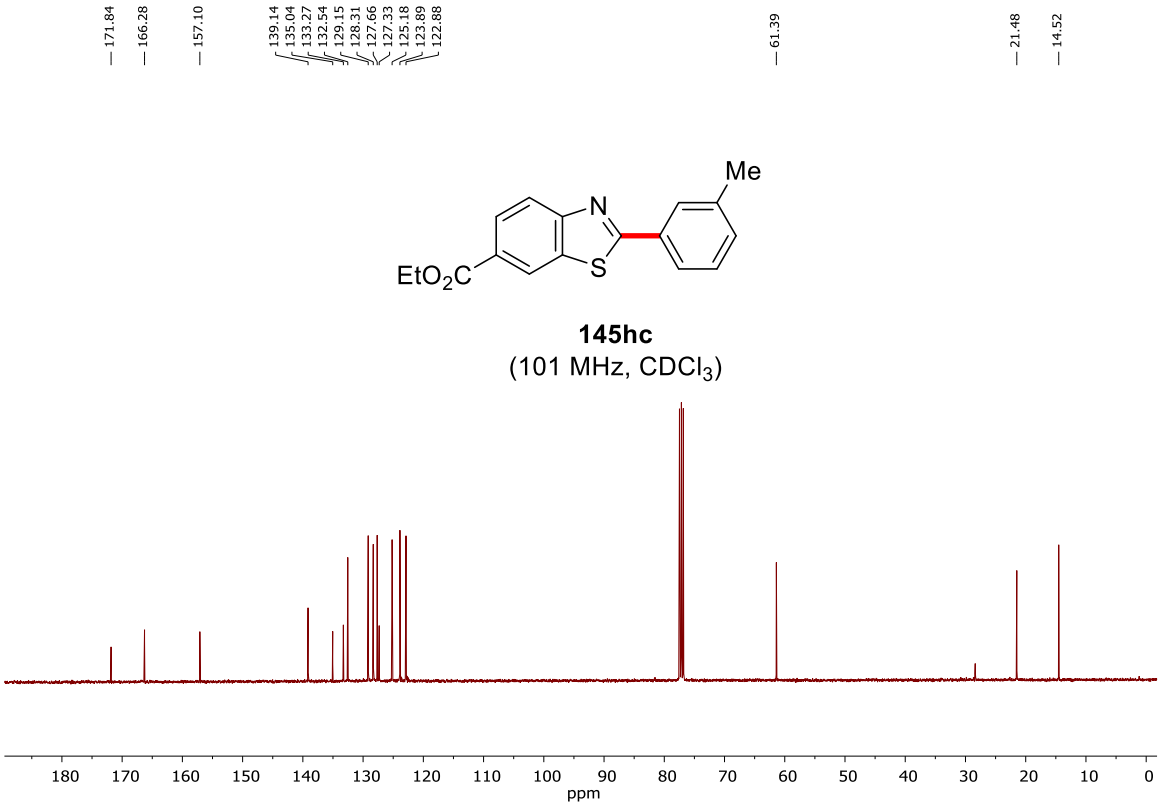

145hc
(101 MHz, $CDCl_3$)

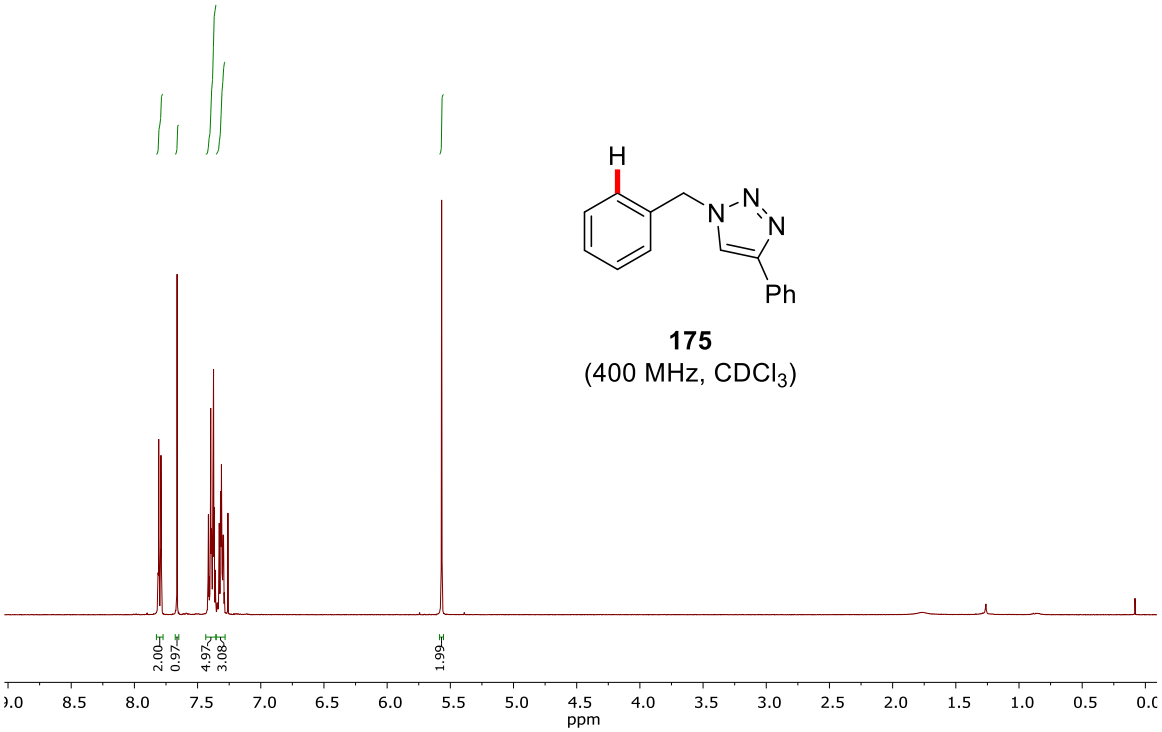

175
(400 MHz, $CDCl_3$)

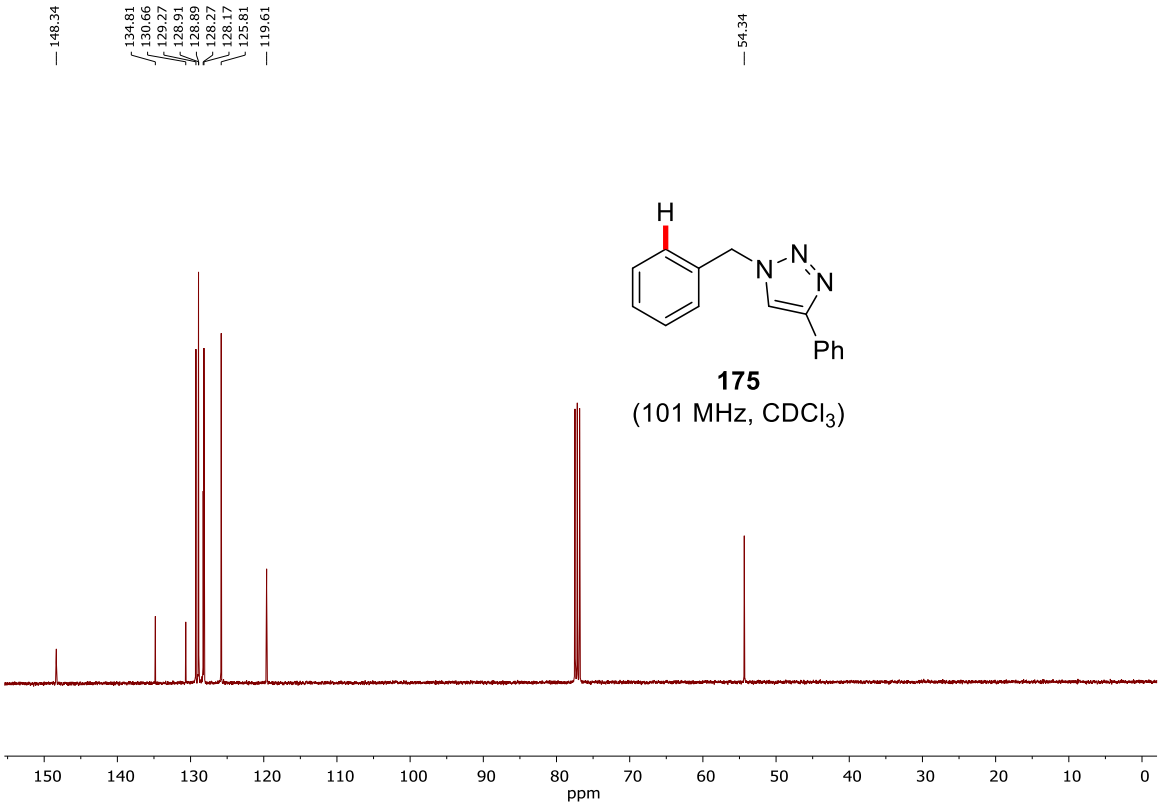

175
(101 MHz, $CDCl_3$)

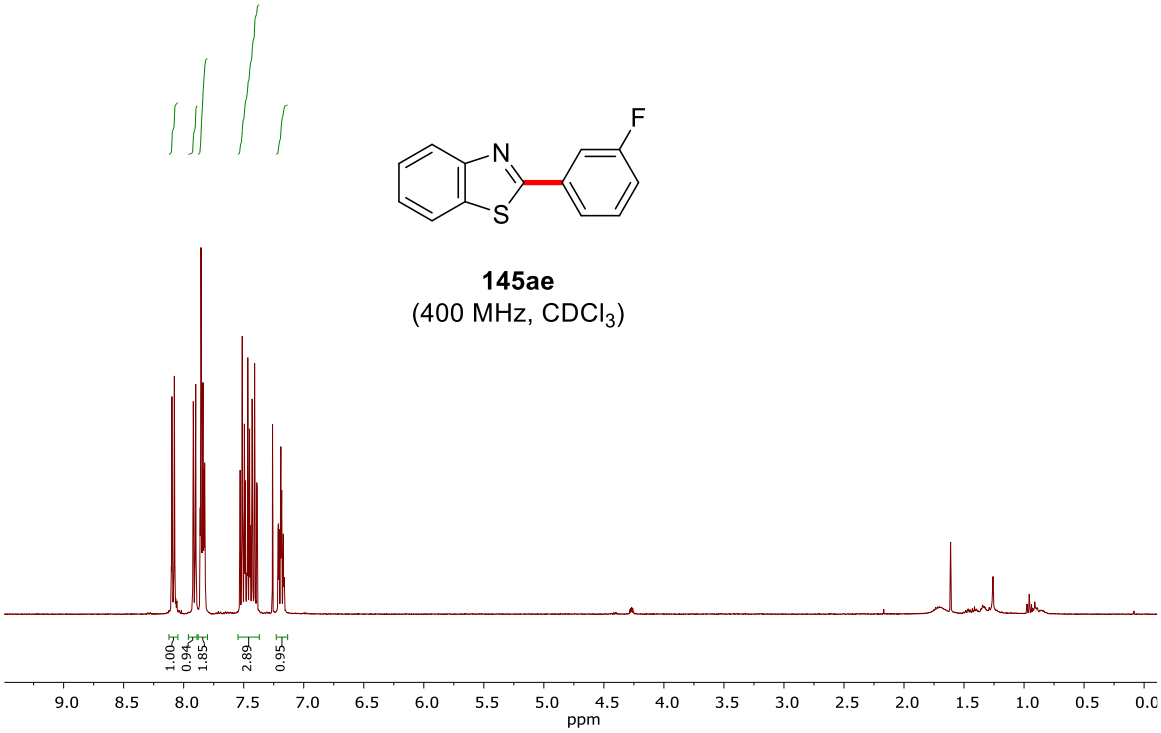

145ae
(400 MHz, $CDCl_3$)

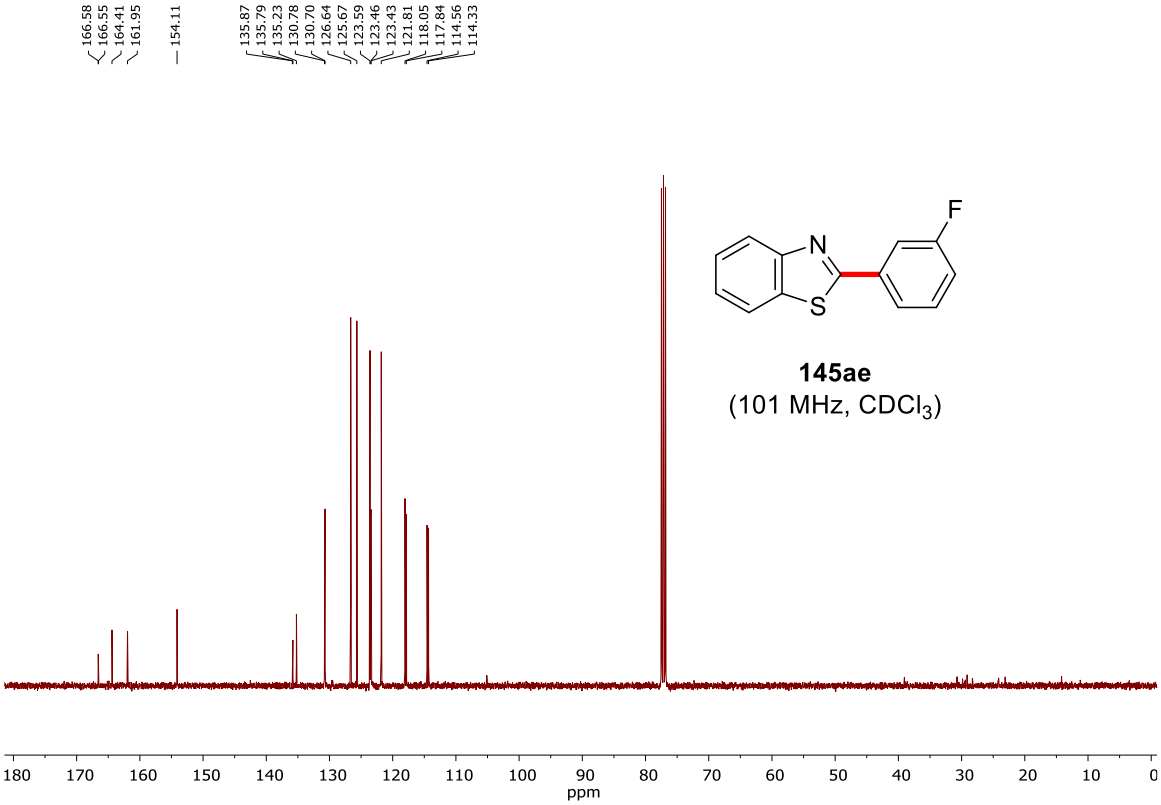

145ae
(101 MHz, $CDCl_3$)

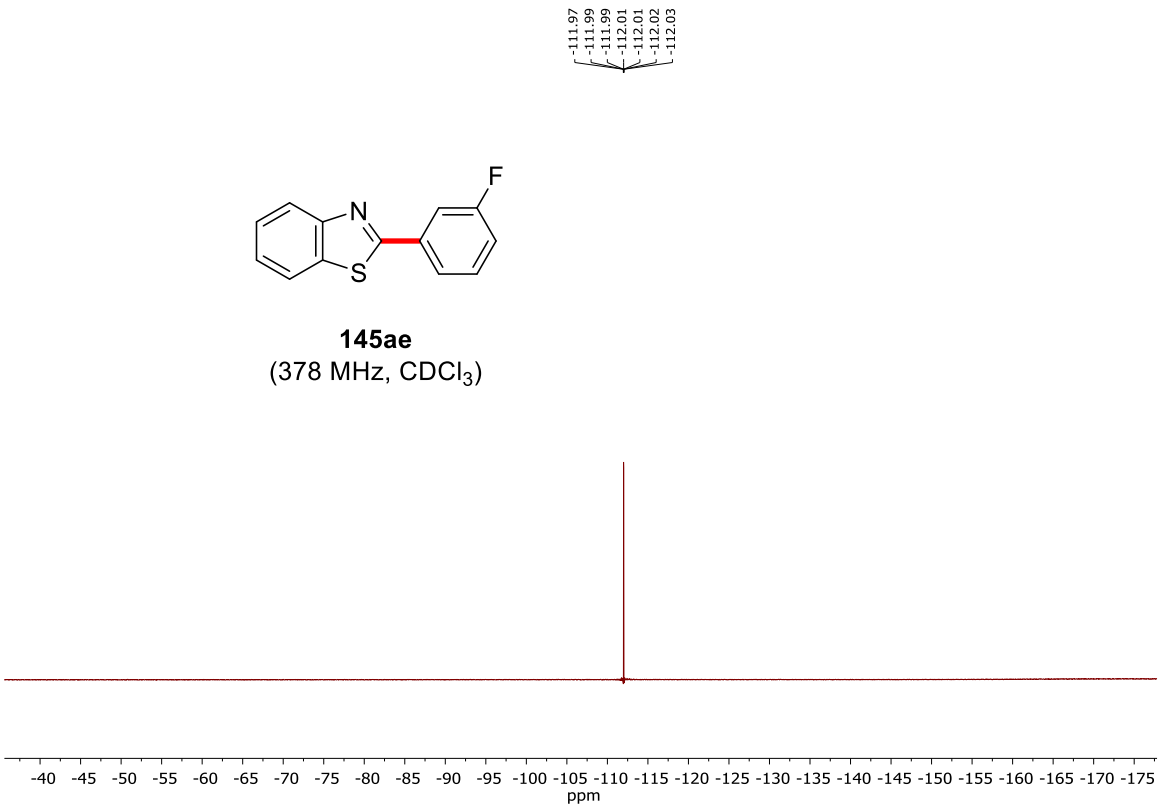
-111.97
-111.99
-111.99
-112.01
-112.01
-112.02
-112.03
F
N
S
145ae
(378 MHz, CDCl3)
-40 -45 -50 -55 -60 -65 -70 -75 -80 -85 -90 -95 -100 -105 -110 -115 -120 -125 -130 -135 -140 -145 -150 -155 -160 -165 -170 -175
ppm

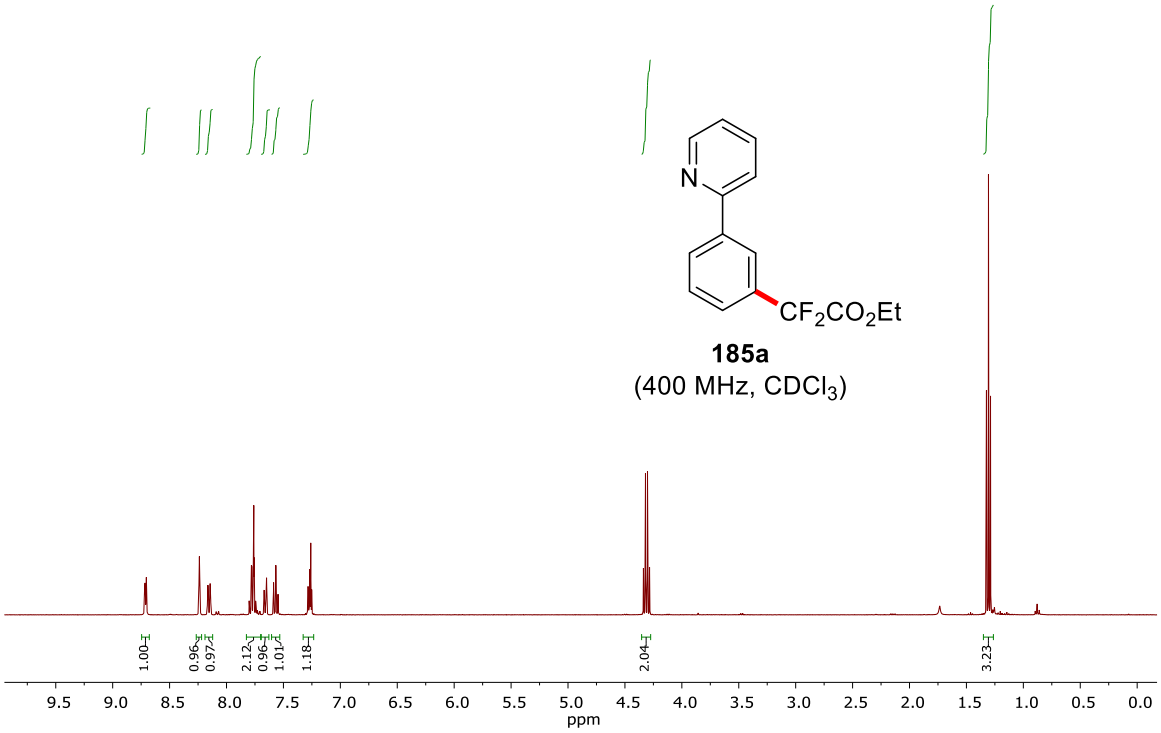
N
CF2CO2Et
185a
(400 MHz, CDCl3)
1.00
0.96
0.97
2.12
0.96
1.01
1.18
2.04
3.23
9.5 9.0 8.5 8.0 7.5 7.0 6.5 6.0 5.5 5.0 4.5 4.0 3.5 3.0 2.5 2.0 1.5 1.0 0.5 0.0
ppm


164.64
164.29
163.94
156.30
150.02
149.97
140.15
137.04
133.81
133.56
133.30
129.61
129.59
129.58
129.29
127.28
126.11
126.05
125.99
124.14
124.08
124.01
122.80
120.76
116.02
113.51
111.01
63.33
14.03

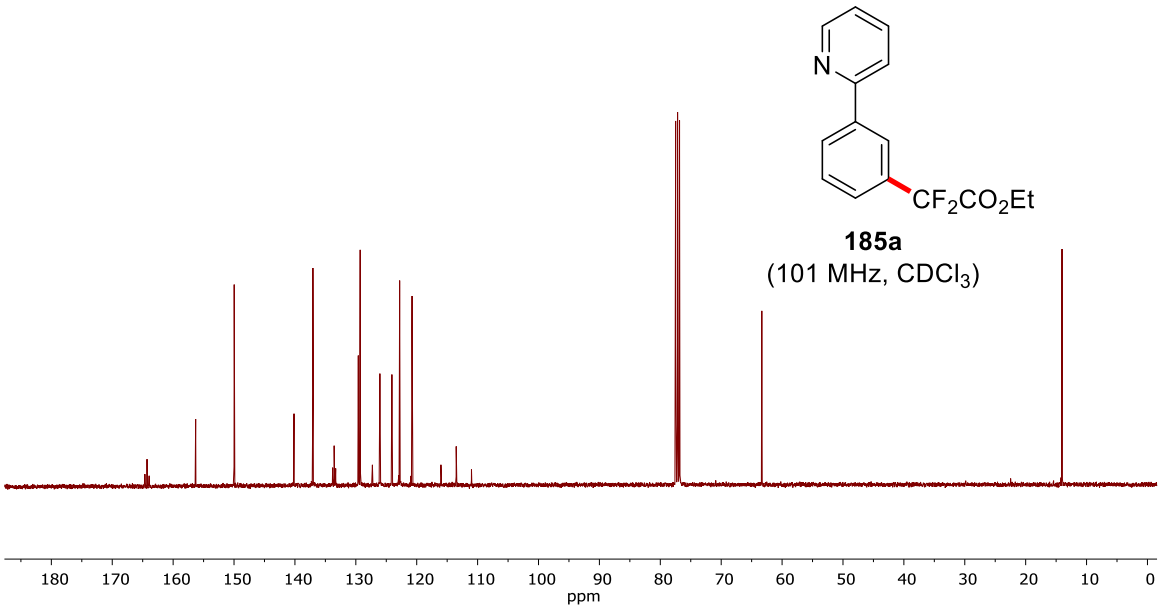
N
CF2CO2Et
185a
(101 MHz, CDCl3)
180 170 160 150 140 130 120 110 100 90 80 70 60 50 40 30 20 10 0
ppm

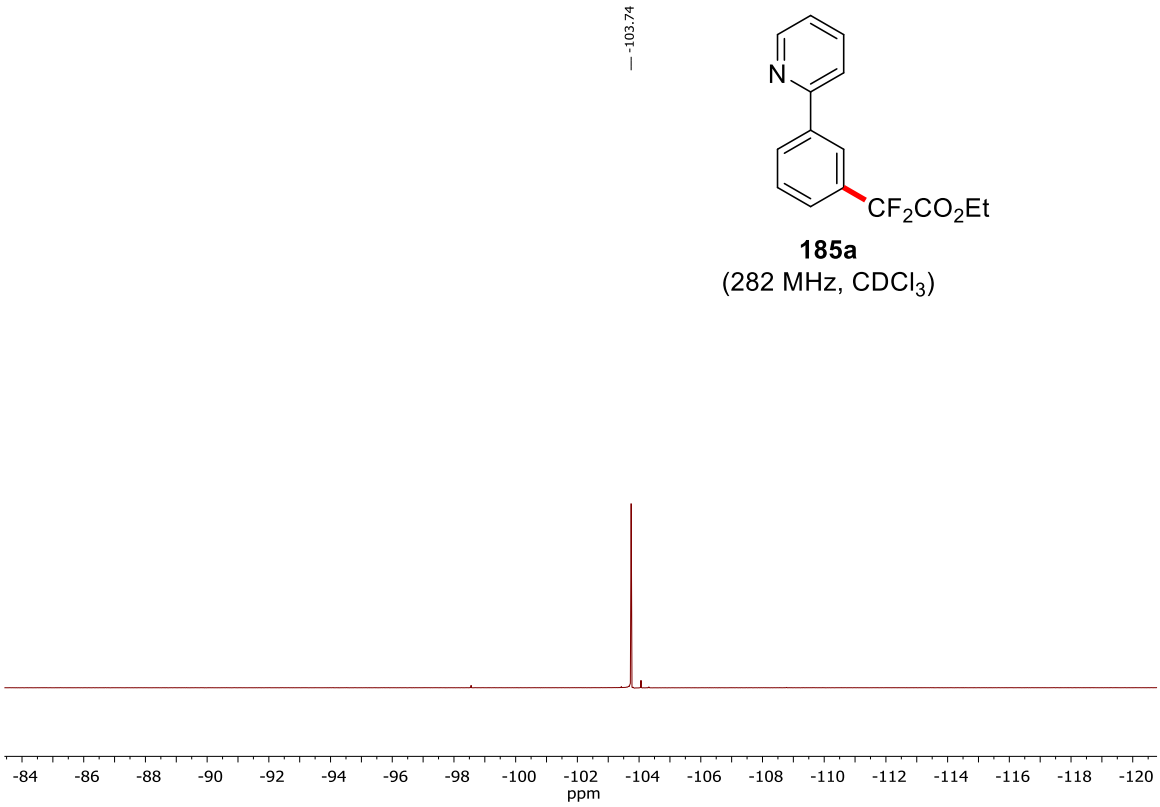

185a
(282 MHz, $CDCl_3$)

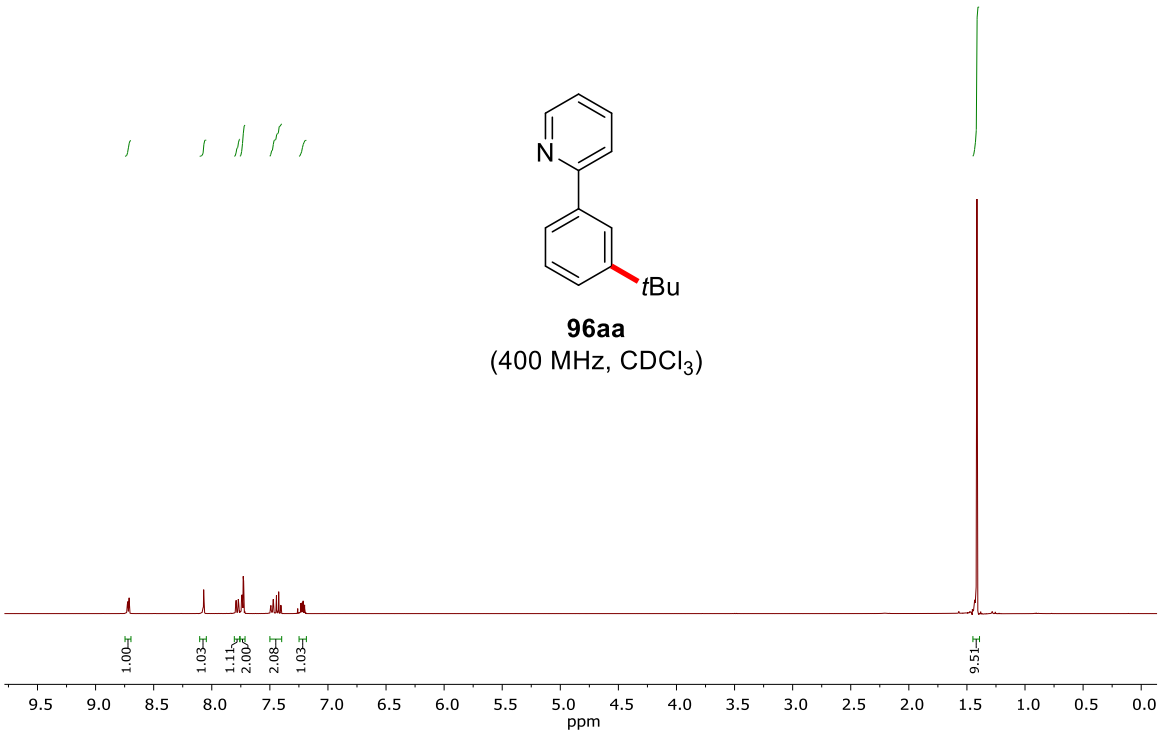

96aa
(400 MHz, $CDCl_3$)

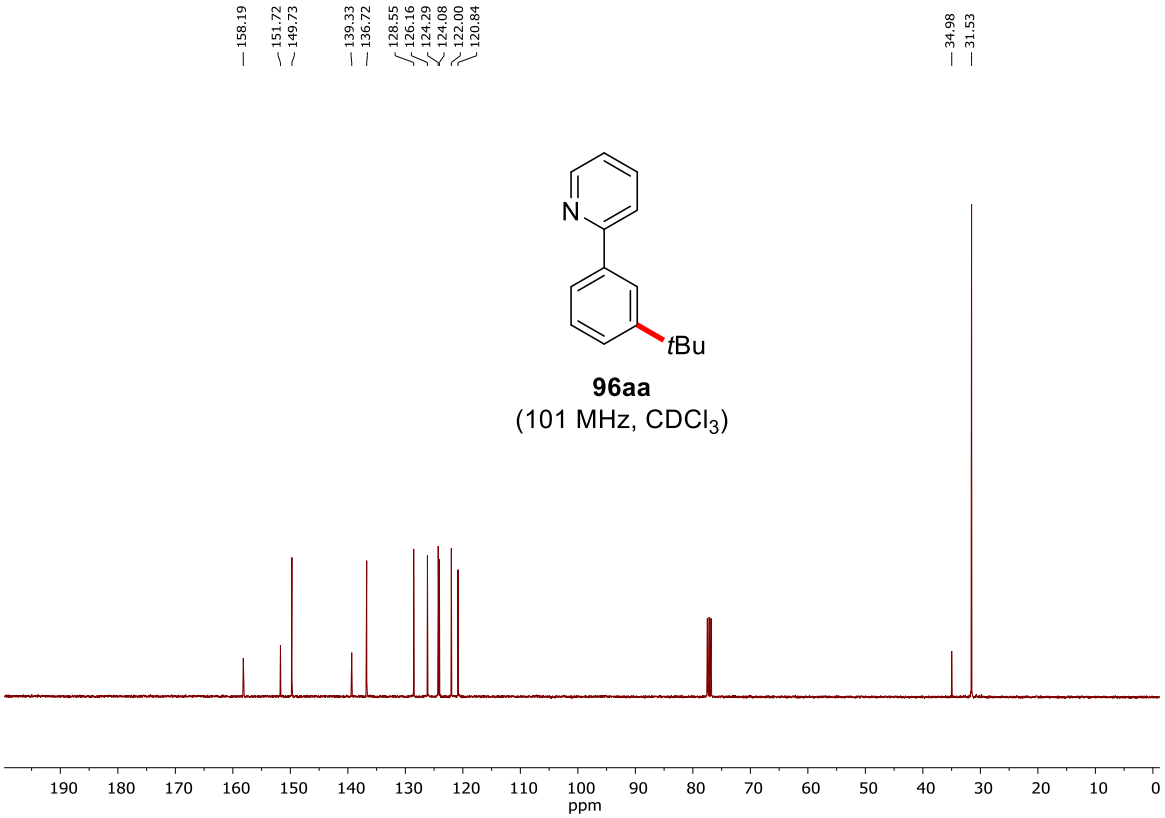

96aa
(101 MHz, $CDCl_3$)

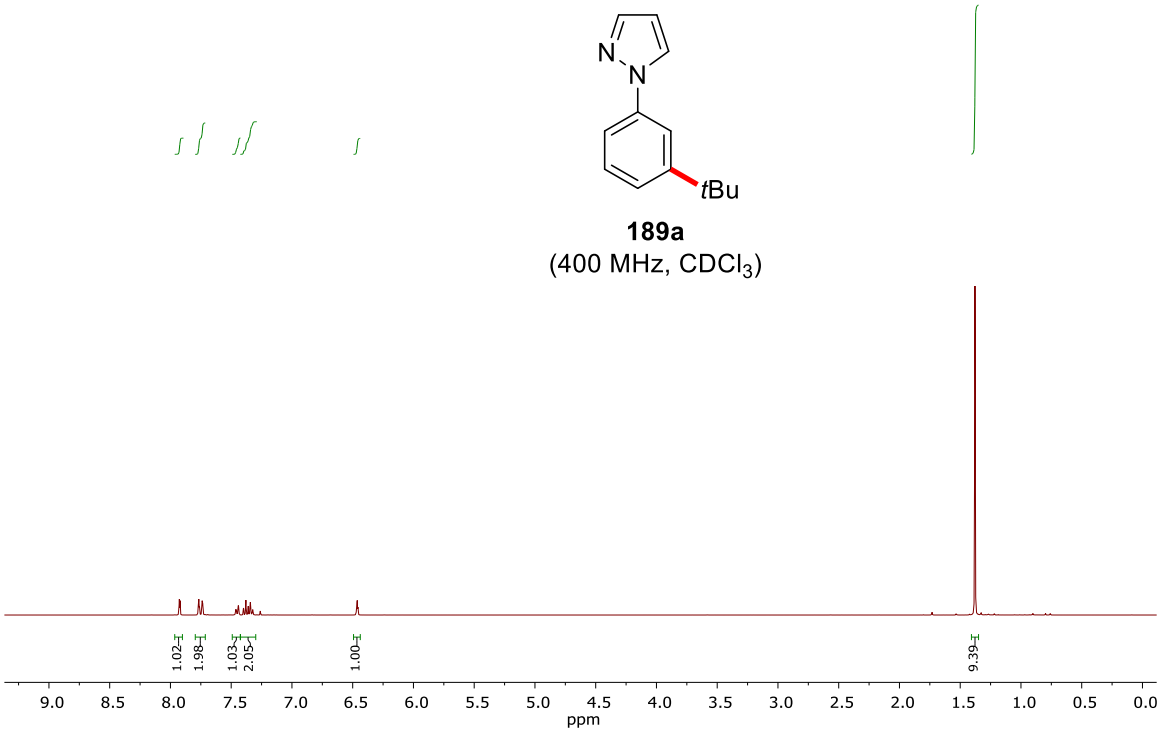
tBu
189a
(400 MHz, CDCl3)
1.02
1.98
1.03
2.05
1.00
9.39
ppm

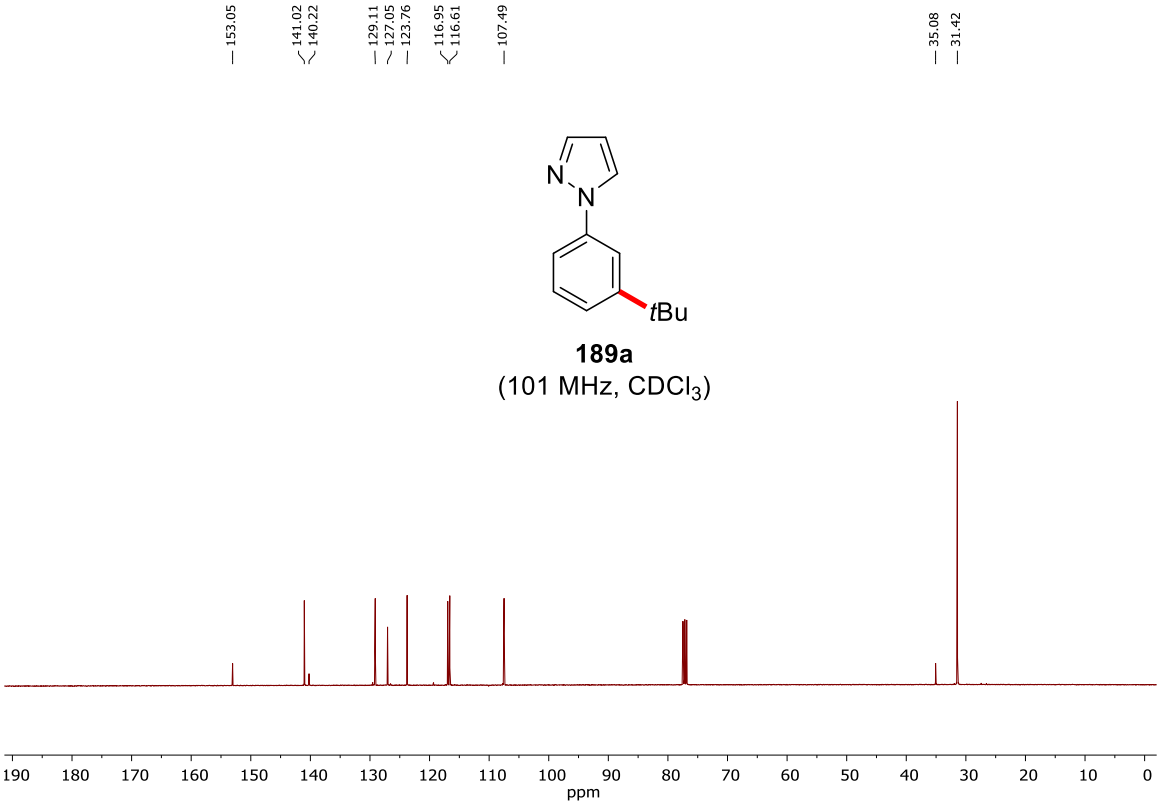
153.05
141.02
140.22
129.11
127.05
123.76
116.95
116.61
107.49
35.08
31.42
tBu
189a
(101 MHz, CDCl3)
ppm

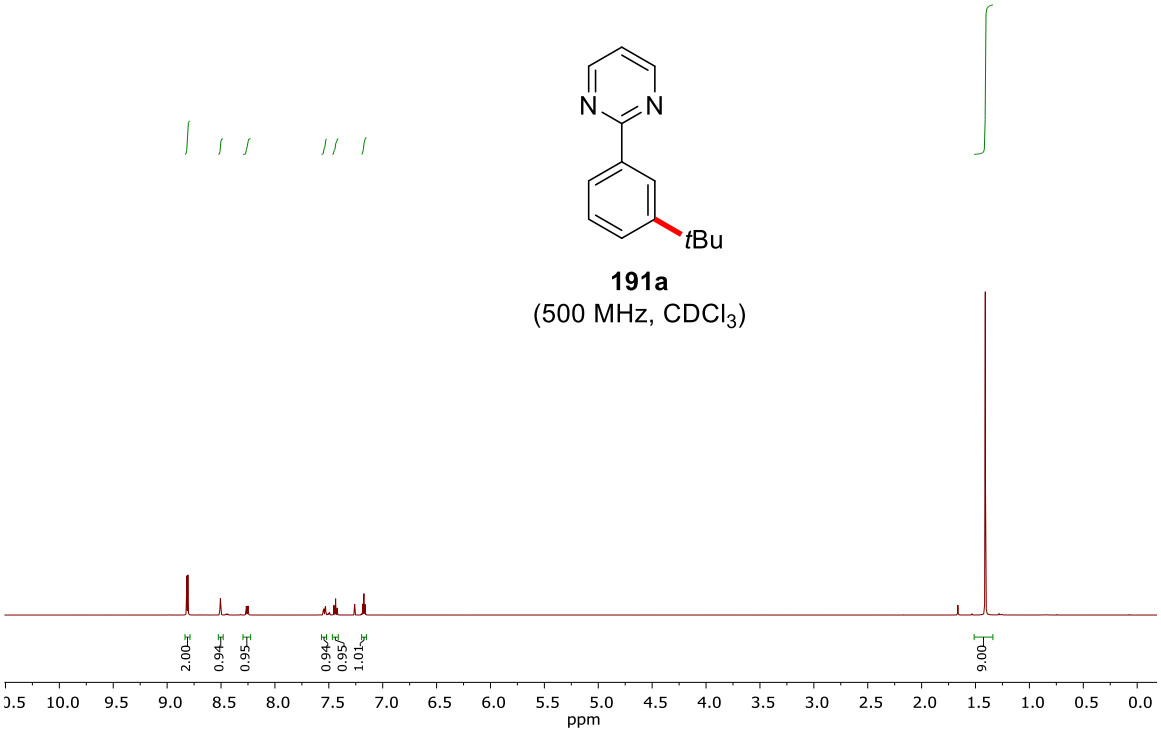

191a
(500 MHz, $CDCl_3$)

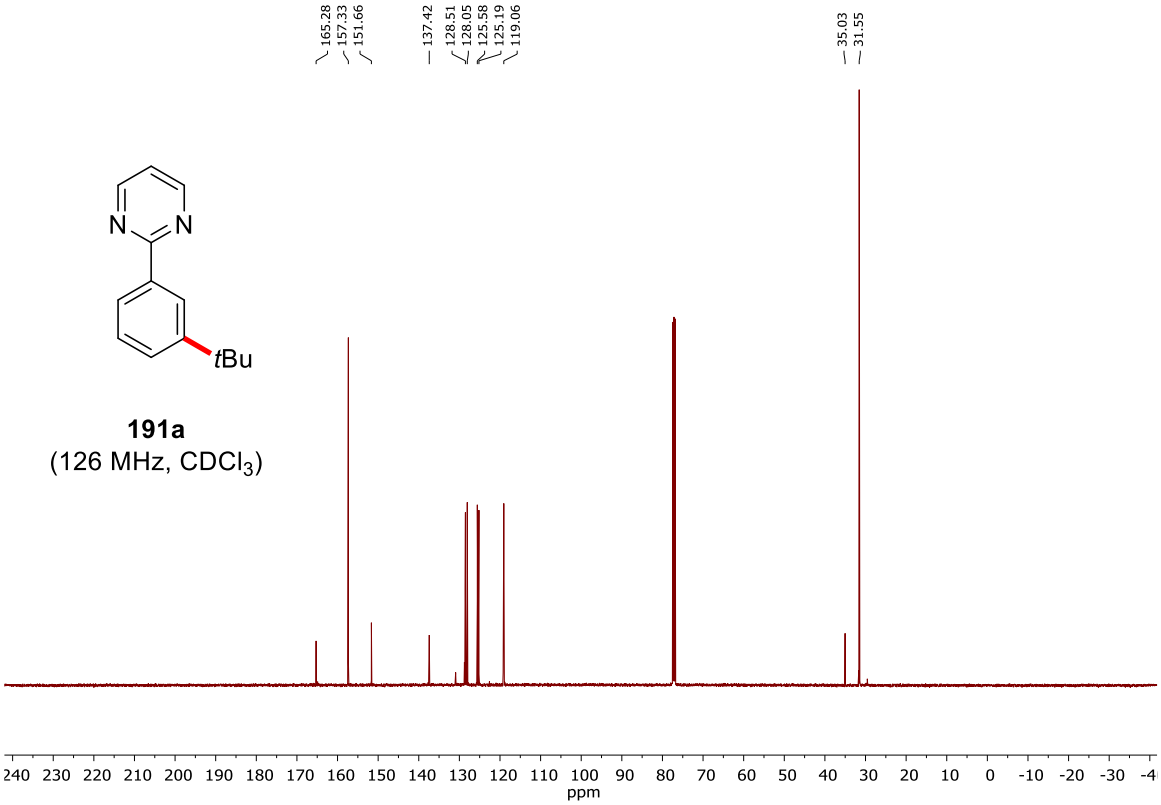

191a
(126 MHz, $CDCl_3$)

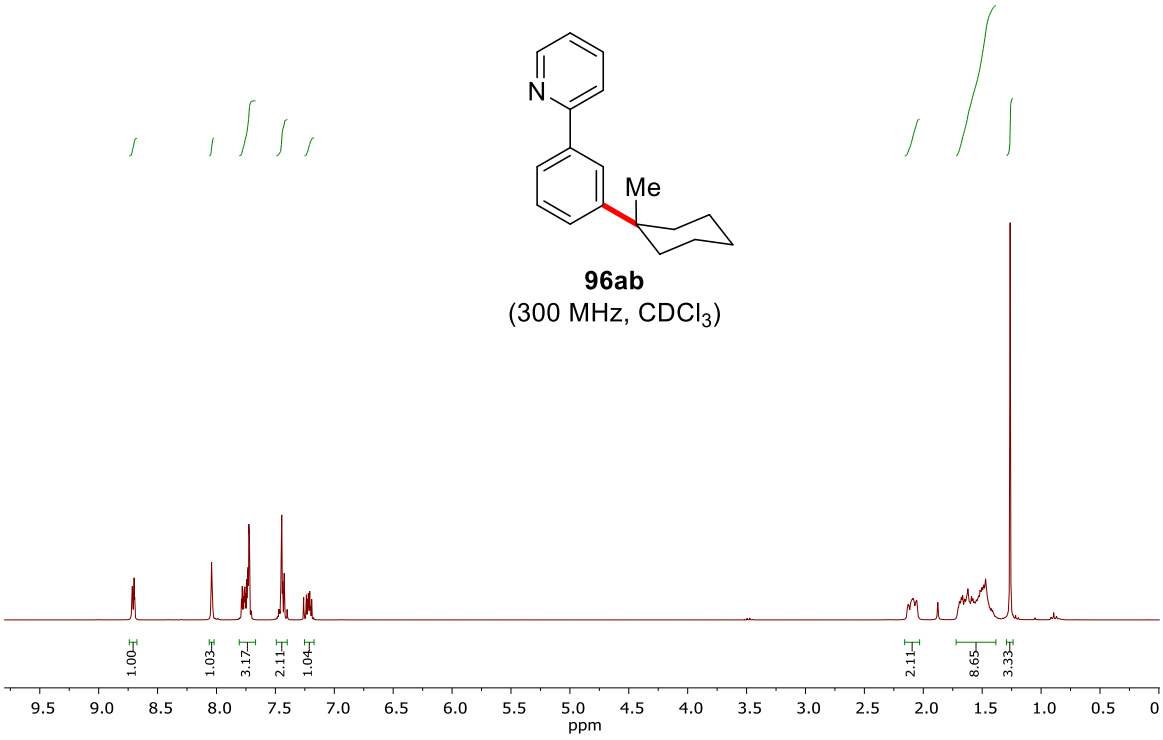

96ab
(300 MHz, $CDCl_3$)

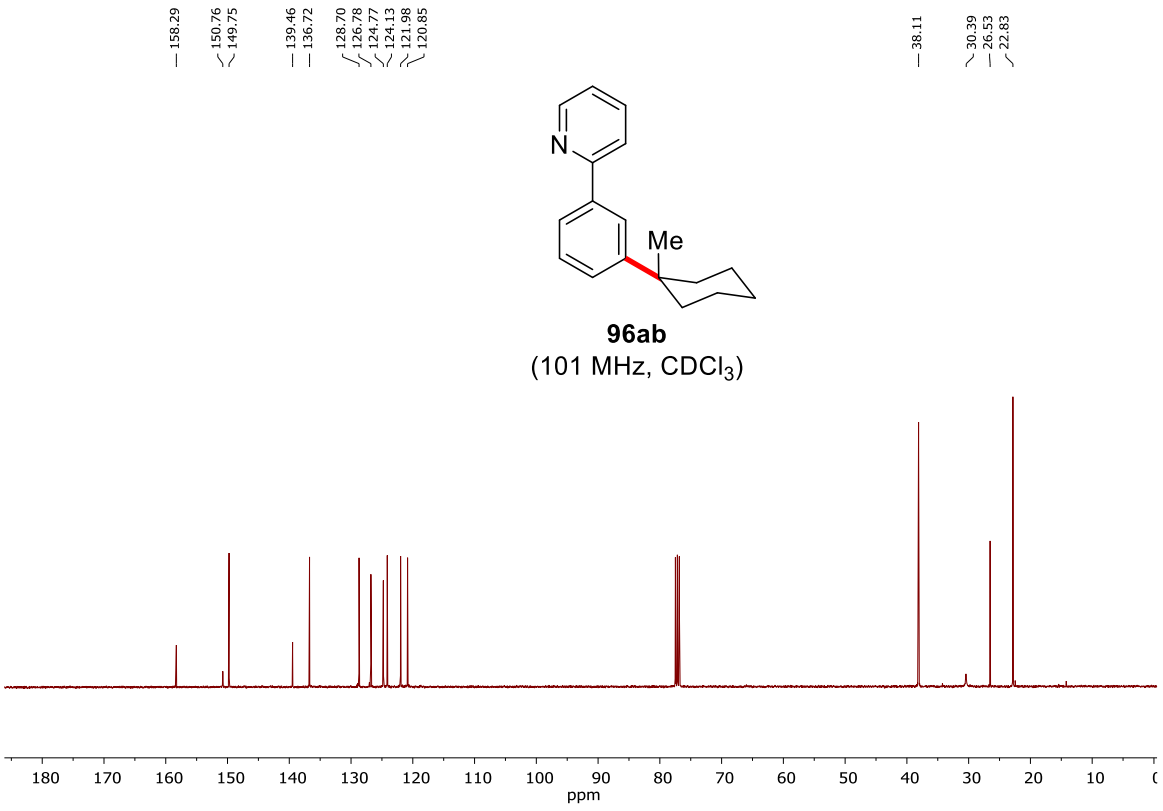

96ab
(101 MHz, $CDCl_3$)

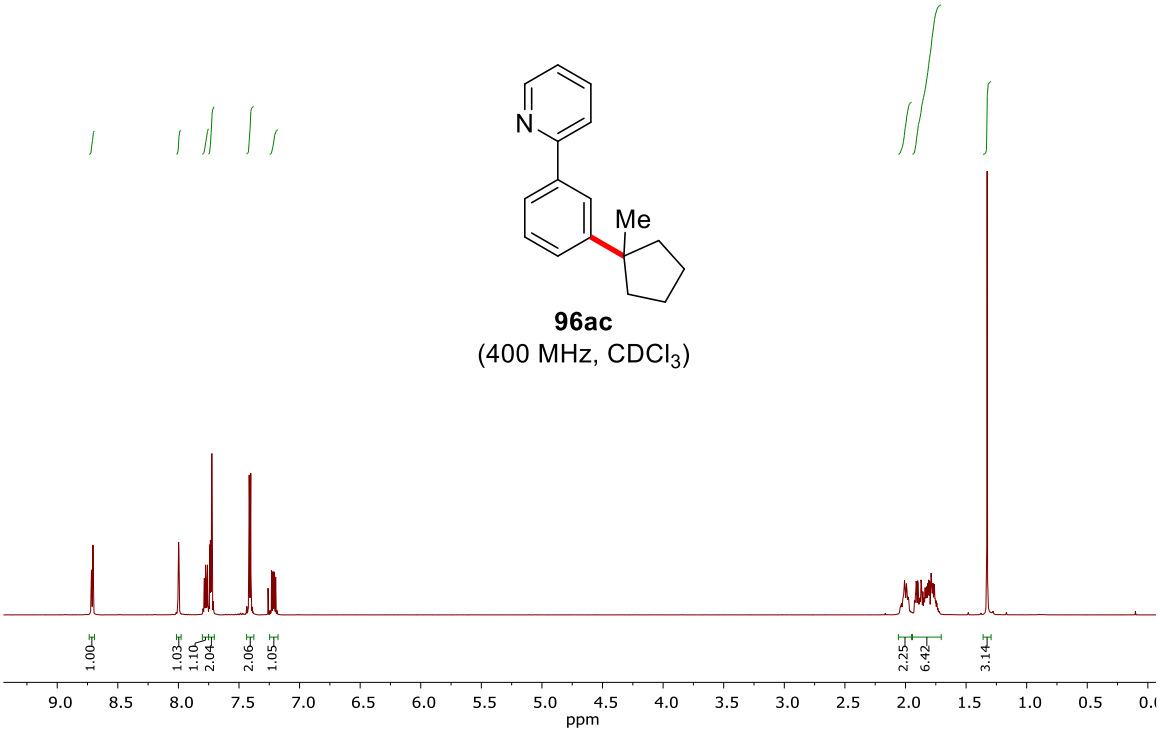

96ac
(400 MHz, $CDCl_3$)

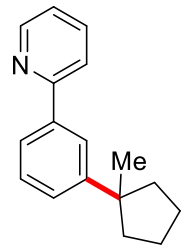

96ac
(101 MHz, $CDCl_3$)

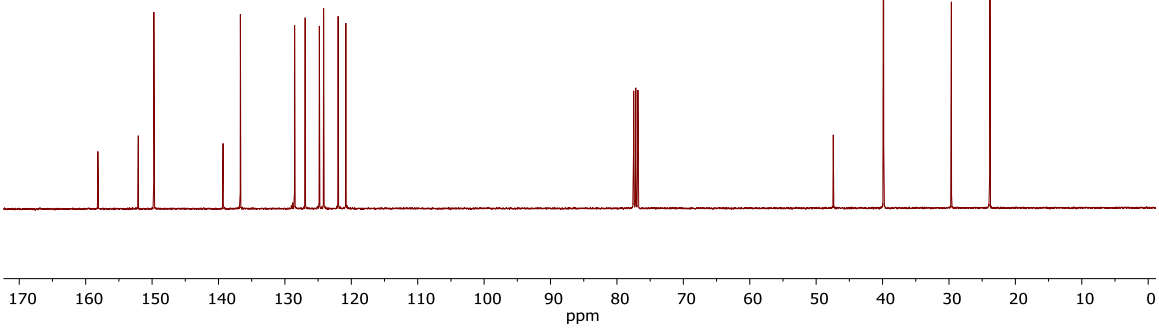

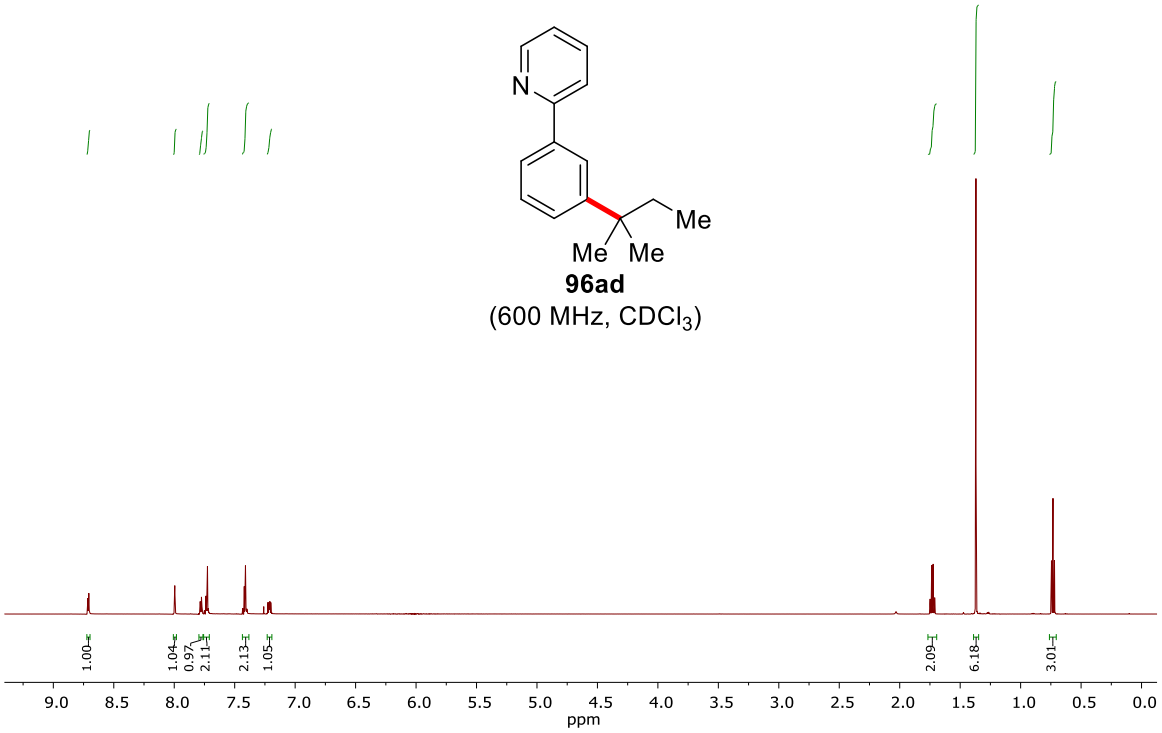
N
Me
Me
Me
96ad
(600 MHz, CDCl3)
1.00
1.04
0.97
2.11
2.13
1.05
2.09
6.18
3.01
9.0
8.5
8.0
7.5
7.0
6.5
6.0
5.5
5.0
4.5
4.0
3.5
3.0
2.5
2.0
1.5
1.0
0.5
0.0
ppm

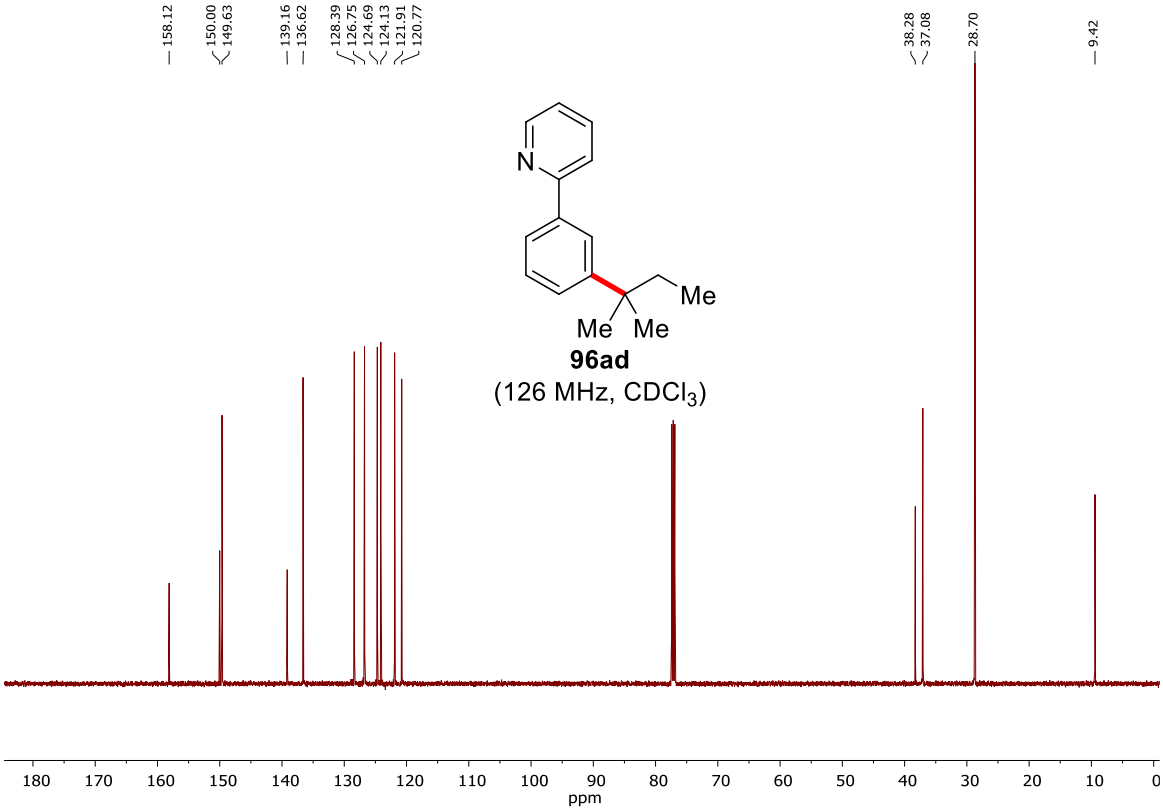
158.12
150.00
149.63
139.16
136.62
128.39
126.75
124.69
124.13
121.91
120.77
38.28
37.08
28.70
9.42
N
Me
Me
Me
96ad
(126 MHz, CDCl3)
180
170
160
150
140
130
120
110
100
90
80
70
60
50
40
30
20
10
0
ppm

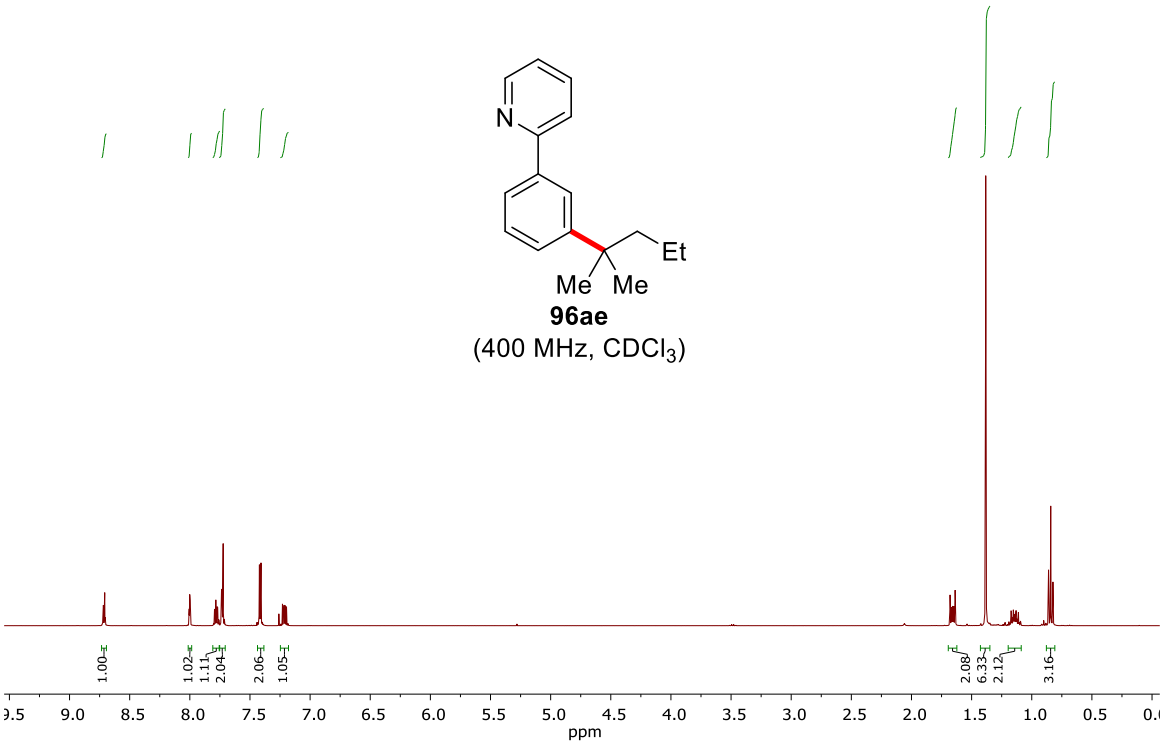
N
Et
Me Me
96ae
(400 MHz, CDCl3)
1.00
1.02
1.11
2.04
2.06
1.05
2.08
6.33
2.12
3.16
ppm

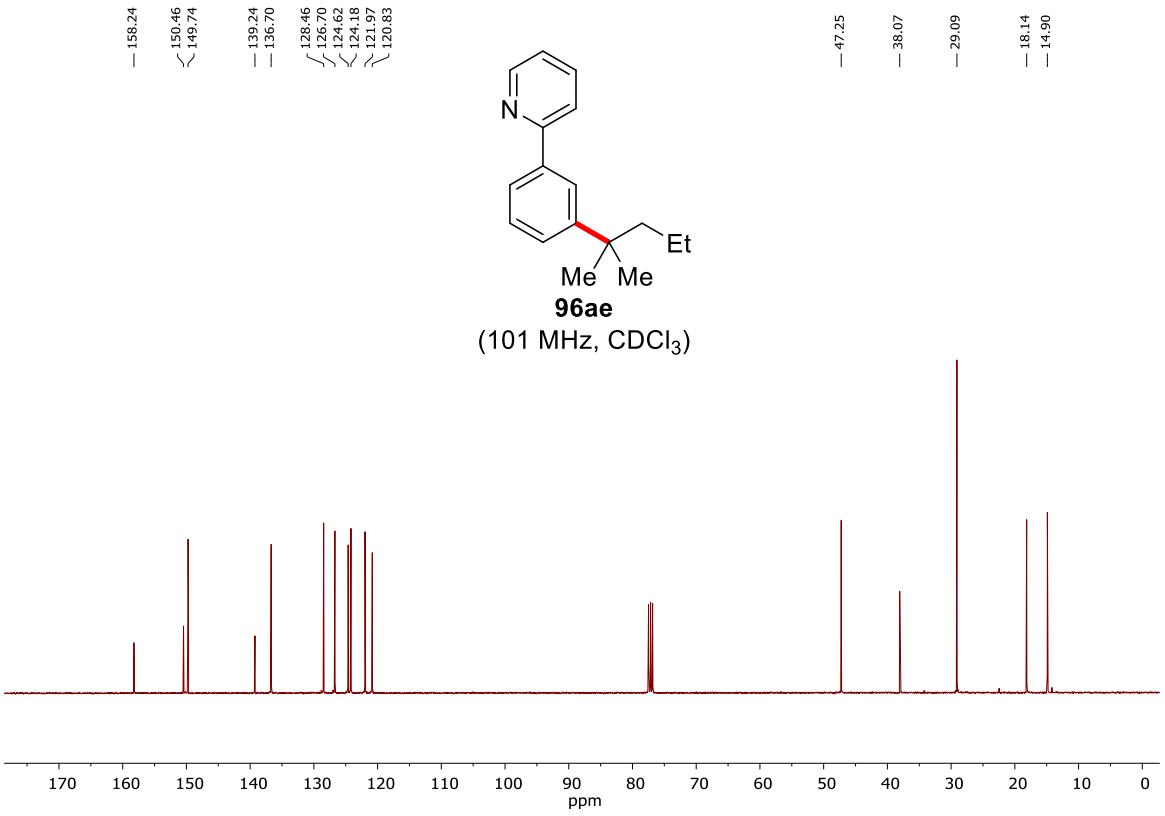
158.24
150.46
149.74
139.24
136.70
128.46
126.70
124.62
124.18
121.97
120.83
47.25
38.07
29.09
18.14
14.90
N
Et
Me Me
96ae
(101 MHz, CDCl3)
ppm

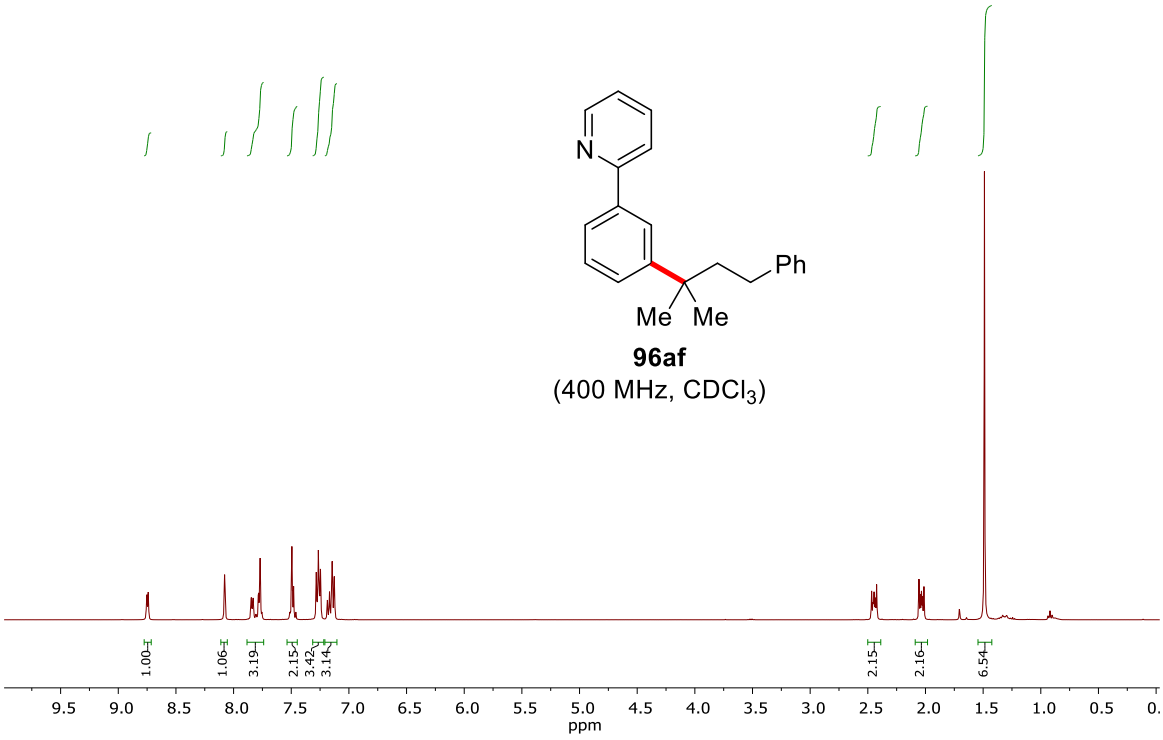

96af
(400 MHz, $CDCl_3$)

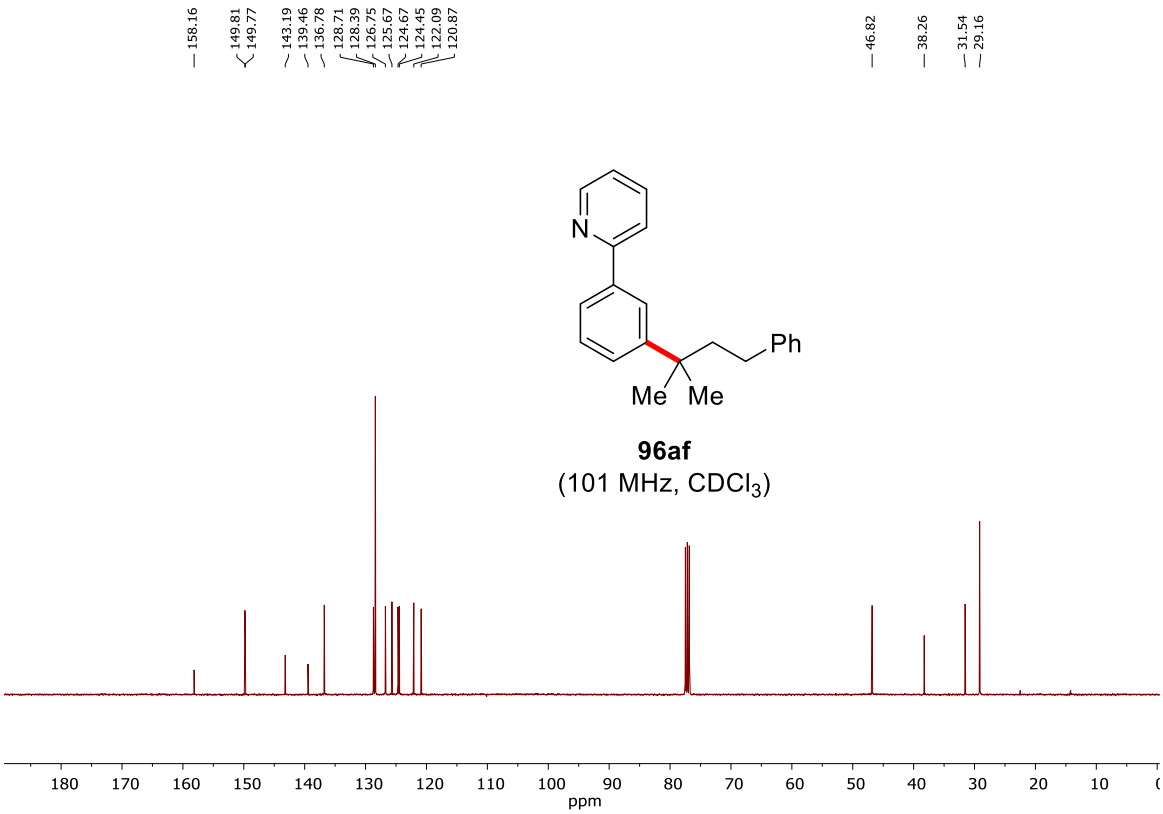

96af
(101 MHz, $CDCl_3$)

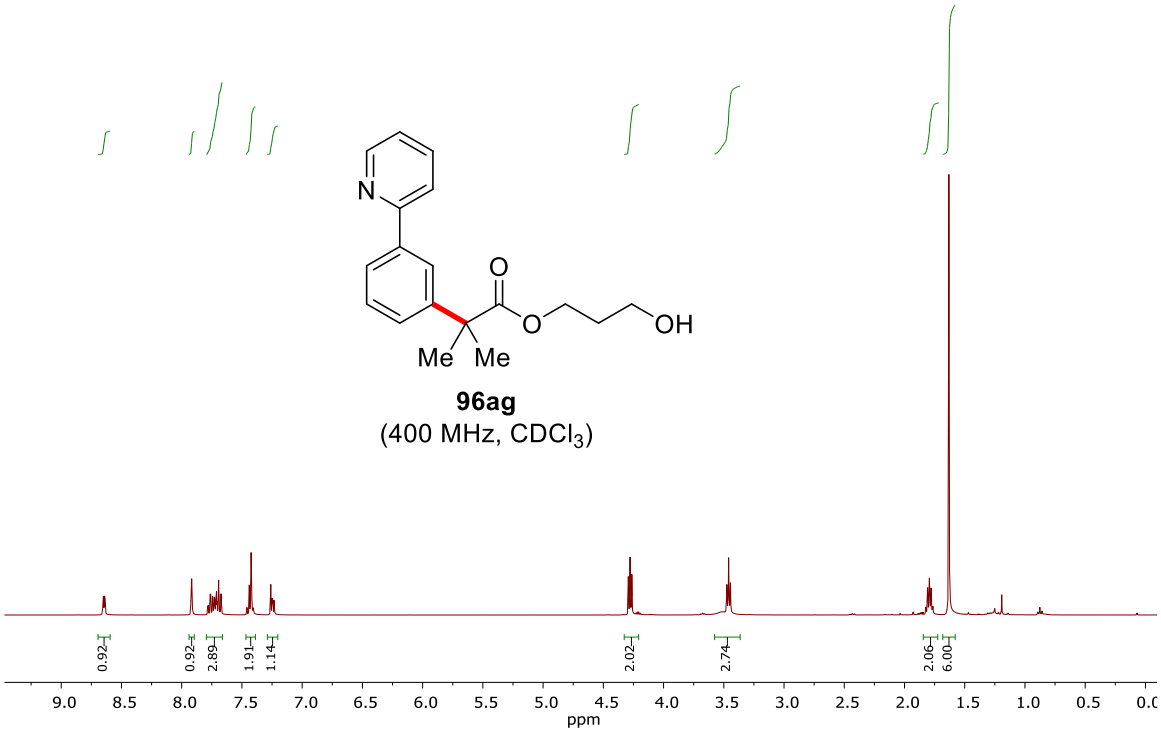

96ag
(400 MHz, $CDCl_3$)

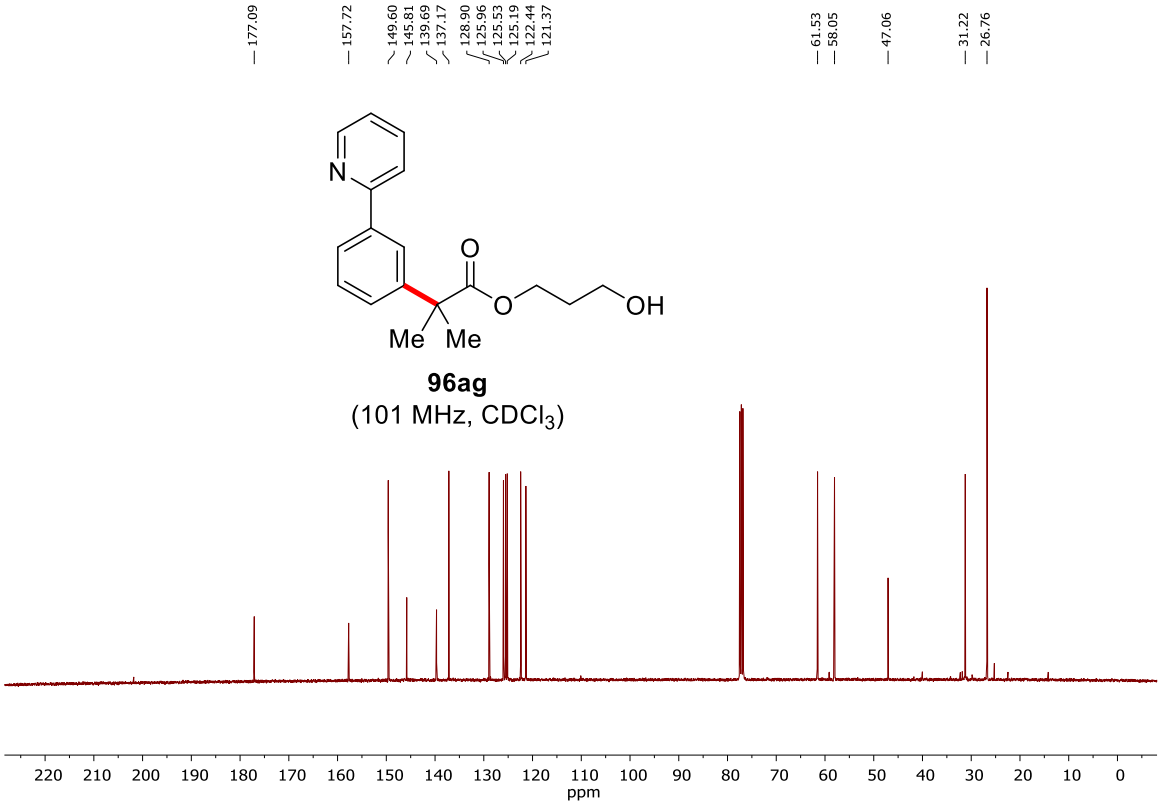

96ag
(101 MHz, $CDCl_3$)

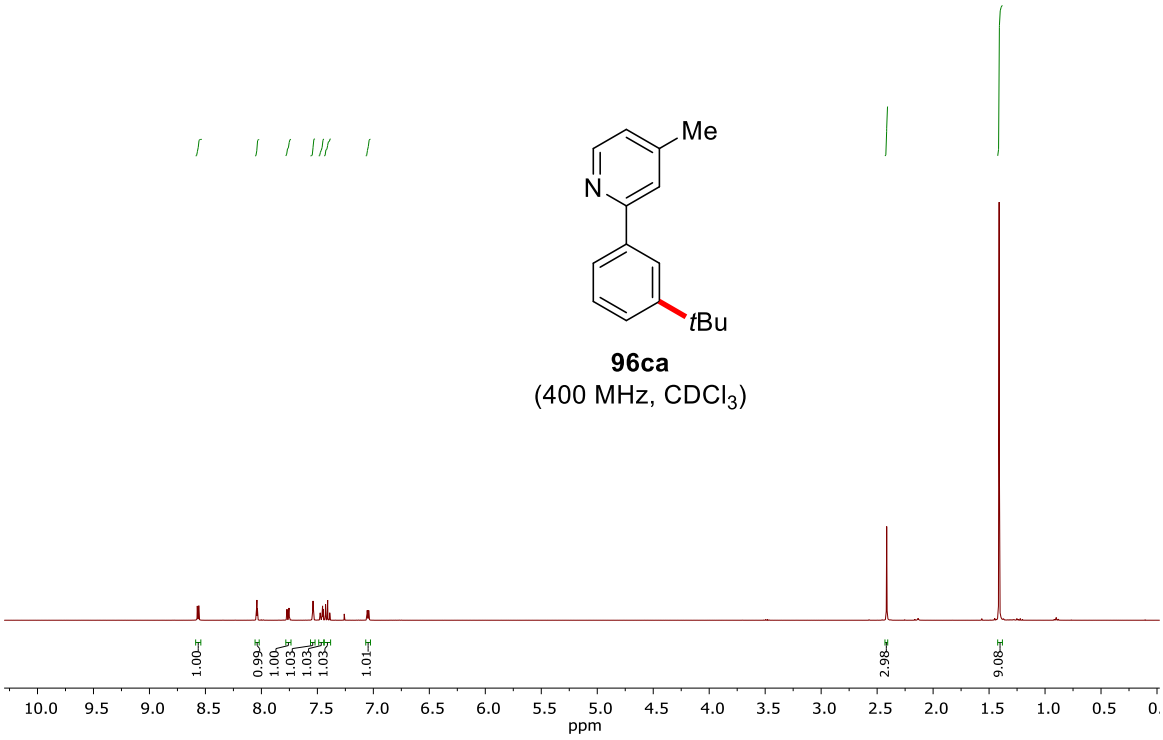

96ca
(400 MHz, $CDCl_3$)

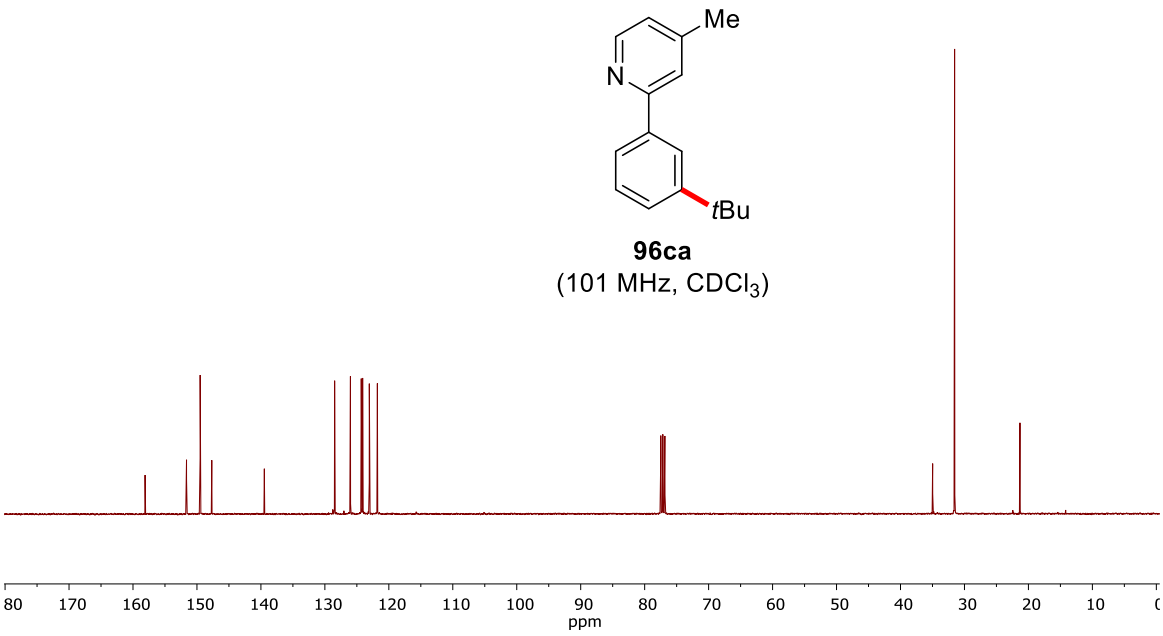

96ca
(101 MHz, $CDCl_3$)

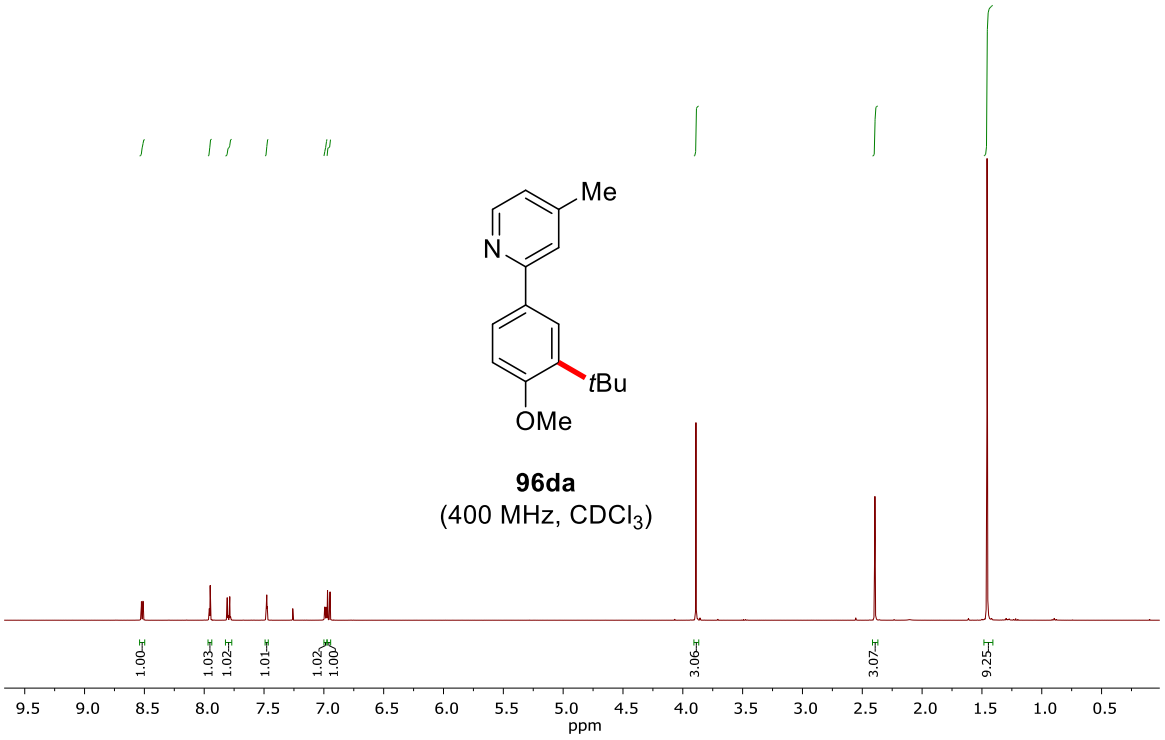

96da
(400 MHz, $CDCl_3$)

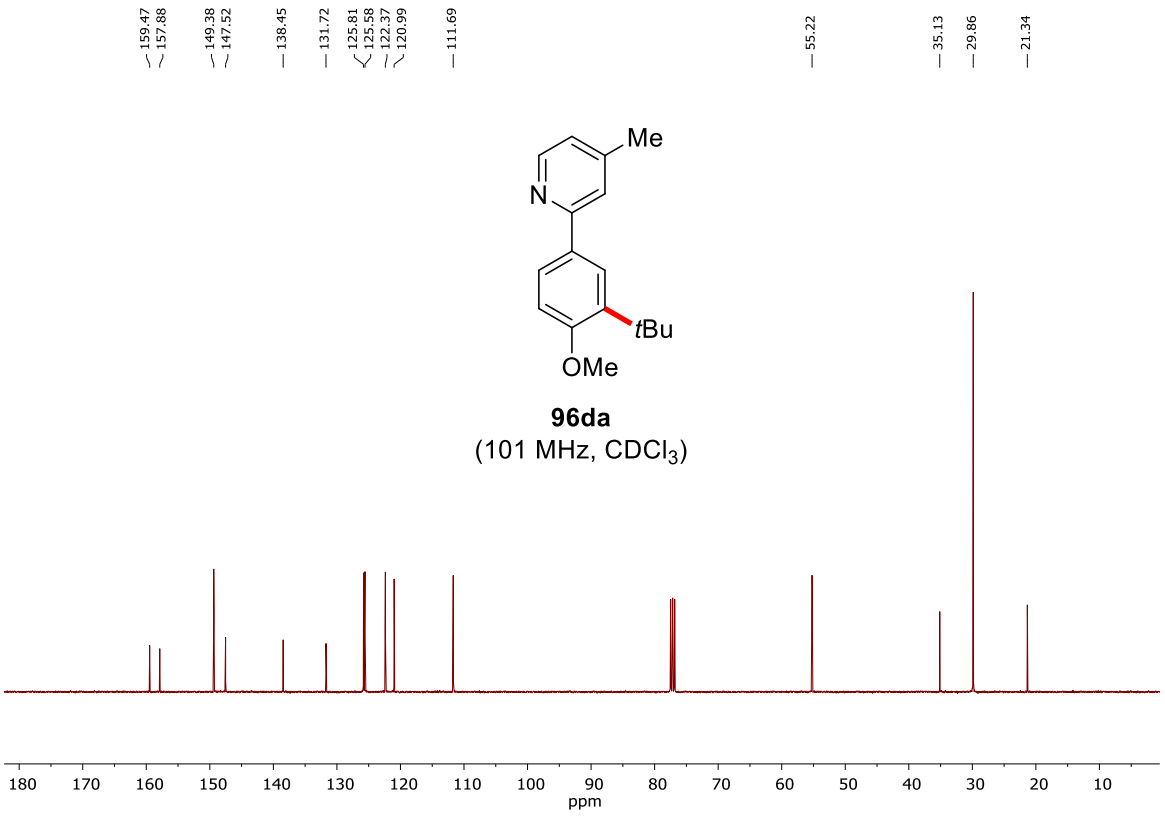

96da
(101 MHz, $CDCl_3$)

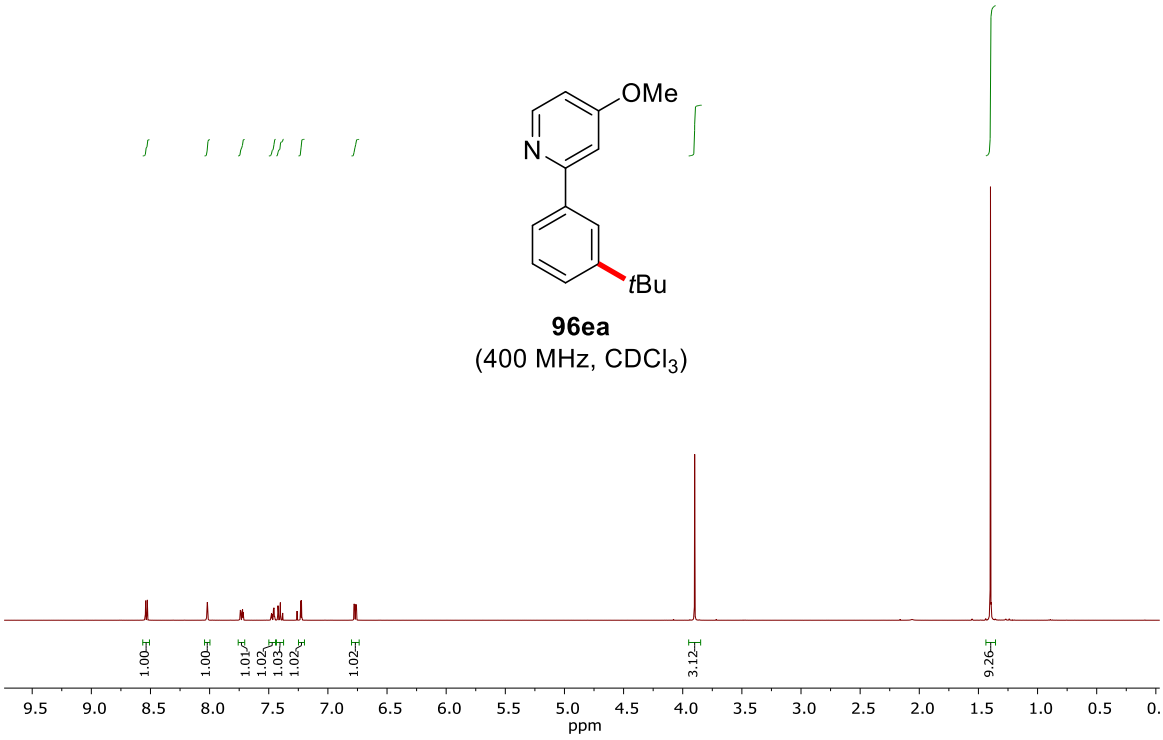

96ea
(400 MHz, $CDCl_3$)

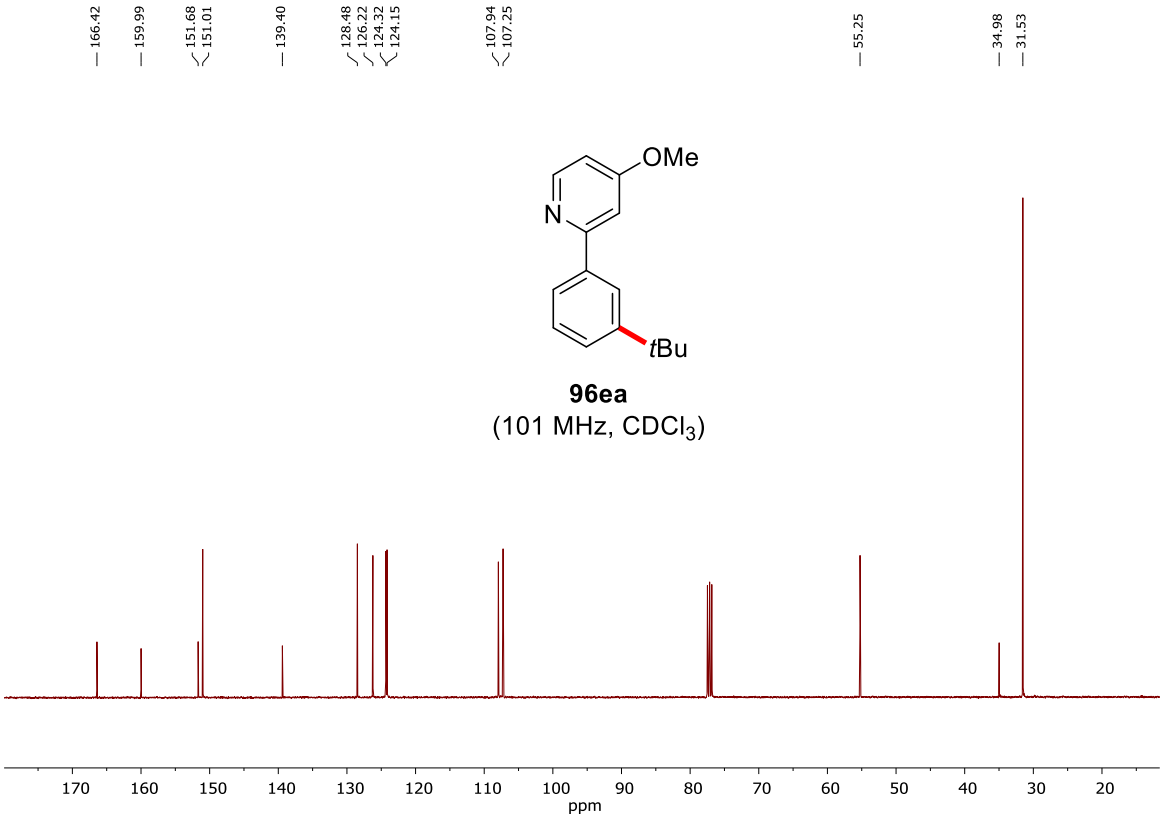

96ea
(101 MHz, $CDCl_3$)

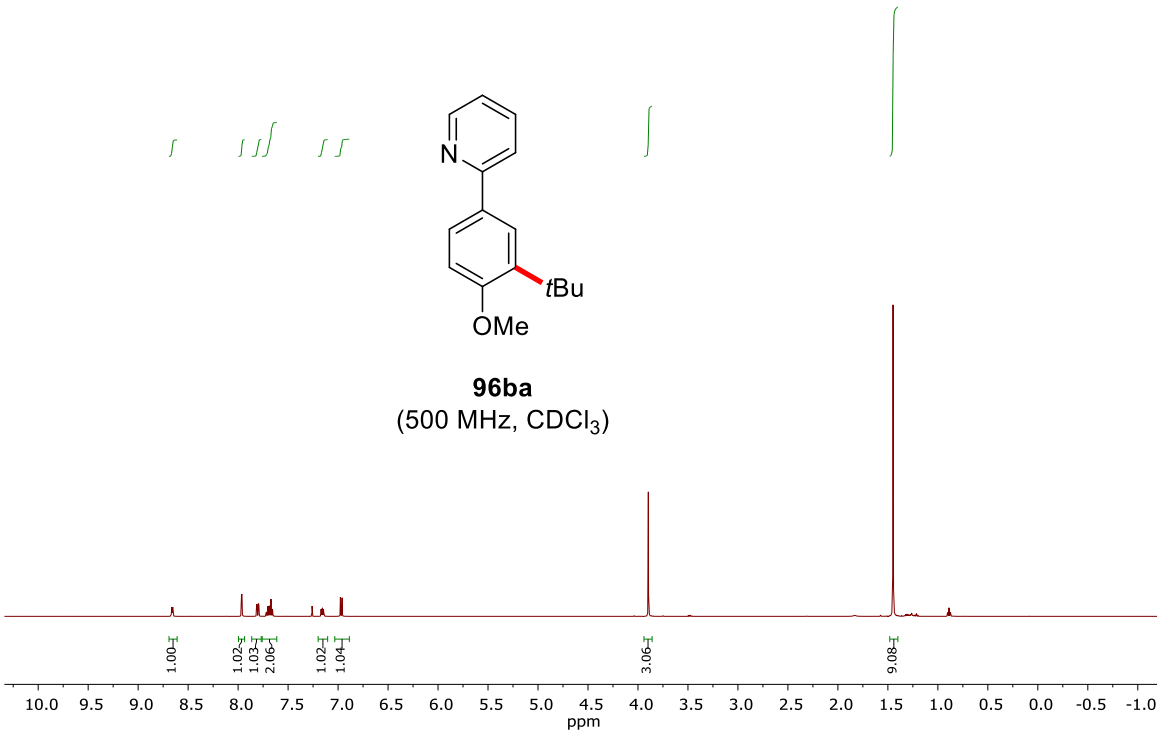

96ba
(500 MHz, $CDCl_3$)

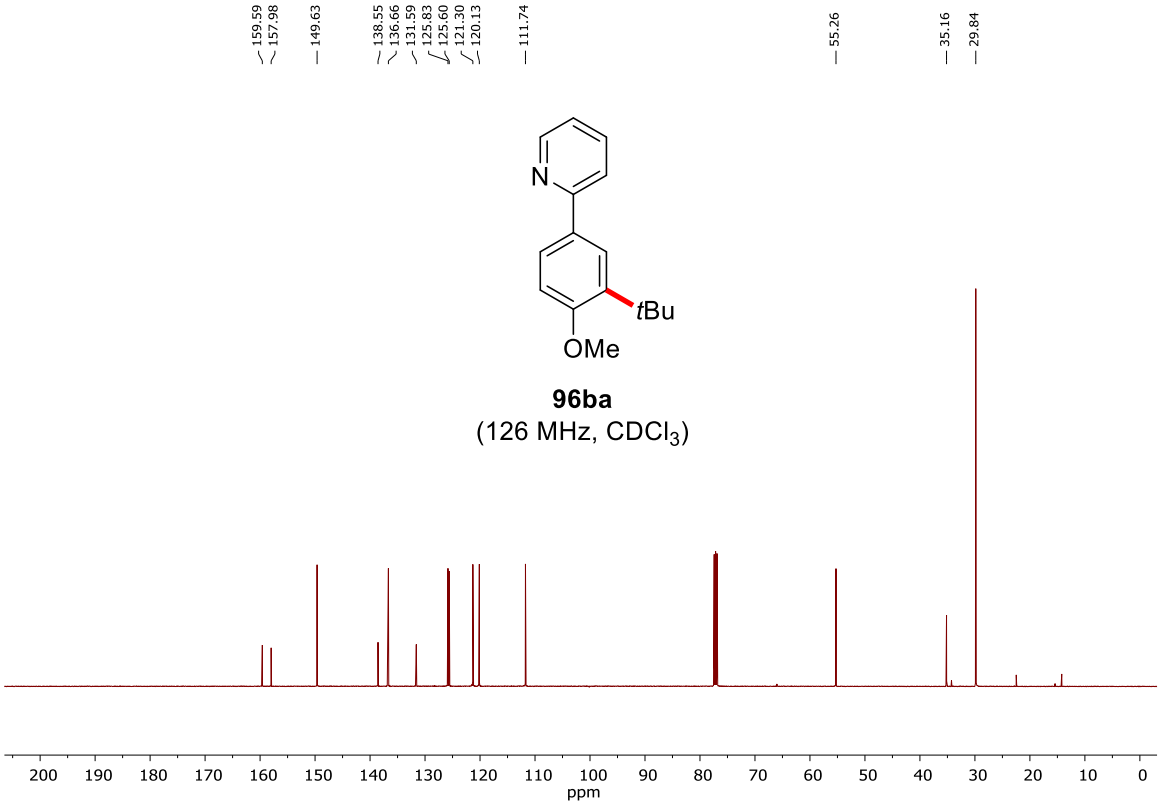

96ba
(126 MHz, $CDCl_3$)

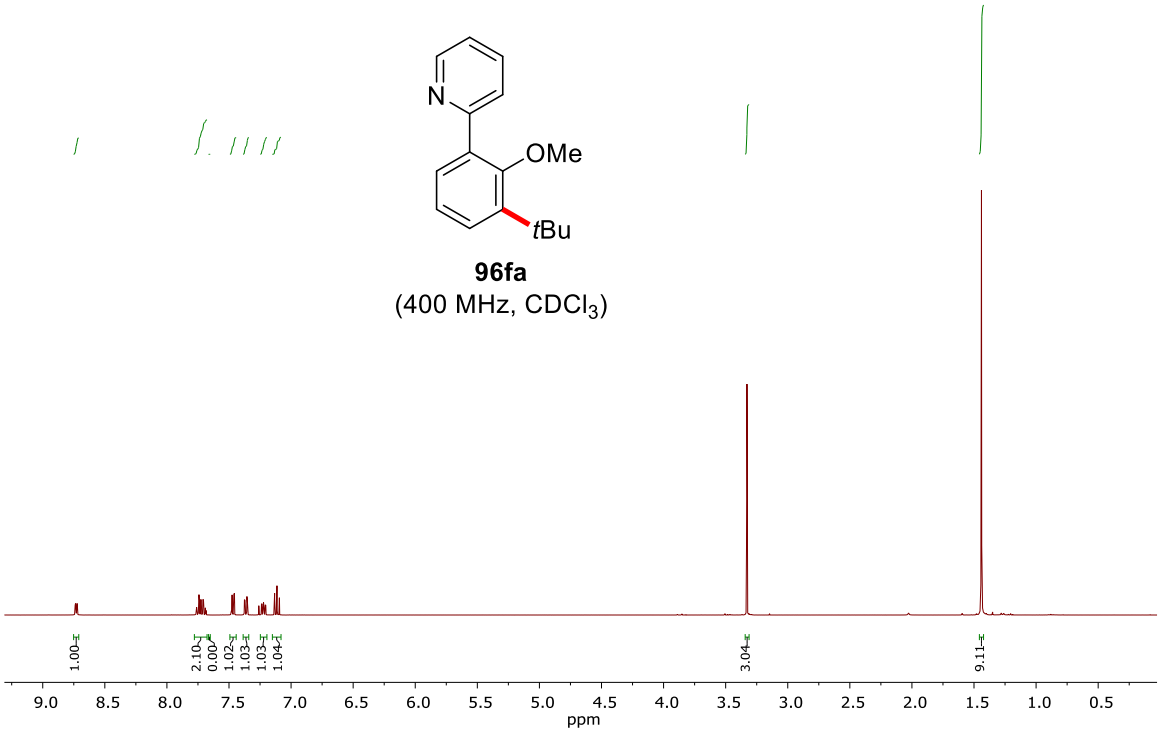

96fa
(400 MHz, $CDCl_3$)

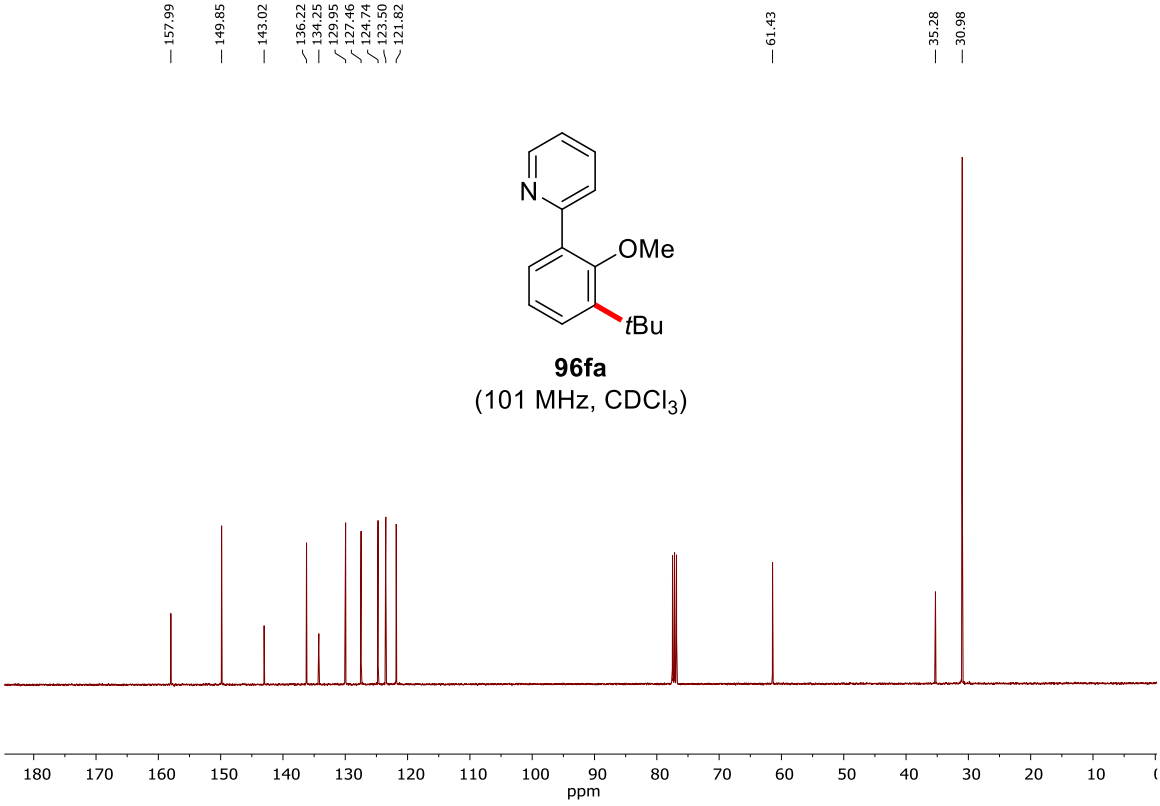

96fa
(101 MHz, $CDCl_3$)

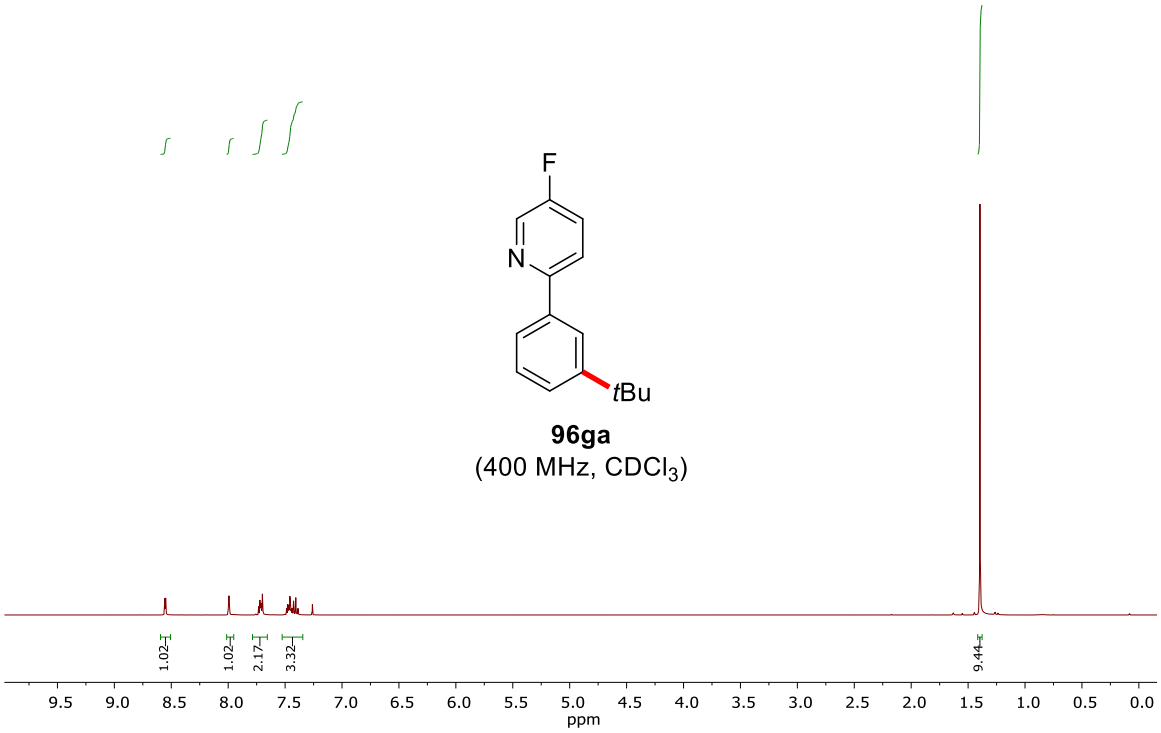

96ga
(400 MHz, $CDCl_3$)

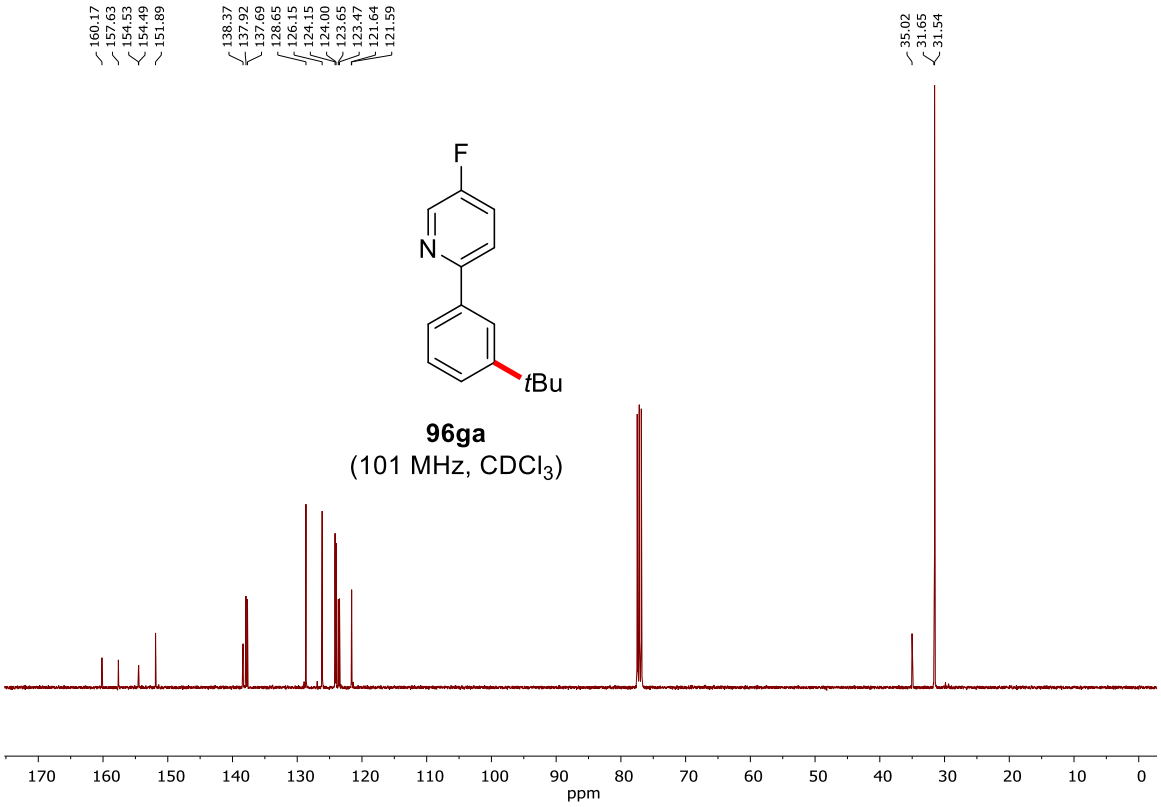

96ga
(101 MHz, $CDCl_3$)

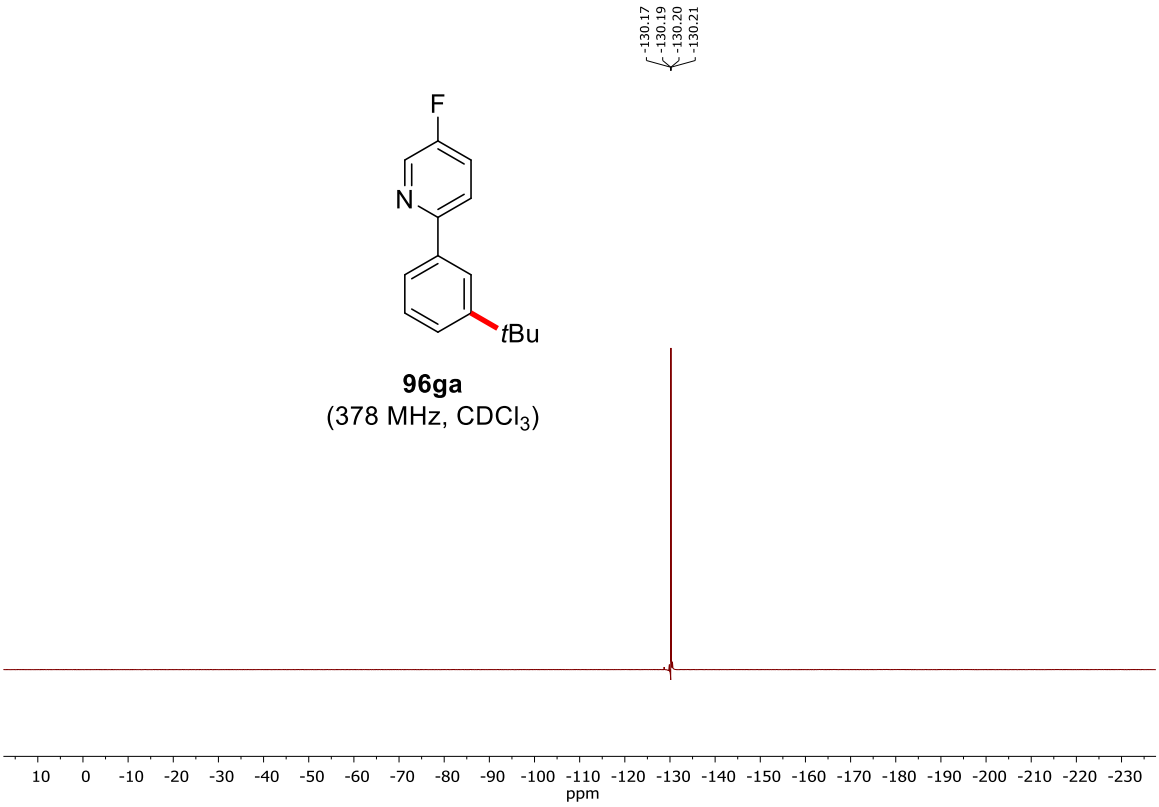

96ga
(378 MHz, $CDCl_3$)

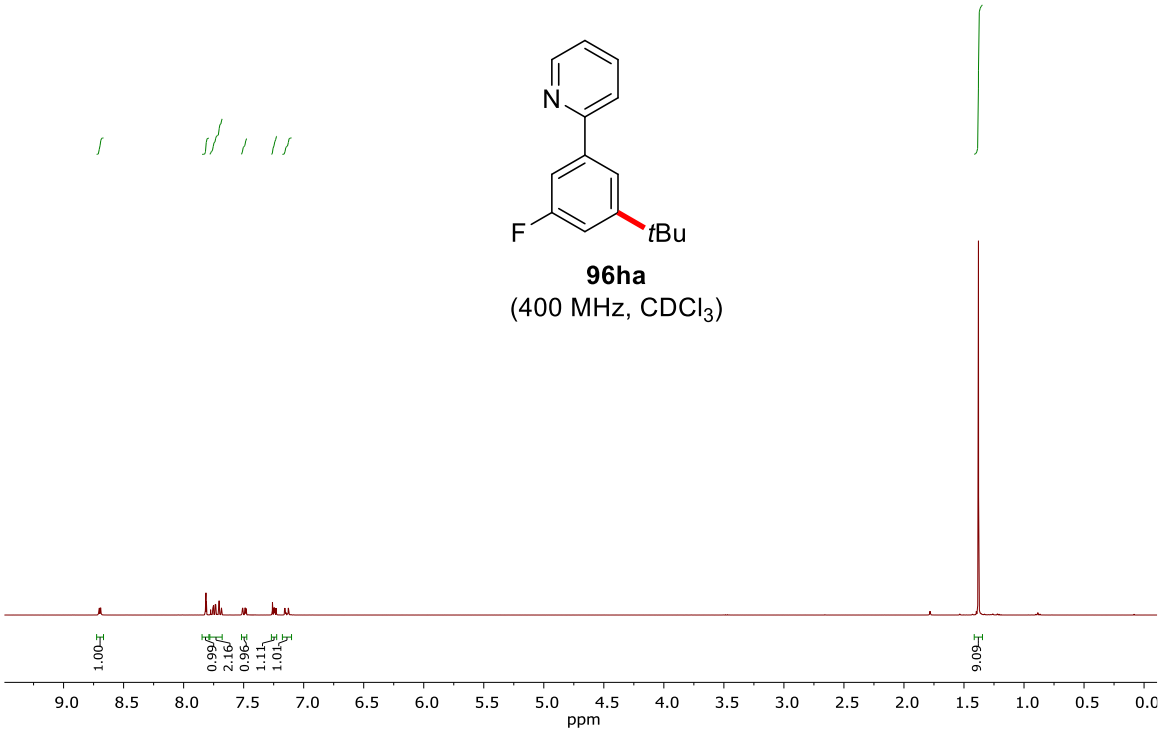

96ha
(400 MHz, $CDCl_3$)

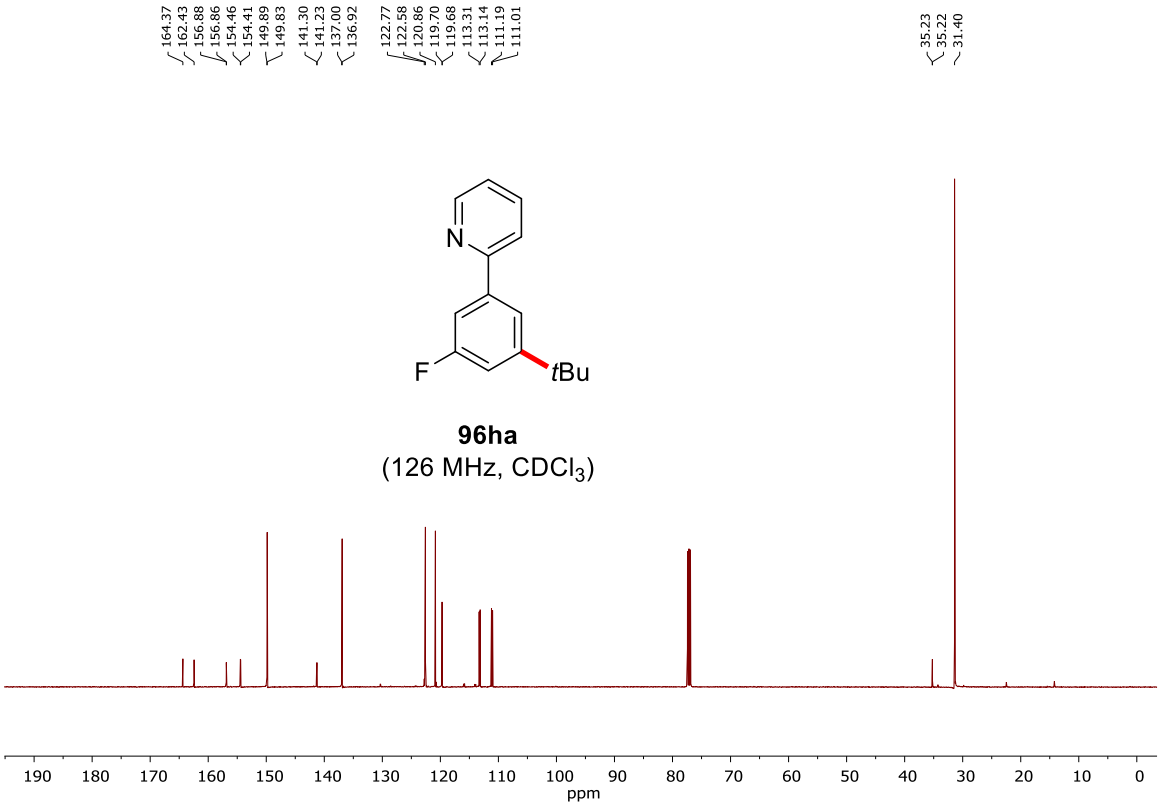

96ha
(126 MHz, $CDCl_3$)

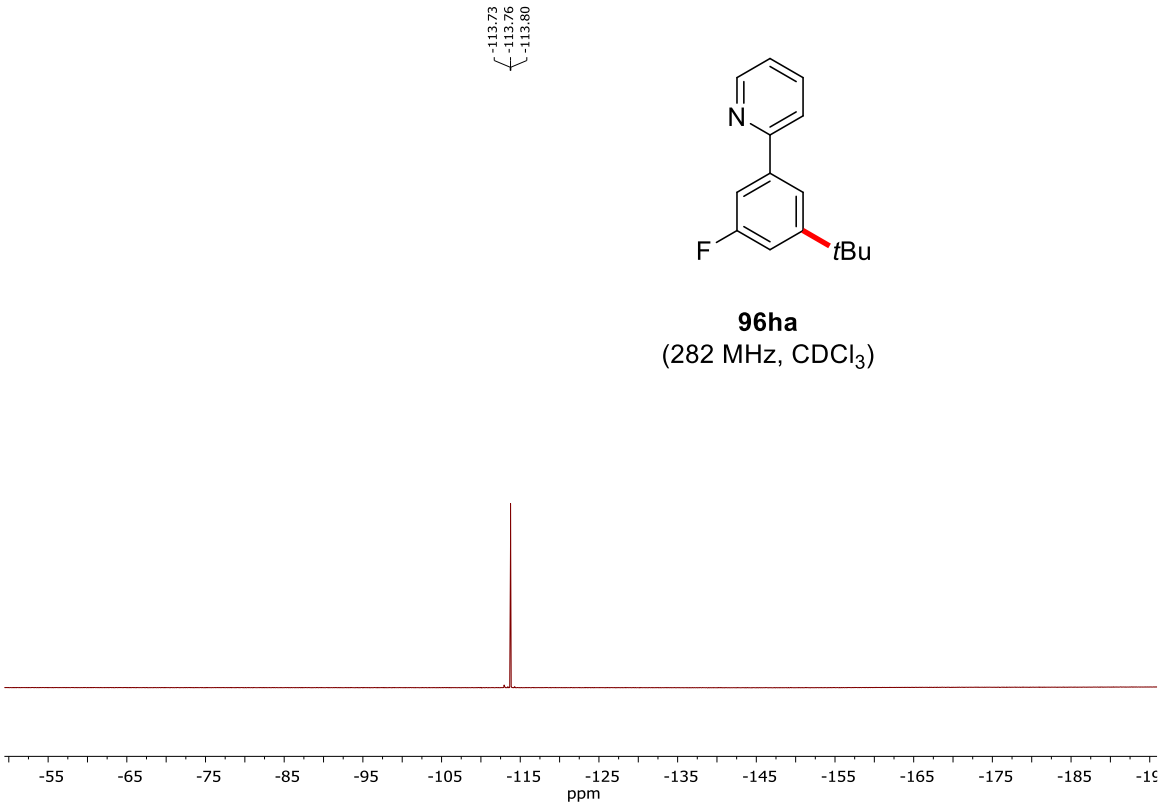

96ha
(282 MHz, $CDCl_3$)

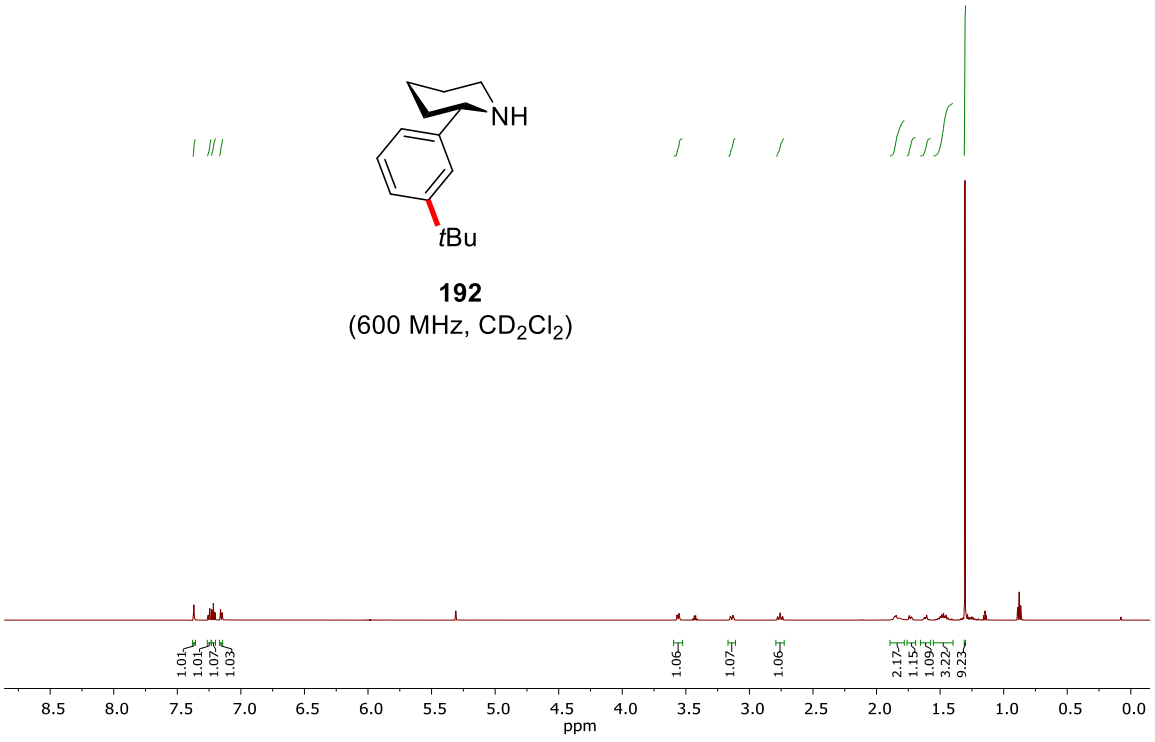

192
(600 MHz, CD_2Cl_2)

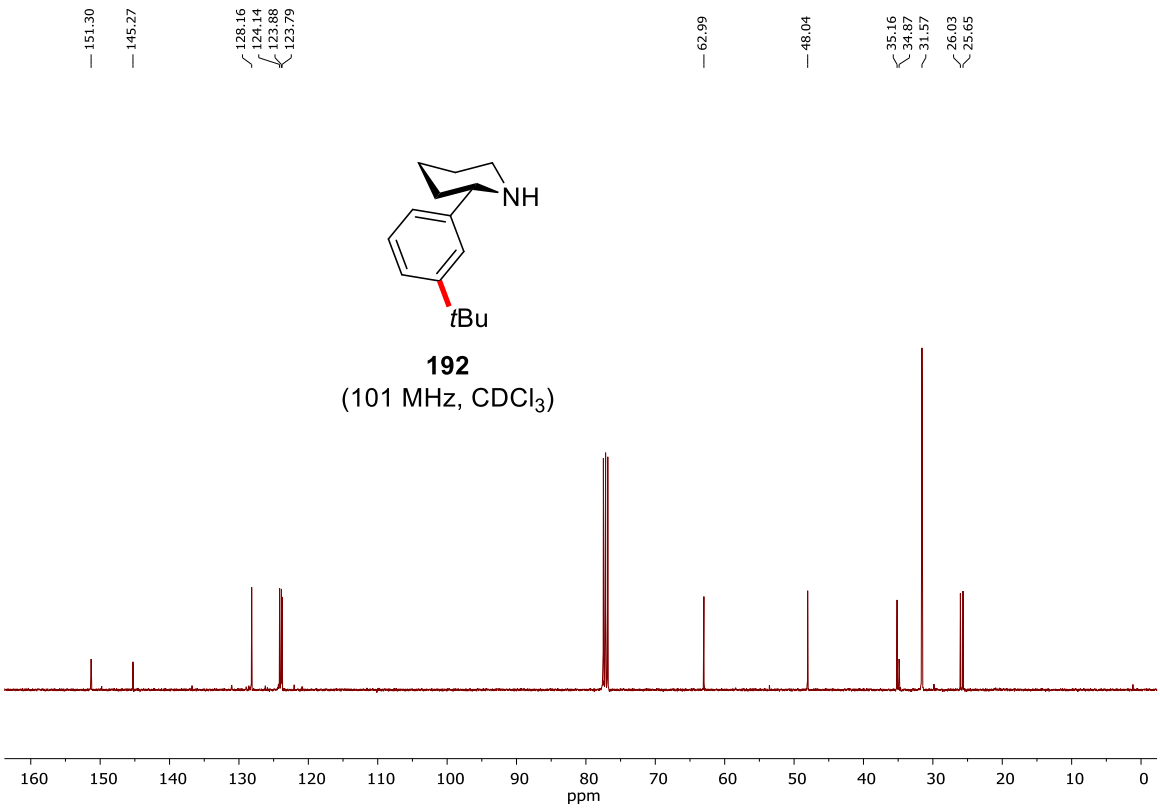

192
(101 MHz, $CDCl_3$)

Erklärung

Ich versichere, dass ich die vorliegende Dissertation im Zeitraum von Oktober 2015 bis Oktober 2019 am Institut für Organische und Biomolekulare Chemie der Georg-August-Universität Göttingen

auf Anregung und unter Anleitung von

Professor Dr. Lutz Ackermann

selbstständig durchgeführt und keine weiteren als die angegebenen Hilfsmittel und Quellen verwendet habe.

Göttingen, den 04.10.2019

_____

Julian Koeller

Curriculum Vitae

Personal Information

Name:	Julian Koeller
Date of Birth	28.06.1989
Place of Birth	Göttingen
Nationality:	German

Academic Education

10/2015–present	**Doctoral Candidate** Georg-August-University School of Science Göttingen Mentor: Professor Dr. Lutz Ackermann Title: Development of Photo-Induced C–H Activation by Copper and Ruthenium Catalysis
10/2012–08/2015	**Master of Science** in Chemistry Georg-August-University Göttingen Master Thesis: Cobalt(III)-Catalyzed C–H Allylation and Alkyne Annulation Mentor: Professor Dr. Lutz Ackermann
10/2009–09/2012	**Bachelor of Science** in Chemistry Julius-Maximilians-University of Würzburg Bachelor Thesis: Synthesis of Labelled Dioncoquinone B Derivatives Mentor: Professor Dr. Dr. h.c. mult. Gerhard Bringmann

Prior Education

08/2001–06/2008	Felix-Klein-Gymnasium Göttingen Abitur completed in 2008

Teaching Experience

10/2018–03/2019	Teaching assistant for the course “Chemie für Human- und Zahnmediziner”
04/2018–09/2018	Teaching assistant for the course “Organisch-Chemisches Praktikum für Lehramtskandidaten und Dipl. Biologen”
10/2017–03/2018	Teaching assistant for the course “Chemie für Human- und Zahnmediziner”
04/2017–09/2017	Teaching assistant for the course “Organisch-Chemisches Praktikum für Lehramtskandidaten und Dipl. Biologen”

10/2016–03/2017	Teaching assistant for the course “Analytik in der Organischen Chemie”
04/2016–09/2016	Teaching assistant for the course “Organisch-Chemisches Praktikum für Lehramtskandidaten und Dipl. Biologen”

Publications

7) P. Gandeepan, J. Koeller, K. Korvorapun, J. Mohr, L. Ackermann, "*Visible-Light for Ruthenium-Catalyzed meta-C–H Alkylation at Room Temperature*" *Angew. Chem. Int. Ed.* **2019**, *58*, 9820–9825.
6) J. Koeller, P. Gandeepan, L. Ackermann, *"Visible-Light-Induced Decarboxylative C–H Adamantylation of Azoles at Ambient Temperature" Synthesis* **2019**, 51, 1284–1292.
5) R. Mei, J. Koeller, L. Ackermann, *"Electrochemical Ruthenium-Catalyzed Alkyne Annulations by C−H/Het−H Activation of Aryl Carbamates or Phenols in Protic Media" Chem. Commun.* **2018**, *54*, 12879–12882.
4) P. Gandeepan, J. Koeller, L. Ackermann, *"Expedient C–H Chalcogenation of Indolines and Indoles by Positional Selective Copper-Catalysis" ACS Catal.* **2017**, 7, 1030–1034.
3) F. Yang, J. Koeller, L. Ackermann, *"Photo-Induced Copper-Catalyzed C–H Arylation at Room Temperature" Angew. Chem. Int. Ed.* **2016**, 55, 4759–4762.
2) H. Wang, J. Koeller, W. Liu, L. Ackermann, *"Cobalt(III)-Catalyzed C–H/N–O Functionalizations: Isohypsic Access to Isoquinolines" Chem. Eur. J.* **2015**, 21, 15525–15528.
1) M. Moselage, N. Sauermann, J. Koeller, W. Liu, D. Gelman, L. Ackermann, *"Cobalt(III)-Catalyzed Allylation with Allyl Acetates by C–H/C–O Cleavage" Synlett* **2015**, 1596–1600.

Conferences

3) Annual Meeting of Chemical Society Located in Taipei
   Kaohsiung (Taiwan), 2018
2) International Center for Advanced Studies of Energy Conversion (ICASEC) Summer School Göttingen (Germany), 2017
   Poster presentation
1) Annual Meeting of the workgroup on sustainable chemistry (GDCh)
   Karlsruhe (Germany), 2016
   Poster presentation

_____
Date, Signature